Australian Government
Geoscience Australia

2009 Australian Geothermal Energy Conference
Geothermal Downunder - Clean Energy from the Ground Up

Proceedings of the 2009 Australian Geothermal Energy Conference

Budd, A.R. and Gurgenci, H.

Record
2009/35

GeoCat # 69699

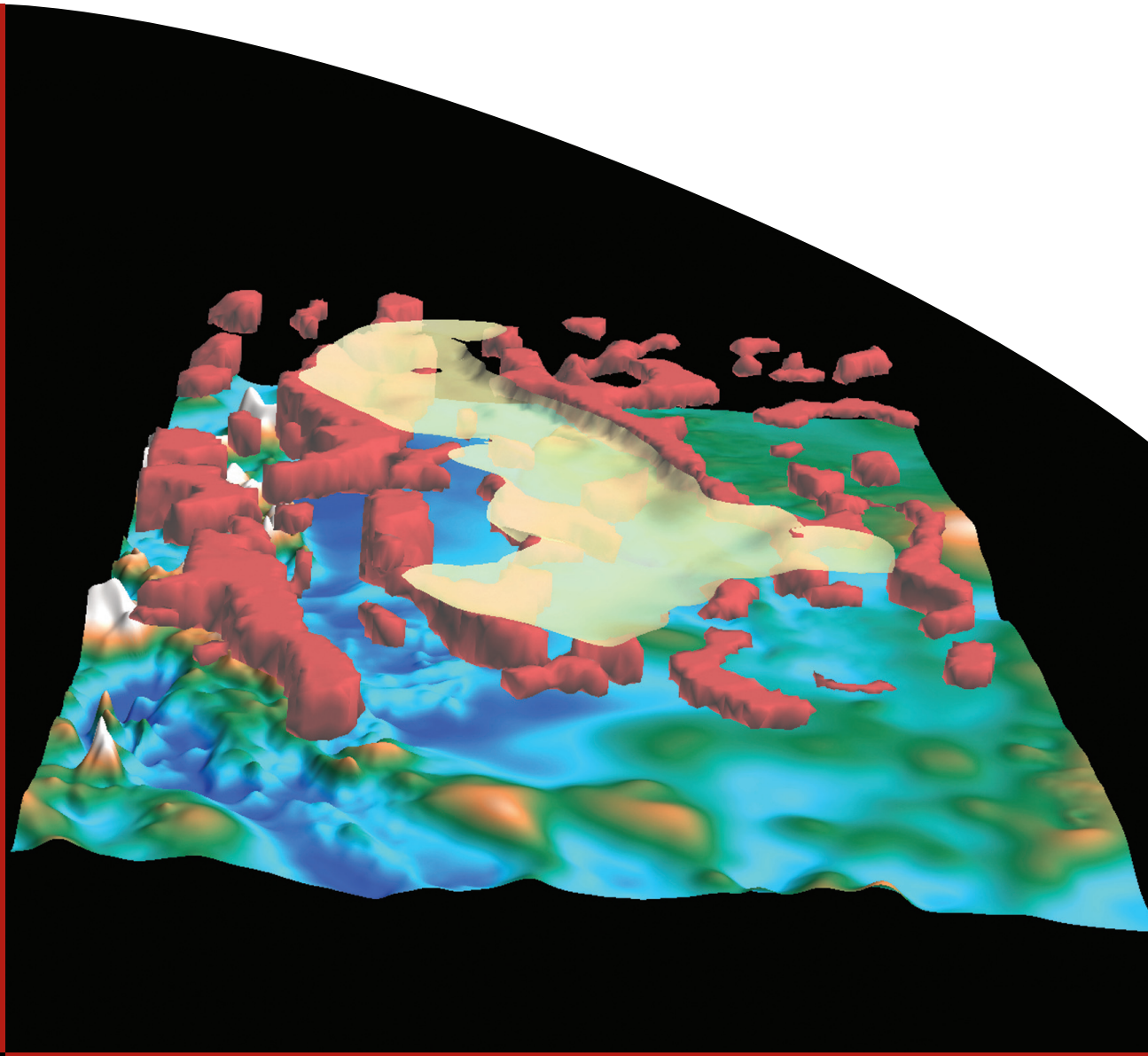

Proceedings of the 2009 Australian Geothermal Energy Conference

GEOSCIENCE AUSTRALIA

Record 2009/35

Edited by

Anthony Budd [1] and Hal Gurgenci [2]

1 Geoscience Australia, GPO Box 378, Canberra, ACT 2601

2 Queensland Geothermal Energy Centre, The University of Queensland, St Lucia 4072

Australian Government
Geoscience Australia

2009 Australian Geothermal Energy Conference
Geothermal Downunder - Clean Energy from the Ground Up

Department of Resources, Energy and Tourism
Minister for Resources and Energy: The Hon. Martin Ferguson, AM MP
Secretary: Mr John Pierce

Geoscience Australia
Chief Executive Officer: Dr Neil Williams PSM

ISSN 1448-2177
ISBN 978-1-921672-28-6

GeoCat # 69699

Recommended bibliographic reference: Budd, A.R. and Gurgenci, H. (editors), 2009. Proceedings of the 2009 Australian Geothermal Energy Conference, Geoscience Australia, Record 2009/35.

Recommended bibliographic citation: Chen, D. B. and Wong, G. 2009. Aims of a Basic EGS Model for the Cooper Basin, Australia, in: Budd and Gurgenci (editors), Proceedings of the 2009 Australian Geothermal Energy Conference, Geoscience Australia, Record 2009/35.

Cover illustration: 3D image of gravity inversion modelling in the are between Mt Isa and the Georgetown Inlier, Queensland, viewed obliquely from the south. The red bodies enclose regions of low density interpreted as granites located at depth beneath Millungera Basin sediments, the base of which is shown as the yellow surface. The interpreted granites are shown projected above an image of the Bouguer Gravity field, from which the inversion model was generated. Courtesy of Alison Kirkby, Geoscience Australia.

The Convenors would like to thank the following sponsors for their kind support:

Platinum Sponsors

Weatherford DRILLING INTERNATIONAL

Gold Sponsors

petratherm

GEODYNAMICS LIMITED

PANAX GEOTHERMAL

FINLAYSONS

Silver Sponsors

GreenRock Energy

TORRENS ENERGY LIMITED

KUTh ENERGY

Australian Government
Department of Resources, Energy and Tourism

Government of South Australia
Primary Industries and Resources SA

Queensland Government

General Trade Industries Pty Ltd

PARSONS BRINCKERHOFF

Bronze Sponsors

HOT DRY ROCKS PTY LTD
Geothermal Energy Consultants

senergy

Government of Western Australia
Department of Mines and Petroleum

Geological Survey of Western Australia

HERRENKNECHT VERTICAL

tiger Energy Services

PLANET GAS LIMITED

CSIRO

BAKER HUGHES

clean energy AUSTRALASIA

Greenearth Energy Ltd.

granite power

LUCAS BAUER RESOURCES

SKM SINCLAIR KNIGHT MERZ

WWW.3D-GEO.COM 3D GEO

HALLIBURTON

CES Cowell Electric

Wednesday Happy Hour | Conference Dinner | Thursday Happy Hour

Quantec Geoscience

activated logic STRATEGY INVESTMENTS COMMUNICATIONS

Schlumberger

Introduction

This volume is a compilation of Extended Abstracts presented at the 2009 Australian Geothermal Energy Conference, 11-13 November 2009, Hilton Hotel, Brisbane, organised by the Australian Geothermal Energy Association and the Australian Geothermal Energy Group.

This Conference is the second dedicated conference organised by the geothermal energy community in Australia. The first conference in August 2008 was made possible by seed funding from the Australian Government under the Sir Mark Oliphant International Frontiers of Science and Technology Conference funding scheme. This conference is made possible by the sponsoring companies acknowledged earlier and paying delegates.

This Conference is being held at a time of continuing rapid growth in all sectors of the geothermal community, but also following a time of restricted financing availability due to the Global Financial Crisis. The number of companies engaged in exploration stands at 48, the number of leases held or applied for is 386, and the value of the work program for these companies exceeds $1.5 billion between 2002-2013. The Australian Geothermal Energy Association serves as the peak industry representative body. The Australian Code for Reporting Exploration Results, Geothermal Resources and Geothermal Reserves has been in effect for over a year, and the second edition will be launched at this conference. The Universities of Queensland, West Australia, Adelaide and Newcastle have active established geothermal research programs. The Australian Government has continued its strong support of the sector through the international Partnership for Geothermal Technology, Geothermal Industry Development Framework and Technology Roadmap, the Geothermal Drilling Program, and the Onshore Energy Security Program.

This volume of Extended Abstracts is organised under five headings:

- Exploration
- Underground Science and Technology
- Power Conversion Technologies
- Legislation, Policy and Infrastructure
- Direct and Low-temperature Use

As editors of these proceedings, we first would like to thank the Technical Committee who have been very generous with their time to review the submissions and to work with the authors of the accepted submissions to improve the quality of the Abstracts and the presentations.

We also thank the Conference Chair Tony Hill and the rest of the Organising Committee who were brave enough to take on the job organising this second event on behalf of the Australian Geothermal Energy Association and the Australian Geothermal Energy Group. Jem Hansen and Impact Environment Conferences have done an excellent job in assisting the organisation.

We also thank again the sponsoring companies for their generous support.

We thank Geoscience Australia for publishing the proceedings.

Finally, we thank all delegates without whose participation none of this is worthwhile.

Anthony Budd

Hal Gurgenci

Conference Organising Committee

Tony Hill (Chair), Primary Industries and Resources South Australia
Dr Andrew Barnicoat, Geoscience Australia
Dr Graeme Beardsmore, Hot Dry Rocks Pty Ltd
Rod Bresnehan, Clean Energy Australiasia
Dr Anthony Budd, Geoscience Australia
Peter Green, Geological Survey of Queensland
Professor Hal Gurgenci, Queensland Geothermal Energy Centre of Excellence
Susan Jeanes, Australian Geothermal Energy Association
John King, Petratherm Ltd
Alan Knights, Green Rock Energy Ltd
Kumar Thambar, Queensland Office of Clean Energy

Program Technical Panel

Dr Anthony Budd (Chair), Geoscience Australia
Dr Bridget Ayling, Geoscience Australia
Delton Chen, Geodynamics Ltd
Gareth Cooper, Hot Dry Rocks Pty Ltd
Neal Evans, Geoscience Australia
Des Fitzgerald, Intrepid Geophysics
Ed Gerner, Geoscience Australia
Helen Gibson, GeoIntrepid
Professor Hal Gurgenci, Queensland Geothermal Energy Centre of Excellence
Alison Kirkby, Geoscience Australia
Alan Knights, Green Rock Pty Ltd
Chris Matthews, Torrens Energy Limited
Tony Meixner, Geoscience Australia
Professor Behdad Moghtaderi, The University of Newcastle
Professor Klaus Regenauer-Lieb, The University of Western Australia
Peter Reid, Petratherm Ltd
Michel Rosener, Geodynamics Ltd
Dr Catherine Stafford, Granite Power Ltd
Dr Adrian Williams, Geodynamics Ltd
Dr Doone Wyborn, Geodynamics Ltd

Conference Organisers

Jem Hansen & Dawn Hallinan
Impact Environmental Conferences
Ph: 02 6583 8118 Fax: 02 6583 8065
ausgeothermal@impactenviro.com.au

www.ausgeothermal.com

Exploration

Underground Science and Technology

Power Conversion

Direct/Low-temperature Use

Legislation/Policy/infrastructure

The Portable Electronic Divided Bar (PEDB): a Tool for Measuring Thermal Conductivity of Rock Samples

Anson M. Antriasian
Hot Dry Rocks Pty. Ltd.
Level 4, 141 Osborne Street, South Yarra, Victoria, 3141
anson.antriasian@hotdryrocks.com

The thermal conductivity of a geological formation is an essential physical property to be determined when attempting to understand and model heat flow. The Portable Electronic Divided Bar (PEDB) is an effective tool in measuring thermal conductivity, and is currently playing an important role in the development of heat flow modelling of Australian geothermal resources.

The PEDB is an electronic apparatus that produces a temperature gradient across a specially prepared rock sample; and with its precision heat flow monitoring system, it allows thermal conductivity of a rock sample to be determined via the application of Fourier's Law. A simple spreadsheet allows direct temperature measurements—utilizing thermocouples—to be recorded and interpreted to provide an absolute thermal conductivity value within ±3.5%. Measurements are rapid, taking from 5 to 15 minutes per sample.

In addition to uniaxial thermal conductivity measurements, biaxial and triaxial measurements can be made with the PEDB, allowing for studies of thermal conductivity anisotropy. Cylindrical core as well as irregularly shaped rock samples can be measured.

The Divided Bar was first described as a steady-state tool used to measure the thermal conductivity of materials by Benfield in 1939 (Beardsmore and Cull, 2001). The Portable Electronic Divided Bar (PEDB) is a development of Benfield's divided bar operating principal, utilizing advancements in technology to create a high accuracy (±3.5%), light-weight (less than 5 kg), small size (260 mm x 310 mm x 450 mm) and low power consumption (less than 200W), low noise production device.

In the field it is valuable for measuring the thermal conductivity of rock samples immediately after recovery from drilling, maintaining as closely as possible the rock's in-situ porosity and moisture content.

For use in laboratory settings, the space that is required is the corner of an office desk, a single AC power outlet, and a PC and logging device.

Keywords: PEDB, portable electronic divided bar, thermal conductivity, heat flow, anisotropy

Thermal Conductivity and Heat Flow

Observing Fourier's Law:

$$Q = \lambda \times \beta \qquad (1)$$

Q, λ, and β are heat flow (W/m^2), thermal conductivity (W/mK), and thermal gradient (K/m), respectively.

The heat flow of a site can be derived by utilising a combination of: 1) thermal conductivity measurements to define λ; and 2) down-hole temperature logging to define β. Determining heat flow requires consideration of the geologic formations from which the thermal conductivity samples came, and so rock samples that are to be tested for thermal conductivity must be carefully chosen to ensure they are appropriately representative of those geologic formations, with attention paid to characteristics such as lithology and porosity.

If thermal conductivity measurements from several geological formations are taken, it is possible to develop a down-hole profile of thermal conductivity.

Calculation of Thermal Conductivity

Thermal conductivity of a rock sample, as measured by a PEDB, is determined by:

$$\lambda = \frac{d}{R} \qquad (2)$$

λ = thermal conductivity

d = thickness of the sample in mm

R = (A (ΔT- c))/(a (diameter + b))

A = surface area of sample in mm^2

a, b, c, are calibration constants determined during the calibration process.

ΔT is defined by:

$$\Delta T = \frac{T_2 - T_3}{(T_1 - T_2) + (T_3 - T_4)} \qquad (3)$$

T_1, T_2, T_3, T_4 = temperatures of PEDB plates as shown on Figure 1.

The thermal conductivity of each rock sample is calculated using the measurements of the three values d, A, and ΔT, where ΔT is the ratio of the temperature drop across the sample relative to the sum of temperature drops across the polycarbonate layers within each plate-pair—a unit-less quantity.

The measurements of *d* and A are made utilising precision callipers; the measurement of ΔT is made utilising the PEDB, a PC, and a digital logging device.

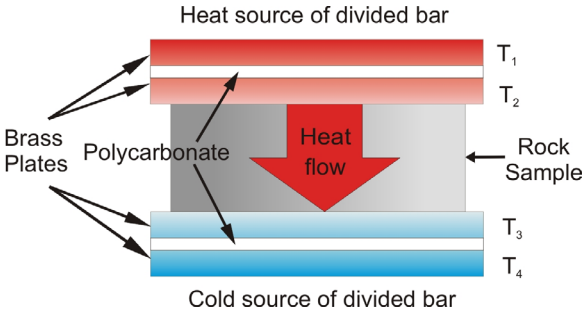

Figure 1: Diagram showing principal components of the plates of the PEDB. Each brass plate is fitted with a separate thermocouple; ΔT is the ratio of the temperature of the plates of the PEDB: $\Delta T = (T_2-T_3)/((T_1-T_2)+(T_3-T_4))$. The heat source is above the top pair of brass plates, and the cold source is below the bottom pair; the consequence is that heat flows across the rock sample.

The PEDB

Power supply

The PEDB has a 'universal' power supply, capable of being powered by mains sources that are within 100-250 VAC, 45-70 Hz. Portability of the PEDB can be achieved by using a sine-wave generator, a sine-wave inverter rated for 200 W from a power source such as an automobile, or from a DC source.

Plates of the PEDB

Two pairs of highly thermally conductive plates—brass in the case of the PEDB—are used, each with a layer of polycarbonate in between, comprising a brass-polycarbonate-brass assembly that resembles a sandwich, as shown in Figure 2. Each of these assemblies has a thickness of approximately 7mm and a diameter of 65 mm. One of the assemblies is situated on top of the rock sample—thermally connected to a heat source—and the other assembly is below the sample—thermally connected to a cold source. Such an orientation prevents: 1) convection from occurring between the plates and; 2) resultant introduced uncertainties.

Within each of the four brass plates is embedded a thermocouple with its welded joint located in the centre of the brass plate. Thus the temperatures of each brass plate can independently be measured and used to determine λ.

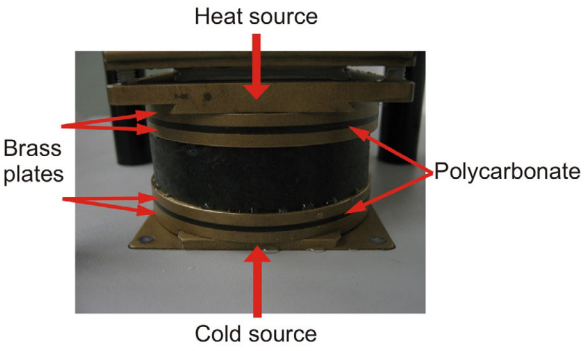

Figure 2: The plates of the PEDB. An HQ sized rock sample is in place and ready for thermal conductivity measurement. Each pair of plates is brass, with a polycarbonate layer in between. Above the upper plate is a heat source, and below the lower plate is the cold source--a thermal gradient across the sample is created; the ratio of the temperature drops across each of the polycarbonate layers and the sample is

Sample preparation

The PEDB measures the thermal conductivity of consolidated drill core. Samples measured for thermal conductivity can be any size up to a diameter of to 65 mm (approximate size of HQ core is 60mm). The samples should be cut so that the two faces of the sample produced are approximately parallel, although precise parallelism is not essential, owing to a swivel-head which allows for measurement of samples that are not perfectly parallel (Figure 3); sample preparation is consequently easier than with systems that do not allow for sub-parallel sample faces.

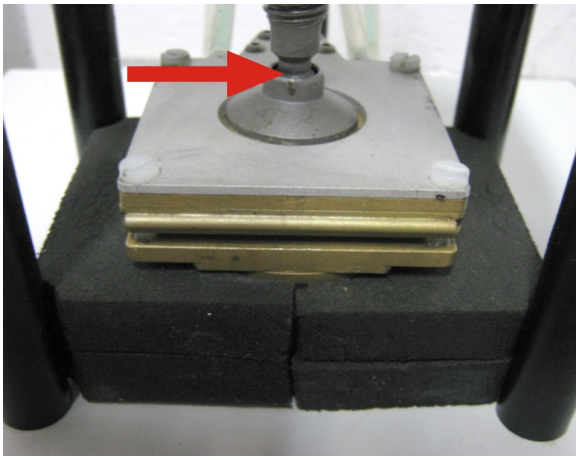

Figure 3: The swivel head (indicated by arrow) of the PEDB allows for thermal conductivity measurements of samples to be made without necessitating perfect parallelism between sample faces. Additionally, the black insulation shown is effective in minimizing thermal loss from the sample.

It is however essential that the faces of the rock sample are flat. This can be accomplished by using a flat grinding wheel and lap-wheel combination, which has been HDRPL's preferred

method for processing thermal conductivity samples thus far. The system of sample preparation should be standardized. Generally, polishing to a fine grade up to 600-grit is recommended.

If the samples being measured for thermal conductivity were saturated with water *in situ*, all efforts should be made to preserve the inter-pore water within the core sample. If this is not practicable, then the sample should be re-saturated before measurement via vacuum saturation. In such cases the samples are subjected to a vacuum for a standardized time before being submerged in water and returned to atmospheric pressure for a standardized time, whereafter they can be measured for thermal conductivity.

Importance of sample preparation quality

It has been observed that samples prepared with sub-flat faces or surface irregularities can return significantly lower measured thermal conductivity values. Examples of surface irregularities that have resulted in significant decrease in apparent thermal conductivity are:

- Convex sample faces resulting from worn grinding and polishing wheels.
- Grooved sample faces left over from the rock-sawing process; chips that have fractured from the sample during cutting.
- Pitted surfaces resulting from preparation of weakly consolidated rocks susceptible to “plucking” of grains.
- Sub horizontal fractures and/or joints.

As zones of low thermal conductivity and high water/air content that are created either within the sample itself or along the sample/plate contact, these irregularities effectively impede the heat flow across the sample. Careful efforts—implemented during sample selection, preparation, and measurement—are essential for producing representative thermal conductivity results. The overwhelming majority of core samples that have been encountered by the author during conductivity measurement have provided useful samples for reliable thermal conductivity measurements, when carefully prepared.

Relevance of size and shape of samples tested in the PEDB

Irregularly shaped rock samples can be measured. The accuracy of thermal conductivity measurements is independent of sample shape so long as thermal loss around the perimeter of the sample is minimized. Generally, the thermal loss that may exist for a sample would increase as its surface area increases, but this tendency is effectively controlled with the use of thermal insulation around the PEDB plates and rock sample (Figure) which prevents environmental air circulation from interfering with thermal conductivity measurements.

Figure and Figure 5 show examples of measurements that were made on differently shaped rock samples. In both cases, samples were ground flat, polished, and were of a variable siltstone lithology. Variation in thermal conductivity was 5% or less from the mean in both cases, consistent with normal inter-sample variation.

The dimensions of a rock sample that must be measured when calculating thermal conductivity are thickness and heat flux cross-section. Thickness is measured with precision calipers. Heat flux cross-section can found by measuring the surface area of the rock sample’s face, either by calculating from core diameter, or by tracing the sample and measuring the surface area of the tracing digitally (via scanner and digital graphics software) or on to graph paper. Experiments have shown that variations in results of measurements made via the tracing method and via the calculation from diameter method are within 0.7% variation from the mean.

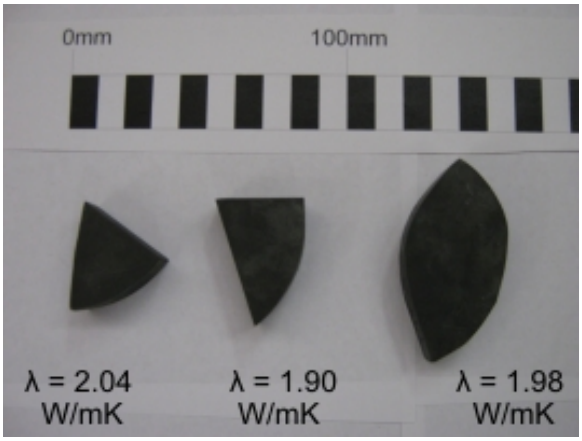

Figure 4: Although varying significantly in size and shape, these samples—which were taken from the same rock specimen—provide consistent results. Their conductivities are 2.04, 1.90, and 1.98 W/mK respectively, representing a range of 3.5% from the mean conductivity of 1.97 W/mK.

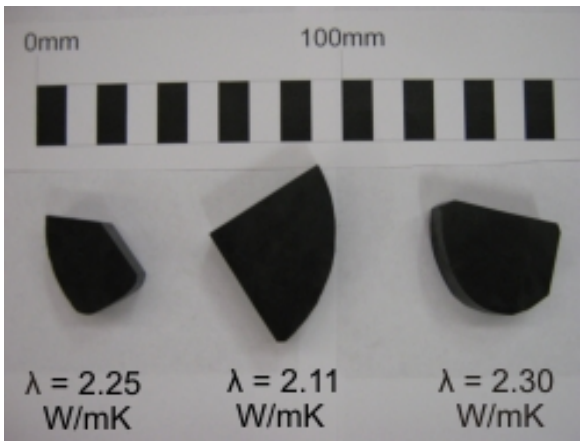

Figure 5: Although varying significantly in size and shape, these samples—taken from the same specimen—provide consistent results. Their conductivities are 2.25, 2.11, and 2.30 W/mK respectively, representing a range of 5% from the mean conductivity of 2.22 W/mK.

Mean Sample Temperature of the PEDB

The PEDB operates best when the mean sample temperature is near the environmental air temperature. To facilitate field operations, the PEDB is capable of operating at a range of mean temperatures, from approximately 10–35°C, and has an indication system showing when the mean temperature approximates the environmental temperature.

Thermal conductivity for rocks is dependent upon temperature, generally becoming less conductive with increasing temperature, at a rate of approximately 0.16% per degree Celcius (Vosteen and Schellschmidt, 2003). This must be kept in mind when determining the thermal conductivity of geological formations, where the *in-situ* temperature is greater than that at which the laboratory tests were made.

Equilibration Process

Once the sample is placed between the plates of the PEDB and slight pressure is applied to the sample via the hand-operated clamp, a temperature gradient is imposed across the sample and thermal equilibrium typically occurs within 5–15 minutes. The time required is dependent upon sample thickness and surface area, and upon the thermal characteristics of the rock sample—most importantly, thermal diffusivity. A sample will equilibrate relatively quickly if it is thin, and has a high surface area and thermal diffusivity. Alternatively, a sample will take longer to equilibrate if it is very thick, and has a low surface area and thermal diffusivity. Figure 6 and Figure 7 represent 1000 seconds of recorded data from the same thermal conductivity measurement.

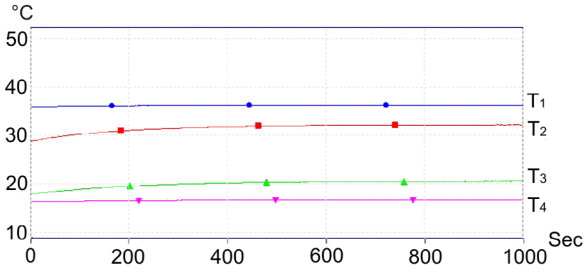

Figure 6: Example of data collected during thermal conductivity measurement; the horizontal axis is time, measured in seconds, and the vertical axis is temperature measured in °C. Each plot represents the temperature of a plate of the PEDB, T_1–T_4, where the hot plate (T_1) in this case is approximately 35°C, the cold plate (T_4) is approximately 17°C, and the intermediate plates (T_2 and T_3), after having a rock sample placed in between them, gradually increase in temperature until thermal equilibrium is reached.

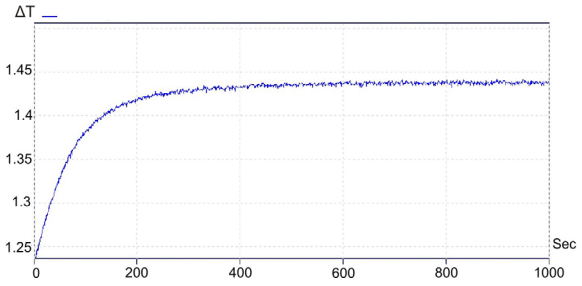

Figure 7: Example of data collected during thermal conductivity measurement; the horizontal axis is time, measured in seconds, and the vertical axis is ΔT. In this example, the sample measured for thermal conductivity is fully equilibrated after approximately 600s, to a ΔT value of 1.44.

Calibration of the PEDB

The PEDB is calibrated using a set of standards of known thermal conductivity. These standards are of differing thicknesses and surface areas, enabling the PEDB to be used for measuring diversely shaped samples, and samples with a range of thicknesses and surface areas.

During calibration, standards are placed in the PEDB individually and measurements are made of the four plate temperatures T_1–T_4 and the derived ΔT value once the standard has reached thermal equilibrium.

Measurement of thermal conductivity anisotropy

Anisotropy is the characteristic of a material to behave differently in one direction with respect to another. Rocks can be thermally anisotropic, and in so being can exhibit different thermal conductivity in different directions.

Typically, thermal conductivity measurements are made along the long axis of a core specimen. During such testing, it is the expectation of the heat flow modeller that the core specimen was

taken from a bore that was drilled nearly vertically, and therefore was sufficiently parallel to Earth's heat flow that the need for understanding how heat travels laterally across the core specimen is negated.

Testing for thermal conductivity anisotropy of a rock sample involves biaxial or triaxial measurements. The preparation of cube-shaped samples allows thermal conductivity to be measured along each axis of the same sample; thus, one sample can provide the minimum data required for the creation of an ellipsoidal thermal model. Alternatively, three orthogonally oriented samples can be prepared from a common specimen, collectively providing data for the creation of an ellipsoidal thermal model.

For foliated meta-sedimentary specimens, the tendency has been observed (Figure 8) for thermal conductivity to be greater parallel to the foliation, compared to perpendicular to the foliation. In this paper, λ_1 is nominated as the axis of greatest thermal conductivity, while λ_2 is nominated the axis of least thermal conductivity, and it is assumed that there is an elliptical gradation between λ_1 and λ_2.

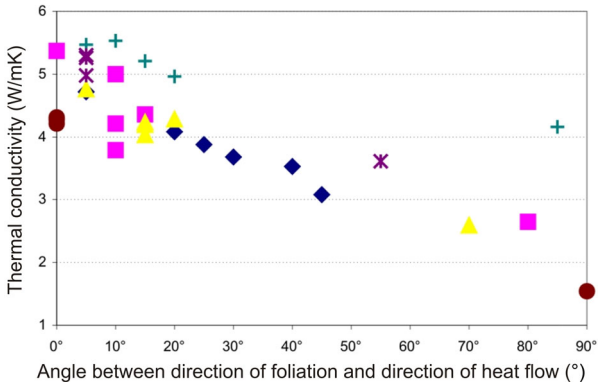

Figure 8: Summary of thermal conductivity data from six meta-sedimentary rock specimens; the six differently shaped symbols indicating the different specimens studied. Each specimen was measured for thermal conductivity at several angles with respect to the specimen's foliation. The vertical axis is thermal conductivity (W/mK); the horizontal axis is the angle between the foliation of the rock sample, and the direction of heat flow across the rock sample while within the PEDB, measured in degrees (°), where 0° indicates heat flow parallel to the planes of foliation, and 90° indicates heat flow perpendicular to the planes of foliation. A relationship is shown to exist between the magnitude of thermal conductivity and the direction of heat flow with respect to the specimen's foliation.

Results of anisotropy testing

The results of two extreme cases of rock thermal conductivity anisotropy are shown in Figure 8 and discussed below.

A foliated meta-sediment, Specimen A had a mean conductivity of 4.26 W/mK parallel to foliation, and a mean conductivity of 1.44 W/mK perpendicular to foliation. That is a variation of 50% from the mean conductivity of 2.85 W/mK. The anisotropy factor for Specimen A expressed as λ_1/λ_2, is 2.96.

Another foliated meta-sediment, Specimen B, had a mean conductivity of 5.37 W/mK parallel to foliation, and a mean conductivity of 2.65 W/mK perpendicular to foliation. That is a variation of 34% from the mean conductivity of 4.01 W/mK. The anisotropy factor for Specimen B expressed as λ_1/λ_2, is 2.03.

In both cases, λ_1 was parallel to the rock specimen's foliation, while λ_2 was perpendicular to the rock specimen's foliation. In addition, λ_1 and the foliation were within 5° of parallel to the bore in both cases. Since the bores that these samples originated from were vertical, the thermal conductivities that would be most relevant to the heat-flow modeller—for the location within the geological formation from which the specimens came—would be those that were parallel to Earth's heat flow, and in these cases parallel to λ_1. The conductivity values most relevant for heat flow modelling of geological formations represented by specimens A and B, would be 4.26 W/mK and 5.37 W/mK respectively.

Calculation of variability in thermal conductivity

But what if the bores, foliation, and the direction of λ_1 discussed immediately above were NOT parallel to Earth's heat flow, and happened to be dipping at 45° instead, as it might in a steeply-dipping mineral exploration bore? In such a case, Earth's heat flow is now no longer parallel with the bore, but is 45° to it; and consequently, the thermal conductivity vector of the rock specimen most relevant to the heat flow modeller is that which is parallel to the direction of Earth's heat flow. Using an elliptical thermal conductivity blending model, where λ_1 and λ_2 are the vectors representing the greatest and lowest thermal conductivities respectively, the resultant thermal conductivity vector for 45° can be determined.

The elliptical model is derived beginning with the equation for an ellipse:

$$1 = \frac{x^2}{a^2} + \frac{y^2}{b^2} \qquad (4)$$

$x = \lambda \cos \theta$

$y = \lambda \sin \theta$

$a = \lambda_1$

$b = \lambda_2$

λ = resultant thermal conductivity when heat flow is at angle θ

λ_1 = vector of greatest thermal conductivity

λ_2 = vector of least thermal conductivity

θ = angle in (°) between the direction of Earth's heat flow and λ_1

Substituting variable into Equation (4) gives:

$$1 = \frac{\lambda^2 \cos^2 \theta}{\lambda_1} + \frac{\lambda^2 \sin^2 \theta}{\lambda_2} \quad (5)$$

Solving for λ in Equation (5) gives:

$$\lambda = \sqrt{\frac{1}{\frac{\cos^2 \theta}{\lambda_1} + \frac{\sin^2 \theta}{\lambda_2}}} \quad (6)$$

By applying the λ_1 and λ_2 data from the results of anisotropy testing into Equation (6), the equivalent uniaxial thermal conductivity of the rock samples A and B can be determined:

Sample A:

λ_1 = 4.26 W/mK and λ_2 = 1.44 W/mK

The resultant λ when λ_1 is dipping at 45° is: 1.93 W/mK

Sample B:

λ_1 = 5.37 W/mK and λ_2 = 2.65 W/mK

The resultant λ when λ_1 is dipping at 45° is: 3.36 W/mK

Significance of variability in thermal conductivity

The resultant λ of sample A and B at 45° is 1.93 and 3.36 W/mK respectively. These values are significantly different than either of their respective λ_1 or λ_2 values.

Sample A

55% variation from λ_1 (4.26 W/mK)

34% variation from λ_2 (1.44W/mK)

Sample B

37% variation from λ_1 (5.37 W/mK)

27% variation from λ_2 (2.65 W/mK)

When entered into a heat flow model, this variation in measured thermal conductivity may result in significant variation of calculated heat flow.

While bores drilled purposefully for geothermal energy exploration may as a rule be vertical, bores such as those used for minerals exploration may be significantly non-vertical owing to the efforts of the exploration program to maximize the likelihood of hitting a target lode. Thus, care should be taken when utilizing core from non-vertical bores for geothermal data, ensuring that thermal conductivity anisotropy is accounted for when developing heat flow models.

Limitations of the PEDB

The PEDB is not calibrated for measuring conductivities of samples larger than 65 mm in diameter. Larger core or hand specimens can however be accommodated by cutting them to a suitable size.

The PEDB provides thermal conductivity measurements at mean temperatures from 15–35°C. Considerations of the geological formation's *in-situ* temperature should be made, since thermal conductivity in rocks is a property that generally decreases with increasing temperature.

Conclusions

The PEDB is effective in measuring thermal conductivity of rock specimens:

- Rapidly and on a production scale
- In remote locations and in the laboratory
- Using variable power supplies
- That have a non-standardized size and shape
- Triaxially for thermal conductivity anisotropy studies
- In parallel (two PEDB's can be operated simultaneously)

References

Vosteen, H.D. and Schellschmidt, R., 2003. Influence of temperature on thermal conductivity, thermal capacity and thermal diffusivity for different types of rock. Physics and Chemistry of the Earth, 28, 499–509.

Beardsmore, G.R. and Cull, J.P., 2001. Crustal Heat Flow, A Guide to Measurement and Modelling, 108 pp.

Modelling in Geothermal Exploration

Graeme R Beardsmore*
Hot Dry Rocks Pty Ltd
Level 4, 141 Osborne Street, South Yarra VIC 3141

In geothermal studies we often have to draw conclusions and make decisions using uncertain or incomplete data sets. In such circumstances, we are compelled to rely on 'modelling'. Modelling takes many forms and is used for many purposes, from temperature prediction to cash flow prediction.

Equations typically modelled in geothermal studies include the heat flow equation, phase change equations, fluid dynamics equations, Rayleigh number equations, project valuation equations or hydro-geo-mechanical equations. Models of geothermal systems are often constrained by geophysical measurements, observations of structural trends, geochemical signatures, flow rate observations, or temperature measurements.

Thermal modelling sheds light on probable temperatures at depth prior to expensive drilling. Reservoir modelling, likewise, helps predict the performance of future geothermal production wells, with increasing confidence as reservoir properties are constrained. Economic modelling, however uncertain, is essential to make informed investment and project development decisions.

Keywords: Modelling, Inversion, Stored Heat, Numerical Simulation, Economic Modelling

Introduction

In geothermal studies we often have to draw conclusions and make decisions about complex systems using uncertain or incomplete data sets. In such circumstances, we are compelled to rely on 'modelling' to make sense of the data. But modelling, itself, often presents us with an assortment of possible methods. This paper briefly covers some of the common instances where modelling is required in geothermal; the type of data required; the range, strengths, and weaknesses of the different available modelling methods; and what stages in the development process each might be appropriate.

The authoritive online dictionary '*wiktionary.com*' defines a 'model' as "(1) A person who serves as a subject for artwork or fashion, usually in the medium of photography but also for painting or drawing. (2) A miniature representation of a physical object. (3) A simplified representation (usually mathematical) used to explain the workings of a real world system or event."

Some individuals in the industry may fit definition (1), but the processes we use to make sense of disparate geothermal data fall into definition (3). The purpose of models is to assist predictions about variables that are beyond the current reach of measurements. Models might be used to help predict the location of undiscovered heat sources, the temperature and reservoir conditions at un-drilled depths, or the income from a geothermal development at some time in the future.

"Real world systems" that can be modelled in geothermal studies include:

- Geological structures
- Underground temperatures (°C)
- Response of fracture networks to stress
- Well productivity (MWt)
- Generation capacity (MWe)
- Cash flow for a project

All modelling should be based on observations or measured data. Models based on 'estimated' or 'assumed' values do not add value to a project because the outputs of any model are only as reliable as the inputs. If the inputs are poorly constrained, so are the outputs.

Models must also conform to the laws of physics, such as conservation of mass and energy. A robust model is a mathematical representation of a system that honours all relevant governing equations, and is consistent with *all* observed or measured data. We say that these known data '*constrain'* the model.

Models can be developed around many different governing equations and be constrained by many different types of data. Relevant governing equations in geothermal studies may include the heat flow equation, phase change equations, fluid dynamics equations, Rayleigh number equations, project valuation equations or hydro-geo-mechanical equations. Models of geothermal systems are often constrained by geophysical measurements, observations of structural trends, geochemical signatures, flow rate observations, or temperature measurements.

Modelling terms that are commonly used, but rarely explained, include:

- *1D*, *2D*, *3D*, 4D, *2.5D* etc
- *Forward modelling* versus *inversion*
- *Stored heat* versus *numerical simulation*
- *Hydro-geo-mechanical modelling*
- *Economic modelling*

The following sections explain each of these terms and how they relate to “real world systems”.

1D, 2D, 3D, 4D, 2.5D etc

The “D” in these terms means “dimension”—usually spatial dimension. The first three dimensions are the three orthogonal dimensions of space (or ‘length’, ‘width’ and ‘depth’). The fourth dimension is (usually) time. 1D modelling is sufficient for processes that happen in a straight line. If a process intrinsically encompasses an area or a vertical section, then a minimum of 2D modelling is required. Processes involving volumes of rock or space require 3D models, while 3D processes that change through time have to be represented by 4D models.

‘2.5D’ modelling refers to when a system effectively only varies in two dimensions, but is assumed to extend infinitely and unchanged into the third dimension. Thus, for example, a three dimensional block can be entirely represented by a two dimensional cross-section.

1D modelling

An example of 1D modelling is predicting the temperature (T_z) at a particular depth (z) when we know surface heat flow (**Q**) and assume vertical conductive heat transfer in the crust (Figure 1).

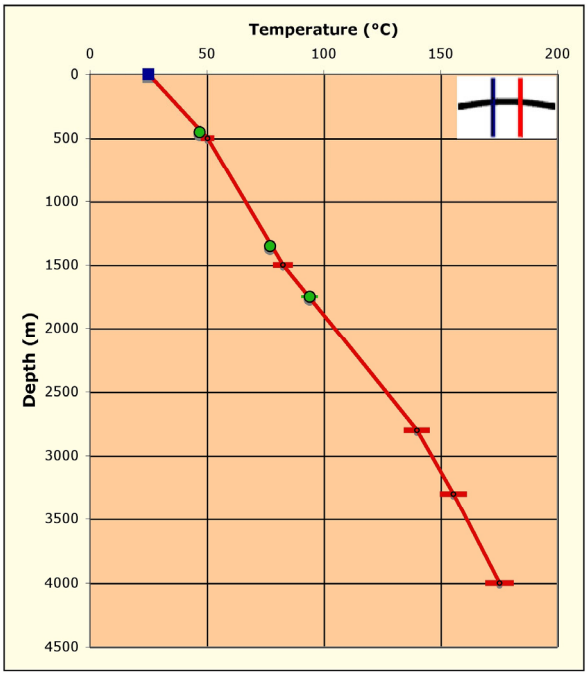

Figure 1. 1D conductive heat flow model of temperature increase with depth. Only one dimension (‘depth’) is modelled, with results (‘temperature’) plotted on the x-axis. Constraining temperature data shown in green.

The governing equation for this is:

$$T_z = T_0 + \mathbf{Q}.\Sigma\mathbf{R} \qquad \textbf{Eq 1}$$

where T_0 is the surface temperature and $\Sigma\mathbf{R}$ is the cumulative thermal resistance (physical thickness divided by thermal conductivity) between the surface and depth, z. All the energy transfer occurs vertically so the system can be represented in a single dimension.

1D models have the advantage that they are easy to comprehend, are computationally relatively simple, do not require much computer memory or processing power, and deliver rapid results. They are appropriate for rapid regional reconnaissance, or in situations where data may only be available for a single location. Their disadvantages include the fact that very few natural processes are truly one-dimensional, so certain simplifications are inherent in the models.

2D Modelling

Some problems are too complex, or inherently areal or spatial in scope, to reduce to 1D. An example might be modelling the thermal effect of convection in a permeable layer. This requires at least a 2D space to represent the vertical and horizontal movement of water and heat (Figure 2).

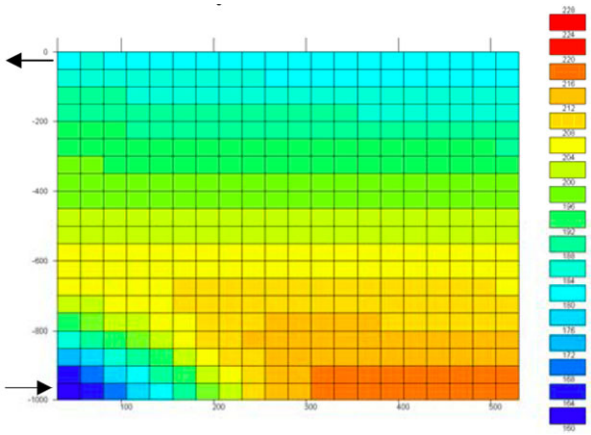

Figure 2. 2D model of temperature (°C) distribution where cool water enters the bottom left of the model and exits at the top left. The axes represent the physical dimensions, and the result (temperature) is represented by cell colour. This could not be modelled in 1D. After Wang *et al*. (2009).

Higher Dimensional Modelling

The real world is inherently four-dimensional. Everything exists in three-dimensional space and time. The higher the dimension of modelling, therefore, the closer a model can approximate ‘reality’. However, higher dimensional modelling comes with significant challenges.

It is usual to break each dimension of a model into sub-sections and to treat each subsection as a discrete unit. In a 1D model, this may result in several tens or hundreds of discrete units making up the total length of the model. In 2D, each dimension might be divided into several tens or hundreds of units, resulting in hundreds to tens of thousands of individual ‘cells’. For instance, the example in Figure 2 shows the model area divided into 20 units in each dimension, resulting

in 400 discrete cells. The number of cells is multiplied further with 3D or 4D modelling, to the point where models (e.g. Figure 3) regularly require millions of cells to adequately define the model space.

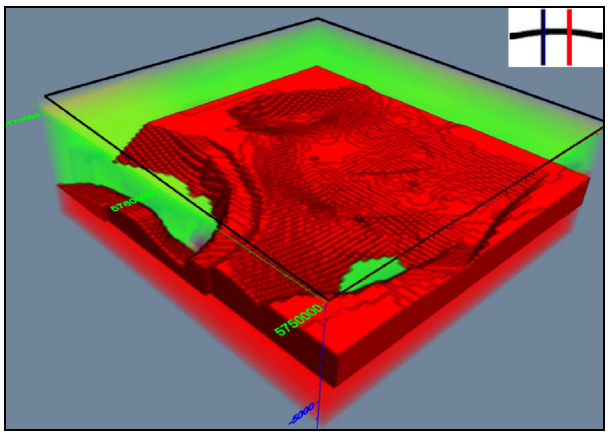

Figure 3. 3D representation of a geological layer. Three orthogonal axes are displayed, with a particular variable ('rock type') represented by colour. There are over one million individual cells in this model.

Storing and manipulating information about millions of cells in a computational process requires significant computing power and/or time. It is not unusual for a typical desktop computer to take several days, or even weeks, to solve a single 3D model. In addition, the number of boundary conditions and variables required to fully define a 3D model is typically higher than lower dimensional problems.

Boundary Conditions

Spatial-type models of any dimension need boundary conditions to constrain a solution. Boundary conditions provide a starting point for the mathematical solution of the particular governing equation under investigation.

Forward Modelling / Inversion

The terms '*forward modelling*' and '*inversion*' refer to fundamentally different ways of interpreting measured data. In '*forward modelling*', an operator builds a geological model and assigns properties and boundary conditions that represent a 'best guess' about the true nature of the piece of crust under investigation. The model is then solved and the results are compared against known measurements of certain parameters. If the results do not closely match the observations, the model is manually altered and the process repeated until a good match is achieved.

'*Inversion*' starts with the known measurements. The operator effectively tells the model what is known, and the inversion process then derives the appropriate boundary conditions or particular values for variables to match the known data.

3D conductive temperature modelling can be used to illustrate these two approaches. Conductive heat flow modelling typically relies on a geological model to represent the structure and lithological variation with the piece of crust under investigation. The different geological units of the model are assigned properties including (as a minimum) thermal conductivity. Surface temperature is almost always used as one of the thermal boundary conditions, and there is an assumption of zero heat flow through the sides of the model. A second thermal boundary condition is always required at either the top or base of the model to fully constrain the solution to the conductive heat flow equation. The nature of the second boundary condition and how a solution is derived effectively distinguishes forward modelling from inversion modelling.

Forward modelling of 3D conductive heat flow has been practiced since the advent of digital computers (e.g. Sams and Thomas-Betts, 1988; Gibson *et al*., 2008). Its strength lies in its relative simplicity and ability to quickly reach a solution for temperature distribution that satisfies a small number of surface heat flow observations. It is appropriate in situations where very little is known about surface heat flow, or for conceptual modelling to explore the effect of different parameters on subsurface temperature distribution.

Forward modelling inherently requires the operator to assume a thermal boundary condition (typically 'constant temperature' or 'constant heat flow') at the base of the model. However, there is no geological reason to expect either heat flow or temperature to be constant across any particular depth surface. In fact, the whole premise of geothermal exploration is that heat flow and temperature are not laterally constant at depth!

Inversion modelling comes into its own when the number of surface observations increases beyond two or three. In this situation, it is unlikely that a simple basal condition will yield a solution that closely satisfies all the available data. But an inversion process inherently starts with the surface data and derives the temperature distribution that best accounts for the observations. This process results in conditions at the base of the model that are rarely constant temperature or constant heat flow (Figure 4).

Stored Heat / Numerical Simulation

Table 2 of the 'Geothermal Lexicon' (AGEG, 2008) includes 'stored heat' and 'numerical simulation' as options for estimating Geothermal Resources and Geothermal Reserves. The Lexicon goes on to describe the two different methodologies in some detail. The methods are mutually independent and represent two very different ways of assessing the potential of a geothermal play.

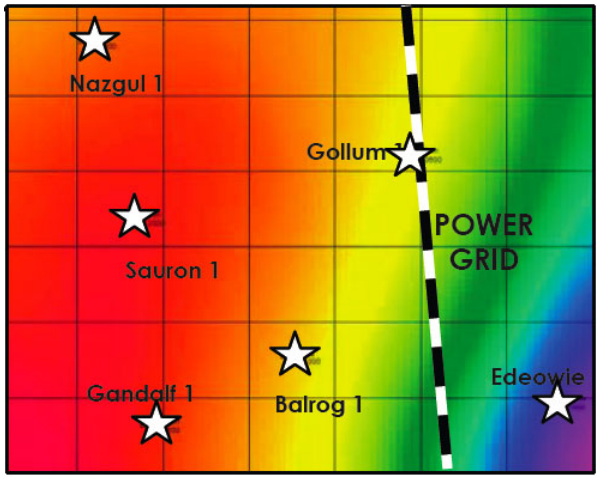

Figure 4. Inversion modelling of conductive heat flow. The colours represent modelled temperature at 5,000 m depth beneath an area approximately 50 km x 40 km. The model was constrained by heat flow measurements at the six locations shown. Both heat flow and temperature vary significantly across the model. After Torrens Energy (2008).

A 'stored heat' evaluation is a technique for estimating the total heat energy contained within a target volume of rock. The method requires the estimation of the volume, density, specific heat capacity and temperature of the target reservoir formations. These parameters are sufficient to estimate the absolute amount of thermal energy in the rock. The proportion of that energy that might ultimately be extracted depends on the lowest economically extractable temperature ('cut-off temperature'), the application to which the energy will be applied, and the efficiency with which the energy can be extracted.

The 'stored heat' approach quantifies the resource base—that is, it addresses the question, "How much thermal energy is in this geothermal play?" It does not address any aspect of extracting the energy, except for a consideration of the ultimate end use of the energy. It also does not address possible recharge of the thermal energy during extraction. 'Stored heat' is a useful concept at the early stages of resource estimation and play evaluation, but is of limited use for detailed project planning.

'Numerical simulation' lets us investigate some of the practical issues surrounding the extraction of thermal energy. Unlike 'stored heat' assessments, 'numerical simulation' incorporates a time element. At the early stages of field development, it allows us to model the flow of fluid (liquid and/or gas) and heat for different extraction strategies, and investigate how they impact on the life of the resource in terms of achievable power output, reservoir temperature and pressure (Figure 5). Later in the life of the project, the models can be refined using actual production data like thermal draw down to develop a predictive understanding of the response of the reservoir to production.

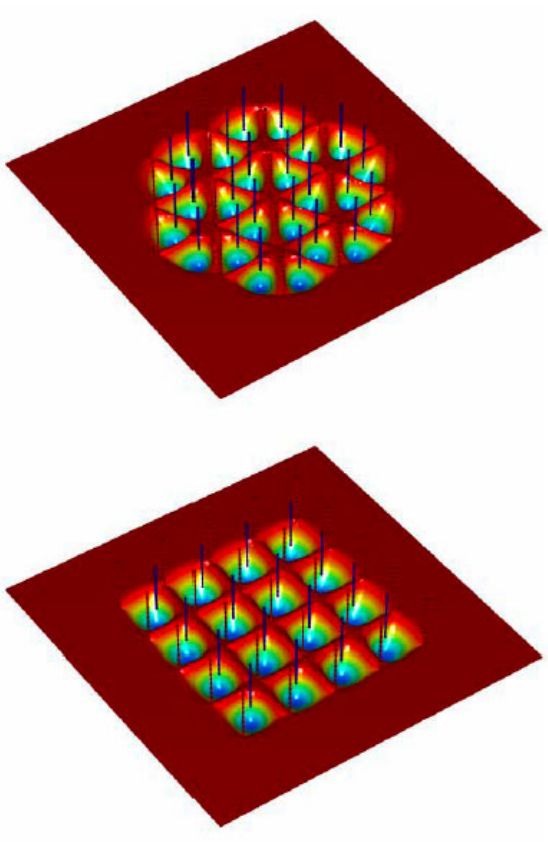

Figure 5. Predicted temperature distribution in an EGS reservoir after 20 years of production using a hexagonal (top) and square (bottom) well pattern. Results from numerical simulation. After Vörös *et al*. (2007).

Numerical simulation is the best way to investigate parameters such as power output through time, the effects of reinjection on reservoir temperature and pressure, improvements in productivity achievable through permeability enhancement, the impact of pumping on reservoir productivity and lifetime, and similar issues. Numerical simulation, therefore, has a role to play at all stages of a project's life.

Hydro-geo-mechanical modelling

Coupled hydro-geo-mechanical modelling is the frontier of EGS numerical investigations. The growth of an EGS reservoir during hydraulic stimulation and the geo-mechanical behaviour of a reservoir during production are incredibly complex processes that currently defy realistic numerical modelling. To get an idea of the complex systems at interplay during an EGS project, consider the following:

When water is injected into a fractured rock, many processes take place. The pressured water increases the pore pressure in the fractures and effectively jacks the fracture open. Eventually, the friction on critically orientated fracture is reduced to the point where the two sides of the fracture can slip against each other in response to the tectonic stress field. This slippage alters the local

stress field in the matrix in the vicinity of the fracture and the pressure within the pores. At the same time, the thermal shock of the cool injected water on the hot fractured rocks causes thermal shrinking of the rock matrix, which in turn also affects the local stress field. As the high-pressure water near the borehole works its way into the rock fabric, the volume of rock affected by the hydraulic stimulation increases, and the local stress field, pore pressures and temperatures continuously adjust and readjust to the hydraulic and thermal changes. As the injected fluid accumulates in the fractured rock, even the bulk volume of the rock increase.

The exact reaction of the rock and fracture system to the injected water depends on the density and orientation of all the fractures; the strength of the rock; the thermal expansion coefficient, specific heat capacity, density and thermal conductivity of the rock; the pressure and temperature of the injected fluid; the initial magnitude and orientation of the local stress field; the stiffness of the fractures; all of which are difficult to quantify.

Developing code to explicitly model the overwhelmingly complex system of interacting forces and flows is effectively impossible. It is physically impossible to provide the computing power and memory to store and process all the essential variables and governing equations on the many different required scales. The problem must be tackled in individual pieces, or by using a 'lumped variable' approach.

One example is 'UDEC[1]' (Universal Distinct Element Code). UDEC models a rock mass as a series of impermeable blocks separated by discontinuities (joints). The joints form boundaries between the blocks, and impose their own boundary conditions. UDEC models the physical displacement of the blocks in response to a stress field. Solutions satisfy the laws of conservation of momentum and energy. UDEC simulations can provide the following useful outcomes:

- Identification of the orientation of fractures most likely to shear during stimulation.
- An estimate of the pre-stimulation hydraulic conductivity and anisotropy of the fractured rock (e.g. Figure 6).
- An indication of potential reservoir growth and fluid flooding directions.
- An estimate of stress magnitudes at the target depth and the injection pressures required for hydraulic stimulation.
- Results provide the basis for more complex models to simulate the lifetime performance of an EGS project.

[1] UDEC™ is a Trademark of Itasca International

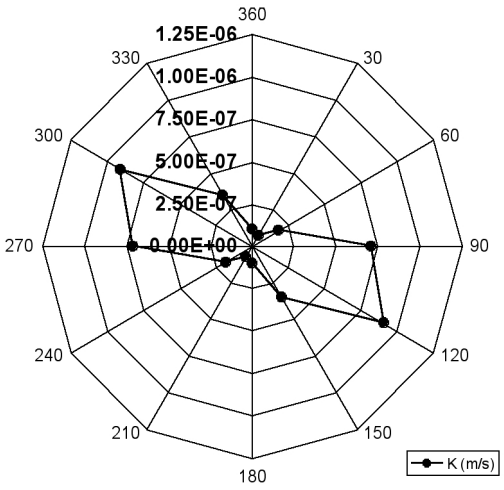

Figure 6. UDEC model results of the horizontal planar hydraulic conductivity (K) ellipse for a fracture network at a specific depth (stress) level.

Economic Modelling

Economic modelling aims to simplify the multitude of factors that affect the ultimate profitability of a project into a few basic assumptions. Unlike the modelling discussed earlier in this document, economic modelling is primarily about estimating cash flow through time, with little reference to spatial or volumetric details.

Many parameters can be estimated through economic modelling. Parameters such as the 'Levelised Cost of Power', 'Net Present Value' and 'Expected Monetary Value' allow the relative values of different geothermal plays, or different strategies for developing the same play, to be assessed. The sensitivity of project value to variables such as discount rates, electricity price, operating costs, drilling costs, distance from the grid, and so forth, can be explored through economic models. Likewise, the impact of policy measures such as Renewable Energy Certificates, Geothermal Drilling Program grants, and so forth, can also be explored.

Economic modelling is a powerful tool for informing investment decisions and for project planning, but the critical input variables often relate to future economic conditions and are very difficult to constrain. Regardless, economic modelling should be used from very early in a project's life in order to identify the key drivers for the economic success of each individual project. In some cases that may be low development costs, while in others it may be high power sale price.

Conclusions

Modelling in all its forms and guises is a vital and valuable tool in making sense of the often scarce and uncertain data inherent in geothermal studies. Thermal modelling sheds light on probable

temperatures at depth prior to expensive drilling. Reservoir modelling, likewise, helps predict the performance of future geothermal production wells, with increasing confidence as reservoir properties are constrained. Economic modelling, however uncertain, is essential to make informed investment and project development decisions.

At each stage of development, the sophistication of the modelling should refect the amount and reliability of the available data. Simple 1D models may be appropriate when little information is available, while more complex, multi-dimensional models are better for extracting the maximum value from larger, more reliable data sets.

References

AGEG (Australian Geothermal Energy Group) (2008). Geothermal lexicon for resources and reserves definition and reporting—Edition 1. AGEG Geothermal Code Committee, August 2008. 105pp.

Gibson, H., Stuwe, K., Seikel, R., FitzGerald, D., Calcagno, P., Argast, D., McInerney, P. and Budd, A. (2008). Forward prediction of spatial temperature variation from 3D geology models. In: Blevin, J.E., Bradshaw, B.E. and Uruski, C. (Eds), Eastern Australasian Basins Symposium III, Petroleum Exploration Society of Australia, Special Publication, 425-430.

Sams, M.S. and Thomas-Betts, A. (1988). 3D numerical modelling of the conductive heat flow of SW England. Geophysical Journal, 92, 323-334.

Torrens Energy (2008). 780,000 PJ inferred resource, Parachilna Project, South Australia. Statement to the Australian Securities Exchange, 20 August 2008. 4pp.

Vörös, R., Weidler, R., de Graaf, L. and Wyborn, D. (2007). Thermal modelling of long term circulation of multi-well development at the Cooper Basin hot fractured rock (HFR) project and current proposed scale-up program. Proceedings: Thirty-Second Workshop on Geothermal Reservoir Engineering, Stanford University, Stanford, California, January 22–24. SGP-TR-183.

Wang, Z., McClure, M.W. and Horne, R.N. (2009). A single-well EGS configuration using a thermo-siphon. Proceedings: Thirty-Fourth Workshop on Geothermal Reservoir Engineering, Stanford University, Stanford, California, February 9–11. SGP-TR-187.

A Geothermal Play Systems approach for exploration

A.R. Budd, A.C. Barnicoat, B. F. Ayling, E.J. Gerner, A. J. Meixner, A. M. Kirkby.
Geoscience Australia, GPO Box 378, Canberra 2601, ACT, Australia

Hot Rock exploration and development has progressed rapidly in Australia in the last decade. A wealth of pre-competitive geological data acquired by government surveys and mineral and petroleum explorers is available in Australia, but heat flow data specific to geothermal exploration is sparse. A methodology is presented that sets out the key parameters required in Hot Rock exploration. Mappable practical proxies corresponding to these parameters can utilise existing geological datasets. Australia has an enviable amount of geological data that is publicly available, and this can be used to show that many parts of the continent are attractive Hot Rock exploration areas.

Keywords: Hot Rock, exploration, Australia, geothermal play systems

Introduction

Mineral Systems Analysis or Petroleum Play Systems are well established in their respective industries. Exploration methods for conventional geothermal systems are likewise well established. To date, most EGS or Hot Rock projects (in Australia at least) have used compilations of bottom-hole temperatures to identify prospective geothermal systems. These data are mostly restricted to petroleum exploration areas. As a result, with few exceptions only areas of historical petroleum potential in Australia have been identified as having geothermal potential, whether Hot Rock or hydrothermal. The other obvious data type for temperature prediction (heat flow) is poorly constrained in Australia with only ~150 publicly-available measurements.

Hot Rock systems are not restricted to the geological settings favorable for oil and gas accumulation and preservation. Therefore, it is to be expected that there are areas of Australia with untested Hot Rock geothermal potential. Geoscience Australia is deriving a Geothermal Plays System approach, modeled on the 'Exploration Science' methodology of Mineral Systems Analysis (Barnicoat 2008), to formulate a framework for Hot Rock exploration. This approach links the key physical and/or chaemical parameters of the geological system under consideration, with mappable 'practical proxies' to define exploration criteria. It is a scalable approach that works for terrain selection, area selection and drill target selection.

To derive the key components necessary to form an accumulation of heat in a Hot Rock geothermal play, a systematic approach is desirable. From these key components, the geological, geophysical and geochemical data necessary for exploration should be identifiable. Importantly, 'practical proxies' should be able to be developed, which utilize existing datasets to make informed assumptions regarding missing data. This would enable Hot Rock exploration in Australia to progress.

Method

Hot Rock systems comprise a heat source, an insulating layer, and sufficient permeability – either natural or enhanced - to enable sufficient flow of fluid through the heat reservoir. Temperature and flow rate are the two essential parameters describing the potential output of a geothermal system.

The steady-state equation for temperature (1) shows that the important determinants of temperature are: thermal conductivity λ, depth-integrated heat generation A, mantle or basal heat flow Q_m and the crustal thickness under consideration Z.

$$T = \int \frac{A_z + Q_m}{\lambda} d_z \qquad (1)$$

In most areas of Australia, this temperature equation cannot be solved by input of direct measurements. Estimates must be used based on inference from other datasets that may have been acquired for other purposes, and as such are practical, proxy measurements. Further, some of these proxies translate readily to mappable features that have concerned petroleum and mineral exploration geologists for many years. Increasingly in Australia, 3D geological maps are being made at various scales that already contain many of the mapped proxy data necessary for Hot Rock exploration, and these may be practically utilized for predicting the thermal structure of the upper crust.

Thermal conductivity

The thermal conductivity of rocks varies according to composition, grainsize, porosity and temperature. Basic geological mapping and logging of drill core or chips will record lithology, and this information can be used to estimate grainsize, porosity and composition. Porosity may be determined from density measurements and well data. In a simplistic first-pass assessment, the effect of temperature may be ignored as its influence is smaller than effects from composition, grainsize, or porosity. In more advanced problem-solving models, it may be solved-for iteratively.

Heat Generation

Heat generation is a property that is dependent on composition. Uranium, thorium and potassium are the main radiogenic elements that contribute to heat generation. The density of a rock is also an important variable. The heat generation of a rock is given by the equation of Rybach (1988):

$$A = 10^{-5} \rho(9.52U + 2.56Th + 3.48K) \qquad (2)$$

where ρ = density in kg m^{-3} and U, Th and K are the concentration of uranium and thorium in parts per million and potassium in weight percent.

Geochemical analyses of whole-rock samples plus determination of density will fully solve the equation. In Australia, geochemical data is often analyzed for a sample although density is generally not. In such case, density must be estimated based on lithology, the determination of which will be aided by geochemistry. In detail, the heat production of a rock also depends on its age. In Australia, where recent active volcanism is lacking, high-heat-producing granites are generally the only rocks capable of creating a sufficient additional heat flow in the upper crust to cause significantly elevated temperature necessary for viable Hot Rock geothermal systems, although low conductivity cover may allow temperatures in radiogenic lithologies to reach economic values. High-heat production granites often occur as deeply (>3 km) buried plutons and are not directly sampled. Granite plutons, suites and supersuites share a genetic lineage that potentially enables some constraints to be placed on unsampled plutons.

Mappable practical proxies for heat production (from granites) can therefore be utilized from mapping geochemistry, geochronology and geophysics (gravity, magnetic, radiometrics, seismic surveys) by: (1) mapping trends of granites from outcrop to beneath insulating materials using geophysical interpretations; (2) using the chemistry (either measured or inferred from radiometrics) of outcropping granites to calculate heat production; and (3) estimating the depth and area (and therefore volume) of buried granites using constraints supplied by seismic surveys and interpretation of gravity and magnetic potential field data (see Meixner *et al*. this volume).

In Australia, the general nature of granites in geological provinces is quite well known and continues to be refined. For example, it is known that late Archean granites in the Yilgarn Craton are high-heat producing (Cassidy *et al*. 2002), as are the more felsic members of numerous supersuites of the Paleozoic of eastern Australia (eg Chappell *et al*. 2000). Proterozoic granites in Australia generally have high U, Th and K compared to granites of older and younger periods, and many Proterozoic supersuites are high heat producing (Budd *et al*. 2001, McLaren *et al*. 2003).

At a national scale, the newly released Radiometric Map of Australia (http://www.ga.gov.au/minerals/research/national/radiometric/index.jsp) shows the surface distribution of K, U and Th for over 80 per cent of the continent (Figure 1). This new radiometric map has been produced by leveling more than 450 individual surveys collected over the past 40 years and compiling them into a single seamless image. This dataset readily shows areas of high U, Th and K, some of which may correlate to high-heat-producing granites. Heat production may also be estimated from gamma logs or from seismic velocity.

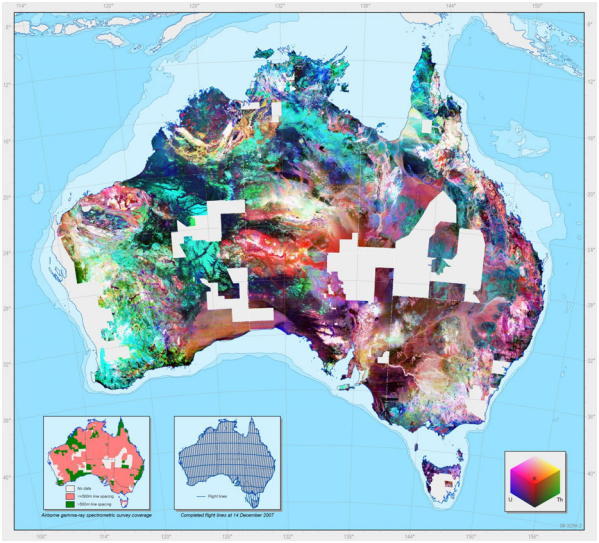

Figure 1: A clip-out of the Radiometric Map of Australia, First Edition (Minty et al. 2008). The ternary radiometric image shows the concentrations of the radioelements potassium (K), uranium (U) and thorium (Th) at the Earth's surface as measured using the airborne gamma-ray spectrometric method. The image is a false color composite using the colors red, blue and green to represent K, U and Th respectively.

These various mappable proxies for heat production are supported by extensive publicly-available datasets, and are readily incorporated into both 2D GIS and 3D maps.

Mantle/Basal heat flow and section depth

In comparison to some other parts of the world, the broad thermal structure of the Australian crust is understood in great detail only in small areas. Sass and Lachenbruch (1979) and Cull (1982, 1991) examined information on heat flow in Australia, but with less than 150 heat flow measurements across the entire continent, the data available are insufficient to be definitive. From this work, it was recognized that several areas of Proterozoic crust have anomalously high heat flow (and include abundant high-heat-producing granites). Several studies have

examined the occurrence of this high heat flow, heat production and implications for tectonic evolution, including (but not limited to): McLaren *et al*. (2006) in the Mount Painter Province, South Australia; Neumann *et al*. (2000) in the area of the South Australian Heat Flow Anomaly; and Sandiford et al (2001) in central Australia. Even with these studies, considerable further work is required to be done throughout Australia to better understand the application of *heat flow province* understanding as outlined by Roy *et al*. (1968).

Information on crustal structure is central to understanding the overall thermal structure of the crust and for deriving mantle heat flow. Seismic reflection surveys directly map crustal structure, and provide information on the potential range of lithologies and hence heat generation and thermal conductivity. Seismic velocities derived from the data also have implications for thermal structure including temperature and heat generation. Seismic velocity is a proxy for density, which may assist in the mapping of granite volumes and therefore potential heat production. Australia has a good database of seismic reflection surveys, and surveys are being continually acquired.

Other parameters

Once the temperature of a potential geothermal Hot Rock reservoir is constrained, the next concern is whether a fluid can pass through the reservoir at the necessary velocity and volume (flow rate) to extract the required energy from the reservoir and transport it to the surface. Darcy's law describes the flow of a fluid through a porous medium:

$$q = \frac{-\kappa A}{\mu}\frac{(P_b - P_a)}{L} \qquad (3)$$

where q is the total discharge (units of volume per time, e.g., m³/s) and is equal to the product of the permeability (κ units of area, e.g. m²) of the medium, the cross-sectional area (A) to flow, and the pressure drop ($P_b - P_a$), all divided by the dynamic viscosity μ (in SI units e.g. kg/(m·s) or Pa·s), and the length L the pressure drop is taking place over.

Of most interest during a resource evaluation phase is the permeability of the target reservoir or formation. Other than direct measurement, mappable practical proxies for this include predicted lithology and seismic velocity.

As Hot Rock developments usually include reservoir engineering to enhance reservoir permeability, mapping the stress regime at that crustal level is of interest. This is mapped either directly through borehole measurement, medium- to long-term passive seismic monitoring using an Australia-wide seismic monitoring network, short-term passive seismic monitoring using temporary array deployments, or indirectly through surface neotectonic kinematic indicators. The Australian Stress Map (Hillis and Reynolds, 2000) showing the crustal stress regime is available at http://www.asprg.adelaide.edu.au/asm/ (Figure 2) and has provided useful information for geothermal explorers in the early stages of their developments.

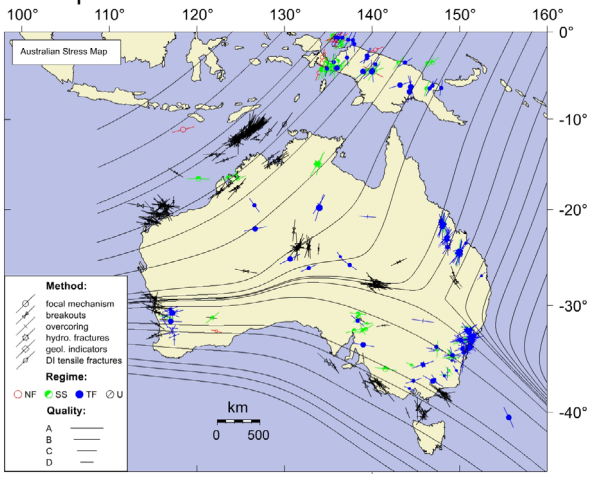

Figure 2: Stress trajectories calculated from the Australian Stress Map (Hillis and Reynolds, 2000). The stress trajectories indicate the orientation of the maximum horizontal stress at each point along the trajectory, but they do not imply information about magnitudes.

Conclusion

In Hot Rock exploration in Australia, it is possible to link the fundamental geothermal parameters to the exploration process by means of the geological expression of the fundamental processes and the application of a scale-dependent mapping of these into exploration decision making.

The most important step in the process is translating the understanding of the process and the key parameters controlling the process into factors that can be determined spatially. Hot Rock geothermal exploration in Australia is in its infancy and with some exceptions has been based on the database of bottom-hole temperatures from petroleum drilling. By incorporating national-scale datasets into a Geographical Information System, a relatively rapid assessment of Hot Rock geothermal plays can be done at a regional scale. This will inform both exploration programs (and therefore lower risk) and pre-competitive data acquisition programs.

A companion paper (Meixner *et al*. this volume, *Establishing Hot Rock Exploration Models - From Synthetic Thermal Modeling to the Cooper Basin 3D Geological Map*) describes the use of thermal modeling of 3D geological datasets as a more detailed way of assessing geothermal prospectivity at a regional scale. Australia has extensive publicly-available geological datasets, and with the understanding of how to practically apply these to geothermal exploration in combination with the tools to perform 3D thermal modeling, the assessment of Hot Rock

geothermal play assessments will highlight Australia as an attractive candidate for geothermal investment.

References

Barnicoat A.C. 2008. The mineral systems approach of the pmd*CRC. Geoscience Australia Record 2008/09, 1-6.

Budd, A.R., Wyborn, L.A.I. & Bastrakova, I.V. 2001. The metallogenic potential of Australian Proterozoic granites. Geoscience Australia Record 2001/12, pp 154 + 2 CD-ROMs.

Cassidy, K.F., Champion, D.C., McNaughton, N.J., Fletcher, I.R., Whitaker, A.J., Bastrakova, I.V. and Budd, A.R. 2002. Characterisation and metallogenic significance of Archaean granitoids of the Yilgarn Craton. AMIRA Project P482/Meriwa Project M281. Minerals and Energy Research Institute of Western Australia Report 222.

Chappell, B.W., White, A.J.R., Williams, I.S., Wyborn, D. & Wyborn, L.A.I. 2000. Lachlan Fold Belt granites revisited: high- and low-temperature granites and their implications. Australian Journal of Earth Sciences, 47/1, 123-138.

Cull, J.P. 1982. An appraisal of Australian heat flow data. Bureau of Mineral Resources Journal of Australian Geology and Geophysics, 7, 11-21.

Cull, J.P. 1991. Heat flow and regional geophysics in Australia. In: Cermáck, V. and Rybach, L. (eds.) Terrestrial Heat Flow and the Lithosphere Structure, Springer-Verlag, Berlin, 486-500.

Hillis, R.R. and Reynolds, S.D. 2000. The Australian Stress Map. Journal of the Geological Society (London), 157, 915-921

McLaren, S., Sandiford, M., Hand, M., Neumann, N., Wyborn, L. and Bastrakova, I. 2003. The hot southern continent: heat flow and heat production in Australian Proterozoic terranes. In: Hillis, R.R. and Muller, D. (eds.) Evolution and Dynamics of the Australian Plate. Geological Society of Australia Special Publication 22, 151-161.

McLaren, S., Sandiford, M., Powell, R., Neumann, N. and Woodhead, J. 2006. Paleozoic intraplate crustal anatexis in the Mount Painter Province, South Australia: timing, thermal budgets and the role of crustal heat production. Journal of Petrology, 47/12, 2281-2302.

Minty, B.R.S., Franklin, R., Milligan, P.R., Richardson, L.M. and Wilford, J. 2008. Radiometric Map of Australia (First Edition), scale 1:15 000 000, Geoscience Australia, Canberra.

Neumann, N., Sandiford, M. and Foden, J. 2000. Regional geochemistry and continental heat flow: implications for the origin of the South Australia heat flow anomaly. Earth and Planetary Science Letters, 183, 107-120.

Roy, R.F., Blackwell, D.D. and Birch, F. 1968. Heat generation of plutonic rocks and continental heat flow provinces. Earth and Planetary Science Letters, 5, 1-12.

Rybach, L. 1988 Determination of heat production rate, in: Haenel, R., Rybach, L. and Stegena, L. (eds.) Handbook of Terrestrial Heat-Flow Density Determination, Kluwer Academic Publishers, 125-142.

Sandiford, M., Hand, M. and McLaren, S. 2001. Tectonic feedback, intraplate Orogeny and the geochemical structure of the crust: a central Australian perspective. In: Miller, J.A., Holdsworth, R.E., Buick, I. and Hand, M. (eds.) Continental Reactivation and Reworking. Geological Society, London, Special Publication 184, 195-218.

Sass, J.H. and Lachenbruch, A.H. 1979. The thermal regime of the Australian continental crust. In: McElhinny, M.W. (ed.) The Earth – its Origin, Stucture and Evolution. Academic Press, New York, 301-352.

What target to drill? Geothermal Pre-Drill Play Evaluation (PDPE): Understanding the nexus between project risk and value

Gareth T. Cooper*, Graeme R. Beardsmore and Luke Mortimer
Hot Dry Rocks Pty Ltd, PO Box 251, South Yarra, VIC, 3141.
* Corresponding author: Gareth.Cooper@hotdryrocks.com

Geothermal exploration and development in Australia is rapidly evolving and many companies will soon be at a critical juncture of deciding which targets to drill and likely well locations. Although the global petroleum sector has evolved a detailed system of prospect evaluation and risking, the same level of discipline has not yet been formalised in the geothermal sector, where play evaluation decisions are largely focused on cost, rather than value and risk.

Geothermal systems in Australia can be characterised by four aspects of geological risk (P_g) - heat flow, thermal resistance, reservoir and water. These risks can be condensed, on further modelling, to temperature risk (P_t) and flow rate risk (P_w). When combined with perceived drilling, engineering and other risks (P_e), these factors form the basis of a simple risk-based evaluation system that can be applied to geothermal plays anywhere in the world.

Combining cash flow considerations allows for the estimation of Net Present Value (NPV) for each play. The product of risk and NPV (the Expected Monetary Value, EMV) provides a more robust and considered assessment of the relative 'risked-value' of a geothermal play.

Keywords: Drilling, Levelised Cost, Risk, NPV, EMV

Introduction

Many geothermal energy explorers in Australia are rapidly approaching a phase of the exploration cycle where an informed decision needs to be made regarding the siting of either a deep 'proof-of-concept' development well, or a moderate-depth exploratory well. In most cases multiple plays will be available within a single tenement or group of tenements and explorers must make a critical decision between them, which may have wide-reaching impact.

The prevailing decision making process within the geothermal sector is to make relative empirical assessments of sites based on known geology (but usually biased by perceptions of temperature alone) and then to further constrain site-selection based on cost, usually expressed in the immediate term as drilling cost, and in the long-term as the project Levelised Cost of Electricity (LCOE). This cost-based approach has some significant flaws, which may be misleading at the best.

The use of a cost-based approach (such as LCOE) alone for site evaluation encompasses neither project risk nor revenue and can therefore lead to erroneous perceptions of relative value - and misguided decisions on drill site location.

In contrast the petroleum sector has evolved a mature and formalised system of project evaluation, which encompasses the inherent geological and commercial risks of a prospect. The assessed value of the prospect (eg. Magoon and Dow, 1994; Otis and Schneidermann, 1997) is usually quantified as the Net Present Value (NPV). The combination of risk and value is the Expected Monetary Value (EMV) of the project, and this risked-value approach more accurately defines the relative worth of projects.

This study describes a risk-based approach to assessing the value of a geothermal project in the Australian context, synonymous with the approach used by the petroleum sector. The study demonstrates how project NPV can be combined with risk via a simple decision tree, to ascertain the EMV of a geothermal project.

The dilemma

A geothermal explorer (hypothetical) has a series of potential 'plays' across GEL7000 and must make a decision to drill one play in the next 6 months. Each target has slightly different characteristics, pros and cons. Two targets (A and B) are schematically shown in Figure 1.

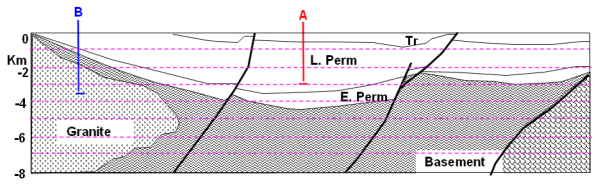

Figure 1: Schematic section showing two hypothetical geothermal plays. Play A is a HSA play targeting 160°C at 3 km depth and Play B is an EGS play targeting 185°C at 3.5 km depth.

Target A is a HSA play with a target sandstone aquifer at 3 km depth. The modelled conductive heat flow in the vicinity of A is 85 mW/m^2, giving a reservoir target temperature of 160°C. Target B is an EGS play with a target granite reservoir at 3.5 km depth. The modelled conductive heat flow in the vicinity of B is 110 mW/m^2, giving a reservoir target temperature of 185°C. Both plays are about

the same distance from the national electricity grid and have similar market potential. The exploration company would like to establish a 10 MWe binary power plant, and although initially attracted to Target B due its high surface heat flow and potentially high reservoir temperature, it is now uncertain about the relative value of Target B compared to the shallower Target A.

Which target offers the best value?

Geothermal systems risk and the exploration and development cycle

Australia is unique amongst the world of geothermal exploration and development in that it is mainly driven by capital investment via public share issues. Costs and timing are, therefore, strongly influenced by the capital-raising cycle. Most Australian geothermal exploration activities can be summarized in a five-year cycle (Figure 2), although longer periods may be expected for more complex projects.

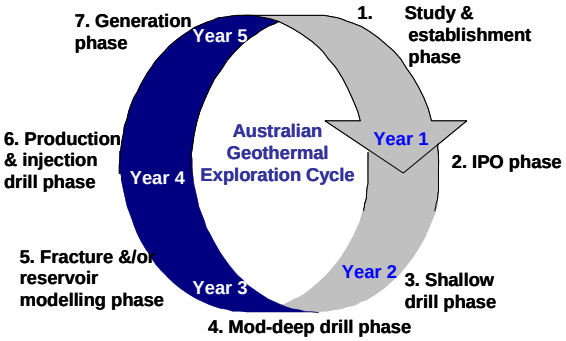

Figure 2: The Australian Geothermal Exploration Cycle showing the progress of activities typical in a five-year exploration cycle leading to the establishment of a small 'proof-of-concept' plant by the end of year 5 (idealised).

By the time most companies reach the moderate-depth drilling phase (Phase 4) in about year 3 of the cycle, they need to have some form of analysis of the value of their plays by which they can make a decision about drilling location, target type and target depth. Anecdotal evidence suggests that, to-date, much of this decision process is empirical, ad-hoc, or (at best) lacks documented systematics.

Whilst petroleum and geothermal systems have a number of differences, there is no reason why the geothermal sector cannot benefit from a risk-based approach as used in the petroleum sector. In the case of the petroleum system, total geological risk (P_g) is defined by:

$$P_g = P_{ch} \times P_s \times P_r \times P_{cl} \quad \text{(Eq 1)}$$

The four aspects of petroleum system risk are shown in Table 1., along with suggested equivalent risk categories for geothermal.

Table-1 Comparison of geological risk categories

Petroleum System	Geothermal System
Charge (P_{ch})	Heat flow (mW/m^2)
Seal (P_s)	Thermal resistance (m^{2}K/W)
Reservoir (P_r)	Reservoir
Closure (P_{cl})	Water

By assigning a probability value (P) to each of the risk categories in Equation 1, petroleum companies derive a relative, but nevertheless useful, risk ranking for their prospects.

Conductive geothermal systems in Australia can be assessed against four discrete aspects of geological risk (Cooper and Beardsmore, 2008). In the early phases of the exploration cycle, companies should undertake a comprehensive Geothermal Systems Assessment (GSA) to identify the key risks in their plays and the relative degree of these risks.

The key geological risks can be summarised as follows:

Heat flow: Probability that heat flow measurements or assumptions reliably characterise the play under investigation. Estimated from geographic coverage and 'uncertainty' of heat flow estimates.

Thermal resistance: Probability that thermal resistance and heat transfer mechanism beneath the level of well intersects are as assumed (purely conductive, convective component, advective component).

Reservoir: Probability that reservoir properties and volumetric extent are as assumed. Estimated from geographic coverage, data type and reservoir type.

Water: Probability that water supply or chemistry may adversely impact on the project.

The above risk variables are defined by measurable factors with intrinsic distributions. For example, in petroleum exploration reservoir risk (P_r) incorporates the distributions of porosity, permeability, area and net:gross thickness data. These factors are typically combined in Monte-Carlo simulations to define the overall probability distribution of reservoir risk. This process provides a disciplined and uniform approach to help mitigate exploration/drilling risks (Capen, 1992; Rose, 1992).

Some aspects of risk in the geothermal system share varying degrees of co-dependence. For example, heat flow and thermal resistance risk share a common link via rock thermal conductivity measurements. It is perhaps more useful to combine geological variables of the geothermal system into just two simple risk categories which

are first derived from the four factors in Table 1. These two risk categories are:

P_t – target temperature risk, and,

P_w – flow rate risk

Pre-Drill Play Evaluation (PDPE) – a simple geothermal risk tool

The concepts outlined in the following paragraphs define a process that may be termed a geothermal *Pre-Drill Play Evaluation* (PDPE). Different geothermal plays will have different Expected Monetary Value (EMV). In simple terms, the net EMV is a proxy for 'risked value' and can be used to rank a series of geothermal plays to determine the lowest-risk, highest-value drilling location. The work path for a PDPE is schematically shown in Figure 3.

A Geothermal Systems Assessment (GSA) should be the first significant activity for an exploration company with new ground, so that the four key geological risks (P_g) can be defined and quantified (Cooper and Beardsmore, 2008). These four risks can be subsequently refined into temperature risk (P_t) and flow risk (P_w), which are quantitatively estimated through heat flow and hydro-geomechanical modelling, respectively.

In a conductive geothermal setting, the probabilistic distribution of reservoir temperatures is a function of the standard deviation of surface heat flow and the uncertainties of rock thermal conductivities. A 3D earth model with estimated surface heat flow of 90±10 mW/m^2 may have a normally distributed probability curve with a mean heat flow of 90 mW/m^2 and standard deviation (σ) 10 mW/m2. Thus the 'P90' value (ie 'true' heat flow is 90% likely to exceed this value) is 2σ less than the mean, or 70 mW/m^2, while 'P10' would be 110 mW/m^2. In some cases, the analyst may believe that heat flow risk is not normally distributed, and may define P90 and P10 according to a different distribution, perhaps based on a log-probability plot of regional heat flow data.

The risk that heat flow is not purely conductive is addressed through hydraulic reservoir modelling, by assessing the thermal stability of conductive models when populated with permeability data. A threshold, or 'critical', permeability is identified for key layers, beyond which spontaneous convection might occur. The analyst is then in a position to quantify the risk that the critical permeability may be exceeded. This is the risk that temperature may be overestimated.

Likewise, the outcomes of hydraulic reservoir modelling, using tools such as TOUGH2 and FEFLOW finite element code, determines the likely distribution of well flow rates for a given distribution of porosity, permeability, pressure, fluid viscosity, well and pump design variables.

Combined, the temperature and flow rate probability distributions allow a direct assessment of probable well power output for different geothermal plays, well patterns, design parameters, or other variables. The outcome is a probability based picture of well output. Geological risk is directly apparent from the median value and the shape and width of the probability distribution curve. The well productivity (typically time-variable) feeds directly into economic models for the expected revenue stream, which are combined with cost estimates to derive the Net Present Value (NPV) of a play.

The NPV, however, does not address non-geological risks. The most significant non-geological risk in a geothermal program is *engineering risk* (P_e). This is largely the explorer's

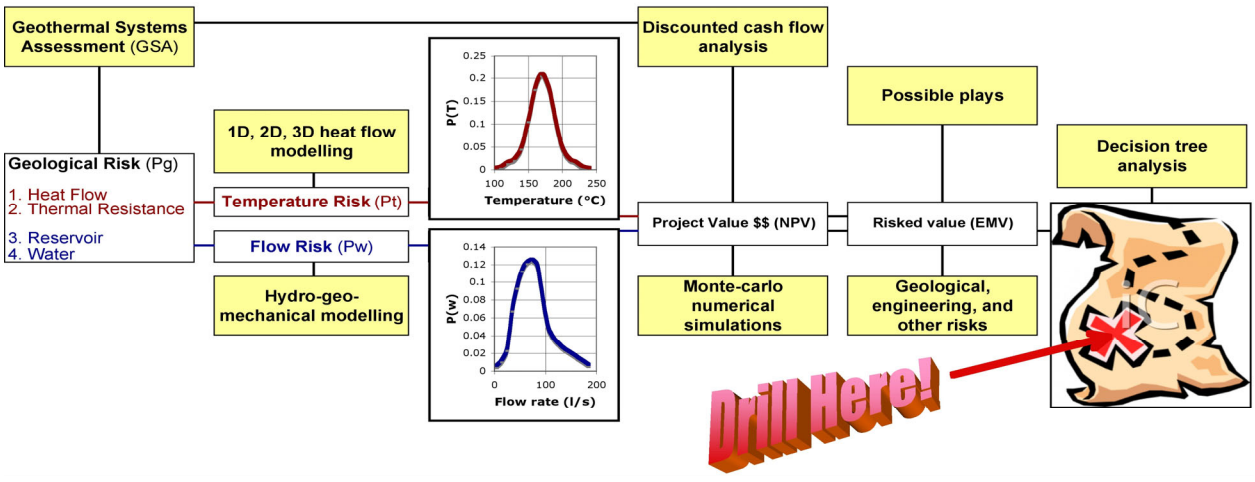

Figure 3: A simple flow chart for a geothermal Pre-Drill Play Evaluation (PDPE). Quantifiable geological risks are incorporated with the NPV. The product of all risks and NPV results in the net EMV, which can be used to decide target priority.

perception of the chance (probability) of experiencing trouble-free drilling. This may be influenced by play type (EGS or HSA), drilling depth, lithology, temperature, logging capabilities etc. The product of geological risk (P_g) profile and the engineering risk (P_e) largely defines the geothermal exploration and development risk. Other risks (eg perceived sovereign risk) can also be addressed at this stage. The product of NPV and risks is the net EMV of a play.

Incorporating project value into the decision making process

The *Levelised Cost of Electricity* (LCOE) is a standard measure of the cost of energy over a project life and is used to compare the relative costs of various forms of energy (eg. coal, solar, wind, geothermal). It is defined as the sum of all discounted project costs over a stated lifetime divided by the sum of discounted net electricity generation. It has been used in the geothermal sector as a project evaluation tool, but LCOE alone does not incorporate information about the relative risks involved in a project.

Example

In the hypothetical example discussed earlier (Figure 1), the exploration company has assessed the LCOE for plays A and B.

Play A has a shallower target reservoir and lower drilling costs than Play B. However, the lower reservoir temperature in Play A means that net well output is expected to be about 0.7 MWe less per well, compared to Play B. Consequently both projects have a similar LCOE of about $115/MWh over a 20 year project life, discounted at 10% (Table 2).

Table-2 Comparison of parameters for hypothetical plays A and B

Parameter	Play A	Play B
Play type	HSA	EGS
Reservoir temp. (P50)	160°C	185°C
Modelled flow (P50)	100 l/s	90 l/s
Expected net MWe/well	4.6	5.3
LCOE ($MWh)	$115	$115
NPV ($ million) 20 years	$20	$30
Geological Risk (P_g)	0.53	0.44
Engineering Risk (P_e)	0.80	0.50
Net EMV ($ million)	$8.4	$6.6

The LCOE, however, only tells the company the 'break even' price for the electricity produced. It does not reveal the relative value of the two plays. After modelling expected flow rates, thermal draw down and pressure draw down over 20 years using TOUGH2 and FEFLOW, the company found that the higher expected net MWe production for Play B resulted in a NPV of $30 million, compared to $20 million for Play A. Consequently, based on NPV alone, Play B appears to offer better lifetime value (Table 2).

In assessing the relative geological and engineering risks (including reservoir engineering) of each play, however, the opinion of the exploration company is that Play B (EGS) has a much lower probability of success compared to the more conventional Play A.

The net EMV for the 'success case' for each play is the product of NPV, P_g and P_e, so Play A has a more attractive net EMV than Play B. Although both plays have similar costs (LCOE) and Play B has an attractive NPV, the perceived risks for Play B are much higher, such that the 'risked-value' is poorer. Consequently, in this instance, the company decides that Play A provides better long-term value.

Discussion

A Pre-Drill Play Evaluation (PDPE) incorporates all available information about a geothermal play, its geological and engineering risks, its probable costs and revenue stream. Geological uncertainty is minimised through an early and thorough Geothermal Systems Assessment (GSA). The GSA process identifies the geological variables (heat flow, thermal resistance, reservoir and water) with the greatest uncertainty (risk), which allows targeted exploration to reduce those risks.

Other, non-geological, risks are, to a large extent, subjective and may be perceived at different levels by different people. Parameters such as 'drilling risk', 'sovereign risk' etc should be quantified through a process of discussion and careful consideration to incorporate a range of views.

There will very likely be widely different opinions about drilling risk for EGS, convection risk in permeable sediments, sovereign risk in developing nations, and other. It may be that probability distributions are derived for each of these risks, rather than simple 'median' values. EMV may then, also, be derived as a distribution with P10, P50 and P90 values. This is a valid alternative to the process outlined above.

If undertaken in a methodical and inclusive manner, a PDPE will naturally reach a consensus view for the exploration (or investment) company about the relative 'risked-value' of potentially very disparate geothermal plays.

Conclusions

The methodical application of a risk-based assessment system, similar to that used by the petroleum sector, will assist geothermal exploration and investment companies to appraise the relative value of different geothermal

plays. When risks are combined with cash flow projections, the net EMV for each play can be ranked to produce an inventory of drilling or investment options. This approach is distinctly different from a cost-based approach.

The use of a 'risked-value' approach to geothermal exploration and investment decision-making provides internal company discipline for drilling decisions and some surety for investors who are familiar with existing and similar systems in the petroleum sector.

References

Capen, E., 1992. Dealing with exploration uncertainties. In: Steinmetz, R., (Ed), The Business of Petroleum Exploration, Treatise of Petroleum Geology, Handbook of Petroleum Geology, American Association of Petroleum Geologists, Tulsa, Oklahoma, 29-62.

Cooper, G.T. and Beardsmore, G.R.: Geothermal systems assessment: understanding risks in geothermal exploration in Australia. Proceedings of PESA Eastern Australasian Basins Symposium III, Sydney 14–17 September, (2008), 411–420.

Magoon, L.B. and Dow, W.G., 1994. The Petroleum System. In: Magoon, L.B. and Dow, W.G. (Eds), The Petroleum System – from source top trap, American Association of Petroleum Geologists, Memoir 60, 3-24.

Otis, R.M. and Schneidermann, N., 1997. A Process for evaluating exploration prospects. American Association of Petroleum Geologists, Bulletin 81, 1087-1108.

Rose, P.R., 1992. Chance of success and its use in petroleum exploration. In: Steinmetz, R., (Ed), The Business of Petroleum Exploration, Treatise of Petroleum Geology, Handbook of Petroleum Geology, American Association of Petroleum Geologists, Tulsa, Oklahoma, 71-86.

The 3D Basement and Thermal Structure of the Gunnedah Basin

Cara R. Danis* and Craig O'Neill
Gemoc Macquarie University, Sydney, NSW, Australia
* Corresponding author: cdanis@els.mq.edu.au

With the development of geothermal resources by in the Cooper Basin, South Australia, interest in sedimentary basins for potential resources has intensified. In Eastern Australia sedimentary basins not only host large deposits of coal, they are closer to large population centres with established infrastructure. The 3D architecture and geothermal potential of such sedimentary basins has so far not been assessed in great detail, however the assessment of temperature at 5km and heat flow in these Basin systems by Budd (2007) indicates some potential in the Sydney-Gunnedah-Bowen Basin System. This paper focuses on the Gunnedah Basin and aims to better constrain the 3D structure and thermal evolution of the Basin and presents a 3D depth to basement model, derived from regional gravity modelling, density measurements, borehole and seismic information, and basement temperatures from thermal modelling.

Keywords: Gunnedah Basin, 3D depth to basement, thermal modelling.

Geological Background

The Gunnedah Basin, part of the Sydney-Gunnedah-Bowen Basin (SGBB), began as an extensional rift basin in the Late Carboniferous to Early Permian towards the end of the Hunter-Bowen Super Cycle (Glen, 2005). The extensional tectonic regime initiated half-graben like structures and produced large quantities of rift volcanics (Tadroz, 1993) which overly the basement rocks of the Lachlan Fold Belt. Basin fill, including coal bearing deposits, localised in rapidly subsiding troughs separated by highlands and ridges consisting of silicic and mafic volcanics with the northerly orientated Boggabri Ridge effectively acting as a principle sediment source and dviding the Gunnedah Basin into two sub basins, Maules Creek and Mullaley. At the end of the Hunter-Bowen Super Cycle in the Late Permian, the SGBB developed into a foreland basin followed by a period of convergence, uplift and erosion. Final filling of the Gunnedah Basin (235 to 230Ma) was dominated by detritus shed from the New England Orogen (Glen, 2005). Vitrinite reflectance data suggest the removal of up to 2km of Triassic and Permian sediments between 227Ma and 235Ma. Compressional movement of the Hunter-Mooki Fault resulted in the development of a number of high relief anticline (Glen, 2005). During the Jurassic-Cretaceous the epicontinental Surat Basin developed over the northern and western parts of the Gunnedah Basin.

The geology, stratigraphy and structural history are well documented by Tadroz (1993) and drilling in the basin has reached top of basal rift volcanics in many areas and defines the stratigraphy thickness over an extensive area. This provides good geological controls for gravity modelling of the Gunnedah Basin, with the only main variable the top of the Lachlan Fold Belt.

Methodology

Gravity modelling of the Gunnedah Basin used eight profiles derived from the Gravity Anomaly Grid of the Australian Region 2008 (Fig. 1), available for download from Geoscience Australia. These profiles were modelled using the interactive potential-field modelling package ModelVision Pro v8.0 supplied by Pitney Bowes ®. Model profiles were constructed similarly to Guo *et al*., (2007) for density values, body extent and total model depth. The upper 5km of the models are constrained by over 60 boreholes for key stratigraphic layers such as the base of Jurassic, top of rift volcanics and were available top of the Lachlan Fold Belt. Increasing density with depth is accounted for with a change in density for sediments >300m deep, as determined by the measure borehole densities of Guo *et al*. 2007 and density measurement of 185 core samples drilled from hand samples of representative key geological units using:

$$D = [(A \times \partial_L)/(A - B)] + C$$

where D is density (g/cm^3), A is dry weight (g), B is wet weight (g), ∂_L is liquid density and C is the air buoyancy constant of 0.0012. All depths to stratigraphy derived from the gravity modelling were converted to metres Australian Height Datum (mAHD) and gridded in Surfer v8.0 supplied by Golden Software ® producing surfaces for the 3D model at a 0.05 degree interval.

Thermal models for the basin were developed using an existing, extensively benchmarked research finite element code *Ellipsis* (Moresi *et al*., 2003). Distinct layers from the gravity models were imported as different materials into the code, which solved the time-dependent energy equation with constant temperature top and bottom boundary conditions. The thermal properties for each material layer is outlined in Table 1, and are aggregates of measurements on each unit/rock type. The main free parameter in these models was the bottom temperature condition at 5km,

which was estimated from the National temperature at 5km map (eg. Budd *et al*. 2007) to be ~180^{o}C, and fine tuned to match existing temperature data for the Gunnedah Basin.

Table 1. Thermal Properties

Rock Type	Density (kg/m^3)	Conductivity (W/m-K)	Heat Production (µW/m^3)
Basement	2700	3	2
Mafics	2900	3	0.5
Sediments	2500	2	1.25
Coal Measures	1500	0.3	1.25

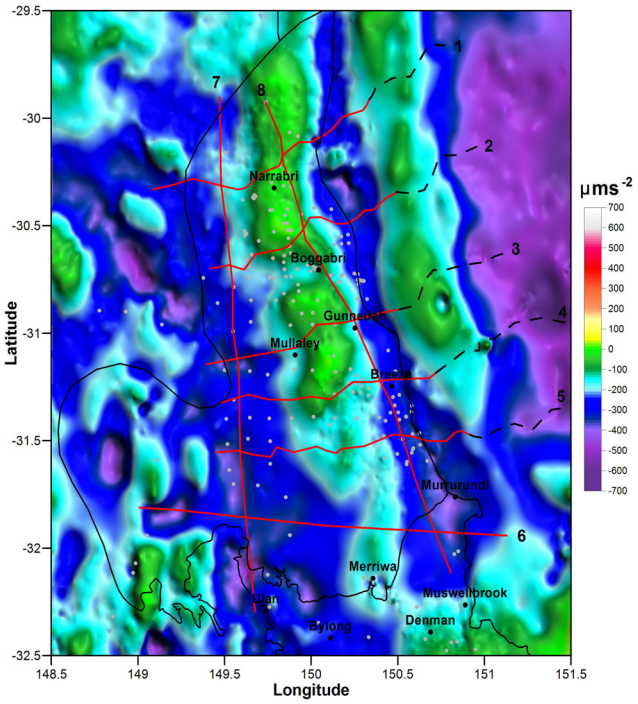

Figure 1: Gravity anomaly map for the Gunnedah Basin (outlined in black) with NE relief using a 0.01 degree grid spacing in Surfer ®. Gravity profile locations shown by red lines, extension of profiles black dashed lines and boreholes grey circles. Grid data available for download from Geoscience Australia.

Gravity Modelling

The geometry of the Gunnedah Basin during modelling was initially based on the work of Guo *et al*. (2007), however borehole and seismic constraints required a review of this. The final model geometry derived for the profiles correlates well with the recently published work of Krassay *et al*. (2009). Presented in Figure 2 are the six east-west profiles. The densities of the key structural units are Jurassic 2.31t/m^3, Tertiary Volcanics 2.88t/m^3, Gunnedah Sediments <300m depth 2.38t/m^3, >300m 2.54t/m^3, Granite 2.59t/m^3, Lachlan Fold Belt 2.60t/m^3 and 2.70t/m^3 and basal rift volcanics 2.95t/m^3.

From the gravity modelling a 2.5-3km deep channel runs through the central part of the basement of the Gunnedah Basin. The overlying basal rift volcanics fill the basement channel and in some areas reach a thickness of up to 3km thick. The Rocky Glen Ridge forms a clean structural high to control the western extent of the rift volcanics whilst the Hunter-Mooki Fault truncates them at depth in the east. To the north

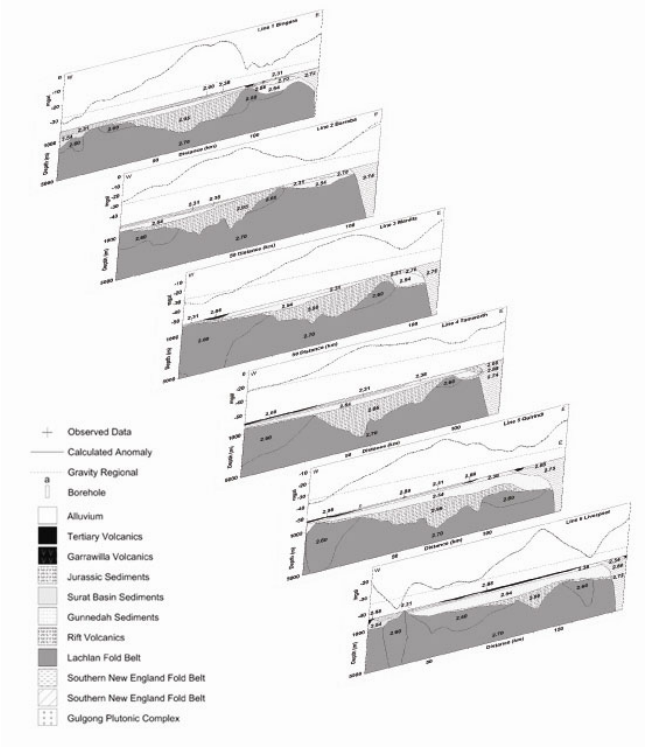

Figure 2: 2.5D E-W Gravity model profiles through the Gunnedah Basin. Model depth shown is 5km, profiles stacked to view NE.

and south the basal volcanics appear continuous into the Bowen and Sydney Basins.

3D Depth to Basement Model

The basement of the Gunnedah Basin is defined here as the metamorphic rocks of the Lachlan Fold Belt, which includes metasediments, granites and volcanics. Using borehole information, and the gravity model profiles a 3D basement structure of the Gunnedah Basin is interpolated in Figure 3. In addition to interpolating the top of the Lachlan Fold belt the Permian Coal Measures interval is also interpolated from borehole information. As the coal measures act as a thermal blanket in basin geometry it is necessary to determine their extent and thickness for the thermal modelling of temperature at depth.

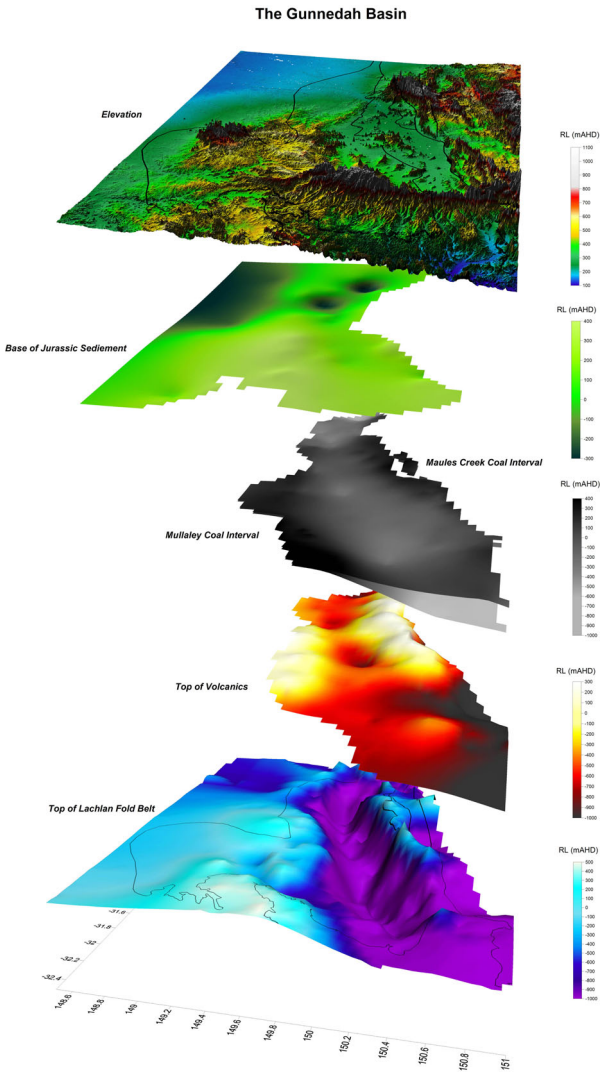

Figure 3: 3D basement structure of the Gunnedah Basin, showing the top of the Lachlan Fold Belt, Top of Volcanics, top and base of Permian coal interval, base of Jurassic and surface elevation from 90m SRTM satellite data.

Thermal Modelling

Thermal models were constructed for six lines (Gravity Lines 1-6), using the thermal properties listed in Table 1, which are derived from published values for each lithology or composite lithology, and the boundary conditions listed in the methodology. The heat production in the basement is taken from representative Lachlan fold belt granites immediately adjacent to the Gunnedah Basin (OZCHEM database). The initial thermal profile is linear between the top and bottom temperatures, and is allowed to evolve in response to the conductivity and heat production structure of the crustal units until equilibrium is reached. We use the finite element code Ellipsis (Moresi et al., 2003) to solve the non-steady state heat equation with internal heat sources in two dimensions.

The model's boundary conditions were refined using limited available temperature data from the Gunnedah Basin. The two data points within the Gunnedah region from the only available continent-scale compilation (Cull, 1982) suggest heat flows in the range 50-80mW/m^2 are appropriate for the Gunnedah Basin - within the range of our models (~70 +/- 10 mW/m^2). Many publicly available down-hole temperature measurements were made in non-equilibrium conditions shortly after drilling, and so are of limited value in constraining the steady-state thermal structure of the crust. Our recent measurements in the southern Gunnedah area suggest temperatures of around 60^{o}C at 1km, or a geothermal gradient of around 0.048 ^{o}C/m.

Figure 4a illustrates the temperature field and material configurations of two of the thermal models, from Lines 2 and 6. Surface heat flux is shown at top of Figure 4a. The critical difference between the two Lines is the thickness of the coal sequences in Line 6. These economic coal measures, whilst interbedded with the sedimentary sequence, have, on bulk, a significantly lower thermal conductivity than the surrounding basins sediments. This results in a blanketing effect and a thermal refraction of heat flow around the insulating coal measures. As a result, despite the highest basement temperatures occurring beneath the thick coal and mafic volcanic units, the highest surface heat flow and near surface temperatures are exhibited around the periphery of the coal. This demonstrates the danger of extrapolating near-surface heat flow measurements to depth without considering 2 and 3-D thermal effects.

We have also stacked and gridded the 2D cross-sections to obtain a 2.5D model of the basement temperatures across the entire Gunnedah basin, shown in Figure 4b. The temperatures at the top of the basement were obtained for each individual profile, this data was then gridded, and draped across our model for the basement architecture. The highest basement temperatures occur in the deeper portions of the basin, particularly under the thickest coal and mafic units. The basement temperatures range from ~105-165^{o}C, with the highest temperatures occurring at the northern and southernmost extents of the basin. Higher temperatures again extend deeper within the crystalline basement.

The model presented here considers thermal conduction only, it does not take into account advective effects, or the effects of varying surface temperature conditions. It does include variable near surface topography, though the effects of this are negligible here given the relief and extent of the Gunnedah Basin. The most critical part of this modelling is establishing a lowermost thermal boundary condition for the model. This boundary condition can, potentially, take the form of a temperature or heat flux constraint. In either case the uncertainty and variability of this parameter

are very large. Here we have combined available deep borehole temperature constraints and heat flux measurements, including some of our own measurements, to converge on a lower boundary condition (ie. T-180^{o}C at 5km) which is most consistent with the regional thermal constraints. This value, and perhaps the model, may be refined as improved steady-state deep borehole temperature measurements of this region become available.

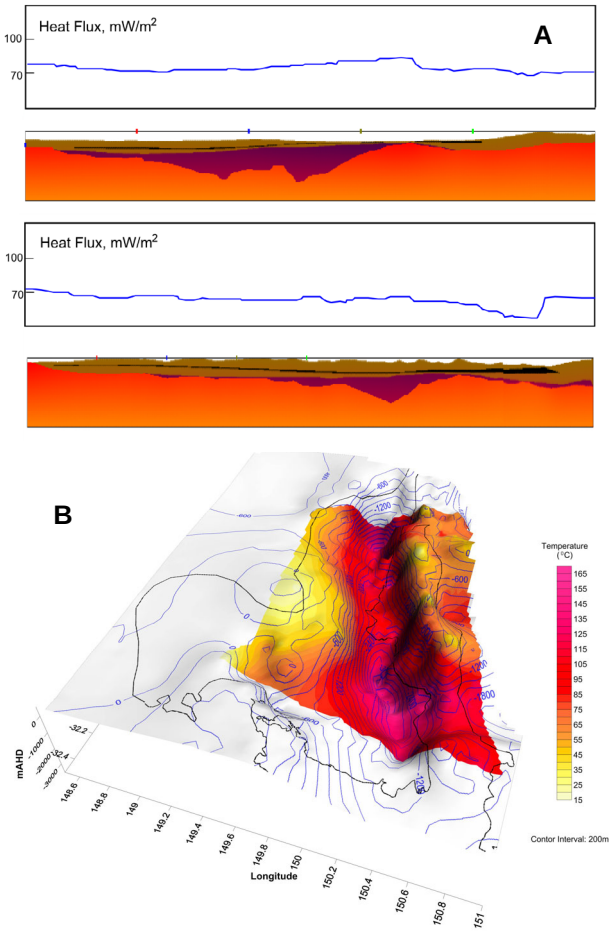

Figure 4: a) 2D cross sections of the modelled temperature field of Lines 2 and 6. Different colours represent different materials, which from top to bottom are basin sediments, interbedded coal measures, mafic volcanics, and Lachlan fold belt basement. Colour gradients represent temperatures. Surface heat flux is also plotted.

b) Temperatures at the top of the Lachlan Fold Belt basement, interpolated from 2D profiles, draped over the basement architecture. Basement contour interval is 200m AHD.

Summary and Discussion

The 3D structure of the Gunnedah Basin is characteristic of a typical rift basin. This provides a deep central channel in the basin where up to 3km of sediments and volcanics have accumulated over basement with temperatures of 105-165°C.

Our modelling demonstrates the importance of 2/3D effects - particularly the distribution of low conductivity sediment cover - in determining basement temperatures. Temperatures may be elevated beneath blanketing sediments, but this may not be evident in shallow borehole temperature measurements. Instead heat may be refracted around such insulators, giving heat flux anomalies at the edge of thick low-conductivity sediment cover. This highlights a potential complication in extrapolating shallower borehole temperatures to depth as per the Austherm07 database. While a good starting point for regional temperatures at depth, it is essential to compare modelled temperature results, using accurate basin geometries, with regional borehole data to ascertain the validity of the model's boundary conditions, and the reproducibility of the subsurface temperature field.

The potential for geothermal resources in the Gunnedah Basin based on this initial work is strongest in the northern and southern most parts of the basin where the coal/sediment blanket provides thermal insulation. In these areas temperatures deeper within crystalline basement are expected to be hotter.

References

Budd, A.R., 2007, Australian radiogenic granite and sedimentary basin geothermal hot rock potential map (preliminary edition), 1:5 000 000 scale. Geoscience Australia, Canberra.

Cull, J.P., 1982, An appraisal of Australian heat flow data. BMR Journal of Australian Geology & Geophysics v.7, p. 11-21.

Glen, R.A., 2005, The Tasmanides of eastern Australia in Vaughan, A.P.M., Leat, P.T., and Pankhurst, R.J., ed., Terrane Processes at the Margins of Gondwana: Geological Society, London, Special Publications 246, p. 23-96.

Guo, B., Lackie, M.A., and Flood, R.H., 2007, Upper crustal structure of the Tamworth Belt, New South Wales: constraints from new gravity data. Australian Journal of Earth Sciences v.54, p.1073-1087.

Krassay, A.A., Korsch, R.J., and Drummond, B.J., 2009, Meandarra Gravity Ridge: symmetry elements of the gravity anomaly and its relationship to the Bowen-Gunnedah-Sydney basin System. Australian Journal of Earth Sciences v.56, p. 355-379.

Moresi, L., Dufour, F., Muhlhaus, H.-B., 2003, A Langrangian integration point finite element method for large deformation modeling of viscoelastic geomaterials. J. Comput. Phys. v.184, p. 476–497.

Tadroz, N.Z., 1993, The Gunnedah Basin, New South Wales: Geological Survey of New South Wales, Memoir Geology 12, 649.

Understanding Risks and Uncertainties in Geothermal Modelling: Constraining Thermal Conductivity Models

Davey J. E., Preston J. C. & Keetley J. T.
3D-GEO, level 5, 114 Flinders Street, Melbourne, Victoria 3000, (03) 96398028

Prediction of the rate at which temperature increases with depth in a sediment pile is an important tool in the evaluation of many geothermal prospects. Such prediction is typically carried out by geothermal modelling based on assumptions that can be made with regard to the interplay of heat-flow and lithological conductivity, from which estimates of geothermal gradient, and therefore absolute temperature, can be derived. Approaches to such modelling work may differ widely, with a correspondingly wide range of outcomes, bringing into question the reliability of geothermal modelling as a predictive tool.

This paper focuses on addressing some of the uncertainties and risks associated with thermal modelling.

Keywords: Geothermal modelling, conductivity, heat-flow.

Thermal Modelling

The thermal conductivity of a rock directly determines the efficiency (or otherwise) with which heat is propagated through it. This conductivity is lithology-dependent, and varies from layer to layer in a sediment pile according to the nature of the various lithologies present and their degree of compaction. The geothermal gradient within any single lithological unit results from the interplay of heat-flow with the thermal conductivity of that unit, broadly expressed thus:

$$Q/K = G$$

where

Q = heatflow (mW/m^2)

k = conductivity (cals/cm/sec)

G = geothermal gradient ($^oC/km$)

The temperature-depth profile at a given location in a sedimentary basin can therefore be thought of as the vertical summing of the geothermal gradients established within the individual layers within the sediment pile. Such a profile is, as we shall see, rarely linear.

Two primary methods are used for modelling geothermal systems based on the above relationship between heat-flow, conductivity and temperature:

- In the absence of existing well data, shallow (200-500m) wells are drilled, down-hole temperatures recorded, and conductivities measured in the laboratory from down-hole samples. The depths from which the temperatures and samples were taken, and the temperatures and conductivities appropriate to those depths, provide values for k and G in the equation described above, permitting a calculation of a notional value of heat-flow (Q) that can then be applied to the base of the sediment pile over the local area. The geothermal gradient that is obtained in the shallow section is typically extrapolated, or projected, to depth in the subsurface in order to provide estimates of drilling depths that would be required to reach commercially viable temperatures (typically 150 ^oC). This is referred to herein as the "***projected approach***"; and
- Where down-hole temperature and lithostratigraphic data are available from adjacent wells, such data can be input to a commercially available burial-history modelling software package, of the kind routinely used in petroleum exploration for the prediction of the degree and timing of source rock maturation, reservoir temperatures, and other mitigating geothermal properties. Such packages typically contain default thermal conductivities for end-member lithologies that can be mathematically averaged to reflect lithological mixtures as necessary, and thus do not rely on the laboratory measurement of conductivities on down-hole samples. Since such packages also take into account burial-compaction effects (in particular, increase in conductivity with increasing compaction), permitting the calculation of a temperature-depth profile from which predictions of depths to key isotherms can be made. This is referred to herein as the "***calculated approach***".

While both methods can be adapted to specific cases, both contain considerable uncertainties that can affect the predicted temperatures.

Projected versus Calculated Models

Thermal conductivity varies with rock type and properties (such as porosity), the latter being highly dependent on depth of burial, chiefly as a result of compaction. Assumptions concerning thermal conductivity measurements are therefore very important in thermal modelling, especially since stratigraphy, and therefore burial history (depth through time), show great lateral variation. Therefore, thermal modelling is necessarily location-specific, and generates a temperature-depth profile unique to the local

geology. However, the assumptions made about conductivity are very different according to the two approaches outlined above.

The projected approach uses input values of conductivity (k) measured directly on samples from shallow wells (200-500m), combined with measured temperatures and values of heat-flow (Q), to generate a geothermal gradient (G) in the shallow section that is then linearly extrapolated to depth (2000-5000m).

By contrast, the calculated approach takes, as its starting point, a stratigraphic sequence to depths of 2000-4000m, typically intersected by petroleum exploration wells or interpreted from seismic data tied to such wells. These sequences are entered into commercially available modelling software packages that utilise default (published), lithology-specific input conductivities that are made to vary with progressive burial and resulting compaction. A value of heat-flow is then calculated in such a way that, when it is applied to the lithological column, the resulting depth-temperature profile matches the down-hole temperatures (Horner-corrected for circulation effects) measured in the well at the time of drilling. This results in a predictive depth-temperature profile that is more accurately calibrated to the known temperature conditions at depth. The heat-flow calculated at the well location, by virtue of its constraint by measured temperature data, can then be used in offset locations more reliably than if it were derived from shallow, relatively uncompacted samples. Such modelling techniques are routine in the petroleum exploration industry.

A comparison of the outcomes typical of these two approaches was made on wells from the Perth Basin, Bass Basin and the Vulcan Sub-basin.

In the well from the Perth Basin (Figure 1), two down-hole temperatures (Horner-corrected for drilling circulation effects) were available together with a comprehensive stratigraphy. These data were input to Genesis^{TM}, a commercially available interactive thermal modelling package used by 3D-GEO Pty Ltd. Heat-flow input to the base of the sediment pile was varied until a temperature-depth profile (in blue) was obtained that was commensurate with, and therefore calibrated to, the measured down-hole temperatures.

The two most important features of the predicted temperature-depth curve are (a) its non-uniform slope as it responds to changes in lithological conductivity from one formation to the next, and (b) the general steepening of the slope (decrease in geothermal gradient) with depth as it responds to increasing lithological conductivity with increasing compaction (porosity-reduction).

The predicted depth-temperature profile (in blue) is compared in Figure 1 to that which might result from the "projected" approach (red dotted line), which may have been required had the well, and the data available from it, not existed. According to this approach, a temperature-depth profile derived at shallow levels is extrapolated linearly downwards. As Figure 1 shows, in the shallower part of the sequence (above 2500m), both curves approximately coincide, and match the shallower down-hole temperature. However, as you go deeper in the profile, the temperature-depth profile projected linearly from the shallow section deviates significantly from the calculated (blue) curve. At the bottom of the hole, the blue (calculated) curve intersects the measured down-hole temperature (approx 142^{o}C), while the projected curve indicates a temperature of 160^{o}C, some 18^{o}C higher than that measured. Another result is that the depth to an economic target of 150 ^{o}C varies by 540 m between the two models. Figure 1. Comparison between the projected and calculated approach from the Perth Basin.

The projected approach therefore has the very obvious effect of being too optimistic in its estimate of the drilling depths required to reach commercially desirable temperatures. A comparison of the two modelling approaches in the Durroon Sub-Basin in southern Australia and the Vulcan Sub-Basin in the Timor Sea show a similar relationship (Figure 2). The calculated curve fits well with measured temperature, whereas the projected linear profile deviates significantly. Here, two linear temperature profiles are compared to the calculated trend, one based on 300 mssf (in red), the other from 500 mssf (in purple). Both profiles deviate significantly from the calculated curve at depth, with up to 1.2 km difference between where the predicted gradients intersect the target 150^{o}C. (Note that two corrected BHTs were available from the well, the calculated curve being calibrated to the more reliable one based on other calibration data. The higher of the two temperatures, which is considered to be over-corrected, coincidentally fits with the profile projected from 500m).

An example from the Vulcan Sub-Basin in offshore NW Australia shows a similar comparison with the 300-500 mssf extrapolations (Figure 3), with a similar outcome (significant overestimation of temperature by the "projected" approach).

The calculated approach is only possible where deep well data are available, and, like all modelling exercises, is prone to numerous sources of error in terms of its input assumptions. However, it does at least take account of the non-uniform nature of temperature-depth profiles with depth. While, in

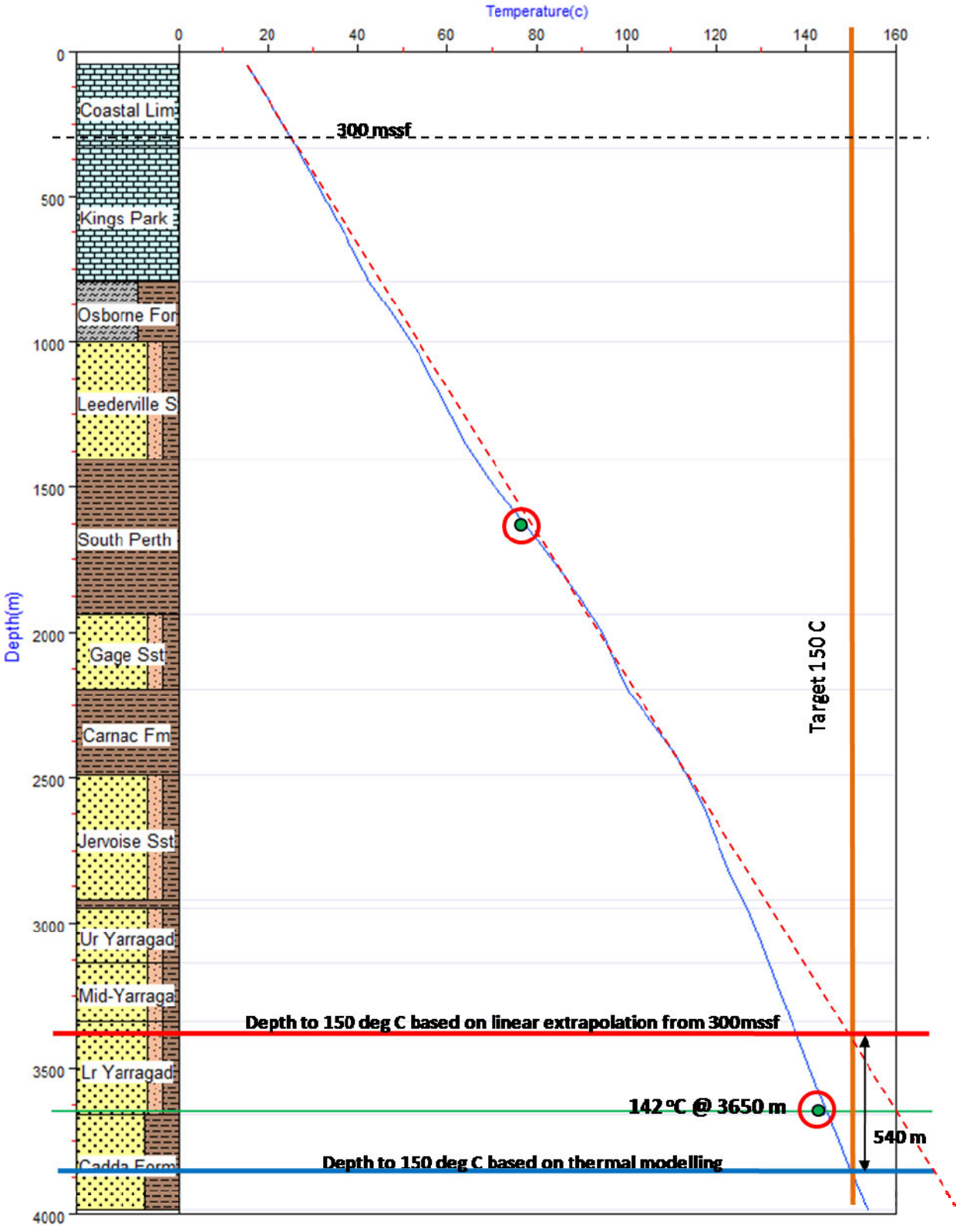

Figure 1. Comparison between the projected and calculated approach from the Perth Basin.

defence of the projected approach, it might be said that it is useful in areas in which no deep-drilling data are available, it is clear from the comparisons shown in Figures 1, 2 and 3 that it is almost inevitably prone to under-estimation of the drilling depths required to reach temperatures of commercial significance. Otherwise put, if the wells shown in these figures had not existed, and the projected approach was applied to the problem of predicting depths to 150°C, the results would have been grossly misleading.

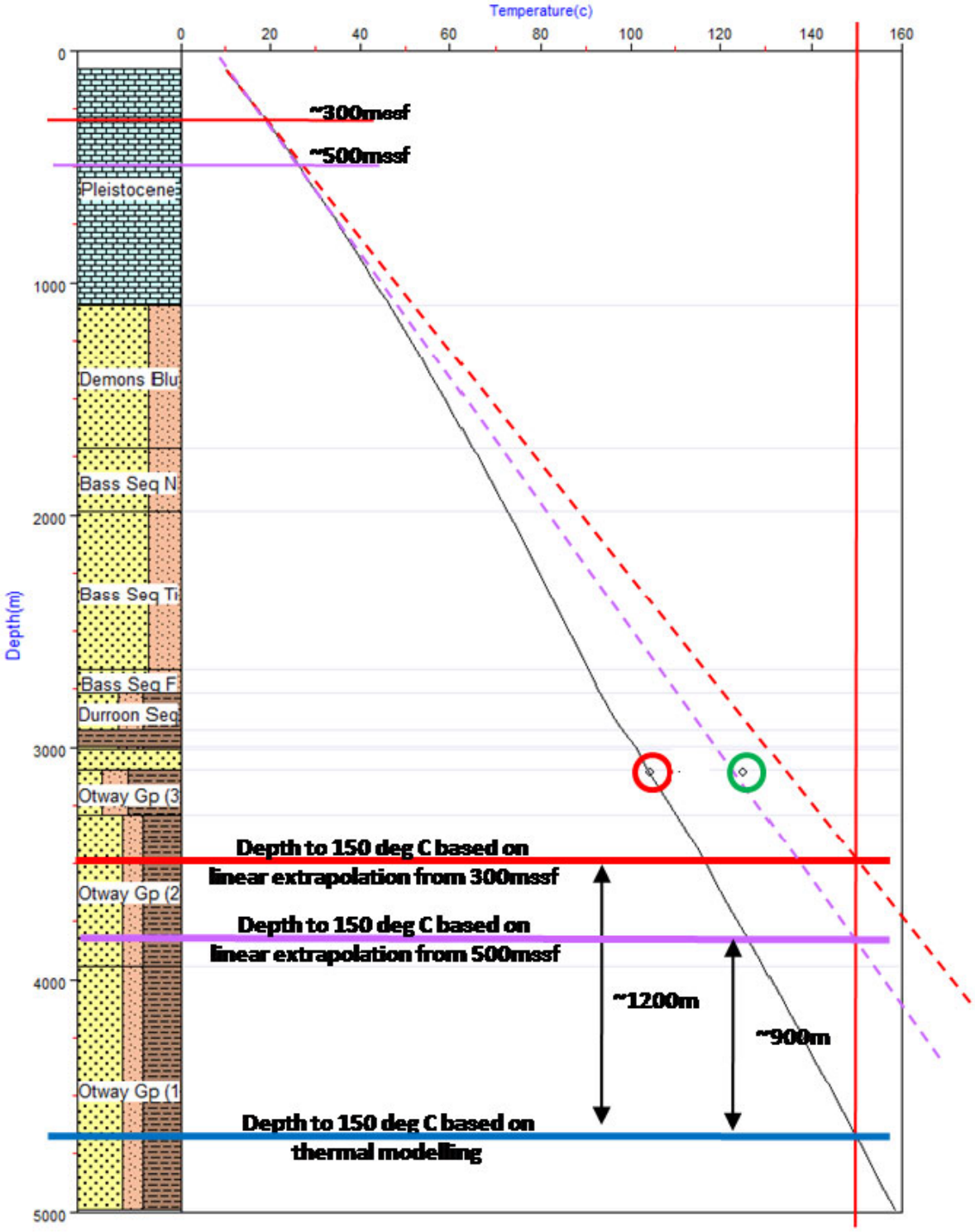

Figure 2. Comparison between the projected and calculated approach from the Durroon Sub-basin. Modelled approximately to basement. Red temperature plot corresponds to Horner corrected temperature. Green temperature plot corresponds to an arbitrary 25% correction applied by the previous modelling attempts.

Conclusions

For the reasons outlined above, the calculated approach accounts for variations in conductivity with both lithostratigraphy and depth (and therefore compaction), and uses measured down-hole temperatures to constrain and calibrate the magnitude of heat-flow being conducted through the sediment pile. The resulting depth-temperature profile is therefore necessarily more consistent with geothermal gradients observed basin-wide. By contrast, the "projected" approach may predict, depth for depth, significantly higher temperatures compared with the "calculated" approach, mainly because the conductivities acquired at shallow levels are anomalously low, and are assumed to be continuous with depth (unaffected by lithological variation or burial-compaction). The

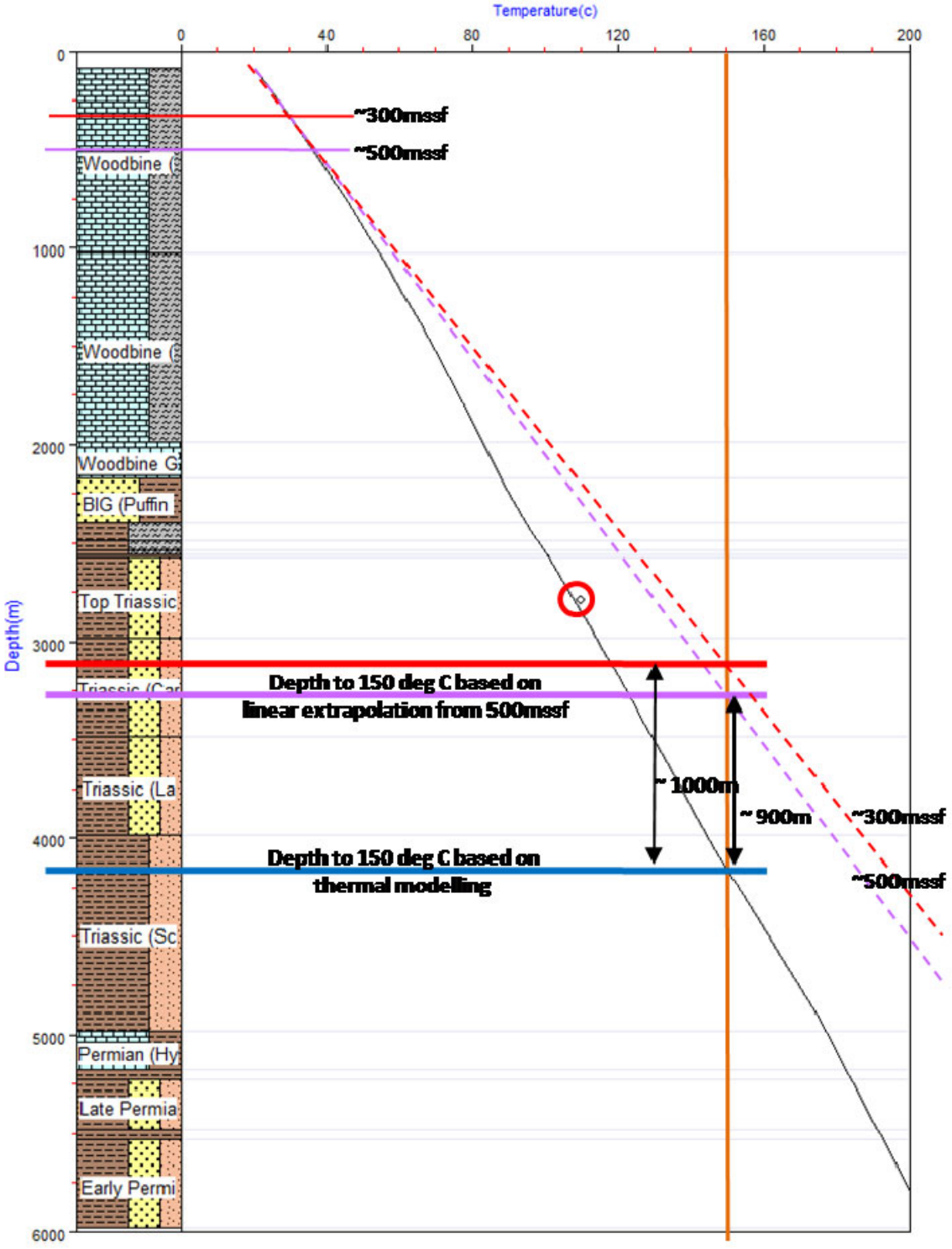

Figure 3. Comparison between the projected and calculated approach from the Vulcan Sub-Basin. Profile modelled to approximate basement.

temperatures predicted at depth by linear extrapolation may therefore significantly higher than those predicted by the "calculated" method, and as such are in danger of predicting the economic target (eg. 140 or 150 ^{o}C) at optimistically shallow levels, and of overestimating geothermal potential.

While both methods have considerable risks and uncertainties associated with them, and while measuring the conductivity in the projected

approach may seem more precise, it is likely to be less accurate than the temperature estimates obtained from the "calculated" approach. However, the "projected" technique may be best suited for areas where calibration data are limited.

References

F. Ascencio, F. Samaniego and J. Rivera, Application of a spherical–radial heat transfer model to calculate geothermal gradients from measurements in deep boreholes, Geothermics 35 (2006), pp. 70–78

Yuan Y. Zhu W., Mi L, Zhang G., Hu S. and He L. 2008. "Uniform geothermal gradient" and heat flow in the Qiongdongnan and Pearl River Mouth Basins of the South China Sea. Marine & Petroleum Geology, 26 (7) 1152-1162.

The Penola Project – Australia's First Hot Sedimentary Aquifer Development

Lambertus de Graaf*, Ron Palmer, Ian Reid
Panax Geothermal Ltd, PO Box 2142, Milton, QLD 4064
*Corresponding author: bdegraaf@panaxgeothermal.com.au

Panax Geothermal Ltd ("Panax") holds the geothermal rights covering four Hot Sedimentary Aquifers (HSA) within troughs or sub-basins in the Otway Basin in southeast South Australia, covering an area of more than 3,000 km^2. The Limestone Coast Geothermal Project is designed to demonstrate that conventional geothermal resources within Australia's hot sedimentary basins can be used to generate large amounts of competitively priced, zero-emission, base-load power. Due to an existing comprehensive database acquired by the petroleum industry, the initial development of its Limestone Coast Geothermal Project is focused on the Penola Trough (GEL223).

The first well, Salamander-1, is the first in a series of wells in the development of a 50 MWe geothermal power plant, which could become the first grid connected geothermal power plant in Australia.

A Pre-Feasibility study has also been completed to assess the total cost per MWh of power produced after taking into account all plant and pump requirements. This study found that electricity can be sustainably generated at a total cost (capital and operating) of AUD$63 per MWh. The Penola Trough has been subjected to intensive oil and gas exploration, including 27 deep petroleum wells with wireline logging and conventional core measurements of reservoir porosity and permeability. In addition, there are 271 km^2 of 3D seismic and a significant amount of 2D seismic data. These data are available as part of the Open File data base and studies have shown that the over 1,000m thick Cretaceous Pretty Hill Formation (sandstones) of the Penola Trough has the capacity to deliver geothermal waters of >140˚C at high volumes, sufficient for the operation of a commercial, medium temperature geothermal power plant. The generating potential is large, as is evidenced by a recent independent Geothermal Resource assessment, which has estimated a "Measured Geothermal Resource" of 11,000 PJ for the Penola Trough.

Introduction

Panax Geothermal Ltd ("Panax") holds eight Geothermal Exploration Licences (GELs), over four Hot Sedimentary Aquifers (HSA) within troughs or sub-basins in the Otway Basin in southeast South Australia, covering an area of more than 3,000 km^2 (see figure 2). The Limestone Coast Geothermal Project is designed to demonstrate that conventional geothermal resources contained within Australia's sedimentary basins have the capacity to generate large amounts of competitively priced, zero-emission, base-load power. The initial development of its Limestone Coast Geothermal Project is focused on the Penola Trough (GEL223, see figure 2), as this trough has a comprehensive exploration database acquired by the petroleum industry.

The Penola Project is located in Geothermal Exploration Licence (GEL) 223, approximately 40 km north of Mount Gambier in South Australia.

The Penola Trough is a sub-basin or trough in the on-shore Otway Basin area of south-eastern South Australia. It is one of several sedimentary troughs and represents an area of thick sediment and relatively recent volcanic activity as indicated by the presence of extinct volcanoes such as those associated with the Mount Gambier region 40km to the south. It is an area of anomalously high heat flow (see figure 3).

The Penola Trough (GEL 223) has been selected for the first deep well because this trough has an extensive data-base of the target productive wells, reservoir, based on more than 20 deep petroleum many of which have intersected the target reservoir, as well as extensive seismic data, including 271 km^2 of 3D seismic.

The Geothermal Reservoir

The target reservoir is the Cretaceous Pretty Hill Formation, a member of the Crayfish Group (see figure 1). The good reservoir quality of the Pretty Hill Formation sandstones has been known from petroleum activities for some time. Gas was first discovered in the trough in 1987 in Katnook-1. These gas discoveries are mainly restricted to the top 25m of the formation, trapped beneath Laira Formation shale. This is relevant and significant because the Laira Formation shale has a low thermal conductivity and is assumed to be a thermally insulating unit, overlying the Pretty Hill Formation target reservoir.

As part of the drilling of the petroleum wells, a significant amount of wireline logging, core sampling and resulting petrophysical evaluation were undertaken in the Pretty Hill Formation. The porosity of the target Pretty Hill Formation section was determined by Panax based on wireline logs calibrated to porosity samples from conventional cores and sidewall cores.

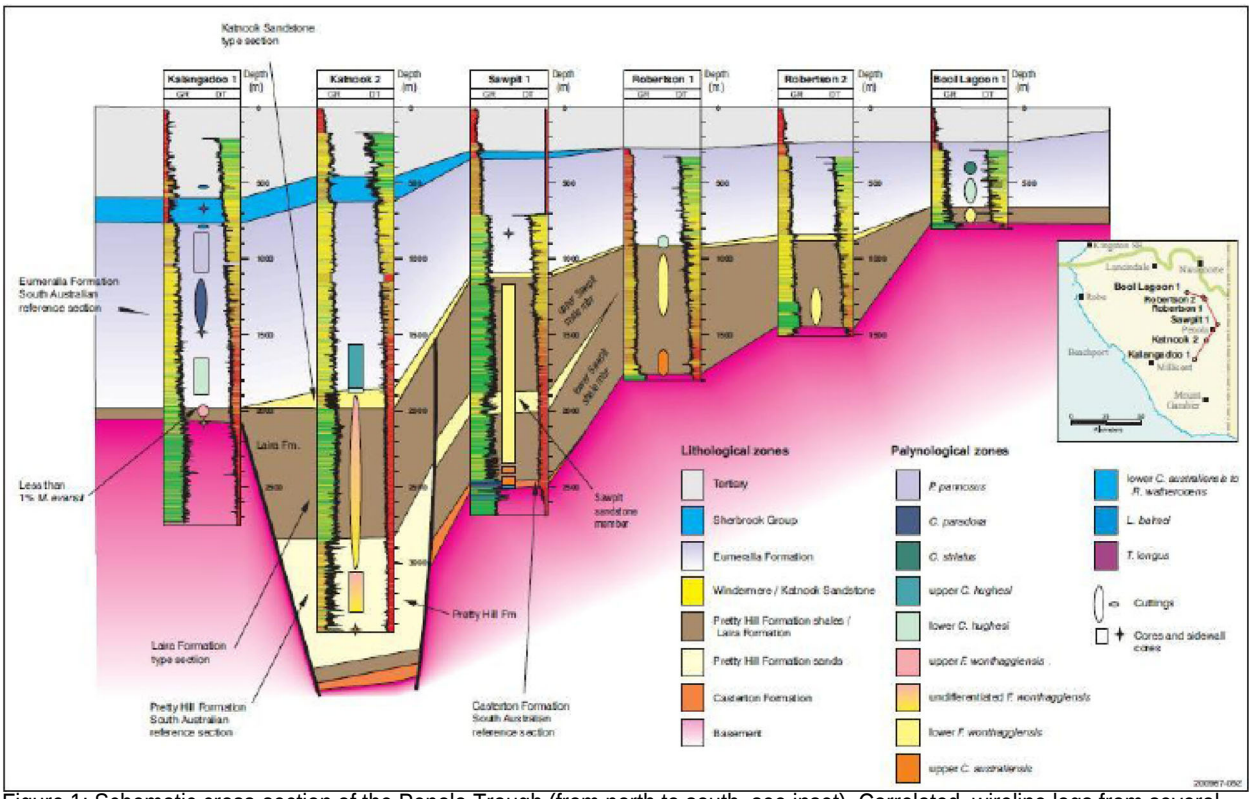

Figure 1: Schematic cross-section of the Penola Trough (from north to south, see inset). Correlated, wireline logs from several wells are also shown. The target reservoir formation, the Pretty Hill Formation, attains maximum thickness in the Katnook Graben (near the Katnook 2 well). After Boult et al. (2002).

We have estimated a total transmissivity (permeability thickness product) of 10-50 Darcy.metres (D.m) depending on well and thickness of Pretty Hill Formation penetrated.

The availability of well data, combined with the available 3D seismic data gives the Penola Geothermal Project a significant degree of credibility and reduced technical uncertainty in regards to the existence of suitable geothermal reservoirs.

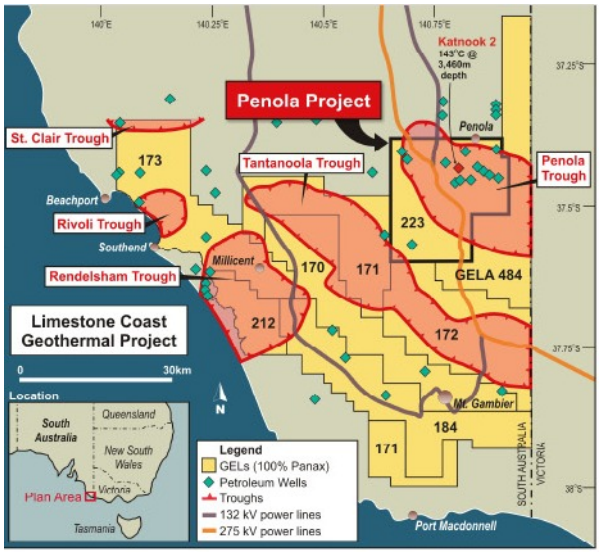

Figure 2: Outline of Sub-basins or troughs of the Limestone Coast Geothermal Project.

Geothermal Resource Estimation and Temperature Determination

Hot Dry Rocks Pty Ltd (HDRPL) undertook a geothermal resource assessment across geothermal tenements owned by Panax, adhering to the Australian Code for Reporting of Exploration Results, Geothermal Resources and Geothermal Reserves, 2008 edition (the Code) (Beardsmore, 2009). The geothermal resource summary in table 1 shows the relatively large overall potential of the Limestone Coast Geothermal Project.

The Penola Trough stands out as being the only trough with indicated and measured resources, courtesy of reservoir information derived from previous petroleum wells and 3D and 2D seismic data. The outline of the measured resource in the Penola Trough is shown in figure 4.

Within most of the Penola Trough, consistent with observations in well Katnook 2, modelling predicts that the temperature is relatively constant around 160°C at 4,000m.

Location and Infrastructure

GEL 223 is located within 50km of Mt Gambier, close to the township of Penola (figure 5). GEL 223 is transected by a transmission network of 275kV and 132kV power grid lines. Indications are there is sufficient capacity at two local substations to facilitate a low cost option (AUD$1-$2 million) for connecting the Demonstration Plant of the Penola Project

Limestone Coast Geothermal Resources					
Trough	**Measured (PJ)**	**Indicated (PJ)**	**Inferred (PJ)**	**Total (PJ)**	**Report Date**
Penola	11,000	32,000	89,000	132,000	18/02/2009
Rivoli & St. Clair			53,000	53,000	28/01/2009
Rendelsham			17,000	17,000	28/01/2009
Tantanoola			130,000	130,000	31/03/2009
Total	**11,000**	**32,000**	**289,000**	**332,000**	

Table 1: Estimated Geothermal Resource within the Pretty Hill Formation and deeper reservoir units for the Penola Geothermal Play. Resource estimates rounded to two significant figures (Beardsmore, 2009; for full reports please refer to the Panax website: www.panaxgeothermal.com.au)

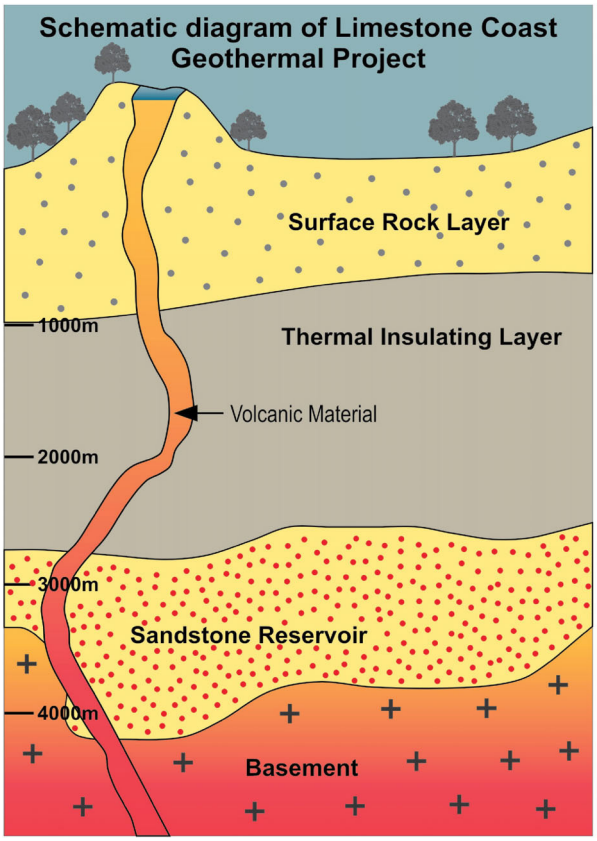

Figure 3: Schematic diagram of the Limestone Coast Geothermal Project.

Seismic Interpretation

Seismic interpretation of the 3D seismic datasets has allowed a confident delineation of the top of the Pretty Hill Formation and the base of the rift. The seismic data was also processed to provide more information on the reservoir quality than from the well data alone. An 'acoustic impedance' inversion of the 3D seismic was undertaken to better identify the prospective reservoir section.

Pre-Feasibility Study

Panax compiled a Pre-Feasibility Study of the Penola Project to determine the total costs per MWh of power generated from brine produced from the Pretty Hill Formation reservoir to provide an assessment of the economic viability of this project. The total cost per MWh is considered to be the cost per MWh of power generated after taking into account all plant and pump requirements.

The Penola Project power generation is based on the production of 175kg/sec of brine (=166.4k gallons/hr (US)), at a temperature of 145˚C (293˚F) from each production well, and an injection temperature of 70˚C (158˚F). This Base Case using a standard binary organic rankine cycle binary geothermal power plant, has an estimated Gross output of 6.7 MWe and Net output of 5.9 MWe and a net/net output of 4.5 MWe.

The development is divided up in three stages:

- a **Demonstration Plant** based on one production well
- the **Phase 1 Plant** based on a total of three production wells; and
- the **Phase 2 Plant** based on a total of ten production wells.

A summary of the output and total cost per MWh for the three stages and a summary of the total capital and operating costs per MWh is listed in tables 2 and 3 below:

	Output MW	$ MWh
Gross	67.0	42
Net Plant	59.0	48
Net Plant/Net Pumps	45.0	63

Table 2: Penola Project Summary of Base Case Output Gross, Net Plant and Net Plant/Net Pumps, Total Costs per MWh

The cost per MWh produced after plant and pump power demands (i.e. net plant, net pumps) is estimated at AUD$63 per MWh. The cost of connecting the Penola Project power generation to the grid (based on independent expert advice) adds approximately AUD$2 to the total cost per

MWh generated, a direct reflection of the excellent infrastructure location of this project.

Capital & Operating Costs per MWh (Phase 2 Plant, AUD$'s)	
Capital Costs	$51
Operating Costs	$12
Total Costs	**$63**
Grid Connection	$2
Total	**$65**

Table 3: Penola Project Capital and Operating Costs per MWh Phase 2 Plant (67 MW).

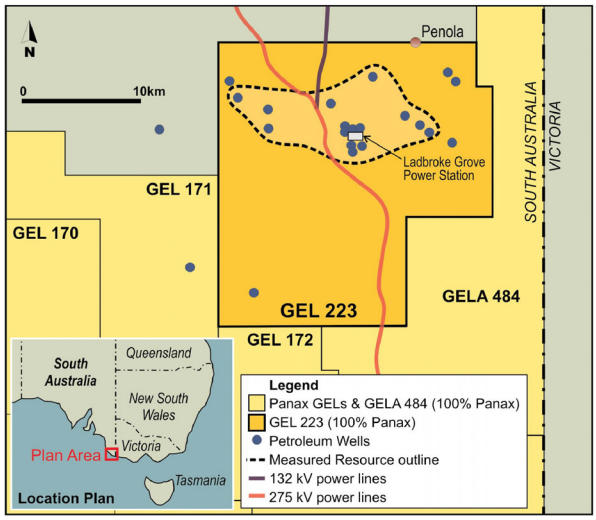

Figure 4: Surface outline of the Measured Geothermal Resources of the Penola Project.

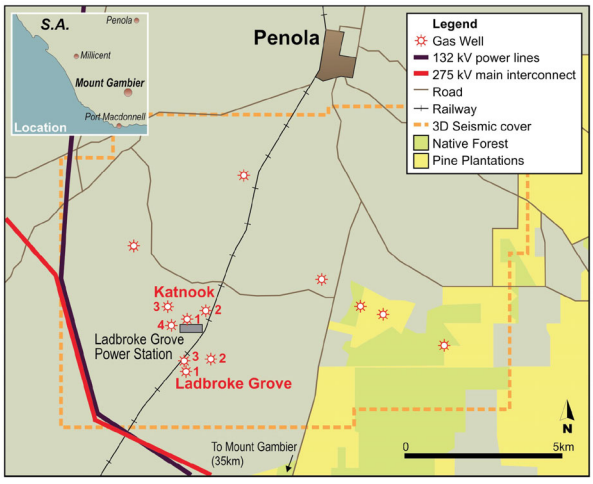

Figure 5: Penola Project – Location & Infrastructure.

Conclusion

It can be concluded that the Penola Project represents a commercially attractive geothermal development proposition targeting a hot sedimentary aquifer which is well known from previous petroleum exploration. A pre-feasibility study indicates that a competitive total cost per MWh of AUD$63 can be achieved. Further, the plans for drilling the first well in the project, Salamander 1, are well advanced. Overall, the Penola Project has the scope to be of national significance in the quest to reduce carbon emissions through providing competitively priced, zero emission, base-load power, and to be the first grid connected geothermal electricity generator in Australia.

References

Beardsmore, G.R., 2009: Limestone Coast Project: Penola Geothermal Play, Statement of Geothermal Resources, Internal report.

Beardsmore, G.R, 2009: Limestone Coast Project: Tantanoola Geothermal Play, Statement of Geothermal Resources, internal report.

Beardsmore, G.R, 2009: Limestone Coast Project: Rendelsham Geothermal Play, Statement of Geothermal Resources, internal report.

Beardsmore, G.R, 2009: Limestone Coast Project: Rivoli - St Clair Geothermal Play, Statement of Geothermal Resources, internal report.

Boult, P.J., White, M.R., Pollock, R., Morton, J.G.G., Alexander, E.M., and Hill, A.J., 2002, Lithostratigraphy and environments of deposition, in J., B.P., and Hibburt, J.E., eds., The petroleum geology of South Australia, Volume Vol 1: Otway Basin, Primary Industries and Resources South Australia (PIRSA).

Water Requirements in Deep Geothermal Systems

Jim P. Driscoll
Hot Dry Rocks Pty Ltd, Level 4, 141 Osborne Street, South Yarra, VIC, 3141.
jim.driscoll@hotdryrocks.com

The working fluid in a geothermal system is the medium through which heat is extracted from the sub-surface realm and brought to surface.

Access to a working fluid is one of four critical risk areas that need to be addressed when undertaking Geothermal Systems Assessments.

Surface water and groundwater are regarded as the most viable supplies of working fluid, although there is scope for the use of water co-generated from hydrocarbon operations. The use of CO2 as a working fluid has also been suggested, and research into this field continues.

Water is a valuable commodity, and it is essential that water access issues be addressed in the early stages of planning a geothermal project. Rainfall in Australia is unevenly distributed, both seasonally and geographically.

An outline of the full life cycle water requirements of a deep geothermal energy project is presented. Distinctions are made between Engineered Geothermal Systems and Hot Sedimentary Aquifers.

Keywords: Water, Working Fluid, Geothermal Systems Assessment, HSA, EGS, Reservoir, Canning Basin

Introduction

Access to a working fluid should be addressed during the initial exploration stage of a geothermal project rather than just being considered during the developmental and production phase. This is due to public concerns about water security, and also to water-use being subject to increasingly stringent regulatory frameworks.

Working fluid risk was identified by Cooper and Beardsmore (2008) as being one of four critical risk areas that need to be addressed when undertaking a Geothermal Systems Assessment of an area.

Cordon and Driscoll (2008) quantified the volumes, rates and quality of water required at successive stages of exploration, development and production of geothermal resources in a South Australian context, and these data are transferrable to geothermal projects elsewhere in Australia.

Exploration and development programs tend to follow similar paths, with each stage having its own water requirements. During the initial stages of a geothermal exploration program, it is usually necessary to drill a series of shallow heat flow holes to delineate the most prospective parts of an area. Once the company has achieved a level of confidence in defining their potential geothermal resource, deep geothermal resource drilling is planned and marks the beginning of the development stage as it is currently accepted that the first deep exploration well is converted into either an injection well or production well.

Climate

Australia's rainfall is highly variable, both seasonally and geographically, as demonstrated in data derived from the Bureau of Meteorology (Figures 1 and 2). Figure 1 details the 30 year average rainfall in Australia whilst Figure 2 shows the variability of rainfall in Australia over the previous 36 months.

Consequently, surface water volumes and groundwater recharge is extremely variable on a year-by-year basis. The Federal Government completed an assessment of Australia's water resources, including water availability, allocation and use, management and development, and water quality. These data were published in 2000 as part of the *Australian Natural Resources Atlas* (www.anra.gov.au/water).

Surface Water

The Australian Natural Resources Atlas (2000) divided surface water resources into 12 drainage divisions, 246 river basins and 325 surface water management areas.

It can be seen from Figure 1 that much of Australia is classed as arid (annual rainfall <250 mm) or semi-arid (annual rainfall 250-500 mm). In such areas, rainfall occurs sporadically and is often concentrated and intense—causing both local and widespread flooding. Evaporation rates tend to be high to extreme, leading to surface water drying out very quickly.

Even in areas where there is greater annual rainfall, evaporation rates can be extreme during the summer months when surface water often dries up entirely. The importance of groundwater as a constant source of water is therefore apparent.

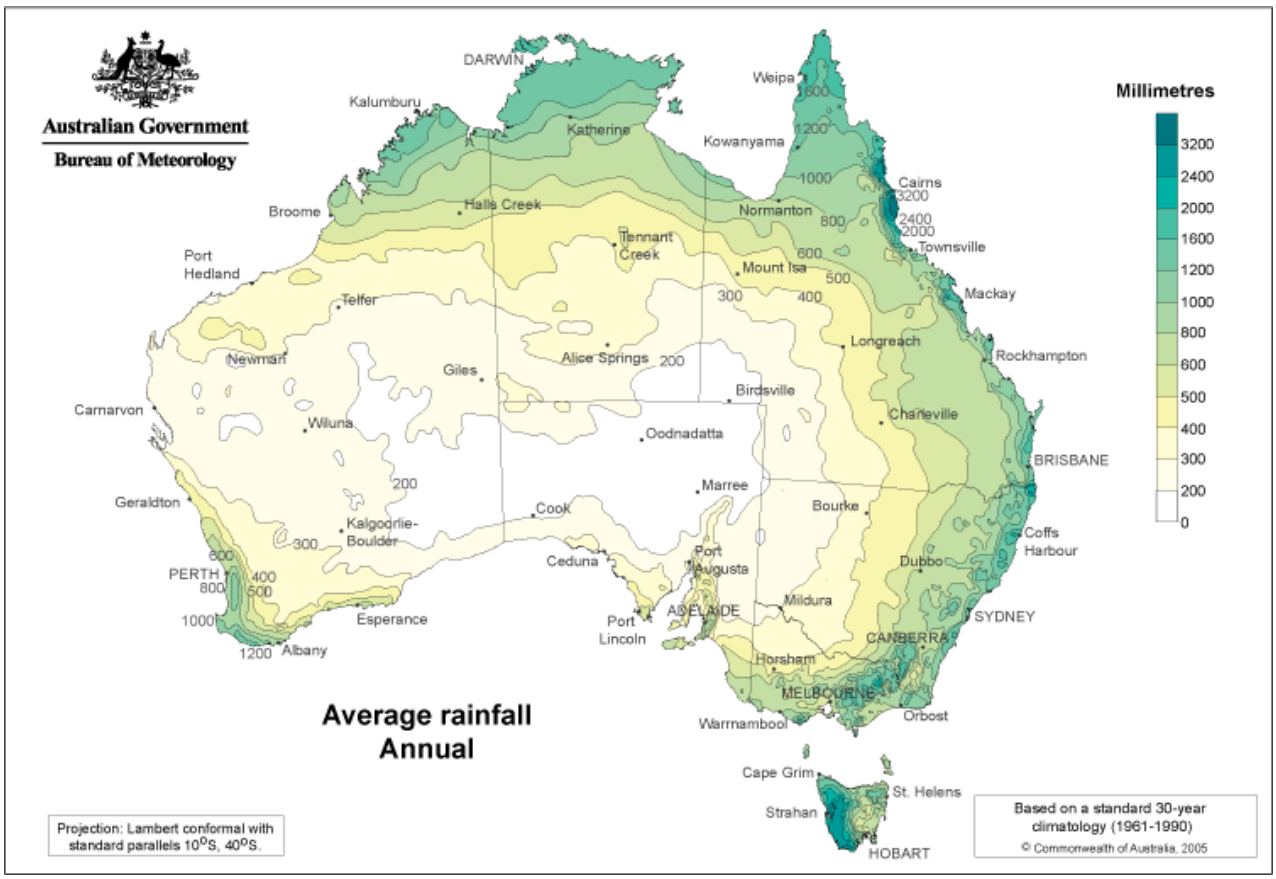

Figure 1. Average annual rainfall in Australia based on 30-year average 1960-1990 (sourced from www.bom.gov.au).

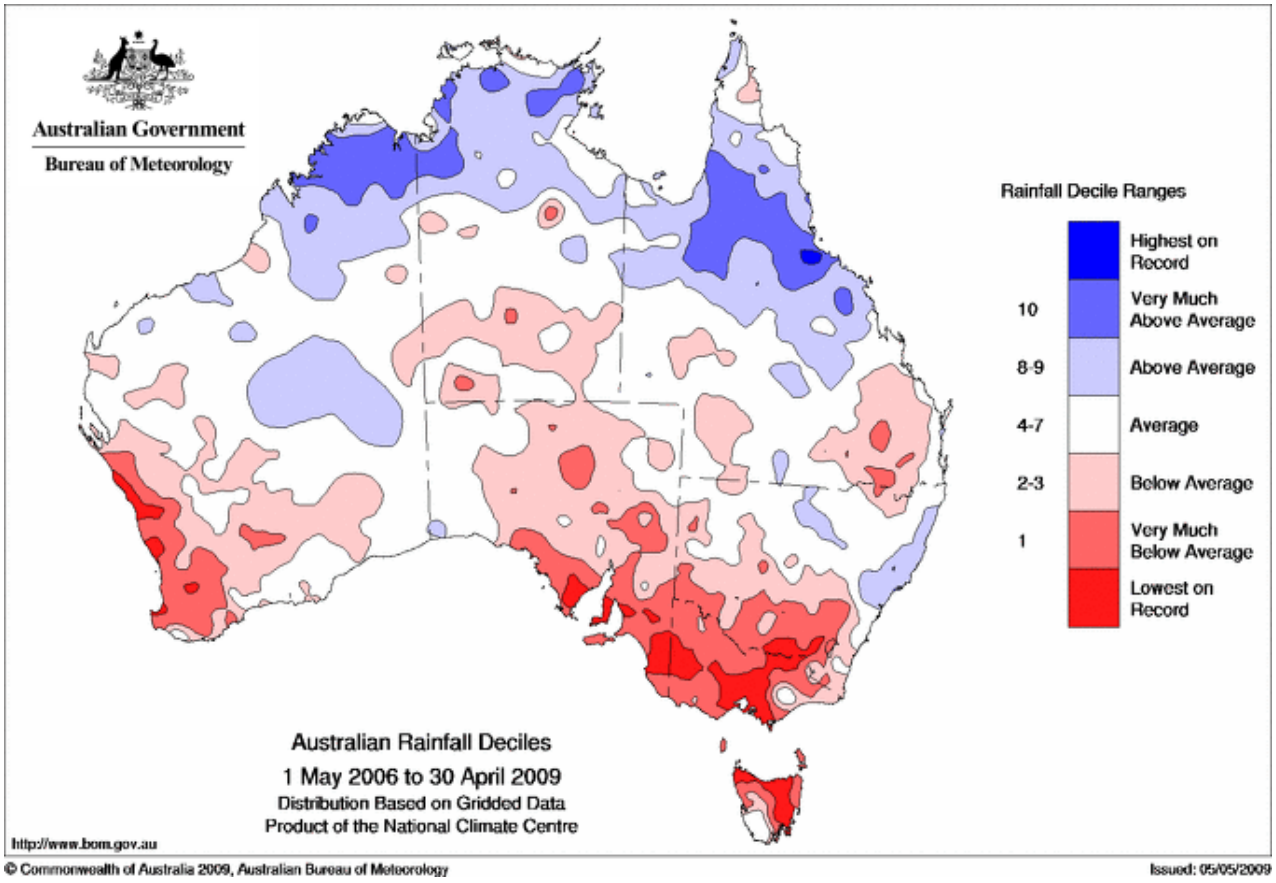

Figure 2 Rainfall deciles for 36 month period 1st May 2006 to 30th April 2009 (sourced from www.bom.gov.au).

The Australian Natural Resources Atlas (2000) concluded that 26% of Australia's surface water management areas (SWMAs) were at a high level of development and approaching or beyond sustainable extraction limits (Table 1).

Development status	Number (%) of SWMAs
Low development (<30% of nominated sustainable flow regime)	195 (60%)
Moderate development (between 30% and 70% of nominated sustainable flow regime)	46 (14%)
High development (between 70% and 100% of nominated sustainable flow regime)	50 (15%)
Overdeveloped (>100% of nominated sustainable flow regime)	34 (11%)

Table 1. The level of development of Australia's 325 SWMAs. The surface water sustainable flow regime is defined as the volume and pattern of water diversions from a river that includes social, economic and environmental needs. Sourced from the Australian Natural Resources Atlas, 2000.

It is also worthy to note that 55% of Australia's water is supplied by SWMAs that are considered overdeveloped.

Groundwater

The availability of groundwater is generally controlled by two important parameters: the type of strata that hosts the aquifer (i.e. whether it is a sedimentary or fractured rock aquifer system) and the degree of connectivity of the voids (whether they be fractures within the rock, or pore throats in sedimentary grains). Sedimentary aquifers typically yield at higher rates and store a greater volume of water compared to fractured rock aquifers.

A further controlling factor in groundwater availability is the rate of recharge to the aquifer system versus the rate of extraction. Regions of high rainfall typically have significant volumes of groundwater available in shallow aquifer systems (assuming an aquifer is present). In drier climatic regions, aquifers tend to be located at deeper levels below the Earth's surface, and are often associated with large volumes of water still resident from the geologic past. Present day replenishment rates in these arid to semi-arid areas are typically low.

The Australian Natural Resources Atlas (2000) divided groundwater resources into 69 groundwater provinces and 538 groundwater management units (GMUs).

Development status	Number (%) of GMUs
Low development (<30% of nominated sustainable yield)	274 (53%)
Moderate development (between 30% and 70% of nominated sustainable yield)	81 (16%)
High development (between 70% and 100% of nominated sustainable yield)	104 (20%)
Overdeveloped (>100% of nominated sustainable yield)	57 (11%)

Table 2. The level of development of Australia's 516 GMUs (note: 22 GMUs were not assessed). The groundwater sustainable yield is defined as the volume of water extracted over a specific timeframe that should not be exceeded to protect the higher social, environmental and economic uses associated with the aquifer. Sourced from the Australian Natural Resources Atlas, 2000.

Great Artesian Basin (GAB)

The Great Artesian Basin (GAB) covers an area of over 1,711,000 km2 (Figure 3), and has estimated water storage of 8.7 million GL, although only a very small proportion of this water is recoverable from bores.

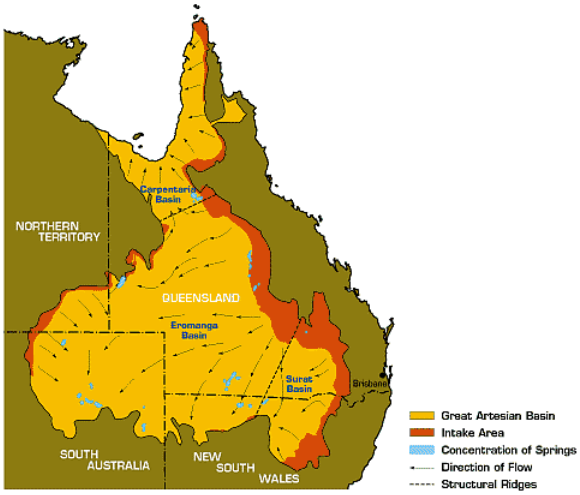

Figure 3. Map of the GAB highlighting intake areas, direction of flow and concentration of springs (source http://www.nrw.qld.gov.au).

The GAB consists of alternating layers of water bearing (permeable) sandstone aquifers and non-water bearing (impermeable) siltstones and mudstones. This sequence varies from less than 100 m thick on the outer extremities of the GAB to over 3,000 m in the deeper parts. Water temperatures vary from 30°C in the shallower areas to over 100°C in the deeper areas, controlled primarily by depth of burial.

Throughout most of the GAB, groundwater generally flows to the south-west, although more to the north-west and north in the northern section. The rate at which it flows through the sandstones varies between 1—5 m/yr. Recharge

by infiltration of rainfall into outcropping sandstone aquifers occurs mainly along the eastern margins of the GAB, and specifically along the western slopes of the Great Dividing Range. Natural discharge occurs mainly from mound springs in the south-western area. These springs are natural outlets through which the groundwater flows to the surface.

Some of the oldest waters are found in the south-western area of the GAB. These have inferred ages of up to 2 million years (dating back to the base of the Pleistocene). The sedimentary rocks that make up the GAB were deposited during the Jurassic and Cretaceous Periods (195–65 million years ago).

Coproduced Fluids

In some areas of oil and gas development, high temperatures are coupled with high volumes of water produced as a by-product of hydrocarbon production. This is of particular significance to the Cooper Basin where geothermal licences for a number of companies overlap with existing hydrocarbon operations. Each oil and gas field has a large evaporation pond to house water co-produced from the extraction of hydrocarbons, so water sources are spread throughout the basin area. The size of the ponds varies depending on fluid rates to surface. Further assessment of water sources co-produced by hydrocarbon operations could prove beneficial to geothermal energy projects in these areas.

In the United States, water is produced from massive water-flood recovery fields and from most mature hydrocarbon areas; the disposal of this co produced water is an expensive problem (Tester *et al*., 2006). Curtice and Dalrymple (2004) estimated that co-produced water in the United States amounts to at least 40 billion barrels per year, primarily concentrated in California and states bordering the Gulf of Mexico.

The key factors required for successful geothermal electrical power generation include sufficiently high fluid rates from a well or group of wells in relatively close proximity to each other, at temperatures in excess of 100°C.

Carbon Dioxide as a Working Fluid

Whilst most geothermal operators consider water to be the optimal working fluid, there is ongoing research into other fluids such as super-critical CO2 (Brown, 2000; Pruess, 2006). Whilst CO2 has many benefits including being a non-polar fluid, low viscosity at temperatures and pressures within the reservoir, and a large buoyancy effect; there are several drawbacks such as a lower heat capacity and large frictional losses (due to gas-phase flows in the production well-bore) which leads to lower thermodynamic performance within the system (Atrens *et al*., 2009).

Working Fluid Risk

Regulatory processes will always be an inherent risk in the Australian context given the increasing value being applied to water resources. However, the main technical risks are the volumes of water required to initially charge an Engineered Geothermal System (EGS), and the quantities of water needed to sustain any ongoing circulation losses during development and production.

Until recently, it was thought water chemistry issues would not adversely impact geothermal projects in Australia so long as operators controlled the quality of water introduced to the system. However—as the April 2009 incident at Geodynamics' Habanero Project demonstrated—corrosion may be an issue where natural fluids are produced. Whilst unfortunate, the identification of this risk does allow for companies to incorporate mitigating strategies in designing their wells and associated infrastructure.

Water Requirements

Engineered Geothermal Systems (EGS)

The water requirements for EGS projects are determined by the volume required to initially charge the system, and volumes required to sustain the system once water losses are accounted for.

Cordon and Driscoll (2008) surmised that the development stage would require 280,000 m3 of water based on the assumption that an EGS module consists of one injector (1st well) and two producers (2nd and 3rd well) of 8.5" open-hole diameter. Wells are typically drilled to a depth of 3,000–5,000 m and modelling studies suggest a separation between wells of 600 m would be optimal to create sufficient volume heat exchangers that operate for a period of approximately 20 years.

Thirty one separate stages were identified by Cordon and Driscoll (2008) in the development phase of the project, each with varying water requirements.

Once the exploration well has been drilled, a series of small-scale injection tests are used to assess the undisturbed hydraulic properties in the open section of the well. These tests may include slug tests (to study the response of the well-aquifer system to an impulse in flow), production tests (which yield information on the pressure and temperature conditions deep in the well where a future heat exchanger is planned) and low-rate injection tests (determine the

hydraulic properties of the un-stimulated open-hole section of the well).

The next phase of development is to stimulate or create a reservoir in the well via initiation of shearing within joints at a predetermined depth. The stimulation involves injecting water in steps with increasing flow rates; and a post-stimulation test is undertaken to evaluate the enhancement of permeability in the reservoir

Once the stimulation and the post-stimulation test of the well is completed, an assessment is made to see if the extent and quality of the reservoir is suitable for progressing to the next stage, the targeting and design of a 2nd well to intersect the reservoir. During the drilling of the 2nd well, wellhead pressure on the 1st well is monitored for any pressure response from the drilling activities in the 2nd well. Once the 2nd well is completed, similar tests to that carried out in the 1st well are required to determine the extent of the hydraulic link between the wells.

A small-scale circulation test between the two wells using tracers is carried out to evaluate the reservoir properties. Should hydraulic data indicate impedance within the reservoir, then remedial treatments can be implemented to improve reservoir connectivity between the wells.

A decision to drill the third well is made once the stimulation and post-stimulation tests in the second well indicate the extent and quality of the reservoir. Again, a series of tests are conducted between all three wells to confirm that circulation is established and that reservoir characteristics are acceptable to the business plan.

Finally, circulation tests with increasing flow rates are undertaken to move the project from the development stage to the production stage.

As there are very few operational EGS's in the world, hydrothermal projects are generally used as analogies to provide an estimate of water usage for the production phase of geothermal energy projects. In a typical, successful hydrothermal reservoir, wells can produce 5 MW or more of net electric power through a combination of high temperatures and high flow. For instance, a well in a shallow hydrothermal reservoir producing water at 150°C needs to flow at about 125 kg/s (~125 l/s) to generate 4.7 MW (Tester *et al*., 2006) of net electric power to the grid.

Hot Sedimentary Aquifers (HSA)

HSA systems differ from EGS projects in that there are substantial volumes of water inherently within a naturally occurring reservoir. Primary porosity and permeability are seen to decrease with increasing depth due to the effects of compaction (Figure 4). There is thus a trade off between temperature and the flow rate potential of the reservoir at depth. In instances where the target isotherm lies at depths where compaction processes have destroyed a significant proportion of the primary porosity and permeability, hydraulic stimulation procedures, similar to those described in the previous section, would be engaged to enhance reservoir properties.

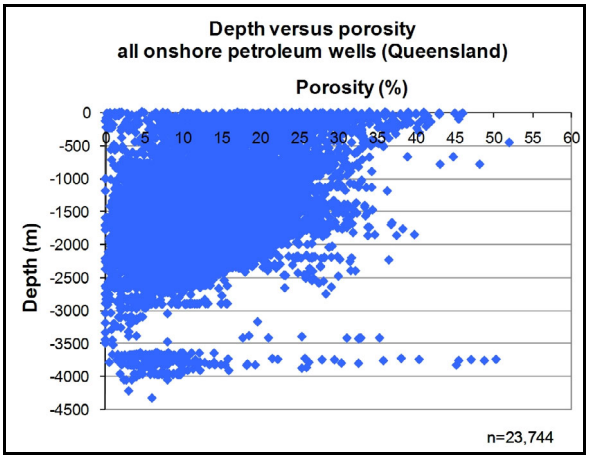

Figure 4. Depth versus porosity plot for all onshore petroleum wells in Queensland

In order to commercially exploit a HSA geothermal resource, detailed knowledge of the aquifer and water-flow characteristics needs to be ascertained. Flow characteristics are especially important in order to ensure reinjection does not cool the system and exhaust the resource too quickly. Two criteria need to be fulfilled: high yielding aquifers and hot water within the aquifer.

HSA systems utilise water at temperatures typically between 100°C and 150°C. Water at this temperature will not flash spontaneously into steam at sufficient pressures to turn electricity generator turbines; thus binary cycle electricity generation is utilised. The heat contained within the water is transferred to another medium with a lower boiling-point, termed the 'working' or 'binary' fluid. The high-pressure vapour of the binary fluid can then be used to turn a turbine.

Driscoll *et al*. (2009) noted in their Canning Basin geothermal assessment several high-yielding aquifers, most notably the Grant Group sandstones which extend throughout much of the basin and are several kilometres thick in places. Two GMUs, the Desert and the Wallal GMU, cover the vast majority of the Canning Basin, and both have very low to minor development of the Grant Aquifer with high sustainable yields (218 and 296 Gl/yr respectively). Assuming the geothermal system requires flow rates of 100 l/s, the water is reinjected back into the same aquifer, and there is 2% water loss, then water requirements would be ~64 Ml/yr for production. The Grant Aquifer

can therefore be regarded as having excellent development potential.

Summary

Changes in rainfall distribution and intensity have been well documented in Australia. Geothermal operators will need to offer creative solutions to acquire and secure their water supplies over the lifetime of the project.

Access to groundwater is limited and regulated, so advanced planning is required by companies.

References

Atrens, A., Gurgenci, H. and Rudolph, V., 2009. Exergy Analysis of a CO2 Thermosiphon. In: Proceedings of the Thirty-Fourth Workshop on Geothermal Reservoir Engineering, Stanford University, SGP-TR-187.

Australian Natural Resources Atlas, 2000 (www.anra.gov.au/water).

Brown, D., 2000. A Hot Dry Rock geothermal energy concept utilizing supercritical CO2 instead of water. In: Proceedings of the Twenty-Fifth Workshop on Geothermal Reservoir Engineering, Stanford University, 233–238.

Cooper, G.T and Beardsmore G. R., 2008. Geothermal systems assessments: understanding risk in geothermal exploration in Australia. In: Blevin, J.E., Bradshaw, B.E. and Uruski, C. (Eds), Eastern Australasian Basins Symposium III, Petroleum Exploration Society of Australia, Special Publication, 411–420.

Cordon, E. and Driscoll, J.P., 2008. Full Life-Cycle Water Requirements for Deep Geothermal Energy Developments in South Australia. Department of Primary Industries and Resources (South Australia) and the Australian School of Petroleum, 50 pp.

Curtice, R.J. and Dalrymple, E.D., 2004. Just the cost of doing business. *World Oil* 77–78.

Driscoll, J.P., Mortimer, L., Waining, B., Cordon, E. and Beardsmore, G.R., 2009. Geothermal Energy Potential in Selected Areas of Western Australia (Canning Basin). 87 pp. http://www.dmp.wa.gov.au/801.aspx

Pruess, K., 2006. Enhanced geothermal systems (EGS) using CO2 as working fluid—A novel approach for generating renewable energy with simultaneous sequestration of carbon. Geothermics, 35, 351–367.

Tester, J. *et al*., 2006. The Future of Geothermal Energy – Impact of Enhanced Geothermal Systems (EGS) on the United States in the 21st Century, MIT Press, pp. 2-29; 5-3.

Approaches for identifying geothermal energy resources in coastal Queensland

Melanie Fitzell*, Stephanie Hamilton, Jim Beeston, Len Cranfield, Kate Nelson, Chris Xavier and Peter Green.
Queensland Mines and Energy, 80 Meiers Road, Indooroopilly QLD 4068
*Corresponding author: melanie.fitzell@deedi.qld.gov.au

The Coastal Geothermal Energy Initiative is a Queensland Government Program designed to investigate sources of hot rocks close to existing transmission lines along the east coast of Queensland where modelled crustal temperatures at 5km are generally <150°C. The modelled low temperatures in this coastal region could reflect insufficient and poorly distributed data rather than an absence of suitable geothermal targets. The initiative involves a series of drill holes for the specific purpose of taking downhole temperature readings and obtaining cores for measurement of thermal conductivity to calculate heat-flow. The drill holes are to be sited in areas considered to have potential to contain hot rocks. Selection of these areas is based largely on an understanding of the geological setting and history of this part of Queensland. This paper highlights five different geological targets identified for further investigation. These targets include an extrapolated buried granitoid, inferred granitoids from geophysical anomalies, and three sedimentary basins that contain either low thermal conductivity coal or oil shale. A variety of techniques have been used in the assessment of these targets, involving the integration of different geological and geophysical data.

Keywords: Queensland, Coastal Geothermal Energy Initiative, Texas beds, Stanthorpe, Tarong Basin, Styx Basin, Hillsborough Basin, geothermal exploration

Background

In June 2007, the ClimateSmart 2050 *Queensland climate change strategy 2007: a low-carbon future* was released, embracing a commitment to investigate sources of hot rocks for geothermal energy close to existing transmission lines. The Coastal Geothermal Energy Initiative (CGEI) is the project that has been established to undertake this investigation. The CGEI is a cooperative project between the Office of Clean Energy and the Geological Survey of Queensland, within the Department of Employment, Economic Development and Innovation (DEEDI).

CGEI will obtain continuous temperature logs in the purpose drilled holes to augment existing data. These holes will be cored from surface to total depth of 300-320m and then be allowed to re-equilibrate before being logged. Thermal conductivity measurements will be taken from core samples to calculate heat-flow.

Coastal regions of Queensland have not been previously considered to be prospective for geothermal energy as modelled crustal temperatures are generally <150°C (Chopra & Holgate, 2005). These low temperatures could reflect a lack of data in the appropriate areas.

The absence of temperature and heat-flow data highlights the need for a different approach to identifying geothermal energy resources in coastal Queensland. The CGEI is the first government program in Australia designed to directly target gaps in temperature and heat-flow data coverage across the state.

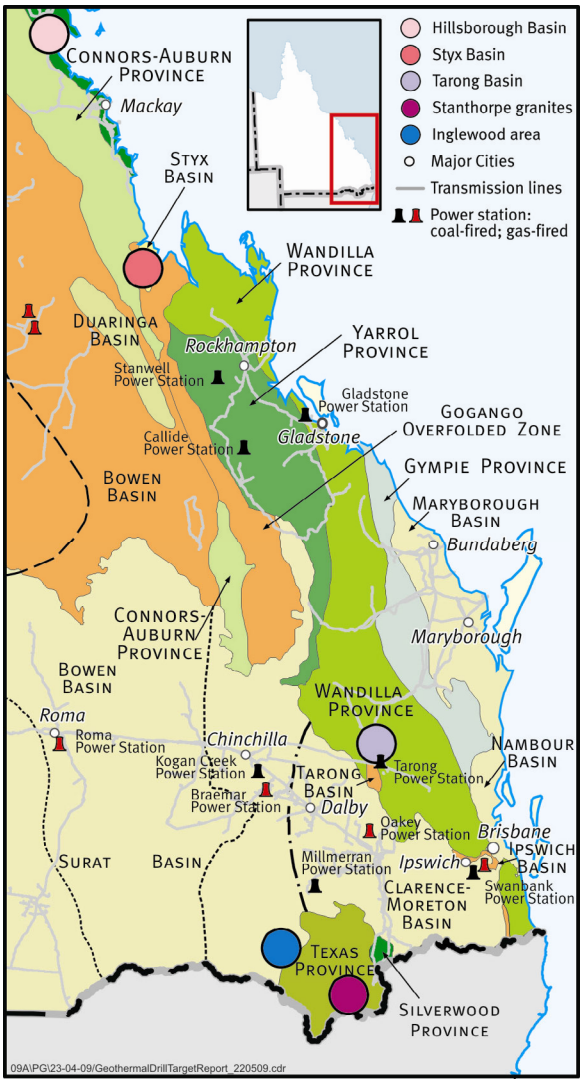

Figure 1: Map showing locations of five geological targets for assessment in the CGEI.

Initially, target areas were identified from an understanding of the geology and tectonic history of eastern Queensland. These areas were considered to have the potential to have elevated temperatures at a shallow depth. No specific geothermal-energy model has been applied to their selection.

Detailed assessment of the target areas is being undertaken using the available geological and geophysical data. Geophysical modelling is being undertaken over target areas where geophysical datasets are suitable, to better define the geothermal target.

Heat production values referred to in this paper have been calculated from whole-rock geochemistry data of granitoids across the state. A heat-production equation (Rybach, 1988) has been used to determine locations of values greater than five microwatts per cubic metre ($\mu W/m^3$).

This paper presents five examples (Figure 1) of the types of geological targets to be tested and the approaches used in their assessment. These targets include an extrapolated buried granitoid, inferred granitoids from geophysical anomalies, and three sedimentary basins that contain low thermal conductivity lithologies such as coal or oil shale.

Inglewood area

Geological Outline

In the Inglewood area, Jurassic-Cretaceous rocks of the Clarence-Moreton and Surat Basins unconformably overlie Carboniferous Texas beds basement. These rocks are unconformably overlain by Tertiary-Quaternary flow remnants of the Main Range - Lamington Basalt Province. Mesozoic units that outcrop/subcrop over the area include the Marburg Subgroup (Lower-Middle Jurassic), the Walloon Subgroup (Middle Jurassic) and the Kumbarilla beds (Middle Jurassic-Early Cretaceous).

The Texas beds form part of the Texas Subprovince, within the central part of the New England Orogen. The turbidite-dominated Texas beds are intruded by Permian-Triassic mainly I-type plutons assigned to the New England Batholith.

Regional Geophysics

The regional magnetic data highlight the structural grain of the western limb of the Texas Megafold. The most obvious surface features are strongly magnetic and magnetically altered rocks in the Texas beds, and moderate to strongly magnetic basalt lavas. These units contrast with the weakly magnetic Clarence-Moreton and Surat Basin successions. Unexposed, moderate to strongly magnetic granitoid intrusions vary in shape and size. The most prominent of these is located west of Inglewood and forms the basis of this investigation. The Stanthorpe Granite farther east also has a moderate to strong positive total magnetic intensity (TMI) response, and is high-heat producing. A number of unexposed, non-magnetic granitoid intrusions have also been interpreted in the Inglewood area (Purdy et al., 2005).

Target Rationale

The premise to be tested is that Carboniferous accretionary wedge rocks and Mesozoic fluvio-lacustrine rocks are insulating a high-heat producing intrusion.

The target is a north-south trending, elliptical, magnetic anomaly west of Inglewood (Figure 2). This anomaly (~90km^2) has a strong positive TMI response. Preliminary modelling demonstrates that the magnetic anomaly may be explained by a diapiric-shaped pluton intruding basement, with the most magnetic material occurring more than 500m below the surface. Donchak et al. (2007) suggested a Permian-Triassic age range for this magnetic unit.

A water supply bore drilled on the anomaly bottomed in Marburg Subgroup at 227m. No bottom-hole temperature was taken. If the unit is high-heat producing and there is sufficient insulation, it could be a viable geothermal target.

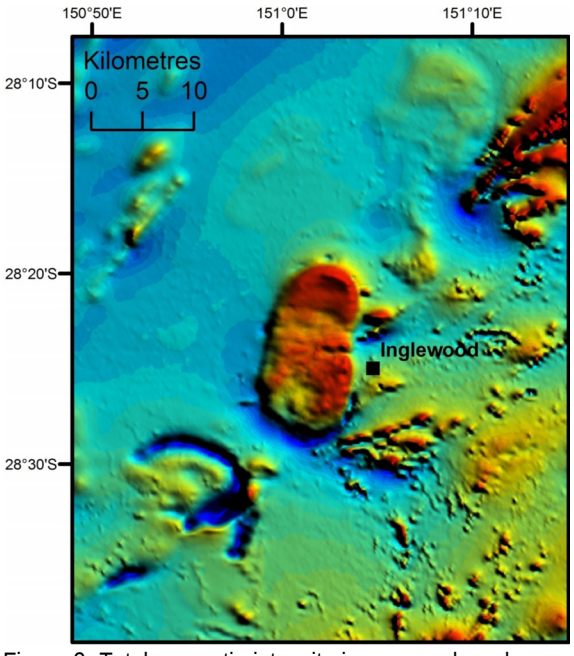

Figure 2: Total magnetic intensity image – colour drape of the Inglewood area.

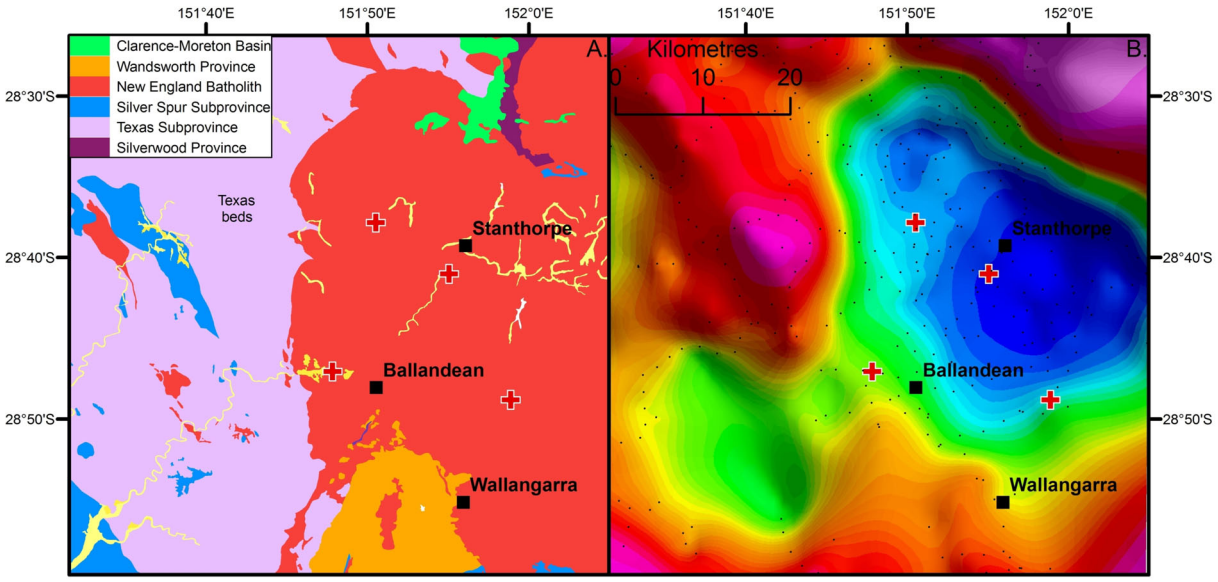

Figure 3: A. Structural elements map of the Stanthorpe area. B. Regional Bouguer gravity image (National Gravity Database). Regional gravity trend removed. Red crosses denote heat-production values greater than 5 µW/m³. Note irregular gravity station spacing.

Stanthorpe area

Geological Outline

Another target area of the CGEI is the Stanthorpe area, in the Texas region of south-east Queensland. The Texas beds (Carboniferous) form the most extensive unit in this region (Figure 3A). The unit is dominated by volcaniclastic turbidites, altered mafic volcanics, and limestone. Granitic rocks (Permian-Triassic) intrude the Texas beds. Intrusions are mainly I-type plutons assigned to the New England Batholith. The most widespread bodies of granite crop out in the Stanthorpe area, where they are mapped as the Ruby Creek Granite (Early Triassic), the Ballandean Granite (Late Permian-Early Triassic) and variants of the Stanthorpe Granite (Early Triassic). The Ruby Creek Granite and Stanthorpe Granite are leucogranites; the Ballandean Granite is dominantly monzogranite.

Regional Geophysics

The highly evolved Stanthorpe and Ruby Creek Granites of the Stanthorpe complex show mainly white tones on a ternary radiometric image, indicating enrichment in all three radioactive elements. The Stanthorpe Granite has three high-heat production values (max. 6.15 µW/m^3), and the Ruby Creek Granite one high-heat production value (6.31 µW/m^3) (Figure 3).

As part of a preliminary geophysical assessment, local-area stretching techniques have been applied to regional Bouguer gravity data from the National Gravity Database. The effects of regional trend have been removed. Figure 3B shows an enhanced stretch of anomalies in the Stanthorpe area.

Target Rationale

The target for investigation is an area where Stanthorpe complex granites extend under insulating cover. The Texas beds may have facilitated the development of a steep thermal gradient relative to surrounding areas.

Although gravity station spacing is sparse, a second gravity low to the west is likely to be granite. The Ruby Creek Granite crops out over part of the anomaly. Tin/polymetallic deposits in this area are hosted within hornfelsed Texas beds, capping very shallow-level and possibly extensive plutons of the Ruby Creek Granite (Donchak et al., 2007).

The continuation of high-heat producing granites under cover favours the Stanthorpe area as a geothermal energy source. Geophysical modelling will be used to infer the dip of granite contacts and to better define the geothermal target.

Tarong Basin

Geological Outline

South-east Queensland contains a number of isolated, coal-bearing, intermontane basins that formed during the extensional phase of the Late Triassic (e.g. Callide, Tarong and Ipswich Basins). These basins are underlain by a range of older rocks of variable derivation, which in most cases can only be determined with uncertainty by extrapolation from outcrops on the margins of the basins.

The Tarong Basin, an arguably 1.86 kilometre deep accumulation of conglomerate, pebbly sandstone, sandstone, shale and coal is of interest owing to the presence of the radiogenic

granites within the Boondooma Igneous Complex (Late Permian to Early Triassic) to the west and north-west of the basin.

This basin contains coals of moderate rank with a maximum vitrinite reflectance (R^o, max) of 0.68%, which suggests that they were subject to higher temperatures in the past.

Regional Geophysics

The regional gravity coverage broadly outlines the extent of the basin as a north-north-west trending graben (Figure 4). The Boondooma Igneous Complex crops out along the western margin of the basin and is also coincident with a well defined gravity anomaly to the north-west. Sediments of the basin have been locally derived from granitic rocks of the Boondooma Igneous Complex, and basal conglomerates contain granitic boulders and cobbles. Consequently, these sediments have a high radiometric signature on a ternary RGB image.

Although it is unknown what underlies the Tarong Basin, the gravity response does not rule out the presence of granitic basement under the coal-measures sequence. Geochemical analyses suggest heat production from radiogenic granites of the Boondooma Igneous Complex can be considered to be moderate.

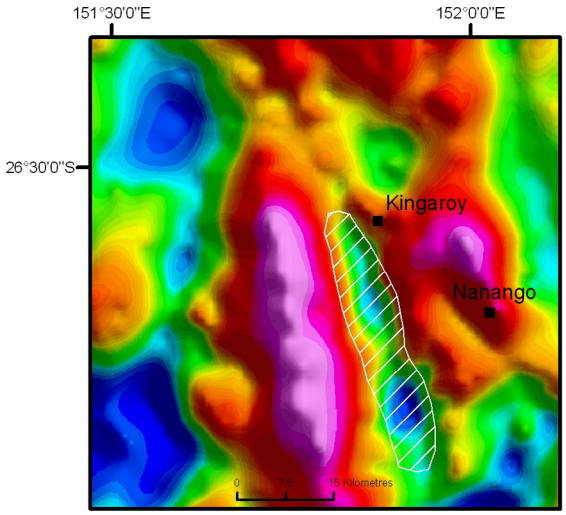

Figure 4: Regional Bouguer gravity image over Tarong Basin and Boondooma Igneous Complex (National Gravity Database). Regional gravity trend removed.

Target Rationale

The Tarong Basin has been selected as a potential geothermal target owing to the thickness of the sedimentary succession and the presence of coal to act as an effective insulator. Based on the available geological and geophysical data, the Boondooma Igneous Complex is present to the west and north-west and is interpreted to underlie the western part of the basin. The combination of Boondooma Igneous Complex at depth and the sedimentary cover provided by the infill of the Tarong Basin suggests that this is a valid geothermal target.

Hillsborough Basin

Geological Outline

A number of narrow, linear, fault-bounded Tertiary grabens occur along the Queensland coast. These structures developed during an active phase of extension associated with the opening of the Tasman and Coral Seas, beginning in the Late Cretaceous (Day et al., 1983).

The Hillsborough Basin is defined by a north-west south-east asymmetrical graben, extending from Proserpine area offshore to Cape Hillsborough. The basin is also interpreted to extend north from Proserpine to Edgecumbe Bay.

Basin infill (Paleocene-Middle Oligocene) consists of minor conglomerate, sandstone, siltstone, oil shale with volcanics and volcaniclastics in the basal sequence. Acid volcanics and sediments crop out at Cape Hillsborough (Cape Hillsborough beds) and may be correlate to the lower part of the basin sequence (Gray, 1973).

Campwyn Volcanics? (Late Devonian-Early Carboniferous) were intersected in an exploration well in the southern onshore part of the basin and are interpreted to form basement. North of Proserpine basement can only be inferred from rocks exposed adjacent to the basin margin. Carmila beds (Permian) crop out along the north-western margin and Edgecumbe beds (Carboniferous) and silicic volcanic rocks of the Whitsunday Volcanic Province (Cretaceous) are exposed along the north-eastern margin.

Oil shales and lignites are present within the sedimentary sequences of the Hillsborough Basin and include the McFarlane Oil Shale deposit.

Regional Geophysics

A seismic refraction and reflection survey over the southern onshore part of the Hillsborough Basin resulted in definition of an asymmetrical syncline with a maximum stratal thickness of 2100m (Gray, 1973). The basin deepens to the north-east and is bound by the Proserpine Fault. The south-eastern flank slopes more gently and basin infill onlap basement. The deepest part of this structure (south of Proserpine) is coincident with a well defined gravity low anomaly (Figure 5).

A second, weaker gravity low occurs to the north of Proserpine. An early oil shale exploration drill hole (PDD01) intersected approximately 509m of Tertiary rocks, indicating the basin continues

to the north-west. Interpretation of the gravity coverage suggests a ridge separates the sub-basins.

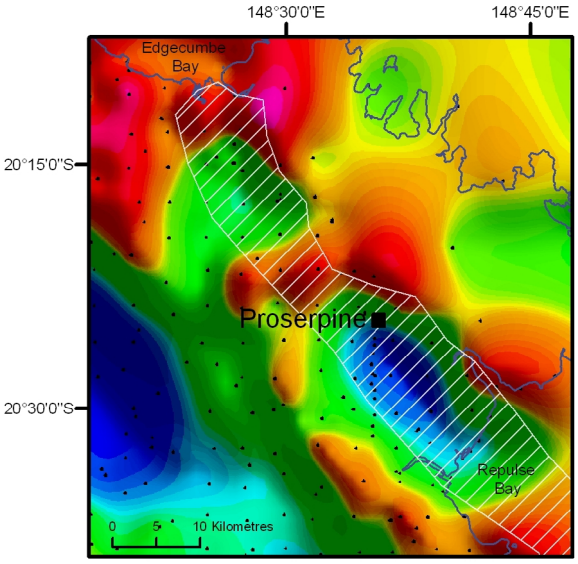

Figure 5: Regional Bouguer gravity image (with gravity stations) over the north-western (onshore) Hillsborough Basin (National Gravity Database). Regional gravity trend removed. Note lack of gravity stations in the east**.**

Target Rationale

The Hillsborough Basin has been selected as a potential geothermal target owing to the thickness of the sedimentary succession, particularly in the southern onshore part of the basin, and inferred high-heat-flow conditions induced by an extensional history. The presence of siltstone and oil-shale sequences may be an effective insulator.

The extensional history of the basin suggests there may be a significant amount of heat remaining within the lithosphere. Cooling may have been slowed by the presence of a thick sedimentary sequence. The target philosophy will be to determine the effectiveness of siltstone and oil-shale sequences as insulators. Geophysical modelling may be used to advance this geological assessment and to better define the geothermal target.

Styx Basin

Geological Outline

The Styx Basin is a small Early Cretaceous sag(?) basin, straddling the central Queensland coast near St Lawrence.

The Styx Coal Measures are predominantly fluvial, with occasional marine incursions, and comprise fine-grained sandstone, mudstone, conglomerate and coal-bearing units (Malone, 1970). The Styx Coal Measures unconformably overlie a folded sequence of Permian Back Creek Group and Boomer Formation of the Bowen Basin. Sediments and volcanic rocks of the Carmila beds (Early Permian) underlie Bowen Basin strata. Styx Basin sediments onlap Permian strata to the west, and are faulted against the Back Creek Group to the east. Adjacent to the fault, Cretaceous strata have been folded and faulted.

The nature of the basement rocks beneath the Bowen Basin in this area can only be inferred from exposed rocks outside the basin. The Connors Arch (Late Devonian-Late Carboniferous) is exposed to the west and consists predominantly of silicic volcanic rocks of the Connors Volcanic Group, which have been intruded by Late Carboniferous granites. It is plausible to infer Connors Arch rocks may form basement to Permian strata underlying the Styx Basin.

The Connors Arch is separated from the basal strata of the Bowen Basin by the Carmila beds. The Carmila beds and Bowen Basin strata have been deformed as part of the Gogango Overfolded Zone.

Numerous coal seams occur within the Styx Coal Measures, but they are generally variable in thickness and lateral extent (Svenson & Taylor, 1975). Coals are considered high volatile bituminous coals with vitrinite reflectance (R^o, max) between 0.8-0.95%, indicating a history of higher temperature.

Regional Geophysics

The regional gravity data reflect the location of the Styx Basin and underlying Permian strata of the Bowen Basin as a gravity-low anomaly. The basin deepens to the north and is reflected by a decrease in gravity values.

The Back Creek Group is characterised by a ‘hot’ radiometric signature (moderate to high in all three channels), appearing as whitish on a composite RGB radiometric image (Figure 6) (Withnall et al., 2009). Carboniferous granitic intrusions of the Connors Arch also exhibit a radiogenic (enriched in all three radioactive elements) signature on the ternary radiometric image (Figure 6). Geochemical analyses of radiogenic granitic rocks in the southern part of the Connors Arch suggest heat production can be considered to be moderate. Some felsic volcanic units within the Connors Volcanic Group also show a high radiometric signature.

Target Rationale

The target for investigation in the Styx Basin includes insulating sedimentary strata overlying radiogenic units of the Permian Back Creek Group and inferred radiogenic granites of the Connors Arch.

The Styx Basin is unlikely to have been deeply buried considering the relative stability of eastern Queensland since the Early Cretaceous. Therefore, the high rank of the coals is unlikely

to have been achieved through deep burial. An elevated heat flow seems a more likely explanation to produce a higher rank at a shallow depth. The elevated heat flow suggests contribution from several sources, including the Back Creek Group and, potentially, granitic intrusions of the Connors Arch. If the Permian Bowen Basin and Cretaceous Styx Basin sedimentary rocks provide effective insulation, then the radiogenic granites of the Connors Arch could be a prime geothermal target.

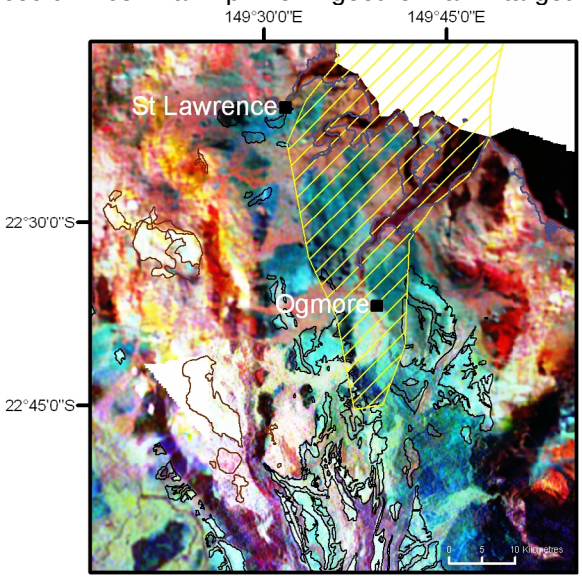

Figure 6: Ternary radiometric image over the onshore part of the Styx Basin and surrounding area. Units of the Back Creek Group are shown by a black outline. Maroon outline denotes Late Carboniferous granitic intrusions of the Connors Arch which have whole-rock geochemical data.

Summary

The Coastal Geothermal Energy Initiative will investigate sources of hot rocks close to existing power transmission lines along the coastal area of Queensland. The major aim of the initiative will be to increase knowledge of the crustal temperatures in selected areas along the coast. It is the first government program in Australia designed to directly target gaps in temperature and heat-flow data coverage in Queensland. The work program will identify potential geothermal targets where high temperature and heat flow may be present. The initiative will test these targets by obtaining temperature and thermal conductivity data within these areas via a cored-drilling program.

No specific geothermal-energy model has been applied to the selection of areas. Five examples of the types of targets that are currently being assessed, through the integration of different geological and geophysical data, are addressed.

Future work will include geophysical modelling of these targets and expanding the assessment process to include other geological settings likely to contain potential geothermal targets.

References

Chopra, P. and Holgate, F., 2005, A GIS Analysis of Temperature in the Australian Crust, Proceedings World Geothermal Congress 2005, Antalya, Turkey, 24-29 April 2005.

Day, R.W., Whitaker, C.G., Murray, C.G., Wilson, I.H., and Grimes, K.G., 1983, Queensland Geology, Geological Survey of Queensland, Publication 383.

Donchak, P.J.T., Bultitude, R.J., Purdy, D.J., and Denaro, T.J., 2007, Geology and mineralisation of the Texas region, south-eastern Queensland: Queensland Geology, 11.

Gray, A.R., 1976, Hillsborough Basin, Queensland, in Leslie, R.B., Evans, H.J., and Knight, C.L., eds., Economic geology of Australia and Papua New Guinea. Australasian Institute of Mining and Metallurgy, Monograph Series No. 6. Vol. 3 Petroleum, p.460-464.

Malone, E.J., 1970, St Lawrence, Qld, 1:250 000 geological series. Bureau of Mineral Resources, Australia, Explanatory Notes SF55-12.

Purdy, D.J., Donchak, P.J.T., and Pascoe, G.S., compilers, 2005, Inglewood, Sheet 9141, Queensland: 1:100 000 Geological Series, Natural Resources and Mines, Queensland, Brisbane.

Rybach, L., 1988, Determination of Heat Production Rate, in Haenel, R., Rybach, L., and Stegena, L., eds., Handbook of Terrestrial Heat-Flow Density Determination, p.125-142.

Svenson, D., and Taylor, D.A., 1975, Styx Basin, Queensland, in Traves, D.M., and King, D., eds., Economic geology of Australia and Papua New Guinea. Australasian Institute of Mining and Metallurgy, Monograph Series No. 6. Vol. 2. Coal, p.324-327.

Withnall, I.W., Hutton, L.J., Bultitude, R.J., von Gnielinski, F.E., and Reinks, I.P., 2009, Geology of the Auburn Arch, southern Connors Arch and adjacent parts of the Bowen Basin and Yarrol Province, central Queensland, Queensland Geology, 12.

Remote sensing of heat: A Review of potentially useful methods and instruments in the quest for innovative exploration approaches

Desmond FitzGerald.
Intrepid Geophysics, Unit 2, 1 Male Street, Brighton, Victoria, 3186, Australia.
* Corresponding author: des@intrepid-geophysics.com

Direct sensing of surface radiant heat, and buried temperature anomalies by remote methods deserves more attention because of the potential uses these methods can offer the geothermal exploration industry. Many instruments and methods exist, but their data have been largely ignored to date.

This paper provides a review of available, and yet to be tested methods, and their relative merits. In summing-up, focus is aimed at methods to measure surface radiant heat. There are ongoing challenges with data interpretation, new mathematical methods and software development.

Finally, a calibration range is advocated in one or more of Australia's more prospective regions for the purpose of testing and consolidating better use of geophysical methods, and developing diagnostic tools kits for exploration.

Keywords: Surface radiant heat, heat flow anomalies, Aster, airborne survey, SQUID, 3D modelling, Curie.

Introduction

There is only token use of remote sensing technology in Australia for heat resource exploration. This seems strange given that field mapping, sampling and drilling are orders of magnitude more expensive. It is also true that the quantitative values from remote sensing are not believed by some workers, to reflect reality.

In estimating a thermal resource for a project via 3D modelling, one is required to input surface temperature, heat flow constraints, and rock property constraints (i.e., thermal conductivities and heat production rates). For all of these inputs, direct measurements need to be obtained to enable thermal modelling and interpolation of results but all of these inputs are typically under-sampled in the project area. The danger here is that local variation in geology and heat flow is generally not being accounted for. Therefore other methods to complete the picture of required inputs are required. This paper suggests complementary inputs can be achieved though acquisition of a well-calibrated and high resolution remotely sensed surface radiant heat map.

To reiterate the merits of this proposal:

1. Measuring any independent variable that reflects a property of the sub-surface geology will always make a contribution to the 3D geology earth model. So along with gravity, magnetics and radiometrics, why not measure surface radiant heat, as a potential means of understanding relative surface heat flow?
2. The rock properties required for a heat resource calculation are typically under sampled even though the variability is generally very high. Proxy measurements of surface heat flow, from remotely sensed surface radiant heat, may help elucidate populations of rocks with similar properties.

A common counter argument to the proposed use of surface radiant heat maps is that what happens at surface has little to do with what might be happening at a depth of say 3 kilometres, where, for e.g., there could be sedimentary layers "blanketing" the resource. Figure 1 illustrates this point. Different thermal gradients will exist in rock units of different thermal conductivity. This is the essence of the "hot dry rock" geothermal energy resource.

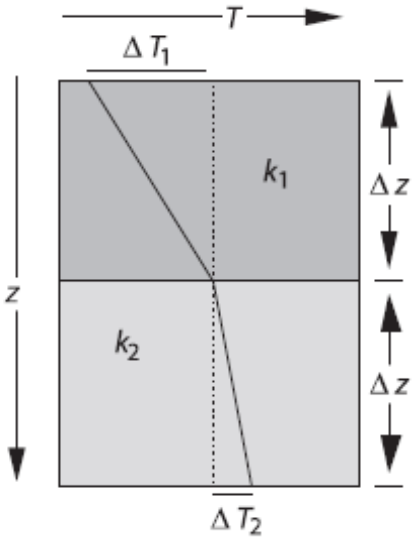

Figure 1. Cartoon illustrating how the geothermal gradient changes with depth if a low conductivity layer (k1) overlies a high thermal conductivity layer (k2). This is a special case of what is more generally known as heat refraction.

Like any other geothermal energy resource, this requires elevated rock temperatures to occur at anomalously shallow depths. For instance, this is achieved if a highly radioactive granite (with medium to high thermal conductivity) is thermally insulated from above by sedimentary cover of low thermal conductivity.

The current thrust in Australia is to find high value EGS resources that could provide significant base load electricity economically. Finding lower temperature heat and hot water resources for direct use (e.g., Cottesloe swimming pool, in W.A.) also has significance for the Australian economy long-term.

Both of these geological scenarios will have distinct surface signatures in terms of heat flow, holding clues to the thermal regime existing below, eg., a negative or a positive surface heat flow anomaly. Surface pattern recognition will be part of the improved innovative exploration methodology. In summary, remote sensing of surface radiant heat has an important part to play in the exploration of both geothermal energy scenarios.

Earth's Heat Loss

In this section we review some principles of Earth's heat flow balance.

Earth's heat loss at present is about:

- 74% from plate activity,
- 9% from hot spots, and
- 17% from radiogenic heat lost from continental crust.

Typical heat flows at the Earths surface are between 0.001 W m^{-2} and 0.1 W m^{-2}. The mean heat flow of all continents *qc* and that of the oceans *qo* , are:

qc = 0.065 W m^{-2}

qo = 0.101 W m^{-2}

(Stein, 1995, Stüwe, 2007).

This energy is directly emitted at the surface, together with heat being absorbed and re-emitted from external sources (see Figure 2). The direct sensing of this surface radiation (Figure 2), or "surface radiant heat" (the adopted terminology for this paper) is problematic, because the contribution of Earth heat loss is very small relative to all other factors. This is analogous to measuring gravity anomalies in an aeroplane, for which there are now several viable systems.

Figure 2 shows a cartoon of the inputs and outputs of the surface heat balance and gives approximate quantities during normal daylight hours. This model comes from NOAA and is a summary of the annual energy budget for the atmosphere.

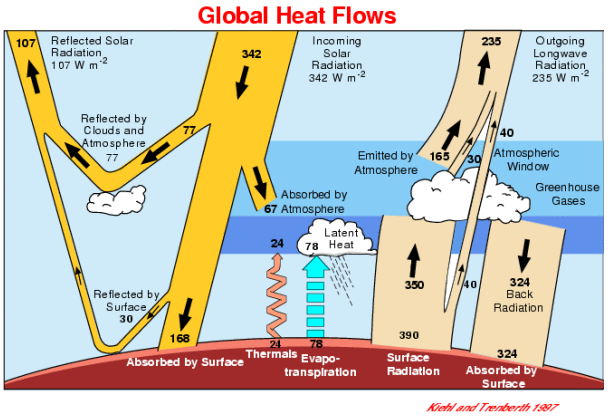

Figure 2. Global heat flows in Watts m^{-2} during daylight hours. Critically, night-time or pre-drawn readings of surface radiation contain a far-reduced component of reflected solar radiation.

Periodic Surface Temperature Fluctuations

Temperatures at the surface of Earth vary both in time and in space: daily and annual temperature fluctuations cause temporal variations and adiabatic gradients cause variations with surface elevation. While both may not be important in Australian geothermal energy problems, they are considered briefly here because they are important to account for when interpreting remotely sensed surface radiant heat (along with other surface effects such as moisture).

The relevance of temporal fluctuations may be studied by assuming that the diurnal or annual temperature variation at the surface is simply described by a cosine function:

$$T = \Delta T \cos(ft) \text{ at } \textit{the surface}$$

where *f* is the frequency (i.e. 1 per day or 1 per year).

For these boundary conditions, there is an analytical solution of the heat flow equation given by:

$$T = T_0 + \Delta T e^{\left(-z\sqrt{f/(2\kappa)}\right)} \cos\left(ft - z\sqrt{f/(2\kappa)}\right)$$

where T_0 is the starting temperature at t = 0, f is the frequency (e.g. 1 per year) and ΔT is the annual temperature amplitude (e.g. 20 °C between summer maximum and mean annual temperature).

Annual fluctuations only influence temperatures at depths down to about 5 metres. Thus, annual and daily temperature fluctuation have to be accounted for in any remote sensing work and removed before 3D modeling is performed.

A review of existing, potentially useful methods and instruments

Satellite sensing of surface radiant heat

There are many contexts where either satellite, airborne or surface measurements clearly indicate unambiguous temperature anomalies in the sub-surface geology. Scenes gathered at night-time using thermal imagery are often quite good indicators of large scale sub-surface temperature anomalies.

ASTER, Landsat and NOAA satellite systems are used extensively by remote sensing specialists to help map geology. A considerable part of the measured signal is from the thermal infra-red (TIR) spectrum. For example, in Figure 3 below, a strongly negative thermal anomaly is imaged on surface in the Middle East. Here sub-surface hydrocarbons (poor thermal insulators) are creating a localised low heat flow anomaly that can be imaged on surface. Therefore, *from surface imagery alone* the ability to image thermal conductivity contrasts and gain clues about the possibility of strong heat refraction in occurring at depth, demonstrated here.

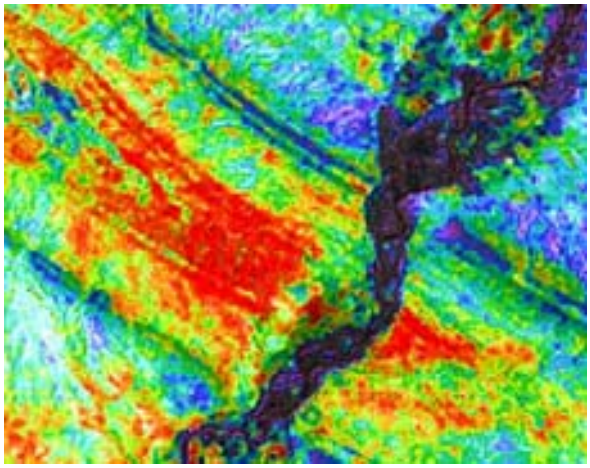

Figure 3. Night-time thermal imagery shows a strong negative (cold) thermal anomaly in the core of an anticline in the Middle East. In this case, sub-surface hydrocarbons with a low thermal conductivity are causing this surface expression.

Extensive use of ASTER NTIR or night-time thermal infra-red data from the northern Flinders Ranges (Beverly Mine Project area), has been used by Stamoulis 2006. This is a first attempt to minimize the effects of daytime temperatures on emissivity. In this example, paleo-channels have been located due to their lower sediment temperature, which is thought to be due to their higher moisture content (related to higher permeability and porosity in fluvial sediments). Figures 4a & 4b demonstrate the identification of temperature contrasts from the ASTER pre-enhanced temperature map. Surface expressions of palaeo-channels are not always evident from elevation, but their presence has been supported by field observations and drillhole data (Stamoulis 2006).

This work has been followed up in 2007 by Hou et. al. and now includes a publication of a state wide paleo-channel map. Temperature maps available as higher end ASTER products require minimal processing and can be integrated with existing data.

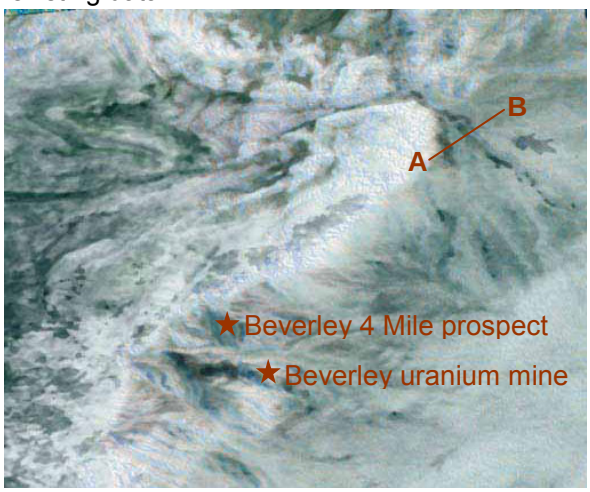

Figure 4a (after Stamoulis 2006). Aster NTIR system image from the Beverly project in the North Flinders Ranges. Dark areas indicate cooler temperatures. In areas of high elevation, colour contrasts are likely to indicate lithology variation. A-B refers to the profile in Fig 4b.

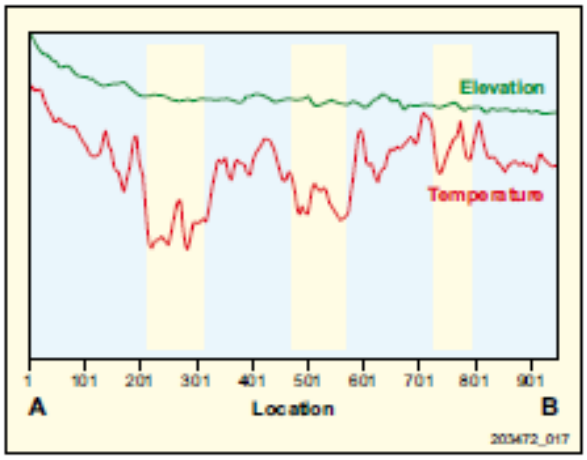

Figure 4b (after Stamoulis 2006). Sediment temperature contrasts are apparent despite no correlation with elevation, and these indicate the location of paleo-channels which are confirmed by drillhole data.

Several groups have developed technology for adjusting the Aster signal to correct for “Black Body” radiation in order to predict surface temperatures and/or heat flow associated with the outcropping geology. The RASTUS system by Neil Pendock is one example.

Black body effects must be removed from each Aster spectrum before the TIR imagery can be meaningfully interpreted. This is achieved by fitting and removing a blackbody curve from each of the TIR spectrums.

Afterwards, two outputs are available: a temperature image and a blackbody corrected data set. An example of this processing from India is shown below in Figure 5.

Further research can provide important information such as understanding temperature variations and properties of outcropping units. Applying such new knowledge will further improve interpretations where ASTER NTIR data is used and exploration targets will be better defined. ASTER data is very cheap to acquire compared to almost any other datasets.

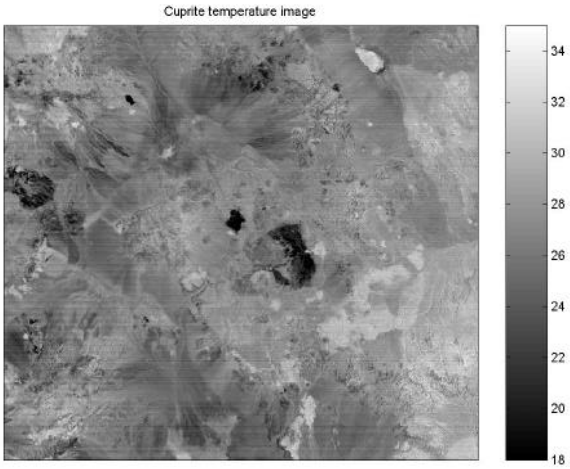

Figure 5 shows an example of a surface temperature map derived from pre-dawn Aster data using the RASTUS system. It shows over 16 degrees centigrade variation on the surface (temperature scale in ºC).

Air Airborne sensing of magnetism for Curie T depths

The continental scale estimate of the temperature at 5 km depth mapped for Australia is due for another upgrade. This time the aim should be to extrapolate from the isolated deep well observations as before, but to also add in a blended contribution from the estimate of the depth to the Curie temperature (approximately 560 degrees).

This estimate can be made using the aero-magnetic observations and seeking the bottom or greatest depth to magnetic basement. While this is very dependent upon the quality of the observed magnetic data, we are fortunate in Australia, to have arguably the best observed regional magnetic datasets. If any country can get it right, Australia should be first. There is scope for new algorithms to emerge for this task.

Airborne sensing of past and present high heat alteration effects

Another approach is to look at surface expressions of mineralogy that indicate where high heat alteration conditions have existed in the past. The mineralogy can be directly sensed using the reflectance of light and analysing wave-lengths (hyper spectral). Regional mapping can be used to differentiate granites through mica chemistry and mafic mineral content. (e.g., Pilbara Geology Mapping, WA.)

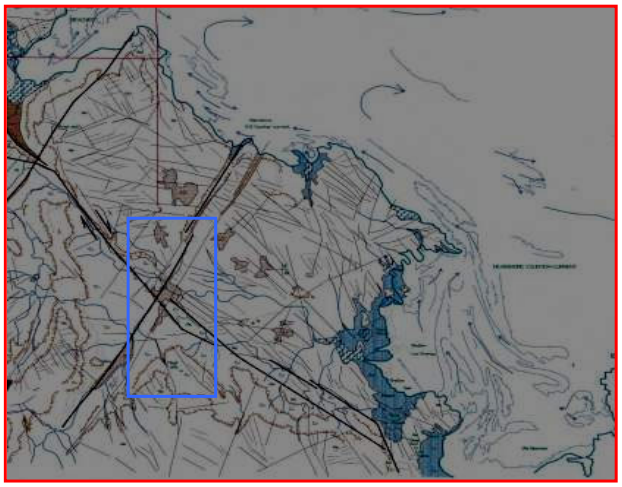

Structure Control Of Alteration?

Above map of structural features derived from interpretation of 1:25,000 aerial photographs. Blue box shows location of scanner image.

Right Mineral index image pyrophyllite/ dickite/ sericite superimposed on the structural map.

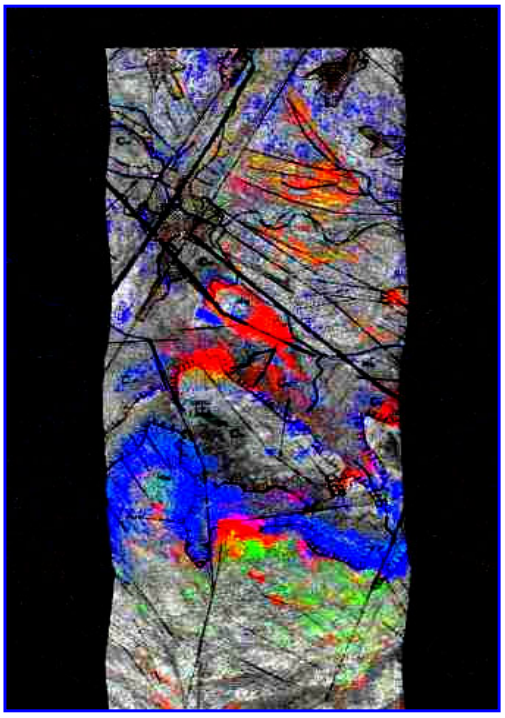

Figure 6. These images show methods adopted in the North Kimberley to analyse whether locations of mineral systems are controlled by structural features, or by alteration zones. Images courtesy of HyVista Corporation.

The HYVISTA system has been used in the North Kimberley region of Australia for the detection of hydrothermal alteration associated with deep-seated high temperature granites. The question, "When did this alteration occur?" is not resolved by this sytem.

Airborne sensing of radiometrics

The daughter products of natural radioactive decay in and around granitic rocks, includes radon gas. This is routinely observable during gamma ray airborne surveying, in Australia where there is granitic outcrop, on days of no rain and little wind.

This is thought of as noise and routinely discarded. The entire raw radiometrics surveying record for Australia contains quite a bit of this information. No systematic use of this record has been contemplated to date, with the possible exception of Geoscience Australia's OESP Geothermal Programme.

Ground sampling of radiometrics

Another daughter product from deep-seated radioactive decay is helium. This is not easily detected from an airborne system, but instruments do exist for ground surveying. This class of instrument is a chemical sniffer rather than an instrument based upon spectroscopy. Hot Dry Rocks market such an instrument.

Alternatively the direct detection of radon gas as an exploration tool is being used routinely in Namibia using the RADONTEX© system.

Exploration Tools for the Future

Innovations in remote sensing instruments

The pursuit of remotely-sensed data to help constrain deep sub-surface temperature predictions prior to drilling is not new, and is not restricted to the geothermal industry. For example, Shell are investigating various methods to help devise world temperature-depth maps in relation to sedimentary basins hosting hydrocarbons. Multidisciplinary approaches will eventually led to technology advances, benefiting a range of industries.

Many types of instruments are available. With the advent of SQUID (Super Conducting Interference Device) devices, the sensitivity and response time are now such that viable observation systems for direct measurement of surface radiant heat are evolving, and these are significantly more useful.

The classical direct heat measurement instruments are:

- Thermometer – temperatures and gradients
- Bolometer–surface radiant heat. This is the term coined by Langley of CIA fame for such an instrument which he invented in 1886.

Importantly, in the presence of significant water vapour, a bolometer is opaque to radiant heat through much of the thermal infrared band, as illustrated in figure 7 below.

Therefore, the greater the column of air, the more the heat signal would be attenuated, so satellite measurements are the least ideal. Low flying aircraft based systems are a good compromise for surveying.

A downward looking "telescope" that is in fact a bolometer, will yield more sensitive and precise measurements. At least 5 of the frequency peaks in Figure 7 should be chosen for measurement.

The German group IPHT from Jena manufacture such an instrument that would be very suitable. This instrument has never been deployed upon an aircraft, but rather on satellites. It is expected a prototype may emerge in 2010.

What To Measure?

There are many sceptics to the notion of remote sensing of surface radiant heat and temperature. They claim that surface temperatures, in a spatial sense, do not vary very much when averaged over several days.

Remote sensing work using thermal infra red bands from satellite systems such as Aster indicate that there are significant spatial anomalies in surface radiant heat and temperature associated with locally outcropping geology (Figure 5).

These two positions (above) are not irreconcilable – we look to physics to explain how both observations can co-exist.

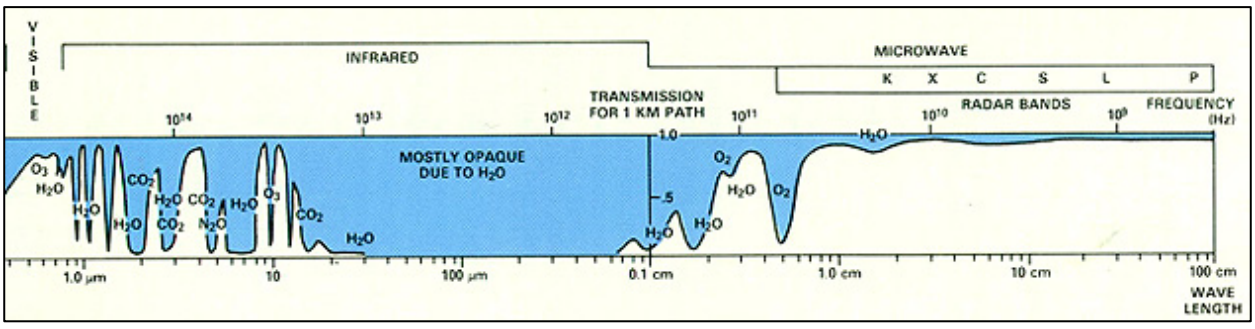

Figure 7. Shows the electro-magnetic spectrum and highlights in the thermal bands, those frequencies that cannot be measured due to water.

For those familiar with gliding, thermals form over "Black Bodies" and strong updrafts can exist over areas of high heat emittance even though surface temperatures may not vary greatly.

Known obstacles to the remote sensing of surface radiant heat

Among the obvious issues to overcome are:

- effect of evapo-transpiration
- Albedo effect
- Black body corrections
- ground water and its influence in masking
- clarification of transient vs. steady state measurements
- what quantity is being measured and how does it compare with other measurements using different physical principals

There are already many examples of published techniques for dealing with these issues. For example, the US Geological Survey via Ken Watson (1992) has investigated removal of the Albedo using innovative Fast Fourier Transform filtering techniques.

There are many examples in observational geophysics where the anomaly to be measured is less than 10^{-5} of the gross amplitude. Heat anomalies are just another challenge of this nature.

Overcoming these and other challenges including: data interpretation and software development are all required to ensure proposed future methods deliver useful outcomes for EGS explorers in Australia.

A Proposal For An Australian Calibration Range

My proposal to the AGEG community is to set up calibration ranges in at least two settings representative of Australian conditions.

Examples of other calibration ranges are available from the work of our overseas counterparts (Figure 7), but we require our own range to test specific geological and geophysical issues arising here on the Australian continent, where we are leading the world in EGS exploration.

In conventional geothermal systems, there is usually an easily discernable expression of near surface heat. Figure 8 shows a calibration or test range set up in Nevada by the US Geological Survey (Kratt, et. al. 2008). Here Aster satellite data, pattern drilling of short length test holes, some deeper drilling and locations of known "hot" geological structures such as geysers are shown.

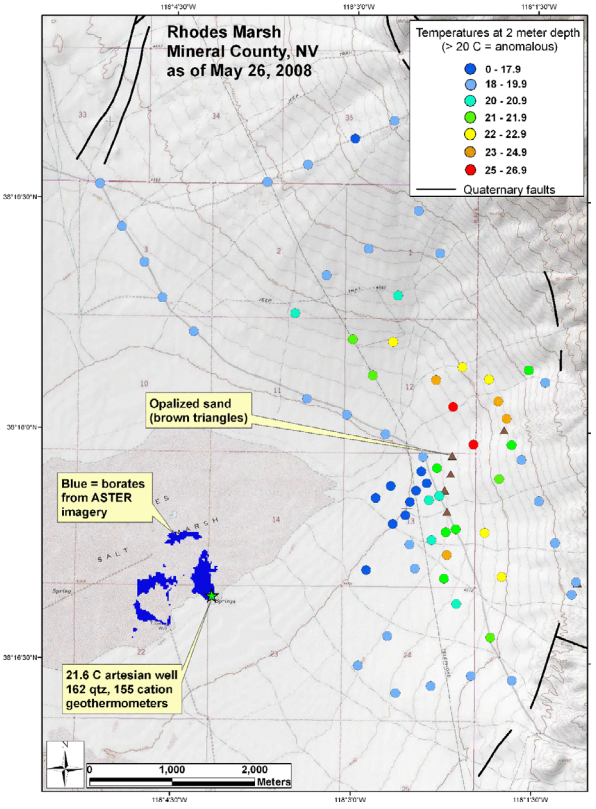

Figure 8. Shows the general layout for what can be described as a calibration range in Nevada, USA.

Two calibration ranges are proposed for Australia:

Range 1

Northern Flinders Ranges (South Australia) where there are known high-heat producing granites, due to radiogenic contribution. The aim is to conduct a detailed field mapping exercise to acquire surface heat and temperature measurements and rock properties on say a 200m grid basis for a 5km x 5km area. The study area should cover both exposed and covered granites. The weather conditions, time of day, cloud cover and soil moisture are also factors to be recorded.

Range 2

Onshore PortCampbell (south-western Victoria) where there are suspected oil seeps associated with faulting. There are also many deeper oil exploration wells in this area.

An initiative to get the ball rolling could be funded by government sources. All datasets go in to the public domain and any party that wants to try out their technique in the test range can have access to all the past data.

Acknowledgements

Ed Biegert from Shell, Houston (SIEP), Mike Hussey from HYVISTA, Neil Pendock and Vicky Stamoulis. Chris Matthews is thanked for his review comments.

References

Christopher K., Coolbaugh M., Sladek C., Zehner R., Penfield R., and Delwiche B., 2008, A New Gold Pan for the West: Discovering Blind Geothermal Systems with Shallow Temperature Surveys, GRC *Transactions*, Vol. 32.

Hou B., Fabris A., Keeling J. and Fairclough M. 2007, Cainozoic palaeochannel-hosted uranium and current exploration methods, South Australia MESA Journal 46 Department of Primary Industries and Resources South Australia, Adelaide.

Keihl and Trenberth, 1997, Earth's annual global mean energy budget. *Bull. Amer. Met. Soc.*, **78**, 197-208.

Stamoulis V., 2006. ASTER night-time thermal infrared data: interpreting subsurface features from high resolution data. South Australia MESA Journal 43 Department of Primary Industries and Resources South Australia, Adelaide.

Stein, C. 1995, Heat Flow of the Earth. Global Earth Physics, A Handbook of Physical Constants. AGU Reference Shelf 1.

Stüwe, K 2007, Geodynamics of the Lithosphere: An Introduction. 2nd Edition. Springer.

Watson, K., 1992, A 2D FFT program for image processing with examples: U.S. Geological Survey Open-File Report 92-265, 74 p.

Practical aspects of 3D temperature and heat flow modeling for exploration of EGS energy plays

Helen J. Gibson[1*], Kurt Stüwe[2], Ray Seikel[1] and Desmond FitzGerald[1].
1 Intrepid Geophysics, Unit 2, 1 Male Street, Brighton, Victoria, 3186, Australia.
2 Karl-Franzens-University,Universitätsplatz2 A-8010 Graz, Austria.
* Corresponding author: helen@intrepid-geophysics.com

Realistic temperature and heat flow modelling relies on the ability to make calculations directly from well-constrained 3D geology models (Gibson et. al. 2008, Meixner and Holgate, 2008). Correct treatment of topography is another key concern for modelling heat flow patterns that replicate those measured in the real world (Stüwe and Hintermüller, 2000; Braun, 2003).

Commencing with a synthetic 3D geology model, featuring high topographic relief and variable scenarios of thermal conductivity contrasts, we present results from thermal modelling employing an explicit finite difference method to solve for temperature in the steady state. Our solver scheme populates a Cartesian voxelised grid with resulting in-situ temperatures, heat flow values and temperature gradients.

Our synthetic model is a test-bed for the Köflach district of Eastern Austria for which a 3D GeoModeller[1] geology model is currently under construction. The Köflach model will demonstrate realistic 3D temperature and heat flow modeling, verified against measured insitu temperatures and heat flow data, whilst always obeying topographic effects. The existence of thermally insulating lignite beds at Köflach lends itself as a possible analogue for Enhanced Geothermal System (EGS) plays which also typically require the existence of shallow insulating horizons to set-up a scenario of anomalously high heat occurrence, at accessibly shallow depths. This work also has implications for geothermal energy exploration in Eastern Australian's coal-bearing basins.

Keywords: Enhanced Geothermal Systems, 3D GeoModeller[1], geothermal module, topography, Köflach, thermal insulator.

Introduction

This extended abstract presents: 1) a review of heat flow modeling in GeoModeller including the simplifications, assumptions and boundary conditions employed; 2) explanations and derivations of the temperatures and other outputs written to 3D voxets; 3) presentations of results from a synthetic geology model featuring high topographic relief and variable thermal conductivity contrasts; and 4) an introduction to the geology of Köflach, Eastern Austria and a description of the aims and objections of this case study which is now underway.

Heat Modelling in 3D GeoModeller

An accessible method for rapid calculation of the spatial variation of temperature, heat flow and geothermal gradients - directly from a complex 3D geology model – is now available within 3D GeoModeller This software (developed by BRGM and Intrepid Geophysics) is well renowned for its ability to model sophisticated geology in association with detailed digital elevation models (DEMs), and now also recently provides a geothermal module.

The solved equation in GeoModeller combines terms that account for conduction, heat production and advection (Stüwe, 2007). See Table 1. Furthermore, the equation solves for the steady state 3D temperature field under consideration of spatially variable thermal conductivity. Implementation of the heat transport equations in GeoModeller is covered in previous work by Gibson et. al. (2008).

Mode of heat transfer	Process	Accounted for in 3D GeoModeller
Conduction	Diffusion	Yes
Heat Production	Radioactive decay	Yes
	Mechanical work (friction)	No
	Chemical reaction	No
Advection	Fluids	Yes, simple[1]
	Erosion	No
	Deformation	No
	Magma	No

[1]Currently only one dimensional scenarios involving advection of heat by fluids can be solved in GeoModeller but development is on-going.

Table 1: Of the main processes of heat transfer (centre) three of these (diffusion, radioactive decay, and advection by fluids) are accounted for in GeoModeller because together they contribute the majority of measurable heat in settings devoid of significant present-day tectonism, seismicity, metamorphism or volcanism.

The solver currently adopts an explicit finite difference approximation scheme that has the advantage of being able to utilize a readily-prepared Cartesian voxelised grid from the smooth 3D geology model. (Note that model-voxelisation is also need for geophysical inversion, but is a simplification of GeoModeller's normal operational mode that uses a potential

field method to calculate smooth 3D geology boundaries from contact and orientation data.)

For 3D temperature, finite difference approximation is solved with a Gauss-Seidel iteration scheme continuing until one of the following occurs: Either the sum of the residual errors is smaller than the user-defined maximum value (maximum change in temperature in any one cell, from one iteration to the next), or a user-defined number of iterations has been performed (where one iteration is defined to have occurred when the solver has acted in every voxel).

Topography and Boundary Conditions

In solving for temperature GeoModeller honors all thermal boundary conditions, and any known temperatures (fixed) that are internal to the project (e.g. temperature well-logs).

As illustrated in Figure 1 (after Stüwe and Hintermüller, 2000) and demonstrated by our results below, topography is a key concern for accurate 3D temperature prediction (also Braun, 2003). Treatment of topography during thermal modeling can approach (but not equal) the detail of the original DEM by ensuring fine resolution in the discretization scheme.

Currently, a constant surface temperature is applied at the topography boundary, but soon a grid-input of variable heat flow on surface (or a constant value) will also be an option for users. This will be a useful improvement, because measured heat flow values can then define the upper boundary rather than an assumed surface or paleo-surface temperature. Working exclusively with heat flows in this way can negate the concern for a dis-equilibrium state so one can concentrate on “heat in the system now”, regardless of its thermal equilibration status.

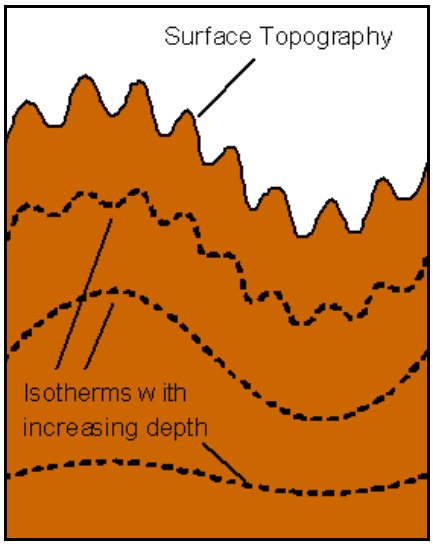

Figure 1: Schematic illustration of the influence of surface topography on isotherms showing that temperature distribution is highly influenced by topography in the shallow-subsurface, and less influenced at depth (after Stüwe K. and Hintermüller M., 2000).

On the four vertical sides of the geology model, Neumann type boundary conditions apply. That is, we apply zero heat flow boundary conditions reflecting the assumption that all lithologies are mirrored beyond the model boundary.

Either constant heat flow, or constant temperature is applicable to the bottom boundary of the model. We suggest this treatment is satisfactory in most scenarios, but if there is evidence for variability, then a more meaningful treatment may be to expand the vertical extent of the model, into depth zones where isotherms are predicted to flatten-out (as is the conventional approach taken amongst many modelers), rather than implement a spatially variable boundary condition.

3D Temperatures and Other Outputs

The solver in GeoModeller populates a Cartesian voxelised grid (.vo format) with estimated in-situ temperatures, heat flow values, and temperature gradients. Output values are valid for the center-point of the given cell/voxel. Derivations of outputs are given in Table 2, below.

3D temperature and other outputs in GeoModeller	
Temperature	(°C) Solved for every cell/voxel centre by Finite Difference approximation
Vertical Heat Flow	(Wm^{-2}) Flow of heat measured in energy per time per unit area. Solved for each cell/voxet centre with respect to the centre of the cell immediately above.
Vertical Temperature Gradient	(°Ckm^{-1}) Change of temperature over a distance. Solved for each cell/voxel centre with respect to the centre of the cell immediately above.
Total Horizontal Temperature Gradient	(°Ckm^{-1}) Change of temperature over a distance of one cell to 4 neighbours in the horizontal plane. Equal to the square root of the sum of the squares of the horizontal temperature gradients in the x and y directions. (An expression of gradient strength with no expression of direction within the horizontal plane.)

Table 2: Definitions and derivations of solved values for temperature, heat flow and geothermal gradients as implemented in GeoModeller.

Test-bed Temperature Modeling

Synthetic geology model + forward run set-up

Figure 2 shows our synthetic geology model built in GeoModeller. The model features topographic relief of up to 7,500m and comprises two geologic units with a simple conformable relationship.

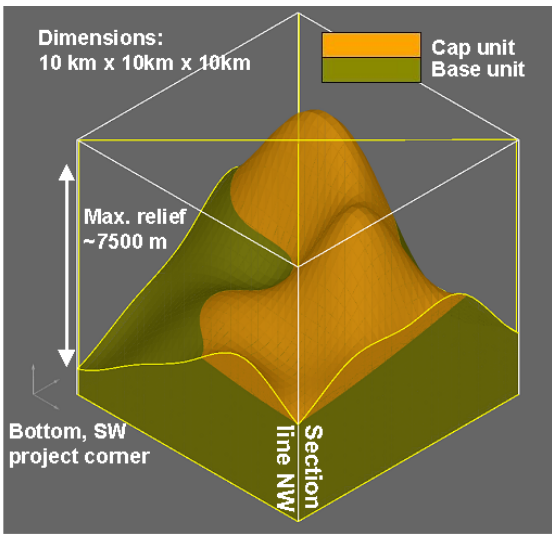

Figure 2: Synthetic solid geology model showing project extents and the maximum topographic relief. The intersection of the DEM with the project bounds are shown in yellow. The model comprises two geology units with a conformable relationship.

Discretization of the smooth geology model in Figure 2 followed a scheme by which 100 cells where created in the x, y, and z directions, and hence (dividing these by the model dimensions in Figure 2) the cell sizes were 100m, square. Total number of voxels was therefore 1,000,000.

The mean thermal rock properties listed in Table 3 for each geology unit were applied to the discretized model. A constant heat production rate was used, but thermal conductivities of the two units were varied in the execution of three separate forward runs.

Geology unit	Physical properties:	
Run #	Thermal conductivity W $m^{-1}K^{-1}$	Heat production rate Wm^{-3}
Cap unit		
Run 1	1.5	3.0 x 10-6
Run 2	3	3.0 x 10-6
Run 3	1	3.0 x 10-6
Base unit		
Run 1	3	3.0 x 10-6
Run 2	3	3.0 x 10-6
Run 3	5	3.0 x 10-6

Table 3: Thermal rock properties of the geology units in the synthetic model, for 3 forward runs estimating temperature, heat flow and gradients.

Set boundary conditions for all 3 runs were: 20ºC for the topography surface, and 0.03 Wm^{-2} for the bottom of the model. Maximum iterations were set at 20,000 and maximum residual tolerance was set at 0.0001ºC. Heat capacities were assumed constant at 1000 J kg °C.

Three thermal modeling runs of the synthetic model were executed. The set-up parameters for all runs were identical except for the thermal conductivities (TC) of the two geology units (see Table 3). Run 1 explored a moderate degree of TC contrast between the capping unit and the underlying geology, Run 2 explored the effects of no TC contrast, and Run 3 explored a strong TC contrast (Table 3).

Results of test-bed modelling

3D temperatures predicted in Run 1, are shown in Figure 3. Clearly, the strong topographic relief of the geology model has had a dominating effect on temperature distribution. The temperature range of the 3D voxet for Run 1 is 20.0 to 76.2°C (Table 4). This range is little different for Run 2 (the case of no TC contrast), but ~16°C wider than the temperature range for Run 3 (strong TC contrast).

Temperature results are further displayed in 2D in Figure 4 where again the strong impact of topography on temperature distribution is evident in all runs. Note the asymmetry of the heat distribution (in all runs) whereby temperatures are raised shallower in the section below the more gently sloping shoulder of the mountain (right-side of figures), but pushed down in proximity to the highly sloped shoulder (left-side of figures).

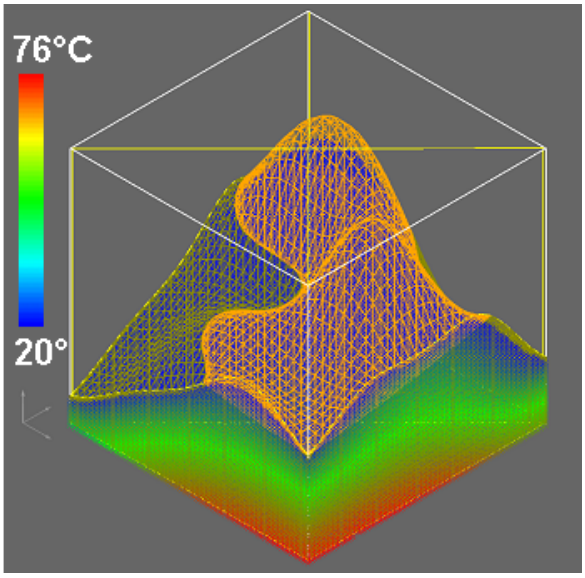

Figure 3: Run 1, 3D temperature voxet (1 million nodes) imported to the synthetic geology model space in GeoModeller. Visual-cut off of the mesh was set to 20.5ºC to allow the topography wire-frame to be viewed (All airspace is otherwise 20ºC, obeying the surface boundary condition.)

Additionally, increased heating of the section at, and below, the capping unit is noted in Runs 1 and 3, as expected, due to the low TCs assigned

to this unit (hence a thermally insulating layer) in combination with higher TCs in the units below.

Results of vertical heat flow for the 3 runs are given in Table 4 and Figure 4. By range they are: 0-0.389, 0-0.382 and 0-0.388 Wm^{-2} respectively. Compared with world-wide surface heat flows (generally between 0.030 and 0.120 Wm^{-2}) the ranges include extremely high values, but we caution that the distributions are skewed to the lower values in all runs (mostly <0.040 Wm^{-2}). Very high values of modeled heat flow only occur where extreme topography has played a part in juxtaposing very high temperature rocks near surface in a deeply incised valley location, in the synthetic model. (See Figure 4, 2nd row.)

3D voxet results by range – synthetic model			
	Run 1	Run 2	Run 3
Temperature (°C)	20.0 - 76.2	20.0 - 73.1	20.0 - 57.0
Vertical Heat Flow (Wm^{-2})	0 - 0.389 (most <0.040)	0 - 0.382 (most <0.040)	0 - 0.388 (most <0.040)
Vertical Temperature Gradient ($°Ckm^{-1}$)	0 - 128.3 (most <20)	0 - 127.4 (most <20)	0 - 77.7 (most <10)
Total Horizontal Temperature Gradient ($°Ckm^{-1}$)	0 - 80.9 (most <15)	0 - 80.3 (most <15)	0 - 60.1 (most <10)

Table 4: Resulting ranges for temperature, heat flow and geothermal gradients solved in 3D for the synthetic geology model, in three independent forward thermal modeling runs.

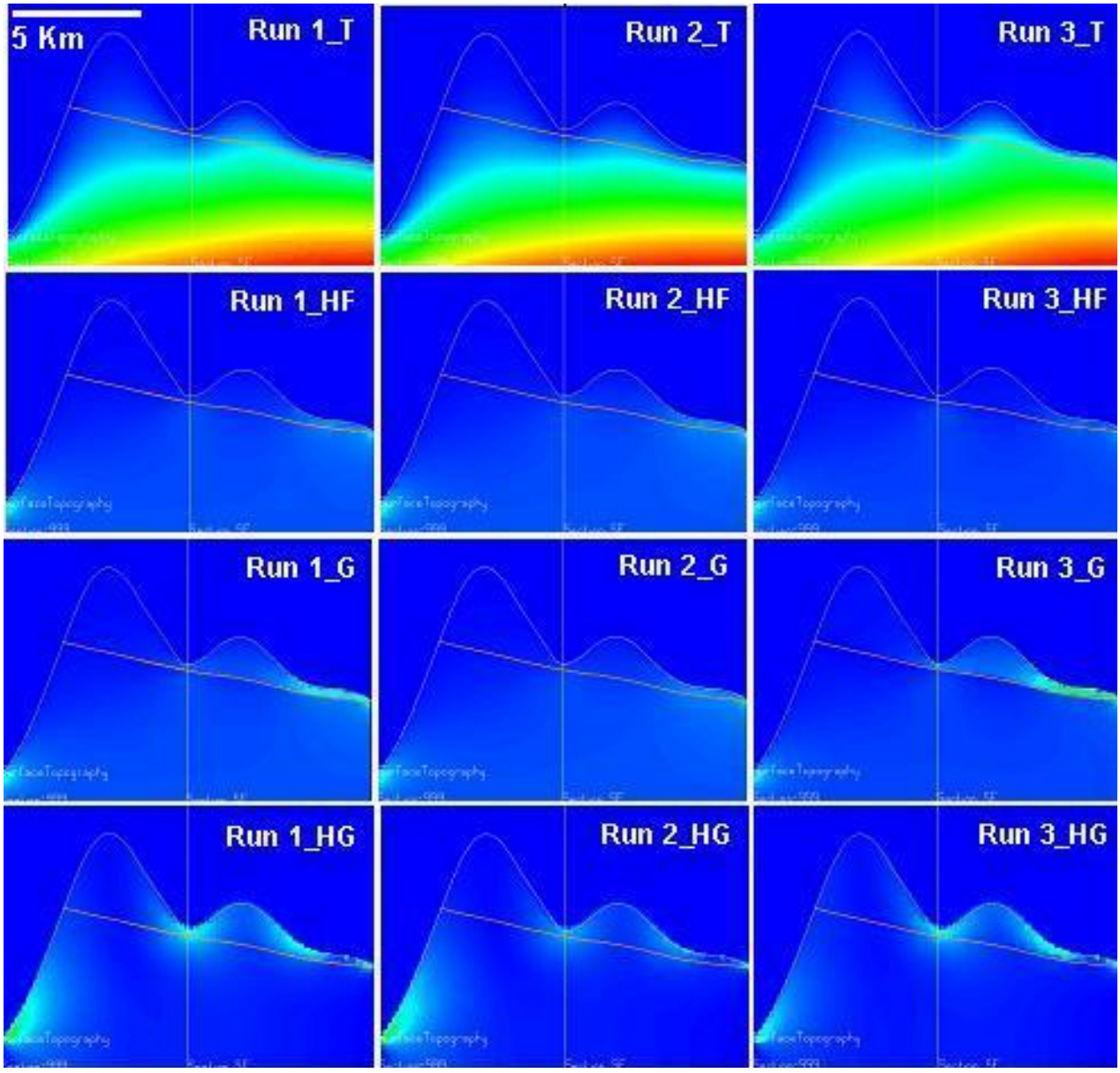

Figure 4: 2D results derived from the 3D voxets, for Section Line NW of the synthetic model (see Figure 2). The left column shows results for Run 1, the centre column are results from Run 2, and the right column are results from Run 3. (T=temperature, HF=vertical heat flow, G=vertical temperature gradient, HG=total horizontal temperature gradient) The set-up parameters for all runs were identical except for the TCs of the two geology units which vary (see Table 3). An outline of the intersection of the DEM with section Line NW is shown in every panel. Also shown is a line representing the geology boundary in the synthetic model.

Vertical temperature gradient results for the 3 runs are given in Table 4 and Figure 4 (3rd row). By range they are: 0-128.3, 0-127.4 and 0-77.7 °Ckm^{-1} respectively. Similarly, large modelled ranges have resulted, but again most values are skewed to a lower range (<20°Ckm^{-1}).

Total horizontal temperature gradient results are shown in the bottom row of Figure 4 above, with ranges given in Table 4 (0-80.9, 0-80.3 and 0-60.1 °Ckm^{-1} respectively in runs 1, 2 and 3). Again large modelled ranges have resulted, but most values are skewed to lower ranges (see Table 4).

For the synthetic model, the highest vertical temperature gradients, and the highest total horizontal gradients occur: a) in shallow sub-surface areas where increased heating at and below the capping unit has occurred due to low TCs of this unit in combination with a contrasting higher TC in the underlying unit (Runs 1 and 3), and b) where extreme topography has caused juxtaposition of high temperature rocks near surface in a deeply incised valley (locations where a strong slope in topography occurs).

Köflach Case Study: Parallels with EGS plays in Eastern Australian Basins

Whilst the Köflach area of eastern Austria is traditionally known for its coal and not for EGS energy exploration, the existence of thermally insulating lignite beds lends itself as a possible analogue for Enhanced Geothermal System (EGS) plays which typically require the existence of a shallow insulating horizon to set-up a scenario of anomalously high heat occurrence, at accessibly shallow depths.

EGS exploration is now being carried out in Australia by a large number of companies, not only in inland basin settings (eg., Cooper Basin), but also in basins throughout eastern Australia where extensive coal seams are common. Our work will have implications for EGS plays in both settings.

Our 3D model of the Köflach area (when finalized) will portray diverse geology including crystalline basement, overlain by weakly metamorphosed units of the Graz Paleozoic and in turn overlain by Neogene sediments of the Styrian Basin, including coal seams.

This geologic package will ensure strong thermal conductivity contrasts in an area of high topographic relief and will therefore be a challenging case study for the geothermal module in 3D GeoModeller. Using this example we will demonstrate realistic 3D temperature and heat flow predictions verified against measured insitu-temperatures and heat flow data – at all times obeying topographic effects.

Conclusions

- Plausible 3D temperature, heat flow and thermal gradient modelling results have been achieved in our test-bed case of the synthetic geology model.
- The strong topographic relief of the synthetic model has had a dominating effect on temperature distribution.
- Thermal conductivity contrasts have had a lesser impact on heat distribution than topography, but this is probably because scenario testing of the latter parameter was taken to an extreme.
- Increased heating of the section at and below the capping unit occurred, as expected, due to the low thermal conductivity assigned to this unit in combination with higher thermal conductivities in the unit below (hence establishing a thermally insulating layer).
- Generally, vertical heat flow values for the synthetic model are <0.040 Wm^{-2}. However, very high values of modelled heat flow occur where extreme topography has played a part in juxtaposing very high temperature rocks near-surface in a deeply incised valley location.
- Generally, vertical temperature gradients for the synthetic model are <20°Ckm^{-1}, while total horizontal temperature gradients are <15°Ckm^{-1}. Much higher values of both occur: a) in the shallow sub-surface when increased heating at and below the capping unit has occurred, and b) where extreme topography has caused juxtaposition of high temperature rocks near-surface in a deeply incised valley (locations where a strong slope in topography occurs).
- Having satisfied test-bed thermal modeling of the synthetic geology model, GeoModeller will now be applied to thermal modeling of the Köflach area, Eastern Austria – which similarly features high relief terrain and strong thermal conductivity contrasts.
- The thermally insulating lignite beds of the Köflach area are likely to be a good analogue for Enhanced Geothermal System (EGS) plays which typically require the existence of a shallow insulating horizon to setup a scenario of anomalously high heat occurrence, at accessibly shallow depths.
- EGS exploration in Australia is likely to benefit from this work, because practical aspects of thermal modeling demonstrated here can be replicated in any exploration programme and hence the risk of exploring for heat can be reduced at the pre-deep drilling stage.

Footnote

[1]3D GeoModeller is a commercial software developed by BRGM and Intrepid Geophysics.

For further information visit:
http://www.geomodeller.com/

References

Braun, J., 2003, Pecube: A new finite element code to solve the 3D heat transport equation including the effects of a time-varying, finite amplitude surface topography, Computers and Geosciences, v. 29, p. 787-794.

Gibson, H., Stüwe, K., Seikel, R., FitzGerald, D., Calcagno, P., Guillen, A., and McInerney, P., 2008, Forward prediction temperature distribution direct from 3D geology models, Proceedings, Australian Geothermal Energy Conference, Melbourne 2008.

Meixner, T., and Holgate, F., 2008, The Cooper Basin 3D Geological Model: A test-bed for thermal modelling, Proceedings, Intrepid Geophysics Geothermal Modelling Workshop, Adelaide 5-6 November 2008.

Stüwe, K., 2007, Geodynamics of the Lithosphere. An Introduction. 2nd edition. Springer Verlag, 493p.

Stüwe, K., and Hintermüller, M., 2000, Topography and isotherms revisited: The influence of laterally migrating drainage divides. Earth and Planetary Science Letters, v. 184, p., 287-303.

Exploring Eastern Tasmania: A Novel Geothermal Province

Fiona L. Holgate*, Hilary K.H. Goh, Graeme Wheller and Roger J.G. Lewis
KUTh Energy Limited, 35 Smith Street, North Hobart, 7000
*Corresponding author: Fiona.Holgate@kuthenergy.com

Over the past two years KUTh Energy Limited has undertaken geothermal exploration across its tenements in eastern Tasmania. The initial phase of this program is now nearing completion and has yielded a variety of results. Although not previously recognised as geothermally prospective, a program of systematic heat flow mapping has now revealed the presence of a significant surface heat flow anomaly in the central Midlands area. Values of high (>90mWm^{-2}) heat flow are found to be spatially associated with the sub-cropping extension of high-heat-producing granite bodies. A series of sedimentary units, extensively intruded by dolerite sills, lie above the granite and combine to provide the insulation necessary for a classic Enhanced Geothermal System (EGS) target. Bisecting the northern portion of the heat flow anomaly is the Tamar Conductivity Zone (TCZ), a region of high crustal electrical conductivity that has been mapped in detail by recent magneto-telluric survey work. This feature, which may indicate the presence of large-scale fracture permeability in the crust, remains open directly along strike from the region of highest recorded heat flow.

Keywords: Tasmania, heat flow, magneto-telluric

Exploration Methods & Results

To effectively explore Eastern Tasmania for its geothermal potential a variety of techniques were required that were capable of discerning key elements of the EGS target beneath extensive Jurassic dolerite cover. Critical amongst these were the magnitude and distribution of heat flow, the depth of insulator (depth to top granite), the quality (thermal properties) of the insulator and the location and nature of the TCZ. The size of the area under investigation further necessitated that any technique used should be economically applicable at a regional scale. To meet these needs, an exploration program was devised that comprised shallow drilling for surface heat flow determination, gravity interpretation, rock property determination and magneto-telluric (MT) data acquisition.

Surface Heat Flow Determination

A program of pattern drilling of shallow boreholes was designed to investigate surface heat flow across the tenement area. Holes were drilled on a 20km grid spacing at 36 locations. In all cases the holes were percussion drilled to 100m with diamond core cut to total depth at ~250m. Heat flow estimation was performed by Hot Dry Rocks Pty Ltd and was based upon application of 1D thermal modelling. Data used in the modelling was collected by Hot Dry Rocks and comprised precision down hole temperature logs and thermal conductivity values determined from core samples using a divided bar apparatus.

At the time of writing, surface heat flow data were available for 31 holes with five holes still outstanding (Figure 1). Heat flows determined to date are of high quality and reliability with analytical uncertainties typically <5%. The data are spatially consistent, defining a large area (>4100km^2) of anomalously high heat flow (>90mWm^{-2}) in the central portion of the tenement area.

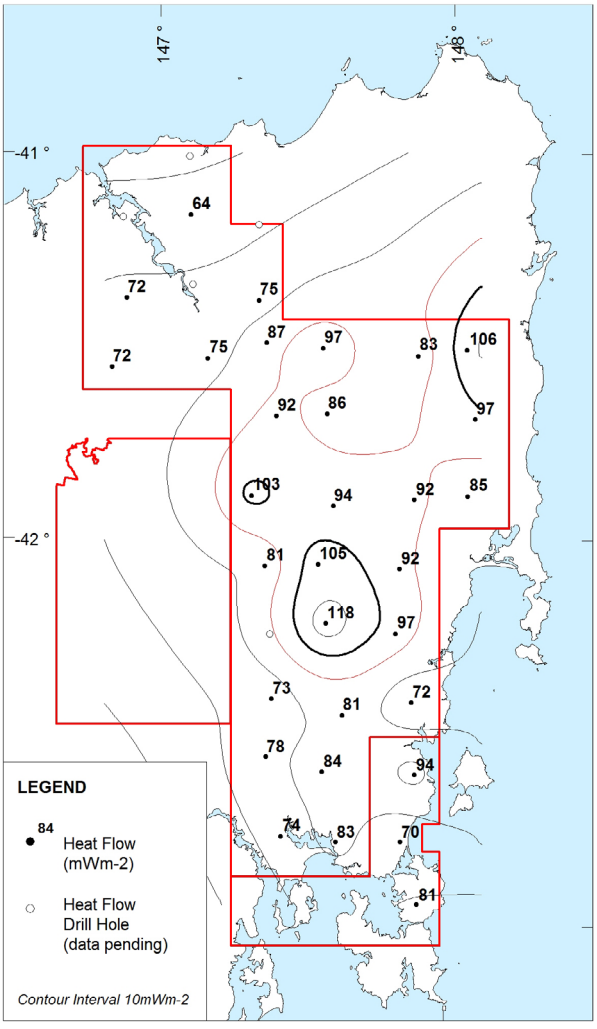

Figure 1: Contoured surface heat flow field for Eastern Tasmania based upon new data acquired during KUTh Energy's recent exploration program. The 90mWm^{-2} contour, shown in red, encloses an area of over 4100km^2 inside the tenement area (outlined in bold red).

Gravity Interpretation

Estimation of the depth to top granitoid was undertaken by Dr. David Leaman using source

modelling of gravity data and following the method of Leaman and Richardson (2003). An infill survey of ~500 gravity stations was undertaken to improve the regional gravity coverage across the tenement area. These data were used to create an updated version of the Tasmanian mantle source model MANTLE03. This model was in turn used to determine the residual Bouguer gravity anomaly from which the depth and shape of top granitoid was interpreted (Figure 2).

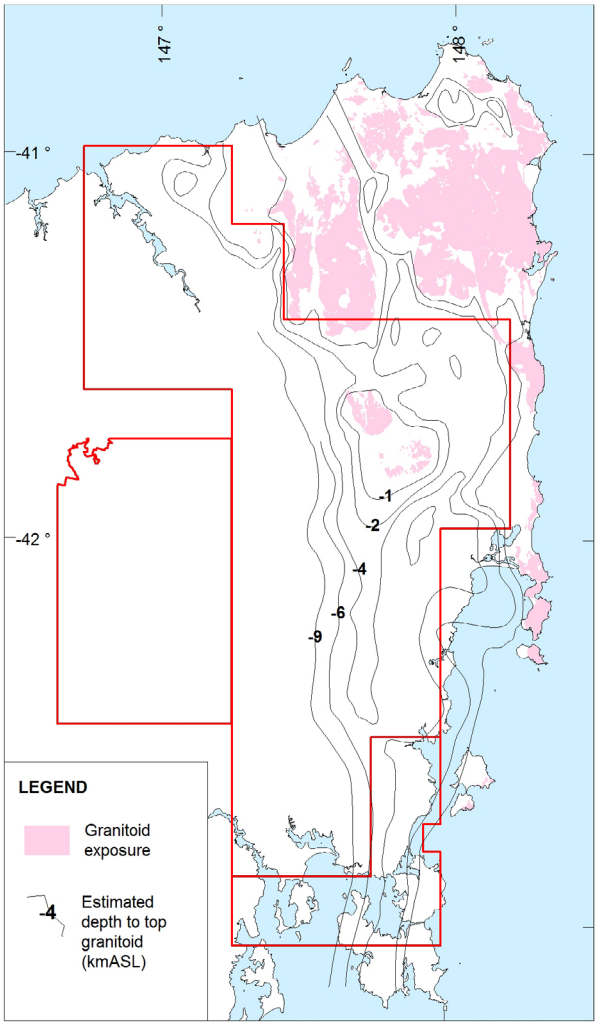

Figure 2: Contoured surface showing estimated depth to top granitoid. Image combines new data derived from KUTh Energy's gravity data acquisition with the existing contours of Leaman and Richardson (2003).

Rock Property Determination

Rock units predicted to overlie the granites in significant thicknesses are Jurassic Dolerite, Tasmania Basin sediments (Parmeener Supergroup) and the Ordovician-Devonican Mathinna Supergroup. Thermal conductivity values determined from these rocks by divided bar analysis from KUTh drill core are summarized in Table 1 together with data from an independent study of this region (H. Goh, 2008). These results confirm the relatively good insulating properties of both the Dolerite and the Tasmania Basin sediments. Predictably, the turbidite sequences of the Mathinna Supergroup display variable thermal conductivities, depending upon rock type and grainsize. Of particular interest in these units, however, was the observation of a strong thermal anisotropy associated with the development of fold axial cleavage (Figure 3). This effect, which was observed most strongly in fine-grained mudstone and shale, serves to significantly reduce the insulating advantage of the fine-grained lithologies wherever heat flow is directed along the cleavage plane.

Unit	Lithology	n	Mean	2σ
Jurassic Dolerite	dolerite	97	2.17	0.35
Parmeener (Tasmania Basin)	sandstone	17	3.54	1.85
	siltstone/mudstone	19	2.39	1.83
Mathinna				
	sandstone	8	4.48	1.27
		24	*4.38*	*1.48*
	siltstone/mudstone	18	3.64	1.24
		16	*3.44*	*1.28*
	shale	*18*	*2.71*	*1.36*
Devonian Granite	granite	*31*	*3.48*	*0.4*

Table 1: Thermal conductivity values (W/mK) determined from core for Eastern Tasmanian rocks. Values in italics are taken from Goh (2008). All values are from wet samples.

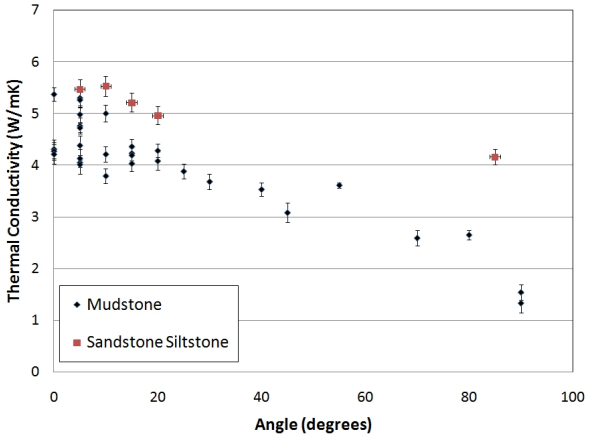

Figure 3: Thermal conductivity versus foliation angle (0° = vertical foliation) for the Mathinna Supergroup. Results indicate a strong thermal anisotropy that is most distinct in the finer grained lithologies.

Magneto-Telluric Survey

An MT survey, comprising 96 stations located at 1km intervals along two E-W lines, was undertaken to better constrain the nature and location of the TCZ anomaly (Figure 4). Full tensor time series data were collected by Moombarriga Geosciences for ~12 hours at each site to ensure resolution of apparent resistivity and phase data in the range 300-0.01Hz.

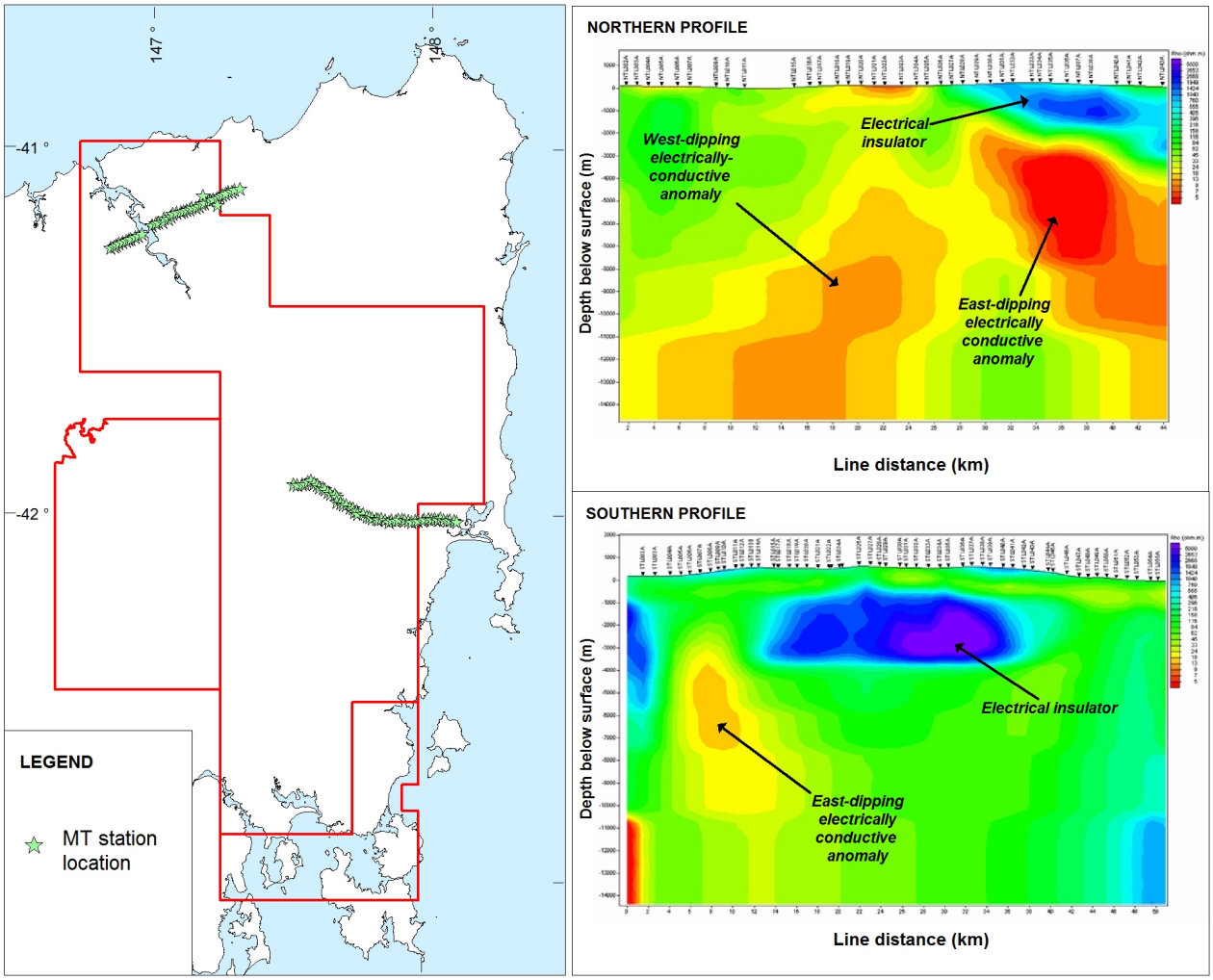

Figure 4: MT survey location and 2D modeled profile results for two lines across Eastern Tasmania. Models are inversions of TM and TE shifted data. Resistivity range 5ohm.m (red) to 6000ohm.m (purple), maximum depth below surface is 14km, line distance northern line = 44km, southern line = 50km.

2D modelling of data generated by this survey was performed by Dr Adele Manzella of the *Consiglio Nazionale delle Ricerche-Istituto di Geoscienze e Georisorse* (CNR-IGG) in Italy. Data were found to be of high quality with relatively few incidences of major signal noise. As part of the modelling Dr Manzella applied a systematic process of data validation to identify, correct or remove poor or biased data. A manually derived 'static shift' correction was applied to compensate for distortion effects produced in the electromagnetic field by near-surface features.

The 2D models produced by Dr Manzella for this survey are presented in Figure 4. In both cases these models have been refined by the use of *a priori* constraints regarding the location of resistive bodies determined in 1D inversion models. No assumptions were made regarding the location, size or intensity of electrically conductive anomalies or of the nature or distribution of the existing geology. Comparisons of TE, TM and joint TE-TM inversion models for the two lines indicated a good agreement for the northern line whilst the southern line displayed significant differences indicating these data are influenced by 3D effects.

The models derived from the MT data indicate the presence of large electrically conductive bodies within the crust in the vicinity of both survey lines. In the northern profile, a strong east-dipping conductive body is observed at a depth of 2.5km and is interpreted to have a thickness of no less than 2km. This body, together with a weaker west-dipping conductor, confirms the presence of the 'Tamar Conductivity Zone' (TCZ) in this region.

An east-dipping electrically-conductive anomaly is also identified at the western end of the southern MT profile at a depth of 3.5 - 4km. This body lies directly along strike from the east-dipping feature identified in the northern profile and is interpreted to be an extension of the TCZ along the Tamar Lineament (Figure 5).

An electrically insulating anomaly is seen located to the east of the interpreted east-dipping TCZ anomaly in both the northern and southern

profiles. At present the identity of the geological feature causing this anomaly remains speculative.

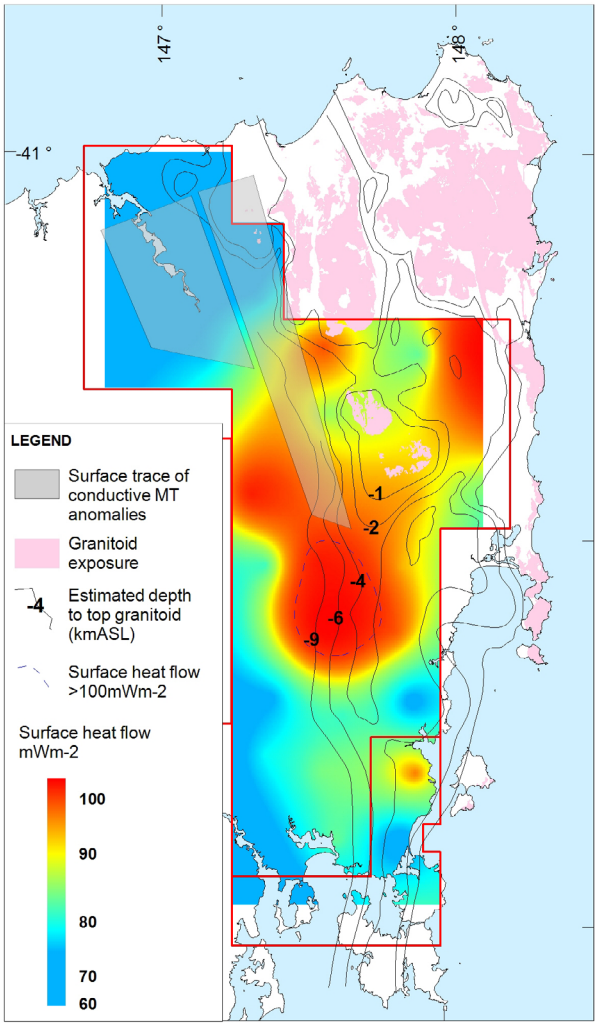

Figure 5: Data compilation of KUTh Energy Ltd's new geothermal exploration results in Eastern Tasmania.

Discussion

Collation of new and existing data for Eastern Tasmania indicates the presence of a significant thermal anomaly in the centre of this region (Figure 5). A large area of elevated heat flow (~4100km^2 >90mWm^{-2}) is seen to spatially coincide with the predicted extension of known granite bodies 3-4km under cover. Flat-lying Mesozoic cover sequences of the Tasmania Basin and intrusive Jurassic Dolerite sills provide up to 1km of good insulating cover at surface. Beneath these lie the deformed flysch of the Palaeozoic Mathinna Supergroup, the insulating qualities of which have been shown to depend upon the orientation of its structural grain. Evidence from field mapping in the north-east indicates that the Mathinna comprises an older recumbently folded unit in the West which is juxtaposed against younger upright folded sequences in the East (Powell *et al*., 1993). Recent data suggests that the contact between these units is faulted implying that the older strata may occur at depth in the east (Reed, 2001; D. Seymour *pers. comm*.). This in turn suggests that the Mathinna section at depth will contain a mixture of upright and horizontal foliations and its bulk properties are therefore likely to be those of a moderate to good thermal insulator. Combined, these data confirm the potential of this area as a Hot Rock or EGS development target. Further geothermal modelling work to estimate a thermal resource and predict temperature distribution with depth in this area is now underway.

MT survey work has confirmed the existence of the Tamar Conductivity Zone in the north and increased its known extent into the south where it remains open along strike from an area of very high heat flow (>100mWm^{-2}). Whilst the nature of this feature is not uniquely defined, its geometry and location suggest that it is a crustal scale structure, most likely a fault or fracture system. It is plausible that this system may be permeable, containing electrically conductive fluid and/or hydrothermal alteration minerals. The possibility of a southern extension of this feature, and of its relationship to the area of very high heat flow, remains open. Further MT survey work is currently in progress to address these issues by better defining the 3D conductivity structure of the southern region.

Summary

A program of systematic geothermal exploration undertaken across Eastern Tasmania has identified a significant new geothermal province. A broad area of anomalously high heat flow (>90mWm^{-2}) is found to spatially coincides with high-heat-producing granite at depth beneath insulating cover. Hot Rock or EGS prospectivity in this area may be further enhanced by the potential for *in situ* fracture permeability associated with the Tamar Conductivity Zone. This feature, which has been detected by an MT geophysical survey, remains open along strike from an area of very high heat flow (>100mWm^{-2}). These targets will be further delineated by exploratory work as part of KUTh Energy's ongoing Tasmanian work program.

References

Goh, H.K.H., 2008, Properties of north-eastern Tasmanian rocks for geothermal exploration, University of Tasmania, Honours Thesis, *unpublished*.

Leaman, D.E. and Richardson, R.G., 2003, A geophysical model of the major Tasmanian granitoids, *Tasmanian Geological Survey Record*, 2003/11.

Powell, C. McA., Baillie, P.W., Conaghan, P.J. and Turner, N.J., 1993, The mid-Paleozoic turbiditic Mathinna Group, northeast Tasmania, *Australian Journal of Earth Sciences*, 40, 169-196.

Reed, A.R., 2001, Pre-Tabberabberan deformation in Eastern Tasmania: a southern extension of the Benambran Orogeny, *Australian Journal of Earth Sciences*, 48, 785-796.

Assessment of Otway Basin Hot Sedimentary Aquifer systems for geothermal and water uses

Cedric Jorand*, Andrew Krassay, Lisa Hall, Stephen Hostetler, and Tom Loutit
FrOG Tech Pty Ltd, 17F, Level 1, 2 King Street, Deakin ACT 2600

The Otway Basin, spanning the southern parts of Victoria and South Australia (Figure 1), is the location of a new regional geological and geothermal study by FrOG Tech Pty Ltd. In partnership with P.I.R.S.A., Geosciences Victoria and Geoscience Australia, the study integrates potential field and seismic data, information from both hydrocarbon exploration and water wells and thermal data to understand the nature of onshore and offshore Otway Basin Hot and Warm Sedimentary Aquifers and their inter-connections. The initial targeted formations within the fault controlled depocentres are Upper Jurassic to Lower Cretaceous synrift and postrift, nonmarine, interbedded sandstones, shales and coals of the Otway Supergroup aquifers.

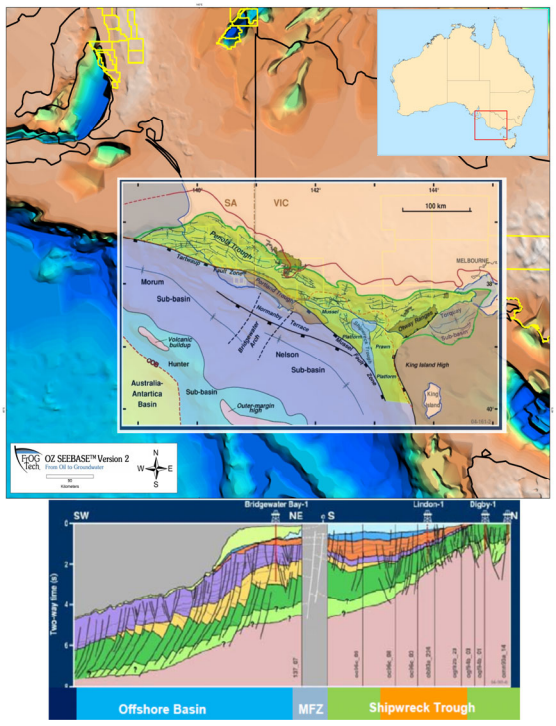

Figure 1: Location of the Otway Sedimentary Basin and a cross-section from the onshore to offshore Otway Basin.

Previous Work

To date, there are no geothermal studies at the regional scale of the entire basin. The current Australian-scale temperature map (Austherm08, 5 kilometres depth) is the result of interpolating dispersed onshore well temperature data and as such it is not appropriate for regional analysis of onshore and offshore sedimentary basins. In both states, small scale geothermal studies have been conducted by government geological surveys and consultants (e.g. Jenkin, 1962; Thompson, 1978, 1979; Nahm & Reid, 1979; Akbarzadeh & Thompson, 1984; King *et al.*, 1987; the Sustainable Energy Authority of Victoria (SEAV), 2005, Driscoll 2006.), but have not been linked into a regional framework.

The project

This ongoing project will integrate Otway Basin geofabric (hydro-thermal and tectono-stratigraphic properties) studies with a detailed geothermal resource calculation.

This study intends to create for the first time, an attributed geological framework for the entire Otway Basin encompassing interpretation of terranes, basement composition/lithology, tectonic event-response, definition and description of deep and shallow potential aquifer/aquitard pairs contained in the economically exploitable geothermal window to the megasequence level.

This abstract summarised the main results of the Phase I of this project that focused on the characterisation of the deep Otway Basin Cretaceous aquifers and the underlying basement.

Otway basin basement topography

The SEEBASE™ basement surface in the Otway basin has been refined since OZ-SEEBASE™ was released in 2004, based on the most recent available geophysical surveys. The new SEEBASE™ of the Otway Basin is a model of basement topography and provides a new view of the Otway Basin geometry and a context which can be used to better understand the basin depocenters structural development together with the sedimentary facies distribution. It was constructed by combining a structural interpretation with depth information derived from potential field datasets, seismic data, FrOG Tech's seismic interpretation, wells, and published cross-sections. The present SEEBASE™ (Figure 2) is a regional model at ~1:2,500,000 scale. The sediment and basement thickness have been derived from the depth-to-basement interpretation and will be used for the next step, heat flow modeling.

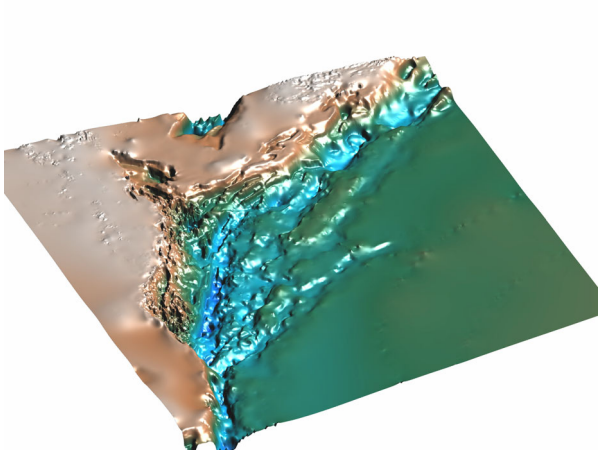

Figure 2: 3D perspective view from the East of the Otway Basin SEEBASE™ (basement topography).

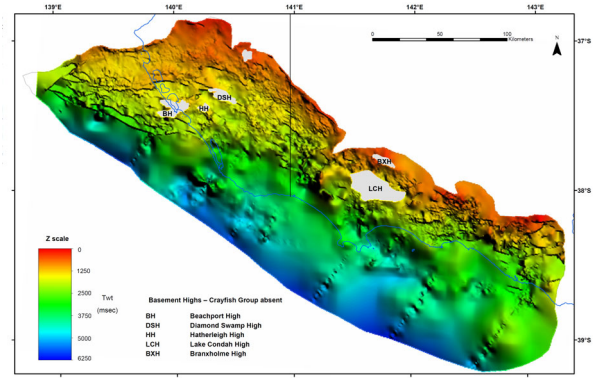

Figure 3: 3D time structure map of the top of the Crayfish Gp.

Seismic Interpretation

Seismic profile analysis has permitted identification of the structural signature for 3 main extensional phases contemporary with deposition of the 3 key supersequences (Crayfish, Eumeralla, Sherbrook). The magnitude and type of structural control has been described for each phase. Analysis of timing, displacement, patterns and intersection relations of interpreted seismic faults allows definition of 3 different main sets of faults.

Thanks to seismic-well ties, the different aquifers have been characterized by their specific seismic and sedimentary facies, gamma ray log signature and seismic horizon geometry and amplitude. This characterization allows the study of the vertical distribution of the potential reservoirs in the Penola, Digby, Mocamboro, Ardonachie, Worong, Koroit troughs and in the Tyendarra Embayment. Porosity and permeability qualifiers based on well-tie have been attributed along the stratigraphic chart.

Isopachs of the supersequences have been constructed using the structure time surfaces for top basement, top Crayfish Group (Figure 3), top Pretty Hill sandstone, top Eumeralla and top Sherbrook at basin scale.

Aquifer characteristics

Six sandstone-rich reservoirs or potential deep aquifers have been identified:

1. The basal Late Jurassic to earliest Cretaceous nonmarine sandstones of the Crayfish Group, sometimes informally described as the “McEachern Sandstone”.

2. The thick, well developed fluvial channel and bar sandstones of the “Sawpit Sandstone”.

3. The Pretty Hill Sandstone is the thickest and most extensively developed Crayfish Group sandstone-dominant unit.

4. The fine-grained sandstones within the Laira Formation, known as “intra-Laira sandstone”.

5. The laterally discontinuous, lenticular channel sandstones of the Katnook Sandstone.

6. The regionally extensive, thin, sheet-like Windermere Sandstone.

The best regional aquifer is the Pretty Hill Formation. It is the thickest (up to 870m) and most extensively developed, but its porosity is strongly facies-dependent (channels = high, floodplain = low). Although thinner, the Sawpit sandstone shows similar characteristics and potential. Alternatively, the Katnook and MacEachern sandstones are more localized, but show higher porosity and permeability values with local thicknesses > 200m.

Compilation of deep water bores salinity data shows that low salinity water is present within the deep aquifers of the Otway Gp.

In parallel, first-pass maps of shallower aquifers in the Wangerrip, Nirranda and Heytesbury groups have also been produced from regional bores/wells databases.

Temperatures

Temperature data from more than 270 wells have been compiled, assessed or re-assessed to attribute confidence values and generate a preliminary linear temperature gradient map at the scale of the Otway basin that will help to target the aquifers that will be the focus of Phase II. The values stored in this temperature database will also serve as a reference for Phase II heat flow modelling. Preliminary linear gradient map shows that the higher gradient values are found in the Penola, Tahara, Morenda and Elingamite troughs. As the number of reliable temperature values in wells diminishes quickly with depth, maps of projected temperature at the top of the deep aquifer surfaces have to be considered with care. Nonetheless temperature at the top of the Crayfish Gp, the shallowest of the targeted deep

aquifers gives values that are locally higher than 100°C along the Victorian coastline.

Conclusion

These preliminary results are encouraging concerning the geothermal exploitation of the deep aquifers in the Otway Basin that seems to be economically viable for a large range of direct-use purposes throughout the basin and potentially locally also for power generation.

But, the Phase I of this project has also shown the limitation of the direct linear gradient temperature approach for the deep aquifers. In phase II, a definition/revision of rock hydraulic properties of each selected aquifer-aquitard pair and prediction of radiogenic heat flow derived from the basement composition and thickness from SEEBASETM to Moho will be performed. These inferred heat flow values together with available estimates of heat flow and corrected temperature at depth will be used to reassess temperature gradients using thermal conductivities derived from mixed-lithology calculations. Heat in place maps, including the errors maps, will be then derived in order to better define the geothermal plays and their associated risks. In addition to the definition of the geofabric and geothermal resources, the project will aim to produce a comprehensive conceptual groundwater model of the Otway Basin. The model will detail groundwater recharge, discharge and the links between the shallow, onshore groundwater resources used for consumptive purposes (e.g. agriculture, environmental services and town water supplies) and the deep groundwater resources available for geothermal, petroleum and carbon capture and storage.

References

Akbarzadeh, A. and Thompson, B. R., 1984. An overview of the potential and applications of geothermal energy in Victoria, and proposed future actions. Victorian Solar Energy Council and Department of Minerals and Energy (Unpubl.).Melbourne, Australia.

Driscoll, J. A preliminary regional assessment of Victoria, Australia. AESC2006, Melbourne, Australia.

Jenkin, J. J. 1962. Underground water in East Gippsland. Underground water investigation report 6. Department of Mines, Victoria, 16 pp.

King, R.L., Ford, A.J., Stanley, D.R., Kenley, P. R., and Cecil, M. K., 1987. Geothermal Resources of Victoria. Department of Industry Technology and Resources and Victorian Solar Energy Council. Melbourne, Australia. 134pp.

Sustainable Energy Authority Victoria, 2005. The geothermal resources of Victoria. pp. 99.

Thompson, B. R., 1978. On the thermal waters of the Gippsland Basin and the problems associated with the study of high temperature aquifers. In: Hydrology of great sedimentary basins; Proceedings of the Budapest Conference, 1976.

Annales Instituti Geologici Publici Hungarici.

Thompson, B. R., 1979. Geothermal gradient maps of the Gippsland Basin and the occurrence of high temperature aquifers. Geological Survey of Victoria Unpublished Report 1979/140.

Multiuse-use 'triple play' hot sedimentary aquifer (HSA) potential of Victoria, Australia

Robert King, Mark Miller,
Greenearth Energy Ltd, PO Box 24, Collins Street West, Melbourne 8007

Greenearth Energy Ltd holds geothermal exploration permits to the east and west of Melbourne, Victoria Australia. These permits are located on the Otway and Gippsland basins that straddle the southern part of the State. The basin fills range up to 6 km thick and form an insulating blanket over Palaeozoic basement rocks.

Geothermal gradients are somewhat elevated, with heat flows up to 100 mW/m^2 in places, and projected temperatures of 150 ^{o} C at around 3 kilometres (km) depth.

Sandy units at the base of the basin sequences offer potential for Hot Sedimentary Aquifers (HSA) while longer term Engineered Geothermal Systems (EGS) prospectivity exists in Palaeozoic granites beneath the insulating sedimentary cover. The HSA's are a triple play with potential for electricity generation, direct heat applications and potential CO_2 sequestration sites.

A geothermal resource has been estimated for the area south of Geelong, encompassing both HSA and EGS geothermal plays. A proposal has been modelled for a 10.7 MW and 48 MW geothermal development accessing part of the HWA geothermal resource.

Introduction

Greenearth Energy Ltd (Greenearth) is a small listed Australian Geothermal explorer. It has geothermal exploration permits near Melbourne Australia (Figure 1) that underlie the industrial hub of southeastern Australia. These areas have a significant greenhouse gas footprint. To the east of Melbourne, in Gippsland, the permits include the Latrobe Valley area, the State of Victoria's power generation hub with over 6000 MW of brown coal fired electricity generation. To the west of Melbourne a permit covers the Geelong region, the most carbon constrained community in Australia. Major industry includes an aluminium smelter, cement works and a brown coal fired power station.

Greenearth has established inferred resources in both its Geelong and Gippsland permits. To the southwest of Geelong an inferred resource of 260,000 PJ is calculated (Beardsmore, 2008), encompassing both a hot sedimentary aquifer resource (HSA) and a deeper engineered geothermal system (EGS), while in the Gippsland area a small inferred geothermal resource of 39,000 PJ is estimated (Beardesmore, 2009).

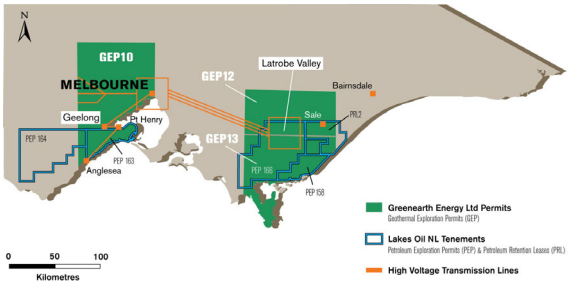

Figure 1: Greenearth Energy Ltd permits.

The Australian Government has set a target that 20 % of all energy generation by 2020 will be from renewable sources (Department of Climate Change, 2008). This could mean that approximately 45,000 gigawatt-hours from renewable energy sources will be required by 2020.

The thick sedimentary basins running east and west of Melbourne, the higher than normal heat flows in the basin margin areas and the potential for thick sandy sequences in the temperature depth widow of 3-4 km make the Greenearth permits prospective for geothermal development of hot sedimentary aquifers.

Geological and geothermal description

A Mesozoic rift basin established along the south-eastern margin of Australia during Gondwana separation. To the west of Melbourne is the Otway Basin, stretching 500 km, while the Gippsland Basin is located to the southeast of Melbourne.

Both basins have undergone significant petroleum exploration with the offshore part of the Gippsland Basin being a major hydrocarbon province.

While the detailed stratigraphic nomenclature varies between the two basins, the overall sedimentary history is similar. Sedimentation commenced in the early Cretaceous with fluvial sediments (Pretty Hill/Rintouls Creek) deposited onto the rifting basement. This is overlain by thick non-marine volcanogenic sandstones and siltstones. These sediments are in turn unconformable overlain by a series of marine sediments spanning the late Cretaceous to mid Tertiary (Duddy, 2003; Holdgate and Gallagher, 2003).

The geothermal potential is associated with the initial sedimentary basin fill which offer permeability potential. Faulting is extensive in the basins with major faults bounding half grabens, originally normal and then subsequently

reactivated as reverse faults. Faulting in or adjacent to any sandy basal units, in particular fracture zones, should provide access to broader reservoir areas (Figure. 2).

Latrobe Valley and Gippsland

In the Gippsland area the base of the sedimentary basin is in the range 3000-4000 m or deeper. The basal units (Rintouls Creek Sandstone and Tyers Conglomerate) have known porosity and offer a geothermal target where they are most deeply buried.

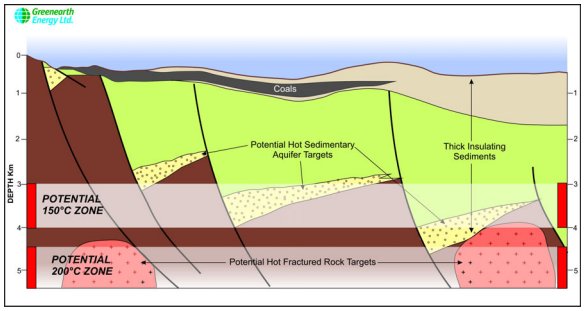

Figure 2: Schematic geological model for Hot Wet Aquifer, Otway and Gippsland basins.

Heat flow investigations show that there is a trend of elevated heat flow through the Latrobe Valley area. Measurements on 10 wells returned estimates up to 101 +/- 26 mW/m^2 (Figure. 3) (Walsh, 2009a). One of the most significant temperature projections is that at the Loy Yang-2 well, drilled in 2005 to 1443 m and re-entered in 2008 for precision temperature logging to 713m. From the original well composite log, measured and fair estimates of conductivity were applied to different layers. The resulting thermal conductivity profile yielded a heat flow of 90 mW/m ^{2}.

Based on this information a heat flow model was used to predict the temperature beneath the well. Well log data from the adjacent Loy Yang-1 well was able to give the stratigraphy to a depth of 1735 m. and a scenario was modelled down to 3500m. An estimated temperature of 150 ^{0} C was achieved at a projected depth of 2900m +/- 400m (Fig. 4) (Walsh, 2009b, Greenearth Energy Ltd, 2009).

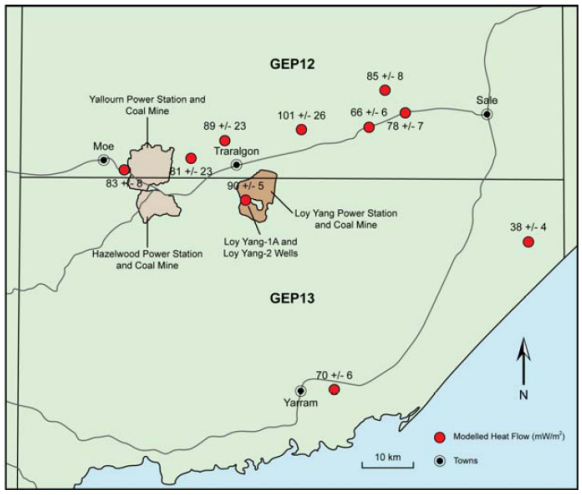

Figure 3: Summary of heat flow investigations. The Latrobe Valley area shows heat flows well above the global average.

Any porous sandy sediment at that depth in the Latrobe Valley area provides an exploration target for hot wet sedimentary aquifer style geothermal resources. In the Latrobe Valley brown coal generation hub opportunities exist for both electricity generation as well as direct heat application for drying brown coal or pre-heating boiler feed water.

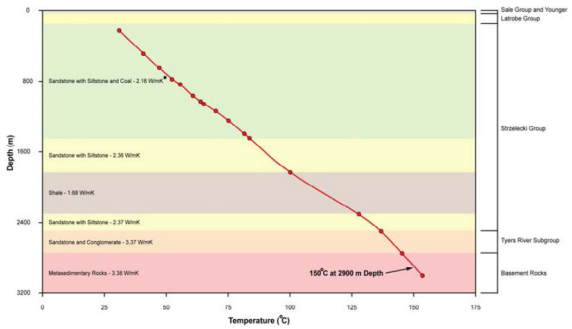

Figure 4: Modelled temperature of Loy Yang-2 Well

These same units also offer potential targets for investigation as CO_2 sequestration reservoirs. The brown coal electricity generation in the Latrobe Valley area produces around 60 mtpa of CO_2. The sandy units, located at depths of 2.5 km or deeper beneath the power generation area, warrant further investigation of their ability to act as onshore CO_2 storage sites.

Geelong area

In the Geelong area the basal parts of the insulating sedimentary cover (Crayfish Group/ Pretty Hill Sandstone) reaches depths of 4000-5000 m (St John, 2007). Just to the west of the permit boundary the Pretty Hill Sandstone is 615m thick.

This area has potential for both Hot Sedimentary Aquifers(HSA) geothermal plays in the shallower sand-prone beds of the early Cretaceous Crayfish Group as well as Engineered Geothermal Systems (EGS) geothermal plays in the Palaeozoic basement.

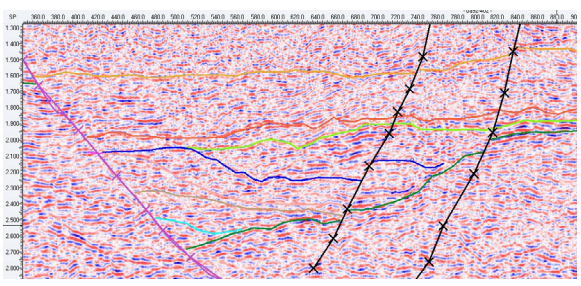

Figure 5: Seismic line OGF 92-402 showing distribution of possible sand prone units. Yellow – top E1, blue – top F, brown – base F, light blue – top Casterton A.

Seismic mapping has identified the distribution of two possible sand-prone units in the early Cretaceous CrayFish Group. These two sequences are described as units F and E1 (Figure. 5) and may constitute viable sedimentary aquifers. Both units show characteristic syn-dypositional growth towards the major bounding faults with unit F reaching a maximum thickness of about 600 m and unit E1 reaching a maximum thickness of about 700 m (Cooper and Waining, 2008; Cooper, Waining and Pollington, 2008) (Figure 6).

Inferred Resource estimates have been made on three reservoir targets. The targets fall into two categories of geothermal reservoir-:

- buried sedimentary aquifers (Hot Sedimentary Aquifers –HSA) type plays, targeting sandstones units in the Crayfish Group (E1 and F reservoirs); and
- Engineered Geothermal System (EGS/HDR), targeting Palaeozoic basement.

The HSA targets were defined via sequence stratigraphic methods incorporating 2D seismic with local and regional well data from the Otway Basin. The EGS target has been defined by the seismic data and constitutes the basement beneath the insulating Otway Basin sediments.

A stored heat method was used to estimate a HSA inferred geothermal resource of 40,000 PJ and the EGS inferred resource of 220,000 PJ. The resource covers an area of 462 km^2 and is contained in 656 km ^{3} volume of rock. The resource estimate complies with the Australian code for reporting exploration results geothermal resources and geothermal reserves (2008 edition).

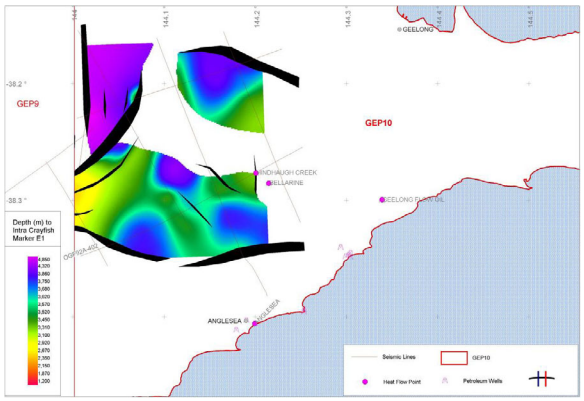

Figure 6: Depth map of the E1 marker, the top of the potential reservoir unit in the Crayfish Group. Distribution is controlled by early Cretaceous growth faults.

This work has led to the development of a HSA commercial model for geothermal based electricity generation southwest of Geelong.

This model assumes that a portion of the inferred HSA geothermal resource of 40,000 PJ present in Geothermal Exploration Permit (GEP) 10 is available to utilize for power generation.

Wells intersecting the Pretty Hill Sandstone in the wider Otway Basin show variable porosity and permeability. Based on this limited data, it is feasible that the Pretty Hill Sandstone may have porosity in the range 10-15 % and average permeability of 50-150 mD at the target depth of 3450 m (Fig. 7). It would be expected that the reservoir unit would need to have a thickness of > 100 m of permeable rock to achieve a permeability-thickness function (Darcy-metre) required for commercial flows.

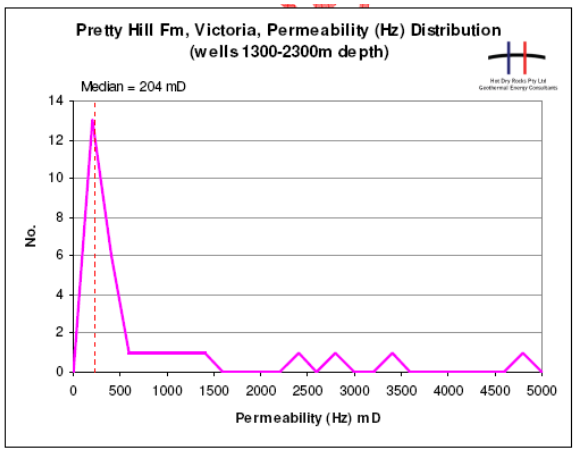

Figure 7: Frequency distribution of horizontal permeability from core samples for the Pretty Hill at Waracburunah-2, Hawkesdale-1, Garvoc-1, Pretty Hill-1, and Woolsthorpe-1. The distribution is strongly log-normal with a median 204mD

A 1D conductive heat flow model on data from the Bellarine-1 well and extrapolated to basement from seismic data illustrate that the geothermal working fluid (150 ^{o} C) is intersected at about 3040m with a heat flow of 90 +/- mW/m^2 (Fig. 8).

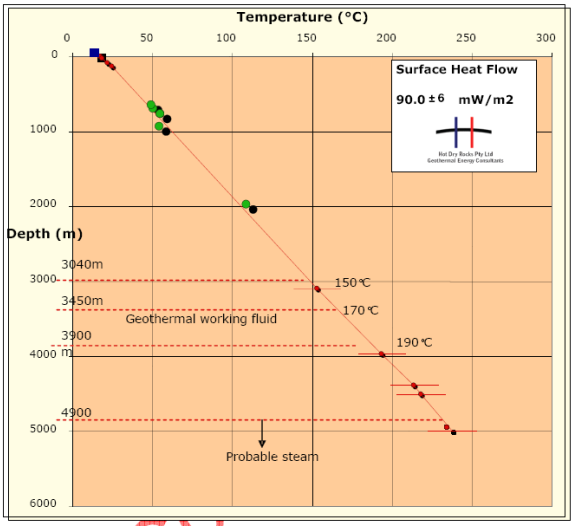

Figure 8: Sample conductive 1D heat flow model based on temperature data from Bellarine-1 and measured thermal conductivity data for all major lithologies in GEP 10. The model has been extrapolated on based on seismic depth grids.

A target geothermal resource temperature of 170 degrees centigrade at the modest target depth of 3,450 metres with an assumed flow rate of 100 litres per second, should yield sufficient heat flow to build an operating geothermal power plant.

There are several possible sites for a geothermal power plant in GEP 10 and a potential site was selected approximately 10 kilometres north-northwest of the Anglesea Coal Mine, 9.5 kilometres from the Anglesea– Point Henry electricity transmission line.

A commercial study modelled the costs and outcomes that may reasonably be expected for developing a 10.7 megawatt (MW) geothermal power plant. Similarly the study modelled an expansion to establish a 48 MW geothermal plant (Cooper, Waining and Pollington, 2008).

Borrowing costs were amortised over the life of the projects (20 years). Costs were discounted as has the generation (MWhr) to calculate the levelised cost (LEC) of both scenarios.

The commercial model shows that over a 20 year life for the proposed geothermal power plant:

. The levelised cost of electricity (LOCE) would be in the range of $96-114 per MW hour.

Generation of attractive pre-tax revenue and discounted cash flows for the project.

Result in a displacement of at least 1.2 million tonnes and up to 7.3 million tonnes of carbon dioxide “greenhouse gases” emitted by conventional power stations.

Conclusion

Greenarth Energy Ltd has geothermal exploration permits that underlie the industrial hub of southeastern Australia. The permits contain in excess of 6000 MW of brown coal fired electricity power generation with the Latrobe Valley power stations alone having a greenhouse gas footprint in excess of 60 mtpa.

The southern Victorian Cretaceous-Tertiary sedimentary basins that straddle the permits have substantial seismic and well data from previous petroleum exploration. Heat flows vary, however, in places values of up to 100 mW/m^2 were recorded. In the Geelong and Latrobe Valley area temperatures are estimated to reach 150 ^{o} C at around 3 km depth. The basal units of the sedimentary pile, where they occur in the 3-4 km depth range have potential to contain hot sedimentary aquifers that may be suitable for power development using organic rankin cycle technology.

The high moisture content of the brown coals used for electricity generation may present opportunities for direct heat application using geothermal fluids to dry coal. Given the high level of greenhouse gas emission in the permit areas, these same units are a target for further research as to their capacity to also act as reservoirs for greenhouse gases.

In the Geelong area good seismic coverage has enabled the calculation of an inferred geothermal resource. A site was selected near the Anglesea power station for a conceptual geothermal development. At this location the potential reservoir is interpreted to be 1000m thick commencing at around 3.5 km depth.

The costs and outcomes for conceptual 10.7 megawatt (MW) and a 48 MWgeothermal power plant were modelled. The plants would produce 1.65 and 7.41 GWh of renewable electricity. The levelised cost of electricity (LOCE) would be in the range of $96-114 per MW hour.

Acknowledgements

Much of this paper has drawn extensively upon reports to Greenearth Energy Ltd by Graeme Beardsmore, Gareth Cooper, Denis Walsh and Ben Waining of Hot Dry Rocks Pty Ltd. They are duly acknowledged for their contribution.

References

Beardesmore, G., 2008, Greenearth Energy Ltd, statement of estimated geothermal resource, Anglesea, GEP 10 as at 04 December 2008. (Release to the Australian Stock Exchange by Greenearth Energy Ltd), 9pp

Beardesmore, G., 2009, Greenearth Energy Ltd, statement of estimated geothermal resource, Wombat, GEP 13 as at 18 December 2008. (Release to the Australian Stock Exchange by Greenearth Energy Ltd), 9pp

Department of Climate Change, Australian Government, 2008, Fact Sheet, Australian Government renewable energy target (December 2008), 1p

Duddy, I. R., 2003, Mesozoic, in Geology of Victoria, (Ed W.D. Birch). *Geological Society of Australia, Victorian Division Special Publication 23,* pp239-286.

Cooper, G. T. and Waining, B., 2008, Interpretation of selected 2D seismic reflection lines in the Otway Basin (GEP 10) and related sequence mapping. Report prepared for Greenearth Energy by Hot Dry Rocks Pty Ltd., 63pp

Cooper, G. T., Waining, B. and Pollington, N. J., 2008, Renewable energy Project: concept development for geothermal power plants, GEP 10, Geelong area Victoria. Report prepared for Greenearth Energy by Hot Dry Rocks Pty Ltd, 31pp

Greenearth Energy Ltd., 2009, High modeled temperatures benearth the Loy Yang power stations, Latrobe Valley, Victoria. Australian Stock Exchange Release, (27 May 2009), 2pp

Holdgate, G. R., and Gallagher, S. J, 2003, Tertiary, in Geology of Victoria, (Ed W.D. Birch). *Geological Society of Australia, Victorian Division Special Publication 23,* pp289-335.

St John, P., 2007, Independent geological expert's report. In Greenearth Energy Ltd Prospectus, pp32-47

Walsh, D, 2009a, GEP 12 & 13 temperature logging and heat flow investigation. Prepared for Greenearth Energy Ltd by Hot Dry Rocks Pty Ltd (unpublished), 43pp

Walsh, D, 2009b: Loy Yang-2 temperature correction and projection. Prepared for Greenearth Energy Ltd by Hot Dry Rocks Pty Ltd (unpublished), 5pp

Progress at the Paralana EGS Project in South Australia

King J.P[1], Reid P.W.[1*] Bendall B[2],
[1]Petratherm Ltd. 106 Greenhill Rd, Unley South Australia 5066,
[2]Primary Industries and Resources, South Australia. 101 Grenfell St, Adelaide 5001
* Corresponding author: preid@petratherm.com.au

The Paralana EGS Project, located 600km north of the city of Adelaide in South Australia, provides a natural laboratory for the development of an Engineered Geothermal System (Figure 1). Anomalously high heat production basement rocks provide the local heat source and are overlain by a thick sedimentary package, informally termed the Poontana Basin (Figure 2), within a favourable in situ stress regime. Early exploration drilling indicates an elevated geothermal gradient and heat flow at the project site. Petratherm Limited, in joint venture with a major oil and gas (Beach Petroleum) and power industry energy utility (TRUenergy), are initially seeking to build a 3.75 - 7.5 MWe commercial power development to supply a local mine.

A local microseismic monitoring network has been deployed to record background seismicity prior to drilling of the first deep well into the resource, which commenced drilling on the 30th June 2009. An innovative strategy for development of the EGS reservoir is planned, involving massive hydraulic stimulation of multiple target zones within the sedimentary overburden. This paper will provide a technical update on progress at the Paralana EGS site.

Keywords: Geothermal, Stimulation, Drilling, Micro seismic monitoring.

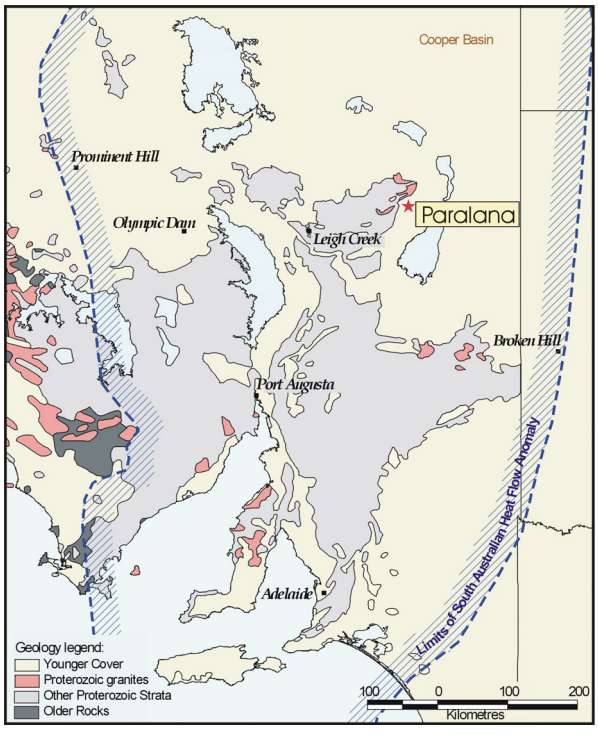

Figure 1: Regional Locality Map and extent of SAHFA (SAHFA modified from Neumann *et. al* . 2000)

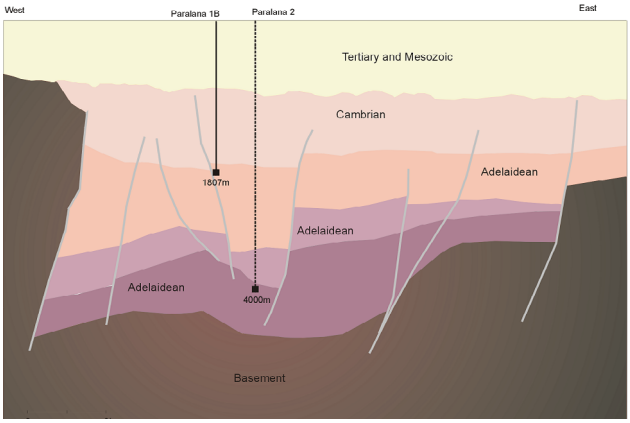

Figure 2: Cross-section of the informally termed Poontana Basin

Heat exchanger development plan – the HEWI model

One of the principal limiting factors in commercialising EGS has been the inability to manufacture a heat exchanger of sufficient size and fluid production rate. Existing technical difficulties in achieving a robust sub-surface heat exchanger in EGS applications generally relate to the practice of developing the sub-surface heat exchanger within the heat producing granite rock. Granite is by nature an impermeable and mechanically strong rock. As a result it is inherently difficult for fluid to flow through granite, or to mechanically fracture the rock to develop an effective reservoir artificially. By comparison, the rocks which make up the overlying insulating sediments tend to have greater naturally occurring porosity and permeability, are mechanically weaker, and more susceptible to induced chemical and mechanical stimulation if enhancement of the reservoir is required.

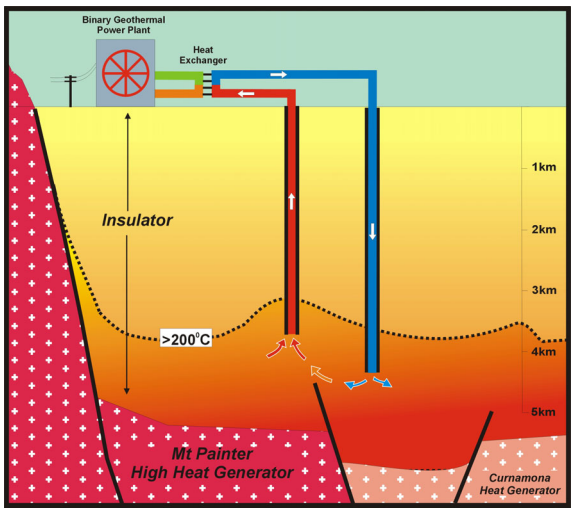

Figure 3: Schematic diagram demonstrating the basic concept of an Enhanced Geothermal System using the HEWI (Heat Exchanger Within Insulator) model

The Heat Exchanger Within Insulator (HEWI) model (Figure 3) aims to exploit naturally permeable and porous insulating sedimentary rocks above the granite heat source. Where intrinsic permeability is inadequate, the HEWI approach will deliver greater control over the reservoir development through the hydraulic stimulation of these units. This strategy more closely approximates the systems successfully used in petroleum reservoirs and conventional geothermal projects. This enables the application of techniques for stimulation and geochemical mitigation developed in these industries.

Multi-Zone Stimulation

Historical hydraulic fracture stimulations have generally been single massive stimulations in an open hole. The limitation of this method is that the operator has minimal control over the location and distribution of the developing fracture network, with most fractures propagating at the base of the casing shoe near the top of the open hole section. The inability to selectively initiate propagation of fractures in the remaining open hole section means the development of the heat exchanger has been severely compromised.

Given that the development of a complex, thick, interconnected fracture network is the optimal configuration for the engineered reservoir, it follows that undertaking multiple stimulation operations initiated at different levels in the well could achieve the desired outcome. Such an operation would enable greater control; both in terms of the location of initiation of fracturing in the well bore, and the potential to develop stacked multiple fracture horizons within suitable single or multiple geological units.

Drilling Status

In 2007 Petratherm established a joint venture with Beach Petroleum who elected, under the terms of the Joint Operating Agreement, to "operate" the drilling and stimulation of the Paralana #2 well. This was designed as an injection well, allowing drilling comfortably within current technical limits. Selection of a rig capable of drilling to the target 4000m depth and handling the casing strings of the well design demanded a 2000 HP rig and the joint venture contracted Weatherford Drilling International to provide a new-build rig. Rig delivery was delayed by manufacturing capacity and subsequently by Hurricane Ike's effects on the US Gulf. Manufacturing was transferred to Dubai and the rig was delivered to site in May 2009 Rig-up and final certification allowed spud on the 30th June 2009 (the time of writing this abstract).

Figure 4: WDI Rig #828 at Paralana #2 Location

The well is designed as an injection well, with an 18-5/8" x 13-3/8" x 9-5/8" x 7" casing programme. A 20-3/4"-3k x 13-5/8"-5k x 11'-10k wellhead assembly will be installed with an 11"-10k x 7-1/16-10k adaptor-seal flange allowing installation of a full-bore 7-16"-10k valve for stimulation and later installation of a 4-16" xmas tree. All casing annulus seals are RCS metal-to-metal with preliminary elastomer seals in the slip and seal assemblies.

Figure 5: Paralana #2 Wellhead at Wood Group Warehouse after inspection

Drilling is planned to take approximately four months and will be followed with logging of the 8-1/2" section and casing. The 7" casing will be set to total depth and cemented to surface. Preliminary reservoir modelling and well log results will be used to identify the units to stimulate and to develop final plans for the stimulation programme.

A local microseismic monitoring network deployed in late 2008 to record background seismicity prior to drilling was augmented in October 2009 with additional sondes placed in deeper boreholes to provide the planned level of monitoring and data acquisition for the stimulation programme.

Stimulation of the Paralana #2 well is expected to commence later in 2009.

TRUenergy joined the joint venture in 2008 and will provide power generation, transmission and marketing resources to the project's development.

References

Neumann, N., Sandiford, M., & Foden, J. (2000) Regional geochemistry and continental heat flow: implications for the origin of the South Australian Heat Flow anomaly. Earth and Planetary Science Letters, 183, 107-120.

Geothermal Energy in the Perth Basin

Adrian Larking & Gary Meyer
Green Rock Energy Limited
www.greenrock.com.au

In 2008, the Government of Western Australia amended the onshore Petroleum Act to include rights to explore for and produce geothermal energy. The first geothermal exploration rights under this legislation were granted to Green Rock Energy in the Perth Basin at the end of July 2009 after a process of application by tender. The Perth Basin straddles the south western coast where most of Western Australia's population and power infrastructure is located. This favourable location close to markets together with the Perth Basin's geological potential to contain large geothermal resources presents the opportunity to supply energy for electricity production and direct use including air-conditioning and desalination of water.

The Perth Basin is a 1,000 kilometre long geological rift containing a thick sequence of sediments in places up to 15 kilometres deep. With its thick sequences of sandstones and the presence of thermal insulating sediments and coals the Perth Basin has potential to house geothermal energy resources in the form of hot sedimentary aquifers (HSA).

The highest known heat flows in the Basin have been determined from petroleum wells in or near producing oil and gas fields in the northern Perth Basin. Green Rock Energy holds 6 Geothermal Exploration Permits (GEPs) there near high voltage power grids where some heat flows exceed 100mW/m^2. Temperatures in hot sedimentary aquifers at depths less than 4,000 metres should be sufficient for the commercial generation of electricity provided sufficient geothermal water flow rates can be achieved.

In the central Perth Basin, where Green Rock Energy holds another two Permits, heat flows are generally lower and geothermal waters are expected to be commercially suitable for direct heat uses rather than electricity generation. In and near Perth low enthalpy geothermal energy resources have been intersected in numerous water bores drilled to 1,000 metres deep into highly permeable aquifers. Within Green Rock Energy's Permit GEP 1 in the western suburbs of the city of Perth geothermal energy recovered from aquifers less than 1,000 metres. This geothermal water is used to heat a number of major swimming centres including the Challenge Stadium Aquatic Centre where the World Swimming Championships have been held twice in the past decade.

At its Perth Permit, GEP1, Green Rock Energy plans to recover geothermal water to power air-conditioning and heating at the main campus of the University of Western Australia. Geothermal energy will be used directly to replace electricity currently used for air-conditioning at the University campus. To achieve this objective the Company proposes to drill one production and one injection well to depths between 2.5km and 3kms deep into sandstone aquifers. Preparatory work is underway to enable this drilling to be carried out in 2010. Drilling wells to these depths should not present any particular difficulty as there is abundant history of petroleum wells drilled without significant problems in the Perth Basin. The laterally consistent stratigraphy makes geological expectations and the drilling prognosis reasonably predictable in the Perth Basin.

Commercial viability will depend on obtaining adequate geothermal temperatures and water flow rates from the sandstone aquifers at depth. Geothermal water temperatures of between 80ºC and 100ºC are required for commercial operation of the absorption chillers which will provide chilled water for the campus. Temperatures at the target depths should be adequate as indicated by heat flow estimates determined from temperatures measured by Green Rock in deep water bores within and adjacent to the Permit. A 208 metre drill hole recently completed at the UWA campus confirmed the estimated heat flows beneath the campus.

To confirm the sub-surface structural geology and flow potential from sediments beneath the University campus the Company evaluated existing seismic surveys and data from petroleum wells adjacent to the Perth Permit and completed a gravity survey near the proposed well sites. Hydrodynamic flow modelling has also been carried out to model the effects of temperature drawdown and re-injection on the reservoirs over time. This has indicated that geothermal production will be sustainable over decades using the targeted permeabilities and proposed production and injection well configuration.

Geothermal Energy Prospectivity of the Torrens Hinge Zone: Evidence from New Heat Flow Data

Chris Matthews*, Bruce Godsmark.
Torrens Energy Limited. PO Box 506, Unley, SA, 5035.
* Corresponding author: chris.matthews@torrensenergy.com

The Torrens Hinge Zone is a long but narrow (up to 40 km wide) geological transition zone between the relatively stable Eastern Gawler Craton "Olympic Domain" to the west and the sedimentary basin known as the Adelaide Geosyncline to the east. It was hypothesized from first principles that the Torrens Hinge Zone should be prospective for high geothermal gradients due to the likely presence of high heat flow and insulating cover rocks. A method to test this hypothesis was devised, which involved the measurement of heat flow on a pattern grid using purpose drilled wells, precision temperature logging and detailed thermal conductivity measurements. The results of this structured test have validated the hypothesis, with heat flow values over 90 mW/m^2 recorded in several wells drilled. With several kilometres thickness of moderate conductivity sediments overlying the crystalline basement in this region, predicted temperatures at 5000 m are up to 300^{o}C in some areas.

Keywords: Australia, Heat Flow, Thermal Gradient, Thermal Conductivity, Torrens Hinge Zone, Adelaide Geosyncline, Delamerian Fold Belt, Gawler Craton, Curnamona Craton, Engineered Geothermal Systems, Geothermal Exploration.

Introduction

For an area to be prospective for geothermal power generation there must exist high average geothermal gradients that indicate high temperatures at depths which can be economically drilled. In addition the heat must be able to be economically exploited. This requires the existence of suitable reservoir rocks with either high natural porosity and permeability, or the conditions that allow permeability to be artificially enhanced. Favourable economics are also driven by location, and the cost of bringing the power to market competitively. Geothermal resources are non transportable, making it desirable that resources be located proximal to a market.

There is a strong economic incentive to locate Enhanced Geothermal Systems (EGS) resources closer to the transmission system in southern Australia. In summary, the following criteria are optimal for a resource to be viable for economic geothermal power generation:

- High average geothermal gradient
- Suitable reservoir conditions, or the ability to economically engineer them
- A proximal market for the generated power

The surface heat flow and broad thermal conductivity structure (and thus the temperature field) of most of Australia are currently poorly understood. Preliminary estimates (e.g. Somerville et al, 1994; Chopra & Holgate, 2005) provided broad approximations of the Australian continent temperature field, but suffered from a sparse geographic distribution of heat flow and thermal conductivity data. Over most of the continent, these data are not available at sufficient spatial resolution to allow temperature modelling to a high degree of confidence.

South Australian Heat Flow Anomaly

The South Australian Heat Flow Anomaly (SAHFA; Neumann et al., 2000) is a region defined loosely by lines of longitude in the central to eastern part of the state of South Australia, encompassing reported elevated heat flow values, but also a number of low values evident in two higher resolution studies.

Prior to 1989 less than 30 published heat flow values were available for the whole of South Australia with, in many cases, hundreds of kilometres between measurements (Matthews & Beardsmore, 2007). This dataset enabled only the most basic understanding of the SA heat flow regime, and required sweeping assumptions to be made about the nature of the heat flow between data points. Two subsequent studies by Houseman et al (1989) and Matthews & Beardsmore (2007) collected heat flow data to a much greater spatial resolution in parts of the SAHFA.

Houseman et al. (1989) revealed that heat flow is variable by a factor of more than two in the Olympic Dam area, and that the highest values correspond to the locations of the Olympic Dam and Acropolis ore bodies, which represent shallow crustal radioactive heat sources (Figure 1). It is estimated that the mantle-derived component of heat flow (q_r) in the eastern Gawler Craton "Olympic Domain" (Figure 1; Ferris et al 2002), is as low as 20–30 mW/m^2 (Neumann et al., 2000). Therefore, the bulk of the surface heat flow anomalies in the Olympic Dam area must be due to the crustal component (q_c) of heat flow.

Matthews & Beardsmore (2007) obtained a similar spread of results in the south eastern corner of South Australia to that of the Olympic Dam study, with heat flow varying by a factor of three over the region. Furthermore, the Padthaway Ridge, a shallow crustal geological feature containing Palaeozoic heat producing granitoids - corresponds to the zone of highest heat flow.

The Olympic Dam and eastern South Australia examples illustrate that the SAHFA is not a zone of

consistently high heat flow, and that it may be little different to the previously proposed Central Australian heat Flow Province (CAHFP e.g. McLaren et al., 2003). The concept is consistent with the idea that the Proterozoic CAHFP crust has a ubiquitous value of q_r, with broadly uniform tectonothermal history and heat production depth scale (Roy et al., 1968).

Geological Setting

The Torrens Hinge Zone

The study area is located within the Torrens Hinge Zone (THZ). Preiss (2005) described the THZ as a "zone of syn-sedimentary faulting and flexuring which separates the Gawler Craton [in the west]… from the rifted basins of the Adelaide Geosyncline to the east."

Preiss (2000) described the Adelaide Geosyncline (AG) as "a deeply subsident Neoproterozoic to Middle Cambrian basin complex…with a record of at least five major successive rift cycles." The Neoproterozoic portion of the geological time scale during which these sediments were deposited is locally known as the Adelaidean Period (Mawson & Sprigg, 1950), and the five rift cycles are broadly allocated to five sub-periods, named from oldest to youngest: Willouran, Torrensian, Sturtian, Marinoan and Cambrian (See Appendix 2).

The THZ is essentially a region of overlap between the Gawler Craton and Adelaide Geosyncline (Figure 1). Over the whole of the THZ, the Adelaidean and Cambrian sedimentary sequences are underlain at depths between 2,500 and 7,000m (de Vries et al, 2006), by the dominantly Mesoproterozoic Gawler Craton Olympic Domain (Ferris et al., 2002). In the south, the Palaeoproterozoic Barossa Complex (e.g. Preiss, 1993) also underlies the THZ.

To the east in the Adelaide Geosyncline proper, the sediments have been variably deformed by the Cambro-Ordovician Delamerian Orogeny (e.g. Preiss, 2000); with that region now part of the Delamerian Fold Belt (DFB). The competent nature of the Olympic Domain basement may have protected the THZ region from the full effects of the Delamerian Orogeny. Thus, while the Adelaide Geosyncline is now within the DFB, the THZ remains a "meridional belt of gentle folding" (Preiss, 2000; see Appendix 1).

Close to Port Augusta the earliest rifting phase of the Adelaide Geosyncline is marked by the extrusion of the mafic Beda Volcanics at around 827 Ma (Preiss, 2000).

Torrens Energy has undertaken two seismic surveys: one in the Parachilna Play, the other near Port Augusta, and the results (see Appendix 1) have confirmed the geometry of the Torrens Hinge Zone in the areas surveyed.

Thermal Conductivity in the THZ

As stated earlier, the Adelaide Geosyncline is a Neoproterozoic to Cambrian basin complex. The Geosyncline contains "a semi-continuous record of shallow-water sedimentation from the basal… rift succession with its associated basalts, through the shallow water sedimentary sequences of the Torrensian, the Sturtian, the Marinoan and the Ediacaran into the Early Cambrian…" (Foden et al, 2001).

Dominantly Proterozoic in age, the sediments of the Adelaide Geosyncline are generally more metamorphosed and less porous than most equivalent Phanerozoic sedimentary units, and this has previously led them to be overlooked as potential thermal insulators. Furthermore, the majority of the geographic distribution of these units is in the Adelaide Geosyncline proper, and as such the sediments there have undergone significant orogenic deformation and metamorphism during the Palaeozoic.

The vertical thermal conductivity of a rock can be greatly affected by factors such as the presence of tectonic fabrics or the tilting of bedding planes due to deformation (Clauser & Huenges, 1995; Beardsmore & Cull, 2001).

Thus the effects of deformation very likely reduce the thermal insulating ability of the sediments in the Adelaide Geosyncline region to the east of the THZ due to the effects of the Delamerian Orogeny. However, as discussed above, the THZ was largely shielded from the deformation associated with the Delamerian Orogeny and therefore also the majority of the negative effects of anisotropy on vertical thermal conductivity.

While sedimentary rocks are generally considered the best insulators, mafic volcanics also have low thermal conductivity. Thermal conductivity measurements on Holocene vesicular basalt rocks from South Australia were published by Matthews & Beardsmore (2007), with two values averaging 1.58 W/mK. A total of 19 samples were analysed from core samples of the mafic Neoproterozoic Beda Volcanics, located in the region immediately north of Port Augusta. The harmonic mean of thermal conductivities is 2.51 ± 0.26 W/mK (Musson & Alesci, 2007). The elevated thermal conductivity of these samples relative to their Holocene equivalents may be due to alteration and metamorphism plus the removal of most of the original vesicular porosity. However, the measured values indicates that the Beda Volcanics are still good insulators.

Structured Heat Flow Measurement Programme

As with other potential fields, the amplitude and wavelength of surface heat flow and temperature distribution are directly related to the magnitude and depth of the heat source. An intra-crustal heat

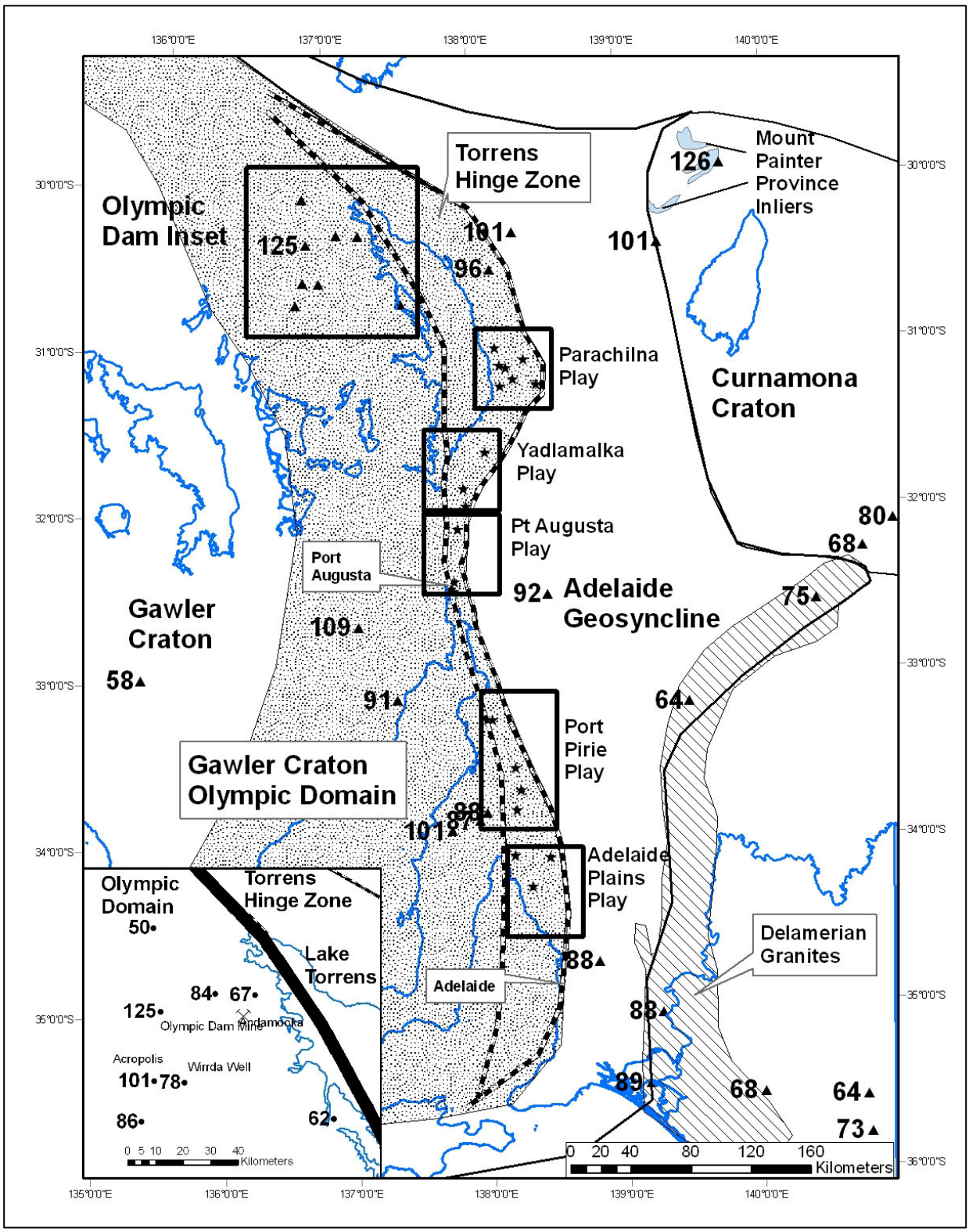

Figure 1: Key geological elements of central South Australia. The Torrens Hinge Zone is a narrow elongate transition zone between the Eastern Gawler Craton and the Adelaide Geosyncline. Heat Flow values are too widely spaced to gauge the true nature of the SA Heat Flow Anomaly. The inset shows values measured by Houseman et al (1989). Key: Triangles = Historic published heat flow values for the region; Stars = Torrens Energy wells. See figures 2a & 2b for heat flow results for Torrens Energy wells.

source should produce a surface heat flow anomaly with a wavelength in a similar order of magnitude as the depth of burial (e.g. Matthews & Beardsmore, 2006). Due to the status of the heat flow data set in Australia, with most values spaced hundreds of kilometres apart, it has been previously impossible to adequately delineate crustal heat flow anomalies.

The depth to crystalline basement in the THZ is estimated to be between 2.5 and 7 km depth (de Vries et al 2006). An effective test of this hypothesis therefore required heat flow data to be collected at a maximum spacing of about 10–15 km to facilitate reasonable accuracy for mapping of heat flow distribution (although this does not necessarily allow for local variations in lithology or rock thermal conductivity which can also contribute variation to surface heat flow distribution).

To test the hypothesis that the THZ contains areas of high heat flow and therefore likely high average geothermal gradients, a heat flow drilling campaign was designed in the Torrens Energy Geothermal Exploration Licences (GELs). Figures 2a and 2b show the locations of heat flow wells.

Data Collection

Each well was designed to reach a depth where the rock is competent enough to be fully cored for around 200m of continuous downhole depth. This involved rotary mud drilling through the mostly unconsolidated Cainozoic clays and sands, found to be up to 400 m deep, followed by diamond coring through the underlying Cambrian and Neoproterozoic sedimentary sequences.

Thermal Gradient Data

A temperature log from within each heat flow well was taken by measuring temperature at discrete depth intervals (0.05 - 2.00 m) from the surface to the bottom of each well. Sufficient time (at least five weeks) was allowed following completion of drilling activities to ensure thermal equilibration (Beardsmore & Cull, 2001). Temperatures were measured to a precision of ±0.001◦C and an absolute accuracy of ±0.01◦C using truck mounted logging tools either from Torrens Energy's in-house logging equipment or contracted from the South Australian Government Department of Water Land Biodiversity and Conservation (DWLBC).

Geothermal gradient varies with lithology. Heat flow remains constant across a geological boundary, and there is an inverse relationship between geothermal gradient and thermal conductivity.

Thermal Conductivity Data

The vast majority of the purpose-drilled heat flow wells contained at least 200m of continuous core section. To allow representative thermal conductivity profiles to be established, core samples were taken every seven to 14 metres on average throughout the cored section.

Up to three specimens were prepared and measured from each sample using a steady state divided bar apparatus.

Heat Flow Estimation

Heat flow can only be modelled over intervals with coincident thermal gradient and thermal conductivity data.

The following methodology was adopted to reach a heat flow determination for each well.

Three assumptions were made. These were that:

- Each conductivity value is representative of the rocks from which the sample was extracted.
- The boundary between one conductivity value and the next is the midpoint between measurement points.
- A dominantly conductive regime exists.

The thermal conductivity profile for each well was then used to model a theoretical temperature profile that would result from a given magnitude of heat flow in a conductive heat flow regime. The observed temperature log was plotted against this theoretical profile, and the magnitude of heat flow was adjusted until the modelled temperature profile best matched the logged temperatures.

Results

In total, 18 purpose-drilled wells and four existing wells returned 18 new heat flow values in the Torrens Hinge Zone, with two results pending and two inconclusive results, providing heat flow coverage for an area of approximately 6,500 km2 at a spatial resolution suitable for investigating heat sources in the basement.

The results of the heat flow study are presented in Table 1 and Figures 2a & 2b, and formed the major constraint for the hypothesis test.

The results of this structured test have validated the hypothesis, with heat flow values over 90 mW/m2 recorded in several of the wells drilled.

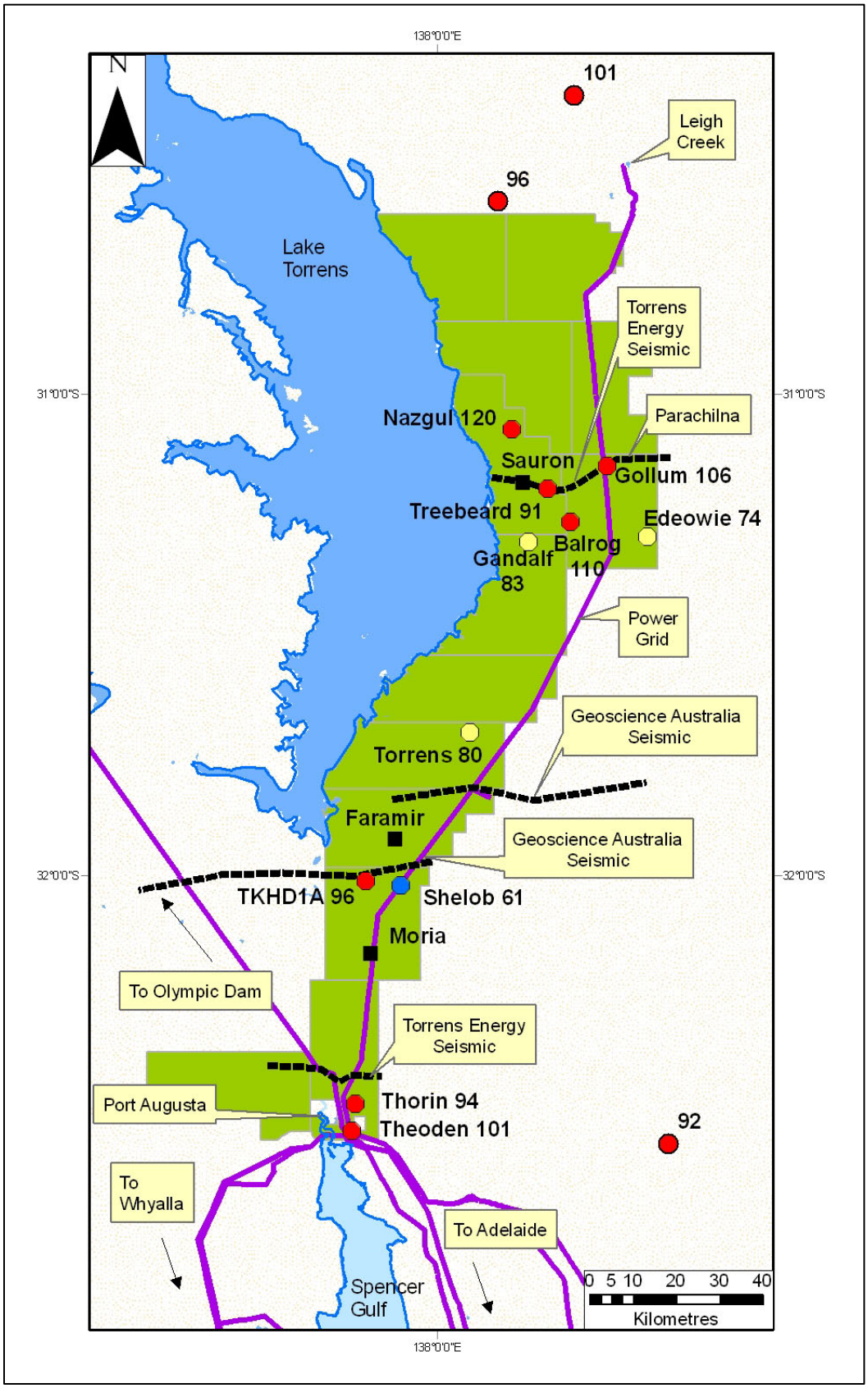

Figure 2a: Torrens Energy's northern tenement areas. The Parachilna Play was the first drilled by the Company, with the Port Augusta region drilled shortly after. Historical heat flow values are unnamed but labelled, with Torrens Energy heat flow wells named and heat flow values labelled. Key to all wells: Blue = < 70 mW/m^2; Yellow = 70 - 89 mW/m^2; Red = ≥ 90 mW/m^2. Black squares represent wells which are either awaiting results or have returned inconclusive results. See Table 1 for values.

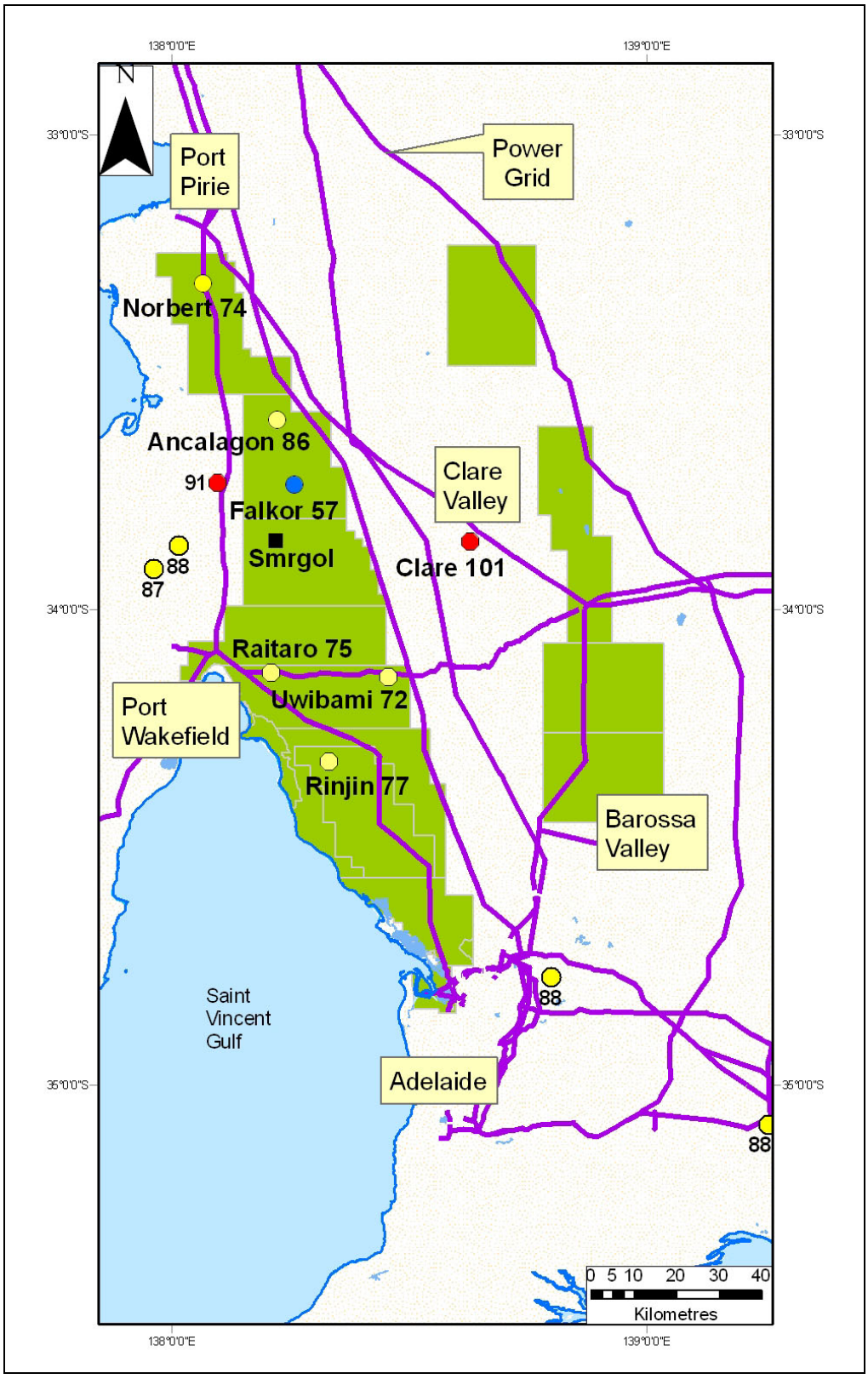

Figure 2b: Torrens Energy's southern tenement areas. The tenements are located in prime infrastructure position, stretching right to inside the city limits of Adelaide. Historical heat flow values are unnamed but labelled, with Torrens Energy heat flow wells named and heat flows labelled. Key to all wells: Blue = < 70 mW/m^2; Yellow = 70 - 89 mW/m^2; Red = ≥ 90 mW/m^2. Black squares represent wells which are either awaiting results or have returned inconclusive results. See Table 1 for values.

Discussion

Torrens Energy used the heat flow and thermal conductivity data to create temperature/depth models for several of the regions that were drilled. The primary tool utilized to estimate temperature was a 3D temperature inversion software module developed through collaboration between Torrens Energy and Hot Dry Rocks Pty Ltd.

Inputs into the software included:

- The 3D geological model of the region in question
- Extensive thermal conductivity measurements undertaken, plus the assignment of textbook values where necessary, with thermal conductivity values assigned to geological units in proportions based on published and interpreted geological data.
- Published data about internal heat generation in the rock column.
- Precision surface temperature and surface heat flow measurements.

The temperature modelling software operates on the principle of 'inversion'. Known information about surface temperature and surface heat flow is entered into the software module. The software then computes in three dimensions the simplest distribution of temperature that fits the observations, while respecting the laws of conductive heat transfer and the thermal properties of the geological strata. The temperature dependence of thermal conductivity is also taken into account.

Torrens Energy derived 3D temperature models in this manner for three of its projects – the Parachilna, Port Augusta and Yadlamalka Plays (Figure 1).

Well	Heat Flow (mW/m^2)
Edeowie 1	74
Gollum 1	106
Sauron 1	Inconclusive
Nazgul 1	120
Balrog 1	110
Gandalf 1	83*
Treebeard 1A	91**
Torrens 1	80
TKHD1A	96
Shelob 1	61
Moria 1	Inconclusive
Theoden 2	101
Thorin 1	94
Rinjin 1	77
Uwibami 1	72
Raitaro 1	75
Norbert 1	74
Ancalagon 1	86
Falkor 1	57
Smrgol 1	Pending
Faramir 2	Pending
CLR 105 (Clare)	101

Table 1.

Surface heat flow measured in wells from this study.

**Gandalf 1 displayed a departure from a simple conductive heat flow inversion model. The best fit conductive model can be found by applying a heat flow of 116 mW/m^2 in the interval 375-433 m depth, and 83 mW/m^2 in the interval 433-545 m.*

***Treebeard 1A heat flow value is preliminary*

Conclusion

It was hypothesized from geological and conductive heat flow principles that the THZ is likely to be a region of high average geothermal gradients and thus prospective for EGS geothermal energy.

The heat flow drilling campaign designed to test the idea returned results that have validated this hypothesis.

With several kilometres' thickness of moderate conductivity sediments overlying the crystalline Eastern Gawler Craton basement in this region, plus its proximity to existing power infrastructure, the Torrens Hinge Zone is now considered prospective for economic EGS development.

Acknowledgements

The authors wish to acknowledge several people. Dr Graeme Beardsmore from Hot Dry Rocks Pty Ltd and Monash University provided guidance on the measurement and modelling of thermal gradient, thermal conductivity and heat flow in the study. Hot Dry Rocks, Alex Musson, Andrew Alesci and Lyndon Parham carried out thermal conductivity measurements on existing rock samples using Torrens Energy's divided bar apparatus, housed in a laboratory at the University of Adelaide. Prof. Mike Sandiford from the University of Melbourne imparted valuable knowledge on the nature and distribution of heat flow and temperature in Australian Proterozoic terranes. Last but not least, the staff and directors of Torrens Energy Limited (especially Christine Sealing, John Canaris and Dennis Gee) are thanked for collaborating to facilitate the heat flow study.

References

Somerville, M., Wyborn, D., Chopra, P., Rahman, S., Estrella, D. and Van der Meulen, T., 1994, Hot Dry Rocks Feasibility Study, Energy Research and Development Corporation, Report 243, 133pp.

Beardsmore, G. R., and Cull, J. P., 2001 Crustal heat flow; a guide to measurement and modelling. Cambridge University Press 324pp.

Chopra, P.N. & Holgate F. 2005 A GIS analysis of temperature in the Australian Crust. Proceedings of the World Geothermal Congress, 2005, Antalya, Turkey 24-29 April 2005, 7 pp.

Clauser, C. & Huenges, E., 1995 Thermal Conductivity of Rocks and Minerals. In: T. J. Ahrens (ed), Rock Physics and Phase Relations - a Handbook of Physical Constants, AGU Reference Shelf, Vol. 3, 105-126, American Geophysical Union, Washington.

Cull, J. P., 1982 An appraisal of Australian heat-flow data. BMR Journal of Australian Geology and Geophysics 7, 11–21.

Dalgarno, C. R. and Johnson, J. E., 1966 PARACHILNA map sheet. 1st Edition. South Australia Geological Survey Geological Atlas 1:250,000 Series, sheet SH 54-13.

de Vries, S., Fry, N. & Pryer, L. 2006 OZ SEEBASE Proterozoic Basins Study. Report to Geoscience Australia by FrOG Tech Pty Ltd.

Ferris, G. M, Schwarz, M. P. and Heithersay, P., 2002 The Geological Framework, Distribution and Controls of Fe-Oxide Cu-Au Mineralisation in the Gawler Craton, South Australia. Part I - Geological and Tectonic Framework. In - Porter, T.M. (Ed), 2002 - Hydrothermal Iron Oxide Copper-Gold & Related Deposits: A Global Perspective, volume 2; PGC Publishing, Adelaide, 9-31.

Foden, J., Barovich , K., Jane, M. & O'Halloran, G. 2001Sr-isotopic evidence for Late Neoproterozoic rifting in the Adelaide Geosyncline at 586 Ma: implications for a Cu ore forming fluid flux. Precambrian Research 106, 291–308.

Houseman, G. A., Cull, J. P., Muir, P. M., & Paterson, H. L., 1989 Geothermal signatures and uranium ore deposits on the Stuart Shelf of South Australia: Geophysics 54, 158–170.

McLaren, S., Sandiford, M., Hand, M., Neumann, N., Wyborn, L., & Bastrakova, I., 2003 The hot southern continent, heat flow and heat production in Australian Proterozoic terranes. Geological Society of Australia, Special Publication 22, 151–161.

Matthews, C. G. & Beardsmore, G. R., 2006 Heat flow: A uranium exploration and modelling tool? MESA Journal 41 Primary Industries & Resources South Australia, 2006, 8-10.

Matthews, C. G. & Beardsmore, G. R., 2007 New heat flow data from south-eastern South Australia. Exploration Geophysics, 38, 260-269.

Mawson, D. & Sprigg, R. C., 1950 Subdivision of the Adelaide System. Australian Journal of Science 13, 69–72.

Musson, A. & Alesci, A., 2007 Thermal conductivity, magnetic susceptibility and specific gravity measurements of core samples of the Adelaide 'Geosyncline' cover sequence. Unpublished report prepared for Torrens Energy Limited, 32pp.

Neumann, N., Sandiford, M. and Foden, J., 2000, Regional geochemistry and continental heat flow; implications for the origin of the South Australian heat flow anomaly. Earth and Planetary Science Letters, 183 (1/2), 107–120.

Preiss, W.V., 1993 Basement inliers of the Mount Lofty Ranges. In: Drexel J. F. Preiss W. V. & Parker A. J. eds. The Geology of South Australia, Geological Survey of South Australia Bulletin 54(1), 51 – 105.

Preiss, W.V., 2000 The Adelaide Geosyncline of South Australia and its significance in Neoproterozoic continental reconstruction. Precambrian Research, 100, 21–63.

Preiss, W. V., 2005 Mineral Explorers Guide, Primary Industries and Resources South Australia DVD Publication.

Roy, R. F., Blackwell, D. D., & Birch, F. Heat generation of plutonic rocks and continental heat-flow provinces. Earth & Planetary Science Letters, 5, 1-12, 1968.

Appendix 1: Seismic Surveys and Results.

Parachilna Seismic Survey, completed January 2009

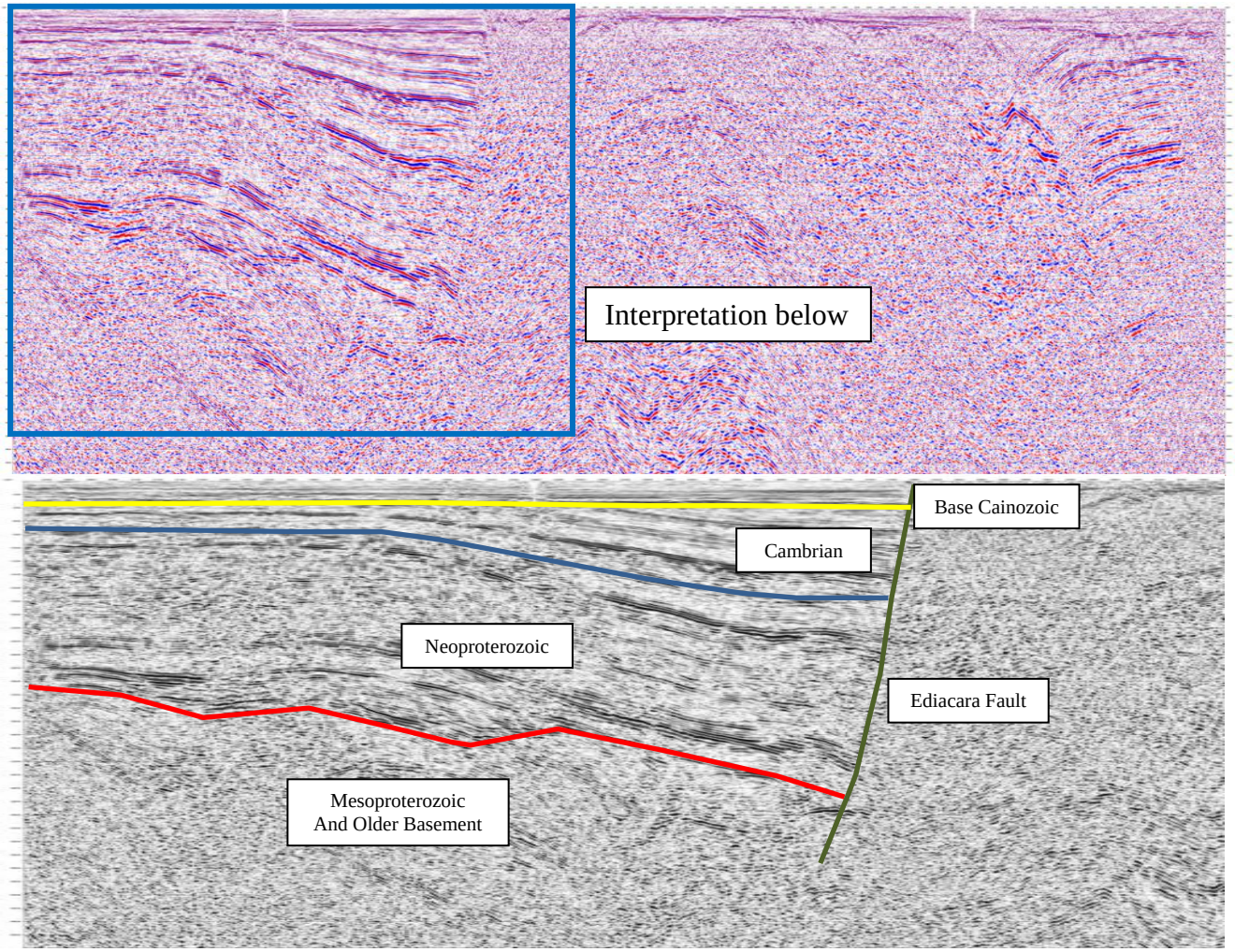

Port Augusta Seismic Survey, completed May 2009

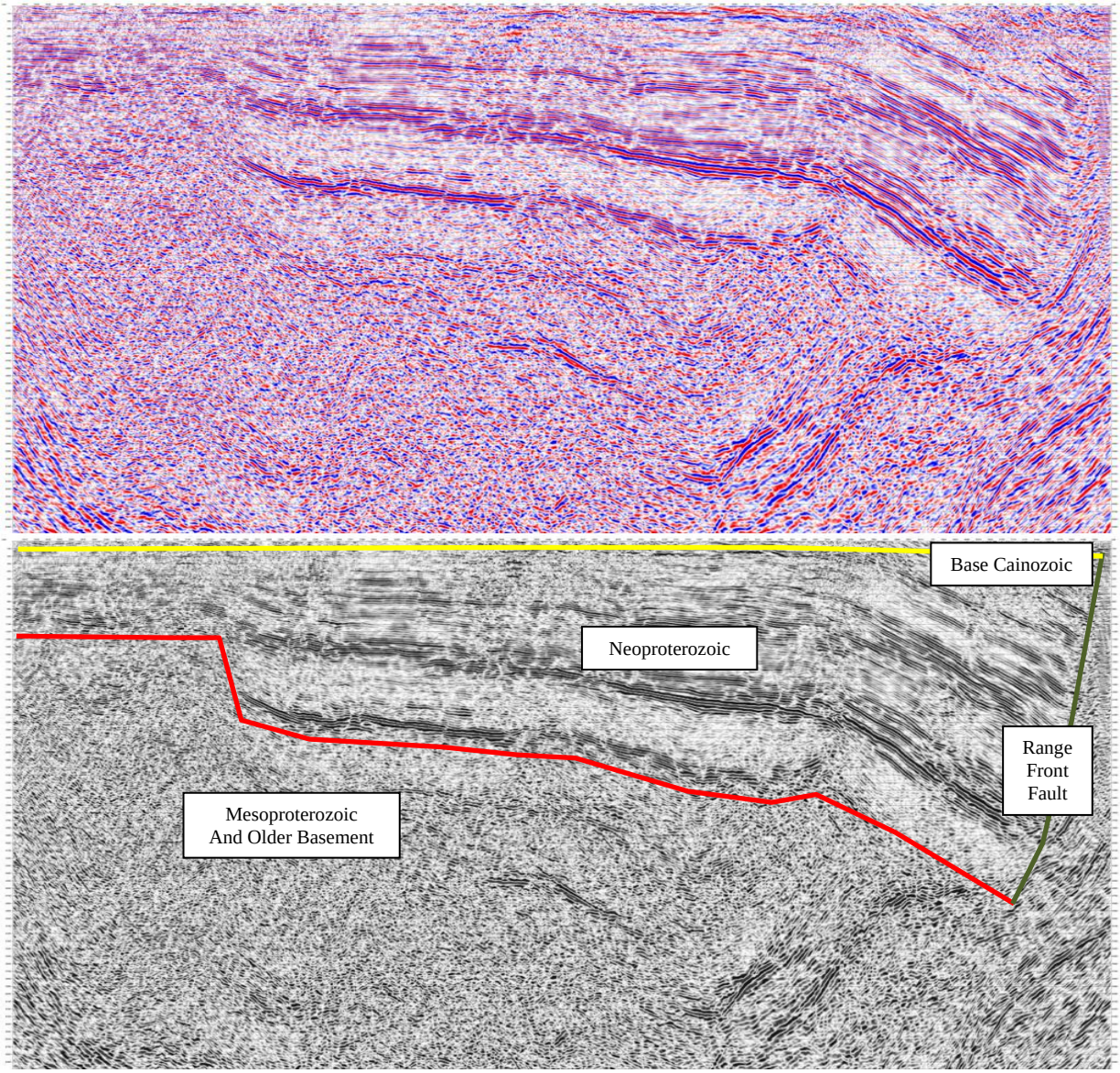

Appendix 2: Generalised Stratigraphic Column for the Torrens Hinge Zone

Torrens Hinge Zone General Stratigraphy		
Age	**Group**	**Common Units Present**
Pleistocene/Holocene	Pirie-Torrens Basin	Undifferentiated Clays and Gravels
Oligocene-Miocene	Pirie-Torrens Basin	Neuroodla Formation
Eocene	Pirie-Torrens Basin	Cotabena Formation
Middle Cambrian	Lake Frome Group	Pantapinna Formation Balcoracana Formation Moodlatana Formation
Middle Cambrian	Unnamed Group	Wirrealpa Limestone Billy Creek Formation
Early Cambrian	Hawker Group	Wilkawillina Limestone Parachilna Formation
Neoproterozoic (Adelaidean, Late Marinoan)	Wilpena Group Pound Subgroup	Rawnsley Quartzite Bonney Sandstone
Neoproterozoic (Adelaidean, Late Marinoan)	Wilpena Group	Wonoka Formation Bunyeroo Formation
Neoproterozoic (Adelaidean, Late Marinoan)	Wilpena Group Sandison Subgroup	ABC Quartzite (incl. Corraberra Sandstone) Brachina Formation (incl. Tregolana Shale) Nuccaleena Formation
Neoproterozoic (Adelaidean, Early Marinoan)	Umberatana Group Yerelina Subgroup	Elatina Formation/Whyalla Sandstone
Neoproterozoic (Adelaidean, Early Marinoan)	Umberatana Group Upalinna Subgroup	Trezona Formation Wilmington Formation Angepena Formation Etina Formation
Neoproterozoic (Adelaidean, Late Sturtian)	Umberatana Group Nepouie Subgroup	Brighton Limestone Tapley Hill Formation (incl. Woocalla Dolomite Member)
Neoproterozoic (Adelaidean, Early Sturtian)	Umberatana Group Yudnamutana Subgroup	Wilyerpa Formation Appila Tillite Other equivalent Sturtian Glacials
Neoproterozoic (Adelaidean, Late Torrensian)	Burra Group Unnamed Subgroup	Saddleworth Formation
Neoproterozoic (Adelaidean, Middle Torrensian)	Burra Group Mundiallo Subgroup	Skillogalee Dolomite
Neoproterozoic (Adelaidean, Early Torrensian)	Burra Group Emeroo Subgroup	Rhynie Sandstone
Neoproterozoic (Adelaidean, Willouran)		Beda Volcanics Backy Point Formation Callanna Group
Mesoproterozoic Eastern Gawler Craton		Pandurra Formation Gawler Range Volcanics Hiltaba Suite Granitoids
Palaeoproterozoic		Barossa Complex

Establishing Hot Rock Exploration Models: From Synthetic Thermal Modelling to the Cooper Basin 3D Geological Map

Tony Meixner[1*], Stephen Johnston[1], Alison Kirkby[1], Helen Gibson[2], Ray Seikel[2], Kurt Stüwe[3], Des FitzGerald[2], Nick Horspool[1], Richard Lane[1] and Anthony Budd[1]
1 Geoscience Australia. GPO Box 378, Canberra, ACT, 2601
2Intrepid Geophysics, Unit 2, 1 Male St, Brighton VIC 3186
3Universitaet Graz, Heinrichstr. 26 A-8010, Austria
* corresponding author Tony.Meixner@ga.gov.au

A large number of exploration models for Hot Rock geothermal energy plays in Australia are based on high-heat producing granites (HHPG) in combination with overlying low-conductivity sedimentary rocks providing the insulator necessary to accumulate elevated temperatures at unusually shallow (therefore accessible) depths. Unknowns in this style of geothermal play include the composition and geometry of the HHPG and its thermal properties and the thickness and thermal properties of the overlying sediments. A series of 3D geological models have been constructed to investigate the range of geometries and compositions that may give rise to prospective Hot Rock geothermal energy plays.

A 3D geological map of the Cooper Basin region, which contains known HHPG beneath thick sedimentary sequences, and the Millungerra Basin region east of the Mt Isa Inlier, have been constructed from gravity inversions constrained by geological data. The inversion models delineate regions of low density within the basement that are inferred to be granitic bodies. Thermal forward modelling was carried out using GeoModeller software by assigning measured and estimated thermal properties to the mapped lithologies.

An enhancement of the GeoModeller software allows input of thermal properties to be specified as distribution functions. Multiple thermal simulations were used to estimate the in-situ heat resource, thus reducing the exploration risk. The two thermal modelling techniques can be used as a predictive tool in regions where little or no temperature and geological data are available.

A series of synthetic 3D maps were constructed using different granite geometries beneath varying thicknesses of cover sediments. The gravity, heat flow and vertical temperature gradients were forward modelled using typical density contrasts, heat production rates and thermal conductivities. Geothermal explorers in the Cooper Basin region can now use the results of the density modelling to identify the geometries and depth of burial of potential HHPG bodies, and also use the results of the thermal modelling to predict heat flows and temperature gradients associated with the bodies.

Keywords: 3D map, thermal modelling, stochastic, Cooper Basin, high-heat producing granites, inversion modelling

Introduction

Hot Rock geothermal exploration methods used in Australia are significantly different to those used for conventional geothermal plays elsewhere in the world. Hot Rock geothermal energy plays essentially comprise a heat source and an insulating layer. In Australia, high-heat producing granites (HHPG) are often the presumed heat source, while low-conductivity sedimentary rocks provide the insulator necessary to create an accumulation of heat and elevated temperatures. Other elements of a hot rock geothermal play such as porosity, permeability and fracture-networking are also crucial, though these can sometimes be artificially enhanced by hydrofracturing or chemical treatment to achieve the required permeability.

There are two fundamental unknowns surrounding the minimum requirements to produce an Australian style Hot Rock geothermal play. The first unknown is the amount of heat production required, which is linked to the concentration of radiogenic elements, and the volume and geometry of HHPGs. The second unknown is the thermal insulation required from the overlying basin sediments, which is a function of the thickness and thermal conductivity of the overlying sediments above a given granite.

To investigate the range of geometries and compositions that may give rise to Hot Rock geothermal systems, two linked processes have been undertaken in this study. Firstly, thermal modelling has been conducted using a 3D geological map from a well-constrained area. Secondly, a series of synthetic models have been constructed for 3D temperature and heat flow modelling.

Cooper Basin 3D geological map

A summary of the geology of the Cooper Basin region is provided in Meixner and Holgate (2009a,b). In brief, significant volumes of Big Lake Suite (BLS) granodiorite intrude basement (Figure 1). Thick sedimentary sequences in the Cooper and overlying Eromanga Basins provide a thermal blanketing effect for these anomalously high-heat producing BLS intrusions, resulting in temperatures up to 270° C at depths less than 5 km. The region, which straddles the

Queensland/South Australia border, is coincident with a prominent geothermal anomaly (Cull and Denham, 1979; Cull and Conley, 1983; Somerville et al., 1994) (Figure 2). The region also forms part of a broad area of anomalously high heat flow which is attributed to Proterozoic basement enriched in radiogenic elements (Sass and Lachenbruch, 1979; McLaren et al., 2003). Australia's first commercial Enhanced Geothermal System (EGS) is under development at Habanero-1 and Habanero-3 near Innamincka (Figure 1).

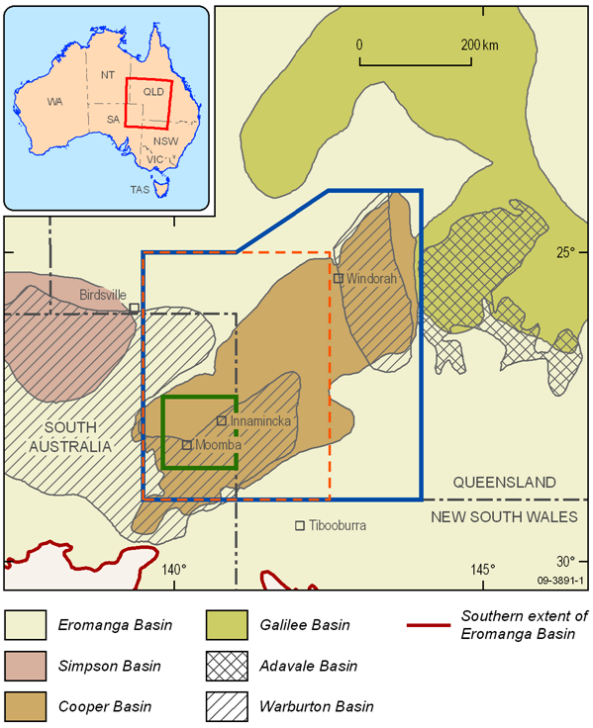

Figure 1. Location of the Cooper Basin region, showing the spatial extents of the stacked Warburton, Cooper and Eromanga Basins. The red dashed box indicates the extent of the original 3D map, the blue outline indicates the extent of the extended 3D map, and the green box indicates the extent of the test-bed thermal model.

A 3D geological map for the Cooper Basin region was constructed as part of a previous study (Meixner and Holgate, 2009a,b). The map, which covered an area of 300 by 450 km (Figure 1), was based in part on 3D inversions of Bouguer gravity data using the method of Li and Oldenburg (1998). The geometries and densities of the Eromanga and Cooper Basin, derived from well and seismic data, as well as gravity 'worms' (Archibald et al., 1999) were used to constrain the inversions. The 3D map delineates regions of low density within the basement of the Cooper/Eromanga Basins that are inferred to be granitic bodies. This interpretation is supported by spatial correlations between the modelled bodies and known granite occurrences from drill holes in the area. Figure 3 shows a density section through the inversion model. The densities of the Eromanga/Cooper Basin sediments and the granitic bodies were constrained to narrow ranges based on measured and inferred values, while the density of the basement was left unconstrained. A perspective view of the interpreted sub-sediment granitic bodies in the 3D map is shown in Figure 4.

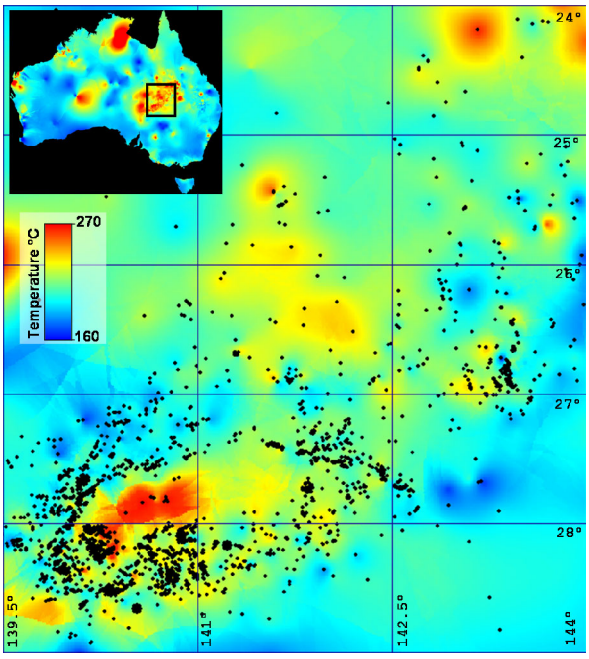

Figure 2: Predicted temperature map at 5 km for the Cooper Basin region, based on bottom hole temperatures, after Chopra and Holgate (2005). Well locations are shown.

For the present study, the 3D map was extended 150 km to the east and 100 km to the north in order to cover the entire Cooper Basin region (Figure 1). In addition, the map includes more detailed subdivisions for the Eromanga (Van Der Wielen, in prep) and Cooper Basin stratigraphies, based on data from ~1000 wells. The greater stratigraphic detail allowed for enhanced geological constraint during the gravity inversion modelling, as well as significantly better control on the assignment of thermal conductivities to individual geology units during the thermal modelling process. Delineation of the sub-sediment granitic bodies, for this extended version of the 3D map, was carried out using the methodology described in Meixner and Holgate (2009a,b). The original 3D inversions used single density values for the Eromanga and Cooper basins that were derived from a refraction seismic survey in the study area (Collins and Lock, 1990). The present study used an averaged density value for each individual stratigraphic unit derived from well density logs. The use of enhanced density constraints for the sedimentary section enhances the credibility of the density variations derived for the basement unit, and therefore provides a more accurate delineation of interpreted granitic bodies.

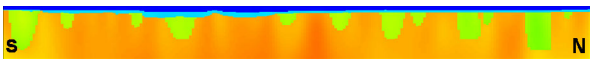

Figure 3: North-south density section through the litho-constrained gravity inversion model. Eromanga Basin sediments (dark blue: 2.3 +/- 0.2 g cm-3), Cooper Basin sediments (light blue: 2.5 +/- 0.2 g cm-3) and the granitic bodies (green: 2.6 +/- 0.2 g cm-3) were constrained to a narrow density range, while the basement (yellow-red: 2.65-2.75 g cm-3) was left unconstrained. The section is 450 km long and 20 km deep.

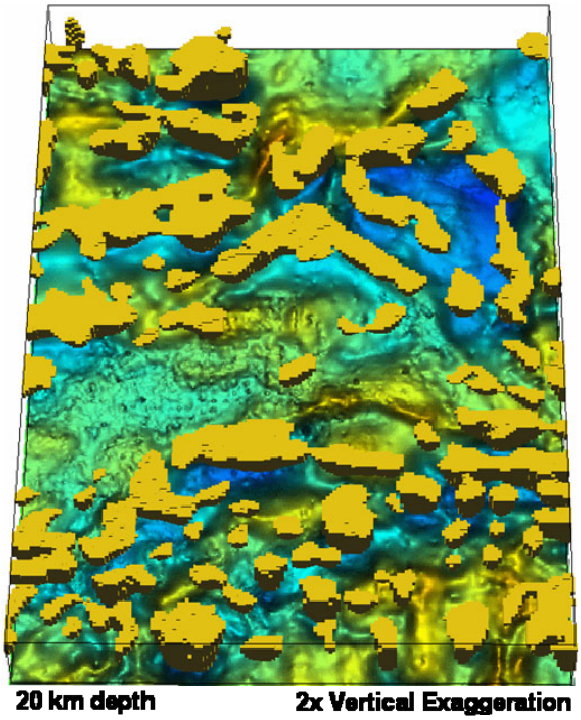

Figure 4: Cooper Basin region 3D map viewed obliquely from the south showing the inferred sub-sediment granitic bodies, overlying an image of gravity data.

Cooper Basin thermal forward modelling

A region 188 by 144 km, by 16 km in depth was extracted from the initial Cooper Basin 3D map and used as a test region (Figure 1) for modelling the temperature, heat flow and geothermal gradients. The test region was populated with thermal properties (heat production rates and thermal conductivities) for each lithology and boundary conditions were approximated (mean surface temperature) or assumed (Neuman-type side boundaries, constant basal heat flow). Initial heat production rates for the granites and sediments and thermal conductivities for the sediments were sourced from published literature (Beardsmore, 2004; Middleton, 1979).

Temperature predictions were generated on a discretised version of the model within GeoModeller[1] using the method described by Seikel et al. (2009). Temperatures were solved by explicit finite difference approximation using a Gauss-Seidel iterative scheme implemented until either: a) the sum of the residual errors fall below a specified threshold; or b) a specified maximum number of iterations were reached – whichever occurred first. The thermal quantities computed were: temperature, vertical heat flow, vertical temperature gradient and total horizontal temperature gradient.

Results of the test-bed thermal modelling were compared to 21 corrected bottom hole temperature (BHT) measurements (Chopra and Holgate, 2005), as well as 30 modelled 1D heat flow measurements (Beardsmore, 2004) from wells in the test area. A number of thermal models were generated by minimising the temperature differences between the BHTs and the modelled temperatures, as well as minimising the difference between the measured and modelled heat flow measurements. Vertical temperature sections through the final test-bed thermal model are shown in Figure 5. The sections show a clear rise in temperature at shallow depth in the north of the model that is coincident with a HHPG intersected by wells.

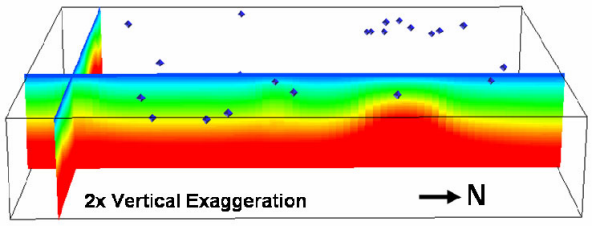

Figure 5: Vertical sections through the 3D temperature model showing the locations of the BHT data (dark blue). Modelled temperatures range from 27° (blue) to 390° (red).

The thermal modelling has provided constraints on the possible thermal conductivity and heat production properties of the basement, as well as a predicted value of mean heat flow into the base of the model. This information, together with additional thermal conductivity measurements from drill core, were then used in a thermal model of the extended 3D map to predict the temperature, thermal gradient and heat flow in regions where little or no temperature data exists.

Cooper Basin stochastic thermal modelling

In order to explore the uncertainty of estimates of heat resources within the Cooper Basin region, we have used an approach based on the generation of multiple models. These models will reflect the full population of viable alternatives, consistent with the expected thermal property probability distribution functions (for thermal conductivity and heat production rate) – but with fixed geological geometries.

The initial voxet model of preferred geology (discretised from the continuous geology model) was generated in GeoModeller. From this initial voxet model, multiple models containing the plausible ranges of varying thermal properties

were produced. Following forward 3D temperature calculations, the family of voxet-model outcomes (3D results for temperature, heat flow and geothermal gradient) were then interrogated by statistical methods to yield the probability estimates of the in-situ heat resource for the Cooper Basin.

To implement this approach we are developing a new solver strategy for the steady-state heat equation that can be scaled to the larger volumes of rock in this study. A fast solver for the inhomogeneous heat equation in free space, following the time evolution of the solution is being developed using Fourier domain techniques. The method we are developing is up to 1000 times faster than the commonly used finite difference and finite element methods. It can also solve much larger problems. This simulation work builds on the work of Li and Greengard, (2007) and Osterholt et al. (2009).

The Millungera Basin 3D geological map

The previously unknown Millungera Basin (Korsch and Huston, 2009), to the east of the Mt Isa Inlier was identified in the 2006 Mt Isa (Hutton, et al., 2009) and 2007 North Queensland seismic surveys (Korsch et al., 2009). Geological relationships suggest that the age of the basin, which underlies the Carpentaria-Eromanga basins, lies between the Mesoproterozoic and Early Mesozoic. Non-reflective zones below the base of the Millungera Basin that are interpreted as granite, also coincide with gravity lows. Based on this interpretation, the region may host potential Hot Rock geothermal plays given the high-heat producing nature of nearby granites of the Williams Batholith (Hutton, et al., 2009) and the thick sequences, up to approximately 3900 m, of potentially insulating Millungera sediments.

A 3D geological map (192 by 315 km, 20 km depth extent) is currently being constructed over the Millungera Basin using similar methodologies to the Cooper Basin study. This 3D map will form the basis for thermal modelling in order to gain a better understanding of the thermal properties of a region that contains no heat flow measurements and few down-hole temperature measurements.

Synthetic modelling

A key dataset for geothermal energy exploration in Australia is the gravity anomaly map of Australia (Murray et al., 1997). Buried granites typically exhibit a negative gravity anomaly in relation to the crystalline basement they intrude, due to their lower relative density. A total of 648 unique granite models have been produced, based on differing diameter circular granites (5 km, 10 km, 20 km, 30 km, 50 km and 70 km), with different depth extents (2, 4, 6, 8, 10 and 12 km) embedded in basement. These models also include different depths of burial of the granite/basement beneath sediments (varying from 1000 m to 6000 m, in 1000 m increments) as well as three different density contrasts between the granites and basement (Figure 6).

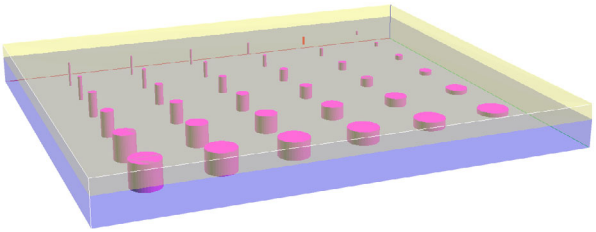

Figure 6: Synthetic model showing a series of granites embedded in basement and overlain by 6 km of sediments. Granite diameters range from 5 to 70 km. Granite thicknesses range from 2 to 12 km.

Forward modelling the gravity signatures from this wide range of starting models produces a comprehensive range of gravity anomalies. A geothermal explorer, interested in identifying unknown potential HHPG beneath a sedimentary basin, will be able use gravity anomaly maps to identify gravity lows and then match their observed anomaly with a likely style of modelled anomaly (and associated geometry, depth of burial and density contrast).

Due to the non-uniqueness of interpretations of gravity data, the explorer may not be able to pin-point a single model because a number of differing geometries and density contrasts could produce a similar gravity anomaly. The explorer will, however, have a range of potential granite geometries for use in predicting temperature and heat flow. As more geological knowledge is gained about a particular region, such as the thickness of sediments and/or density contrast between the granite and basement, the number of modelled granite geometries that match the observed data will become restricted.

Once potential granite geometries have been identified, the 3D thermal models can be used to predict surface heat flow and vertical temperature gradient. For a selected granite geometry the explorer can then choose from a range of inputs (five different heat production rates for the granites and five different thermal conductivities for the overlying sediments) to predict the likely heat flow and thermal gradient over the granite body. In all, a total of 5400 unique geothermal scenarios were produced from 216 unique granite/sediment geometries. The gravity and thermal anomaly are displayed in graph form in order to condense the results so they are easier to interpret and use.

Summary

Case study 3D maps and thermal models, such as the Cooper and Millungera Basin studies, incorporate all available geological knowledge into a 3D map. Often little or no information is known

about the basement composition beneath sedimentary basins. Inversion of gravity data is, therefore, a valuable tool for identifying regions of low density within the basement that are potentially due to granitic bodies, which in turn may be acting as a viable heat source for a hot rock geothermal energy play.

Thermal forward modelling and stochastic thermal modelling of 3D maps, which contain both potential heat sources and thermally insulating cover, can be used as a predictive tool to identify the locations of potential geothermal plays. Where case study models do not exist, synthetic modelling provides a systematic approach to the interpretation of exploration datasets.

References

[1]GeoModeller is a commercially available software package and has been produced by Intrepid Geophysics and Bureau de Recherches Géologiques et Minières (BRGM). www.geomodeller.com.

Archibald, N., Gow, P., and Boschetti, F., 1999, Multiscale edge analysis of potential field data: Explor. Geophys., 30, p. 38-44.

Beardsmore, G.R., 2004, Thermal modelling of the Hot Dry Rock geothermal resource beneath GEL99 in the Cooper Basin, South Australia: Sydney: 17th Aust. Soc. Explor. Geophys. Conference. Extended Abstracts.

Chopra, P., and Holgate, F., 2005, A GIS Analysis of Temperature in the Australian Crust: World Geothermal Congress, Turkey, 24-29 April 2005, Abstracts.

Collins, C.D.N., and Lock, J., 1990, Velocity variations within the upper crustal basement of the central Eromanga Basin: Bureau of Mineral Resources, Geology and Geophysics, Canberra. Bulletin, 232, p. 177-188.

Cull, J.P., and Denham, D., 1979, Regional variations in Australian heat flow: Bureau of Mineral Resources, Journal of Australian Geology and Geophysics 4, p. 1-13.

Cull, J.P., and Conley, D., 1983, Geothermal gradients and heat flow in Australian sedimentary basins: Bureau of Mineral Resources, Journal of Australian Geology and Geophysics 8, p. 329-337.

Hutton, L.J., Gibson, G.M., Korsch, R.J., Withnall, I.W., Henson, P.A., Costelloe, R.D., Holzshuh, J., Huston, D.L., Jones, L.E.A., Maher, J.L., Nakamura, A., Nicoll, M.G., Roy, I., Saygin, I., Murphys, F.B., and Jupp, B., 2009 Geological interpretation of the 2006 Mt Isa Seismic Survey: In: Camuti, K., and Young, D. eds., Northern Queensland Exploration & Mining 2009 and North Queensland Seismic and MT Workshop: Extended Abstracts. Australian Institute of Geoscientists Bulletin No. 49, p. 137-142.

Korsch, R.J., and Huston, D.L., 2009. Geodynamics and Metallogeny of North Queensland: insights from new deep crustal seismic data: In: Camuti, K., and Young, D. eds., Northern Queensland Exploration & Mining 2009 and North Queensland Seismic and MT Workshop: Extended Abstracts. Australian Institute of Geoscientists Bulletin No. 49, p. 57-63.

Korsch, R.J., Withnall, I.W. Hutton, L.J., Henson, P.A., Blewett, D.L., Huston, D.L., Champion, D., Meixner, A.J., Nicoll, M.G., and Nakamura, A., 2009, Geological interpretation of deep seismic reflection line 07GA-IG1 the Cloncurry to Croydon transect: In: Camuti, K., and Young, D. eds., Northern Queensland Exploration & Mining 2009 and North Queensland Seismic and MT Workshop: Extended Abstracts. Australian Institute of Geoscientists Bulletin No. 49, p. 153-158.

Li, J-R., and Greengard, L., 2007, On the numerical solution of the heat equation I: Fast solvers in free space: Journal of Computational Physics 226, p. 1891-1901.

Li, Y., and Oldenburg, D.W., 1998, 3-D inversion of gravity data: Geophysics, 63, p. 109-119.

McLaren, S., Sandiford, M., Hand, M., Neumann, N., Wyborn, L., and Bastrakova, I., 2003, The hot southern continent; heat flow and heat production in Australian Proterozoic terranes: In: Hills, R.R., and Mueller, D.R. eds., Evolution and dynamics of the Australian Plate. Geol. Soc. of America Special Paper 372, p. 157-167.

Meixner, A.J. and, Holgate, F., 2009a, In search of hot buried granites: a 3D map of sub-sediment granitic bodies in the Cooper Basin region of Australia, generated from inversions of gravity data: Adelaide: 20th Aust. Soc. Explor. Geophys. Conference. Extended Abstracts.

Meixner, A.J., and Holgate, F., 2009b, The Cooper Basin Region 3D Map Version 1: A Search for Hot Buried Granites: Geoscience Australia, Record, 2009/15.

Middleton, M.F., 1979, Heat flow in the Moomba, Big Lake and Toolachee gas fields of the Cooper Basin and implications for hydrocarbon maturation: Bulletin – Aust. Soc. of Exploration Geophysics 10(2), p. 149-155.

Murray, A.S., Morse, M.P., Milligan, P.R. and, Mackey, T.E., 1997, Gravity anomaly map of the Australian region (second ed.), scale 1:5 000 000. Australian Geological Survey Organisation, Canberra.

Osterholt, V., Herod, O., and Arvidson, H., 2009, Regional Three-Dimensional Modelling of Iron Ore Exploration Targets, Proceedings: Orebody

Modelling and Strategic Mine Planning Conference, Perth.

Sass, J.H., and Lachenbruch, A.H., 1979, Thermal regime of the Australian Continental Crust, in McElhinny, M.W,, ed., The Earth: its origin, structure and evolution. Academic Press, London, p. 301-351.

Seikel, R., Stüwe, K., Gibson, H., Bendall. B., McAllister, L., Reid, P., and Budd, A., 2009, Forward prediction of spatial temperature variation from 3D geology models: Adelaide: 20th Aust. Soc. Explor. Geophys Conference. Extended Abstracts.

Somerville, M., Wyborn, D., Chopra, P., Rahman, S., Estrella, D., and Van der Meulen, T., 1994, Hot dry rock feasibility study: Energy Research and Development Corporation, Report 94/243. 133pp.

Van der Wielen, S.E., Kirkby, A., Britt, A., Schofield, A., Skirrow, R., Bastrakov, E., Cross, A., Nicoll, N., Mernagh, T., and Barnicoat, A., 2009, Large-Scale Exploration Targeting for Uranium Mineral Systems within the Eromanga Basin. Townsville 10th Soc. Geol. App. Min. Dep Conference. Extended abstracts. in prep.

Hydro-Mechanical Selection Criteria of Engineered Geothermal Systems

Luke Mortimer
Hot Dry Rocks Pty Ltd, GPO Box 251, South Yarra, Victoria 3141, Australia
luke.mortimer@hotdryrocks.com

Stored heat geothermal resource estimates commonly extend across an extensive area and often contain more than one potential Geothermal Play. It is critical that an informed decision be made about which exploration Play has the best chance of commercial success. The decision might be between a deep Engineered Geothermal Systems (EGS) Play and a shallow Hot Sedimentary Aquifer (HSA) Play, or between several potential Plays at different levels. In any case, the critical parameters are resource temperature, depth and potential deliverability. A stored heat resource estimate constrains the first two parameters, leaving deliverability as the key risk.

In the case of HSA reservoirs, deliverability is largely dictated by the preservation of primary porosities and permeabilities at depths below the target operational isotherm. An HSA reservoir target may, however, lie at a depth where compaction processes have destroyed a significant proportion of its primary porosity and permeability. Such reservoirs should then be considered and developed as EGS or partial EGS reservoirs. In the case of EGS reservoirs, deliverability is largely dictated by the inherent hydro-mechanical properties of the reservoir rock and its fracture network, coupled with the *in situ* stress field. This paper summarizes the key datasets and knowledge required to make informed decisions about deliverability and development potential of possible EGS reservoirs.

Keywords: Engineered Geothermal Systems, Discrete Fracture Network, Numerical Modelling, Stress.

Development of an EGS Reservoir

The main mechanism for creating a geothermal reservoir and enhancing its *in situ* permeability is the shearing of pre-existing natural fractures during the process of hydraulic stimulation. This process involves the accommodation of an injected volume of water in fractures opened during elastic compression of the adjacent rock mass, rigid body block translation and permanent fracture dilation in response to shear displacement. These all depend upon the nature of the *in situ* stress field and the inherent properties of the host rock and its fracture network. In particular, shear deformation of pre-existing natural fractures is controlled by the elastic, cohesive, frictional and dilational properties of the host rock and fracture network with preferential reservoir growth and fluid flow occurring along fractures oriented ~parallel to the present-day, maximum principle stress direction. The creation of pure hydraulic fractures during stimulation has been shown to be rare and restricted to the near-well environment.

The critical information required for optimal planning of an EGS development includes:

- The nature of the *in situ* stress field (stress regime, orientation, magnitude and gradient).
- Characterisation of the primary structural features of the target reservoir (fault and fracture density, orientation and connectivity distributions).
- Characterisation of the hydro-mechanical properties of the rock material and fracture network.
- Preliminary identification of faults and fractures amenable to hydraulic stimulation.
- Predicted reservoir growth and anisotropic permeability direction in response to hydraulic stimulation.
- Estimation of fluid injection pressures required for controlled hydraulic stimulation.

The preliminary investigation of these primary features has a major impact on the planning, design, implementation and exploitation of an EGS project. For example, this information can be used to develop reservoir injection and circulation strategies that optimise reservoir growth and production whilst minimising the risk of high flow impedance or short-circuiting. These are also the key datasets required for coupled thermal-hydrogeological-geomechanical modelling of a geothermal reservoir.

Conceptual Reservoir Types

From a purely heat extraction point of view, the best reservoir host rock is that with the highest thermal conductivity (i.e. allows the greatest rate of heat extraction). At a proposed EGS site, the highest thermal conductor could either be the heat source itself (high heat producing granites) or a different rock type within the overlying insulating sequence. However, the ultimate performance of an EGS reservoir is determined by the hydro-mechanical properties and behaviour of the host rocks. These control fluid flow and residence time between injection and production wells. From a hydro-mechanical point of view, there are two

broad types of conceptual EGS reservoir targets; those with zero effective natural permeability, and those with finite but low natural permeability.

Type 1 : Hydraulically tight rocks at depth (approx. ≥ 4km)

Type 1 examples include rock types such as crystalline igneous or metamorphic basement rocks with little to no *in situ* porosity or permeability. These rocks are typically of high stiffness and poor fracture density and occur at depths with relatively high confining pressures. These stronger rock types tend to develop relatively rough fracture surfaces with higher fracture shear strengths and display a strong coupling between shearing and hydraulic conductivity. Potentially these characteristics allow reservoir development during hydraulic stimulation to be more easily constrained with a lower probability of significant fluid losses. However, experience has found that creating a reservoir in stiff and hydraulically tight rocks may also be difficult. They may experience poor circulation due to high flow impedance even after stimulation and may require high injection pressures to open fractures and achieve the necessary fluid volume throughput. This may lead to increased risk of runaway fracture growth, fluid pathway short-circuiting and water losses.

Type 2 : Finite but low permeability rocks at shallower depths (approx. ≤ 4km)

Type 2 examples may include a wide range of rock types that occur within high temperature but relatively shallower depth settings such as in a graben structure (e.g. Soultz). Rocks in these locations generally have higher *in situ* permeabilities and may be more easily stimulated due to lower confining pressures and rock mass stiffness. Reservoir rock types may also include non-crystalline, weaker rock types, such as layered sediments, within the insulating horizon. Layered sedimentary units may contain higher *in situ* permeabilities due to relatively higher fracture densities including bedding planes. The potential disadvantages of Type 2 reservoir targets are that reservoir growth may be more difficult to constrain with an increased probability of fluid losses. Within a sedimentary basin setting additional complexities may arise from an increased probability of chemical alteration from basinal fluids and an increased probability of local stress field perturbations due to major basin structures or interbedded rock types with significant mechanical contrasts.

Hydro-Mechanical Coupling in EGS Reservoirs

The phenomenon of stress-dependant fracture permeability is well documented in studies of deep-seated, fractured hydrocarbon and geothermal reservoirs and nuclear repositories (e.g. Gentier *et al*., 2000; Hillis *et al*., 1997; Hudson *et al*., 2005). Specifically, *in situ* stress fields are known to exert a significant control on fluid flow patterns in fractured rocks with a low matrix permeability. For example, in a key study of deep (>1.7 km) boreholes, Barton *et al*. (1995) found that permeability manifests itself as fluid flow focused along fractures favourably aligned within the *in situ* stress field, and that if fractures are critically stressed this can impart a significant anisotropy to the permeability of a fractured rock mass. Preferential flow occurs along fractures that are oriented orthogonal to the minimum principal stress direction (due to low normal stress), or inclined ~30° to the maximum principal stress direction (due to shear dilation).

Stress-dependent fracture permeability forms as a result of the interplay between normal and shear stresses, which are the components of stress that act perpendicular and parallel to a fracture plane, respectively. In a fractured rock mass, these stresses are highly coupled and can cause fractures to deform. Fracture deformation results in changes in permeability and storage because the ability of a fracture to transmit a fluid is extremely sensitive to its aperture as demonstrated by the “Cubic Law”. This law defines the bulk hydraulic conductivity of a fractured medium in the direction parallel to the fractures assuming that fractures are planar voids with two flat surfaces within an impermeable matrix. For an isolated test interval within a borehole, it is expressed as:

$$K_b = \frac{(2b)^3}{2B}\frac{\rho g}{12\mu} \qquad (1)$$

where K_b is the bulk hydraulic conductivity ($m.s^{-1}$) (where K_b = Transmissivity/test interval), $2b$ is the fracture aperture width (m), $2B$ is the fracture spacing (m), ρ is the fluid density ($kg.m^{-3}$), g is gravitational acceleration ($m.s^{-2}$) and μ is the dynamic viscosity of the fluid (Pa.s).

Anisotropic flow behaviour or flow channelling is particularly strong in low fracture density and low permeability rocks typical of potential EGS Plays. Fluid flow is dominantly controlled by fracture network density, geometry, connectivity and mineralization whilst contemporary stress fields superimpose a secondary influence on pre-existing fracture networks by deforming them further. In numerical modelling exercises, these features are best represented through the use of coupled hydro-mechanical, discrete fracture network (discontinuum) models.

Hydro-Mechanical Characteristics of EGS Reservoirs

This study presents a methodology that attempts to describe the hydro-mechanical character and behaviour of a fractured rock reservoir from a multi-disciplinary approach prior to any hydraulic

stimulation. The results of this methodology can be used to qualitatively to semi-quantitatively rank the EGS suitability of potential reservoir rock unit, to identify potentially permeable structures and to estimate injection pressures and reservoir growth directions during hydraulic stimulation. This multi-disciplinary approach consists of four key components, which include:

- Determination of the *in situ* stress field;
- Geological and hydrogeological characterisation;
- Geomechanical characterisation; and
- Hydro-mechanical modelling.

Determination of the *In Situ* Stress Field

The description of any *in situ* stress field includes the relative arrangement of the three mutually orthogonal principal axes of stress referred to as the maximum (σ_1), intermediate (σ_2) and minimum (σ_3) principal axes of stress. As the Earth's surface is a free surface with zero shear stress the vertical stress (σ_V) is assumed to be one of these principal axes of stress. The other two principal axes of stress consist of the two mutually orthogonal, horizontal stress orientations referred to as the maximum and minimum horizontal principal axes of stress (σ_H and σ_h, respectively). In practice, far-field crustal stress regimes are classified using the Andersonian scheme, which relates the three major styles of faulting in the crust to the three major arrangements of the principal axes of stress (Anderson, 1951). These three major stress regimes are:

(a) Normal faulting stress regime where $\sigma_V > \sigma_H > \sigma_h$;

(b) Strike-slip faulting stress regime where $\sigma_H > \sigma_V > \sigma_h$; and

(c) Thrust faulting stress regime where $\sigma_H > \sigma_h > \sigma_V$.

To estimate the effective stress state (σ') also requires that an estimate of the pore fluid pressures (P_p) within the rock formation, as σ' is defined as the difference between the applied stress (σ) and the internal pore fluid pressure:

$$\sigma' = \sigma - P_p \qquad (2)$$

The effective stress is critical as it controls coupled hydro-mechanical behaviour (or poroelasticity) by affecting fracture deformation processes as fluid pressures act to reduce the stress acting normal to a fracture plane. For example, high effective stresses with relatively low fluid pressures act to close fractures whilst low effective stresses with relatively high fluid pressures act to dilate fractures.

There are several techniques for measuring the magnitude and orientation of *in situ* stresses, among which the following are common (Zoback, 2007):

- Overcoring and strain relief methods.
- Hydraulic fracturing.
- Imaging of (vertical) borehole breakouts and drilling-induced tensile fractures (DITFs).
- Earthquake focal mechanisms.

All of the above techniques assume that σ_V is ~vertical and equivalent to the integration of rock densities to the depth of interest. Pore fluid pressures are often assumed "hydrostatic" and equivalent to the pressure of fluid column at the depth of interest. However, in areas of confined fluid flow, such as deep sedimentary basins, pore fluid pressures can exceed hydrostatic and require direct estimates from techniques that isolate sections of formation such as drill stem tests or through the analysis of drilling mud weights.

Each stress measurement technique has its advantages and disadvantages and any stress field determinations should ideally combine as many of these techniques over the greatest depth interval possible and be quality ranked according to the scheme developed by the World Stress Map (Heidbach et al., 2008).

Knowledge of the stress field and pre-existing fractured rock mass can be used to make preliminary predictions of fracture and reservoir growth directions during hydraulic stimulation. As a generalisation, the three major fracture growth directions are:

(a) Normal faulting stress regime ($\sigma_V > \sigma_H > \sigma_h$) form steep to vertical dipping fractures that strike orthogonal to σ_3.

(b) Strike-slip faulting stress regime ($\sigma_H > \sigma_V > \sigma_h$) form steep to vertical dipping fractures that strike $<45^o$ (commonly 30^o) to the direction σ_1; and

(c) Thrust faulting stress regime ($\sigma_H > \sigma_h > \sigma_V$) form shallow to horizontal dipping fractures that strike ~parallel to σ_2.

Geological & Hydrogeological Characterisation

Where available, the geological context of the study site should include all information pertaining to the geological setting, lithological composition, structure, geometry, weathering, deformation history and stress path for each potential reservoir rock type. For example, if a particular sequence has been metamorphosed, multiply folded or eroded at the surface before re-burial, those events would have significant implications for permeability and joint formation within the affected rock units. Fracture network data can be obtained from a variety of sources including outcrop, drill core and borehole images. Of particular use are

fracture scanline maps or core logs that provide important detail relating to fracture orientation, spacing, length, type, mineralisation and age relationships. Local hydrogeological data could include any reported hydraulic data from a variety of sources including well completion reports, well yields, pump tests, core permeability tests etc. This hydrogeological data compilation adds value as an indication of likely *in situ* permeabilities, hydraulic gradients, flow rates and fluid chemistries that can also provide useful constraints in a numerical model.

Geomechanical Characterisation

The geomechanical properties of a rock mass and fracture network are essential for predicting coupled hydro-mechanical processes as the elastic properties of an intact rock material together with fracture stiffness (strength) and pore fluid pressures control the amount of fracture deformation (dilation, closure and shearing) that may occur under an imposed stress field.

Important intact rock material properties include parameters such as density, bulk moduli, uniaxial compressive strength, tensile strength, cohesion and friction angle. These parameters are commonly estimated from laboratory tests such as drill core triaxial compression or ultrasonic velocity tests or from field based rock mass classifications such as those described by Hoek (2007). Furthermore, rock formations commonly contain a fabric, which may result in a mechanical anisotropy that needs to be determined and accounted for in any numerical model.

Fracture stiffness is primarily a function of fracture wall contact area. Normal stiffness (jk_n) and shear stiffness (jk_s) of a fracture are measures of resistance to deformation perpendicular and parallel to fracture walls, respectively. Normal stiffness is a critical parameter that helps to define the hydraulic conductivity of a fracture via an estimate of the mechanical aperture as opposed to the theoretical smooth planar aperture as described in the Cubic Law. Ultimately, estimates of fracture stiffness attempt to account for more realistic fracture heterogeneity, asperity contact, deformation and tortuous fluid flow. Equations 5 & 6 below describe the simplified relationship between fracture stiffness and fracture deformation (Rutqvist and Stephannson, 2002):

$$\Delta\mu_n = jk_n \, \Delta\sigma'_n \quad (5)$$

$$\Delta\mu_s = jk_s \, \Delta\sigma_s \quad (6)$$

which states (a) that fracture normal deformation ($\Delta\mu_n$) occurs in response to changes in effective normal stress ($\Delta\sigma'_n$) with the magnitude of opening or closure dependent upon fracture normal stiffness (jk_n); and (b) that the magnitude of shear mode displacement ($\Delta\mu_s$) depends upon the shear stiffness (jk_s) and changes in shear stress ($\Delta\sigma_s$).

Estimates of fracture stiffness are derived by a variety of field logging or laboratory tests, which are well documented in comprehensive reviews by Bandis (1993), Barton and Choubey (1977) and Hoek (2007). Standard practice is to derive stiffness estimates based upon fundamental measurements of fracture surface topography profiles and the elastic properties of the intact rock material, although these estimates are affected by many factors including:

- Joint roughness coefficient (JRC) which is a standard measure of a fracture surface topography profile (Barton and Choubey, 1977).
- Joint compressive strength (JCS) corresponding to the compressive strength of the fracture wall rock which can be modified by weathering and mineralization.
- Magnitude of fracture stiffness increasing with increasing effective normal stress.
- Fracture spacing and density and its effect on the partitioning of strain.
- Intact rock material moduli such as Young's modulus (E), shear modulus (G), bulk modulus (K) and Poisson's ratio (ν).
- Test type (e.g. unconfined, triaxial, *in situ* direct shear, laboratory direct shear etc).
- Sample size.
- Definition (e.g. peak, initial or 50% during an applied test).

Fracture stiffness is probably the most difficult of all the geomechanical parameters to characterise accurately principally due to the large number of dependent variables, their heterogeneous nature and the scale dependence of key factors such as the JRC and JCS estimates. It is also often difficult to gain access to sufficient amounts of drill core or outcrop. Typically, these limitations are addressed within numerical models through the use of parameter sensitivity studies and/or geostatistical-based approaches such as, for example, Monte Carlo simulations (de Marsily, G. *et al*., 2005).

Hydro-Mechanical Modelling

The aim of the hydro-mechanical modelling process is to make a preliminary evaluation of the hydro-mechanical character of each prospective reservoir unit at the inferred target depth, stress regime and pre-stimulation stage (i.e. steady state conditions). One example code is the Universal Distinct Element Code (UDEC), which is a 2.5D, distinct element, discontinuum code that represents a rock mass as an assembly of discrete rigid or deformable, impermeable blocks separated by discontinuities (faults, joints etc), which are treated as boundary conditions between the blocks (Itasca, 2004). UDEC

interpolates the physical response and stress-displacement relationship of a fractured rock mass to an imposed stress field, which satisfies the conservation of momentum and energy in its dynamic simulations with fluid flow calculations derived from Darcy's Law (for a comprehensive review of the UDEC governing equations see Itasca, 2004). Based upon a conceptual fractured rock mass model of the potential reservoir target, hydro-mechanical model simulations can provide the following useful information:

- Structural anisotropy of the rock mass via estimates of the fracture deformation distribution across all individual fractures (Figure 1).
- An indication of the pre-stimulation, steady-state, bulk *in situ* hydraulic conductivity and its related anisotropy (Figures 2 & 3).
- An indication of potential reservoir growth and fluid flooding directions.
- An estimate of stress magnitudes at the target depth horizon and an indication of the injection pressures required for hydraulic stimulation.
- Model input parameters and results provide the basis for more complex, coupled thermal-hydrogeological-geomechanical models to simulate the lifetime performance (e.g. pressure and thermal drawdown) of an EGS project.

Ranking of Potential Reservoir Targets

From a hydro-mechanical context, the process of ranking the reservoir suitability for each prospective rock unit will require a qualitative to semi-quantitative assessment of the advantages and disadvantages of both Type 1 and 2 conceptual targets. It is recommended that the ranking criteria include the following factors:

- Favourable fracture set orientations with respect to the *in situ* stress field.
- Degree of fracture network connectivity (e.g. fracture density, length etc).
- Fracture set strengths, mineralisation etc.
- Rock mass stiffness (i.e. deformability).
- Estimated bulk hydraulic conductivity and hydraulic conductivity ellipse.
- Target depth with respect to the pre-defined target isotherm.
- Target depth and its expected stress magnitudes.
- Target rock unit thermal conductivity.
- Target rock unit thickness.

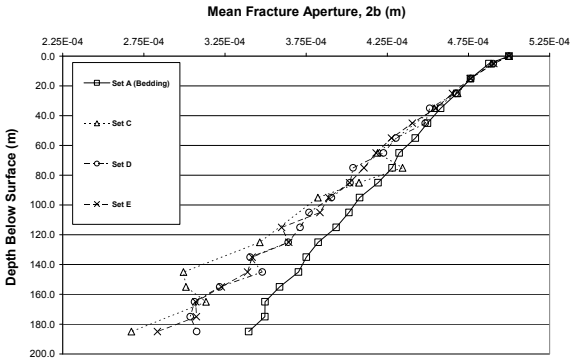

Figure 1 : Example of a UDEC fracture deformation depth profile for individual fracture sets that comprise a larger fracture network. In this example, the initial (at surface) fracture hydraulic apertures were set at 0.5 mm with data points representing the calculated mean fracture aperture for each 10 m thick depth interval. The results show a progressive divergence in the relative amounts of fracture closure (i.e. structural and hydraulic anisotropy) occurring across the individual fractures.

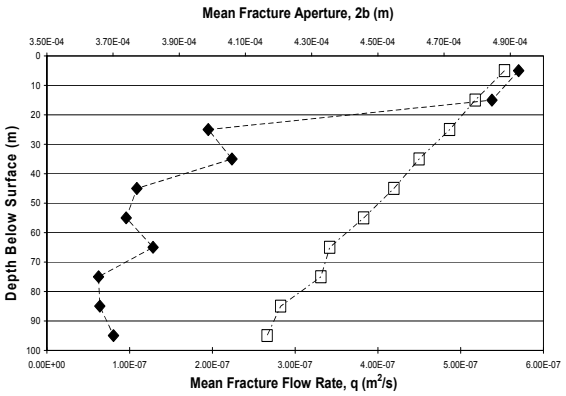

Figure 2 Depth profile example of UDEC estimated mean fracture flow rates (diamonds, lower x-axis) and fracture apertures (squares, upper x-axis). The initial (at surface) fracture hydraulic apertures were set at 0.5mm.

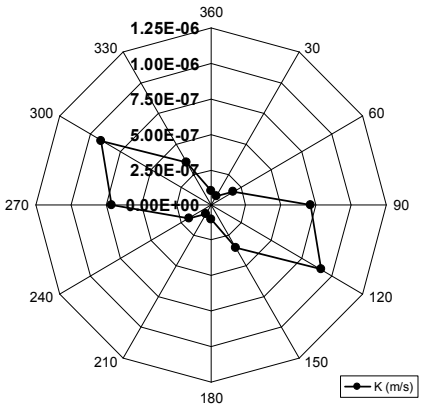

Figure 3 : Example of a UDEC horizontal planar hydraulic conductivity (K) ellipse for a fracture network at a specific depth (stress) level. The degree of ellipse elongation represents the *in situ* hydraulic anisotropy of the fracture network with the elongation direction equal to the maximum K direction.

Conclusion

This study has described how preliminary estimates of the hydro-mechanical properties of a fracture network can be combined with coupled hydromechanical, discrete fracture network models to characterise reservoir potential. This approach has several limitations, which are largely due to the complexities and uncertainties associated with data capture, sample representativeness and spatial confidence, particularly in regard to the geomechanical characterisation of *in situ* rock material and fractures. Furthermore, the computational limitations of codes such as UDEC restrict their practical application to either detailed small-scale (<100m) studies or stochastic representations of larger scale problems. However, the main advantage of this approach is that it provides an alternative method to standard borehole hydraulic tests, can be based upon outcrop or single well data, can be applied at any geological or depth setting and can account for anisotropic fluid flow by explicitly representing fractures and the effects of the *in situ* stress field. The model outputs can be used as valuable parameter inputs for larger scale, "life-of-operation" reservoir models, to identify potentially permeable structures and to estimate required injection pressures and reservoir growth directions during hydraulic stimulation.

There is no "one-size-fits-all" model or methodology and the preference for Type 1 or Type 2 reservoir host rocks is site-dependent, as each rock type has its own unique hydro-mechanical character and behaviour within its present-day geotectonic setting. Ideally, the choice of reservoir rock type should be evaluated in the context of a broader risk-based geothermal systems assessment, which characterises the four aspects of geological risk - heat flow, thermal resistance, reservoir and water. These risks can be condensed, on further modelling, to temperature risk (P_t) and flow rate risks (P_w). When combined with perceived drilling and engineering risks (P_e), these factors form the basis of a simple risk-based assessment system which can be applied to any geothermal prospect/play.

References

Anderson, E. M., 1951. The dynamics of faulting and dyke formation with application to Britain. Oliver and Boyd, Edinburgh.

Bandis, S.C. 1993. Engineering properties and characterization of rock discontinuities. In: Hudson, J. (ed.) Comprehensive Rock Engineering: Principles, Practice & Project, 1, 155-183, Pergamon Press, Oxford.

Barton, N.R. and Choubey, V. 1977. The shear strength of rock joints in theory and practice. Rock Mechanics, 10(1-2), 1-54.

Barton, C. A., Zoback, M. D., and Moos, D., 1995. Fluid flow along potentially active faults in crystalline rock. Geology, 23, 683-686.

de Marsily, G., Delay, F., Goncalves, J., Renard, P, Teles, V. and Violette, S., 2005. Dealing with spatial heterogeneity. Hydrogeology Journal, 13, 161-183.

Gentier, S., Hopkins, D., and Riss, J., 2000. Role of Fracture Geometry in the Evolution of Flow Paths under Stress. In Faybishenko, B., Witherspoon, P.A and Benson, S.M. (eds), Dynamics of Fluids in Fractured Rocks. AGU Geophysical Monograph 122, 169-184.

Hillis, R. R., Coblentz, D. D., Sandiford, M., and Zhou, S., 1997. Modelling the Contemporary Stress Field and its Implications for Hydrocarbon Exploration. Exploration Geophysics, 28, 88-93.

Hoek, E., 2007, Practical Rock Engineering. Online publication. http://www.rocscience.com/hoek/PracticalRockEngineering.asp

Hudson, J. A., Stephansson, O., and Anderson, J., 2005. Guidance on numerical modelling of thermo-hydro-mechanical coupled processes for performance assessment of radioactive waste repositories. International Journal of Rock Mechanics and Mining Sciences, 42, 850-870.

Itasca, 2004. UDEC 4.0 Theory and Background. Itasca Consulting Group Inc., Minnesota.

Rutqvist, J. and Stephansson, O., 2003. The role of hydromechanical coupling in fractured rock engineering. Hydrogeology Journal, 11, 7-40.

Zoback, M. D., 2007, Reservoir Geomechanics. Cambridge University Press.

Thermal thinking: optimal targeting for Australian geothermal explorers

Alexander Musson[1,2 *], Ben Harrison[1], Kate Gordon[1], Sarah Wright[1] and Mike Sandiford[1,2].
[1] School of Earth Sciences, University of Melbourne, Victoria 3010.
2 Melbourne Energy Institute, University of Melbourne, Victoria 3010.
* Corresponding author: alexander.musson@unimelb.edu.au

Introduction

The two foremost criteria that define the viability of a potential geothermal reservoir are: the highest temperature at the shallowest depth, and sustainable geofluid flow rates. In addressing the former, geothermal explorers face a difficult challenge; a challenge starting with scarce or inaccurate thermal datasets extracted mostly from shallow drillholes, and concluding with oversimplified interpretations and underconstrained thermal models.

In the absence of deep drilling, temperature predictions at a target depth of several kilometers require the extrapolation of thermal data obtained from boreholes typically a few hundred metres deep. Because an uncertainty of 1 ºC at a 100 m depth translates to an error of 40 ºC at 4,000 m, it is essential that thermal data from shallow drillholes, in particular heat flow, be well constrained. Often the analysis of heat flow is considered as a one-dimensional steady-state and purely conductive heat transfer problem. This simplified view ignores transient effects and spatial variations which arise from heat and fluid transport as well as the inherent three-dimensional heterogeneity and anisotropy of the geological subsurface. In this context our approach to the problem is to establish a more rigorous evaluation in assessing the nature and significance of primary data. We specifically explore the role of heat refraction and palaeoclimatic transients and its incidence on extrapolation methods. In certain circumstances primary data from shallow boreholes can be evaluated and adequately relied upon for extrapolation at target depth, independently of deep drilling. We propose conceptual models showing why heat refraction, heat insulation, rock anisotropy and palaeoclimate cannot be ignored and how consequently explorers can optimize their geothermal targets.

Keywords: Australia, Latrobe Valley, heat flow modelling, heat refraction, palaeoclimatic corrections, Enhanced Geothermal Systems (EGS), Hot Fractured Rocks (HFR), Hot Dry Rocks (HDR), Deeply Buried Sedimentary Aquifers (DBSA), Hot Sedimentary Aquifers (HSA).

Heat refraction

Because the geological subsurface is not a layer cake, heat refraction occurs due to thermal conductivity contrasts. This lateral variation in the thermal properties of rocks will always result in heat refraction effects and will invariably impact on shallow heat flow fields. When the thermal conductivity contrasts are large, the relationship between temperature at target depth and surface heat flow is complex and non-trivial to understand. For example buried 'insulators' will induce high temperatures at depth, below the insulator; yet will display a negative heat flow anomaly at the surface (Figure 1, Appendix). In the Latrobe Valley (Victoria's Gippsland Basin), the magnitude of the anomaly associated with buried coals is estimated to be – 40 mWm^{-2}, with an inversely correlated temperature anomaly of + 20-30 ºC. This instance highlights the necessity to elucidate the source of heat flow anomalies before they are used to extrapolate temperature to target depth. Furthermore it provides a stringent test with respect to the robustness of primary data obtained from shallow drillholes. If shallow boreholes do not record the anomaly associated with heat refraction, they cannot reflect purely conductive heat flow processes and are therefore of little use in constraining temperature at target depth by extrapolation methods.

Palaeoclimatic corrections

Palaeoclimatic variations over the Late Pleistocene have been extreme, with most proxy data indicating that surface temperatures along southern Australia are now some 6-8°C higher than at the height of the Last Glacial Maximum (LGM) some 18,000-20,000 years ago (Galloway 1965, Miller *et al*. 1997, Barrows *et al*. 2002, Hesse *et al*. 2004, Jouzel *et al*. 2007). Because surface temperatures are warmer now than in the past 100,000 years, surface heat has propagated into the shallow subsurface affecting an otherwise steady state-gradient. This means that temperature gradients are lower today than those of the LGM. This temperature anomaly needs to be accounted for in accurate heat flow modelling. The inversion of downhole temperature is arguably the only direct method that permits to determine palaeoclimatic ground surface temperatures histories from a few hundred years to 100,000 years (i.e. Hotchkiss and Ingersoll

1934, Benfield 1939, Birch 1948, Sass *et al*. 1971, Beck 1977, Clauser 1984, Chapman and Harris 1993, Pollack and Smerdon 2004, Beltrami *et al*. 2005, Rath and Mottaghy 2007). The use of the transient heat conduction equation (Carslaw and Jaeger 1959) with typical values of the thermal diffusivity of rocks (i.e.Touloukian *et al*. 1970, Seipold 1998, Beardsmore and Cull 2001, Mottaghy *et al*. 2008), show that excursions in ground surface temperature for 10, a 1,000 and a 100,000 years ago produce maximum temperature anomalies at depths of approximately 25, 250, 2,500 m respectively. A prescribed time-dependent boundary condition reveals that for every 1 ºC of fluctuation at the ground surface corresponds a heat flow variation of approximately 1 mWm^{-2} at the depth of the anomaly maximum. Although the magnitude of this correction depends on whether the location of the borehole is 'coastal' or 'intracontinental', it has important implications for geothermal modelling since an uncorrected shallow heat flow estimate is most likely an underestimate.

Summary

Often the analysis of heat flow is considered as a one-dimensional, steady-state, purely conductive heat transfer problem, given constant boundary conditions. Because the geological subsurface is neither homogeneous nor isotropic, and because it is subject to various transients, one-dimensional steady-state modelling does not appear robust enough to develop well-constrained temperature or heat flow maps. This holds especially true when thermal data are extracted from shallow-depth drillholes. We propose through this contribution, an ongoing effort of the Geothermal Research Group at the School of Earth Sciences, University of Melbourne, a more rigorous evaluation of the nature and significance of shallow-depth thermal data. We develop theoretical and numerical models that demonstrate the importance of heat refraction and palaeoclimate variations through two-dimensional predictive heat flow modelling.

Appendix

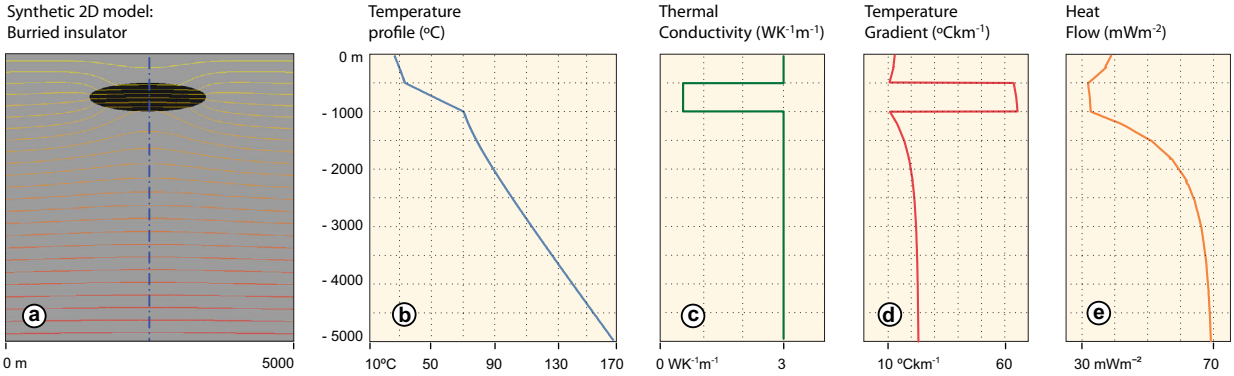

Figures 1a, 1b, 1c, 1d, 1e: Synthetic 2D model (Fig. 1a) by finite element method, depicting a buried insulator placed between a depth of 500 m and a 1,000 m. Boundary conditions are a surface temperature of 17ºC (Fig. 1b) and a bottom heat flow of 70 mWm-2 at z = –10,000 m. The side boundaries are placed in the far-field and are mirror conditions. The thermal conductivities (Fig. 1c) are arbitrarily chosen at 0.5 Wm-1K-1 for the insulator, and 3.0 Wm-1K-1 for the rest of the domain. The thermal conductivity exerts a first order control on the gradient profile (Fig. 1d): to low thermal conductivities correspond large thermal gradients. The heat flow profile (Fig. 1e) demonstrates the large difference between the heat flow at the surface (30 to 40 mWm-2) and that at depth (70 mWm-2), a result of the heat refraction induced by the large thermal conductivity contrast.

References

Barrows, T.T., Stone, J.O., Fifield, L.K. and Cresswell, R.G. 2002. The timing of the Last Glacial Maximum in Australia. Quaternary Science Reviews 21, 159-173.

Beardsmore G.R. and Cull J.P. 2001. Crustal heat flow: A guide to measurement and modelling. Cambridge University Press, New York.

Beck, A.E. 1977. Climatically perturbed temperature gradients and their effect on regional and continental heat-flow means. Tectonophysics, 41, 17-39.

Beltrami, H., Ferguson, G. and Harris, R.N. 2005. Long-term tracking of climate change by under-ground temperatures. Geophysical Research Letters 32, L19707.

Benfield, A.E. 1939. Terrestrial heat flow in Great Britain. Proceedings of the Royal Society of London, Mathematical and Physical Sciences 173, 955, 428-450.

Birch, F. 1948. The effects of Pleistocene climatic variations upon geothermal gradients. American Journal of Sciences 246,729-760.

Carslaw, H.S. and Jaeger, J.C. 1959. Conduction of heat in solids. 2nd Edition. Clarendon Press, Oxford.

Chapman, D.S. and Harris, R.N. 1993. Repeat temperature measurements in borehole GC-1, northwestern Utah: Towards isolating a climate-change signal in borehole temperature profiles. Geophysical Research Letters 20, 1891-1894.

Clauser, C. 1984. A climatic correction on temperature gradients using surface temperature series of various periods. Tectonophysics 103, 33-46.

Galloway, R.W. 1965. Late Quaternary climates in Australia. Journal of Geology 73, 603-618.

Hesse, P.P., Magee, J.W. and van der Kaars, S. 2004. Late Quaternary climates of the Australian arid zone: a review. Quaternary International 118-119, 87-102.

Hotchkiss, W.O. and Ingersoll, L.R. 1934. Post-glacial time calculations from recent geothermal measurements in the Calumet Copper Mines. Journal of Geology 42,113-142.

Jouzel, J., Masson-Delmotte, V., Cattani, O., Dreyfus, G., Falourd, S., Hoffmann, G., Minster, B., Nouet, J., Barnola, J.M., Chappellaz, J., Fischer, H., Gallet, J.C., Johnsen, S., Leuenberger, M., Loulergue, L., Luethi, D., Oerter, H., Parrenin, F., Raisbeck, G., Raynaud, D., Schilt, A., Schwander, J., Selmo, E., Souchez, R., Spahni, R., Stauffer, B., Steffensen, J.P., Stenni, B., Stocker, T.F., Tison, J.L., Werner, M. and Wolff, E.W. 2007. Orbital and millennial antarctic climate variability over the past 800,000 years. Science 317, 793-796.

Miller, G.H., Magee, J.W. and Jull, J.W.T. 1997. Low-latitude glacial cooling in the Southern Hemisphere from amino-acid racemization in emu eggshells. Nature 385, 241-244.

Mottaghy, D., Vosteen, H. D. and Schellschmidt, R. 2008. Temperature dependence of the relationship of thermal diffusivity versus thermal conductivity for crystalline rocks. International Journal of Earth Sciences 97, 435-442.

Pollack, H.N. and Smerdon, J. E. 2004. Borehole climate reconstructions: Spatial structure and hemispheric averages. Journal of Geophysical Research 109, D11106.

Rath, V. and Mottaghy, D. 2007. Smooth inversion for ground surface temperature histories: estimating the optimum regularization parameter by generalized cross-validation. Geophysical Journal International 171, 1440-1448.

Sass, J. H., Lachenbruch, A. H. and Jessop, A. M. 1971. Uniform heat flow in a deep hole in the Canadian Shield and its paleoclimatic implications. Journal of Geophysical Research 76, 8586-8596.

Seipold, U. 1998. Temperature dependence of thermal transport properties of crystalline rocks – a general law. Tectonophysics 291, 161-171.

Touloukian, Y.S., Powell, R.W., Ho, C.Y. and Klemens, P.G. 1970. Thermal conductivity, non-metallic solids. Thermal properties of matter, Volume 2. IFI/ Plenum, New York.

Overview of Geothermal Resources and Exploration Activity in Victoria

David H Taylor, Ben C Harrison
GeoScience Victoria, GPO BOX 4440, Melbourne, VIC, 3001
Corresponding author: david.taylor@dpi.vic.gov.au

Victoria currently derives most of its electricity generation from brown coal but is keen to diverse towards lower emission energy sources. Geothermal energy offers the possibility of base load power generation plus direct use thermal applications. Legislation for geothermal resource security was passed in 2005. In 2006 and 2008 two rounds of competitive tendering resulting in about two thirds of the State being placed under exploration by seven different companies. They have pledged to spend close to $370 million over the next five years in the quest to find and develop geothermal resources. Legacy data from petroleum exploration suggests potential for Hot Sedimentary Aquifer (HSA) plays in basins along the onshore margin of Victoria. Elsewhere the geology may support Engineered Geothermal Systems (EGS) plays in the abundant Palaeozoic granites. Magmatic plays may also exist in association with a major episode of recent basaltic volcanism. Governments, Universities and exploration companies are currently collecting basic geothermal data such as heatflow measurements and thermal conductivities to better characterise the potential of geothermal systems in Victoria. A number of Inferred Resources have been declared but deep drilling to appraise these is awaiting funding opportunities.

Keywords: Geothermal, Hot Sedimentary Aquifer, Energy generation,

Background History

The oil shocks of the 1970s piqued interest into alternate energy sources. Town water supplies drawn from thick Cretaceous-Tertiary basins along the Victorian coast showed temperatures of about 50-90C at 1-2km depth. The potential of direct use of this hot water was investigated (King et al. 1987). Petroleum exploration in the same area also occasionally intersected a deeper basal aquifer with temperatures of about 130-150C at 3.5-4km depth (Woollands & Wong 2001). Low oil prices throughout the 1990s suppressed interest in alternate sources but the return of higher prices and concerns around green house gas emissions have again sparked interest in the potential of geothermal energy. Legislation was put in place in 2005 and exploration companies were invited to tender for large permit blocks established across the State in 2006 and again in 2008. To support tender bids, a preliminary review of the geothermal prospectivity was published by the State government geology organisation (Driscoll 2006). This report included a quality-controlled compilation of temperature data from pre-existing groundwater and petroleum bores.

Geological Framework for potential geothermal systems

Geothermal potential depends on the interaction of a number of geological factors. The best resources are likely to exist in regions where high heat flow passes through rocks of low conductivity (good insulation) to create high temperature at shallow depth (Duffield & Sass, 2003).

Unfortunately there is insufficient published heat flow data and hardly any published thermal conductivities to allow a quantitative assessment via these criteria. Instead, the geothermal potential can only be assessed indirectly, in a more qualitative manner, by looking at geological factors which control the geothermal factors. The recent publication of a geothermal systems assessment framework (Cooper & Beardsmore 2008) outlines the four factors that need consideration: (1) a heat producing basement (2) an insulating blanket (3) a fluid to move the heat around with and (4) a reservoir to accommodate the fluid.

Applying this four factor analysis to the major geological provinces of Victoria gives some idea of their relative geothermal prospectivity (Figure 1). The broad diversity in the age and types of rocks across Victoria gives some potential for all three types of geothermal systems: Engineered Geothermal Systems in Hot Rocks; Hot Sedimentary Aquifer; and Magmatic.

Three broad geological/geothermal provinces can be delineated across Victoria: (1) The Palaeozoic bedrock (2) the onshore Otway and Gippsland Basins and (3) the Murray Basin.

The Palaeozoic bedrock consists predominantly of Cambrian to Devonian deep marine siliclastics that have been tightly folded and cleaved at various times in the Palaeozoic (blues, browns and purples of figure 1). These rocks underlie the other provinces. This exposed bedrock gives good insight into the heat producing basement factor. Numerous granites intrude this bedrock (red blobs on figure 1). In west and central Victoria some of them have felsic, fractionated geochemistry with mild enrichment in heat producing elements so the Engineered Geothermal System plays may be possible where

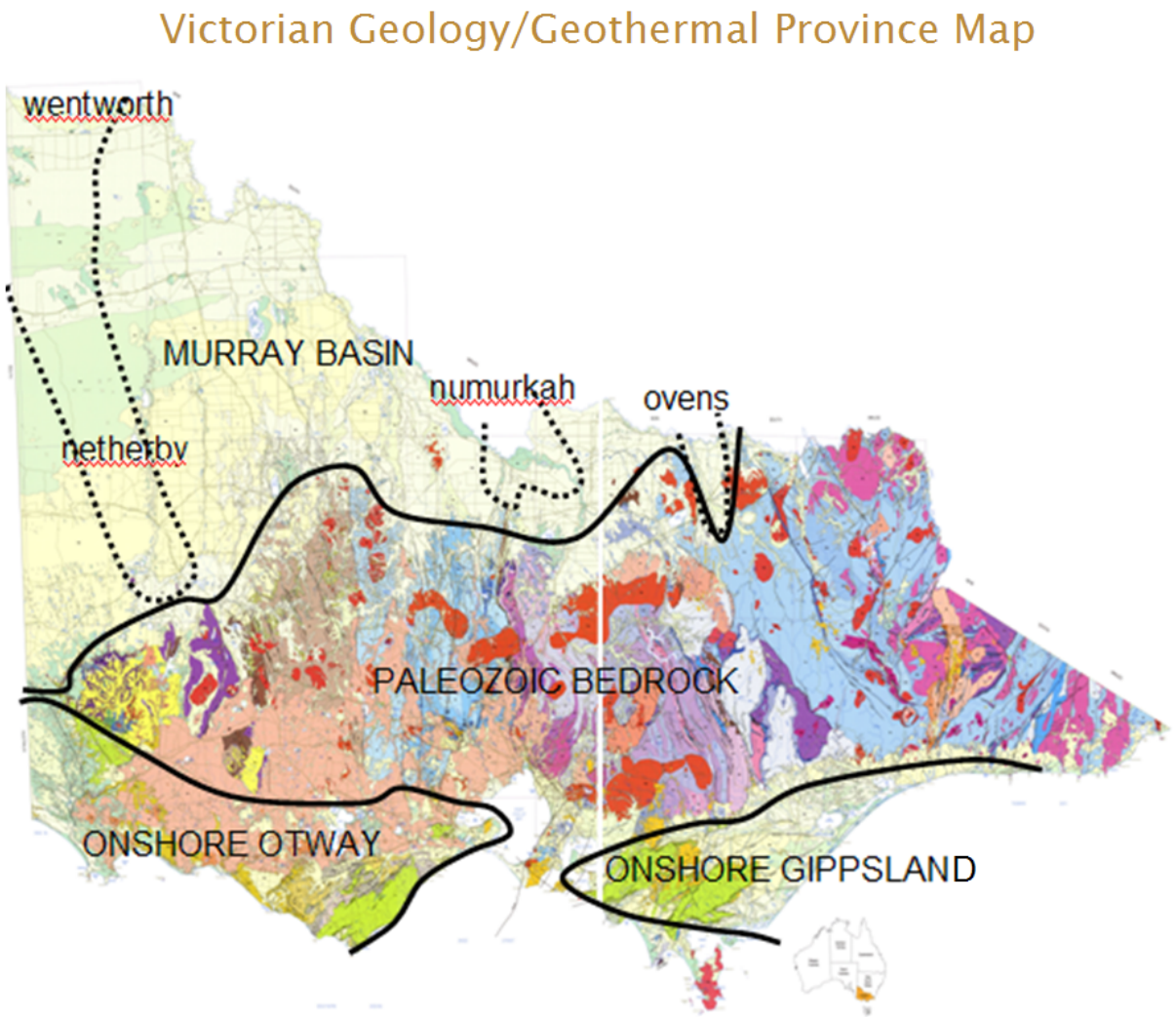

Figure 1: Geological/Geothermal Province map of Victoria based on underlying geological controls. Three broad geothermal provinces of Palaeozoic bedrock, onshore basins, and Murray basin each have a number of potential geothermal play types where factors favourably align.

some granites still lie buried within the bedrock or beneath the adjacent basins? In the southwest, an extensive province of young basalts has erupted onto the bedrock in the last few million to tens of thousands of years (the light pink in figure 1). Thus there is the possibility of Magmatic plays related to residual transient heat anomalies in the upper crust that may exist because of the recent magmatism.

The Onshore Otway and Gippsland Basins are Cretaceous rift basins associated Gondwana break-up (greens and yellow along coast in Figure 1). These basins are well characterised thanks to a long history of petroleum exploration. They contain several kilometres of muddy sediments overlying a coarser grained basal unit. This provides a natural reservoir already charged with hot water beneath an insulating blanket to create an attractive fairway for Hot Sedimentary Aquifer plays. In the Otways this basal unit has been intersected upon the basin floor but in the Gippsland basin this unit has yet to be tested away from the margins, at the depths necessary for a geothermal play. Beneath these basins there is also potential for Engineered Geothermal System plays in places where it is floored by granites.

The Murray Basin is a Tertiary intracratonic sag basin (light greens and yellow inland in Figure 1). It generally contains only a few hundred metres of sandy marly cover. This is insufficient cover to act as a heat blanket but in some places deeper troughs – such as the Wentworth, Netherby, Numurkah and Ovens - exist and can contain up to a couple of kilometres of sediment that is poorly known since there has been limited petroleum exploration here. Alignment of favourable factors over the deeper troughs may allow Engineered Geothermal System or Hot Sedimentary Aquifer plays but the favourability of the geothermal factors in this province has yet to be validated.

Science Research and Company Exploration

Most activity by everyone – government agencies, university academia and exploration companies –

is focussing on collecting the fundamental geothermal data sets of temperature gradients and thermal conductivities to allow heat flow mapping.

GeoScience Victoria is working with GeoScience Australia on the National Geothermal Energy Project (Budd et al., 2008). In the Murray Basin, 7 deep water bores were recently measured to fill a large gap in the national heat flow database. More bores are planned to be entered as access and the national work program permits. In addition to supporting the Federal program, GeoScience Victoria also has some moderate funding to purchase a thermal logger to accelerate State coverage and also allow opportune access to appropriate mineral exploration drill holes etc. Similar to this government work, many of the exploration companies have also been re-entering bores for temperature logging and measuring cores for thermal conductivity so that heat flow calculations and conductive 1-2-3D modelling of their permit areas can be undertaken. Several Inferred Resources of 'Stored Heat' have already been declared and some of these plays are now ready for further appraisal by deep drilling.

Pathways to Resource Development

In the absence of detailed, dedicated geothermal data, most of Victoria can be viewed as 'blue sky' or perhaps 'green fields' at best, in those areas where some legacy petroleum data exists. Most of the Victorian geothermal explorers are small companies with limited amounts of capital and cash-flow to fund their 5 year exploration programs. Ideally, as these companies collect information and decrease risks and unknowns, they could call for more capital through either debt or equity raisings until it becomes probable that a major backer would farm-in for development. The Global Financial Crisis has badly affected this traditional venture capital pathway through to resource development.

At the national level the Federal government has committed a significant amount of funds into a geoscience investigation program and also put up money for co-funding deep appraisal drilling. If these drilling appraisals lead to early success then perceived risks around geothermal energy may lessen and allow easier funding for the whole industry from more the traditional pathway.

Company announcements around Inferred Resources and/or conceptual targets suggest that several thousand MW of electricity generation may be possible but it is still early days for the geothermal industry in Victoria.

References

Budd, A.R., Holgate, F.L., Gerner, E.J., Ayling, B.F. & Barnicoat, A.C., 2008, Pre-competitive geoscience for geothermal exploration and development in Australia: Geoscience Australia's Onshore Energy Security Program, in: Gurgenci and Budd (eds) Proceedings of the Sir Mark Oliphant International Frontiers of Science and Technology Australian Geothermal Energy Conference, Geoscience Australia Record 2008/18, 1-8.

Cooper, GT. & Beardsmore, GR., 2008, Geothermal systems assessment: understanding the risks in geothermal exploration in Australia. Proceedings Eastern Australian Basins Symposium III, Sydney, Australia, September 2008.

Driscoll, J., 2006, Geothermal propsectivity of onshore Victoria, Australia. GeoScience Victoira, VIMP report 85.

Duffield, WA. & Sass, JH., 2003, Geothermal energy: Clean power from the earth's heat. U. S. Geological Survey circular 1249, 36pp.

Graeber, FM., Houseman, GA. & Greenhalgh, SA., 2002, Regional teleseismic tomography of the western Lachlan Orogen and the Newer Volcanic Province, southeast Australia. *Geophysical* Journal International, vol. 149, no. 2, pp. 249--266.

King, RL & Council, VSE 1987, Geothermal Resources of Victoria, Department of Industry, Technology and Resources, Victorian Solar Energy Council.

Woollands, MA., & Wong, D., (eds.) 2001, *Petroleum Atlas of Victoria, Australia*, Department of Natural Resources and Environment.

Mineralogy and Petrology of the Cooper Basin Basement Granites

Van Zyl, J.A.B.[1, 2], Uysal, I.T.[1], Gasparon, M.[2]
[1]Queensland Geothermal Energy Centre of Excellence, The University of Queensland, Queensland 4072, Australia
[2]School of Earth Science, The University of Queensland, St Lucia Queensland, 4072
Email: j.vanzyl@uq.edu.au

The Australian continent is tectonically relatively stable in comparison with other continental settings, the radiogenic heat production within the Australian continental crust is significantly high. One region with particularly elevated heat production is the Cooper Basin. The Cooper Basin is an intercratonic basin that contains Late Carboniferous to middle Triassic sedimentary rocks which are mainly of non-marine origin (Hill and Gravestock 1995).

The Cooper Basin overlies granites, which have intruded the Warburton Basin Sediments (Gatehouse et al, 1995, McLaren and Dunlap, 2006, Sun, 1997). The Cooper basin in turn is overlain by the Eromanga Basin (Gatehouse et al, 1995, Sun, 1997).

This paper focuses on three wells (Table 1) in which granites have been intersected. The aim of this study is to characterise the mineralogy and petrology of these granites that may control the heat production in the Cooper Basin.

The data collected in this study will be used to establish an advanced geochemical/isotopic and geochronological database for improving our understanding of existing geothermal resources, and the definition of an investigation procedure that can be applied as a routine exploration tool for Hot Rock geothermal systems in Australia and in similar tectonic environments worldwide.

Petrography

Ten petrographic thin-sections were made from granites sampled in four geothermal wells that intersect the basement of the Cooper Basin.

Eight of the ten samples are highly altered with the predominant minerals being quartz, and a high birefringent clay mineral (illite based on XRD) with minor oxides. In four of the sections, highly altered plagioclase is present (Big Lake-1 and the three McLeod-1 sections, 3745.2, 3745.9 and 3748.3) exhibiting distinct Carlsbad-Albite twinning.

In all the altered sections, three textures (Figure 1-A) can be identified in terms of mineralogy and grain size. The first texture is the primary granite texture. This is characterised by the large grain size of some quartz grains (> 2mm) and the occurrence of pseudomorphic illite, through the replacement of biotite and strongly altered plagioclase in some of the sections. The primary quartz (Figure 1-C) in the sample exhibits extensive undulose extinction with some prominent striations, with the quartz being highly fractured. The second texture is the pervasive alteration. This is exhibited by finely (< 100µm) inter-grown clay minerals with associated fine-grained quartz. The third texture is an intermediate texture; with the dominance of the larger, more crystalline clay minerals. This third texture is characterised by the clay minerals, which have a grain size between 200 µm to 1 mm.

Table 1: Sample Names and sampling depth

Well Name	Sampling Depth (m)	Alteration
Big Lake-1	3057	Pervasive
Jolokia-1	4905	Minor (sericitisation)
McLeod-1	3745.2	Pervasive
	3745.9	Pervasive
	3748.3	Pervasive
Moomba-1	2847.75	Pervasive
	2848.7	Pervasive
	2851	Pervasive
	2857.4	Pervasive
	2895.2	Minor (sericitisation)

In one of the Big Lake 1 samples, a vein (Figure 1-B) occurs that consists of mainly quartz with some illitic clays. This vein varies in thickness from 80µm to 200µm . The vein postdates the predominant alteration of the sample as it crosscuts all alteration minerals in the section.

Some of the quartz grains (McLeod-1_3745.9, McLeod-1_3748.3, Moomba-1_2847.75, Moomba-1_2848.7, and Moomba-1_2851, Figure 1-D) have small inclusions of unaltered biotite and amphibole (hornblende). It appears that the inclusions may have survived the alteration.

The sample also contains some accessory hematite and zircon. Both these minerals seem to be associated with the third texture, which is dominated by intermediate clay minerals. The zircon is mainly locked within the large clay minerals, with minor zircon grains locked in the large quartz crystals. The zircons, which are observed within the illitic clays, tend to occur as fractured euhedral crystals with some grains

containing minor opaque inclusions. The zircons occur as locked grains in the clay minerals crosscutting the cleavage lamellae. The zircons also tend to occur as grains attached to quartz and clay mineral grains. Some of the zircons are zoned.

The hematite in the sections occurs as elongated anhedral crystals, with a minority occurring as subhedral grains. The elongated hematite occurs as locked particles along the clay mineral lamellae. Some of the hematite (Moomba-1_2851) occurs in distinct areas not included within a particular clay mineral grain. The hematite is being altered to Fe-oxyhydroxides (goethite/limonite) This is indicated by rims around some of the hematite.

Two of the samples, Jolokia-1 and Moomba-1_2895.2, have less pervasive alteration compared with the other eight samples. The alteration in Jolokia-1 appears to have affected only the biotite and amphibole as they have been replaced by a highly birefringent clay mineral. In the Moomba-1_2895.2 (Figure 1-F) section, the biotite and amphibole exhibit only small amounts of alteration, evidenced by the discoloration along the grain boundaries. The plagioclase in both these samples exhibits some degree of alteration as there is some sericitisation. Primary microcline is also present and exhibits similar alteration as the plagioclase. In the Jolokia-1 sample, evidence of eutectic crystallisation of quartz and microcline is present. In both these sections, the opaques and zircon are observed with the clay alteration mineral (Jolokia-1) and the biotite and amphibole (Moomba-1_2895.2).

Hydrothermal alteration and deformation

Thin section optical microscopy shows that the granite samples have been severely fractured, and that the fracturing was accompanied by significant hydrothermal alteration. Fracturing in the granite occurs mostly as irregular micro-fractures and veining as well as planar micro-deformation structures in quartz (Figure 1-G, H). This indicates that the granite has been subjected to a significantly high stress regime of an unknown origin with a subsequent hydrothermal fluid circulation along micro-crack systems. Hydrothermal alteration mineralogy consists largely of a single phyllosilicate phase (illite). In many cases, all feldspars and micas in the granite have been completely altered to illite.

The Distribution and intensity of alteration mineralogy is irregular with depth, with some deeper samples only slightly altered (e.g., Moomba 1 at 2895.20 and Jolokia 1 at 4005 m) in contrast to the shallow granites showing intense fracturing and hydrothermal alteration (e.g., Moomba 1 at 2847.75 m). The alteration mineralogy of the overlying sedimentary rocks consists of mainly illite, and unlike the granite, also some chlorite and kaolinite.

Illite crystallinity

Illite crystallinity values, which were determined by XRD, can be used as a semi-quantitative geothermometer for burial and hydrothermal metamorphism (Frey, 1987; Ji and Browne, 2000). Illite crystallinity is defined as the width of the first order illite basal reflection (10 Å peak) at half height and expressed usually in $\Delta 2\theta$ values. Illite crystallinity values decrease with increasing illite crystallinity. In this study, illite crystallinity values were measured mainly on samples of <2 μm size fraction and they broadly indicate that temperatures during the hydrothermal process in the granite ranged from 250°C (in Moomba 1 and Big Lake 1) to 350°C (in McLeod 1 and Jolokia 1). Crystallinity of the illite in the sedimentary rocks is lower in comparison to those in the granite samples. This together with the occurrence of chlorite and kaolinite indicates that a different fluid chemistry and lower temperature regime has prevailed during fluid flow events in the Cooper Basin sediments than in the underlying granite.

Further work

Our next step will be to constrain the timing of granite generation and hydrothermal alteration events. We hope to achieve this by dating zircon from the granite, and illite found in the sedimentary rocks of the Cooper Basin. Combined studies of geochemistry, alteration mineralogy and geochronology are crucial in establishing spatial and temporal relationships between granite generation, enrichment of heat-producing elements, and secondary thermal and/or hydrothermal alteration events.

Further analyses include additional detailed X-Ray powder Diffraction (XRD), Scanning Electron Microscope Cathodo-Luminescence (SEM-CL), and Electron Microprobe Analysis (EPMA). The XRD will be performed to further constrain the mineralogy of the granite, and EPMA will be performed to constrain the chemical compositions of the major, minor and trace minerals. With this we hope to constrain the mineralogy of the granites and further improve our understanding of their emplacement. With the SEM-CL we hope to constrain the quartz groupings and deformation features observed under polarized light. In conjunction with these analytical measurement ICP-MS will also be conducted on the bulk rock. Here two types of experiments will be conducted; in the 1st all the minerals be dissolved, in the 2nd the zircons will not be dissolved. This approach will assist in establishing whether the U content in the granites is associated to zircon and/or to other mineral phases.

References

Frey, M., 1987, Very low-grade metamorphism of clastic sedimentary rocks, In: *Low Temperature Metamorphism,* (ed. Frey M), p. 9-57. Blackie & Sons, Glasgow.

Gatehouse, C.G., Fanning, C.M. and Flint, R.B., 1995, Geochronology of the Big Lake Suite, Warburton Basin, north-eastern South Australia, *South Australia Geological Survey. Quarterly Geological Notes,* 128, 8-16.

Hill, A.J. and Gravestock, D.I. 1995 Cooper Basin, In Drexel, J.F and Preiss, W.V. (Eds), , The Geology South Australia Vol2, The Phanerozoic. South Australia, Geological Survey, Bulletin 54, p78-87

Ji, Junfeng, and Browne, P.R.L., 2000, Relationship between illite crystallinity and temperature in active geothermal systems of New Zealand, *Clay and Clay Minerals*, v48: p139-144

McLaren, S, Dunlap, J., 2006, Use of $^{40}Ar/^{39}Ar$ K-feldspar thermochronology in basin thermal history reconstruction: an example from the Big Lake Suite granites, Warburton Basin, South, Australia Basin Research, 18, 189–203

Sun, Xiaowen., 1997, Structural style of the Warburton Basin and control in the Cooper and Eromanga Basins, South Australia, Exploration Geophysics, 28, 333-39

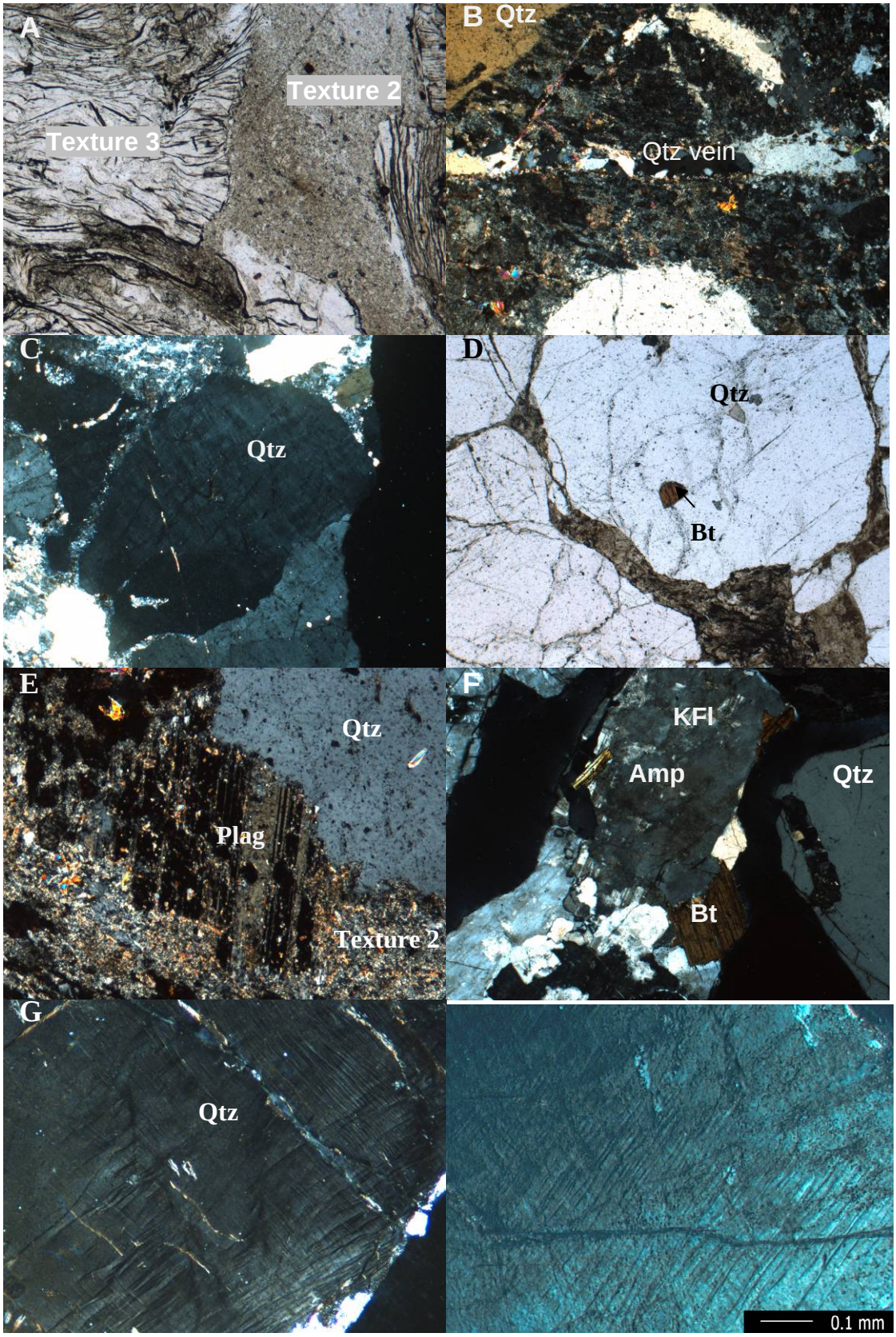

Figure 1: Transmitted light photomicrographs of some of the features observed in the various sections. Field of view in each image is 3417µm for photos A-F. A) A Plane Polarized Light (PPL) image of the relation between Texture 2 and 3. B) Vein in Big Lake-1 3057. C) quartz (qtz) grain with undulatory extinction and with "striations" visible in extinction under crossed Nichols (XPL). D). inclusion of an unaltered Biotite (Bt) in a Quartz grain (PPL),E) Altered plagioclase (Plag) present in Moomba 1 sections. F) Relatively fresh sample from Moomba 1 2895.2, G) Planar micro-deformation structures observed in quartz.

Concept of an Integrated Workflow for Geothermal Exploration in Hot Sedimentary Aquifers

J. Florian Wellmann, Franklin G. Horowitz, Klaus Regenauer-Lieb
Western Australian Geothermal Centre of Excellence, UWA-CSIRO-CURTIN
ARRC 29, Dick Perry Avenue 6165 Kensington
wellmann@cyllene.uwa.edu.au

Geothermal exploration is currently performed in different steps and on different scales, from the initial, large-scale resource estimation going down to local reservoir sustainability analysis for a specific application. With this approach, it is not possible to explore directly for requirements dictated by a geothermal application.

If we, for example, consider the exploration for a direct heat-use application we could require a pumping rate of 100 l/s at a minimum temperature of 70°C. Economic constraints could be a maximum drilling depth and the minimum years lifetime of the system. The direct map-based exploration for the best locations considering these constraints is not possible with the standard workflow.

We present here an approach to overcome this limitation. We combine geological modelling, geothermal simulation and reservoir estimation into one consistent location-based method. Outcomes of this integrated workflow are map-based reservoir and resource analyses that can directly be used as guidance in the exploration for the best possible location of a geothermal application. Our workflow is specifically developed for applications in hot sedimentary aquifers but can be extended to other geothermal settings.

Keywords: Geological Modelling, Geothermal Simulation, Direct Heat Use, Integrated Workflow, Hot Sedimentary Aquifers

Geothermal Exploration

Geothermal exploration for hot sedimentary aquifers usually consists of the following steps (not necessarily in this order):

- Geological Modelling for a resource area
- Resource Base Estimation in a large-scale target area (accessible and useful resources)
- Market analysis and other local considerations (e.g. power lines, infrastructure)
- Above-ground installation and technical application (direct heat use, power generation)
- Detailed resource analysis in a smaller scale (economic resources for a specific application)
- Local reservoir exploration and sustainability analysis
- Financial modelling

Depending on the reservoir type, further analyses are necessary (e.g. stress-field, permeability optimisation, etc.). The single parts of this workflow are usually performed separately and in a sequential order. Our method combines the steps from geological modelling to sustainability analysis which are briefly described below.

Geological Modelling

A structural geological 3-D model is an important basis for geothermal exploration. It allows the visualisation of geological structures in the subsurface and can directly be used to identify relevant areas (e.g. from fault structures, etc.). Also, a 3-D geological model is the basis for other types of analyses, like the geothermal simulation.

A large variety of tools exist to construct geological models, ranging from map-based interpolation of structures (2.5-D methods, e.g. depth to basement maps interpolated from drillhole data) to full 3-D geological modelling that can consider complicated structures like reverse faulting or doming structures (Turner, 2006).

Geothermal Simulation

Numerical geothermal simulation is the next important step in the exploration. Based on physical constraints and subsurface data, a model of the temperature distribution below ground is simulated. This is the basis for the geothermal resource estimation and allows first estimates of drilling depth to a desired temperature.

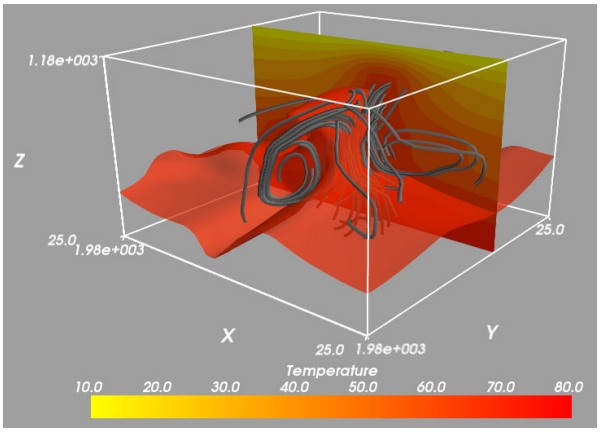

Figure 1: Example of a simulated fluid and heat flow field. The section shows a contour map of temperatures, the plane is a temperature isosurface, and streamlines (gray) indicate fluid flow paths.

Similar to geological modelling, a variety of different methods and codes are available for geothermal simulation. Main differences are the complexity of the simulation, i.e. from simple heat conduction simulation to coupled simulation of fluid and heat to complex multi-phase flow and reactive transport. (Kohl et al., 2007). The application of a code strongly depends on the geothermal reservoir type. In the case of hot sedimentary aquifers, fluid flow has to be considered as a heat transport mechanism and a suitable code should be used.

Geothermal Resource Base Estimation

Standard methods for the quality estimation of a geothermal resource are based on Muffler and Cataldi (1978). They describe several different approaches, most widely known is the volume method, often referred to as "heat-in-place". The total thermal energy contained in a volume V of rock is estimated based on specific heat of rock c_r and fluid c_w, porosity ϕ, density ρ and a temperature difference ΔT:

$$H_{ip} = \left[(1-\phi)c_r\rho_r + \phi c_w\rho_w\right]\cdot V\Delta T$$

The calculation of heat-in-place is usually performed for an estimated total volume, mean temperature and porosity of a resource rock.

Other estimations are possible and depend on the geological situation and geothermal resource type.

The evaluated resource base has to be further subdivided (Fig. 2) into accessible heat, usually defined by the maximum depth of drilling (this is what is usually considered in a standard "heat-in-place" analysis). But not all heat from the accessible heat is actually useful, based on physical limitations, reservoir lifetime and legal and environmental considerations. Finally, only a fraction of the useful heat can be considered as economic, which Muffler and Cataldi (1978) define as the geothermal energy that can be extracted in the lifetime of a reservoir at costs comparable to other energy sources.

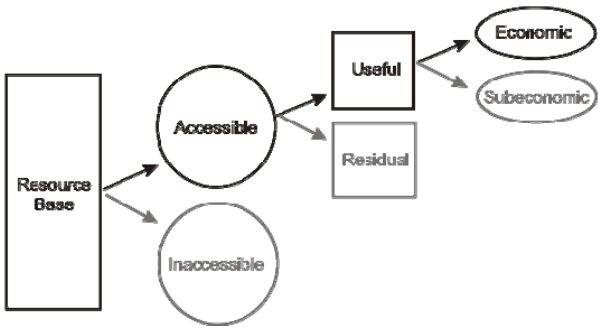

Figure 2: From the broad geothermal resource base to estimation of the economically useable resource (redrawn from Muffler and Cataldi, 1978).

Estimation of Extractable Energy

The amount of extractable heat depends on many geological, physical and technical factors. These are usually combined into a general "recovery factor" as a broad estimation.

For a hot sedimentary aquifer, Gringarten (1978) defines a heat recovery factor, R_g, as a the ratio of extracted heat, $Q_{\max}\Delta t\rho_w c_w\Delta T$, to the total theoretically recoverable heat-in-place as given above. Here Δt is the producing time, the quantity $Q_{\max}$ is the maximum production flow rate that can be maintained either indefinitely (for a truly sustainable system) or over the assumed economic lifetime of the geothermal system and $\rho_w c_w$ is the volumetric heat capacity of water. Writing

$$R_g = \frac{1}{\phi + (1-\phi)(\rho_r c_r / \rho_w c_w)}\frac{Q_{\max}\Delta t}{V}$$

we find the heat recovery factor is dominated by $Q_{\max}\Delta t$ for a porosity of ϕ: the recovery factor is a function of time. The maximum sustainable pumping rate $Q_{\max}$ for a doublet well (pumping and re-injection) over a production time Δt can be analytically estimated from heat and flow equations. Gringarten (1978) presents an analytical approximation and derives the following relationships for the pumping rate Q:

$$Q = \frac{\pi\rho_a c_a}{3\rho_w c_w}\frac{h}{\Delta t}D^2$$

and

$$Q = 2\pi\frac{1}{\ln(D/r_w)}Ts$$

The first equation describes the pumping rate as a function of production time, thickness *h* of the aquifer and distance *D* between pumping and re-injection well. The second equation includes the maximum drawdown *s*, the well diameter r_w and transmissivity *T*. Temperature is implicit in these equations as density of water and transmissivity are a function of temperature.

The combined solution of these equations provides an estimate of the maximum pumping rate $Q_{\max}$ and the minimal distance *D* required between the pumping and re-injection well in the aquifer to avoid a thermal breakthrough during the production lifetime of the doublet.

The result can be considered a very conservative estimate as an application may still be possible after thermal breakthrough for some time. Also, as soon as a natural hydraulic gradient is present, a

layout of the re-injection well downstream from the pumping well will increase the lifetime even more (Banks, 2009).

Limitations of the standard approaches

The presented standard methods to evaluate a geothermal resource and its sustainable application are performed on two different scales. Whereas the heat-in-place estimation is performed for a whole resource, the estimates for a sustainable pumping rate are performed on the local scale. It is not possible to derive a location-based analysis of heat in the subsurface (i.e. how is the total heat-in-place distributed in space) or to analyse a whole area for a required pumping rate (i.e. where can a certain pumping rate be obtained for a minimum time). Thus, the combined analysis of both factors is not possible for a whole resource region.

To overcome this limitation, we present an approach to down-scale the heat-in-place estimation for a regional analysis and to extend the Gringarten estimations to a whole area, all within the context of geological modelling and geothermal simulation.

Integrated Geothermal Exploration

Concept of workflow

In our workflow (Fig. 3), we combine the steps from geological modelling to resource and sustainability estimations.

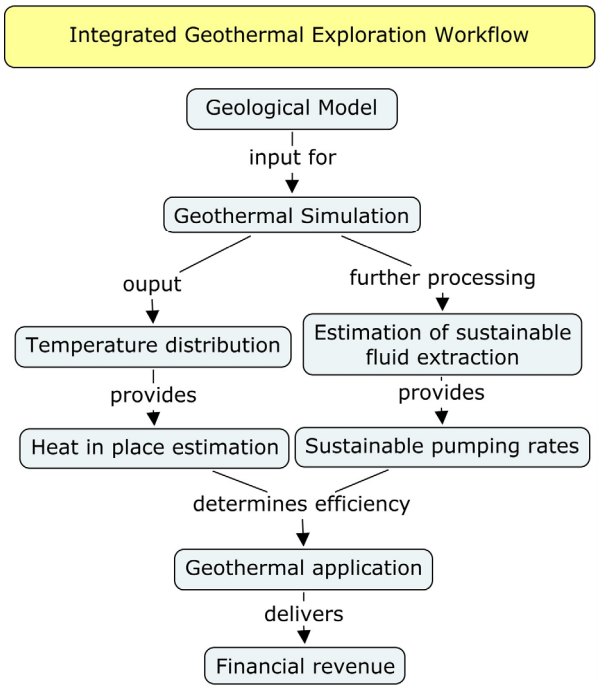

Figure 3: workflow of our approach from geological model to efficiency estimation of geothermal application

The starting point for our workflow is a full 3-D geological model. We use GeoModeller (www.geomodeller.com) for the modelling as it is capable of dealing with complicated 3-D geological settings and provides a very fast and efficient way to create realistic geological models directly based on input data (e.g. Calcagno, 2008). It is thus possible to quickly test several geological scenarios as the starting point for the geothermal simulation.

We link the geological model directly to a geothermal simulation code. The simulation is performed with a fully coupled fluid, heat and reactive transport simulation code (SHEMAT). All relevant physical properties are calculated as a function of temperature in each time step. It is also possible to include anisotropies in thermal conductivity and permeability (see Clauser, 2003 for a detailed description). The simulation code is thus capable of dealing with complex settings (from hot dry rock to hydrothermal) and has been applied to many geothermal simulations (e.g. Soultz-sous-Foret (France), Waiwera (New Zealand)).

Now, we process the results of the geothermal simulation further for two analyses: (1) the distribution of heat in the subsurface and (2) estimation of the sustainable pumping rates. The main difference to the standard approaches is that we create a map view of the distribution of both properties in the whole resource area.

The simulated temperature and fluid flow field and the distribution of physical properties in 3-D are then processed further with a set of programs to derive several characteristic parameters (e.g. transmissivity, mean water density, mean temperature of one formation at depth). Essentially, we analyse the physical properties in the subsurface at every location in space. This is then used as an input for the extended volumetric heat-in-place calculation (following Muffler and Cataldi, 1978) and the well doublet spacing and maximum pumping rate analysis from Gringarten (1978) and Banks (2009), as described above.

The distribution of temperatures, local heat-in-place and the evaluation of sustainable pumping rates in the resource area now directly allows the exploration for a suitable area given the characteristics of a geothermal application. For example, we can now identify areas in the map where we can achieve the required pumping rate for a given minimum temperature and available heat which, in the end, determines the economics of a geothermal application.

Example Model

We apply our workflow for geothermal resource estimation to a full 3-D geological model to local heat-in-place and sustainable pumping rate evaluation. The model is situated in a half-graben setting (Fig. 4). A large normal fault in the east off-sets the basement creating a basin. This basin is filled with several sedimentary formations that are furthermore displaced by normal faults, leading to an internal graben structure. The scale of the model is 8 km x 8 km x 5 km.

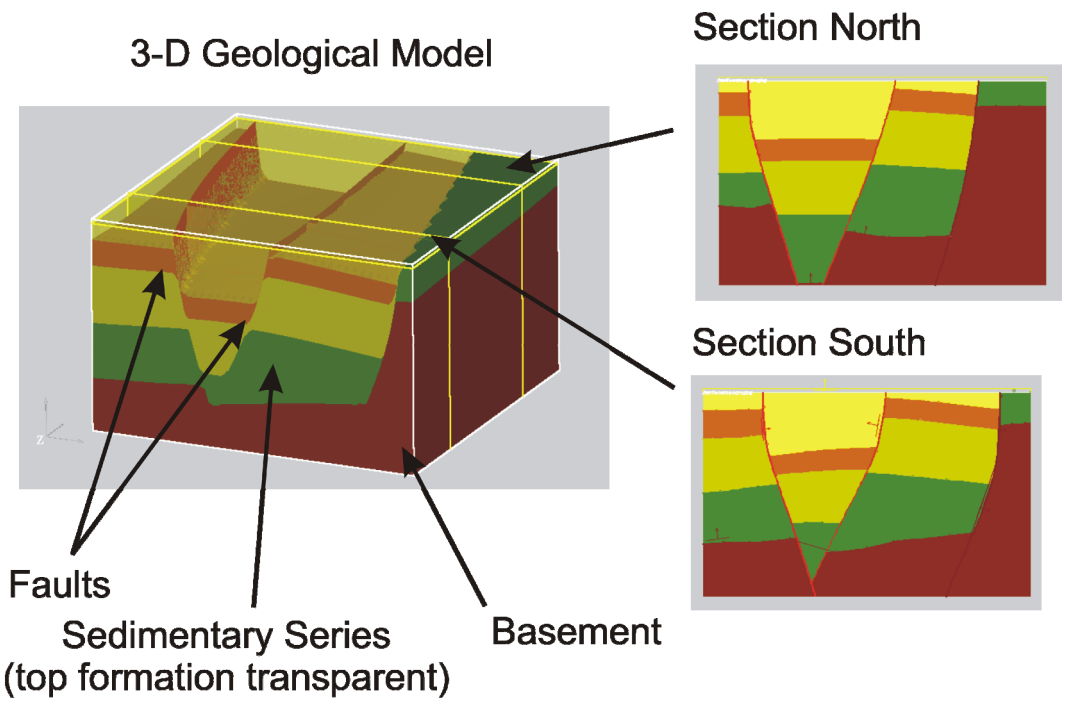

Figure 4: Simple geological model used for the application of the workflow. The structural setting is a half-graben structure; the basin is filled with sedimentary formations that are further cut by faults.

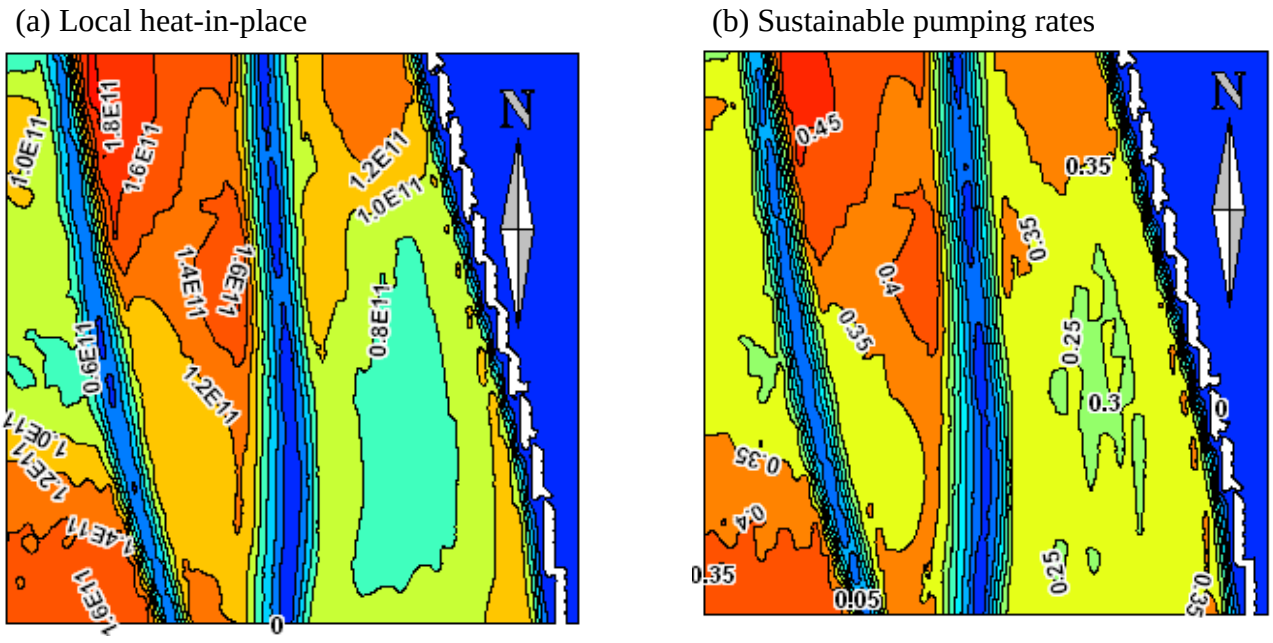

Figure 5: Selected results of our workflow. Analyses are performed for the second lowest sedimentary formation (light green in Fig. 4).

(a) local heat-in-place, normalised to m^2. (b) Sustainable pumping rates [m^3/s] for a production period of 30 years. We can clearly identify the most promising areas.

This structural set-up happens to be similar to areas in the Perth Basin and representative of geological settings in other sedimentary basins. Values for thermal conductivity and hydraulic properties are also similar to formations in the Perth Basin.

Results

The maps in Figure 5 show the most important results of our integrated workflow, i.e. the local heat-in-place and the maximum pumping rate for one formation. These maps are created in a GIS framework and can directly be used for a location-based analysis. We obtain the local heat-in-place in addition to the total heat-in-place which is usually estimated (it would be approximately 5.2E18 J in this example).

The map dimensions are the same as for the model (8 x 8 km). Displayed is the analysis for the second lowest sedimentary formation (light green in Fig. 4). We can see that most of the heat in place (Fig. 5a) is located within the Northern part of the graben. In the same area, we can obtain the highest sustainable pumping rates (here determined for a total lifetime of 30 years). The patterns coincide in this case as we are considering a simple structure with homogeneous permeabilities and thus pumping rates are strongly related to temperature (which is, in this simple case, also reflected by the local heat-in-place pattern). In other cases (e.g. in lower permeability settings like Enhanced Geothermal Systems), we might obtain a completely different picture for local heat-in-place and sustainable pumping rates.

Discussion

We presented an integrated geothermal resource evaluation workflow that combines and extends classical methods. Starting from a full 3-D geological model and relevant physical properties, we simulate the temperature and fluid flow fields and use these as a basis for a variety of estimations. Firstly, we calculate the overall heat-in-place, as defined in Muffler and Cataldi (1978). We extend this classical method to a location-based analysis to identify directly the position of a valuable resource. We also use the results of the simulation for an estimation of a well doublet scheme and sustainable pumping rates, after Gringarten (1978) and Banks (2009) and extend it to a resource-wide estimation. The main benefit of our workflow is that it directly combines these standard methods for a location-based geothermal resource and sustainability analysis.

As the results from our integrated workflow are location-/map-based, it is possible to combine them with other relevant location factors. We can, for example, combine our analyses with a map of the depth of a formation and a maximum drilling depth. Other map-based economic constraints can directly be implemented, e.g. the distance to the market or available infrastructure. Our workflow thus opens up the way to an integration of geological, geothermal, technical and financial considerations within one combined framework.

Furthermore, our workflow can be extended to scenario testing. All the single steps in the workflow are linked. It is thus possible to directly test the effect of a change in the geological model or the physical properties on the estimation of the sustainable pumping rate. This is not possible with common standard approaches.

The results of our simple example model (Fig. 5) are based on several assumptions and simplifications (see Gringarten, 1978, and Muffler and Cataldi, 1978, for a detailed description of their assumptions). The calculated estimations have to be considered in the light of these assumptions. Still, in a recent review of these methods, Banks (2009) points out that they are applicable in many cases and provide a rather conservative estimate. We interpret the numbers as a guideline but the distribution in space as very valuable information as this directly points out the location of a probable geothermal resource.

Our approach is flexible and can be applied in simple and complex settings. The geological modelling is capable of dealing with complicated geological settings, like reverse faulting or overturned folding and doming structures (e.g. Calcagno, 2008). The geothermal simulation can be extended to include reactive transport and species transport (Clauser, 2003). Furthermore, the applied simulation code can also model pumping and re-injection. This will be implemented in the future into our workflow. It will thus be possible to directly validate the effect of long-term pumping in the fluid and heat flow field in complex geological settings in an identified target area.

References

Banks, D., 2009, Thermogeological assessment of open-loop well-doublet schemes: a review and synthesis of analytical approaches: Hydrogeology Journal,

Calcagno, P., Chiles, J. P., Courrioux, G., Guillen, A., 2008, Geological modelling from field data and geological knowledge: Part I. Modelling method coupling 3D potential-field interpolation and geological rules: Physics of the Earth and Planetary Interiors, v. 171, p. 147-157

Clauser, Christoph, Bartels, Jörn, 2003, Numerical simulation of reactive flow in hot aquifers. SHEMAT and processing SHEMAT. Berlin: Springer.

Gringarten, Alain C., 1978, Reservoir lifetime and heat recovery factor in geothermal aquifers used

for urban heating.: Pure and Applied Geophysics, v. 117, p. 297–308.

Kohl, T., Baujard, C., Zimmermann, G., 2007, Modelling of Geothermal reservoirs – an overview: ENGINE Mid-Term Conference, Potsdam, January 2007.

Muffler, P., Cataldi, R., 1978, Methods for regional assessment of geothermal resources: Geothermics, v. 7, p. 53–89.

Turner, K., 2006, Challenges and trends for geological modelling and visualisation: Bulletin of Engineering Geology and the Environment, v. 65, p. 109-127

Exergetic performance and power conversion of a CO_2 thermosiphon

Aleks D Atrens[1]*, Hal Gurgenci[1] and Victor Rudolph[1]
[1] The Queensland Geothermal Energy Centre of Excellence, The University of Queensland, QLD 4072
* Corresponding author: aleks.atrens@uq.edu.au

Engineered geothermal systems (EGS) supply the potential to produce a significant capacity of base-load renewable electricity. In EGS that are not hydraulically connected to a source of water recharge off the opportunity to use CO_2 as a heat extraction fluid instead of H_2O. CO_2 offers the advantages of ease of flow through the subsurface reservoir, an innate buoyancy driving simplifying surface equipment design, and lower dissolution of compounds that lead to fouling in wellbores and surface equipment. These advantages are balanced by higher frictional losses within the wellbores, particularly the production wellbore due to the low density of CO_2 in this process component. Here we explore the results of these advantages and disadvantages on the exergy extracted from the geothermal reservoir, and examine the impact of direct use of CO_2 in power conversion equipment.

Keywords: Carbon dioxide, EGS, enhanced geothermal systems, CO2, thermosiphon

Introduction

The use of CO_2 in EGS has been discussed in a number of previous works (Brown 2000; Pruess 2006; Gurgenci, Rudolph et al. 2008; Pruess 2008; Atrens, Gurgenci et al. 2009a). The use of CO_2 in EGS where CO_2 recovered from the underground reservoir is fed directly into a turbine (known as a CO_2 thermosiphon), is significantly different from H_2O flash or binary plants.

A convenient method for comparing power generation systems with significant internal differences is through the usage of exergy. This provides a measure of the maximum theoretical electricity that can be generated from the system. As such, a comparison of the exergy available at the surface can be used as a rough measure to compare the different designs. Exergy available on the surface Ψ is calculated from:

$$\Psi = m(h_{prod} - h_{inj} - T_0 (s_{prod} - s_{inj}))$$

Where h_{prod} and s_{prod} are the enthalpy and entropy of fluid exiting the production wellhead, h_{inj} and s_{inj} are the enthalpy and entropy entering the injection wellhead, and T_0 is the reference temperature (ambient temperature is used).

The enthalpy and entropy at the injection and production wellheads is calculated by methods described in previous work (Atrens, Gurgenci et al. 2009b).

Exergy Recovery

Fluid flow of CO_2 compared to water as calculated from modelling methods in previous work is shown in figure 1 (for a reservoir of hydraulic impedance as per Soultz-sous-Foret). Much larger flow-rates of CO_2 then H_2O can be achieved due to its lower viscosity in the reservoir, particularly in the region near the injection well (where the viscosity of water is much higher).

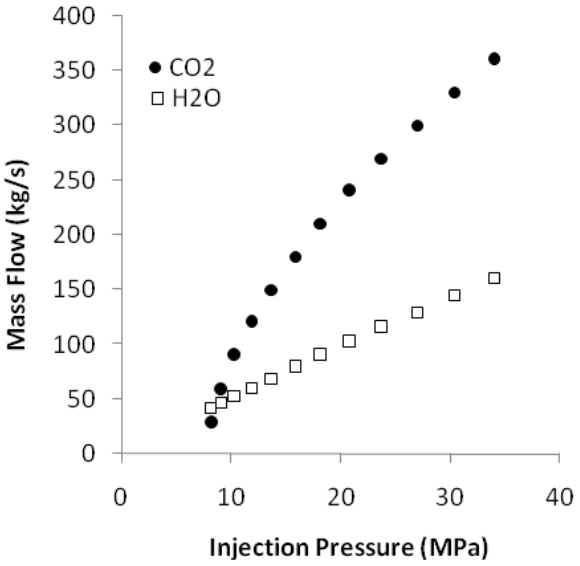

Figure 1: Injected fluid flow-rates

However, due to larger pressure drop in the production well, in conjunction with the lower heat capacity of CO_2 compared to water, CO_2 will extract less exergy than water under most conditions. This situation can be changed through increase in production well diameter size. This change has very large effects on the CO_2, significantly reducing the pressure drop in the production well leading to higher exergy recovery. As well diameters generally used are an appropriate size for the volumetric flows likely for water, the effects on exergy extraction of water are negligible. Exergy extracted for a base reference case, and with two larger diameter casing sizes for CO_2-based systems is shown in figure 2.

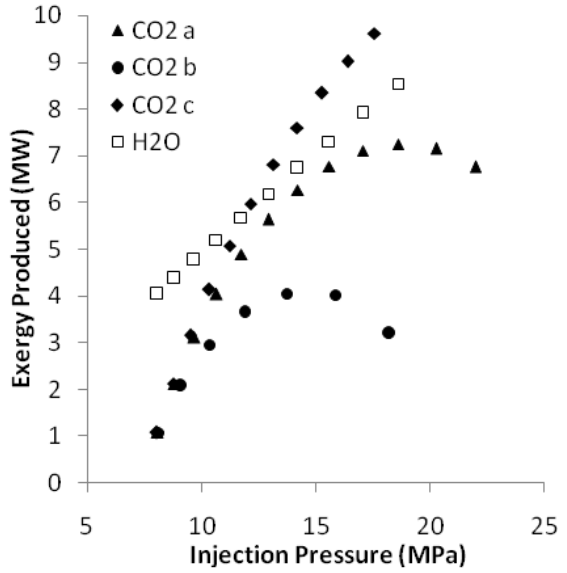

Figure 2: Exergy produced at the surface by the different fluids; (a) for reference casing internal diameter size of 0.2313 m; (b) for internal diameter of 0.3 m; (c) for internal diameter of 0.4 m

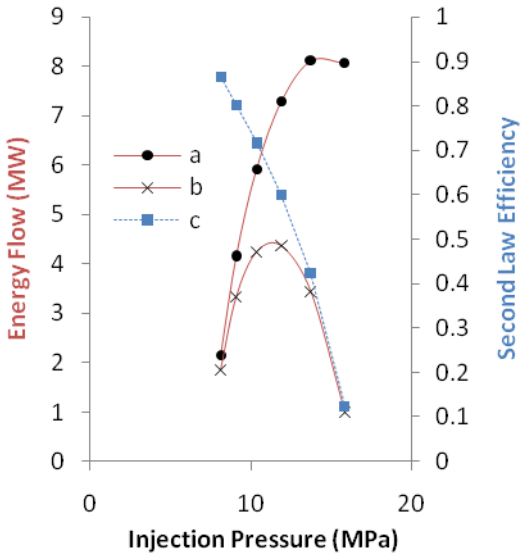

Figure 3: Energy recov ery considerations for CO_2 for the reference case; (a) Exergy produced at the surface; (b) Electricity generated; (c) Second law efficiency of the overall process.

Power Conversion

The ability to extract exergy from the subsurface reservoir is not the only issue of critical importance to an EGS power plant. Also important is the capability to convert the exergy extracted into electricity in an effective manner.

Because CO_2 in a thermosiphon plant configuration is used directly in power conversion equipment, the impact of production pressure on the ability to convert available exergy into electricity is significant. This means that as flow-rates through the subsurface are increased (and exergy extraction is increased), the ability to convert the exergy extracted into electricity is reduced (due to the reduced difference in pressures between the production wellhead and the injection wellhead). This leads to the relationship between turbine work and exergy produced as shown in figure 3. This is based on an assumed isentropic efficiency of the turbine of 85%, while in reality higher isentropic efficiency may be achievable. The second law efficiency shown in this figure represents the proportion of the actual work out of theoretical maximum work achievable in an ideal case.

This relationship can be improved through the addition of a recompression system. In such a case, the turbine exhaust would be designed at a lower operating pressure, and the effluent from the turbine would be recompressed after cooling, and prior to reinjection. The thermodynamic relationship of this process change is shown in figure 4.

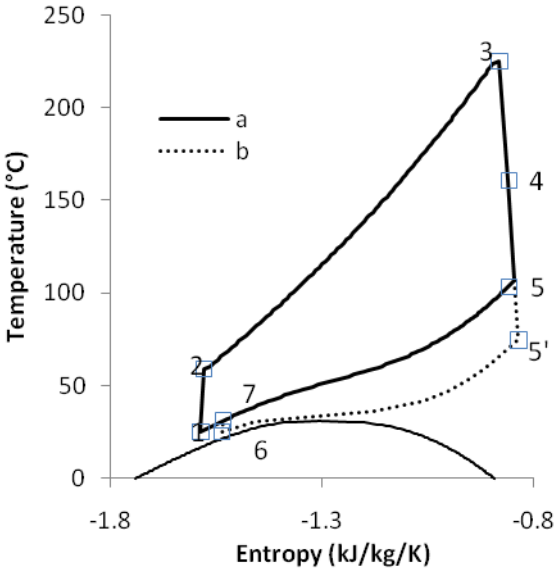

Figure 4: Temperature-entropy diagram showing (a) CO_2-based EGS basic power cycle; and (b) recompression modification. Point (1) indicates the injection wellhead and heat exchanger outlet, point (2) indicates the base of the injection well and the entry to the reservoir, point (3) indicates the base of the production well, point (4) indicates the production wellhead and turbine inlet, and point (5) indicates the turbine exhaust and cooling system inlet. Point (5') indicates the turbine exhaust with recompression modification, point (6) indicates the compressor inlet, and point (7) indicates the compressor outlet.

Process modification in this manner leads to performance as shown in figure 5. This represents a significant improvement in electricity recovery, and indicates a worthwhile process modification.

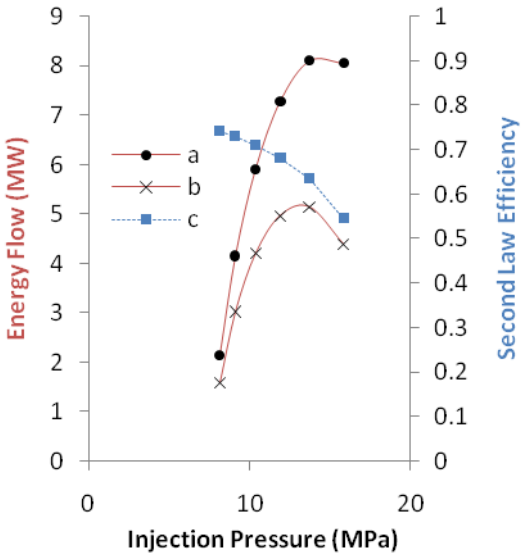

Figure 5: Energy recov ery considerations for CO_2 as in figure 3, with recompression process modification; (a) Exergy produced at the surface; (b) Electricity generated; (c) Second law efficiency of the overall process.

Reference Case

The reference case used in this work utilises data as given in table 1.

Table 1: Reference Case Data

Parameter	Value
Depth (m)	5000
Reservoir Length (m)	1000
Reservoir Temperature (°C)	225
Injection Temperature (°C)	25
Reference Temperature (°C)	25
Min. Reservoir Width (m)	0.73
Max Reservoir Width (m)	251
Depth (m)	5000
Hydraulic Impedance (MPa.s/L)	0.2
Reservoir Pressure (MPa)	49
Wellbore roughness, ε (m)	0.0004
Wellbore Diameter (m)	0.231
Isentropic Efficiency, η_{II}	0.85

References

Atrens, A. D., Gurgenci, H., Rudolph, V., 2009a, CO2 thermosiphon for competitive power generation, Energy & Fuels **23**(1): 553-557.

Atrens, A. D., Gurgenci, H., Rudolph, V., 2009b, Exergy analysis of a CO2 thermosiphon, Thirty-fourth workshop on geothermal reservoir engineering, Stanford University, Stanford, California

Brown, D. W., 2000. A hot dry rock geothermal energy concept utilizing supercritical CO2 instead of water. Twenty-Fifth Workshop on Geothermal Reservoir Engineering, Stanford University, Stanford, California.

Gurgenci, H., V. Rudolph, et al., 2008. Challenges for geothermal energy utilisation. Thirty-Third Workshop on Geothermal Reservoir Engineering, Stanford University, Stanford, California.

Pruess, K. (2006). "Enhanced geothermal systems (EGS) using CO2 as working fluid—A novel approach for generating renewable energy with simultaneous sequestration of carbon." *Geothermics* **35**: 351–367.

Pruess, K. (2008). "On production behaviour of enhanced geothermal systems with CO2 as working fluid." Energy Conversion and Management **49**: 1446-1454.

Radiation associated with Hot Rock geothermal power

David L. Battye*, Peter J. Ashman
School of Chemical Engineering, University of Adelaide, SA 5005.
* Corresponding author: david.battye@adelaide.edu.au

Water in Hot Rock reservoirs is in contact with granites containing radioactive elements (radionuclides). The wider community is generally aware of this fact through publicity by the Australian geothermal industry. It is less clear to the public what radiation hazards may exist for Hot Rock projects, and how significant they may be. The aim of this study was to investigate likely radiation hazards associated with Hot Rock geothermal power, with a particular emphasis on radon emission. The study consisted of a review of literature and quantitative estimates of radon emission and dispersion from a typical Hot Rock reservoir. This information has been used to develop a fact sheet, published by Primary Industries and Resources South Australia (PIRSA, 2009).

Keywords: radiation, radon, radium, uranium, Hot Rock geothermal.

Dissolved radionuclides

The radionuclides of interest are those with long enough half-lives to travel to the surface from the reservoir, including isotopes of uranium, thorium, radium, and radon.

Uranium and thorium in granites are mostly found in monazite, zircon and allanite mineral phases. These phases are highly insoluble under most conditions, therefore the controlling mechanisms for radionuclide release are dissolution at the rock-water interface and alpha-recoil (ejection from the rock due to alpha-decay of the parent radionuclide).

Uranium solubility is a strong function of the oxidising or reducing nature of the geofluid. Uranium contents in granite groundwaters are frequently less than the recommended limit for drinking water (20 μg/L), but may exceed 800 μg/L in oxidising groundwaters (Gascoyne, 1989). Uranium does not emit gamma radiation, therefore it is only hazardous if ingested or inhaled.

The solubility of thorium is low since it tends to form the insoluble hydroxide. Thus, thorium concentrations in groundwaters rarely exceed 1 μg/L (Langmuir and Herman, 1980).

Radium is released from the rock by alpha-recoil, but is readily scavenged from solution by sorption onto mineral surfaces. Cations compete with radium for sorption sites, thus the solubility of radium increases strongly with total dissolved solids (TDS), as indicated by groundwater data shown in Figure 1. Where natural waters exist in Hot Rock reservoirs, they are typically quite high in dissolved solids, eg. TDS = 100 g/L at Soultz (MIT, 2006) and 21 g/L in the Cooper Basin (Wyborn et al, 2004). The TDS of water in an operational field will depend on the extent of dilution of natural water with injected water. At Fenton Hill, substantial dilution was achieved during open-loop operation (Grigsby et al, 1983). On switching to closed loop operation, the TDS reached a steady value of ~3 g/L. Thus, natural water in Hot Rocks may have radium activities at the upper end of the scale shown in Fig. 1, but the activity can be reduced to low levels by dilution of dissolved solids. To gain some perspective on what constitutes “low” levels, we note that groundwater sources for drinking water may contain radium at up to or exceeding 0.5 Bq/L (NHMRC, 2004), a level corresponding to TDS ≈ 5 g/L according to the trend in Fig. 1.

Hot Rock reservoirs are at significantly higher temperatures than the groundwaters for which uranium, radium and thorium data exist. Solubility is typically enhanced by increasing temperature and higher concentrations of these radionuclides than cited above are therefore possible, depending on the other contributing factors. The Hot Rock geothermal literature reports measurements of radon in solution but not other radionuclides of interest. Such measurements in current and future projects would be of scientific value, and would directly address radiation concerns.

Deposition in surface equipment

The Hot Rock geothermal power concept involves circulation of water through an artificial reservoir and surface equipment in a closed loop. Cooling and depressurising of water in surface equipment may lead to solid deposits in the form of scales and sludges. There is potential for these deposits to be radioactive due to inclusion of precipitated radionuclides. This problem is encountered in the oil and gas industry, where highly saline produced waters with significant dissolved radium are handled. These waters tend to be saturated with barium and strontium sulphates, which precipitate as scales and sludges. Dissolved radium readily substitutes for barium and strontium in the solids, creating a radioactive waste material which must be periodically removed. Workers are exposed to gamma radiation, which is able to penetrate pipe and vessel walls. Additionally, inhalation of radioactive dust is an exposure hazard when removing the deposits. Hamlat (2001) provides estimates of radiation doses received by workers in the oil and gas industry which suggest that the

exposure is low - generally < 1 mSv per year - compared with the Australian occupational dose limit of 20 mSv per year (ARPANSA, 2002), provided that appropriate protective measures are taken. This level of exposure is less than the average background radiation dose in Australia of 1.5 mSv per year (ARPANSA, 2009).

The levels of dissolved solids, radium, and of strontium and barium sulphates are expected to be lower for Hot Rock waters than generally encountered in the oil and gas industry. Hence, lesser quantities of radioactive deposits are anticipated, with lower concentrations of precipitated radium. The gamma radiation hazard associated with solid deposits may therefore be small compared to that managed in the oil and gas industry. The data of Fisher (1995) in Fig. 1 is representative of waters produced from oil and gas fields, which frequently have TDS in excess of 100 g/L. Diluted water circulating in Hot Rocks is expected to have at least 10 times less TDS than this, and therefore 7 times less radium activity according to the trend in Fig. 1. The same reduction in radioactivity of the barium and strontium sulfate deposits can be expected. Considering that the occupational radiation exposure in the oil and gas is already relatively low, the exposure from Hot Rock geothermal power plants is therefore likely to be very small. However, the ALARA (As Low As Reasonably Achievable) principle of radiation protection will still apply, which calls for monitoring of exposure and protective measures. In particular, workers involved with removing solid deposits from equipment will need to avoid inhaling dusts.

Radon

Radon is an inert radioactive gas which is formed by the alpha-decay of radium. It is normally present at low levels in ambient air. The average radon level in Australian homes is 10.5 Bq/m^3 (ARPANSA, 2009). The decay products of radon can lodge in the lungs if inhaled, exposing them to ionizing radiation and increasing the risk of lung cancer. The action limits for radon in air are 200 Bq/m^3 in dwellings and 1000 Bq/m^3 in workplaces (ARPANSA, 2002).

In a geothermal reservoir, radon enters solution predominantly by alpha-recoil and remains dissolved until its decay. The maximum radon content is achieved when the rates of solution and decay are equal This occurs if the residence time of water in the reservoir exceeds 25 days (^{222}Rn has a half life of 3.8 days). Radon activity in water was a maximum of 500 Bq/L at Fenton Hill (Grigsby et al, 1983) and 200 Bq/L at Rosemanowes (Richards et al, 1992).

Radon emission and dispersion

Radon emissions will occur during open-loop circulation testing of newly created reservoirs, from uncontrolled flows of geothermal water, or from venting of light gases from steam condensers.

If the Hot Rock reservoir is assumed to consist of planar, parallel fractures with even spacing, the radon emanation rate, R (atoms/s) is given by:

$$R = \frac{2FV}{S}$$

where F is the radon flux from fracture surfaces (atoms s^{-1} m^{-2}), V the fractured rock volume (m^3) and S the fracture spacing (m).

The radon flux from plane surfaces of Carnmenellis granite cubes in water was measured at 30 atoms s^{-1} m^{-2} by Andrews et al. (1983). The granite had an average uranium content of 13.5 ppm, and we have assumed that a similar flux value is appropriate for Cooper Basin granites, which typically contain 16 ppm of uranium (Geoscience Australia, 2008).

Kruger (1995) inferred a mean fracture spacing of 50 m from circulation tests at the Rosemanowes site.

Steady-state emission of radon from a field can be estimated by assuming that the emission rate at the surface is equal to the emanation rate. Decay of radon in the reservoir is neglected. Assuming the above cited values for fracture spacing and flux in the Cooper Basin, this method yields an emission rate of 1.2 billion atoms (2520 Bq) per second, per cubic kilometer of fractured rock.

Radon is emitted from steam-venting stacks during circulation testing, therefore downwind radon levels are of interest. A simple Gaussian dispersion model was used to predict the maximum radon activity at ground level downwind of a single emission source with respect to effective emission height (physical vent height plus an allowance for plume rise), and wind speed. Results for a 1 km^3 reservoir are shown in Figure 2. Radon levels are generally negligible for emission heights of 10 m or more, except in calm conditions (wind speeds less than 1.8 km/h). In the latter case, levels are expected to be less than the action limit for dwellings.

During an uncontrolled flow of geothermal water from a well, the effective emission height is close to ground level, eg. 2-5 m. Figure 1 suggests that for a 1 cubic kilometre reservoir, downwind radon levels would be significant but not exceeding the workplace action limit except under calm conditions. However, it should be remembered that Figure 1 is based on a steady-state emission rate. If the water in the reservoir has been still for a period, its radon content will be higher than during circulation. Therefore the initial emission rate will initially be higher than the steady-state value. For example, if still water in the reservoir

attains a radon level of 500 Bq/L, then a sudden flow of 50 L/s will cause an initial emission rate of 25,000 Bq/s, a value 10 times the steady value assumed for Figure 1 and therefore increasing downwind radon activities by the same factor.

Calm conditions usually occur at night in central Australia and may last several hours. Estimates suggest that during calm periods radon emission may be a significant hazard for the area within 200 m downwind of an uncontrolled flow. However, the simple Gaussian dispersion model results become spurious as wind speed approaches zero, and more advanced dispersion models are required to more accurately predict radon levels in calm periods.

Acknowledgements

This work was commissioned by Primary Industries and Resources SA (PIRSA). We wish to thank Alexandra Long and Michael Malavazos of PIRSA for their guidance throughout the project.

References

Andrews, J.N, 1983, Dissolved radioelements and inert gases in geothermal investigations, Geothermics, v. 12, no. 2/3, p. 67-82.

ARPANSA, 2009, Background radiation fact sheet, http://www.arpansa.gov.au/pubs/baseline/bg_rad.pdf (retrieved June 2009).

ARPANSA, 2002, Radiation Protection Series No. 1, http://www.arpansa.gov.au/publications/Codes/rps.cfm (retrieved June 2009).

Fisher, R., 1995, Geologic, geochemical and geographic controls on NORM in produced water from Texas oil, gas and geothermal reservoirs, Final report, US Department of Energy Report DOE/MT/92011-12.

Gascoyne, M., 1989, High levels of uranium and radium in groundwaters at Canada's Underground Research Laboratory, Lac du Bonnet, Manitoba, Canada, Applied Geochemistry, v. 4, p. 577-591.

Geoscience Australia, OZCHEM database, http://www.ga.gov.au/gda/ (retrieved October 2008)

Grigsby, C.O., Tester, J.W, Trujillo, P.E., Counce, D.A., Abbot, J., Holley, C.E., and Blatz, L.A., 1983, Rock-water interactions in hot dry rock geothermal systems: Field investigations of in situ geochemical behavior, Journal of Volcanology and Geothermal Research, 15, p. 101-136.

Hamlat, M.S., Djeffal, S., Kadi, H., 2001, Assessment of radiation exposures from naturally occurring radioactive materials in the oil and gas industry, Applied Radiation and Isotopes, 55, p. 141–146.

Kruger, P., 1995. Heat extraction from HDR geothermal reservoirs. Proceedings of the World Geothermal Congress, 1995, Florence, Italy, Vol. 4, pp. 2517-2520.

Langmuir, D. and Herman, J.S., 1980, The mobility of thorium in natural waters at low temperatures, Geochimica et Cosmochimica Acta, 44, p. 1753-1766.

MIT, 2006, The Future of Geothermal Energy, http://geothermal.inel.gov (retrieved October 2008).

NHMRC, 2004, Australian Drinking Water Guidelines, http://www.nhmrc.gov.au/publications/synopses/eh19syn.htm (retrieved June 2009).

PIRSA, 2009, Fact Sheet: Radon and Naturally Occurring Radioactive Materials (NORM) associated with Hot Rock Geothermal Systems, http://www.pir.sa.gov.au/__data/assets/pdf_file/0013/113341/090107_web.pdf (retrieved September 2009).

Richards, H.G., Savage, D. and Andrews, J.N., 1992, Granite-water reactions in an experimental Hot Dry Rock geothermal reservoir, Rosemanowes test site, Cornwall, U.K., Applied Geochemistry, v. 7, p. 193-222.

Wyborn, D., de Graaf, L., Davidson, S., and Hann, S., 2004, Development of Australia's first hot fractured rock (HFR) underground heat exchanger, Cooper Basin, South Australia, PESA Eastern Australasian Basins Symposium II, Adelaide, p. 423-430.

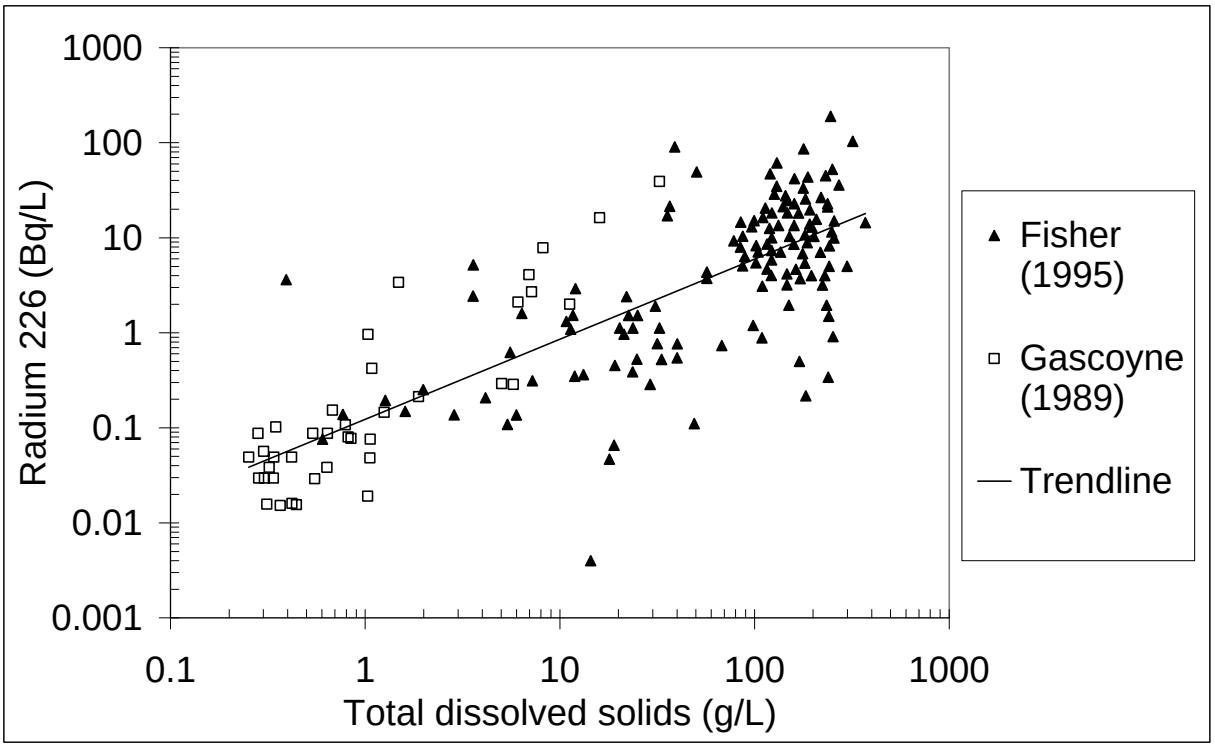

Figure 1: Radium-226 activity versus total dissolved solids in groundwaters. Fisher (1995): Oil, gas and geopressured-geothermal wells in Texas. Gascoyne (1989): Granite groundwaters, Whiteshell Research Area, Canada.

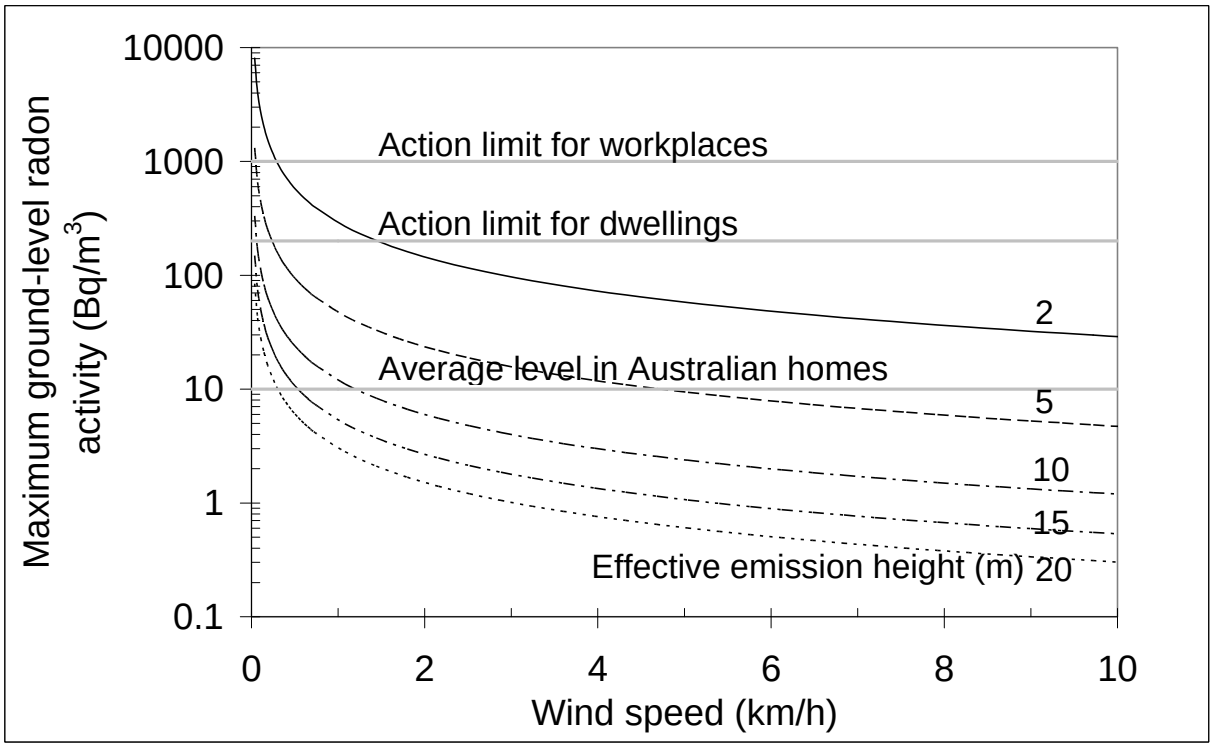

Figure 2: Maximum ground-level radon activity directly downwind of a single emission source, with respect to wind speed and effective emission height. Assumes an emission rate of 2520 Bq/s, based on steady-state emission from 1 km^3 of fractured rock, 50 m mean fracture spacing, 30 atoms s^{-1} m^{-2} radon flux from fractures, and neglecting decay of radon. To determine radon levels at another emission rate, E (Bq/s), multiply the radon level in the plot by E/2520.

Silica deposition in Enhanced Geothermal Systems

Donny S. Bhuana[1], Peter J. Ashman[1*], Graham J. Nathan[2]
Centre for Energy Technology
[1] School of Chemical Engineering, The University of Adelaide.
[2] School of Mechanical Engineering, The University of Adelaide.
* Corresponding author: peter.ashman@adelaide.edu.au

Central Australia has one of the hottest rock resources on earth, making it a potential region for developing geothermal energy using Enhanced Geothermal Systems (EGS). However, this technology is yet to be proven under local conditions and so relatively little field data or experimental data relevant to local conditions are available. Nevertheless, much can be learned from the global experience due to the operation of conventional geothermal energy plants, i.e. those using heat from volcanic activity. The amount of heat that can be extracted from high-temperature underground reservoirs using water as a working fluid in a closed loop is significantly limited by the onset of silica precipitation and subsequent scaling of heat exchanger surfaces and fouling of reservoirs as the water is cooled. The precipitation rate of amorphous silica is relatively rapid, resulting in potential deposition if the water is cooled below its saturation temperature. With the present level of understanding, experimental determination of deposition rates in individual fields is ultimately required to determine the scaling potential of a given geothermal brine. However, in the absence of such data under conditions of relevance to EGS operational conditions, a simplified mathematical approach is employed to predict the deposition rate of silica under idealised conditions. This is seen as a first step in developing a rigorous model of the behaviour of silica in EGS. Such a model would allow the optimisation of silica management strategies and allow new methods of silica removal and/or control to be devised, evaluated and assessed, prior to experimental investigations, at low cost.

Keywords: Hot dry rock, silica fouling, silica deposition rate, silica polymerization

Silica Scaling

Solid silica is present within geothermal reservoirs as quartz, and the concentration of silica in the brine at the exit of the reservoir, typically 300-700 mg/kg SiO_2, is controlled by the solubility of quartz at the reservoir temperature (Fournier and Rowe, 1966). On cooling the brine becomes supersaturated with respect to amorphous silica and silica either precipitates from the brine as amorphous silica or polymerises to form colloids which may stay in solution or may deposit onto surfaces. The fouling of heat exchanger (and other) surfaces can lead to decreased thermal efficiency, increased maintenance costs due to cleaning and increased operational costs due to expensive abatement strategies.

The mechanism of silica precipitation and deposition is quite complex and poorly understood (Brown and Bacon, 2009). Following an induction period (Gunnarsson and Arnórsson, 2005; Bohlmann *et al.*, 1980), monomeric silica begins to polymerize. At high degrees of super-saturation, polymerisation occurs via rapid homogeneous nucleation. Supercritical silica particles grow by further reaction with silicic acid and eventually coagulate or flocculate to produce a gel, followed by a cementation of the particles in the gel by chemical bonding and further molecular deposition among the silicic acid particles (Weres *et al.*, 1982). The polymerization process will continue until the concentration of monomeric silica reduces to the saturation concentration of amorphous silica at the fluid temperature. The deposition process following the polymerized silica is known as particle deposition, which produces white, fluffy, scale with dry density of about 0.95 g/cc. At lower concentrations of dissolved silica, slow homogenous nucleation can occur with direct deposition of dissolved silica on solid surfaces being the dominant polymerisation process (Weres *et al.*, 1982). Deposits that are formed by direct precipitation of monomeric silica are more destructive and difficult to remove, producing hard, vitreous, dark coloured scale, with the density of about 2.0 g/cc. Some studies have identified that monomeric silica is more likely to precipitate and deposit than polymeric silica (Bohlmann, 1980; Gunnarsson and Arnórsson, 2005). A number of factors effect the polymerization rate of amorphous silica in geothermal brine, including pH, temperature, salt concentration, residence time, and the presence of certain ions.

Prediction of the silica deposition rate

Reinjection aquifers in Enhanced Geothermal Systems (EGS) have been considered to be the area with the greatest risk of having silica deposition problem. Predicting polymerisation and deposition rates of dissolved silica in the EGS reinjection aquifer is complex due to a lack of data from operating sites. A number of factors should be taken into account in modelling the real conditions, such as fluid mechanics, heat and mass transfer. Here we have taken a very simplified approach using experimental data for the precipitation of monomeric silica obtained under ideal conditions.

A schematic diagram of the system model is shown in Figure 1. A closed loop binary cycle is assumed with a reservoir depth of 5000 m. Only the flow of brine in the reservoir and through the heat exchanger (30 m length) is considered. Water exits the heat exchanger at temperature T_{s1} = 90°C and is returned to the reservoir, via the reinjection well. The brine is heated to temperature T_R = 270°C at the exit of the reservoir and returns to the surface reaching the heat exchanger at temperature T_s = 260°C. The temperature profiles in the production well (2°C/km) and heat exchanger (5.67°C/m) are assumed to be linear. The temperature profile in the reinjection well is calculated using simple heat transfer assumptions and follows the method of Yu et al. (2009).

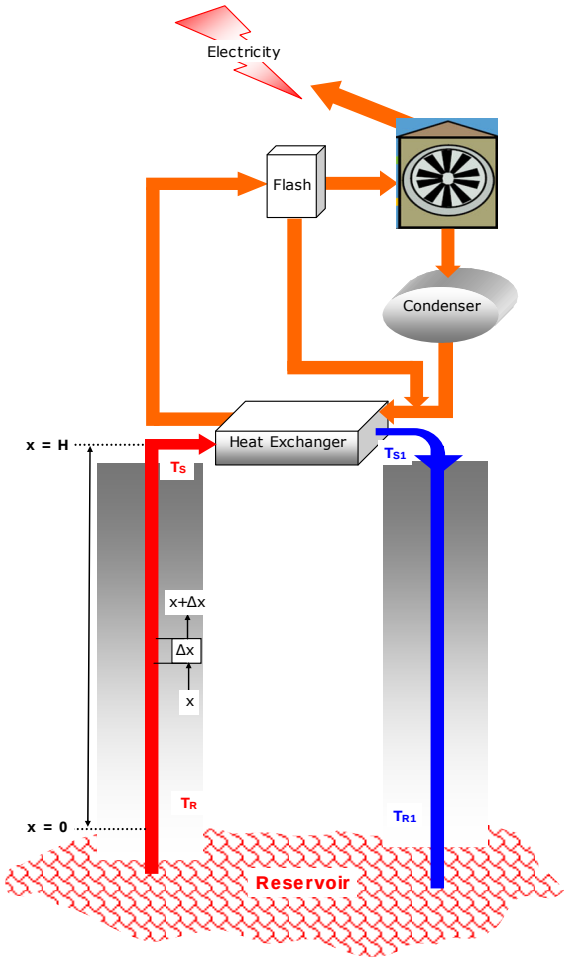

Figure 1: Schematic diagram of the mathematical simulation

The kinetics of amorphous silica precipitation have been determined by Rimstidt and Barnes (1980) for 0-300°C. For the reversible reaction:

$$SiO_2(s) + 2H_2O(l) \leftrightarrow H_4SiO_4(aq)$$

the net precipitation rate, for dilute solutions, may be expressed as:

$$r'_{SiO_2} = -k_+(1 - Q/K) \qquad \text{mol.L}^{-1}\text{.s}^{-1}$$

where k_+ is the forward rate constant, K is the equilibrium constant and Q is the activity quotient:

$$Q = (a_{H_4SiO_4})/(a_{SiO_2})(a_{H_2O})^2$$

where a_i is the activity of species i. The quantity Q/K indicates the degree of saturation or the *saturation ratio* (S).

Rimstidt and Barnes (1980) provide expressions for k_+ and K, as a function of temperature allowing the precipitation rate of amorphous silica to be simply calculated as a function of temperature and the concentration of silica in solution. Here, silica in solution is assumed to be in equilibrium with solid quartz at the reservoir temperature and its concentration is determined using the expression of DiPippo (2008).

The precipitation rate of amorphous silica is plotted in Figure 2 as a function of temperature and for silica concentrations of 550, 675, 745 and 800 ppm, which correspond to quartz equilibrium concentrations at reservoir temperatures of 270, 300, 320 and 340°C, respectively. As temperature decreases, the degree of saturation, S, increases and so the predicted precipitation rate increases until a maximum is achieved. With further decrease in temperature, the forward rate constant (k_+) decreases faster than S and so the net rate of precipitation decreases. As a consequence, for temperatures below about 50°C, the precipitation rate is small, despite the large extent of supersaturation and this, potentially, provides a mechanism by which silica deposition may be controlled or minimised.

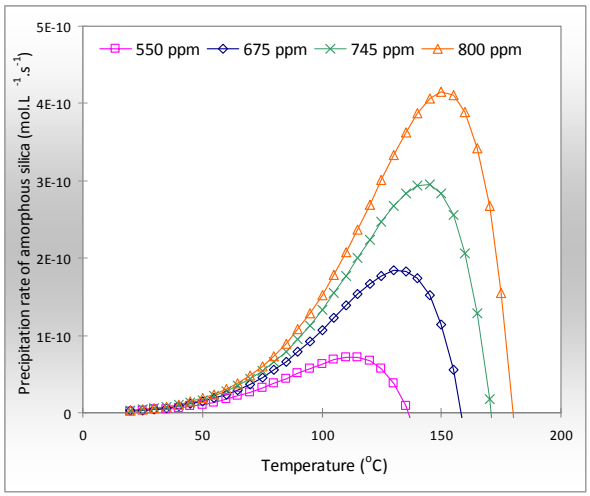

Figure 2: Precipitation rate of amorphous silica as a function of temperature and silica concentration.

Simulation results and discussion

The precipitation rate of silica in the heat exchanger is plotted in Figure 3 as a function of heat exchanger tube length. At the heat exchanger inlet, the geofluid temperature is well above the saturation temperature and the

precipitation rate is negligible. As the temperature decreases below 140°C, which occurs at approximately 22 metres, the geofluid becomes saturated with respect to amorphous silica and the precipitation rate increases substantially. The highest rate of precipitation in the heat exchanger occurs at 26 metres, corresponding to a temperature of 113°C. Thus, the final 25% of the heat exchanger is susceptible to fouling due to silica deposition.

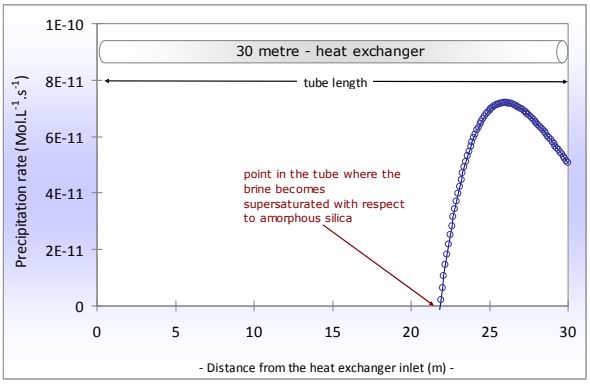

Figure 3: Precipitation rate as a function of temperature in the heat exchanger for [SiO_2] = 550 ppm

The precipitation rate of silica and the geofluid temperature in the reinjection well is plotted in Figure 4. At shallow depths, the geofluid in the reinjection well continues to cool due to the lower temperature of the surrounding earth. The precipitation rate of silica decreases accordingly and reaches a local minimum at a depth of 330 m corresponding to a minimum temperature of 83.3°C. With increasing depth, the precipitation rate increases to a maximum at a depth of 1350 m, which occurs at a temperature of approximately 112°C and corresponds to the maximum precipitation rate for [SiO_2] = 550 ppm shown in Figure 2. At greater depths, the temperature increases further and the precipitation rate decreases as the extent of supersaturation decreases. Thus, the upper 30% of the reinjection well is susceptible to fouling due to silica precipitation.

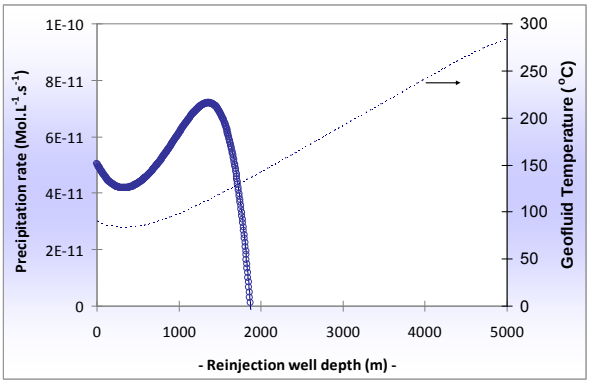

Figure 4: Precipitation rate and geofluid temperature (RH axis) as a function of depth in the reinjection well for [SiO_2] = 550 ppm

Silica polymerisation

The disappearance of monomeric silica from solution may also occur via a polymerisation reaction that proceeds quite rapidly following an initial induction period. Bohlmann *et al.* (1980) report that the induction period, τ_i, may be calculated as a function of the supersaturation ratio and the pH of the solution as:

$$\ln \tau_i = \left[\ln \frac{1}{\ln(C/Ce)} \right]^8 + 4.8 - 2.3(\mathrm{pH} - 4.5)$$

Figure 5 is a plot of the calculated induction period, as a function of the supersaturation ratio, for pH = 5, 6 and 7. At any supersaturation ratio above about 1.5, the induction period is quite rapid and occurs in less than 1 minute for neutral pH. Thus, the polymerisation of silica is expected to contribute substantially to the precipitation of silica from solution.

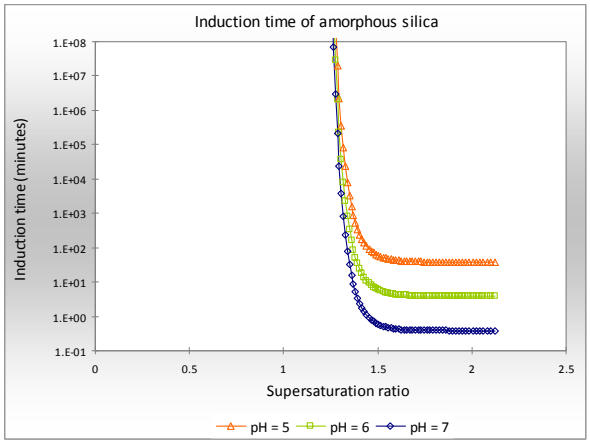

Figure 5: Calculated induction period for amorphous silica as a function of supersaturation ratio and pH

The present study assumes that amorphous silica in solution is removed primarily via precipitation of monomeric silica. The rapid induction times indicated in Figure 5 suggest that under at least some conditions the polymerisation reaction will be a significant contributor to the removal of silica. Thus, there are limitations of the present work when applying these calculations directly to practical enhanced geothermal systems. Furthermore, theoretical based models of precipitation, such as those of Rimstidt and Barnes (1980) that have been determined in the laboratory under ideal conditions, predict rates that are about three orders of magnitude slower than rates observed in the field (Carroll *et al.*, 1998).

The present work may be considered as a preliminary step towards the development of a more rigorous model of silica behaviour in EGS. Future work will include a more detailed description of the precipitation and polymerisation rates, based on empirical relationships

determined under more realistic conditions (e.g. Bohlmann *et al.*, 1980 and Weres *et al.*, 1981).

Summary

Silica deposition occurs both via direct precipitation of amorphous silica and polymerisation of dissolved silica to form colloids. In both cases, the final solid product may lead to persistent deposits on heat exchanger surfaces or to fouling of the reservoir due to entrainment of fine particles. Precipitation rates have been calculated as a function of temperature in the heat exchanger and reinjection well for conditions corresponding to a typical EGS installation. The maximum rate of precipitation occurs towards the end of the heat exchanger and in the upper section of the reinjection well, at depths above about 1350 m. Due to high geofluid temperatures, the precipitation rate is calculated to be negligible at depths below 2000 m in the reinjection well. In this study, the rate of precipitation has been calculated based on laboratory data obtained under ideal conditions and the rate of polymerisation has been neglected. Future work will include more detailed descriptions of precipitation and polymerisation based on empirical measurements.

References

Bohlmann, E.G., Mesmer, R.E. and Berlinski, P. (1980). Kinetics of silica deposition from simulated geothermal brines. *Society of Petroleum Engineers Journal*, pp. 239-248.

Brown, K.L. and Bacon, L.G. (2009). Pilot plant experiments at Wairakei Power Station. *Geothermics*, **38**, pp. 64-71.

Carroll, S., Mroczek, E., Alai, M. and Ebert, M. Amorphous silica precipitation (60 to 120^{o}C): Comparison of laboratory and field rates. *Geochimica et Cosmochimica Acta*, **62**, pp. 1379-1396.

DiPippo, R. (2008). *Geothermal Power Plants: Principles, Applications, Case Studies and Environmental Impact*, 2nd edition, Butterworth-Heinemann, Oxford.

Fournier, R.O. and Rowe, J.J. (1966). Estimation of underground temperatures from the silica content of water from hot springs and wet-steam wells. *Am. J. Sci.* **264**, pp. 685-697.

Gunnarsson, I. and Arnórsson, S. (2005). Impact of silica scaling on the efficiency of heat extraction from high-temperature geothermal fluids. *Geothermics*, **34**, pp. 320-329.

Rimstidt, J.D. and Barnes H.L. (1980). The kinetics of silica-water reactions. *Geochimica et Cosmochimica Acta*, **44**, pp. 1683-1699.

Weres, O., Yee, A. and Tsao, L. (1982). Equations and type curves for predicting the polymerization of amorphous silica in geothermal brines, *Society of Petroleum Engineers Journal*, pp. 9-16.

Yu, Y., Lin, T., Xie, H., Guan, Y. and Li, K. (2009). Prediction of wellbore temperature profiles during heavy oil production assisted with light oil. *Society of Petroleum Engineers,* SPE 119526.

Aims of a Basic EGS Model for the Cooper Basin, Australia

Delton B. Chen[1*], Gregory Wong[1]
[1]Geodynamics Limited, PO BOX 2046, Milton, QLD 4064, Australia
[*]Corresponding author: Delton.Chen@geodynamics.com.au

Geodynamics Limited is currently undertaking field development activities to support a proposal for Engineered Geothermal Systems (EGS) in the Cooper Basin, Australia. For feasibility assessment it is essential that the relationship between EGS design variables and both net electrical power and return on investment are understood. This paper presents key aims and concepts of a spreadsheet model that will help provide this information. The model, which is currently in development, is called the Basic EGS Model.

Incorporated into the Basic EGS Model are sub-models that quantify fluid pressures and temperatures at key locations in the system, including within the geothermal reservoir, within the wells, across the heat-exchanger (of the power plant) and across the circulation pump. The model will link the geothermal power result to a generalist sub-model for a range of power plant designs to estimate the net electrical power deliverable to market. The model will then link the net electrical power results to an economic sub-model for calculating financial performance.

The EGS design variables of major interest include (i) well spacing, (ii) well diameter, (iii) well layout, (iv) well depth, (v) well trajectory, and (vi) number and location of stimulated fracture zones. These design variables are discussed in context of their potential impact on geothermal power and economic performance.

Keywords: EGS, Australia, Cooper Basin, model, geothermal, economic, reservoir, fracture, power, sensitivity.

Project and Location

Geodynamics Limited is developing Engineered Geothermal Systems (EGS) near the small town of Innamincka in South Australia (Figure 1). Drilling and related field work began in 2003 and is currently contained within the company's Geothermal Retention Licenses (GRL) 3 to 12, totalling 985 km^2 (Figure 1).

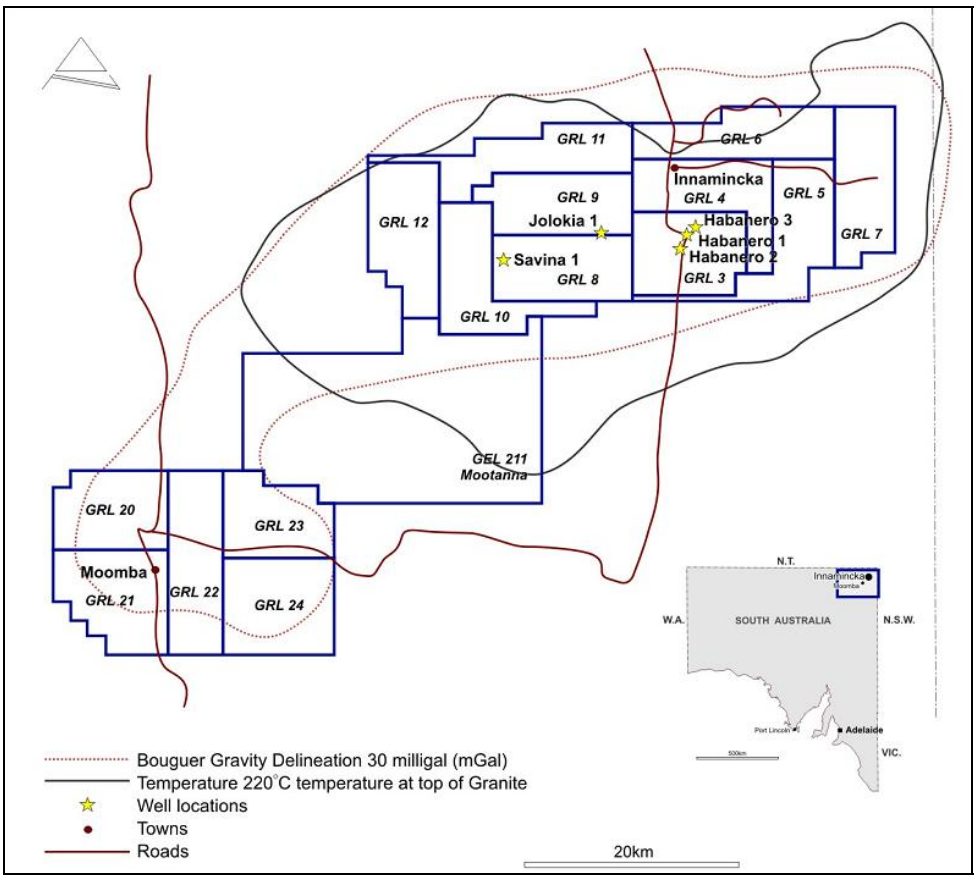

Figure 1. Site location map showing Innamincka and Moomba townships (dots) and the well bore locations (stars). Geodynamics Limited holds the geothermal retention licenses (GRL) and geothermal exploration licenses (GEL) shown. The location of the granite batholith is inferred from gravity and temperature contours.

The company initially aims to supply base-load electricity to a co-located consumer with a commercial demonstration plant (CDP), followed by the development of ten 50 MW_e EGS modules to supply 500 MW_e of electricity to the national grid. Each module will consist of about nine wells drilled to a maximum depth of 5 km, closed-loop pipeline, pump, heat exchanger, air-cooled condenser, and steam-turbine power plant. Multi-layered reservoir stimulation will be needed and the economic life of each module will be about 20 years.

Status of Wells

Five wells have been drilled to date, including: Habanero #1, #2 and #3, Jolokia #1, and Savina #1. At the time of writing the status of the wells were as follows:

- Habanero #1 (4,421 m TVD[1]) is an injection well for the 1 MW_e demonstration power plant.
- Habanero #2 (4,358 m TVD) is shut-in and available for a possible side-track.
- Habanero #3 (4,221 m TVD) was a production well for a 1 MW_e pilot plant until a well rupture on 24 April 2009. On 22 May 2009 the well was controlled and secured with two cement plugs. The precise cause of failure and the future of the well were not known at the time of writing.
- Savina #1 is temporarily suspended and secured with a cemented plug at 2,640 m TVD (100 m above a stuck pipe). The well is available for side-track drilling.
- Jolokia #1 (4,852 m TVD) is temporarily suspended whilst preparations are made for well completion and reservoir stimulation.

The drilling of Habanero #1, #2 and #3 into fractured granite, effective hydraulic stimulations, and subsequent closed-loop flow and tracer tests provided the basis of a proof-of-concept (Grove-White, 2009; Chen and Wyborn, 2009) that brought the company a major step closer to achieving its long-term goal of economically extracting energy from a non-volcanic geothermal resource. The proof-of-concept report was released to the Australian Stock Exchange (ASX) on 31 March 2009 and is available on the internet at http://www.geodynamics.com.au.

Geothermal Resource

The resource is a radiogenic granite (batholith) buried under ~3.7 km of layered sedimentary rock and it extends slightly beyond GRLs 3 to 12 (Figure 1). The company also holds adjacent Geothermal Exploration License (GEL) 211 and GRLs 20 to 24. The target interval for drilling is 3.7-5 km below ground where the granite temperature is approximately 227-284°C. The granite produces heat at a rate of 7-10 μW m^{-3}, and is comprised of 75% SiO_2 and >5% K_2O.

The granite has crystalline medium-to-coarse sized grains and is saturated with brine which is pressured to ~34.4 MPa above hydrostatic. Regional confinement is provided by sedimentary layers that have a very low porosity and low permeability. The granite was glacially eroded during the early-Permian ice age (circa 300 Ma ago) prior to burial. There is no evidence of major faulting in GRLs 3 to 12.

Rock stress at 4 km depth

In the project area the rock stresses at 4 km depth are characterized by: (i) a vertical minimum principal stress of ~90 MPa; (ii) a minor horizontal stress of ~110 MPa; (iii) a maximum horizontal stress of ~140 MPa; and (iv) a pore pressure of ~75 MPa. The maximum horizontal stress is orientated east-west due to present day tectonic compression of the Australian plate. Hydraulic stimulations in this stress field are effective at activating fractures that are orientated sub-horizontally (Grove-White, 2009). This sub-horizontal fracture orientation is considered ideal for heat extraction because it promises the development of vertically-stacked fracture zones within the granite.

The Basic EGS Model

Main Aims

The Basic EGS Model is an empirical-analytical thermo-hydraulic model for constant flow circulation conditions (on a mass per time basis). The term 'Basic' is used in recognition that the final EGS model may need to be better calibrated and refined and expanded in scope to include a combination of mechanical, thermal, hydraulic, and chemical processes in time and space (e.g. Hayashi et al., 1999).

The Basic EGS Model aims to predict the production temperature and pressure (average for all production wells), pump differential pressure, total geothermal power, and total net electrical power over ~20 years for various EGS designs. The Basic EGS Model is coded in a spreadsheet (Microsoft Office Excel 2007) to facilitate rapid development. After the model is reviewed and validated (a work in progress) it may then be used for economic sensitivity analysis.

EGS Design Variables

The EGS design variables of major interest are (i) well spacing, (ii) well diameter, (iii) well layout, (iv) well depth, (v) well trajectory, and (vi) number and location of stimulated fracture zones. Other important variables describe (vii) well cavity

[1] Total Vertical Depth (TVD)

completion (e.g. under-reaming or perforation jetting), (viii) pump efficiency, (ix) pump inlet/outlet pressure limits, (x) heat-exchanger discharge temperature, (xi) power plant geothermal-to-electrical efficiency, and (xii) power plant auxiliary power loads. The effect of well cavity completions may be employed in the future to reduce turbulent friction ('skin') near-field of the wells with the intention of improving well bore productivity and injectivity.

Reservoir Sub-Model

The reservoir sub-model describes the quasi-steady fluid pressure and transient fluid temperature distributions throughout the closed-loop (Figures 2 and 3). The model is limited to a steady circulation rate (mass per time) to simplify the analysis.

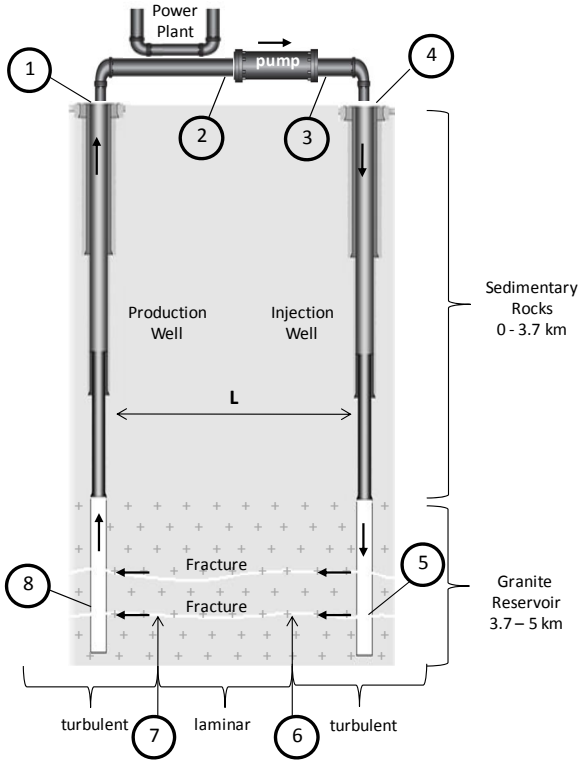

Figure 2: Conceptual fluid flow diagram for EGS based on a producer-injector pair or 'doublet'. The important thermo-hydraulic reference points are numbered.

Referring to Figure 2, the main processes that influence fluid temperature and pressure include: (1-2) pipe frictional pressure loss and temperature drop across the heat exchanger; (2-3) pressure rise forced by the pump; (3-4) pipe frictional pressure loss; (4-5) well bore and constricted[2] frictional pressure drops, hydrostatic pressure change with depth, and temperature rise due to conduction; (5-6) turbulent frictional pressure drop due to radial-diverging flow in fractures and temperature rise due to conduction; (6-7) laminar frictional pressure drop within the fracture network and temperature rise due to conduction; (7-8) turbulent frictional pressure drop due to radial-converging flow in fractures and temperature rise due to conduction; and (8-1) well bore and constricted frictional pressure drops, hydrostatic pressure change with depth, and falling temperatures due to conduction.

Turbulent radial flow near-field of the wells (5-6 and 7-8 in Figure 2) is believed to be responsible for most of the pressure drop in the fractured reservoir. A novel semi-analytical method for modelling pressures losses in the near-field of wells is currently in development. The method, called the Radial Pipe Flow Method (RPFM) (Chen, *in press*), is based on empirical formulae for laminar and turbulent losses in tubular pipes. Preliminary results using the RPFM are promising and the method appears suitable for use in the Basic EGS Model.

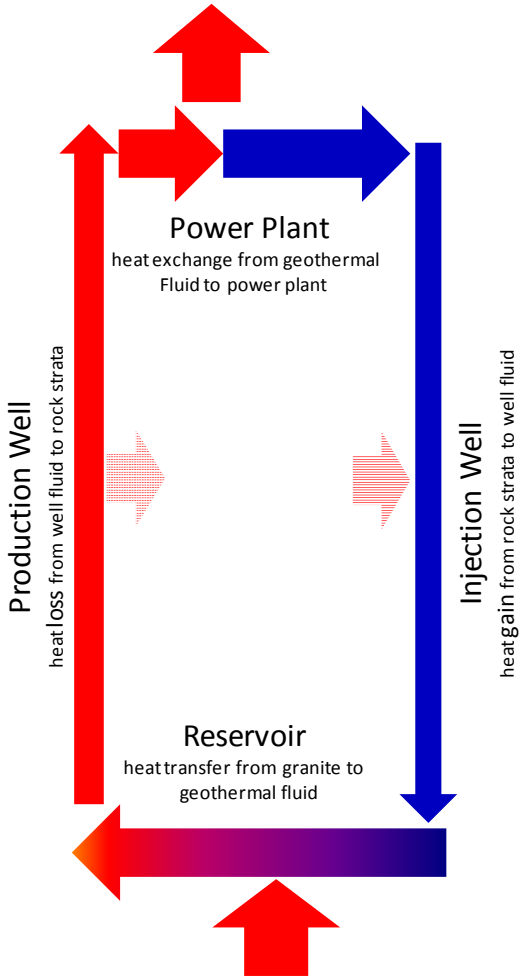

Figure 3: Conceptual heat flow diagram for a single producer-injector 'sweep zone'. The Basic EGS Model is comprised of a collection of 'sweep zones' as a means of approximating the total geothermal power output of multi-well systems. Each sweep zone is analysed individually using a combination of empirical, analytical and numerical methods. Red indicates relatively hot fluid and blue relatively cold fluid.

[2] Constrictions include changes in pipe internal diameter and *vena contracta* at the well-fracture interface.

At every location in the flow system, fluid viscosity and fluid density are influenced by temperature and pressure. Consequently there are physical feedback loops affecting fluid pressure. To address this inherent complexity, the fluid pressure profiles of the production and injection wells are solved iteratively. Furthermore, the pressures at all key reference points in the model (Figure 2) are also solved iteratively to determine the pressures that balance the entire system. A method has been developed for solving system pressures and the preliminary results are promising.

The most simple system diagram for heat flow involves four exchange processes (Figure 3): (i) heat losses to the power plant; (ii) heat gains/losses in the injection wells; (iii) heat gains in the reservoir; and (iv) heat losses in the production wells.

Extracting heat produces a three-dimensional cooling front in the rock that starts at the injection wells and grows towards the production wells (Vörös et al., 2007). Also, the heating and cooling of fluid in the well bores involves three-dimensional 'radial-type' heat flow patterns. These heat transfer processes are generally too complex to be modelled with just analytical methods. The current approach is to utilise the results of detailed numerical modelling studies (Vörös et al., 2007) in combination with analytical methods (Arpaci, 1966). This is achieved by representing numerical results with empirically adjusted analytical equations or 'black-box' empirical equations (a work in progress).

Well Layouts

The multi-well layouts produce spatially and temporally complex fluid flow and heat transport patterns (Vörös et al., 2007). They also need to be carefully designed to ensure sufficient sweep of the reservoir for achieving stated geothermal power targets. In this modelling study, a sweep zones is defined as the planar area of the reservoir that transfers appreciable fluid between neighbouring injection and production wells (Figure 4).

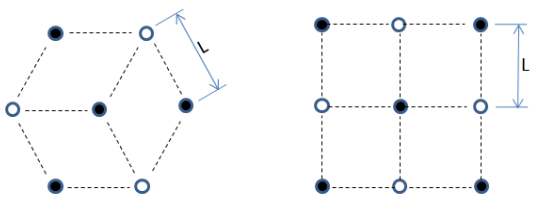

Figure 4: Two plausible EGS well layouts: (a) seven wells on a triangular grid with nine sweep zones, and (b) nine wells on a square grid with twelve sweep zones. Sweep zones are represented as dotted lines, producers as black dots, and injectors as white dots.

The total sweep area is principally controlled by (i) number of wells, (ii) well layout and spacing, and (iii) number of parallel fracture zones. The ratio of sweep zones to the number of wells give a basic indication of the efficacy of a well layout. The current model approximates multi-well heat extraction by representing the reservoir as collection of discrete sweep zones (a work in progress). Each sweep zone is defined by an approximately equivalent rectangular fluid-rock contact area. Preliminary results based on this method are promising.

Well Bore Averaging

The Basic EGS Model simplifies the flow hydraulic problem by representing the multi-well layout with one 'average producer' and one 'average injector' doublet (Figure 2). The averaging method involves spreading the total flow evenly amongst the producers and injectors and calculating the average geometry of the producers and injectors taking into account well design and directional drilling. This well bore averaging technique and the discrete sweep zone method (described above) greatly simplify the modelling task. Validation against a more accurate and proven modelling approach is required.

Power Sub-Model

The Basic EGS Model includes a power sub-model that will provide an estimate of power plant efficiency and auxiliary equipment power load for any plausible geothermal production flow, production temperature, and ambient air temperature.

The main aim of the sub-model is to estimate the main components of the EGS power balance, namely: (i) geothermal power output, (ii) steam turbine power output, (iii) pump power load, and (iv) auxiliary equipment power load. The auxiliaries will include air cooled condensers (as opposed to water cooled) because of water scarcity in the Cooper Basin (Figure 5).

Power plant designs should be tailored to production flow and temperature hence the Basic EGS Model requires a capacity to adapt the power plant design to a wide range of possible production outcomes. The design of power plants also requires specialised engineering skills and software (Thermoflow by Thermaflow, Inc. USA). To circumvent this inherent complexity, the current approach is to collate a range of suitable power plant designs and to develop empirical ('black-box') regression equations for plant gross power supply and auxiliary power load as a function of production flow, production temperature, and ambient air temperature.

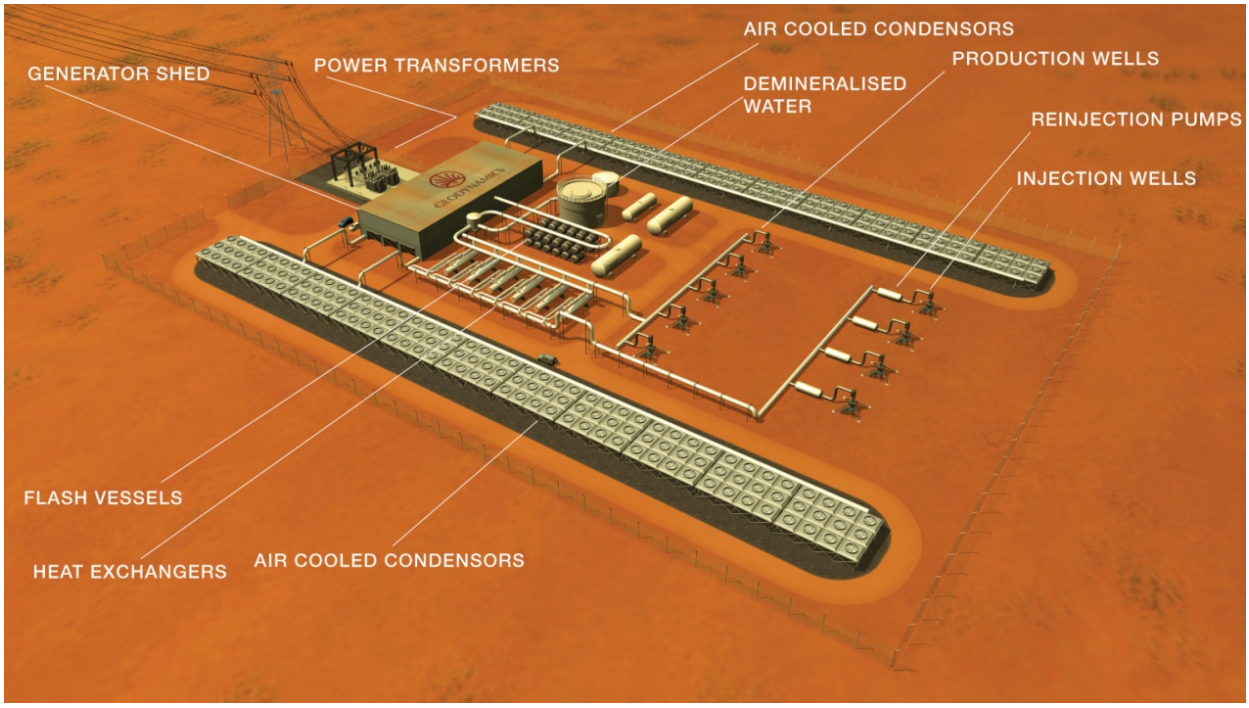

Figure 5: Artist's impression of a 50 MW EGS module comprising four injectors, five producers, steam turbine power plant, heat exchanger, and air cooled condensers.

Economic Sub-Model

The economic sub-model is based on discounted cash flow analysis and calculation of Internal Rate of Return (IRR) over 20-30 years. Of interest is the sensitivity of the IRR to the various EGS design variables. The following are the key economic inputs: (i) drilling cost expectations, (ii) cost of power station and other capital equipment, (iii) operation and maintenance costs, (iv) electricity revenue expectations, and (v) renewable energy certificate revenue expectations. The electricity price expectations are taken from an economic analysis by McLennan Magasanik Associates (2008) for the Australian government's Carbon Pollution Reduction Scheme. The renewable energy certificate revenue expectations are taken from market analysis by McLennan Magasanik Associates (2009).

Implications for EGS Design

The main benefit of the proposed modelling is the ability to rank Cooper Basin EGS designs in terms of revenue potential. The work completed to date has identified a number of optimal design points ('sweet spots'). Two key examples are:

- A peak net electrical power and IRR as a function of pump differential pressure; and
- A peak in IRR as a function of well spacing.

Summary

A basic thermo-hydraulic model for EGS in the Cooper Basin is currently being developed. It is called the 'Basic EGS Model'. It is comprised of sub-models for the reservoir, power plant, and expected economic conditions. Early model results are promising and suggest that the model components are valid and will be accurate enough for economic sensitivity analysis. Although the model is currently a work-in-progress, some preliminary results may be presented at the 2009 Australian Geothermal Conference in Brisbane.

References

Arpaci, V.S., 1966, Conduction Heat Transfer. Addison-Wesley, Reading, Massachusetts, 1966, 351 p.

Chen, D., in press, Concepts of a basic EGS model for the Cooper Basin, Australia, Proceedings of the World Geothermal Congress 2010, Bali, Indonesia, 25-30 April 2010.

Chen, D., and Wyborn, D., 2009, Habanero Field Tests in the Cooper Basin, Australia: A Proof-of-Concept for EGS, Proceedings of the GRC Annual Meeting, 4–7 October 2009, Reno, Nevada, USA.

Grove-White, G., 2009, ASX Announcement 31 March 2009: Stage 1 - Proof of Concept Complete, Geodynamics Ltd., 31 March 2009.

Hayashi, K., Willis-Richards, J., Hopkirk, R.J., and Niibori, Y., 1999, Numerical models of HDR geothermal reservoirs - a review of current thinking and progress, Geothermics, 28, p. 507-518.

McLennan Magasanik Associates, 2008, Impacts of the Carbon Pollution Reduction Scheme on

Australia's Electricity Markets - Report to Federal Treasury, 11 December 2008, Ref: J1565, 75 p.

McLennan Magasanik Associates, 2009, Benefits and Costs of the Expanded Renewable Energy Target – Report to Department of Climate Change, January 2009, 38 p.

Vörös, R., Weidler, R., de Graaf, L., and Wyborn, D., 2007, Thermal modelling of long term circulation of multi-well development at the Cooper Basin hot fractured rock (HFR) project and current proposed scale-up program, Proceedings, Thirty-Second Workshop on Geothermal Reservoir Engineering, Stanford University, Stanford, California, January 22-24, 2007.

Acknowledgements

The authors wish to thank William Cibich, Michael Malavazos, and Alexandria Long at the Petroleum and Geothermal Group of the PIRSA (Primary Industries and Resources South Australia) for sharing EGS model developments and related reports.

Analysis of error sources for estimating geothermal stabilised formation temperatures using analytical and rigorous methods

Espinoza-Ojeda[1], OM, Santoyo[2*], E and Andaverde[3], J
[1]Posgrado en Ingeniería (Energía), Centro de Investigación en Energía, Universidad Nacional Autónoma de México. Priv. Xochicalco s/n, Col. Centro, Temixco, Morelos 62580, México.
[2]Centro de Investigación en Energía, Universidad Nacional Autónoma de México, Centro de Investigación en Energía, Universidad Nacional Autónoma de México. Priv. Xochicalco s/n, Col. Centro, Temixco, Morelos 62580, México. *Corresponding author: esg@cie.unam.mx
[3]Centro de Investigación en Ingeniería y Ciencias Aplicadas, Universidad Autónoma del Estado de Morelos. Av. Universidad No. 1001, Col. Chamilpa, Cuernavaca, Morelos 62210, México.

Analytical and rigorous solutions of 7 heat transfer models were statistically evaluated, for the estimation of stabilized formation temperatures (SFT) of geothermal wells. Linear and cylindrical heat source models were selected to represent the heat flow processes present in wells drilling operations. A statistical assessment of the main error sources involved with these models was comprehensively performed. Analytical and rigorous solutions were evaluated by using comprehensive statistical methodologies which enabled to determine the sensitivity parameters that should be considered for a reliable calculation of SFT, as well as to define the constraints where the analytical and rigorous methods provide consistent SFT estimations.

Keywords: Static formation temperature, bottom-hole temperatures, error propagation, shut-in time, circulation time

Statistical methodology of evaluation

An improved statistical methodology was developed for a better evaluation of the main error sources associated with the most common heat transfer models used for estimating geothermal SFT. The methodology consisted of: (1) Selection of methods, mainly those that simultaneously propose both analytical and rigorous solutions; (2) Creation of a geothermal database with BHT and shut-in time data sets from well drilling logs and synthetic experimental works; (3) Application of different regression models (i.e., OLS and QR) with the algorithms of each selected method to calculate the SFT; (4) Statistical evaluation of the existing relationship (linear or non-linear) between BHT and the time function data of each method; (5) Comparative statistical analysis of the SFT estimates for each method based on the ratio between its analytical and rigorous solutions; and finally (6) Evaluation of accuracy in each method using a statistical comparison analyses between "true" SFT measurements and SFT estimates (inferred from analytical and rigorous solutions).

Selection of methods

Seven methods commonly used for the determination of SFT were selected: (i) the radial source with a conductive heat flow or Brennand method (BM: Brennand 1984); (ii) the cylindrical heat source with a conductive-convective heat flow method (CHSM) proposed by Hasan and Kabir (1994); (iii) the constant linear heat source or Horner-plot method, (HM: Dowdle and Cobb 1975; (iv) the generalized Horner or the Kutasov-Eppelbaum method (KEM: Kutasov and Eppelbaum 2005); (v) the cylindrical source with a conductive heat flow or Leblanc method (LM: Leblanc *et al* 1981); (vi) the cylindrical source with a conductive heat flow or Manetti method (MM: Manetti 1973); and (vii) the spherical and radial heat flow method (SRM) proposed by Ascencio *et al* (1994). The reader is referred to the original references of each method for more details. The analytical methods BM, HM, KEM, LM, and MM were derived from the well-known heat conduction equation (Eq. 1) under radial conditions.

$$\frac{1}{r}\frac{\partial}{\partial r}\left(r\frac{\partial T}{\partial r}\right)=\frac{1}{\alpha}\frac{\partial T}{\partial t} \qquad (1)$$

whereas, the heat conduction equation under spherical-radial dimensionless coordinates (Eq. 2) was used for the SRM method,

$$\left(\frac{\partial^2 T_D}{\partial r_D^2}\right)+\left(\frac{2}{r_D}\right)\left(\frac{\partial T_D}{\partial r_D}\right)=\left(\frac{1}{\alpha}\right)\left(\frac{\partial T_D}{\partial t_D}\right),\ 0 < r_D < \infty \qquad (2)$$

The CHSM method was derived from a heat transfer model, based on transient heat exchange between drilling fluid and rock formation (Eq. 3), under conductive and convective heat flow conditions.

$$\frac{dT_w}{dt}=-\left(\frac{2\pi}{m\,C_{pm}}\right)\left(\frac{r_w U k}{k+rUT_D}\right)(T_w-T_{CHSM}) \qquad (3)$$

As far as these general equations, analytical and rigorous solutions have been proposed in the literature. These solutions are summarized in Table 1 (Appendix).

Geothermal database: BHT and shut-in time data sets

A geothermal database containing eight BHT data sets logged in geothermal borehole drilling operations and three synthetic data sets was created. The BHT data were recorded from borehole drilling reports carried out in various world geothermal sites: (1) Los Humeros geothermal field, Mexico [MXCO, Verma *et al* 2008]; (2) Mississippi petroleum wellbore, USA,

characterized by temperatures with a geothermal origin [USAM, Kutasov 1999]; (3) Larderello geothermal field, Italy [ITAL, Da-Xin 1986]; (4) Kyushu geothermal field, Japan [JAPN, Hyodo and Takasugi 1995]; (5) Norton Sound field, Alaska [COST, Cao *et al* 1988a]; (6) Chipilapa geothermal field, El Salvador [CH-A, González-Partida *et al* 1997]; (7) Roosvelt geothermal field, USA [R #9-1, Crosby 1977]; (8) Oklahoma geothermal field, USA [SGIL, Schoeppel and Gilarranz 1966].

The synthetic data sets used here were compiled from experimental works reported by Shen and Beck (1986) (SHBE), Cao *et al* (1988b) (CLAH), and Cooper and Jones (1959) (CJON). These data sets were used as they have the advantage that these experimental works reported the "true" formation temperatures (*TFT*) or SFT (i.e., SHBE = 80.0°C, CLAH = 120.0°C and CJON = 20.25°C, respectively).

For example, the thermal recovery behaviour (i.e., the BHT behaviour versus shut-in time) of some geothermal boreholes after drilling has been plotted in Figure 1 (a) (MXCO, USAM, ITAL and JAPN) and Figure 1 (b) (COST, CH-A, R #9-1 and SGIL).

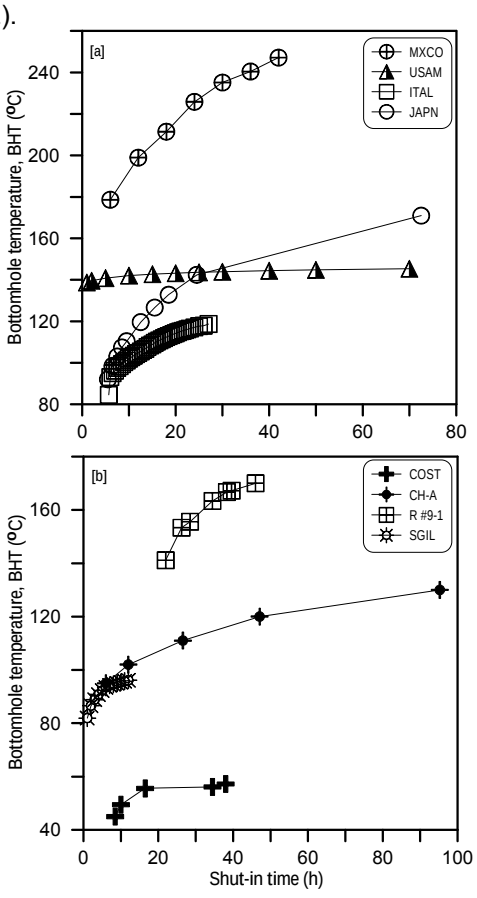

Figure 1: Temperature measurements logged after cessation of the drilling mud circulation (shut-in times).

Regression models (OLS and QR) to calculate the SFT

OLS and QR models were initially used to evaluate either the linear or non-linear relationships between BHT and the time functions of each analytical method, and afterwards, to estimate the SFT from the eight BHT data set selected and three experimental works. For the seven analytical methods under evaluation, the independent variable *x* data is the time function data for each method (BMTF, CHSMTF, HMFT, KEM, LMTF, MMTF, and SRMTF), *y,* the dependent variable, as the *BHT*, and the intercept (*a* or a_w) of any regression model (OLS and QR) will provide the SFT estimates.

Statistical evaluation of the existing relationship between BHT and the time function data of each method

Three well-known statistical tests: (i) sequence of signs by Wald-Wolfowitz; (ii) regression using sequential subsets of an ordered array of data; and (iii) residual sum of squares (RSS); were applied to evaluate the existing relationship (linear or non-linear) between the BHT and the time function data in each analytical method used.

Statistical comparison of the SFT estimates using the analysis of the ratio between analytical and rigorous solutions

For evaluating the prediction capability of the heat transfer models described in this work, the SFT estimates (inferred from their rigorous and analytical solutions) were statistically compared using an extension of the constant linear heat source theory suggested by Drury (1984). Such a theory was originally applied for the evaluation of the HM using the analysis of the ratio between analytical and rigorous solutions (defined as the β parameter), and under shut-in (Δt) and circulation (t_c) times. For these purposes, β parameter and the time ratio for each method was computed. A plot between β parameter and the time ratios $\left(\Delta t / t_c\right)$ was analyzed to evaluate both the similarity of the two solutions and the most suitable shut-in times for a reliable estimation of SFT. For β ratios close to 1, both analytical and rigorous solutions provide similar results, whereas for β ratio values > 1 the analytical solution of the method exceeds its rigorous solution and vice versa.

Evaluation of accuracy using statistical comparison analyses between "true" SFT measurements and SFT estimates

SFT estimates (inferred from the analytical and rigorous solutions of seven methods) were statistically compared with "true" SFT measurements reported in three synthetic experiments (SHBE, CLAH, and CJON) and a long thermal recovery history of the geothermal borehole CH-A. The accuracy of each method

was evaluated, for the first time, from statistical analyses of: (i) *F* and *t-student* statistical significance tests; (ii) deviation percentages ($\%Dev = \{(T_p - T_m)/T_m\}x100$) between measured ("true" SFT) and SFT estimates (predicted by the solutions of the seven methods); and (iii) a linear regression analysis between "true" SFT and SFT estimates (where for an ideal linear correlation, the intercept *a* would be equal zero, and the slope *b*=1).

Results and discussion

Before calculating the SFT using the BHT data logged in geothermal boreholes and synthetic thermal experiments, the time functions of the seven analytical methods were calculated using their respective equations. For example, some of the resulting relationships between the BHT and the HMTF data were plotted in Figure 2, for the first group of borehole data (MXCO, USAM, ITAL, and JAPN). The plots contained in the Figure 2 show the BHT build-up curves (i.e., BHT behaviour versus time function) for the Horner analytical method. These plots were drawn with the goal to observe the existing trend between BHT and time function data. As can be observed and notwithstanding the scale effects, non-linear tendencies are clearly observed for most of the borehole and synthetic BHT-time function data, which preliminarily suggest that a non-linear regression model should be better used for a reliable determination of the SFT, instead of the linear regression model, traditionally adopted as a solution algorithm by all the analytical methods.

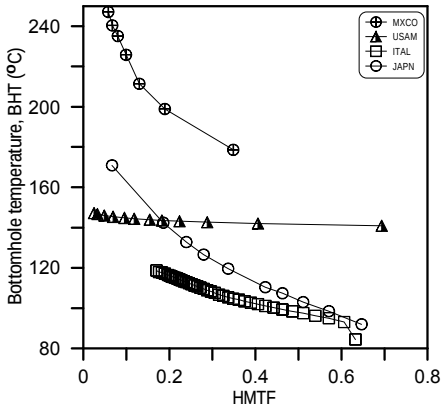

Figure 2: Plots of actual BHT measurements and time functions of the analytical Horner method.

Use of regression models (OLS and QR) to estimate the SFT

OLS and quadratic regression algorithms were individually applied to the BHT build-up data using the equations of the analytical methods under evaluation. As with all observed phenomena, when statistical methods are assumed to apply, there are certain underlying assumptions which may not be valid. The OLS is not a statistically valid model in presence of heteroscedastic errors (in any of the variables to be correlated *x* or *y*), and with *x-y* data that exhibit a non-linear trend, the OLS regression model is still used in geothermal and petroleum applications. This is basically the reason why the OLS model is still under evaluation in this work for the determination of the *SFT*. QR was also applied to calculate the SFT from the intercepts (*a*) of the fitted QR equation ($y = a + bx + cx^2$). According to the non-linear trends observed in most of the thermal recovery histories of boreholes (actual and synthetic), the QR model was a valid statistical fitting tool. The SFT estimates obtained from the OLS and QR for the seven analytical methods have been included in Table 2 (Appendix). Uncertainties of these estimates are also reported.

Rigorous solution

Some authors have reported the rigorous solutions of five analytical methods. Such equations were analyzed and used for determining the SFT using OLS and QR regression models (see Table 3).

Analysis of the β ratio results

The approximate and rigorous solutions for each method were analyzed through a plot between *β* and $(\Delta t / t_c)$ ratios to evaluate the similarity of both solutions. A BHT geothermal data set (CH-A) and the synthetic data sets (SHBE, CLAH and CJON) were used for these evaluations. Figure 3 shows some results. For *β* ratios close to 1, both approximate and rigorous solutions provide similar results. For $\beta < 1$, the approximate solution overestimates the SFT, whereas for $\beta > 1$, the approximate solution underestimates the SFT. Thus, BM, HM, and MM seem to provide acceptable results for SFT because *β* values are close to 1 for most $(\Delta t / t_c)$ ratios (Fig. 3). On the other hand, the SRM_1 gives unacceptable results for most $(\Delta t / t_c)$ ratios.

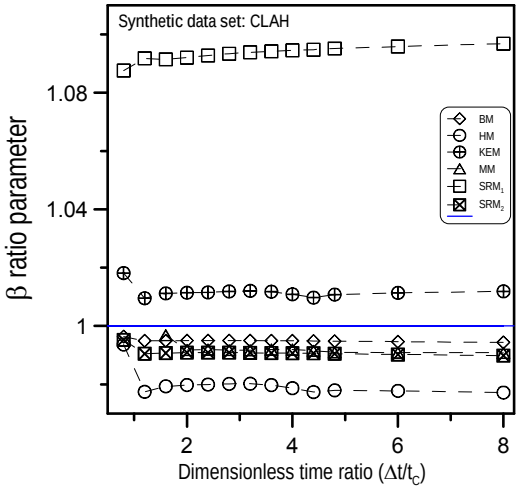

Figure 3: Plot of parameter *β* as function of ratios $\Delta t/t_c$ for synthetic data set CLAH.

Accuracy analysis of the SFT's calculated

A comparison of the SFT estimates provided between the OLS and QR regression models using the seven methods with three synthetic sets (SHBE, CLAH and CJON) and one geothermal set (CH-A) was carried out (see Fig. 4). For all the synthetic data sets the "true" SFT was reported (indicated as reference smoothed lines). As can be observed, for the CLAH data set using OLS, the better estimation was provided by MM, whereas for the QR model, the CHSM and MM provide the best estimations. The SRM systematically provide overestimations of the SFT in both OLS and QR models. Deviation percentages from the "true SFT" were also calculated and represented in Fig. 5.

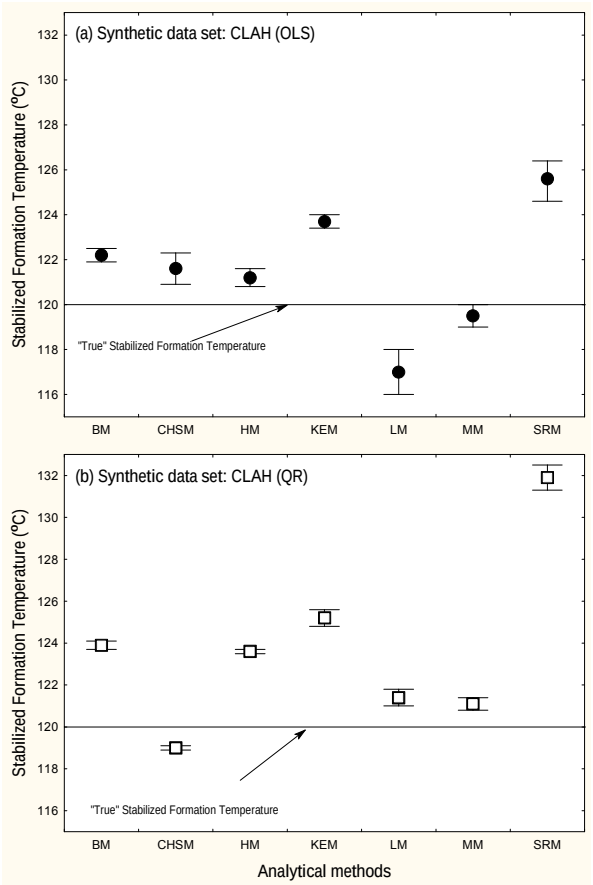

Figure 4: Accuracy evaluation of regression models (OLS and QR) for the determination of the "true" formation temperatures (SFT) using BHT synthetic data set CLAH.

Conclusions

The empirical evaluation of error sources in heat transfer models for the determination of SFT in geothermal and petroleum wells and synthetic data sets was successfully carried out. Seven analytical methods (BM, CHSM, HM, KEM, LM, MM and SRM) were comprehensively evaluated. It was confirmed that the BHT build data logged in actual wellbore drilling operation exhibit a clear polynomial tendency, which suggests the QR as the most suitable regression model to estimate the SFT.

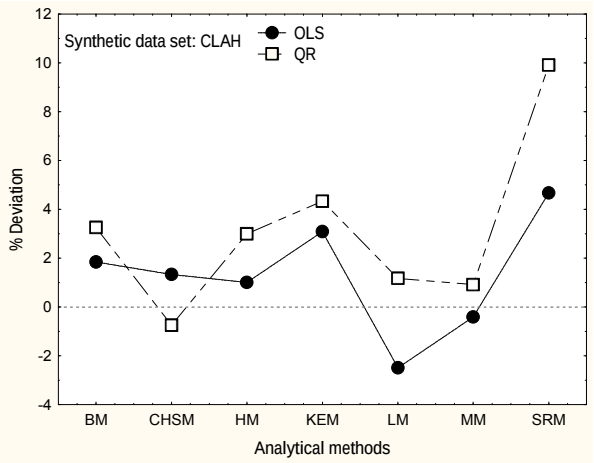

Figure 5: Results of the criterion of evaluation (% deviation) of regression models (OLS and QR) for the determination of the "true" formation temperatures (SFT) using BHT synthetic data set CLAH.

On the other hand, it was also confirmed that the OLS model, traditionally used by some analytical methods for the calculation of the SFT, is statistically an invalid regression model, and therefore must be abandoned. The β ratio results showed that only some approximate solutions (BM, HM, and MM) provide reliable estimations of the SFT. Shut-in and circulations times are fundamental parameters that influence the determinations of SFT, and therefore they must be measured in the field with high accuracy and precision, including the knowledge of their measurement errors.

As a final remark, further research work is still needed to develop new analytical methods with more realistic assumptions of the physical models that can reproduced the heat transfer involved in such processes.

References

Ascencio, F., Garcia, A., Rivera, J., and Arellano, V., 1994, Estimation of undisturbed formation temperatures under spherical-radial heat flow conditions: Geothermics, v. 23(4), p. 317-326.

Brennand, A.W., 1984, A new method for the analysis of static formation temperature tests: 6th New Zealand Geothermal Workshop, New Zealand, p. 45-47.

Cao, S., Hermanrud, C., and Lerche, I., 1988a, Estimation of formation temperature from bottom-hole temperature measurements: COST #1 well, Norton Sound, Alaska: Geophysics, v. 53(12), p. 1619-1621.

Cao, S., Lerche, I., and Hermanrud, C., 1988b, Formation temperature estimation by inversion of borehole measurements: Geophysics, v. 53(7), p. 979-988.

Cooper, L.R., and Jones, C., 1959, The determination of virgin strata temperatures from observations in deep survey boreholes: Geophysical Journal of the Royal Astronomical Society, v. 2, p. 116-131.

Crosby, G.W., 1977, Prediction of final temperature: 3rd Workshop on Geothermal Reservoir Engineering, Stanford University, Stanford, California, p. 89-95.

Da-Xin, L., 1986, Non-linear fitting method of finding equilibrium temperature from BHT data: Geothermics, v. 15(5-6), p. 657-664.

Dowdle, W.L., and Cobb, W.M., 1975, Static formation temperature from well logs - An empirical method: Journal of Petroleum Technology, v. 27(11), p. 1326-1330.

Drury, M.J., 1984, On a possible source of error in extracting equilibrium formation temperatures from borehole BHT data: Geothermics, v. 13(3), p. 175-180.

Gonzalez Partida, E., Garcia Gutierrez, A., and Torres Rodriguez, V., 1997, Thermal and petrologic study of the CH-A well from the Chipilapa-Ahuachapan geothermal area, El Salvador: Geothermics, v. 26(5/6), p. 701-713.

Hasan, A.R., and Kabir, C.S., 1994, Static reservoir temperature determination from transient data after mud circulation: SPE Drilling & Completion, v. 9(1), p. 17-24.

Hyodo, M., and Takasugi, S., 1995, Evaluation of the curve-fitting method and the Horner-plot method for estimation of the true formation temperature using temperature recovery logging data: 20th Workshop on Geothermal Reservoir Engineering, Stanford University, Stanford, California, p. 23-29.

Kutasov, I.M., 1999, Applied Geothermics for Petroleum Engineers: Elsevier Scientific Publishing Company, First ed., 347 p.

Kutasov, I.M., and Eppelbaum, L.V., 2005, Determination of formation temperature from bottom-hole temperature logs-a generalized Horner method: Journal of Geophysics and Engineering, v. 2, p. 90-96.

Leblanc, Y., Pascoe, L.J., and Jones, F.W., 1981, The temperature stabilization of a borehole: Geophysics, v. 46(9), p. 1301-1303.

Manetti, G., 1973, Attainment of temperature equilibrium in holes during drilling: Geothermics, v. 2(3-4), p. 94-100.

Schoeppel, R.J., and Gilarranz, S., 1966, Use of well log temperatures to evaluate regional geothermal gradients: Journal of Petroleum Technology, v. 18(6), p. 667-673.

Shen, P.Y., and Beck, A.E., 1986, Stabilization of bottom hole temperature with finite circulation time and fluid flow: The Geophysical Journal of the Royal Astronomy Society, v. 86, p. 63-90.

Verma, S.P., Pandarinath, K., and Santoyo, E., 2008, SolGeo: A new computer program for solute geothermometers and application in Mexican geothermal fields: Geothermics, v. 37, p. 597-621.

Appendix

Table 1. Analytical and rigorous solutions of the seven analytical methods.

Analytical method	Analytical solution	Rigorous solution
BM	$BHT(t) = T_{BM} - b_{BM}\left(\frac{1}{\Delta t + pt_e}\right)$	$T(r_w,t) = T_f - \frac{B\rho C_p r_w^2 (T_f - T_w)}{2k(\Delta t + p\,t_e)} \exp\left(-\frac{\rho C_p r_w^2}{4k(\Delta t + p\,t_e)}\right)$
CHSM	$BHT = T_{CHSM} + (b_{CHSM}) \cdot [F(t_{eD} + \Delta t_D) - F(t_D)]$	Not reported
	$T_w = T_{CHSM} - b'_{CHSM}\left(e^{\frac{-\Delta t}{\lambda}}\right)$	
HM	$BHT(t) = T_{HM} + (b_{HM}) \cdot ln\{(t_e + \Delta t)/\Delta t\}$	$\Delta T = Q'\left\{Ei\left(\frac{-r_w^2}{4\alpha\Delta t}\right) - Ei\left(\frac{-r_w^2}{4\alpha(\Delta t + t_e)}\right)\right\}$
KEM	$BHT(t) = T_{KEM} + b_{KEM}\, ln(X)$	$\Delta T = Q'\left\{Ei\left(\frac{-r_w^2}{4\alpha\Delta t}\right) - Ei\left(\frac{-r_w^2}{4\alpha(\Delta t + t_e)}\right)\right\}$
LM	$BHT(t) = T_{LM} - b_{LM}\left[1 - \exp\left(-\frac{r_w^2}{4\alpha\Delta t}\right)\right]$	Not reported
MM	$BHT(t) \approx T_{MM} + b_{MM}\, ln\left(\frac{\Delta t}{\Delta t - t_e}\right)$	$T(t) = T_f + \frac{Q'}{4\pi k}\left[Ei\left(-\frac{r_w^2}{4\alpha\Delta t}\right) - Ei\left(-\frac{r_w^2}{4\alpha(\Delta t - t_e)}\right)\right]$
SRM	$BHT(t) = T_{SRM} + (b_{SRM}) \cdot \left(\frac{1}{\sqrt{\Delta t}}\right)$	$T_D = \frac{1}{2}\left\{erf\left[\frac{r_D + 1}{2\sqrt{t_D}}\right] - erf\left[\frac{r_D - 1}{2\sqrt{t_D}}\right]\right\} + \frac{1}{r_D}\sqrt{\frac{t_D}{\pi}}\left\{exp\left[-\frac{(r_D + 1)^2}{4t_D}\right] - exp\left[-\frac{(r_D - 1)^2}{4t_D}\right]\right\}$
		$T_D = erf\left(\frac{1}{2\sqrt{t_D}}\right)$

Table 2. Comparison of stabilized formation temperatures calculated by seven analytical methods (BM, CHSM, HM, KEM, MM and SRM) using eight actual BHT build-up data (MXCO, USAM, ITAL, JAPN, COST, CH-A, R #9-1 and SGIL) and three synthetic data sets (SHBE, CLAH and CJON).

Data set	Regression model	BM	CHSM	HM	KEM	LM	MM	SRM
MXCO	OLS	254 ± 5	249 ± 2	251 ± 6	260 ± 5	249 ± 6	244 ± 6	301 ± 5
	QR	279.4 ± 3.5	253.8 ± 1.3	277.0 ± 3.5	288 ± 3	274.3 ± 3.7	269 ± 4	352 ± 16
USAM	OLS	145.7 ± 0.3	144.8 ± 0.1	146.0 ± 0.4	145.9 ± 0.3	144.8 ± 0.5	146.0 ± 0.4	147.5 ± 0.4
	QR	146.7 ± 0.3	144.7 ± 0.1	147.1 ± 0.3	147.0 ± 0.3	145.5 ± 0.4	147.1 ± 0.3	148.0 ± 0.3
ITAL	OLS	130.6 ± 0.6	127.8 ± 0.6	127.8 ± 0.6	134.2 ± 0.6	124.8 ± 0.6	120.1 ± 0.7	142.2 ± 0.6
	QR	133.4 ± 1.9	123.8 ± 1.4	132.2 ± 1.6	135.8 ± 2.5	130.0 ± 1.3	123.0 ± 0.9	161.9 ± 1.1
JAPN	OLS	172 ± 4	166.3 ± 1.8	167 ± 4	178 ± 3	162 ± 5	157 ± 7	209.9 ± 0.9
	QR	187 ± 2	169.4 ± 1.7	184.7 ± 2.5	192 ± 1	180.1 ± 3.4	162 ± 6	215
COST	OLS	60.3 ± 1.9	57.8 ± 1.4	60.0 ± 1.7	60.9 ± 2.2	59.5 ± 1.4	58.7 ± 1.0	
	QR	53.2 ± 1.2	55. 8 ± 0.6	54 ± 1	51.9 ± 1.7	54.8 ± 0.7	56.3 ± 0.7	
CH-A	OLS	126.1 ± 4.3	124.8 ± 2.9	125.4 ± 4.4	128.0 ± 4.0	125 ± 5	123 ± 5	137 ± 5
	QR	134.8 ± 3.6	127.7 ± 2.7	133.0 ± 3.7	137.5 ± 3.2	133.1 ± 3.8	131.3 ± 4.1	155.5 ± 3.8
R #9-1	OLS	212.3 ± 4.1	175.1 ± 0.9	205.9 ± 3.1	216.6 ± 4.5	198.3 ± 2.1	185.5 ± 0.6	205.1 ± 0.8
	QR	156 ± 10	172 ± 1	168 ± 8	149 ± 12	178 ± 5	185.9 ± 2.4	258.4
SGIL	OLS	100.5 ± 0.1	106 ± 1	99.3 ± 0.2	102.1 ± 0.2	97.0 ± 0.4	97.5 ± 0.2	102.9 ± 0.3
	QR	100.0 ± 0.3	87.7 ± 1.4	99 ± 1	101.1 ± 0.5	99.1 ± 0.2	98.3 ± 0.2	104 ± 1
SHBE	OLS	77.7 ± 0.6	77.4 ± 0.5	75.5 ± 0.7	79.0 ± 0.5	74.1 ± 1.3	75.6 ± 0.9	83.0 ± 0.6
	QR	80.2 ± 0.2	76.2 ± 0.2	80.1 ± 0.2	81.5 ± 0.1	78.0 ± 0.6	78.5 ± 0.5	87.3 ± 0.4
CLAH	OLS	122.2 ± 0.3	121.6 ± 0.7	121.2 ± 0.4	123.7 ± 0.3	117 ± 1	119.5 ± 0.5	125.6 ± 0.8
	QR	123.9 ± 0.2	119.0 ± 0.1	123.6 ± 0.1	125.2 ± 0.4	121.4 ± 0.4	121.1 ± 0.3	131.9 ± 0.6
CJON	OLS	21.42 ± 0.27		20.76 ± 0.10	21.80 ± 0.31	20.05 ± 0.05	19.65 ± 0.11	22.41 ± 0.19
	QR	19.82 ± 0.15		20.24 ± 0.06	19.81 ± 0.14	20.22 ± 0.05	20.16 ± 0.04	20.89 ± 0.14

Table 3. Comparison of SFT calculated by the analytical methods rigorous solutions (BM, HM, KEM, MM and SRM) using seven actual geotermal data set (MXCO, ITAL, JAPN, COST, CH-A, R #9-1 and SGIL), one petroleum data set (USAM) and three synthetic data set (SHBE, CLAH and CJON).

Data set	Regression model	BM	HM-KEM	MM	SRM_1	SRM_2
MXCO	OLS	256 ± 5	254 ± 6	240 ± 6	244 ± 6	285 ± 7
	QR	281.4 ± 3.4	271 ± 11	263 ± 7	266.9 ± 3.9	342 ± 7
USAM	OLS	145.8 ± 0.3	144.4 ± 0.2	144.8 ± 0.2	144.5 ± 0.5	146.4 ± 0.4
	QR	146.8 ± 0.3	145.1 ± 0.3	145.5 ± 0.4	145.1 ± 0.4	148.4 ± 0.3
ITAL	OLS	131.7 ± 0.6	128 ± 1	120.2 ± 0.7	121.8 ± 0.6	143.8 ± 0.8
	QR	133.8 ± 2.1	127.5 ± 2.5	126 ± 1	127 ± 1	148.4 ± 4.3
JAPN	OLS	174.1 ± 3.6	159 ± 3	141 ± 4	156 ± 6	195.6 ± 3.7
	QR	188.4 ± 1.9	164 ± 8	157 ± 3	173.5 ± 4.4	219.8 ± 1.7
COST	OLS	60 ± 2	62.3 ± 2.3	60 ± 1	68 ± 6	64 ± 3
	QR	52.9 ± 1.3	56 ± 5	56.6 ± 1.2	20 ± 22	43.8 ± 3.8
CH-A	OLS	126.2 ± 4.2	118.4 ± 4.4	117.6 ± 3.9	123 ± 5	137.3 ± 4.5
	QR	135.4 ± 3.5	128 ± 5	124 ± 5	130.8 ± 4.2	156.1 ± 3.7
R #9-1	OLS	213.1 ± 4.2	202 ± 10	184.8 ± 1.2	194.9 ± 1.7	237 ± 6
	QR	154 ± 11	107 ± 23	188 ± 5	180 ± 4	118 ± 21
SGIL	OLS	101.6 ± 0.2	100.0 ± 0.2	97.9 ± 0.2	95.9 ± 0.5	103.8 ± 0.2
	QR	99.7 ± 0.4	99.6 ± 0.6	98.9 ± 0.6	97.8 ± 0.2	104.5 ± 0.7
SHBE	OLS	78.3 ± 0.5	84.7 ± 2.4	76.2 ± 0.9	72.6 ± 1.4	81.7 ± 0.9
	QR	80.4 ± 0.2	75 ± 8	78.9 ± 1.1	76.3 ± 0.8	87.4 ± 0.3
CLAH	OLS	122.8 ± 0.2	122.8 ± 0.6	118.4 ± 0.7	115.4 ± 1.1	126.9 ± 0.6
	QR	124.0 ± 0.2	121.5 ± 1.2	121.4 ± 0.4	119.5 ± 0.6	131.9 ± 0.7
CJON	OLS	21.57 ± 0.31	20.93 ± 0.23	19.77 ± 0.08	19.59 ± 0.11	20.87 ± 0.28
	QR	19.69 ± 0.18	19.85 ± 0.18	20.09 ± 0.09	19.99 ± 0.06	19.57 ± 0.29

Field experiments for studying CO_2 mineral trap at high temperature at Ogachi, Japan

Hideshi Kaieda[1*], Akira Ueda[2], Kenji Kubota[1], Hiroshi Wakahama[3], Saeko Mito[3], Kazunori Sugiyama[4], Akiko Ozawa[4], Yoshihiro Kuroda[2], Yoshikazu Kaji[5] , Heigo Suzuki[5] and Hisao Sato[6]
[1] Central research institute of electric power industry, 1646, Abiko, Abiko-shi, Chiba, 270-1194, Japan
[2] Kyoto university, C1-2-155, Katsura, Nishikyo-ku, Kyoto 616-8540, Japan
[3] Research Institute of Innovative Technology for the Earth, 9-2 Kizugawadai, Kyoto, 619-0292, Japan
[4] Mitsubishi Material Techno Corp., 1-14-16 Kudan-kita, Chiyoda-ku, Tokyo 102-8205, Japan
[5] Chuo Kaihatsu Corp., 3-4-2 Nishi-aoki, Kawaguchi, Saitama, 332-0035, Japan
[6] Mitsubishi Material Corp., 1-297, Kitabukuro, Ohmiya-ku, Saitama, 330-8508, Japan
* corresponding author : kaieda@criepi.denken.or.jp

Previous experiments at Ogachi, up until 2007, generated two important results obtained by injecting CO_2 dissolved water into a 1,100 m deep well, OGC-2 at Ogachi in Japan, for which the bottom-hole temperature was measured at about 210 degree C. One result was that Ca concentration of the CO_2 dissolved (3 weight %) water, at a depth of 1,030 m in OGC-2, increased to a maximum of 85.2 mg/L in a few hours. The Ca was considered to be dissolved from rock. The second result was that calcite precipitation on calcite crystal samples was observed when the samples were held at depths of 850 m and 950 m for an hour in the CO_2 dissolved water in OGC-2. In 2008, we reconfirmed that calcite precipitation occurred on calcite crystal samples at a depth of 950 m in OGC-2. From these results, we constructed a model for describing a CO_2 mineral trap mechanism at high temperature. When CO_2 is injected underground at high temperature four zones are created, one is a super critical CO_2 zone, second is a dense CO_2 dissolved water zone, third is a thin CO_2 dissolved water zone, and fourth is a formation water zone. The CO_2 dissolved water zones react with rock. Ca dissolves from rock in the dense CO_2 dissolved water zone by high CO_2 concentration (low pH) but in the thin CO_2 dissolved zone (nearly neutral pH), by mixing with formation water, Ca precipitates as calcite minerals.

Keywords: CO_2, Mineral trap, Geothermal, Calcite, Ogachi

Concept of CO_2 Mineral Trap at High Temperature

Under high temperature conditions, the following reaction can proceed from the upper to the lower of the formula (1) (Gale and Shane, 1905).

$CaAl_2Si_2O_8$ (plagioclase) + H^+ + HCO_3^- + H_2O =$CaCO_3$ (calcite) +$Al_2Si_2O_5(OH)_4$ (kaolinite) (1)

According to Ueda et al., (2005), carbonate-rich rock formations can be observed in most Japanese geothermal fields. Reaction according to formula (1) moves towards the lower side at higher temperatures, reflecting the fact that calcite solubility decreases with increasing temperature. Calcite and kaolinite (clay)-rich rock is produced through the reaction and forms a cap rock for the geothermal reservoir. These considerations, together with the increasing reaction rates at high temperature conditions and the fact that precipitation of carbonate minerals fixes CO_2 suggest that CO_2 sequestration could be practicable by injection into geothermal fields (see Figure 1).

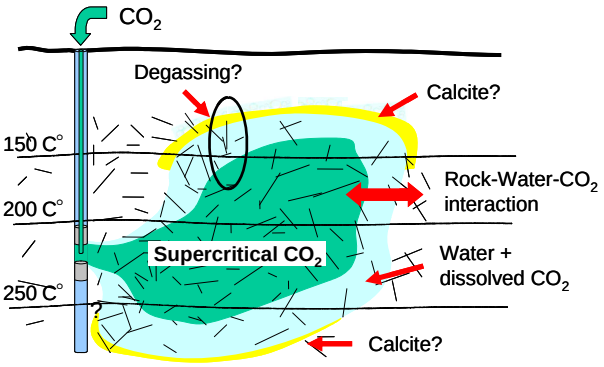

Figure 1: Concept of CO_2 injection into high temperature rock (Ueda et al., 2005)

We have conducted some field experiments from 2002 to 2008 to study CO_2 sequestration in solid minerals by injecting CO_2 dissolved in water into a high temperature borehole, OGC-2, at the Ogachi Hot Dry Rock geothermal site in Japan (Kaieda et al., 2008 and Kaieda et al., 2009). OGC-2 was drilled into granitic rock to a depth of 1,100 m and was cased from the ground surface to 700 m depth. The bottom 400 m interval of OGC-2 was left uncased and the bottom-hole temperature was measured around 210 degree C.

CO_2 dissolved water injection in 2008

The surface water (nearly neutral pH) was injected into OGC-2 at a flow rate of 50 kg/min at atmospheric pressure on September 16th, 2008. During the water injection solid CO_2 (dry ice) blocks of a few centimetres in size were injected at a rate of 0.4 kg/min to create 0.8 weight percent CO_2 dissolved water (see Figure 2). A total of 20 tons of 0.8 % CO_2 dissolved water with a total of about 160 kg-dry ice was injected into the open-hole region between 700 m and 1,100 m (bottom) in OGC-2 and into the surrounding rocks.

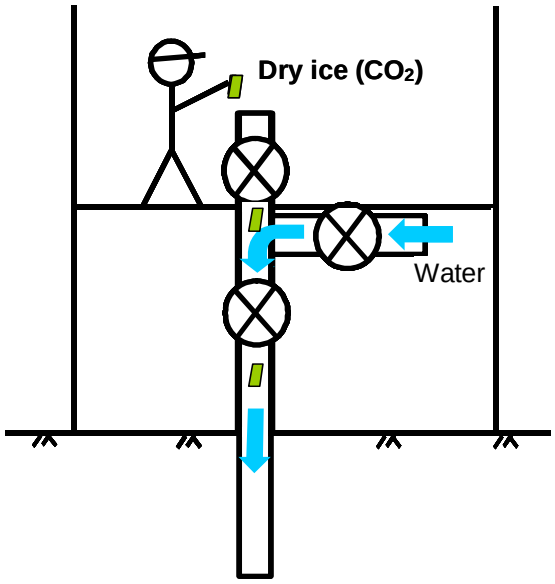

Figure 2: CO_2 (Dry ice) injection with water

Calcite Precipitation Measurement

After the CO_2 dissolved water was injected and replaced pre-existing formation water, a specially designed test sonde (see Figure 3) was inserted into OGC-2 and calcite crystal growth tests were conducted using the sonde. Calcite crystal samples partially covered with Au (Gold) film were set in the sonde to prevent the covered area reacting with the CO_2 dissolved water. He (Helium) gas filled the inside the sonde at an adequate pressure for protecting outside water coming in. A valve (rupture disk) of the sonde breaks when the outside pressure increases high enough relative to the He gas pressure in the

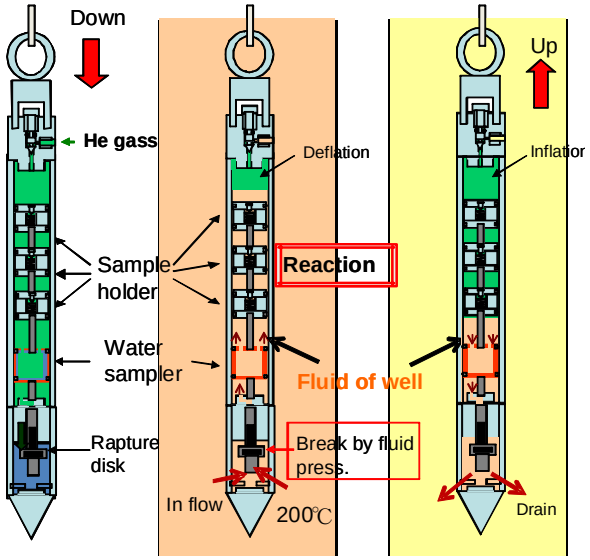

Figure 3: Test sonde for Calcite sample react with fluid in borehole

sonde. In this test we set the valve to break at a pressure of 950 m depth in OGC-2 where the well bore wall was relatively smooth. The sonde was inserted to a depth of 950 m in OGC-2 and held there for an hour. During this hold time CO_2 dissolved water in OGC-2 came into the sonde and reacted with the samples. The sonde was recovered to the surface after the hold time and the CO_2 dissolved water drained from the sonde during retrieval from OGC-2. At the surface the samples were removed from the sonde and the surface features of the samples were observed by stereo micro-scope. Roughness of the sample surfaces was measured by phase shift interferometer, comparing the Au film covered area to the remaining area (see Figure 4).

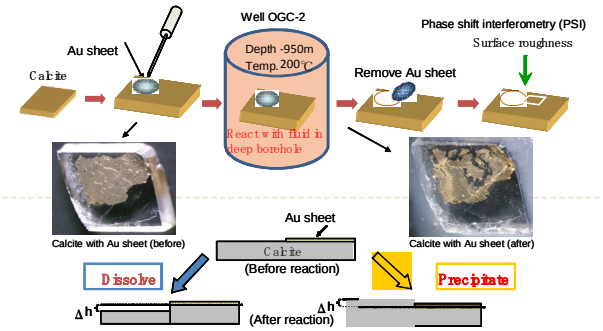

Figure 4: Calcite sample treatment

Calcite Precipitation Results

We conducted calcite precipitation tests five times before and after the CO_2 dissolved water injection from September 15 to 19, 2008. Figure 5 shows an example of the test result which was observed when the crystal test sonde was set 3.6 hours after the CO_2 dissolved water was injected into OGC-2. The top picture of Figure 5 shows an example of the surface feature of the calcite crystal sample from the stereo microscope before the test. X is a horizontal distance in micro-meter and Z is the elevation in nano-meter.The term 'masked' refers to the area covered with Au film. The middle picture shows the sample's surface at the same point as the above picture but following the test. The bottom graph shows the measured roughness of the sample surface along line A to B measured by the phase shift interferometer. The blue line represents the before test condition and the red line represents the after test condition. In the masked area, the roughness of the sample surface is relatively flat both before and after the test, but in the other area elevation of the sample surface was measured to increase after the test to a maximum of about 2,224 nano-meters (2.224 micro meters). This means that the calcite crystal samples grew in the test.

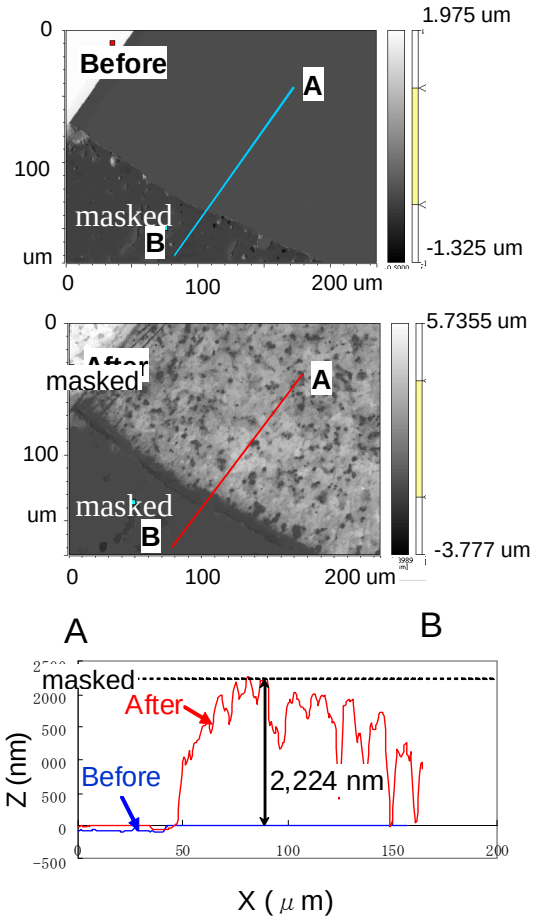

Figure 5: Stereo microscope pictures and the surface roughness along the A-B line of the calcite sample before and after reaction 3.6 hours after CO_2 dissolved water injection into OGC-2. X is horizontal distance and Z is elevation along the A-B line.

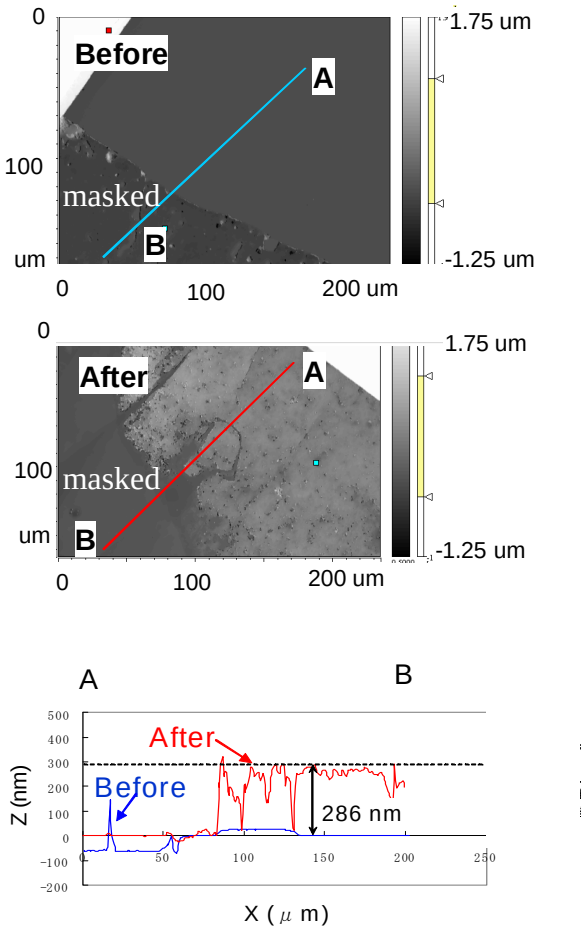

Figure 6: Stereo microscope pictures and the surface roughness along the A-B line of the calcite sample before and after reaction 22.6 hours after CO_2 dissolved water injection into OGC-2. X is horizontal distance and Z is elevation along the A-B line.

Another result is shown in Figure 6. This result was obtained when the test sonde was set 22.6 hours after the CO_2 dissolved water injection into OGC-2. In this test calcite crystal growth was also measured to a maximum of about 300 nano meters (0.3 micro meters).

From the above results, it was considered that CO_2 precipitation on crystals occurred quickly and CO_2 precipitation rate was faster a few hours after CO_2 dissolved water injection but the rate gradually decreased.

The sample dissolutions which were observed just after the CO_2 dissolved water injection in the 2007 tests were not observed in the 2008 tests.

We summarised the reaction process of CO_2 dissolved water with rock as follows: 1) water conditions in the open-hole region in OGC-2 for a few hours after CO_2 dissolved water injection was that of high CO_2 concentration and low pH. For this condition Ca is dissolved from the rock and calcite samples are also dissolved; 2) a few hours after CO_2 dissolved water injection CO_2 concentration decreased and pH increased to near neutral because of mixing with formation water, and calcite solubility decreases with temperature increase. For this condition, calcite precipitates quickly, 3) after Ca and CO_2 precipitation occurred, calcite precipitation rate gradually decreased.

CO_2 mineral trap mechanism at high temperature

Using these results we constructed a model to explain the CO_2 precipitation (mineral trap) mechanism at high temperature. The concept of this mechanism is shown Figure 7.

When CO_2 is injected deep underground (more than 800 m deep) at high temperature, four zones are created. One is a super critical CO_2 zone, second is a dense CO_2 dissolved water zone, third is a thin CO_2 dissolved water zone, and fourth is a formation water zone. Ca dissolves from rock in the dense CO_2 dissolved water zone

by high CO_2 concentration (low pH) but in the thin CO_2 dissolved zone (nearly neutral pH) where mixing with formation water occurs, Ca precipitates as calcite minerals.

To confirm this model, we need to inject super critical CO_2 (not CO_2 dissolved water) into rock and further need to observe the CO_2 concentration distribution in CO_2 dissolved water zone around the super critical CO_2.

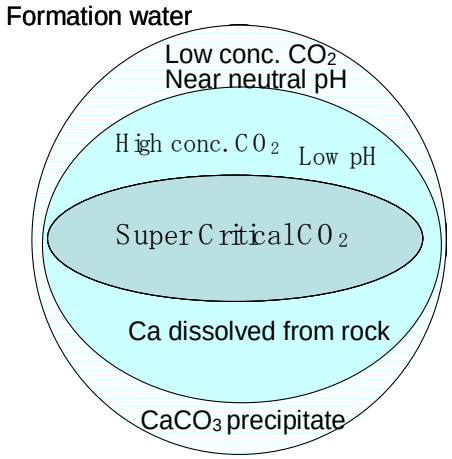

Figure 7: A model for describing the reaction of CO_2 dissolved water with rock around super critical CO_2.

We also think that the following studies are needed as future work: the effect of calcite precipitation on permeability changes of rock: Ca dissolution rate from rock in CO_2 dissolved water; effective Ca volume in rock, and confirmation of calcite precipitation phenomena at different temperatures and with different geology.

We plan to conduct permeability tests of rock in OGC-2 before and after CO2 dissolved water injection in Autumn 2009.

Conclusion

CO_2 dissolved water was injected into an open-hole interval between 700 m to 1,100 m depths of OGC-2 at Ogachi which was drilled into granitic rock. The bottom hole temperature was measured at around 210 degree C. In 2008, we reconfirmed that calcite precipitation occurred on calcite crystal samples which was observed in previous experiments up until 2007. From these results, we constructed a model for describing a CO_2 mineral trap mechanism at high temperature. When CO_2 is injected underground at a high temperature four zones are created, one is super critical CO_2 zone, second is a dense CO_2 dissolved water zone, third is a thin CO_2 dissolved water zone, and fourth is a formation water zone. The CO_2 dissolved water zone reacts with rock. Ca dissolves from rock in the dense CO_2 dissolved water zone by high CO_2 concentration (low pH), but in the thin CO_2 dissolved zone (nearly neutral pH), where mixing with formation water occurs, Ca precipitates as calcite minerals. In 2009 we will conduct permeability tests of rock in OGC-2 before and after the CO_2 dissolved water injection.

Acknowledgement

This research has been conducted as a collaboration work between the Central Research Institute of the Electric Power Industry and Research Institute of Innovative Technology for the Earth in the Research & Development Program "Development of innovative technology for the CO_2 fixation by Georeactor" under the fund from Ministry of Economy, Trade & Industry of Japan.

References

Gales, C. and Shane, H., 1905, About a case of kaolinitisation in granite by a cold CO2 bearing water, Zenlt. Geol. Min. Palisant., 427-467.

Kaieda, H., Ito, H., Kiho, K., Suzuki, K., Suenaga, H. and Shin, K., 2005, Review of the Ogachi HDR Project in Japan, Proceedings World Geothermal Congress 2005.

Kaieda, H., Kubota, K., Wakahama, H., Mito, S., Ueda, A., Ohsumi, T., Yajima, T., Satoh, H., Kaji, Y., Sugiyama, K. and Ozawa, A., 2008, Experimental Study on CO_2 Injection into HDR Geothermal Reservoir, Proceedings, 2008 Australian Geothermal Conference.

Kaieda, H., Ueda, A., Kubota, K., Wakahama, H., Mito, S., Sugiyama, K., Ozawa, A., Kuroda, Y., Sato, H., Yajima, T., Kato, K., Ito, H., Ohsumi, T., Kaji, Y. and Tokumaru, T., 2009, Field Experiments for Studying on CO2 Sequestration in Solid Minerals at the Ogachi HDR Geothermal Site, Japan, Proceedings, Thirty-Fourth Workshop on Geothermal Reservoir Engineering, Stanford University.

Ueda, A., Kato, K., Ohsumi, T., Yajima, T., Ito, H., Kaieda, H., Metcalfe, R. and Takase, H., 2005. Experimental studies of CO2-rock interaction at elevated temperatures under hydrothermal conditions. Geochemical Journal, Vol. 39, pp.417-425.

A Preliminary Study on Fluid-Rock Interactions of the Hot Fractured Rock Geothermal System in Cooper Basin, South Australia

Gideon B. Kuncoro[1], Yung Ngothai[1*], Brian O'Neill[1], Allan Pring[2], Joël Brugger[2]
[1] The University of Adelaide, School of Chemical Engineering, North Terrace, Adelaide, SA, 5000
[2] South Australian Museum, North Terrace, Adelaide, SA, 5000
*Corresponding author: yung.ngothai@adelaide.edu.au

A study of the interactions between rock and circulating fluid is essential to determine the chemical changes and mineral alteration of a geothermal system. Preliminary mineralogical investigation and geothermal experiments have been performed to investigate the hydrothermal alteration of the Habanero geothermal system in the Cooper Basin, South Australia. Samples of drill cuttings from a borehole 5 km deep were contacted with reverse osmosis water in a thermosyphon induced loop reactor at 250°C and 50 bar. Fluid and rock samples were analysed prior to, and after circulation of the water through crushed sample of the rock (100 – 200 µm diameter) for 1, 2, 3, 7, 14 and 21 days. Water analysis was performed using ICP-MS, and rock analyses were conducted using an optical microscope, SEM and XRD. The experimental results indicated that mineral dissolution was more rapid in the early stages of the experiment. This may be a consequence of the dissolution of finer rock particles. SEM observations showed evidence of etching of the mineral surfaces consistent with partial dissolution. XRD results indicated that quartz was stable throughout the experiment, and that the albite-feldspar ($NaAlSi_3O_8$) in the rock had partially dissolved. ICP-MS analysis on the water sample confirmed that some mineral dissolution has occurred. The concentrations of most elements increased with the exception of Ca, Ba and Mg. Future work will quantify concentrations (ppm) of the dissolved minerals.

Keywords: hot fractured rock, fluid-rock interaction, geothermal, Cooper Basin, Habanero

Introduction

Hot fractured rock (HFR) geothermal energy has great potential as a future supply for electric power generation by harnessing stored thermal energy from high temperature granitic rocks in the Cooper Basin and North Flinders Ranges. This route provides opportunities for power generation with minimal greenhouse gas emissions or long-lasting nuclear wastes, at a cost competitive with those for energy generated from fossil fuels if carbon costs are considered. The geothermal heat exchange occurs at great depth, up to 5 km, and the thermal energy source is radioactive decay rather than volcanism (Geodynamics, 2009). Existing reservoir granites are currently in equilibrium with the surrounding ground water. The injection of fresh water to extract thermal energy from the host rock will alter this fluid-rock equilibrium and may cause partial chemical dissolution or mineral species alteration, which may potentially increase the dissolved solids such as silica and other metals in the water. These dissolution products of the components have different equilibria, which will be a function of temperature and pressure, thus precipitation or scaling of pipe work and closure of fractures in the granite body are possible. The saturation of metals in fluid is volume-dependent, where very small volumes of fluid may require slight under-cooling before precipitation occurs. Clearly, characterization of fluid geochemistry is important in the evaluation of the performance of geothermal systems (Grigsby et al., 1989). Moreover, understanding the chemical interactions due to the injection of fluid into hot granite is crucial for problems concerning clogging by precipitation and heat loss caused by dissolution (Azaroual and Fouillac, 1997).

The study of fluid-rock interaction will allow determination of mineral alteration and dissolution of minerals to the circulating water. Unfortunately, relatively little information is available on the rates and chemical mechanisms of mineral reactions in hydrothermal solutions (Posey-Dowty et al., 1986). Furthermore, it is impossible to generalize the actual field experience of mineral deposition in geothermal systems into one consistent theory due to the vast chemical and operational variation between field sites (Robinson, 1982). Therefore, although there have been a number of studies on fluid-rock interactions for different geothermal sites (Rimstidt and Barnes, 1980; Robinson, 1982; Posey-Dowty et al,. 1986; Savage et al., 1987; Grigsby et al., 1989; Savage et al., 1992; Azaroual and Fouillac, 1997; Yangisawa et al., 2005), these are probably not directly applicable to the hot granite-based geothermal systems in the Cooper Basin.

Flow-through Cell

A hydrothermal reaction cell has been developed to observe chemical changes in the host rock and the circulating fluid. A diagram and a photograph of the flow through cell are provided in Figure 1. The cell is designed to operate in a flow-through configuration where the fluid flows continuously inside the cell. The total cell volume is 345 ml. All tubing is made from ¼ inch titanium and connected with standard Swagelok titanium fittings, with the reservoirs in stainless steel

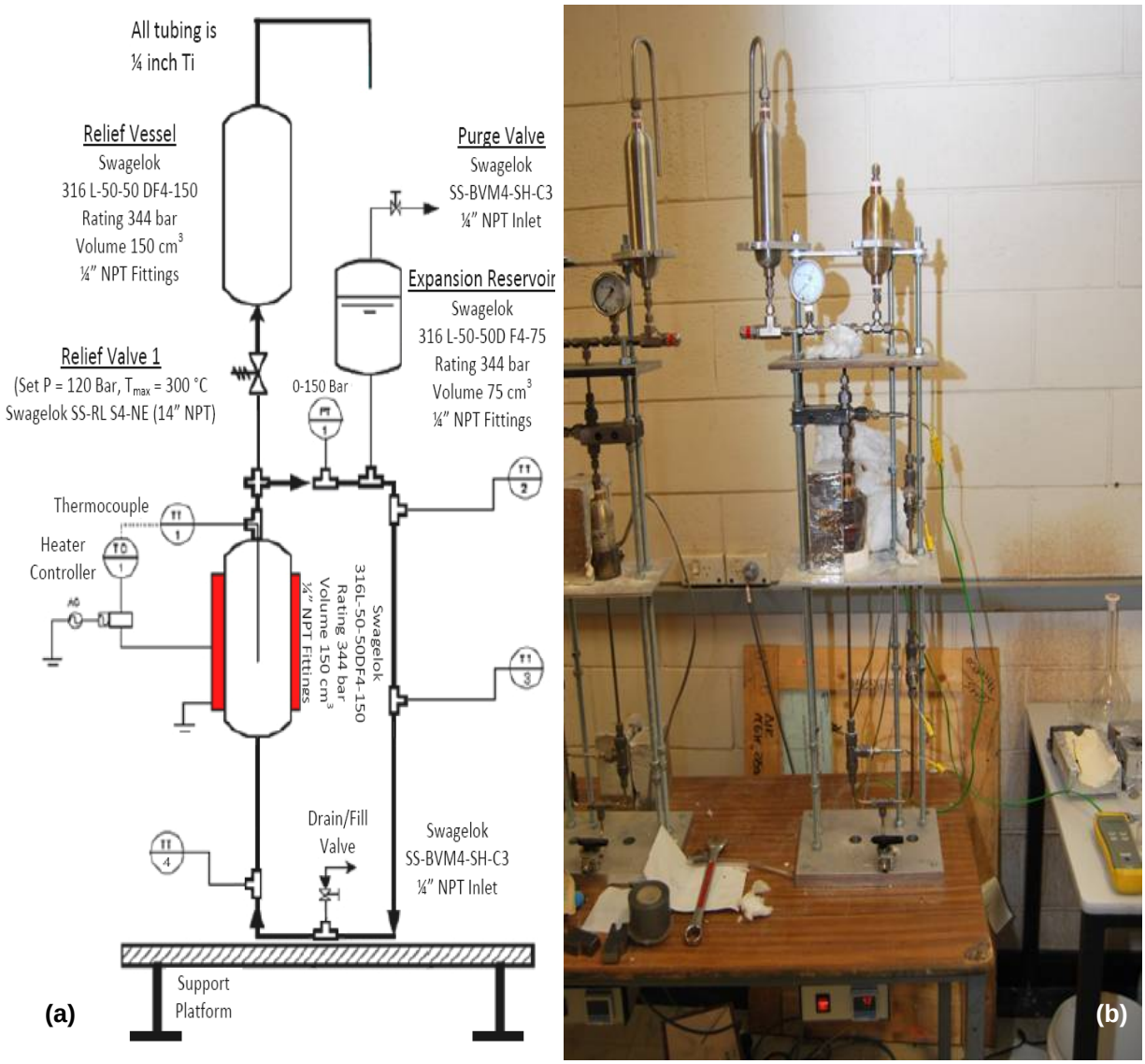

Figure 1: (a) Diagram of the flow through cell (b) Photograph of the geothermal flow through cell

(SS316). The total length of the cell loop is approximately 1800 mm. The volume of the main reservoir is 150 cm^3. A pressure relief system consisting of a relief valve and a relief vessel is employed to the cell for safety. The volume of the relief vessel is 300 cm^3 and the relieve valve was set to open at a maximum pressure of 100 bar. An expansion reservoir is employed to compensate for changes in volume as the fluid is heated. The volume of the expansion reservoir is 75 cm^3. All vessel are rated at 344 bar. Four thermocouples are installed to monitor the temperature changes throughout the cell. A pressure transducer is installed to monitor the pressure. The operating temperature and pressure are 250^oC and 50 bar, respectively. Temperature is controlled by a simple relay controller and two heaters were used and arranged in parallel. The heaters are intact with the main reservoir and insulated with ceramic bricks.

Experimental

Samples of drill cuttings were provided by Geodynamics from the Habanero 3 well. The samples were analysed using optical microscope, scanning electron microscope (SEM) at the Adelaide Microscopy Centre to observe both surface and cross-sectional area, and powder X-ray diffraction (XRD) at the South Australian Museum to identify and semi-quantify the minerals. A preliminary set of experiments to observe the fluid-rock interaction were performed in batch mode. The drill cutting was used as the rock sample. The rock sample was crushed and sieved to give 100 – 200 µm size fraction and approximately 0.7 grams of rock were used in each batch. The sample was contained in a pre-weighed wire basket made from stainless steel and placed in the sample holder of the cell. The cell was filled through a valve in the base of the cell with reverse osmosis (RO) water and then 90 ml of water was drained from the cell to allow for

fluid expansion upon heating. The velocity of the thermosyphon circulating fluid is estimated to be approximately 0.1 m/s. The fluid-rock interaction periods were 1, 2, 3, 7, 14, and 21 days. At conclusion of this interaction period, the rock sample was dried (105°C for 48 hours), cooled in a desiccator, and weighed to determine any weight loss.

The rock samples were analysed using SEM and XRD, and the water samples were stored and preserved with 4% w/w of 1M nitric acid until analysis by ICP-MS to identify the dissolved metals. The silica content was quantified using heteropoly blue method (HACH, 2009).

Results and Discussion

Preliminary results from the geothermal cell experiment illustrate that the dissolution of the rock (% w/w) increases with time (Figure 2).

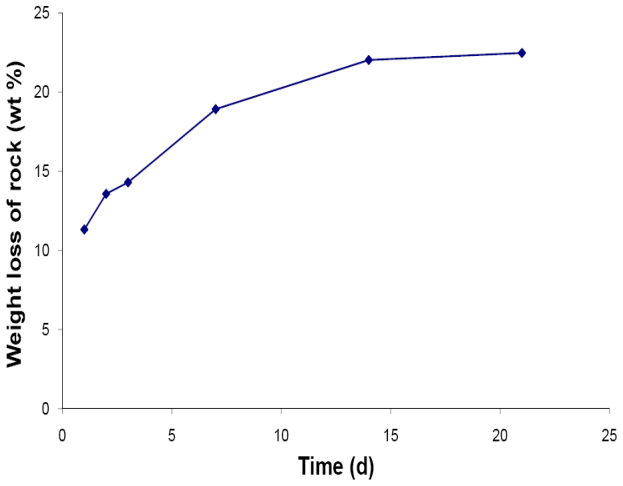

Figure 2: Change in weight loss of rock (% w/w) versus time

However, dissolution appears more rapid in the early stages of the experiment. It is probably an artefact of the rapid dissolution of fine particles present in the rock sample (Savage et al., 1987).

The later stage of the experiment approached a steady state value. However the fluid is not necessarily saturated with minerals (feldspar), but due to the low dissolution reaction rate between the remaining phases causes this behaviour..

Detailed analyses of the mineralogical changes in the host rock are currently underway and will be reported at a later date.

Rock Analysis

Petrographic analysis was performed on the drill cuttings from Habanero 3 well. The rock is a feldspar syenite, containing albite ($NaCa)AlSi_3O_8$, and microcline ($KAlSi_3O_8$) with carbonate alteration, which has been subjected to hydrothermal alterations (Pring, pers. comm. 2009), as shown in Figure 3.

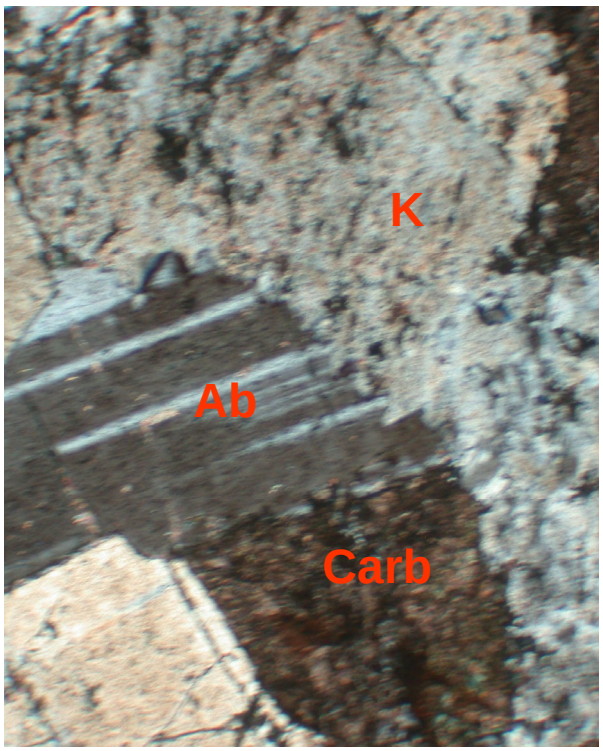

Figure 3: Host rock Habanero 3 – "syenite" consisting of albite (Ab), microcline (K) with extensive carbonate (carb) alteration – field of view 2mm across

SEM images of the surface particles were obtained using the secondary electron detector (SE) of the XL30 in Adelaide Microscopy. The SEM images of the rock sample surfaces before and after the experiments are shown in Figure 4. It can be seen that fine particles adhered on the surface of the starting rock. The fine particles rapidly dissolved during the early stages of the experiments and the roughness of the rock surface also becomes more apparent with longer interactions with the fluid. Etching is evident on the surface of the rocks and again developed in the later stages of the experiment. This indicates that a dissolution reaction has occurred in the interaction period.

SEM analyses of the cross section of the rock samples (images not presented) were also conducted. These images were obtained using the backscattered electron detector (BSE) and analysed using the energy dispersive x-ray spectrometer. The results suggest that the rock is composed of albite-feldspar, microcline and quartz. The feldspar was variably veined and was replaced by patches of fine grained carbonate with a magnesium and iron-rich composition. The rock also contains minor amounts of pyrite (FeS_2), sphalerite (ZnS), fluoropatite ($Ca_5(PO_4)_3F$ and a number of other accessory minerals. Preliminary observation of the SEM analysis on the rock samples after the experiment indicates minimal alteration. However, it was evident that the carbonates have dissolved in the early stages of the experiment.

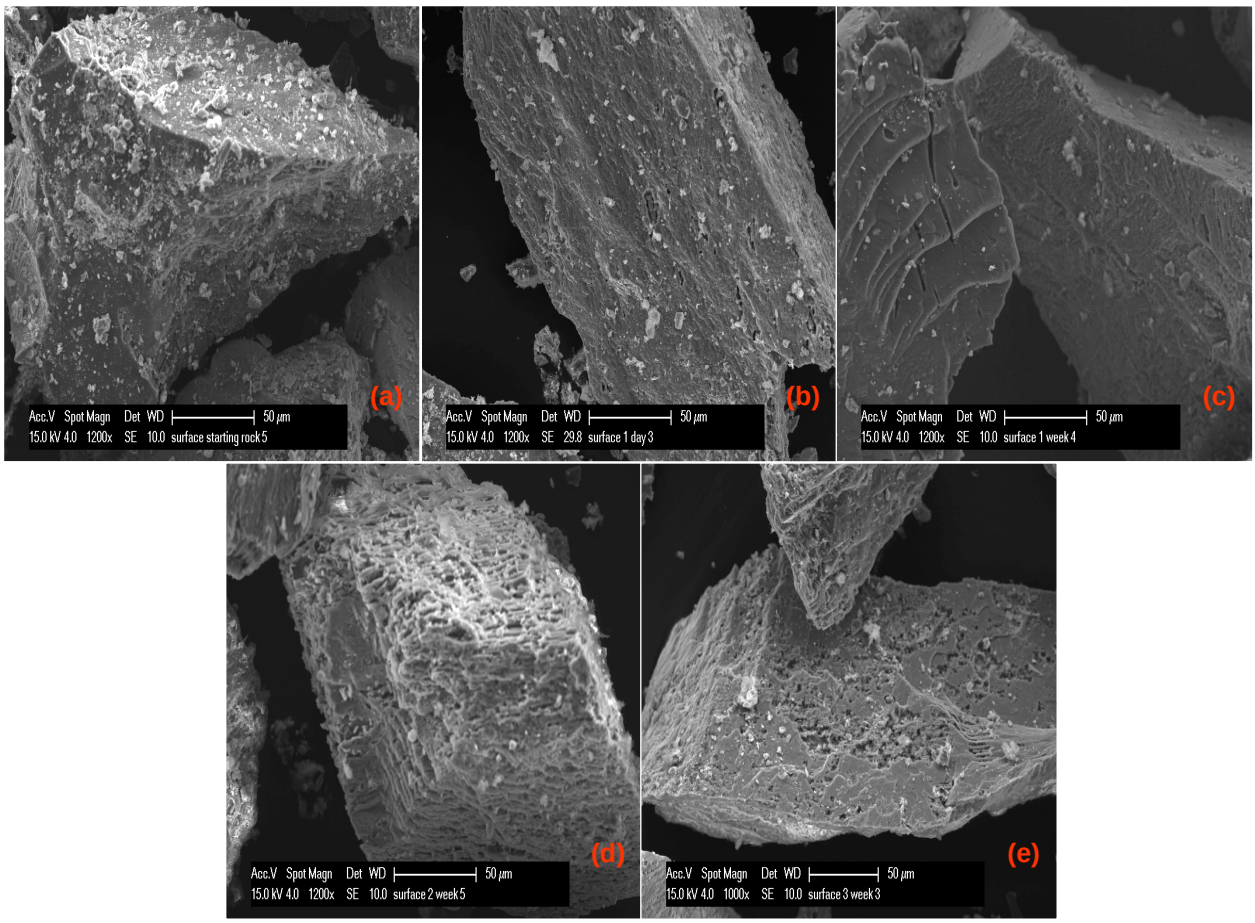

Figure 4: SEM images of the rock sample surface (a) starting rock (b) after 1 day experiment (c) after 1 week experiment (d) after 2 weeks experiment (e) after 3 weeks experiment

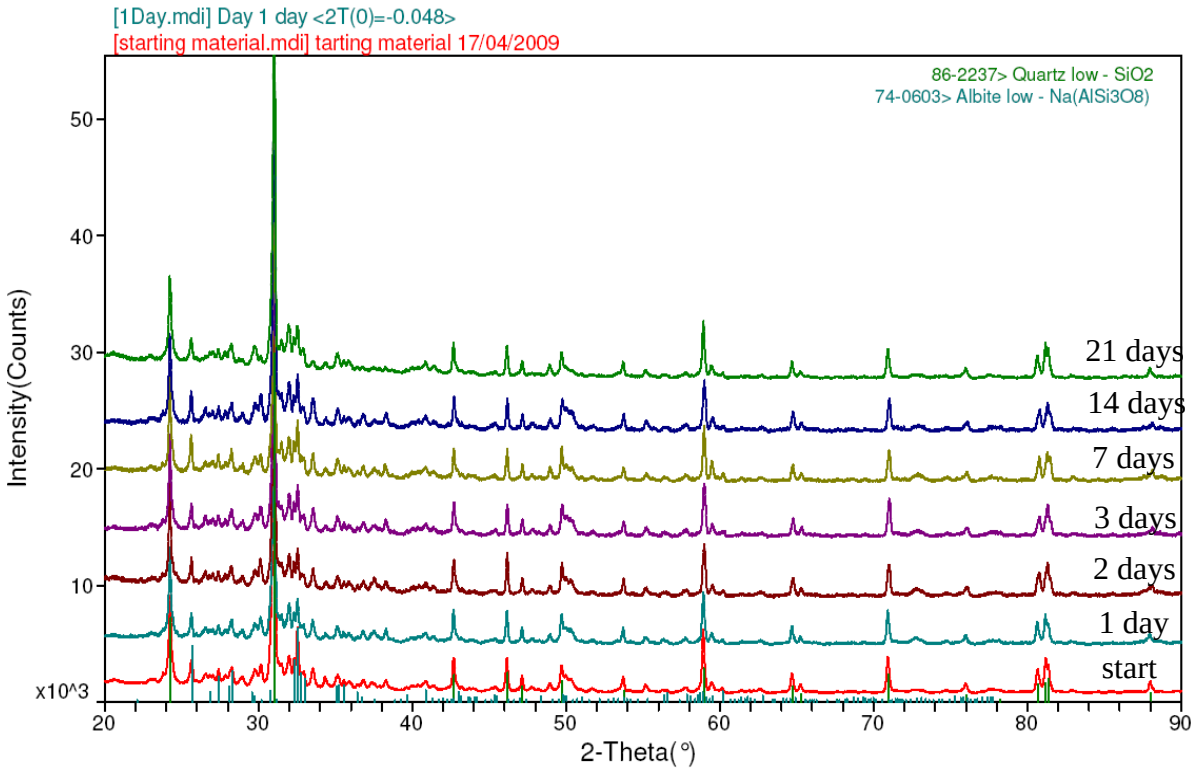

Figure 5: Compiled XRD analysis results from geothermal cell experiments

Traces of iron, manganese, magnesium, and strontium were found in the solutions after the experimental runs. Some of the iron may be contaminants from partial dissolution of metals from the stainless steel basket and/or the stainless steel reservoir of the geothermal cell. The results from the X-ray diffraction analysis of the rock sample from different stages of the experiment are presented in Figure 5. It is seen that the peaks showing intensity do not change significantly in different experimental runs. The lines in the XRD trace for albite and microcline show slight decrease compared to those of quartz, which is quite stable. Quantitative phase analysis using the X-ray diffraction data is planned for future work.

Water Analysis

The initial pH of the water was 5.5. This did not change significantly in all batch experiments. Figures 6 – 9 show the concentration of elements versus time from the ICP-MS analysis on the circulating water after 1, 2, 3, 7, 14, and 21 days of fluid-rock interactions.

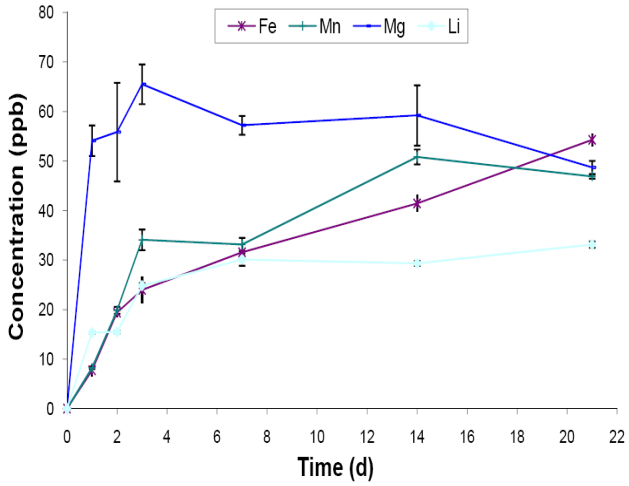

Figure 6: Concentration of Fe, Mn, Mg and Li in experimental liquid versus time

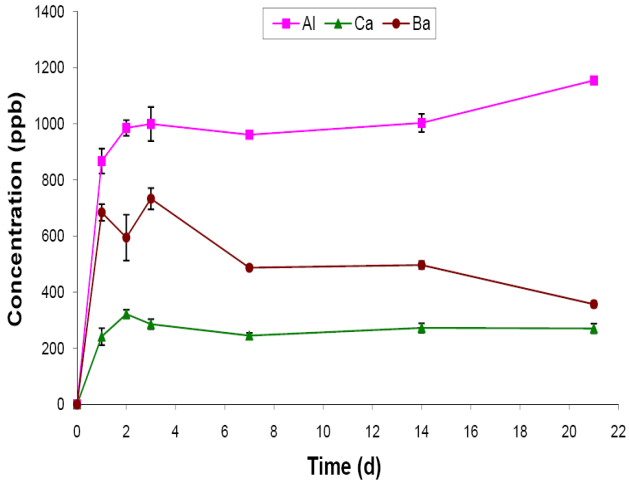

Figure 7: Concentration of Al, Ca and Ba in experimental liquid versus time

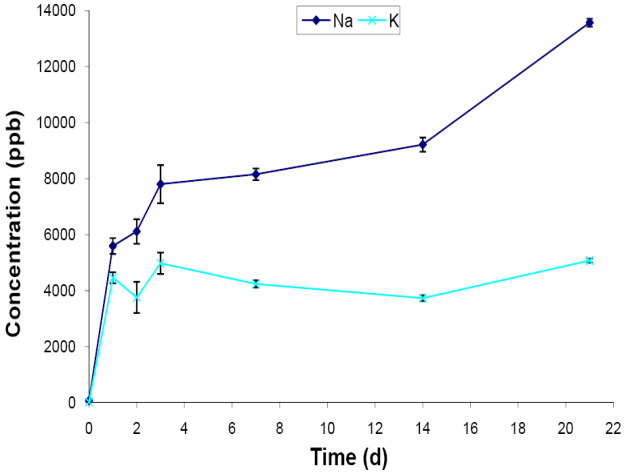

Figure 8: Concentration of Na and K in experimental liquid versus time

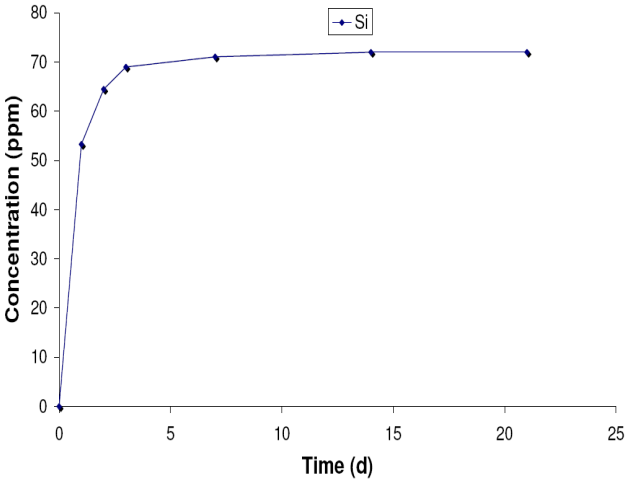

Figure 9: Concentration of Si in experimental liquid versus time (standard deviation 0.0067)

Water analysis results showed that there was enhanced release of the minerals, indicated by the concentration increase of minerals in the liquid phase. The rapid dissolution is probably a consequence to the dissolution of fine particulates which adhere to the mineral grains of the rock sample to the fluid phase (Figure 4a). The use of pure water (very low concentration of dissolved mineral) would also explain the rapid dissolution reaction. The increase in concentration of elements Si, Na, and K in the water would indicate the dissolution of albite and microcline feldspars. The increase in the concentration of Fe and Mn may be the consequence of the carbonate dissolution to the liquid. Traces of Al, Fe, Mn and Mg may be contaminants from the dissolution of accessory minerals. Concentration of all analysed elements showed a net increase during the experiment, except for Ca, Ba, and Mg.

Conclusion

The petrographic and diffraction analysis showed that the rock is composed chiefly of feldspar syenite, quartz, albite and microcline with carbonate alteration. The fluid-rock interaction experiment showed that dissolution reactions occur predominantly in the early stages of the experiment probably due to the dissolution of fine particulates in the rock. In addition, the carbonates have also dissolved in the early stages of the experiment. Results of XRD showed that feldspar experienced a slight reduction; however, quartz remained stable throughout the experiment. Liquid analysis showed higher concentrations of Na, K, Si, and Al compared to other analysed elements. These results suggest that the dissolution reaction occurs primarily for the feldspars.

The dissolution of feldspar would suggest potential silica scaling. The concentration of silica (72 ppm released from 0.7g rock sample) was released to the liquid phase throughout the experiment. Unfortunately the quantification of the minerals has not been concluded, therefore the mass balance and mass transfer rates are still unclear at this stage.

Future Work

The current work has used reverse osmosis water for the fluid-rock interaction and does not represent the actual interaction. Therefore future work will conduct the experiment using a more complex fluid system Na – Cl – H_2O and will progress with the actual fluid from the field. Quantification of the minerals will be performed using electron microprobe to understand the mass transfer occurring in the interaction. Modelling of the fluid-rock interaction will be performed in the later stage of this research using Geochemist Workbench.

Acknowledgments

The research described in this paper has been supported by The Department of Primary Industries and Resources of South Australia (PIRSA) and Geodynamics. The author would like to thank Geodynamics for supplying the drill cuttings, and the South Australian Museum and Adelaide Microscopy for the equipment access.

References

Azaroual, M., and Fouillac, C., 1997, Experimental Study and Modelling of Granite-Distilled Water Interaction at 180°C and 14 Bars: Applied Geochemistry, V. 12, pp. 55-73.

Geodynamics, 2009, Power from the Earth. Habanero 3, http://www.geodynamics.com.au/IRM/Company/ShowPage.aspx?CPID=1403, accessed 10 January 2009.

Grigsby, C. O., Tester, J. W., Trujillo JR., P. E., and Counce, D. A., 1989, Rock-Water Interactions in the Fenton Hill, New Mexico, Hot Dry Rock Geothermal Systems I, Fluid Mixing and Chemical Geothermometry: Geothermics, V. 18, 629-656.

HACH, 2009, DR/2010 Portable Spectrophotometer Procedures Manual. http://www.hach.com/fmmimghach?/CODE%3A4930022286|1, p 767 – 772, accessed September 2008

Posey-Dowty, J., Crerar, D., Hellerman, R., and Clarence, D. C., 1986, Kinetics of Mineral-Water Reactions: Theory, Design, and Application of Circulating Hydrothermal Equipment: American Mineralogist, V. 71, pp. 85-94.

Pring, A., 2009, personal communication.

Rimstidt, J. D., and Barnes, H. L., 1980, The Kinetics of Silica-Water Reactions: Geochimica et Cosmochimica Acta, V. 44, pp. 1683-1700.

Robinson, B. A., 1982, Quartz Dissolution and Silica Deposition in Hot Dry Rock Geothermal Systems, Thesis, Cambridge, Massachusetts Institute of Technology.

Savage, D., Cave, M. R., Milodowski, A. E., and George I., 1987, Hydrothermal Alteration of Granite by Meteoric Fluid: An Example from the Carnmenellis Granite, United Kingdom: Contributions to Mineralogy and Petrology, V. 96, pp. 391-405.

Savage, D., Bateman, K., and Richards, H. G., 1992, Granite-Water Interactions in a Flow-through Experimental System with Applications to the Hot Dry Rock Geothermal System at Rosemanowes, Cornwall, U.K.: Applied Geochemistry, V. 7, pp. 223-241.

Yangisawa, N. Matsunaga, I., Sugita H., Sato, M., and Okabe T., 2005, Scale Precipitation During Circulation at the Hijiori HDR Test Field, Yamagata, Japan: Proceedings World Geothermal Congress 2005, Antalya, Turkey, 24-29 April 2005.

The End Point of Geothermal Developments: Modelling Depletion of Geothermal Resources

J V Lawless
*A W Clotworthy; *G Ussher
Sinclair Knight Merz
PO Box 9806, Newmarket, Auckland, New Zealand: JLawless@skm.co.nz

Any finite quantification of the "capacity" of a geothermal resource implicitly involves a start point and an end point for energy extraction. The issue addressed in this paper is: at what time and why does energy extraction cease from a geothermal resource, and what are the implications for resource assessment?

The point of cessation can be referred to as the "end point" and the reason for cessation as the "failure mode". The objective of this paper is to define the various ways that geothermal energy extraction development can be quantified and might have to cease, and then look at to what extent these can be built into predictive models. Useful insights can be gained from experience in "conventional" geothermal projects based on high temperature naturally convective systems with long operating histories, in excess of 50 years in some cases. This study is theoretical in the sense that to date, no whole geothermal power schemes anywhere have been decommissioned due to the resource reaching the end point and failing (though individual plants have ceased to operate). However, this will eventually be the case.

These issues will became increasingly important in Australia as projects move from Inferred Resource estimates to higher Resource and Reserve categories.

Stored Heat Estimates

In a simple stored heat estimate with no natural heat or fluid recharge over the project lifetime, the implicit assumption is that the project will cease when all of the available energy has been extracted. So the "failure mode" is a temperature decline. This is implicit in all of the Inferred Resource estimates that have been public in Australia so far, since they are all based on stored heat estimates.

In many of those assessments the "cut off temperature" which represents the minimum isotherm for defining the resource volume is based on an assumed power plant inlet temperature, and the "base temperature" which the available energy is referenced to is based on the plant rejection temperature. But even those apparently straightforward assumptions can be significant oversimplifications.

In a system with reinjection, practically speaking energy extraction will have to cease when the fluid coming out of the production wells drops below the minimum inlet temperature requirement of the power plant. But at that time there will be a temperature and pressure gradient laterally through the reservoir from the reinjection to the production wells, so the average resource temperature at that time will be less than the power plant inlet temperature. That average temperature should more logically be the cut off temperature for the stored heat assessment.

The next level of refinement is to consider that because of the change in water viscosity with temperature, the lateral pressure and therefore temperature gradient between the reinjection and productions wells will definitely not be linear, which means the fraction of the resource volume from which energy can usefully be extracted is not just a simple proportion. That could readily be addressed by a dynamic reservoir model, provided suitable data on the formation properties are available for calibration.

A related consideration which has arisen in one recent resource estimate is that the, use of a "cut-off isotherm" may not be the most appropriate method to apply to a series of vertically stacked sedimentary aquifers or horizontally fractured granite, in which heat flow is conductive and not convective, i.e. temperature is stratified, low at the top and high at the bottom, so wells at different depths or wells with multiple feed zones may produce fluid with a wide range of temperatures.

In such a system there could be the freedom to set the cut-off temperature at such a level, which ensures that the mixed geothermal fluid produced at the well head remains above the power plant temperature. Adoption of this approach could mean that the cut-off temperature to define the geothermal reservoir is lower than the power plant inlet temperature. The adoption of a lower cut-off isotherm could be beneficial in situations where the benefits of increasing the total volume outweigh a modest decrease in the temperature of the fluid produced.

Further considerations to take into account are: heat loss up production wells, which could be considerable where wells are deep and flow rates small; heat loss between the wells and power plant; heat loss between the separators (if any) and power plant and reinjection wells; and heat gain down the reinjection wells. There are also power systems aspects to consider such as process and thermodynamic issues as well as parasitic pumping etc. loads. Site-specific

ambient temperatures and humidity will dictate practical cooling options.

Furthermore, if the production temperature declines over the lifetime of the project which is what would be expected in a heat mining operation and is therefore implicit in a stored heat estimate, the power plant efficiency would also drop and the production pumping requirements will change as the fluid density and viscosity changes. That would be exacerbated by reservoir pressure changes. All of these factors can and ideally should be modelled as resource assessments become more accurate, even when just using a stored heat approach.

Dynamic Resource Estimates

An alternative approach is to assume that a certain rate of extraction is indefinitely physically sustainable on a human time scale, in which case the field "capacity" is better expressed as MWth or MWe (making suitable assumptions as to conversion efficiency) rather than PJthermal or MWthermal-years in place and recoverable. This appears to be the case with fields such as Wairakei in New Zealand, where reservoir modelling predicts that extraction will be physically sustainably for at least 100 years – which is perhaps simply an expression of the fact that our perception of the "resource" is too limited in that it does not include the deeper heat source. But even there other factors may come into play which could mean the project cannot in fact sustain output for all of that period.

Based on practical experience of geothermal systems that have been exploited for a long period of time, there are other possible failure modes as follows.

With dynamic reservoir simulation, which is the most common means of assessing appropriate capacity in advanced existing conventional schemes without pumping, the "failure mode" is often predicted to be pressure decline rather than simply temperature decline. In a single phase (liquid) reservoir, pressure decline will be due to draw down in liquid pressure, as in a groundwater aquifer. In a two-phase reservoir such as Wairakei in New Zealand, Cerro Prieto in Mexico, or many of the other high temperature "conventional" projects worldwide which have been exploited, pressure draw down will to some extent be buffered by boiling, but if wells tap two-phase zones, pressures will be linked to temperatures, so can decline if cool water invades the reservoir (as has happened at Ohaaki for example).

In a dry steam system such as The Geysers in California pressure decline can be due to the reservoir drying out. Water loss within EGS projects is an obvious parallel though of a different origin.

Pressure decline has two important consequences. Initially it will cause declines in well mass output (though that may be compensated for by rising enthalpy if boiling occurs so the available energy output actually increases). It is also possible that pressures may eventually fall to the point where steam turbines become inoperable. In both cases considerable unrecovered thermal energy may remain within the reservoir.

To some extent these effects can be countered by drilling make up wells or adopting pumping, but a point of no return may be reached at which drilling further wells is not considered economic.

Linked to and synergistic with reservoir pressure declines, there can be incursion of groundwater, either laterally or from above. This has been well documented and studied in New Zealand resources such as Wairakei, Ohaaki and Kawerau as well as in some fields in the Philippines. As well as chemical monitoring of well production physical and chemical parameters, repeat micro-gravity measurements are an appropriate tool for tracking fluid movements.

Incursion of cool ground waters may be severely detrimental by reducing well enthalpies, as at Ohaaki. But it can also causing undesirable chemical effects such as scaling and corrosion. The ground water above and around high temperature geothermal systems may be high in species such as bicarbonate and sulphate and of low pH, developed by separation, absorbtion and oxidation of gas phases. Wells have failed in New Zealand fields due to external corrosion by such secondary fluids. They can also contribute to scaling in production wells by anhydrite from the admixed sulphate and/or more commonly calcite from the bicarbonate.

Premature reinjection returns to production wells are also a common limiting factor in some developments, and can leading to a low % energy recovery though not usually total failure of the project.

Excessive environmental effects on the surface are another factor that can limit geothermal energy extraction well before thermal energy depletion. At Wairakei in New Zealand for example, many years of geothermal fluid extraction with very limited reinjection have caused severe localised surface subsidence (possibly up to 21m) and increases in thermal activity including hydrothermal eruptions. The possibility of such effects extending into populated areas has been a constraint on further development. At Rotorua, power generation is effectively precluded because of concerns over effects on thermal activity which is crucial to the tourist industry.

Ability to Predict Failure Modes and Model End Points

The ability to predict what will be the failure mode of a geothermal project and hence its end point for resource estimation varies both according to the nature of the reservoir and the amount of knowledge available. At an early (pre-drilling) stage stored heat with its implicit assumption of temperature depletion is the most appropriate tool.

Once exploration wells are drilled and tested, stored heat estimates can be refined, but data may start to become apparent which indicate other possible end points, such as premature reinjection returns. At this stage such effects can be qualitatively modelled by analogies and dynamic reservoir simulation, but probably as a series of "what if" scenarios rather than a definitive quantitative prediction. To do so will require more attention is paid to permeability data than has been typically the case so far.

It is only once some production history becomes available either through operation of a small scale initial power generation scheme or long term well testing, that dynamic reservoir simulation can really come into its own and can be used to give reliable forward predictions.

Implications for Resource Estimation

The methodology for meaningful resource and reserves estimates will change over time as projects become more advanced. While stored heat estimates are adequate for Inferred Resource estimates, more advanced projects and higher resource categories should take into account other possible end points and adjust the estimates accordingly, in many instances most particularly through numerical reservoir simulation.

In many cases this approach will cause the later resource estimate to be lower than the initial ones – though strictly speaking that should not be so if the risks and uncertainties have been considered properly in the initial estimates. That is not always necessarily the case however. At Wairakei for example a significant stimulation of heat and fluid recharge has occurred which has increased the resource available.

EGS & "The Law of Averages"

Peter Leary* & Peter Malin
Institute of Earth Science & Engineering, University of Auckland
58 Symonds Street, Auckland 1142, New Zealand
*Corresponding author: p.leary@auckland.ac.nz

Enhanced Geothermal Systems (EGS) seek to produce high permeability flow systems where Nature has provided only low permeability flow systems. We take a science-based modelling look at the flow heterogeneity character of high permeability geothermal systems to better understand the *in situ* systems EGS is dealing with. Our flow modelling is based on percolation through grain-scale fractures, with grain-scale fracture density η(*x,y,z*) allowed to fluctuate in space on all scale-lengths in line with well-log power-law scaling phenomenology recorded in both sedimentary and crystalline basement rock. Massive hydrofracturing in EGS drill holes can in principle introduce high permeability quasi-planar mega-fractures into our natural poroperm medium but almost certainly EGS induced fractures cannot be expected to completely define the hydraulic connectivity between an induced fracture and the remaining drill holes in the EGS plumbing system. At some point in an EGS volume, the natural fracture hydraulic connectivity is likely to control the fluid system throughput We therefore suggest that it is highly relevant for EGS developments to target crustal volumes in which the natural fracture permeability is higher rather than lower.

For spatially variable porosity φ(*x,y,z*) proportional to fracture density η and spatially variable permeability κ(*x,y,z*) proportional to fracture connectivity factor η!, then the identity δη ~ δ(log(η!)) reproduces the poroperm spatial fluctuation relation δφ ~ δlog(κ) documented in oil and gas field well-core data. We model 3D fluid flow in numerical media constructed for 3 degrees of spatial correlation of grain-scale fracture density: (1) no spatial correlation -- grain-scale density does not cluster and "the law of averages" holds; (2) intermediate spatial correlation -- grain-scale density clusters are diffuse and unpredictable whence the law of averages fails; (3) strong spatial correlation -- grain-scale clustering compartmentalizes rock volumes and the law of averages has rough validity over limited spatial domains. Our flow simulations indicate that geothermal reservoir pressure and flow data are far more likely to resemble case (2) than cases (1) or (3). We infer that, at least for scale-lengths characteristic of geothermal reservoirs, the *in situ* low permeability flow systems that EGS seeks to enhance into high permeability flow systems are likely to be spatially erratic and unpredictable at all relevant scale-lengths, and hence that the resulting EGS flow systems are also likely to be more spatially erratic and unpredictable than expected from "the law of averages". Supplementary fracture-sensitive data, e.g. microseismic and/or MT surveys, can thus be useful in completing EGS projects.

Keywords: fractures, heterogeneity, percolation, permeability, flow modelling

Introduction

To date flow models for both geothermal and hydrocarbon reservoirs have had little predictive value. The failure of reservoir modelling can in good part be attributed to ignoring the pervasive fracture-heterogeneity of crustal rock attested by well-log and well-core fluctuation systematics. *In situ* fluctuation systematics indicate that geofluids flow via spatially erratic fracture-percolation networks that cannot be predicted from traditional small-scale reservoir sampling (Leary 2002).

In geothermal reservoirs, spatially erratic *in situ* percolation flow networks can potentially be mapped using flow data observed at suitably large scale lengths. A possible means of flow-structure mapping is afforded by systematically recording and interpreting inter-well flow connectivity data. Such reservoir model-building tactics supersede the standard approach based on "the law of averages".

The law of averages supposes that for every earth property, variations in one direction are sooner or later balanced out by variations in the opposite direction. The law of averages thus says that reservoir geological formations can be described in terms of "effective medium properties" about which reservoir physical properties fluctuate benignly. Moreover, effective property values can be determined by a few small scale samples. Typically the small-scale samples of formation porosity, say, are taken from well logs and formation permeability samples are taken from well core.

Formation property averaging, however, leads to accurate reservoir flow models only if *in situ* fluctuations of relevant properties are spatially uncorrelated. The necessary and sufficient condition for spatially uncorrelated *in situ* geophysical properties is that spatial fluctuations in these properties have a "flat" or "white" Fourier power spectrum in spatial frequency k, $S(k) \sim 1/k^0$.

Well-logs show, however, that the characteristic spectrum of *in situ* geophysical property fluctuations is $S(k) \sim 1/k^1$ rather than $S(k) \sim 1/k^0$. The necessary condition for "the law of averages" to apply *in situ* is universally and systematically

violated at all relevant wavelengths for virtually all physical properties of crustal reservoirs (Leary 2002).

Percolation phenomenology for spatially correlated grain-scale fracture-density fluctuations

We compute percolation flow of geofluids in a numerical framework capable of embodying well-log fluctuation systematics. In this heterogeneity framework, the spatially fluctuating numerical density $\eta(x,y,z)$ of grain-scale fractures attested by well-log data is modelled by power-law-scaling numerical fluctuations within the model volume.

Numerical fluctuations $\eta(x,y,z)$ are connected to geofluid flow by the empirical relation $\delta\varphi \approx \delta\log(\kappa)$ observed to hold for well-core porosity φ and well-core permeability κ. In this expression, $\delta\varphi$ and $\delta\log(\kappa)$ are respectively the zero-mean unit-variance reductions of the porosity and log(permeability) fluctuation sequences for cored reservoir intervals (Leary & Walter 2008).

The empirical well-core poroperm fluctuation relation $\delta\varphi \approx \delta\log(\kappa)$ is conceptually equivalent to a mathematical identity $\delta\eta \sim \delta(\log(\eta!))$ if fluctuations in porosity are proportional to fluctuations in grain-scale density $\eta(x,y,z)$ and fluctuations in permeability are proportional to the fluctuations in the combinatorial factorial term $\eta(x,y,z)!$ representing the number of ways $\eta(x,y,z)$ grain-scale fractures can combine to produce a percolation pathway. If a rock volume has η grain-scale fractures per unit volume at location (x,y,z) and $\eta + \delta\eta$ grain-scale fractures at location $(x,y,z)+(\delta x,\delta y,\delta z)$, the percolation-related permeability in the two volumes can be expected to vary as the combinatorial terms $\eta!$ and $(\eta+\delta\eta)!$. Stirling's formula, $\eta! \approx (\eta + ½)\log(\eta) - \eta$, applied to the two fracture connectivity expressions reduces to the empirical well-core fluctuation expression $\delta\eta \approx \delta\log(\eta!)$.

Percolation flow in spatially correlated fracture networks

Single phase flow in heterogeneous media is simulated using SUTRA (Voss and Provost 2008), a finite-element solver for Darcy's law in permeability-heterogeneous media, $\partial_t P = \underline{\nabla}\bullet(\kappa(x,y,z)\underline{\nabla}P)$, P = geofluid pressure. Model porosity $\varphi(x,y,z)$ is proportional to numerical fracture density $\eta(x,y,z)$, and model permeability $\kappa(x,y,z)$ is given by the well-core relation $\delta\varphi \approx \delta\log(\kappa)$.

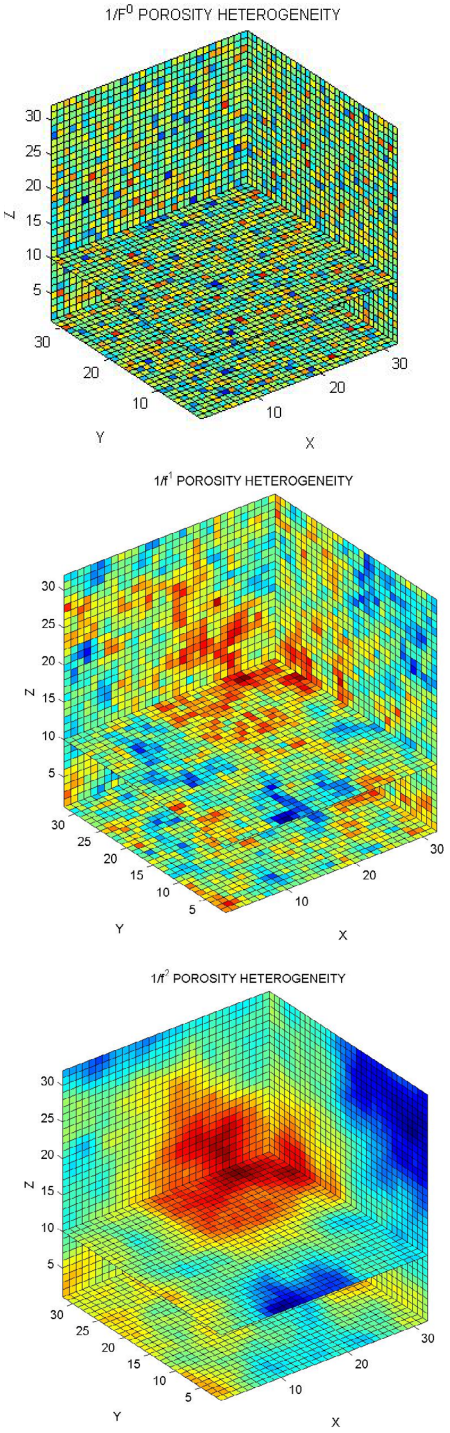

Figure 1a-c: 3D numerical spatial noise distributions with increasing degrees of correlation: (top) uncorrelated white noise, fluctuation power spectrum $S(k) \sim 1/k^0$; (mid) intermediate correlation 1/*f*-noise, power spectrum $S(k) \sim 1/k^1$; (bottom) strong correlation Brownian noise, power spectrum $S(k) \sim 1/k^2$.

To see the effect of spatial correlation on reservoir flow, we compute flow for three degrees of spatial fracture correlation parameterized by power-spectral exponent p, $S(k) \sim 1/k^p$, k = spatial frequency. The degrees of spatial connectivity are: (*i*) $p = 0$, spatially uncorrelated or white noise fluctuations (Figure 1a); (*ii*) $p = 1$, moderately spatially correlated "1/*f*" noise fluctuations (Figure

1b); (*iii*) p = 2, strongly spatially correlated Brownian noise fluctuations (Figure 1c). Each of these 3D numerical heterogeneity constructs has the same mean and standard deviation. The only distinguishing feature is the degree of spatial correlation/clustering of the numbers representing grain-scale fracture density.

Finite-element solutions to fluid flow in and out of elementary digital volumes or cells are robust against spatial variations in the porosity and permeability of cells. The fact that these property spatial variations occur at all scale lengths throughout numerical medium has no effect on the speed or stability of the flow computations. Of course, the greater the number of cells, the more realistic will be a specific flow simulation, but it is currently feasible to run simulations with 64x128x128 = 2^6x2^7x2^7 cells, giving six octaves of vertical fluctuation power and seven octaves of lateral fluctuation power, equivalent to factors 8 and 11, respectively, in amplitude fluctuations.

Flow systematics for $1/k^0$, $1/k^1$ & $1/k^2$ grain-scale fracture density spatial correlation

Simulation pressure histories plotted in Figures 2a-d reflect the distinct character of 1/*f*-noise heterogeneity flow evolution (red traces) compared with those of white noise (black traces) and Brownian noise (blue traces). Each figure represents a different source well flow simulation for the three heterogeneity types. For each source well, a colour-coded quartet of flow history traces shows time-evolving pressure signals recorded at observation wells at four offsets from the source well.

The Figure 2 colour-coded pressure curves show that the different heterogeneity types result in substantially different pressure histories. All pressure histories evolve more or less consistently within a heterogeneity class. The uncorrelated heterogeneity (white noise = black traces = Figure 1a) and strongly correlated heterogeneity (Brownian noise = blue traces = Figure 1c) both generate essentially monotonic pressure evolution. The black curves of uncorrelated heterogeneity are relatively subdued in pressure history difference as expected from a medium that is essentially uniform within a standard deviation about a mean permeability; there is no evidence of flow complexity that might be associated with significant spatial trends in poroperm distribution. The blue curves of Brownian-noise heterogeneity have a stronger degree of temporal evolution that is the same for three of the source-sensor well pairs, but substantially different for the fourth source-sensor well-pair. The amplitude discrepancy is due to three of the sensor wells being inside the Figure 1c high-porosity volume while the fourth sensor well is on the edge of the high porosity volume. In both amplitude cases, however, pressure evolution at the sensor well is monotonic.

These simulation flow data are understandable in terms of simple considerations. Flow in spatially uncorrelated media conforms to the standard statistical expectation that randomness tends to average out. Flow in strongly spatially correlated media tends to be simply diffusive over each range of coherent spatial properties.

The red curves of 1/*f*-noise (Figure 1b) heterogeneity present an unfamiliar degree of flow complexity. The Figure 2a-d observation well pressure histories in red are responding to a consistent but complex spatially-correlated heterogeneity structure, and the spatial complexity generates temporally complex evolution signals. In conspicuous contrast with the monotonic well-pair histories for the uncorrelated and strongly correlated poroperm heterogeneity, 1/*f*-noise poroperm heterogeneity consistently exhibits large-amplitude temporal fluctuations about a diffusion trend history.

If we now compare the three Figure 2a-d pressure history types to a sample of *in situ* pressure histories in Figures 3a-d, we see little evidence in field pressure data for essentially monotonic diffusion-flow characteristic of uncorrelated $1/k^0$ and $1/k^2$ spatial correlation, but see ample evidence for pressure histories that systematically fluctuate about long-term diffusion trends that are modelled by flow simulations in $1/k^1$ poroperm heterogeneous media. The correspondence between *in situ* flow data fluctuations (Figures 3a-d) and model flow data fluctuations (Figures 2a-d) indicates that spatial poroperm heterogeneity based on well-core and well-core empirics has a general validity for *in situ* fractures and fracture-borne percolation flow.

Discussion

The “law of averages” incorporates three working assumptions:

- Fluctuations balance out on all scale lengths;
- No significant trends develop at any scale length;
- Small scale samples yield good indicators of large scale properties.

These working assumptions are highly convenient but are unfortunately formally invalidate for *in situ* spatial fluctuations in reservoir properties recorded by well logs; well logs have power-spectra that scale inversely with spatial frequency, $S(k) \sim 1/k^1$, rather than as the form $S(k) \sim 1/k^0$ required for the law of averages.

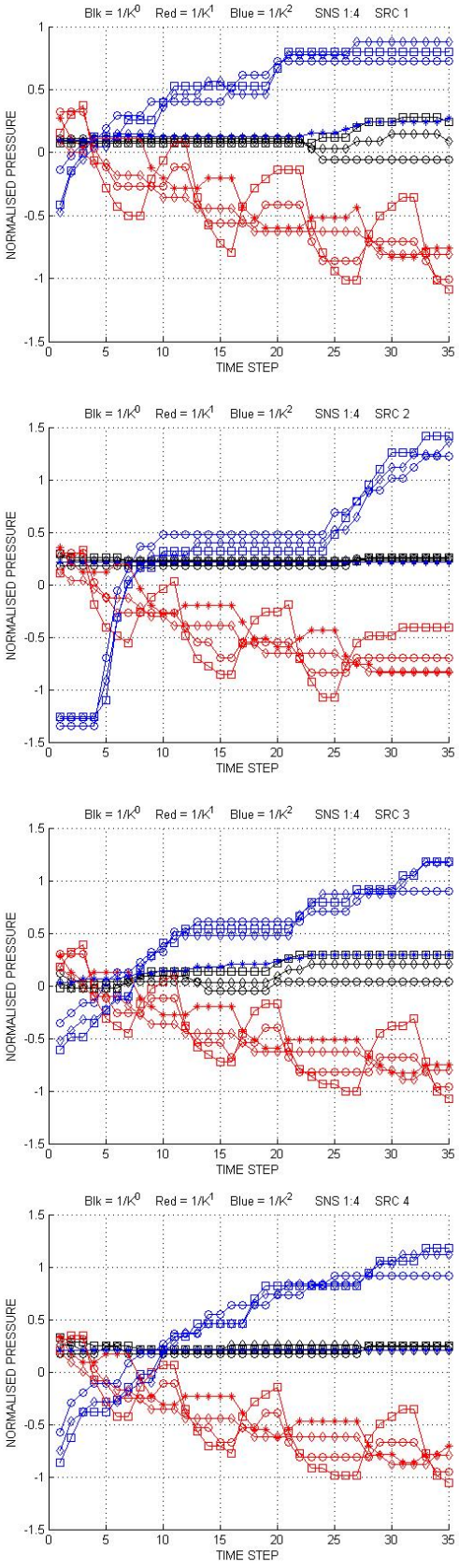

Figures 2a-d: Quartets of simulation flow pressure histories for (top to bottom) 4 different source well locations in Figure 1 numerical reservoir volumes: black traces = Figure 1a; blue traces = Figure 1b; red traces = Figure 1c.

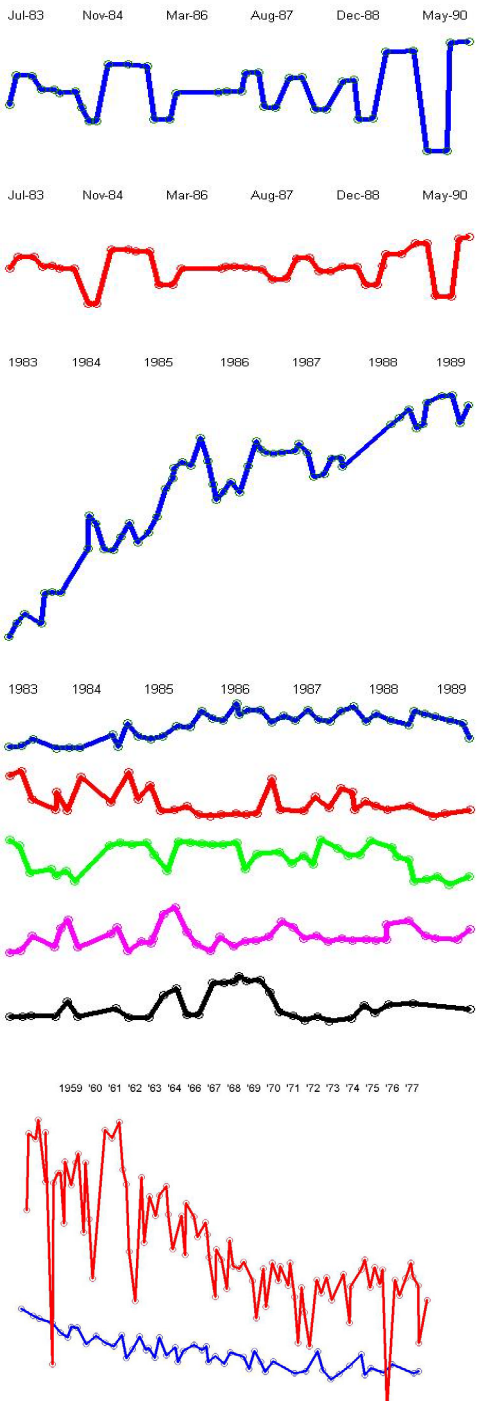

Figures 3a-d: Geothermal field flow-related well data: (a-c) Chloride abundances, Palinpinon field, Philippines (Horne 2008); (d) Pressure and mass discharge (Sorey and Fradkin 1979).

The *in situ* geothermal reservoir flow data of Figures 3a-d go beyond mathematical formalism to give additional and perhaps more practical rebuttal to the law of averages applied to reservoir processes. The different types of *in situ* fracture distributions in Figures 1a-c are seen to have real meaning in terms of reservoir flow. Figure 3a-d *in situ* flow data imply that we can be more confident in understanding that long-range trends in fracture density and fracture connectivity are characteristic

of *in situ* rock permeability over a range of scale lengths characteristic of reservoir flow. It is visually clear from Figures 1a-c that such *in situ* trends cannot be adequately modelled by data averaging (Figure 1a is not a valid smoothed version of Figure 1b), nor can valid statistical inferences about large-scale flow structures be made from acquiring small-scale samples (a few samples from Figure 1a fix the likely values of other samples; this is clearly not true of sample from Figure 1b).

As a general statement, fracture heterogeneity in the form of Figure 1b must be addressed by making suitable *in situ* measurements at the appropriate scale lengths.

Applying this statement to EGS projects seeking to enhance *in situ* fracture permeability, it seems clear that EGS fracture enhancement is best conducted in rock volumes that host large-scale fracture clustering. Even if EGS induced fractures are thought of only in terms of massive planar flow structures, such structures must naturally terminate in country rock. In terms of Figure 1b, country rock volumes with high fracture densities denoted by warm colours are far more promising EGS targets than are rock volumes with low fracture densities denoted by cool colours.

A practical implementation of this statement is to associate *in situ* fractures with earthquake failure and/or fracture-borne fluid electrical conductivity. While it is common to regard with alarm earthquake failure in a reservoir environment, this attitude is likely to be naïve and counter-productive. Enhanced reservoir flow is likely to be essentially concomitant with earthquake failure. Given the comprehensive failure of the law of averages applied *in situ* and the use of small-scale sample to infer large-scale *in situ* flow properties, a more informed point of view would be systematically use micro-earthquakes as an exploration tool to locate *in situ* fracture clusters that are likely to be large-scale permeability systems for which input and output flow can be engineered/enhanced. Microseismicity data can be supplemented by MT detection of electrically conducting volumes at depth.

A compelling logic associates earthquakes with fluid-rich fracture clusters. Such clusters are the weakest and more compliant part of the rock mass, and fluid pressures tend to lower normal frictional stresses that work against slip failure. Seismicity is almost universally induced by the modest crustal loads of water ponded behind dams, indicating that the crust is everywhere near fracture failure. The most fractured crustal volumes being the most likely to fail, microseismicity, either natural or induced, is a likely indicator of fluid-rich fracture systems. Conversely, absence of microseismicity implies a lower potential for *in situ* fracture systems. Exploration wells instrumented with seismic sensor arrays to detect the range and azimuth of background seismicity could be the most direct way to assess EGS prospectivity. Fibre optical seismic sensor technology is on the verge of making seismic assessment of elevated temperature EGS prospects a viable exploration option.

Summary

The law of averages does not apply to the spatial or temporal properties of *in situ* reservoirs. *In situ* reservoir fracture systems have a tendency to develop long-range spatial trends in fracture density that generate localised fracture/flow clusters that could be plausible EGS targets, but such trends can equally be towards low fracture content and therefore unpromising EGS prospects. Because the law of averages fails for reservoirs, small-scale sampling of *in situ* crust has little bearing on the location and/or properties of EGS prospects. EGS prospect assessment can logically be conducted through systematic large-scale microseismic and or MT data acquisition.

References

Horne, R.N., 2008, Geothermal data mining – Value in antiques, Proceedings of 30th New Zealand Geothermal Workshop, New Zealand Geothermal Association, p. 82-90.

Leary, P.C. and Walter L.A., 2008, Crosswell seismic applications to highly heterogeneous tight gas reservoirs, *First Break,* 26, p.33-39.

Leary, P.C., 2002, In: J.A. Goff & K. Holliger (Eds.) *Heterogeneity of the Crust and Upper Mantle - Nature, Scaling and Seismic Properties,* Kluwer Academic/Plenum Publishers, New York, p.155-186.

Sorey, M.J. and Fradkin, L., 1979, Validation and comparison of different models of the Wairakei geothermal reservoir, *Proceedings of 5th Workshop on Geothermal Reservoir Engineering* Stanford, CA, USA (1979), pp. 119–204.

Voss, C.I. and Provost, A.M., 2008, SUTRA Version 2.1, U.S. Geological Survey Water-Resources Investigations Report 02-4231, http://water.usgs.gov/nrp/gwsoftware.

Summary of AGEG Technical Interest Groups Research Projects

Alexandra Long*, Barry A. Goldstein, Tony Hill and Michael Malavazos
Petroleum and Geothermal Group, PIRSA, GPO Box 1671 Adelaide, SA, 5000
* Corresponding author: long.alexandra@saugov.sa.gov.au

The Australian Geothermal Energy Group (AGEG) has the vision that geothermal resources will provide the lowest cost emissions free renewable base load energy for centuries to come. The AGEG is working towards this vision through its Technical Interest Groups (TIGs) which focus on topics that have been prioritised by the Australian geothermal industry. The priorities are thus aligned with those of the International Energy Agency Geothermal Implementing Agreement (GIA) and the International Partnership for Geothermal Technologies (IPGT). Increasingly, priorities are also coming into line with the oil and gas industry with opportunities to drive innovation.

This paper will provide an update and overview of the scope and research findings of projects completed for the AGEG by members since the last Australian Geothermal Energy Conference. Many of the projects focus on topics relevant to the advancement of Enhanced Geothermal Systems (EGS) in Australia, including reservoir characterisation, research and development into power cycle design for the Australian conditions and other studies to reduce the uncertainties surrounding EGS and ensure responsible management of projects.

It is expected that detailed presentations will be given on many of these projects by the project investigators, so this paper intends to provide a brief introduction of each project's aims and to demonstrate the range of research that is covered by the AGEG TIGs.

Keywords: Australia, EGS, Hot Rock geothermal

The Australian Geothermal Energy Group

The AGEG was formed to bring together all parties involved in geothermal development in Australia, in order to work together and cooperatively advance the industry as a whole.

The method of this advancement is through the work of the Technical Interest Groups which are broadly separated into the stages of a geothermal project and so encompass land access and exploration through to power systems and transmission or connectivity to the National Electricity Market. The 12 AGEG TIGs are briefly described in Table 1.

The TIGs have transformed somewhat since their conception in 2007. In particular TIG 2 has formed the joint AGEG and AGEA Resource and Reserves Code Committee, who released and now administers the first uniform geothermal reserves and resources reporting code. The TIG for policy advice has led to the creation of the Australian Geothermal Energy Association (AGEA), the national industry body representing the Australian geothermal industry. TIG 5 has held some informative workshops and has become the AGEA working group on issues relating to the national electricity market which also reports back to the AGEG. The order of the groups has been re-organised such that the first four groups cover best practice protocols and communication and TIGs 5 to 12 cover geothermal technology development (Outlined in red).

TIG 1	Land Access
TIG 2	Reserves & Resources
TIG 3	Policy
TIG 4	Outreach
TIG 5	Getting to Markets
TIG 6	Power Plants
TIG 7	Direct Use
TIG 8	Information & Data
TIG 9	Reservoir Development & Engineering
TIG 10	Exploration & Well Log Technologies
TIG 11	Drilling & Well Construction
TIG 12	Education

Table 1 - The AGEG's Technical Interest Groups

The AGEG and the AGEA have agreed to coordinate research efforts through the AGEG's Technical Interest Groups. This will facilitate Australian companies, research experts and government agencies (including regulators) to convey and take note of international best practices for the full-cycle of below-ground and above-ground geothermal energy operations and stewardship.

The structure of the AGEG and the TIGs is shown in Figure 1. The AGEG's TIGs will have active links to the International Energy Agency's (IEA) geothermal research annexes, the IPGT, and will aim to attain strong linkages to all other reputable international geothermal research clusters, to ensure that Australia's comparative advantages in Hot Fractured Rock (HFR) geothermal resources can be leveraged into accelerated development of high priority geothermal technologies, methods and the sharing of lessons learnt. On this basis, the AGEG and the AGEA have agreed that the AGEG should become the Australian affiliate for the International Geothermal Association.

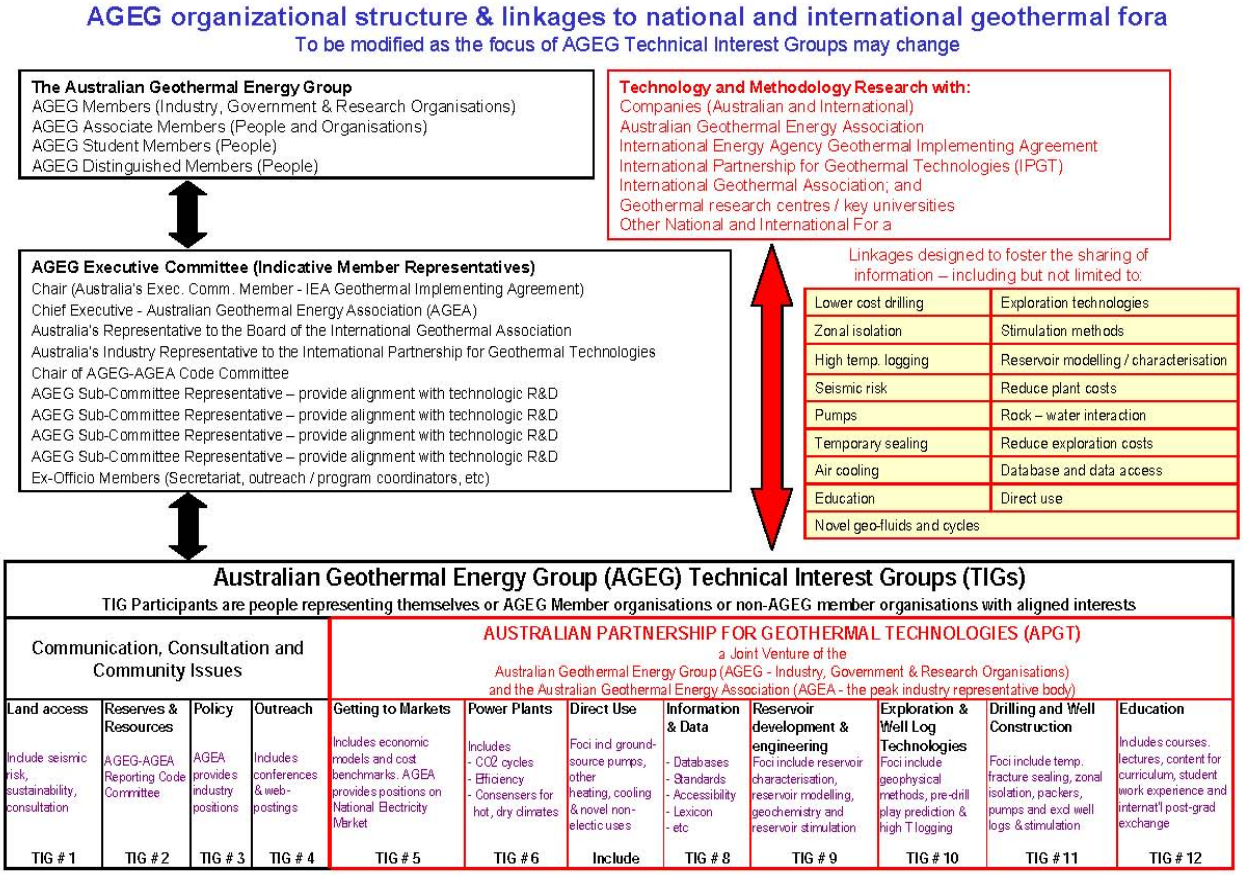

Figure 1: Diagram showing the structure of the AGEG, including the Technical Interest Groups and linkages to national and international geothermal groups.

Further information on the AGEG and its TIGs can be found on the AGEG website at http://www.pir.sa.gov.au/geothermal/ageg

Geothermal Research Projects

Already some significant projects have been completed within the AGEG TIGs with support from the Department of Primary Industries and Resources, SA (PIRSA) tied grants, geothermal company contributions and in-kind contributions from members providing their valuable time.

Completed projects of note include the first uniform code to guide the reporting of geothermal data to the market, The Geothermal Reporting Code and the accompanying Lexicon, which were developed by the Australian Geothermal Code Committee (AGCC) and released in 2008. Since the Code's release a number of operating companies have reported their geothermal exploration results according to the Code. The Code is intended to be a living document and as such a second version is expected to be released in 2009.

Under the TIG for land access and environmental issues, PIRSA commissioned research studies on the potential for induced seismicity associated with the fracture stimulation of EGS wells in the Cooper Basin (Hunt and Morelli, 2006), followed by a report on the analysis and management of seismic risks (Morelli and Malavazos, 2008 and Morelli, 2009). These studies were completed at the Australian School of Petroleum at the University of Adelaide and have been reported on previously.

Further to these research projects, 6 more projects have been completed in the last year and another 5 are expected to be completed by the end of 2009. These projects are described in more detail below and the reports will be made freely available from the AGEG website.

An assessment of radiological hazards in HR geothermal systems

Battye and Ashman (2008) were commissioned by PIRSA to conduct a literature review and some modelling to assess the risk of radiological hazards for HR geothermal systems. The study found that isotopes of Uranium, Radium, Thorium, Radon and Lead will be likely to be present in the circulating ground waters.

The main risks of exposure to these Naturally Occurring Radioactive Materials (NORMs) for a HR geothermal system would be through exposure to radon gas if the geo-fluid and steam are emitted to atmosphere, or exposure to the scales and sludge that may form in the above ground system.

If the HR geothermal power plant is operated in an entirely closed loop configuration then there would be little to no risk of radon exposure. For an open loop situation the levels are probably still below the action levels for workplaces in Australia (1000Bq/m3) but are very dependent on wind speed and the residence time of the geo-fluid in the reservoir, so thorough monitoring should take place to ensure that the exposure is known and there is no risk, or else the risk is managed appropriately.

The other way there could be exposure is from the scales or sludge that may be deposited in the above ground equipment, depending on the geochemistry and the plant conditions. Experience from conventional geothermal systems and from the oil and gas industry shows that these scales and sludge can contain radio-nuclides that have been carried with solid particles suspended in the solution and then deposited, or from particles that precipitate out at surface. Only the Radium isotopes can emit gamma radiation that could penetrate the pipe work. Radium isotopes are less likely to be found in waters with low concentrations of barium and strontium sulphates, and the report states that as the radium concentrations will be expected to be lower than for the oil and gas industry the gamma radiation from these residues would be expected to be at insignificant levels.

The other isotopes that may be present could be hazardous if inhaled as a fine dust, so precautions should be taken during all cleaning operations.

Geochemistry, corrosion and scaling in Hot Dry Rock energy extraction systems

This project investigates an important element of the Hot Rock geothermal energy system. The first objective is to study geo-fluid chemistry and its contribution to the corrosion and scaling in pipes in the above ground equipment of a geothermal power plant. Understanding the fluid chemistry is also vital to maintain open pores within the underground reservoir, by avoiding clogging of the fracture network caused by mineral precipitation.

The project has involved sampling the geo-fluid from a Hot Rock EGS system and also the rock itself to determine the mineralogy and composition of each. The researchers at the University of Adelaide and the Museum of South Australia then intend to re-create the above ground and below ground conditions experimentally. Using a specially designed experimental apparatus they first study the interaction between the geo-fluid and the rock at temperatures and pressures equivalent to those in the geothermal reservoir. The results of these experiments will be used to calibrate and further develop geothermal modelling tools to determine potential scaling and pore blockage issues and consequently possible solutions

Characterisation of Adelaidean rocks as potential geothermal reservoirs (Heat Exchange Within Insulator)

The main objectives of this project are to determine the extent of pre-competitive data available to characterise the reservoir parameters of the Adelaidean formations within the Adelaide Geosyncline. This will involve reviewing and compiling all available data and publications. Further to this, maps would be compiled to show the areas in the region possibly suitable for both geothermal development and geosequestration, with the intention to provide a temperature gradient for the region.

Three dimensional reconstruction of the Adelaide geosyncline – application to geothermal exploration

Backé and Giles (2008) developed a robust integrated methodology to construct a 3D model of the Lake Torrens – Central Flinders zone in South Australia. Using Gocad, they incorporated various tectonic structures (including faults, folds and mini-basins) without geomorphic expression at the surface.

The Gocad model was then exported into 3D thermal modelling software to provide an inferred geothermal resource over the Parachilna area of the southern Flinders Ranges, South Australia.

Full life-cycle water requirements for deep geothermal energy developments in South Australia

Cordon and Driscoll (2008) documented the likely water usage for each stage of geothermal exploration and development, including issues of water loss, and compiled an atlas of water resources for South Australia to assist explorers in understanding the quality, availability and legislative requirements associated with these resources. Although the atlas of this report is for South Australia, the full life-cycle water requirements for deep geothermal energy developments that are outlined in this report are applicable world-wide.

Preliminary assessment of the impact of geo-fluid properties on power cycle design

While the effects of geo-fluids in terms of corrosion and scaling are known, there has not been a thorough assessment of the scope of these issues for Australian geothermal projects, and in particular with reference to the power cycle design to accommodate the Australian conditions. Information on the composition of the water that can be expected for geothermal projects is difficult to find, which causes great difficulty in forward planning for power plant design as these elements greatly affect the choice of systems and materials.

The first project aim was to compile a database of available water composition and quality from a consortium of AGEG members. This aim was revised, for at the time the researchers were completing this section the only available data was from the Geodynamics wells. From this data set, the most difficult set of conditions have been selected and a preliminary design will be completed using these conditions in order to provide guidance for how to manage them. The preliminary design will also allow further investigation of where opportunities lie for geothermal companies to achieve cost savings through better design and highlight areas of further research. This project is expected to be completed in 2009.

Preliminary assessment of the potential for underground cooling on power cycle design

Dally et al. (2009) have reported on a novel concept of using a large underground network of pipes instead of large cooling towers or large air coolers. Large cooling towers are unlikely to be feasible due to their water requirements which previously left large air coolers as the only option. Underground cooling offers the possibility to provide increases in efficiency for power cycles for geothermal plants operating in locations where the ambient temperatures are very high. The concept and initial results of this study have been reported (Dally et al., 2008) and the final report provides further insights.

A thermodynamic model of the underground pipe was used to determine the required length of pipe and depth of burial for a set of harsh conditions and a 5 MW power plant output. The model results were then used to determine the feasibility of such a design. The authors found that a pipe length of 25 km was needed but this would only need to be placed 10 cm deep to be beneficial – this requires a total area of approximately 5 km^2. While this is a large area it was estimated that the cost for the system would be lower than for an air cooled system and provide more constant output including greater power output than a fan/air cooler system during peak daytime temperatures.

State-of-the-art in power cycles for geothermal applications and bottoming cycles

Researchers from Newcastle University and the University of Adelaide are working jointly on this study to compile a detailed comparison of existing geothermal power plants, their performance and operating conditions, compared with the conditions expected for the Australian geothermal industry. Using models of the Kalina, Super critical, flash and Organic Rankine cycles the research aims to estimate modifications that would be required to adapt those existing power plants to Australian conditions.

The development of a geothermal power plant preliminary cost estimator – Stage 1: basic estimates

Stage 1 of this project aims to develop a cost estimator for power generation by a geothermal power plant in Australian conditions. The estimator will initially be designed around a set of assumptions which define the geothermal system, providing the ability for the user to specify the values of certain variables such as the geo-fluid temperature, the ambient conditions, well depth, reservoir porosity and surface pressure. The cost estimator will calculate the average cost of power generation for a specified period and the predicted net power under a range of conditions.

This model will be designed to be used in conjunction with the MIT cost calculator (Herzog et al., 1997), and to include some factors important for the Australian geothermal industry. Important factors include the effect of ambient conditions on the cooling cycle, the water quality and level of treatment required, and the pressure required for reinjection. The model will also be designed to be able to expand over time and include more options for power cycle design, a range of options for working fluids and different cooling systems and corrosion mitigation methods.

Forward prediction modelling of spatial temperature variation from 3D models

This report was prepared by Intrepid Geophysics (2008) and involved the development of a software module in 3D GeoModeller to calculate 3D temperature directly from a 3D geology model. The method for 3D temperature prediction incorporated heat flow contributions from conductive and in situ heat production sources and honoured known boundary conditions.

During the module testing, a simple case of heat advection, honouring a known internal boundary condition was proven. Furthermore, the capacity to compare outcomes of model-generated temperatures, with observed temperatures and heat flows was demonstrated using real–world 3D geology models in the Mount Painter and Cooper Basin regions of South Australia.

The ability to commence a forward 3D temperature run, starting with a non-GeoModeller 3D geology model was demonstrated for the Cooper Basin, South Australia. This project was completed in 2008 and included the provision of an informative workshop.

Alternative carriers for geothermal energy in SA - an investigation of the systems needed to generate hydrogen and methane from a 50 MW geothermal demonstration.

Dickinson et al. (2009) were commissioned jointly by the Electricity Supply Industry Planning Council and PIRSA to assess the system requirements for

hydrogen production as a potential primary electricity load for a geothermal demonstration power plant output.

The objective of this study was to assess the possibility that hydrogen, methanol or synthetic methane production facilities co-located with geothermal energy production could have an attractive benefit to cost ratio. This study concluded that the costs to design and construct a 45MW electrolysis plant and an associated 5 MW refrigeration plant with all of the required pumps and ancillary equipment, could be economically more attractive than using the same geothermal energy to fuel a 50MW capacity power plant to reach distantly located markets via high voltage transmission lines. Locating the electrolysis plant near to existing gas transmission (pipeline) infrastructure suggests that synthetic methane could have the lowest transport costs.

Geothermal Centres of Excellence

Australian geothermal research will now be further strengthened through the work of three geothermal Centres of Excellence. The Queensland Geothermal Energy Centre of Excellence (QGECE) was established in 2008 with support from the Queensland government and the University of Queensland. The Western Australia Geothermal Centre of Excellence (WAGCoE), announced in 2008, is a joint venture between the CSIRO, Curtin University, the University of Western Australia and the government of Western Australia. Given the good results attained with its earlier grants, the South Australian Government announced the first project to be funded from a South Australian (state-based) Renewable Energy Fund will be the South Australian Centre of Excellence (CoE) for Geothermal Research at the University of Adelaide.

Each centre will have areas of expertise which complement the research and expertise of the other centres.

Industry Support for Geothermal Research

The geothermal research projects to date have been completed with support from federal and state governments and co-contributions or in kind support from geothermal companies and research institutes such as universities, Geoscience Australia and the CSIRO. Moving forward geothermal companies will be expected to make contributions to collaborative research in order to continue to progress geothermal technology.

Geodynamics has taken the lead in this endeavor with an announcement this year that the company has committed $5 million over a five year period for their Geothermal Technology Plan (GTP) (Geodynamics, 2009). This significant contribution will leverage private and public sector co-funding to develop geothermal technology which will benefit Geodynamics' Cooper Basin project and the geothermal industry both nationally and internationally.

Conclusion

The Australian geothermal industry has advanced significantly since 2005 and is assisted by supportive government initiatives, the efforts of the Australian Geothermal Energy Association and the collaborative determination of industry priorities and research work through the Australian Geothermal Energy Group.

A number of interesting research projects are underway and have already been completed relating to topics that will aid the Australian geothermal industry, with some projects focussed in the area of EGS or HR geothermal systems and more specifically to adapting to the Australian conditions. All of the outcomes of these research projects and their final reports will be made available through the AGEG website.

References

Australian Geothermal Code Committee (AGCC), 2008, The Geothermal Reporting Code, Australian Geothermal Energy Group, Adelaide, Australia. Available from: http://www.pir.sa.gov.au/geothermal/ageg/geothermal_reporting_code

Battye, D.L. and Ashman, P.J., 2008, an assessment of Radiological hazards in Hot Rock geothermal systems, Consulting report 2008/2314-1, CHEMENGTEST, The University of Adelaide, Australia.

Backé, G. and Giles, D., 2008, Three Dimensional geological modelling of the Adelaide Geosyncline – application to geothermal exploration, Final Report Tied Grant 4.4 for Australian Geothermal Energy Group, University of Adelaide, Australia.

Cordon, E. and Driscoll, J., 2008, Full Life-Cycle Water Requirements for Deep Geothermal Energy Developments in South Australia, Final Report Tied Grant 4.5 for Australian Geothermal Energy Group, prepared by Hot Dry Rocks Pty Ltd, Melbourne, Victoria.

Dally, B.B., Hew, F.L., Nathan, G.J. and Ashman, P.J., 2008, 163-4, Feasibility of Underground Cooling for Geothermal Power Plant Applications, in Proceedings of the Sir Mark Oliphant International Frontiers of Science and Technology Australian Geothermal Energy Conference, edited by Gurgenci, H. and Budd, A.R., Geoscience Australia Record 2008/18.

Dally, B., Nathan, G., Watson, S., Heath, A., Howard, C., and Ashman, P., 2009, Feasibility of Underground Cooling for Geothermal Power cycles, PIRSA Tied grant 6.2 Final report , the University of Adelaide, Australia.

Dickinson, R.R., Battye, D.L. Linton, V.M. Ashman, P.J. and Nathan, G.J., 2009, Alternative carriers for geothermal energy in SA - An investigation of the systems needed to generate hydrogen and methane from a 50 MW geothermal demonstration. Consulting Report CHEMENGTEST 2009/2355, the University of Adelaide, Australia.

Geodynamics, 2009, Geodynamics commits $5 million towards advancing geothermal technology, ASX Announcement 23 April 2009, available from http://www.geodynamics.com.au/IRM/Company/ShowPage.aspx?CPID=1955&EID=82963744&PageName=Geodynamics commits $5 million to geothermal technology

Herzog, H.J., Tester, J.W. and Frank, M.G., 1997, Economic Analysis of Heat Mining, *Energy Sources*, 19, 19-33.

Hunt, S.P. and Morelli, C., 2006, Cooper Basin HDR hazard evaluation: Predictive modelling of local stress changes due to HFR geothermal energy operations in South Australia, Prepared by The University of Adelaide for South Australian Department of Primary Industries and Resources, University of Adelaide Report Book 2006/16, Adelaide, SA.

Intrepid Geophysics, 2008, Forward Prediction of Spatial Temperature Variation form 3D Geology Models, Final Report Tied Grant 9.1 for Australian Geothermal Energy Group, the University of Adelaide, Adelaide, SA.

Morelli, C.P. and Malavazos, M., 2008, Analysis and Management of Seismic Risks Associated With Engineered Geothermal System Operations in South Australia, in Proceedings of the Sir Mark Oliphant International Frontiers of Science and Technology Australian Geothermal Energy Conference, edited by Gurgenci, H. and Budd, A.R., Geoscience Australia Record 2008/18.

Morelli, C.P., 2009, Analysis and Management of Seismic Risks Associated with EGS operations in SA, Final report for the Department of Primary Industries and Resources, SA, Report book 2009/11, Adelaide, SA.

Geothermal Applications: Development of new state of the art drilling rigs for geothermal use

Andy Lukas[1]*, Thomas Steinbrecher[2] and Jörg Uhde[3]
[1] AJ Lucas Group Ltd, Level 2, 394 Lane Cove Road, Macquarie Park NSW 2113.
[2] BAUER Resources Australia Pty. Ltd, P.O. Box 3423, Terrey Hills, NSW 2084
[3] BAUER Resources GmbH, BAUER-Straße 1, DE-86529 Schrobenhausen
* Corresponding author

Geothermal energy is the most promising of renewable energy sources. In Iceland, for example, oil and gas for heating purposes have nearly disappeared from the market, with nearly 85 % of its heat coming from geothermal energy resources. One of the biggest geothermal energy power plants of the world is called "The Geysers" in the North of the US state California. It provides an electrical power of about 1,400 Megawatts and is therefore able to cover the biggest part of the power requirement of San Francisco´s municipal area, which is located 170 km in the South.

Further geothermal energy power plants exist in other countries including, Kenya, Turkey, New Zealand, Philippines, Indonesia, Japan, Mexico, El Salvador, the Carribean and the Azores.

Australia is experiencing an impressive upswing in the field of Deep Geothermal Energy.

Deep Geothermal Energy in Germany

In Germany 3 regions are especially suited for gaining geothermal energy (Fig. 1):

- the North-Germany lowlands,
- the Upper Rhine Graben and
- the South-German Molasse basin.

The first geothermal energy power plant in Germany began operations in Neustadt-Glewe (Mecklenburg-Vorpommern) in November 2003. Hot water of 98 °C from the depth of 2 250 m activates a turbine. The power plant delivers 230 kilowatts of power. Warm water which is incoming after the power generation and which is about 70 °C is fed into the local district heating grid.

The Malm Karst of the Southern German / Upper Austrian Molasse basin is one of the most important hydrogeothermal energy reservoirs in Central Europe. The Malm (Upper Jurassic) which is present throughout almost the whole of the area is a highly-productive aquifer which dips from north to south to increasing depths and temperatures.

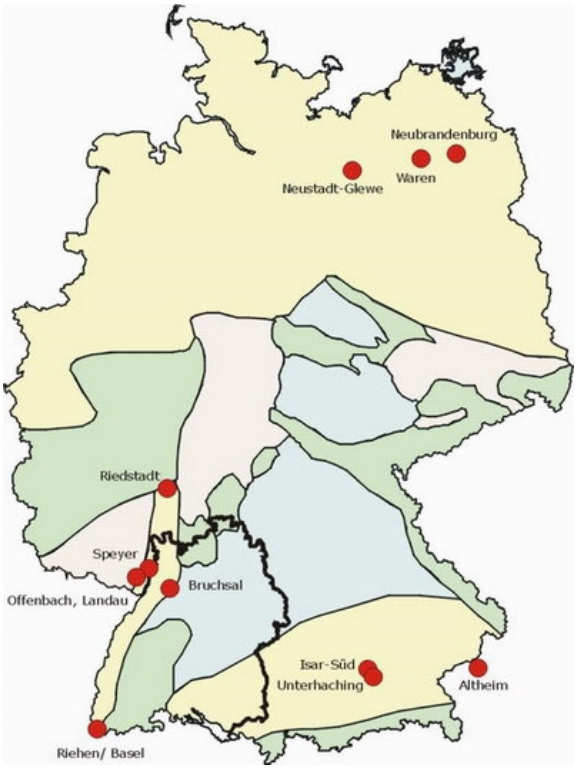

Figure 1: Geothermal Regions of Germany

A Production well to a depth of 3,577m sources a water aquifer with a temperature of 127°C in Unterhaching (Munich). A geothermal energy power plant utilizes these fluids for generating power and long-distance heating.

Almost 100 applications for exploration in geothermal energy in Bavaria show the great interest in deep geothermal energy in the Molasse (Fig. 2). Even the first interstate geothermal powerplant at Braunau/Simbach between Austria and Germany was realised in the Molasse basin.

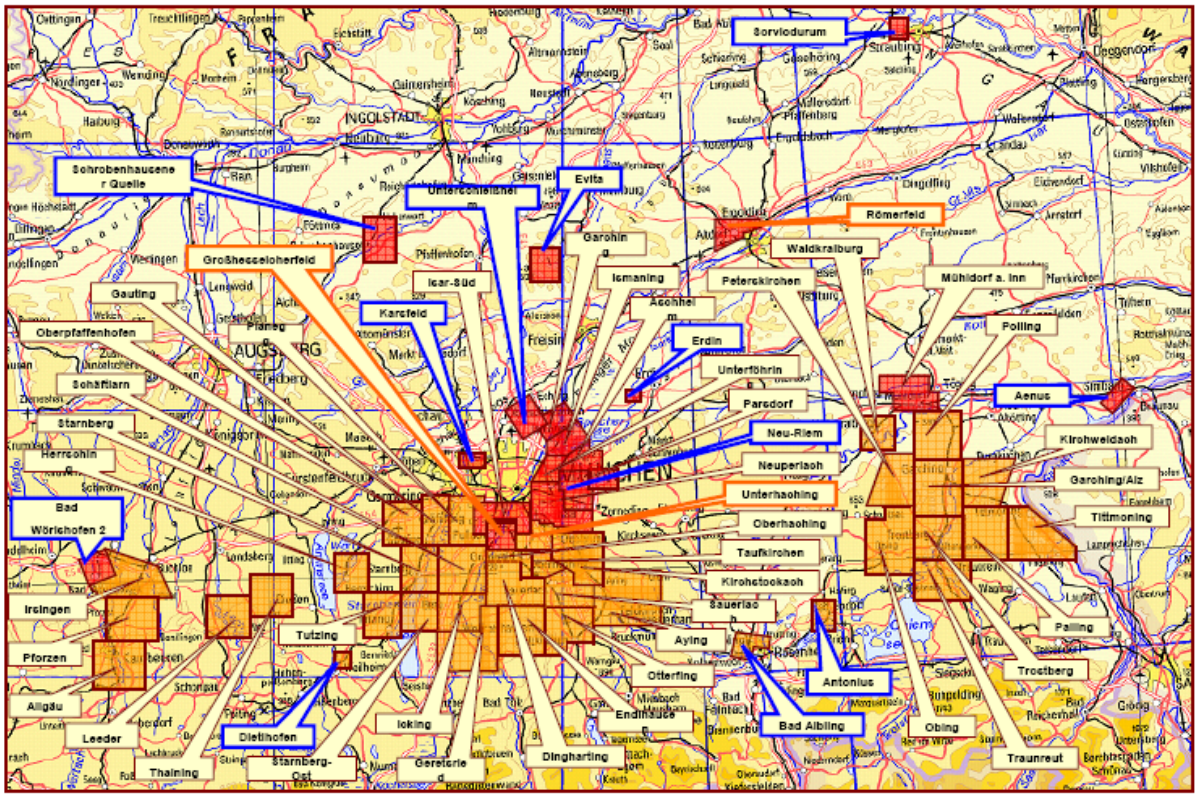

Figure 2: Geothermal projects in the Southern German / Upper Austrian Molasse basin

Many of these projects are currently being drill tested and many others will soon begin drilling operations. The whole potential in South Bavaria is estimated to be about 500 MW. This is approximately 5.6 % of the total Bavarian power use. 3,500 MW of thermal power would have to be added into the thermal energy provision for district heating systems provided that there would be sufficient consumers. Further projects are planned for the Upper Rhine Graben, in the South of Hesse and in Brandenburg.

Expert panel for the seismic risk of geothermal projects established

Following an M_L=2.7 seismic event occurring on August 15th near the site of a geothermal power plant at Landau (Germany) (Fig. 3), the Department of the Environment Rheinland-Pfalz established an expert group to analyse and evaluate the seismic risk associated with the geothermal system. An expert panel with experts who contribute know-how acquired from similar projects, e.g. the Basel and the Soultz-sous-Forêts geothermal systems.

The Landau project will be allowed to continue operating while the review panel deliberates. Like other earthquakes that have been attributed to geothermal plants, the Landau tremor was sudden and brief and was accompanied by a sound that in some cases has been likened to a sonic boom.

There were no injuries and there was no known structural damage to buildings in the city. But the 2.7 magnitude quake has stoked fears and set off debate in the state parliament, which subsidized the construction of the plant, about the method's safety. The officials of the operating company initially denied any responsibility for the tremor and continue to dispute the government's data linking the project to the quake. The panel will, among other things, have to sort through the

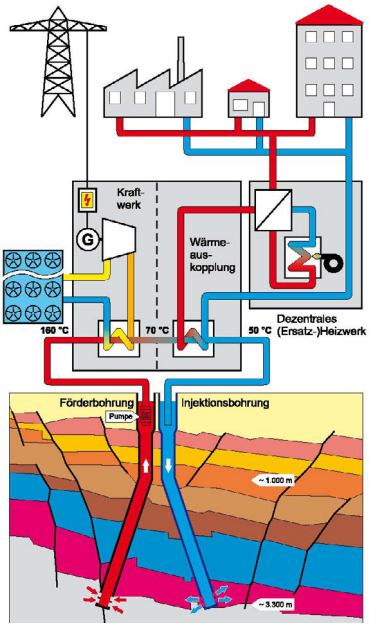

Figure 3: Configuration scheme of the Landau geothermal power plant

conflicting data presented by the company and government scientists. But some experts in the field say they worry that projects like the one in Germany, if the managers deny responsibility for inducing earthquakes or play down the effects on people's lives, could damage the reputation of geothermal energy, even in highly environmentally conscious areas of the world like California or Western Europe.

The demonstration project GeneSys - development of new concepts for the direct use geothermal heat

The GeneSys project of the Federal Institute for Geosciences and Natural Resources (BGR) and the Leibniz Institute for Applied Geophysics - LIAG aims at the development and implementation of new concepts for the direct use geothermal heat. The location Hannover is an exemplary one: Target rocks are the formations of the Mid Triassic. In a depth of 3,700 m to 4,000m, these thick formations have a temperature of 130°C to 160°C. These rocks are a common type for northern Germany. In most cases, their permeability is not sufficient for the conventional production of hot water. Therefore, an artificial fracture will be created in the bedrock which acts as a heat exchanger. The heat energy of the produced hot water will be extracted by a surface heat exchanger and fed into a heating circuit. The cooled down water is then going to be injected into a shallower rock layer via the same borehole (Fig. 4).

Since June 2009 a 4,200 m deep geothermal well is being drilled at the premises of the GEOZENTURM in the city of Hannover. Large scale artificial fractures are going to be created at a depth of approximately 3,800 m which will act as a heat exchanger. This will be followed by a long term test-operation in order to determine the performance of the geothermal system. Coupling the geothermal sub-surface system with the GEOZENTRUMs heating system can provide heat energy for several decades. The GeneSys project Hannover is funded by the Federal Ministry of Economics and Technology.

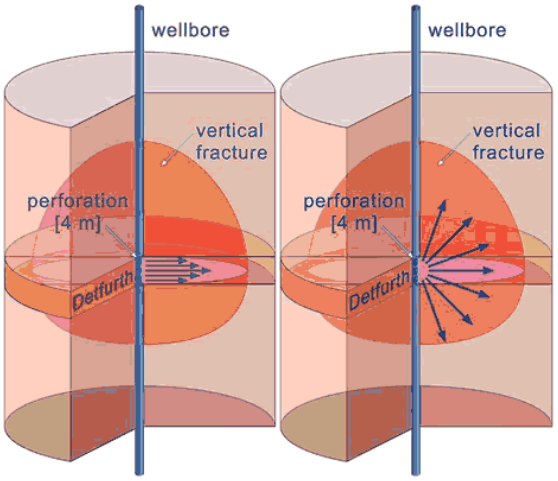

Figure 4: GeneSys project - Schematic illustration of the flow regimes at low (left) and of the flow regimes at high (right) injection rate, due to hydromechanical fracture opening.

The new Bauer Deep Drilling Rigs TBA

Bauer Maschinen are developing new deep drilling rigs which will go into operation between the middle of 2009 and the middle of 2010. The rig family will consist of three types of TBA rigs.

Type	Hook Load [tonnes]	Operating Weight [tonnes]	Power [MW]
TBA 300	250 - 400	500 - 600	3 - 4
TBA 200	150 - 220	200	1.5 - 2
TBA 100	60 - 120	100	1.5

The rigs of the TBA 300 Series are particularly well suited for the installation of deep geothermal boreholes, including directional ones, to around 5000 metres. Projects of this type are to be found in Germany, specifically south of Munich, in Switzerland, Austria and the USA, although important projects are also under development in Australia.

Depending on the geographical areas and the prevailing deposits, Bauer deep drilling rigs are suited for the exploration of onshore oil and gas deposits. The size and type of drilling rig for a particular drilling project is determined by the intended drilling depth, the degree of intentional deviation and also the borehole diameter.

The highly mobile rigs of the TBA 100 Series are ideally suited for all operations associated with the maintenance or overhaul of existing extraction wells. Due to their modular construction, the workover rigs can always be tailored to the exact needs of the client.

By attaching a top drive, the workover rig can also be used for drilling operations.

TBA 300

The TBA 300 (Fig. 5) is a high performance drilling rig that meets the most modern demands. Due to its patented and unique hybrid drive, the design of the rig is optimised for the two most important work processes during deep drilling operations:

- Rapid installation and extraction of the drill string; the installed triple cylinder facilitates trip times up to 400m per hour for maximum drill string loads up to 120 tonnes.
- High-performance installation of drill casings with maximum loads up to 280 tonnes, for which the 8-part main hydraulic winch is optimised.

Figure 5: TBA 300

The combination of both systems – fast trip times for smaller loads as well as slow installation of drill casings for high loads - ensures energy savings of around 30% over conventional systems, where either the hydraulic crowd cylinders or the winch drives have to be designed for both load cases.

The BHS 400 pipe handling system mounted on the side of the deep drilling rig enables drill pipes of all kinds to be installed automatically at speeds up to 400 m per hour without manual intervention. Safety is of utmost importance during all operating procedures on the drilling rigs of the TBA Series. This applies in particular to the trip-in and trip-out processes. The drill pipes, which are stored safely on the drill site in a horizontal position, are placed directly in the drill axis by the manipulator.

During the development of the drilling rigs, it was important to optimise and thus minimise the setting up and transportation processes. All components are fitted with container corner castings and their dimensions also correspond with conventional 20 or 40 ft. containers, enabling fast and secure transportation by standard container lorries. Only a few of these transports exceed normal heights or weights over 20 tonnes (Fig. 6).

To accelerate rig assembly with a greater degree of safety, the heavy duty pins, used for example for connecting the mast sections, are no longer inserted by hand, but with the use of hydraulic cylinders operated from the control station. Then, only the plug-in connections have to be made for the hydraulic hoses and electric cables.

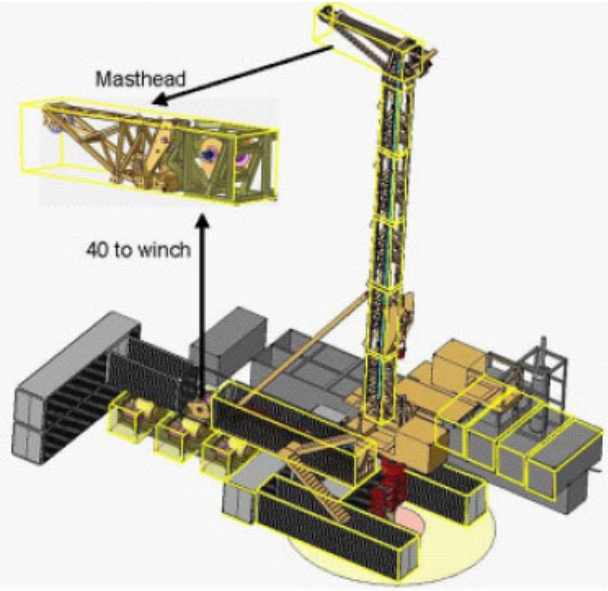

Figure 6: Container-size components

As the mast head and the main winch are transported together, the main hoist rope with a diameter of 40mm can always remain reeved. This reduces rigging and de-rigging times, and significantly increases safety by avoiding this difficult, and at times dangerous, operation.

A further significant innovation is the Bauer top drive TDK 65. Generally operated hydraulically, it can also be equipped with an electric motor at the client's request.

With its installed power of 530 kW, the Bauer top drive develops a torque of up to 65 kNm and a speed of 180 rpm. The top drive is designed for a 3¼" flushing head with pressures of up to 5000 psi. When making connections, the variation in length of drill pipe is allowed for by way of hydraulic cylinders. Commercial elevators with break-out clamps up to 100 kNm breaking torque can be used for installing the drill string.

In order to introduce a new level of safety in this area as well, all Bauer top drives can alternatively be supplied with a clamping and breaking device for drill pipes up to 8" and casings up to 13 3/8" diameter.

For operation of the drilling rig, up to three electrically operated Bauer mud pumps, each with an input power of 900 kW, a maximum delivery rate of 2,450 l/min and a maximum pressure of 5000 psi can be connected and controlled (Fig. 8). These pumps are also fitted into 20" container frames and are, therefore, easy to transport.

Figure 7: Two mud pumps at the rear of the TBA 300

TBA 200

As for the TBA 300, the advantages and innovations of the TBA series are also integrated in the TBA 200 (Fig. 8):

Hybrid drive with crowd cylinders for running in drill pipes and winch pull-down for installing drill casings with corresponding energy saving. The diesel driven power pack with an output of 403 kW serves also as counterweight. Due to the compact design of the entire unit, which is mounted on a frame complete with winch and mast, it is possible to rig or de-rig the drill extremely quickly within approximately one day. The telescopic mast and all other rigging functions are powered via a small integrated power pack even before the main power pack is connected. The TDK 35 can also be equipped with elevator or optionally with clamping head technology.

The pipe handling system mounted on the rig can either be the BHS 400 or the conventional V-Door System with front loading.

Figure 8: Deep drilling rig TBA 200

The VFD container and driller's control cabin are similar to those on the TBA 300. Once again, up to three mud pumps can be connected and operated, although only two mud pumps are generally required for the boreholes of a TBA 200.

Workover rigs

The design concept of the TBA 60 to 120 was also adopted for the workover rig with the result that by simply adding a rotary table and adapting the peripheral equipment, the same rig can carry out both functions – workover or drilling operations.

Mud treatment plants

Bauer Maschinen is also developing, jointly with its subsidiary MAT, the entire mud treatment and separation plant (Fig. 9).

Figure 9: Mud treatment plant TSA 5000

Apart from the conventional technology of slurry regeneration by way of fine screens and centrifuges (as for example in the TSA 5000 with the capacity of 5000 l/min) the latest treatment and separation systems which combine screens, cyclones and centrifuges are also being built. This includes the TSA 4000 with a capacity of 4000 l/min. These latest types of plant have an extremely high output capacity with minimal space requirements.

Conclusion

Drilling for geothermal energy deposits is based on the same technology which is used in the oil and gas industry. The mast, hoisting system, mud pumps (including mud circuit) and the blow-out-preventer are the main components of the drilling rigs. Today the Top-drive-Rotary-systems are applied in modern deep drilling rigs. The BAUER deep drilling rigs are designed both for the emerging markets for the development of geothermal resources and conventional oil and gas drilling.

Power Generation Potential of SC-CO_2 Thermosiphon for Engineered Geothermal Systems

Alvin I. Remoroza*, Elham Doroodchi, Behdad Moghtaderi
[1]Priority Research Centre for Energy, School of Engineering (Chemical Eng.), Faculty of Engineering & Built Environment, University of Newcastle
University Drive, Callaghan, NSW 2308, Australia
* Corresponding author: Alvin.Remoroza@studentmail.newcastle.edu.au

Numerical modelling was conducted to assess thermodynamic properties and power generation potential of SC-CO_2 thermosiphon for Engineered Geothermal Systems (EGS) and compared with H_2O-based EGS with Organic Rankine Cycle (ORC).

Keywords: SC-CO_2 thermosiphon, Enhanced Geothermal System, Hot Dry Rock

Findings from the Simulation

The methodology and reference data (Table 1) adopted in this paper is similar to that used by Atrens et al (2009) for computing the overall flow in an EGS. The calculations are divided into two parts, injection and production sections. The injection calculations include fluid well-bore flow from the surface to the bottom of the injection well and fluid flow through the reservoir. The production calculations only include fluid well-bore flow from the bottom of the production well to the surface.

The following sets of equations with the assumptions of adiabatic flow and negligible kinetic energy at the wellbore, and reservoir Darcy flow of constant cross-sectional area (single channel flow) with linearly increasing temperature were used in the injection calculation;

$$P_{inj} = P_{res} + \Delta P_{f,well} + \Delta P_{f,res} - \rho g \Delta z$$

$$\Delta P_{f,well} = f \frac{\Delta z}{D} \rho \frac{V^2}{2} = f 8 \frac{\Delta z \dot{m}^2}{\pi^2 \rho D^5}$$

$$f = \left[-1.8 \log \left(\frac{6.9}{\mathrm{Re}} + \left[\frac{\varepsilon}{3.7D} \right]^{1.11} \right) \right]^{-2}$$

$$\Delta P_{f,res} = \frac{\dot{m} \mu \Delta L}{\rho \kappa A}$$

In the production section, the adiabatic flow defines the following relationship,

$$P_{prod} = P_{res} - \rho g \Delta z - \Delta P_{f,well}$$

Where V = fluid velocity

$\dot{m}$ = mass flow rate

f = friction factor

ρ = density

$$\mathrm{Re} = \frac{\rho V D}{\mu} = \frac{4\dot{m}}{\mu \pi D}$$

ε = pipe roughness

D = pipe diameter

g = gravitational constant, 9.81 m/s^2

κ = homogenous permeability

A = swept area of the fluid flow in the reservoir

P_{inj} = injection pressure

P_{res} = reservoir pressure at the bottom of the production well

$\Delta P_{f,well}$ = frictional losses at the well

$\Delta P_{f,res}$ = reservoir pressure losses

ΔL = incremental reservoir length

Δz = incremental vertical distance

The total exergy generated from SC-CO_2 thermosiphon EGS was dominated by exergy associated with change in enthalpy. The specific exergy can be expressed as

$$X_H = (h - h_0) - T_0 (S - S_0)$$

Where X_H = exergy associated with change in enthalpy

h = specific enthalpy

S = specific entropy

T = temperature in Kelvin

The subscript 0 denotes initial conditions.

Numerical simulations were carried out using Engineering Equation Solver (EES). EES calculates thermodynamic properties for carbon dioxide using the fundamental equation of state developed by Span and Wagner (1996) and viscosity and thermal conductivity based on the work by Vesovic et al (1990). EES gives thermodynamic properties of water using the 1995

Formulation for the Thermodynamic Properties of Ordinary Water Substance for General and Scientific Use issued by The International Association for the Properties of Water and Steam (IAPWS).

Table 1: Reference values used in the exergy analysis

Parameter	Values (Artens, 2009)	Values (this study)
Reservoir Length	1000 m	1000 m
Reservoir Temperature	225^{0}C	225^{0}C
Reinjection Temperature	25^{0}C	25^{0}C
kA (inverse impedance)	2.1E-19 m^4	2.1E-19 m^4
Reservoir Pressure, P_{res}	Hydrostatic (49.05MPa)	Hydrostatic (49.05MPa)
Wellbore Roughness (ε)	400 micrometer	400 and 40 micrometer
Wellbore Diameter, D	0.2315	0.2315
Reference Temperature	25^{0}C	25^{0}C

Effect of Pipe Roughness

Pipe frictional losses at the injection well are higher for SC-CO_2 than for H_2O because pipe roughness affects CO_2 mass flow rates more than it affect H_2O mass flow (Figures 1 and 2).

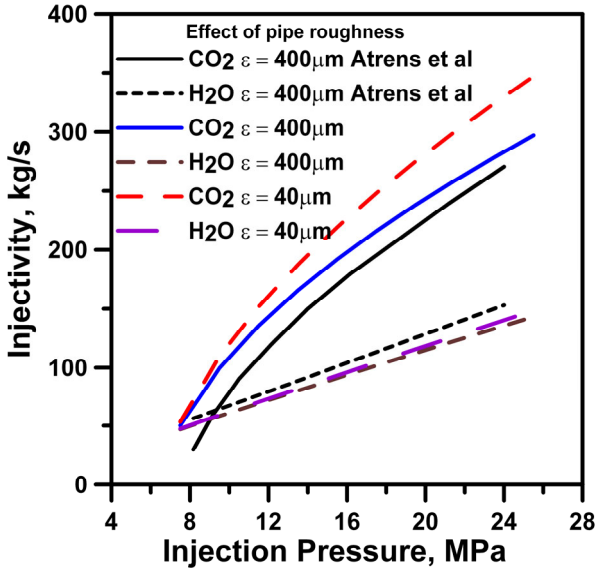

Figure 1: Injectivity of SC-CO_2 and water at different injection pressures and roughness values.

Bottomhole pressures at the injection well with H_2O circulation are, in theory, greater than with SC-CO_2 circulation because (a) H_2O has higher density than CO_2 at the same pressure-temperature conditions, and (b) CO_2 has higher pipe frictional losses than water for the same mass flow rate. Reservoir pressure losses are significantly higher for H_2O than SC-CO_2 thermosiphon based system because of H_2O's higher kinematic viscosity (μ/ρ) at the given T-P domain in the reservoir (plots not shown).

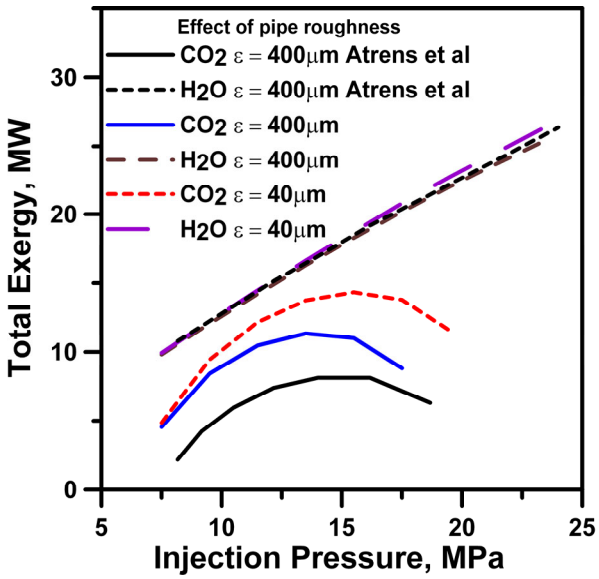

Figure 2: Total exergy provided by SC-CO_2 and water at different injection pressures and roughness values.

Pressure and Temperature Well Profile of the Injection Well

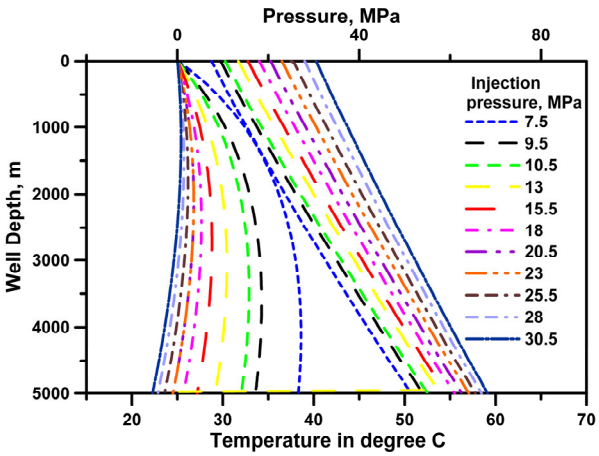

Figure 3: Temperature (left plots, lower X-axis) and pressure (right plots, upper X-axis) well profile at the SC-CO_2 injection well (Note: pipe roughness used is 40 microns).

For SC-CO_2 adiabatic flow at the injection well, the SC-CO_2 temperature at the bottom may be higher (at lower injection pressure) or lower (at higher injection pressure) than the injection temperature (Figure 3). Specific enthalpy of SC-CO_2 is affected by temperature and pressures whereas specific enthalpy of H_2O is affected by temperature and only slightly by pressure (Pruess; 2006, 2008).

Effect of Injection Temperature

Injection temperature affects SC-CO_2 and H_2O in somewhat different ways (Figure 4);

- For SC-CO_2, lowering the injection temperature increases the pipe frictional and reservoir losses due to increased

density and viscosity. However, the gain in the pressure head (i.e. increase in bottomhole pressure) due to increased density is far more than the total losses resulting in net overall gain in buoyant force driving natural convection.

- For H_2O, decreasing the injection temperature actually decreases the pipe frictional losses, slightly increases bottomhole pressure and increases reservoir pressure losses. Overall, reservoir losses are greater than the combined head gain and less pipe frictional losses resulting in slight decrease in injectivity.

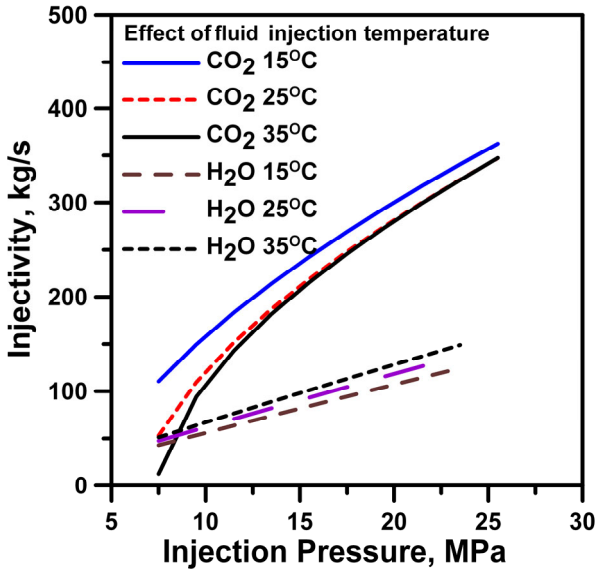

Figure 4: Effect of injection temperature on injectivity.

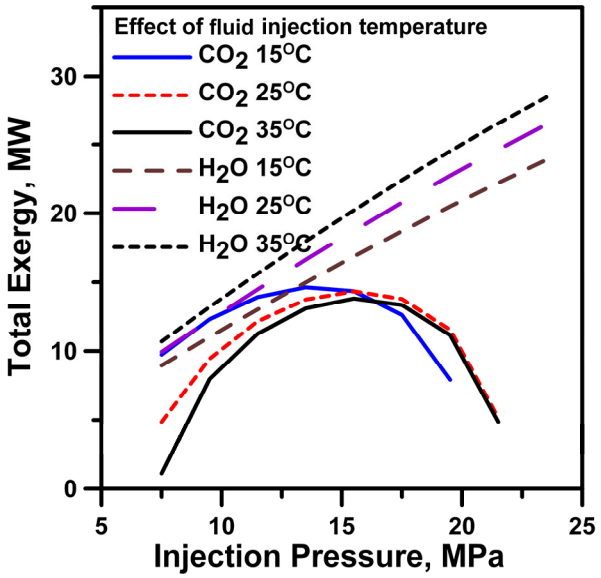

Figure 5: Effect of reinjection pressure and temperature on total exergy.

Whenever reinjection temperature of 15^0C or less are possible, SC-CO_2 thermosiphon based EGS can have slightly higher thermal heat extraction efficiency at injection pressures lower than ~13.0 MPa (Figure 5).

Single Channel versus Radial Reservoir Flow

Radial pressure distribution in the reservoir from an injection well can be described in the following equation

$$P(r) = \frac{\mu \dot{V}}{2\pi K L_R} \ln(r)$$

Where μ = absolute viscosity

$\dot{V} = m/\rho$ = volumetric flow rate of the fluid

K = homogenous permeability

L_R = reservoir depth or thickness

The pressure difference between the injection well face, r_W and the production well located at distance, r_R (equals 1000 m in our previous assumptions) can be approximated using the following equation

$$\Delta P_{f,well} = \frac{\mu * \dot{m}}{2 * \pi * \rho * K * L_R} \ln(\frac{r_W}{r_R})$$

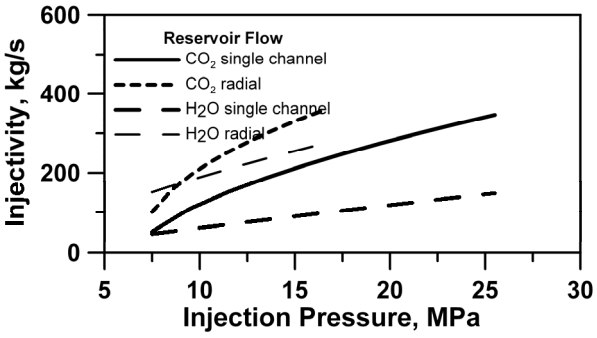

Figure 6: Effect of reservoir flow model choice on injectivity.

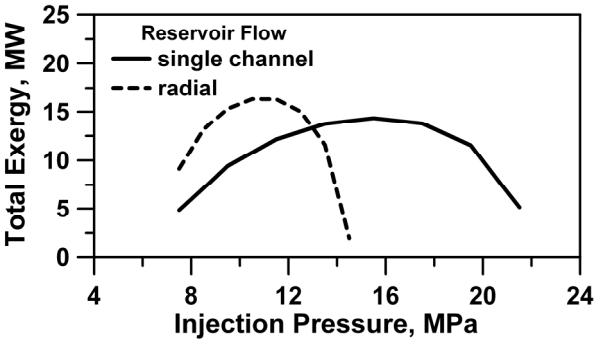

Figure 7: Effect of reservoir flow model choice in total exergy of a SC-CO_2 thermosiphon EGS.

Comparing single channel (constant cross-sectional area, i.e. pipe flow) and radial reservoir flow showed that radial reservoir flow gives higher injectivity and consequently improved total exergy (Figures 6 and 7). This behaviour is due to lower

reservoir pressure losses in radial reservoir flow compared to single channel flow.

Sensitivity of Exergy to Well-Configuration

Well configuration (ratio of the number of injection to production wells) does not significantly affect the injectivity of the fluid but it affects the performance of the production wells. Higher number of production wells lowers the frictional losses because of lower mass flow rates in each well since the mass flow rate of the circulating fluid is equally divided by the number of production wells. For single channel reservoir flow, 1 injection to 2 production well ratio gives the optimum total exergy while the five-spot well configuration (1 injection to 4 production well ratio) gives the optimum total exergy for radial reservoir flow. On the basis of per drilled well (sum of injection and production wells), the doublet configuration (1 injection to 1 production well) gives the highest total exergy both for single channel and radial reservoir flow (Figures 8 and 9).

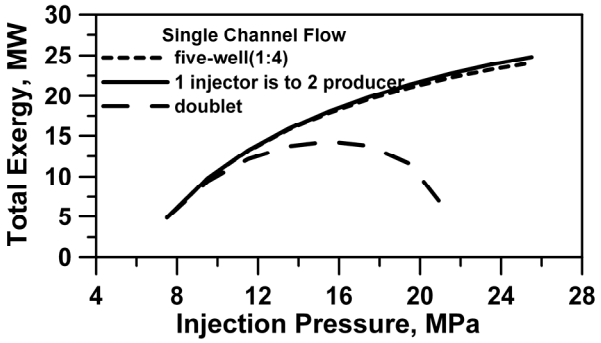

Figure 8: Effect of well configuration on total exergy of SC-CO_2 on single channel reservoir flow.

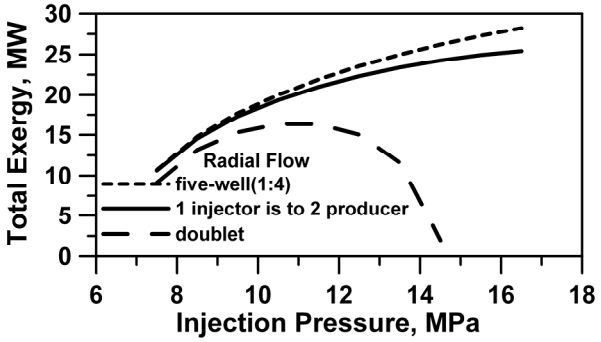

Figure 9: Effect of well configuration on total exergy of SC-CO_2 on radial reservoir flow.

It can be deduced that if five-spot well-configuration is used, the radial reservoir flow model would be more appropriate to implement in numerical modelling. Doublet and 1 injection to 2 production well configurations would command the implementation of single channel reservoir flow modelling. Based on the results, doublet configuration is the most efficient in extracting heat based on the total exergy per drilled well.

H_2O-based EGS with Organic Rankine Cycle versus SC-CO_2 Thermosiphon Power Cycle Analysis

H_2O based EGS can not be used in a thermosiphon power cycle since the production pressure is always lower than the injection pressure.

In SC-CO_2 power cycle analysis, the gross potential electrical power is calculated based on CO_2 isentropic expansion in the turbine with 85% turbine efficiency (Figure 10). Temperature-entropy diagram of a SC-CO_2 power cycle at injection pressure of 7.5 MPa is given in Figure 11. It shows that super-critical CO_2 exists in all stages of the process. Auxiliary power requirement is not included in the calculations, i.e. power used in cooling tower, etc. It is assumed that no pump will be used in the SC-CO_2 thermosiphon power cycle.

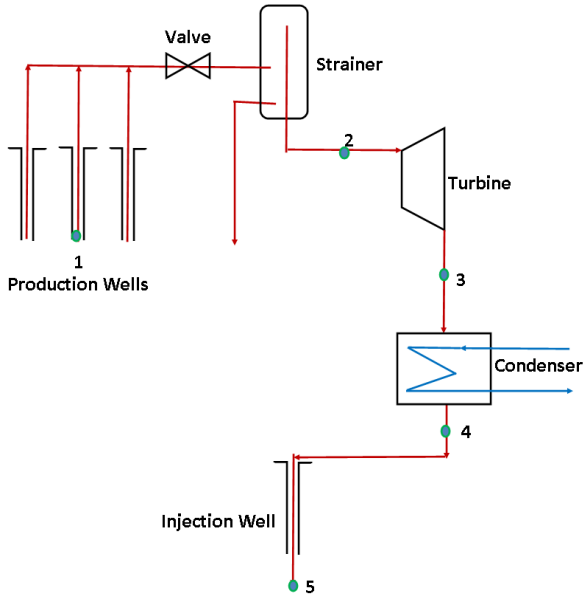

Figure 10: Schematic Diagram of a SC-CO_2 Thermosiphon Power Cycle.

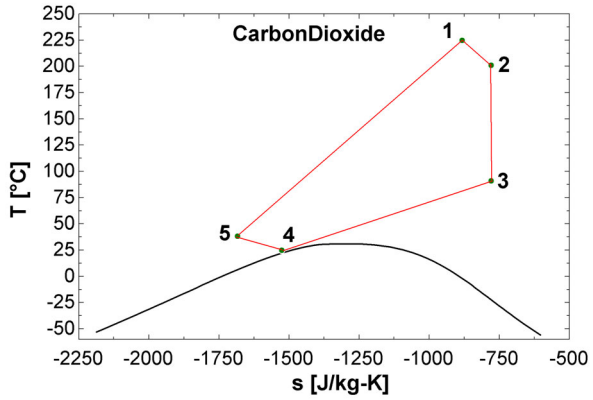

Figure 11 Temperature-entropy diagram of SC-CO_2 thermosiphon power cycle.

Power cycle analysis of H_2O-based EGS ORC (Figure 12) assumes the use of isopentane as the secondary fluid with circulating pump pressure of 2.793 MPa (T_{sat} = 175^{0}C) and condenser pressure of 101.325 kPa (atmospheric condition). This circulation pump pressure is chosen so that existence of two-phase is avoided during expansion at the turbine while giving the maximum power (Figure 13). The pump is assumed to be 75% efficient and isentropic.

The power generated from H_2O based EGS with ORC is calculated as turbine power minus pump power for H_2O injection and circulation of the working fluid and does not include power used in the cooling tower and other auxiliary equipment.

$$W = W_{turbine} - W_{injection} - W_{ORC,circulation}$$

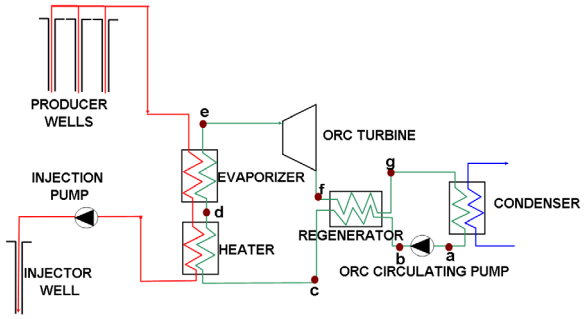

Figure 12: Schematic diagram of binary organic rankine cycle for H_2O based EGS.

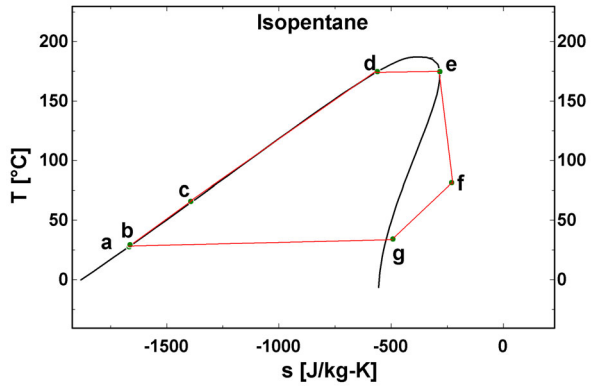

Figure 13: Temperature-entropy diagram of ORC with Isopentane as working fluid.

Power cycle analysis showed that H_2O based EGS is better in mining heat and transferring that heat in secondary fluids for electrical power generation than SC-CO_2 thermosiphon EGS (it maybe different for pump CO_2 EGS because of possible higher injectivity). The optimum power that can be generated from SC-CO_2 thermosiphon is 8.6 MW at 9.5 MPa injection pressure at radial reservoir flow model while for H_2O-based EGS with ORC, the electrical power potential at the same conditions is 25.8 MW. For single channel reservoir flow model, the optimum electrical power potential of a SC-CO_2 thermosiphon is 6.3 MW while for H_2O-based EGS is 9.4 MW. Electrical power potential of H_2O-based EGS linearly increases with injection pressure whereas for SC-CO_2 thermosiphon EGS the relationship is parabolic (see Figure 14).

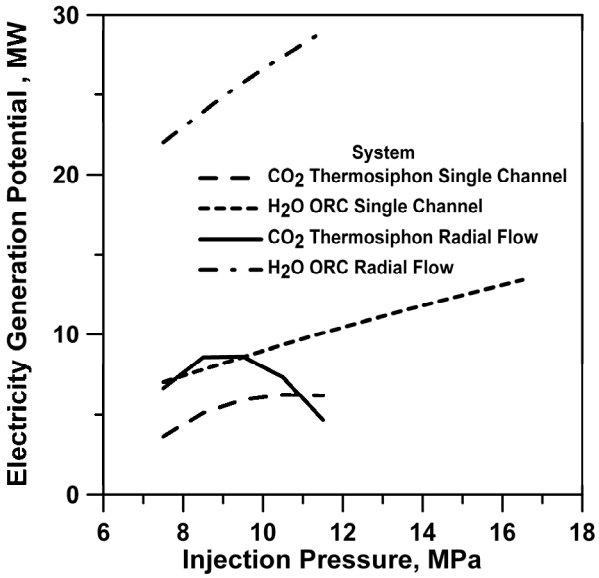

Figure 14: Potential electricity generation comparison of a SC-CO_2 thermosiphon and H_2O based EGS with ORC (assumes 85% turbine efficiency and 75% pump efficiency).

The less number of equipment of a SC-CO_2 thermosiphon power cycle (no injection pump and circulation pump for secondary fluid) and relative inertness of CO_2 with regards to rock-interaction and associated mineral dissolution, precipitation and fouling of equipment warrant further evaluation. However, SC-CO_2 thermosiphon power cycle will require research and development of SC-CO_2 turbine.

Sensitivity of Exergy to Reservoir Depth

The performance of SC-CO_2 thermosiphon EGS on shallower hot dry rock geothermal resource was also investigated. The numerical simulation used single channel reservoir flow model and doublet well configuration, the same resource temperature of 225^{0}C and injection temperature of 25^{0}C, and changing well depth to 3000 m and assuming reservoir pressure at the producer well to 29.43MPa (assumes hydrostatic pressure).

The over-all effect of shallower reservoir depth of the HDR geothermal resource at SC-CO_2 thermosiphon EGS were lower total exergy and lower electricity generation potential due to lower production pressures (Figures 15 and 16). However, SC-CO_2 injectivity increased at shallower HDR geothermal resource depth. The total exergy of H_2O-based EGS increased at deeper reservoir depth but the electricity generation potential were similar.

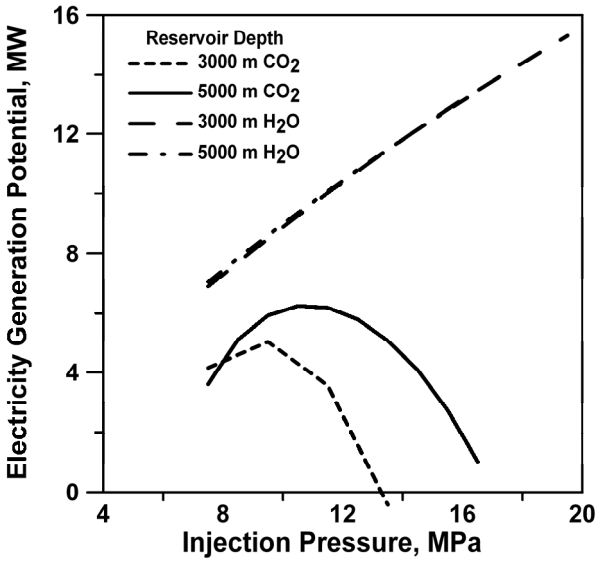

Figure 15: Effect of reservoir depth on SC- CO_2 thermosiphon on electricity generation potential (assumes 85% turbine efficiency).

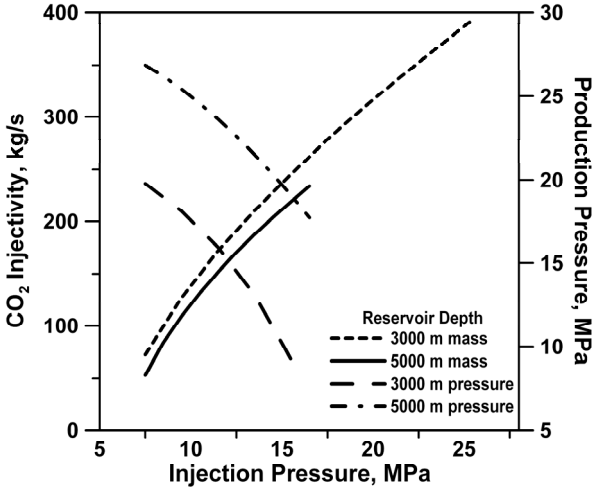

Figure 16: Effect of reservoir depth on SC-CO_2 thermosiphon on injectivity and production pressure.

Recommendations

The less complicated design of CS-CO_2 thermosiphon EGS and relative inertness of CO_2 with regards to rock-interaction and associated mineral dissolution, precipitation and fouling of equipment warrant further economic and geochemical evaluation. Research and development of high efficiency SC-CO_2 turbine is also necessary to prove the viability of this system. The use of pump for SC-CO_2 circulation in EGS may also be investigated.

Economic and thermodynamic analyses over the full life of SC-CO_2 and H_2O based EGS should be carried out to compare their overall environmental and economic performances. One can determine the total amount of CO_2 that will be created and sequestered plus the amount of conventional CO_2 emissions that will be avoided during the entire life cycle of CS-CO_2 thermosiphon and H_2O EGS projects. It appears from this study that H_2O based EGS can generate more electrical power than CS-CO_2 thermosiphon EGS.

The amount of CO_2 that may be sequestered and stored in a SC-CO_2 thermosiphon EGS is only an added ancillary benefit since the amount is negligible compared to the current total CO_2 emission. Another concern will be the issue of possible CO_2 leakage in EGS.

This paper merely present the results of a thermodynamic and power cycle analysis, it does not prove or disprove the viability of using SC-CO_2 circulation EGS.

References

Atrens, A. D., Gurgenci, h. and Rudolph, V. (2008). Carbon Dioxide Thermosiphon Optimisation, in: Gurgenci, H. and Budd, A.R. (eds.), Proceedings of the Sir Mark Oliphant International Frontiers of Science and Technology Australian Geothermal Energy Conference, Geoscience Australia, Record 2008/12,149-152.

Atrens, A. D., H. Gurgenci, and V. Rudolph (2009). CO_2 Thermosiphon for Competitive Geothermal Power Generation. Energy & Fuels 23(1): 553-557.

Atrens, A. D., H. Gurgenci, and V. Rudolph (2009). EXERGY ANALYSIS OF A CO_2 THERMOSIPHON. PROCEEDINGS, Thirty-Fourth Workshop on Geothermal Reservoir Engineering, Stanford University, Stanford, California.

Pruess, K. (2006). Enhanced geothermal systems (EGS) using CO_2 as working fluid - A novel approach for generating renewable energy with simultaneous sequestration of carbon. Geothermics 35(4): 351-367.

Pruess, K. (2008). On production behavior of enhanced geothermal systems with CO_2 as working fluid. Energy Conversion & Management 49(6): 1446-1454.

Pruess, K. and M. Azaroual (2006). On the feasibility of using supercritical CO_2 as heat transmission fluid in an engineered hot dry rock geothermal system. PROCEEDINGS, Thirty-First Workshop on Geothermal Reservoir Engineering, Stanford University, Stanford, California.

Span, R. and W. Wagner (1996). A New Equation of State for Carbon Dioxide Covering the Fluid Region from the Triple-Point Temperature to 1100 K at Pressures up to 800 MPa. J. Phys. Chem. Ref. Data 25: 1509-96.

Vesovic, V., W. A. Wakeham, G. A. Olchowy, J. V. Sengers, J. T. R. Watson, and J. Millat (1990). The Transport Properties of Carbon Dioxide. J. Phys. Chem Ref. Data 19(3): 763-808.

Modelling Reservoir Behaviour during Stimulation Tests at Habanero #1

Baotang Shen *
CSIRO Exploration and Mining
PO Box 883, Kenmore, QLD 4069, Australia
baotang.shen@csiro.au

This study was to characterise the underground heat-exchange reservoir at Habanero #1 well operated by Geodynamics Ltd. Several three-dimensional coupled mechanical/fluid 3DEC models have been studied to understand the rock mass reaction to the stimulation tests that were conducted in November-December, 2003. The microseismic monitoring results by Tohoku University and the falloff test results on 12 December 2003 were used to estimate some key input parameters for the numerical modelling. The seismic results were also used as benchmarks for model verification tests. Different fracture orientations, rock mechanical properties and fluid properties were used in this study to investigate the effect of varying these parameters on rock mass response to fluid injection. The study provided an improved understanding of the fracture system that was activated during the stimulation tests.

Background

A program is being undertaken by Geodynamics Ltd to develop the Hot Fractured Rock (HFR) geothermal energy resource in the Cooper Basin. Habanero #1 was the first well drilled in this program and it reached a depth of over 4,400 m with a bottom hole temperature of over 240°C. Following the completion of the drilling, stimulation of the reservoir was conducted during November-December 2003 by injecting high pressure water into the fractured granite to activate the fractures and hence increase the permeability of the heat exchange reservoir. The response of the reservoir to injection has been monitored by Tohoku University using advanced microseismic monitoring systems. The location and timing of the seismicity associated with fracture movement were then mapped.

Understanding the characteristics of the heat exchange reservoir is the key for the design of ongoing operations. Because of the depth to the granite, there are very limited measurement techniques available that can be used to characterize the reservoir, apart from pressure and injection rate monitoring and microseismic monitoring. Numerical modelling hence becomes an important tool for this purpose.

The aim of the modelling is to provide interpretation and understanding of the reservoir behaviour during the stimulation tests, which will provide guidelines for future circulation tests.

Numerical models

The numerical models use a three-dimensional distinct element code, 3DEC, that can simulate coupled geomechanical-fluid processes and is especially suited to simulating coupled fluid flow and deformation in fractured rock masses (Itasca, 2003). 3DEC has the following main features:

- It simulates the joints/fractures explicitly.
- The fluid flow in the rock mass is considered to occur only in the rock fractures.
- The coupled process between fluid flow and rock fracture deformation is simulated.

In the granitic rock mass targeted for the HFR stimulation and circulation operations, fluid flow is believed to occur mostly in the fractures. Intact rock porosity and permeability is low and rock matrix flow is assumed to be insignificant. In this case, 3DEC is considered to be suitable and hence was chosen for this study.

Based on the seismic monitoring data, two different fracture patterns have been interpreted by different research teams. One interpretation showed that there are four shallow dipping major fractures, see Figure 1 (Wyborn, 2004, personal communication), whereas the other considered there is only one large fracture. The first interpretation has been used in this study.

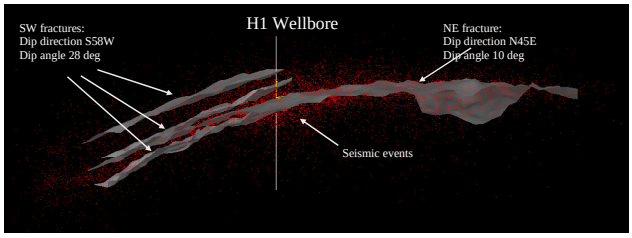

Figure 1. The major fractures delineated from the seismic monitoring data (based on one of the two interpretations). Fractures are shown in three dimensions with a viewing direction from SE to NW.

The four fractures considered may be large scale distinct fractures or they may represent fracture zones with some thickness (say, less than 150m). The limited accuracy on the location of the seismic events, and the fact that seismicity can occur both on and off the major fracture planes, does not permit a definitive location of the fracture planes.

The granite section of the Habanero #1 well was logged for natural fractures. There are three dominant fracture sets:

Set 1 – dip = 28°, dip direction = 238°

Set 2 – dip = 75°, dip direction = 230°

Set 3 – dip = 35°, dip direction = 155°

These fracture sets are considered to be smaller scale fractures intersecting the four major fractures in the reservoir, as shown in Figure 1.

The 3DEC model was constructed with an overall dimension of 4000m (E-W) x 4000m (N-S) x 1800m (depth), see Figure 2.

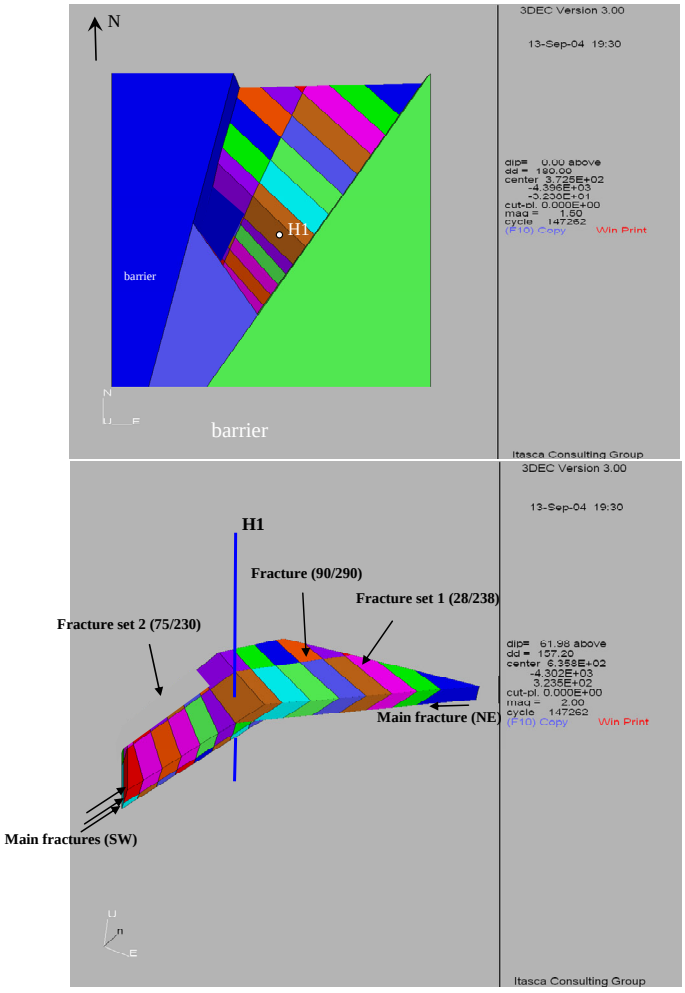

Figure 2. 3DEC model. Top figure – plan view of a 3DEC model (one block was hidden to show the detailed zone). Bottom figure – view of the detailed zone only.

A detailed region is defined as shown in the lower picture of Figure 2. This region is approximately the zone where seismic events have been detected during stimulation operations. The main sub-horizontal fractures delineated in Figure 1 define the upper and lower border of the detailed region. Note that in this model, the north-east trending sub-horizontal fracture in Figure 1 is considered to be a fracture zone with a thickness of approximately 150m, bounded by two 10° dipping fractures at the top and bottom.

The model shown in Figure 2 also includes two fracture sets with spacing of 150m. The 28/238 fracture set is included in the north-east part of the model, and the 75/230 fracture set is in the south-west part. One vertical fracture (90/290) is also included in the model to simulate a hydraulic barrier observed in the microseismic data. All the fracture sets are confined to the detailed region of the model.

The numerical modelling requires detailed mechanical and fluid properties of the rock mass and fluid to be specified. Due to the lack of directly measured data, most of the properties used were estimated based on existing knowledge and past studies for granitic rock (Barton, 1986; Evans, 2004; Choi, 2004, Hillis et al., 1997; Jeffrey, 2004; Shen, 2004). The values of the properties used in this study are listed below:

- Young's modulus = 65GPa
- Poisson's ratio = 0.25
- Friction angle = 33°
- Cohesion = 0
- Dilation = 5°
- Maximum aperture = 93 μm
- Residual aperture = 50 μm
- Fluid density = 990 kg/m^3
- Dynamic viscosity = 0.15×10^{-3} Pa sec
- Bulk modulus = 8×10^5 Pa
- Pore pressure at a depth of 4250m = 74MPa
  Wellbore storage = 2×10^{-8} m^3/Pa
- In-situ stress at a depth of 4250m:
- σ_H = 149MPa (N85E)
- σ_h = 112MPa (N5W)
- σ_v = 98MPa

Model results

Several models with different fracture geometries and input parameters were used in this study. The model which produced the best match to the measurement data is discussed in this section. The best-fit model is judged by matching the numerical results with the following data:

- Falloff test data on 12 Dec 2003.
- Seismic results interpreted by Tohoku University

Matching the falloff test data

The injection-falloff test is a hydraulic test conducted by injecting into the reservoir at a constant rate which produces an associated increase in pressure. The injection is then stopped and the well is shut in with the pressure decline after shut in monitored. This is a standard test method to measure permeability of the reservoir. Longer injection and falloff periods

result in measurement of permeability deeper into the reservoir.

An injection-falloff test was conducted on 12 December, 2003 after the completion of stimulation at Habanero #1. At that time, seismic activities in the reservoir had all ceased which indicated that fracture slip was no longer occurring. The bottom-hole pressure was increased from the in-situ pore pressure (74MPa) to 84.5MPa within about 2 hours by injecting water. Then the well was shut in and pressure dropped back to 74.5MPa within 3 hours. The measured pressure variation is shown in Figure 3.

To match the injection-falloff test results, three key input parameters in the numerical model were adjusted: They are:

- Bulk modulus of the fluid
- Fracture maximum aperture.
- Wellbore storage.

The fluid bulk modulus was found to affect the slope of the pressure build-up curve and the falloff curve; the maximum fracture aperture affects the magnitude of the peak pressure; and the wellbore storage affects the slope of the falloff curve.

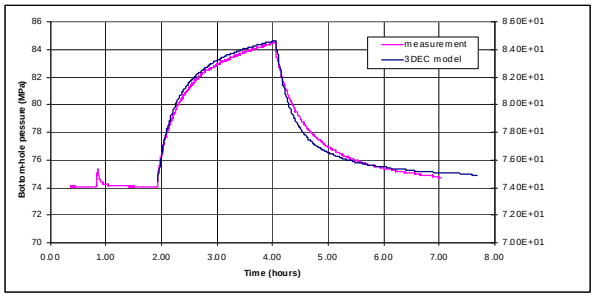

Figure 3. Matching of the numerical results with the measurement data for the falloff test.

The best match was obtained with an apparent fluid bulk modulus of 8×10^5 Pa for the reservoir, maximum fracture aperture of 93 μm and wellbore storage of 2×10^{-8} m^3/Pa, see Figure 3.

The resultant fluid bulk modulus for the reservoir is much lower than that of water at room temperature. The low bulk modulus required for the match is thought to be a result of the 3DEC model neglecting fluid storage in the rock matrix. The maximum fracture hydraulic aperture of 93 μm is equivalent to a permeability-height product (i.e. kh) of 200 md·m to the south-west of the borehole with three parallel main fractures. This agrees with the finding by Evens (2004) that "the far-field kh is 100 md·m or more".

The wellbore storage of 2×10^{-8} m^3/Pa is based on a wellbore volume of 41 m^3 and fluid bulk modulus of 2.0GPa. The 3DEC models did not include the wellbore therefore the effect of wellbore storage had to be considered as a separate effect.

Matching the seismicity monitoring data

The numerical model as shown in Figure 2 was used to investigate the fracture activation during stimulation process. The actual injection operation was done in 4 stages as shown in Figure 4. The 1st stage was the fracture initiation stage, and the 2nd-4th stage are actual fracture stimulation.

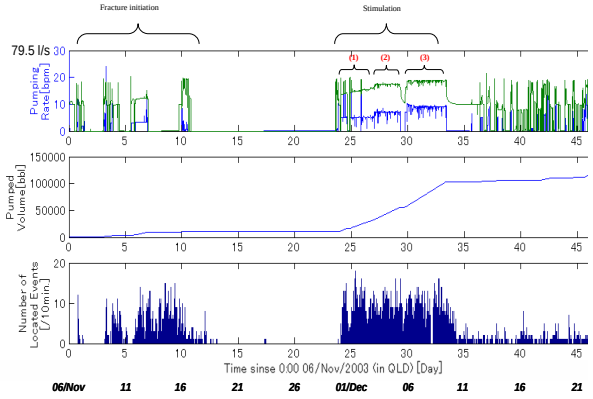

Figure 4. Summary of injection record (after Davidson, 2004).

After completion of the 4 stages of initiation and stimulation in the numerical model, the model results were extracted and processed. The modelled evolution process of fracture sliding was compared with that of microseismic events after initiation stage and stimulation stage as shown in Figure 5 and Figure 6. In the figures, the black dot points indicate the locations of the seismic events obtained from the microseismic monitoring. The red dot points represent the centre of a fracture element which has exceeded its shear strength (i.e. is sliding). Both the measured and predicted results are the cumulative results.

In the fracture initiation stage (Figure 5), the modelled fracture sliding in general matched well the microseismic records. The model results however did not match the isolated cluster of seismic events in the southern side of the wellbore. The run-away seismic cluster could be caused by localised stress concentration or highly conductive fractures in the rock mass. The model did not include any of these special features.

In the stimulation stages (Figure 6), the modelled fracture sliding matched reasonably well with the seismic records, both in the horizontal plan view and the cross section view.

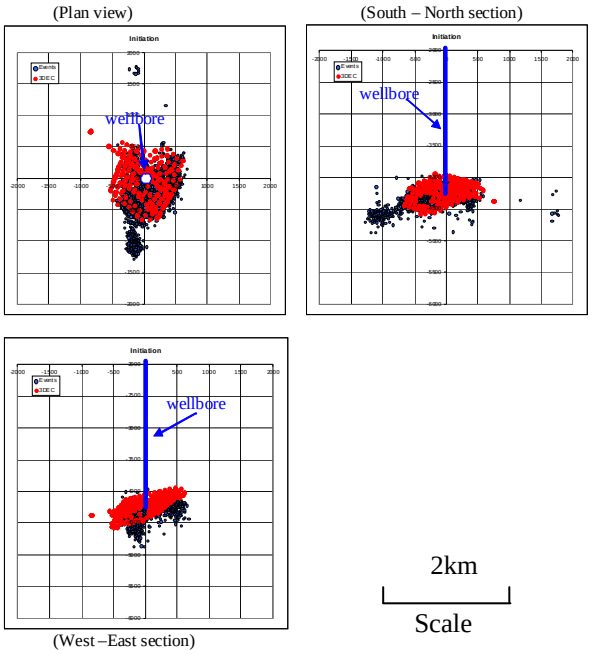

Figure 5. Comparison of the predicted fracture sliding and microseismic monitoring events during fracture initiation.

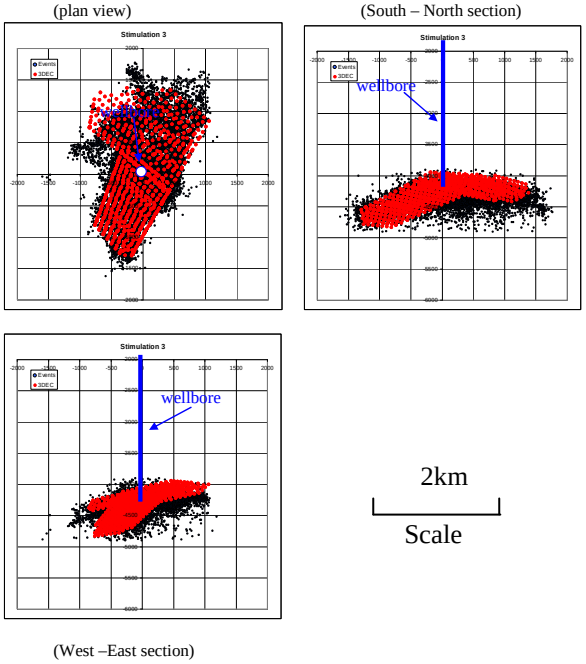

Figure 6. Comparison of the predicted fracture sliding and microseismic monitoring events during stimulation phase 3.

Because the main fractures in the 3DEC model were bounded by the border of the seismic events (except in the northern part where the main fractures extend to the model boundary), it is not surprising that the final locations of modelled fracture sliding matched well with that of the seismic events. However, a good match has also been obtained during the different stages and it is likely that the model is accurately calibrated (although it is possible that other combinations of fracture geometry and input parameters would produce similar matches.)

Injection pressure

The model-predicted time history of bottom-hole pressure of all phases is shown in Figure 7. In general, the predicted injection pressure shows the same trend as that recorded during the actual stimulation tests (see Figure 4). As the injection flow rate increases from 5 bpm (barrel per minute) to 9 bpm, the injection pressure increases accordingly.

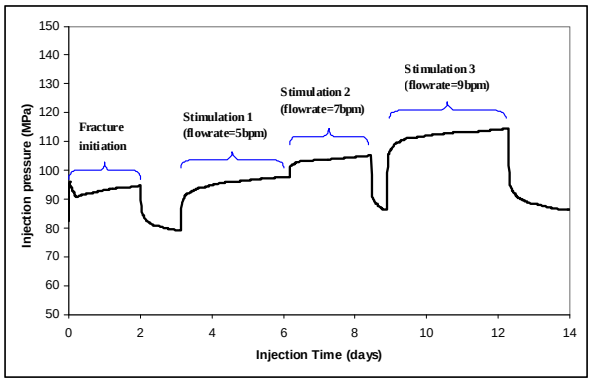

Figure 7. Predicted injection pressure at the wellbore using the 3DEC model.

The predicted magnitude of the injection pressure at the bottom of the wellbore, however, is higher than that calculated using the measured surface pump pressure (with consideration of pressure loss). At the later stage of the injection (stimulation stages 2 and 3), the predicted bottom-hole pressure is actually higher than the overburden stress. Two factors in the numerical model may have contributed to this: (1) The model has fixed boundaries on the top and bottom at a distance of 900m from the injection section. The fixed boundaries may have restricted the opening displacement of sub-horizontal fractures and hence resulted in higher fluid pressure. (2) The current 3DEC version only allows a single maximum fracture aperture defined for both shear and open joints. The maximum aperture of 93μm used in the model may not be suitable for open joints although it is reasonable for shear joints.

Figure 8 shows the predicted fluid pressure distribution in the main fractures when the injection flow rate is 9 bpm at the end of the stimulation tests. The fluid pressure in the immediate vicinity of the injection hole is over 100MPa. Fracture in this area would be opened by such pressure. The pressure dropped below 100MPa at about 50m away from the injection hole, implying fracture shearing rather than opening takes place beyond this distance. Measured pressures were, however, close to or below the fracturing opening pressure for all injection periods.

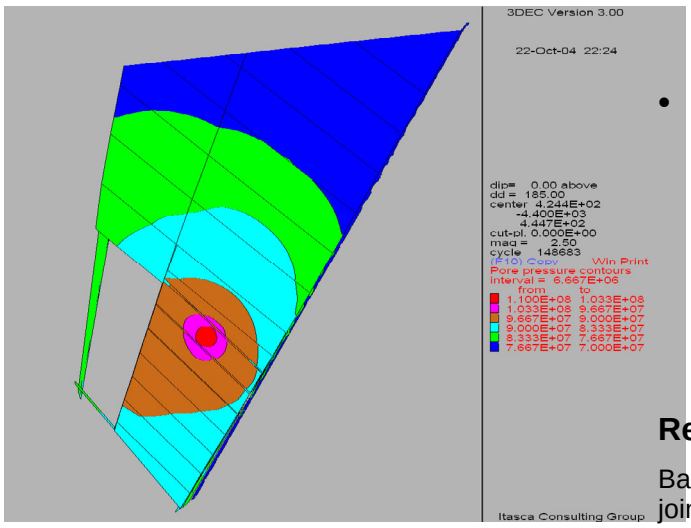

Figure 8. Fluid pressure distribution in the sub-horizontal main fractures at the end of the stimulation test.

Discussion and Conclusions

The study was the first step toward characterisation of the underground heat-exchange reservoir in the vicinity of the Habanero #1 well. The modelling results improved our understanding of the fracture system that has been activated during the stimulation tests. The key findings from this study are:

- To the south-west of the wellbore, the observed seismicity was likely due to fracture sliding along three large parallel fractures with a favourable dip (about 25° - 30°). These fractures were predicted to slide during the early stage of the stimulation tests, agreeing well with the seismic monitoring results.
- To the north and north-east of the wellbore, the observed seismicity was possibly caused by the shear movement in many relatively small fractures in a fracture set with a probable dip (dip/dip direction=28/238). The apparent main fracture with a dip of 10°, delineated from the seismic data, is unlikely to have any major contribution to the seismicity and it was predicted to remain inactive during stimulation tests. This apparent fracture may not exist in the form of a single explicit fracture.
- The fracture permeability in the stimulated zone in south-west is estimated to be around 200md·m (i.e. fracture aperture = 93μm) after stimulation.
- Fracture sets (35/155 and 75/230) which were observed from the borehole log were predicted to remain inactive during stimulation tests. They are unlikely to have contributed to the observed seismicity, although they may have some effect on fluid flow.
- The in-situ stresses inferred from back-analysis of the borehole breakout data are believed to be correct at Habanero #1 site (Shen, 2004). With the horizontal stresses being the major and intermediate principal stresses, the most favourable fracture orientation for sliding is about 28°. This agrees well with observation, particularly in the south-west of the wellbore.

References

Barton, N.R., 1986, Deformation phenomena in jointed rock. Geotechnique. 36, No.2, 147-167.

Choi, X., 2004, 3-Dimensional Finite Element Modelling Study of Habanero #1 CSIRO Petroleum Confidential Report No. 04-035.

Davidson, S.C., 2004, Habanero #1 Stimulation Operation Review. Geodynamics Ltd report.

Evans, K., 2004, Comments to Q-Con's first analysis of the injection test of 12th December, 2003. Report for Geodynamics Ltd.

Hillis R.R., Meyer J.J., Magee M. E., 1997, The contemporary Stress Field of the Nappamerri Trough and Its Implications for Tight Gas Resources. Report of Department of Geology and Geophysics, University of Adelaide, SA 5005, Australia.

Itasca, 2003, 3DEC – Three-Dimensional Distinct Element Code (User's manual). Itsaca Consulting Group, Inc. Mill Place, 111 Third Avenue South, Suite 450. Minneapolis, Minnesota 55401 USA.

Jeffrey, R., 2004, Stimulation of Habanero 1 and positioning of production well. CSIRO Petroleum Confidential Report No. 04-008.

Shen, B., 2004, Using borehole breakout data to estimate in situ stresses in deep granite at Habanero #1 Hot Dry Rock well. CSIRO Exploration and Mining Report 1166C (confidential).

Acknowledgements

The study was sponsored by Geodynamics Ltd. The author wishes to thank Dr Doone Wyborn of Geodynamics Ltd and Mr Steve Davidson for their input to this study.

Magnetotelluric Monitoring Of Geothermal Fluid Flow

Stephan Thiel[1], Jared Peacock[1]*, Graham Heinson[1], Louise McAllister[2]
[1] TRaX, School of Earth and Environmental Sciences, University of Adelaide, SA 5005
[2] Petratherm Ltd, Adelaide, Unley, SA 5061
*Corresponding author: jared.peacock@adelaide.edu.au

Monitoring fluid flow in enhanced geothermal systems (EGS) is vital to reservoir growth and production. Geothermal fluids are innately conductive due to high temperature and pressure and dissolved enhanced ion concentration. This can be exploited by geophysical measurements sensitive to subsurface conductivity changes at several hundreds of meters to a few kilometers depth, such as magnetotellurics (MT). It is proposed that fluid flow can be monitored by measuring subsurface conductivity as a function of space and time using the magnetotelluric method constrained by other geophysical and geological data. 3D MT forward modelling studies demonstrate the feasibility of the method. MT data will be collected in the near future across the EGS site at Paralana, South Australia.

Keywords: Magnetotellurics (MT), geothermal, monitoring, microseismic

Problem:

EGS reservoirs consist of low permeability/porosity rock volumes which need to be stimulated by forcing high pressure fluids into the hot rock layer in order to produce economically feasible amounts of heat. The process of stimulation induces fractures through which fluids can flow and absorb heat. Induced rock fractures can be remotely measured using microseismic methods. Rial et al. (2005) explore shear wave splitting as a viable method to measure microfracture growth. The method is based on the principle that shear waves travelling parallel and perpendicular to the principle fracture plane propagate at different velocities and that change in velocity is proportional to fracture density. However, shear wave splitting analysis cannot provide any information about fluid content nor connectivity of the fracture system. Therefore, another method is needed to complement the microseismic data.

Magnetotellurics passively measures the earth's response to changes in the earth's magnetic field and is sensitive to material properties, primarily the electrical conductivity of rocks and fluids in the subsurface. Hot fluids under pressure with high ion concentrations have enhanced conductivity characteristics, which can be measured with MT. Furthermore, multiple MT surveys over the same grid at different time intervals could produce a time lapse of subsurface fluid movement, effectively monitoring geothermal reservoir fluid flow. Spichak and Manzella (2008) claim that MT is the most effective electromagnetic method for defining conductive reservoirs.

The main goal of this project is to show that magnetotellurics is a viable method for characterising and monitoring enhanced geothermal systems. First, a forward model will be created using existing geological information of the test site. Then, before fractures are induced to produce a reservoir, a grid of MT stations will be set up at the test site such that a 3D resistivity image can be produced from the data. A few MT stations will be deployed permanently during the fracturing process from which conductivity will be measured as a function of time. After fracturing, another survey will be collected with plans to collect more surveys at intervals on the order of months. These surveys will provide spatial subsurface conductivity images as a function of time.

Hypothesis:

Geothermal fluids have enhanced conductivities due to high temperatures and pressures and high dissolved ion concentration. The dissolved ions will be a mixture of initial concentrations of salts as well as ions dissolved into the fluid picked up from lithology. Ussher et al. (2000) demonstrate that there are two conduction mechanisms in clay-rich sediments; firstly, conduction via pore water and secondly, through the double layer of cations. Temperature is the measurement of how fast particles are moving, which means at higher temperatures charges can move faster and easier under the influence of an external electromagnetic field, increasing the conductivity. When these fluids enter the fractured system, conductivity may increase by an order of magnitude or more, which will cause a change in the MT response. MT measurements crossing an area of a fractured system with two perpendicular lines will allow the delineation of the vertical and horizontal extent of the fluid-filled fractured rock. Other material properties of the fluids could also be estimated from the MT response such as temperature, porosity, permeability and salinity (Spichak and Manzella, 2008).

Another interesting phenomenon that might be explored in these surveys is seismoelectric effects due to fracturing. Seismoelectrics is based on the theory that seismic events cause charges to move which creates currents. More precisely, the double layers between pore electrolytic fluids and pore wall geometries emit an electric signal when displaced by seismic activity (Pride and Haartsen,

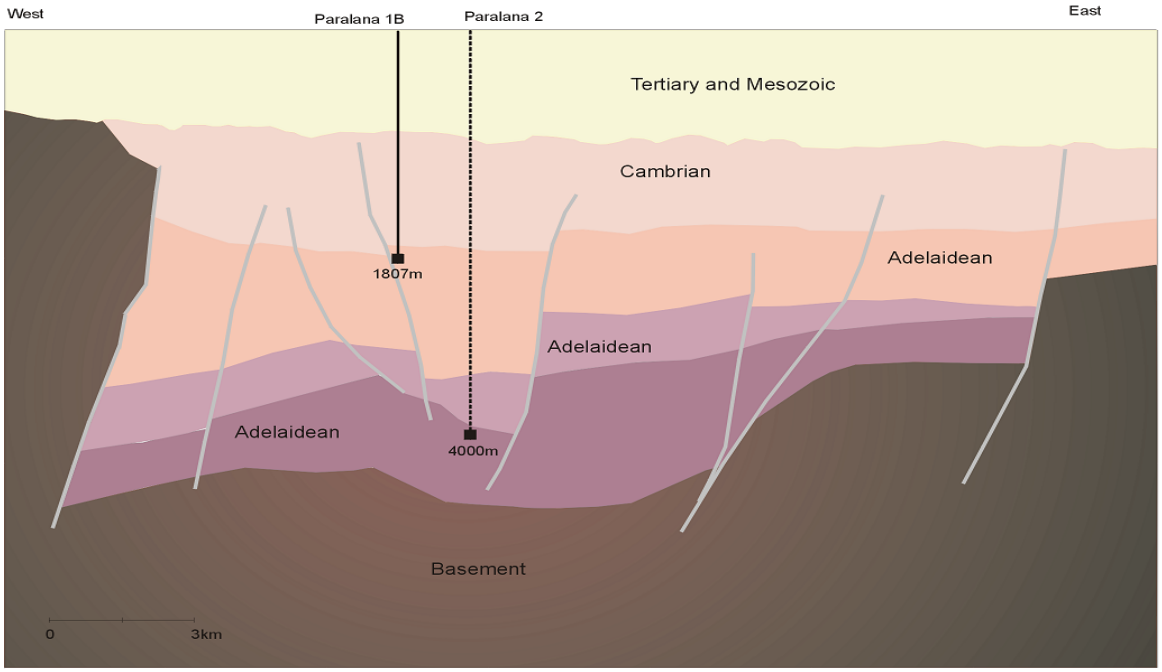

Illustration 1: Interpreted geological cross-section across the EGS site at Paralana.

1996). If the seismic, electric and/or magnetic fields are measured simultaneously, relationships between various material properties can be derived, such as resistivity and seismic velocity (Garambois and Dietrich, 2001, Haines et al., 2007).

The test site at Paralana, South Australia, has a conductive sedimentary layer near the surface with a few hundreds of meters thickness. The sedimentary layer overlies a more resistive basin. Two faults bound the proposed reservoir, which has a lateral extent of a few hundred meters at about 3-4km depth.

Procedure:

First, a geological model of the test site at Paralana will be produced using existing geological information such as regional structures along with well log data. This information will then be used to forward model the MT response of the existing geology before fracturing is induced. This will provide a control with which to compare changes in conductivity of the fractured layer. To simulate fluid injection, a conductive layer will be inserted in the Mt forward model at a depth of the proposed fracturing. A range of conductivity values will be used reflecting expected values calculated from Archie's Law using provided parameters (Archie, 1942). The conductive layer will then "flow" through the model by laterally expanding the conductive area of the forward model in incremented steps. At each step the MT response will be calculated. This will provide information about the type of MT responses predicted for the test site, which will give vital information about the measurement spacing and frequency ranges to be used.

Next, preliminary MT surveys will be collected at the test site in late November to early December 2009. The survey will include two perpendicular 2D lines and a small grid that covers the proposed reservoir. The MT data of the 2D lines will be inverted to obtain a 2D resistivity image of the subsurface underneath the drill site. This will provide constraints of the resistivity distribution in the east-west and the north-south direction. The additional MT sites outside the two 2D lines across will provide additional constraint.

Fracturing will then be induced into the reservoir in January 2010, which should take around one month to complete. A microseismic network will be in place during the fracturing process to monitor seismic events associated with the oping of the fractures. A few MT stations, covering a grid extending over the reservoir and powered by solar panels, will be deployed to collect data while fracturing is induced. This will provide time lapse data as well as detect possible seismoelectric effects when correlated with microseismic data. The data will be downloaded at intervals on the order of weeks and processed to produce 3D images of subsurface conductivity (Newman et al., 2008), from which the extent of the fluid-filled reservoir can be estimated if the resolution permits.

During and after fracturing, MT measurements will be repeated along the two 2D lines and compared to the MT data collected before the stimulation. Thus, this survey will provide information about the change of conductivity as a function of time, and will help to relate the outcomes with the extent of the fluid-filled reservoir.

References

Archie, G., 1942, The electrical resistivity log as an aid in determining some reservoir characteristics: Trans. A.I.M.E., v.146, p. 54-62.

Garambois, S. and Dietrich, M., 2001, Seismoelectric wave conversion in porous media: Field measurements and transfer function analysis: Geophysics, v. 66, p. 1769-1778.

Haines, S. S., Pride, S. R., Klemperer, S. L., Biondi, B., 2007, Seismoelectric imaging of shallow targets: Geophysics, v. 72, no. 2, p. 9-20.

Newman, G. A., Hoversten, M., Gasperikova, E., Wannamaker, P. E., 2008, Three-dimensional magnetotelluric characterization of the Coso geothermal field: Geothermics, v. 37, p. 369-399.

Pride, S., and Haartsen, M. W., 1996, Electroseismic wave properties: Journal of the Acoustical Society of America, v. 100, p. 1301-1315.

Rial, J. A., Elkibbi, M., Yang, M., 2005, Shear-wave splitting as a tool for the characterization of geothermal fractured reservoirs: lessons learned: Geothermics, v. 34, p. 365-385.

Spichak, V., and Manzella, A., 2008, Electromagnetic sounding of geothermal zones: Journal of Applied Geophysics, doi:10.1016/j.jappgeo.2008.05.007.

Ussher, G., Harvey, C., Johnstone, R., Anderson, E., 2000, Understanding the resistivities observed in geothermal systems: Proceedings World Geothermal Congress, Kyushu-Tohoku, Japan, p. 1915-1920.

Completion of Habanero Closed-loop Circulation Test

Doone Wyborn[1*].
[1] Geodynamics Limited. PO Box 2046, Milton, QLD, 4064.
* Corresponding author: doone.wyborn@geodynamics.com.au

Geodynamics has been working towards its "Proof of Concept" Enhanced Geothermal System (EGS) since drilling its first deep well in 2003 into the basement granites beneath the central Cooper Basin, NE South Australia. By 2008 there were two successful wells 560m apart connected by a stimulated fracture system located at a depth of 4,250m where the rock temperature is 247°C.

Initially open loop testing was employed involving production to a pit then re-pressurization back to reservoir pressure with oil industry "frac" pumps. In late 2008 a high pressure pipe line was completed connecting the two wells at surface, and by December 2008, after initial pump failures, a six week circulation was commenced. The circulation involved flow from Habanero 3 using the natural artesian pressure, keeping the fluid at full flowing wellhead pressure through the surface pipeline, cooling the fluid near the re-injection well Habanero 1 with an air cooled heat exchanger, and using a 41-stage centrifugal pump to re-inject the fluid back into the reservoir.

The results of the circulation test and of the associated tracer testing will be presented. The success of the circulation led Geodynamics to announce completion of its "Proof of Concept" in March 2009.

Keywords: Enhanced Geothermal System, circulation test, tracer test, stimulated reservoir.

Background

Geodynamics formed as a single purpose company in November 2000 to develop hot fractured rock (now generally known as Enhanced Geothermal Systems, EGS) geothermal energy from a unique non-volcanic environment represented by basement high-heat-production granites overlain by insulating sediments. Oil industry drilling had identified the central part of the Cooper Basin in an area known as the Nappamerrie Trough as an ideal site for such development. In addition the oil exploration had reported that the stress field is close to overthrust with minimum principle stress vertical. Under such conditions hydraulic stimulation of fractures would in preference take place on sub-horizontal existing natural fractures. These conditions were envisaged to be ideal for large scale multi-well EGS development.

The first well (Habanero 1), drilled in 2003, identified high fluid overpressures in the existing natural fractures, and these overpressures caused difficulty in drilling. In order to control these overpressures the use of heavy drilling mud resulted in mud losses that caused damage to the natural fractures reducing their ability to flow. Habanero 1 was completed to a depth of 4,421m and a fracture system at about 4,250m was stimulated by massive injection in late 2003 where the rock temperature is 247°C.

A second well, Habanero 2 was drilled 500m to the SW of Habanero 1. However difficulty with the existing drilling method and the fracture overpressures resulted in an eventual suspension of a side track in the well with stuck drill pipe left in the hole 79m below the top of the granite at 3,784m. Prior to the sidetrack the well had intersected the stimulated reservoir at a depth of 4,325m and the well flowed at rates up to 20 kg/second with surface flowing temperatures up to 210°C. Pressure responses in Habanero 1 whilst flowing from Habanero 2 indicated strong connection via the fracture system at 4,250m between the wells.

A second massive stimulation from Habanero 1 was completed in 2005 which extended the stimulated reservoir outwards to occupy an area of approximately 4 km^2 in plan view. This reservoir resulted from the injection of 40,000 m^3 of water in total in 2003 and 2005. It was defined by the location of 45,000 micro-seismic events. The 2005 stimulation proved that stimulation created permanent enhanced fracture flow capacity as the 2005 micro-seismic events commenced essentially where the 2003 events finished.

Habanero 3, the new production well was completed in February 2008 at a distance of 560m NE of Habanero 1 or slightly more than 1 km from Habanero 2. The stimulated reservoir was intersected at the predicted depth at 4,181m, and a pressure response at Habanero 1 was observed before drilling parameters were recognised as detecting the intersection.

Immediately after reaching TD of 4,221m the well was logged with the Baker Atlas circumferential borehole imaging tool (CBIL). The tool was deployed to the fracture zone area as quickly as possible and proceeded to log down. The tool managed to log the whole of the fracture zone before the temperature rendered it inoperable at a depth of 4,207m. Its temperature rating is 205°C, but the tool actually continued to operate to a temperature of 220°C, a very commendable performance. The image through the main part of the fracture is shown in the picture below (Figure 1).

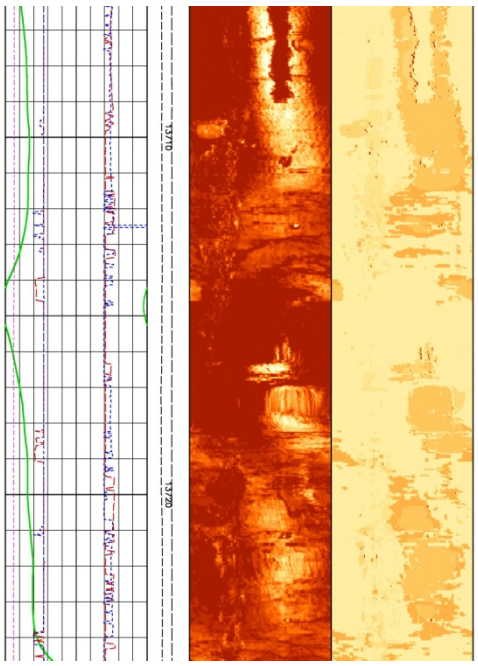

Figure 1 CBIL image of main fracture zone at 4181m (13,716 ft). The dark area in the centre of the image represents a cavity in the borehole formed where a large fracture intersects the wellbore.

Open-Loop Circulation Test

The open-loop flow test was designed to demonstrate communication between Habanero 1 and 3 along the fracture zone stimulated from Habanero 1 in 2003 and 2005, and to determine the impedance or friction loss associated with circulation between these wells. The impedance governed the pumping requirement for closed loop operation, which in turn dictated the operability of the pump that had been purchased for this phase. If the impedance was too high, the pump would not be suitable and a number of remedial actions would need to be effected.

Habanero 3 was drilled to 40m below the main intersection of the reservoir and completed with a 7 inch perforated liner. The rig demobilised with the well left with a mud weighted to accurately balance the fluid overpressure from the fracture zone. The fracture pressure was estimated at 74 MPa at a depth of 4,181m or 34 MPa above hydrostatic. This pressure is the same as the shut-in pressure observed at Habanero 1.

In order to bring the well on to flow a coil tubing unit was used to progressively clean out the mud to water. By the time the coil had reached about 2,000m depth it was clear that the well was flowing so the coil was removed. The well was cleaned of mud and filled with water derived from the fracture system.

Open-loop testing was based on flowing Habanero 3 through a wing valve and two chokes, a fixed sized choke and a variable choke in parallel, with the fluid flashed to low pressure through the chokes and delivered in an 8 inch pipeline to a steam separator. The fluid level in the separator was adjusted by a control valve on the liquid outlet side. In this outlet line there was also placed a magnetic flow meter and electrical conductivity meter. The steam flow rate was measured by a pitot tube located in the steam vent line.

Figure 2 Mud cleanout with coil tubing

Habanero 3 was opened to flow for the first time on 14 March 2008, and to the separator on 15 March.

The open loop testing can be divided into a number of phases as shown in Table 1 below:

Table 1; Open-Loop Operations in 2008

Operation	Date (2008)	Comment
Flow testing from Habanero 3 with Habanero 1 shut-in	14 to 21 March	A stable flow of 16 kg/sec at a flowing pressure of 27 MPa was achieved with a 14mm fixed choke. Wellhead temperature reached 209°C
Main open-loop circulation	22 to 25 March	Injection 18.5 kg/sec at 51.7 MPa (7,500 psi), production of 20 kg/sec at 27.5 MPa, an increase of 4 kg/sec over the earlier test with Habanero 1 shut-in. Temperature reached 212°C
HDC injection	26 March	Slow injection of HDC chemical barite dissolving agent in Habanero 1 to increase injectivity
Post HDC injection	26 March	Injection at 18.5 kg/sec at 50.3 MPa (7,300 psi), an improvement of 1.4 MPa. Expect further improvements with longer injection during closed loop operation.
Stimulation of Habanero 3	18-19 April	Injection of 2,173m^3 of water at injection pressures up to 64 MPa, resulting in 276 microseismic events close to Habanero 3. Expected increase in productivity

During the initial flows from Habanero 3 in mid March, Habanero 1 was shut-in, but pressure was monitored with a highly accurate quartz pressure gauge. Any change in flow conditions at

Habanero 3 was immediately recognised by the Habanero 1 pressure gauge indicating ideal connection between the wells in the main fracture zone (Figure 3).

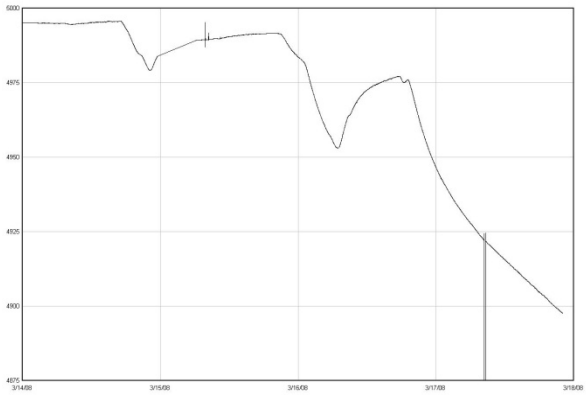

Figure 3. Pressure response of Habanero 1 pressure gauge during flow from Habanero 3 from 14 to 18 March 2008. Pressure on Y axis is in psi.

At the end of the main circulation on 25 March a pressure-temperature-spinner (PTS) logging tool was run to the main fracture and the well was shut-in. The flowing pressure at the fracture was stable during flow at 62.95 MPa, and rose within 20 minutes to 71.5 MPa after shut-in. This rapid rise indicates that most of the friction associated with flow is very close to the well-bore. The bottom hole temperature measured during logging was 244.5°C.

The HDC (barite dissolving agent) injection on 26 March (Table 1) was aimed at the 2,000 barrels of barite-rich drilling mud lost in the fracture system when Habanero 1 was drilled in 2003. Previous well test analysis of Habanero 1 indicated that the mud is inhibiting flow from Habanero 1 into the fracture system. The injection resulted in some improvement in the injectivity of Habanero 1.

Closed Loop Circulation Test

Circulation Impedance

The circulation pump was sized according to the understanding that the injectivity of Habanero 1 would be substantially better with Habanero 3 flowing than with Habanero 3 not flowing. This was a view that had been held since before flow testing of Habanero 2 in 2005, but it was never proven.

During the open loop circulation in March 2008 it became apparent that the injectivity into Habanero 1 was restricted and HDC was used to try to improve this. Once the circulation was achieved this improvement was not as good as hoped. Under the conditions at the time, at a pump design pressure differential of 11 MPa the pump could only deliver around 12 kg/second into Habanero 1. It is most likely that the lack of response at Habanero 1 to Habanero 3 flow is caused by the drilling mud lost around Habanero 1 in 2003.

Despite the injectivity problems of Habanero 1, the pump was capable of carrying out circulation operations that would allow the determination of reservoir parameters from injection of chemical tracers, so preparation for the tracer testing phase began. The six-week circulation and tracer test was likely to improve the injectivity of Habanero 1 because (i) longer term cooling of the fractures immediately surrounding Habanero 1 would result in a contraction of the rock adjacent to the fractures and the fractures would open slightly decreasing impedance, and (ii) it was envisaged that the lost drilling mud in Habanero 1 would be gradually washed further into the reservoir with longer term flow, thus reducing the restriction.

Initial Closed-loop Operations

Start-up closed-loop operations in August 2008 were beset with problems involving (i) blockage of the grit arrestor at Habanero 3, (ii) pump inlet seal failure, (iii) cooling fan vibrations, (iv) generator overheating, (v) leaking plugs, (vi) a flange washout and (vii) gradual loss of efficiency of the air cooler.

The air cooler efficiency loss turned out to be caused by scaling of the antimony sulphide mineral stibnite. The cooling of the formation water from over 200°C to less than 100°C resulted in its precipitation. Fortunately this material is relatively easy to remove as it does not adhere to pipe like other common scales (calcite, anhydrite, and silica).

The pump inlet seal failure required the pump to be sent to Singapore for refurbishment. As a result the circulation test did not commence until December 2008.

Circulation operations

A data logging unit was installed to collect pressure and temperature readings every 30 seconds at a number of points on the system. Flow rate was measured using an orifice plate set immediately after the air cooler, and before the re-injection pump. The orifice plate was calibrated using two turbine flow meters set on a temporary flow line to a pit. During the calibration, flow was directed to the pit via the flow cross on the Habanero 1 wellhead. A sampling panel on a side capillary line was used to collect fluid samples for tracer analysis. The sampling panel also had installed pH, conductivity and dissolved oxygen sensors.

Between the pump and the Habanero 1 wellhead a 700 ml pressure vessel was installed on a 1 inch sideline for collection of fluid at high pressure and at a defined temperature. The chamber was wrapped in a heating blanket that controlled the temperature. This apparatus was designed to measure the polymerisation rate of silica at re-injection temperature. Fluid samples were left in the chamber for a pre-determined period and then

collected and immediately measured for monomeric silica (H_4SiO_4) using the ammonium molybdate method. In this way the rate of polymerisation could be determined to asses the potential for silica scaling in the re-injection well.

By 11 December 2008 the pump had been re-installed after its trip to Singapore. The operation was run for several days to assess reliability of equipment and data collection. In the afternoon of 17 December 2008 the system was shut down for 5 hours while 1000 l of fresh water with 100 kg on 1-3-5 naphthalene tri-sulphonate and 50 kg of fluorescein was injected down Habanero 1. The tracer chemicals were injected using a pressure testing injection pump (the tracer story is described in an accompanying paper at this conference (Yanagisawa et al., 2009)). The pump was then re-started and the six week tracer test commenced.

Operating pressure conditions and flow rates were initially as expected, based on earlier understanding of the drilling mud damage at Habanero 1. The stable flow rate was slightly less than 12 kg/second. During the following weeks the system was shut down for short periods and after each shut down the stable flow rate increased slightly. It was noticed that during initial pump start-up with each shut-down that the pump could inject at a higher flow rate whist the reservoir was pressurizing up. The flow rate during these start-ups was greater than 20 kg/second and it was not until several hours later that the flow rate settled to a stable rate once the injection pressure had also stabilised.

Progressively over the circulation test the stable flow-rate increased so that by the end of the test the flow rate was 15.5 kg/second, and was still increasing. The pump differential of 11 MPa remained essentially the same throughout the test so that the overall circulation efficiency increased by 30% over the test period. Barite and fine granite particles were collected from the flow from time to time indicating clean up of the fracture network, and this most likely explains the increasing efficiency. The high flow rates on pump start-up most effectively contributed to the clean up explaining the slight increases in stable flow after each start-up.

The tracer results (Yanagisawa et al., 2009) indicated a tracer swept pore volume of 18,500 m^3. On the basis of the modelling of stream-lines (Figure 4, unpublished data from our reservoir analysis consultants Q-con GmbH) it can be reasoned that the pore volume of the whole reservoir (black polygon in Figure 4) is close to 40,000 m^3.

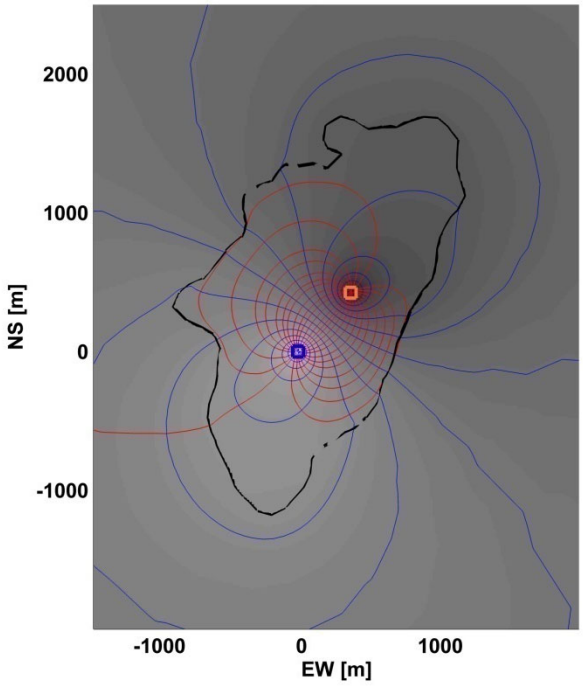

Figure 4; Stream-lines of circulation modelled on the limits of the reservoir based on the stimulation area (black polygon). Red lines represent stream flow, blue lines isobars. Modelling carried out by Q-con GmbH.

The estimated pore volume of the reservoir is approximately equal to the volume of fluid injected during the 2003 and 2005 stimulations. Thus it appears that the stimulation created new pore space about equal to the fluid volume pumped, and that the fracture fluid volume prior to stimulation was quite small. This attests to the effectiveness of stimulation and its necessity.

Summary

The six-week Habanero closed-loop circulation test took place over the period December 2008 to February 2009. The test enabled Geodynamics to announce its “Proof of Concept” in March 2009. During the test the circulation efficiency increased by 30% and this was mainly attributed to the cleaning out of drilling mud lost into the fractures during the drilling of Habanero 1 in 2003. The pore volume of the reservoir is approximately equal to the fluid volume pumped during the stimulations in 2003 and 2005.

References

Yanagisawa, N., Rose, P., and Wyborn D., 2009. Habanero Tracer test in the Cooper Basin, Australia: Key Results for EGS Development. Australian Geothermal Conference 2009, Brisbane.

Enhanced Geothermal Reservoir Simulation

Huilin Xing*, Ji Zhang, Yan Liu, Hans Mulhaus.
The University of Queensland, Earth System Science Computational Centre, St Lucia, QLD 4072.
* Corresponding author: h.xing@uq.edu.au

This paper introduces the current state of art in computer modelling of enhanced geothermal system (EGS) and expends our research efforts in high performance simulation of EGS. We include a brief introduction of our integrated geothermal reservoir simulator PANDAS and its applications in: (a) model benchmark, (b) fracture and permeability evaluation based on recorded microseismic events and (c) simulation and evaluation of a certain multiple well EGS. We demonstrate the usefulness and efficiency of our software PANDAS.

Keywords: enhanced geothermal reservoir, simulation, finite element, permeability, HDR/HFR/HWR, microseismicity.

Introduction

A large amount of research and testing on EGS, such as HDR (hot dry rock), HFR (hot fractured rock) and HWR (hot wet rock) geothermal reservoirs, have been accomplished worldwide in the past 30 years including reservoir construction, fluid circulation and heat extraction. A successful EGS reservoir strongly depends on thermal-fluid flow distribution at any given time. This is primarily determined by: (1) the nature of the interconnected network of hydraulic stimulated joints and open fractures (including both stimulated and natural) within the flow-accessible reservoir region; (2) the mean temperature and pressure in the reservoir; (3) the cumulative amount of fluid circulation (reservoir cooling) that has occurred; and (4) water loss (e.g. Brown et al., 1999). In order to understand, model and predict the thermal power performance of an EGS reservoir, it is necessary to have good measures and understanding of the following two interrelated reservoir properties: (a) the effective heat transfer volume at high temperature; and (b) the fracture/joints and its distribution within the effective heat transfer volume. Both highly affects the reservoir characteristics (i.e. permeability), which are complicated and are functions of the applied reservoir pressure/stress that are controlling the nature and degree of interconnection within the network of fractures.

EGS – A THMC coupled system

A literature survey (e.g. Bjornsson and Bodvarsson, 1990) on thermal, hydrological and chemical characteristics of geothermal reservoirs and their relevant parameters - permeability, permeability-thickness, porosity, reservoir temperature and concentration of dissolved solids and non-condensable gases – suggests that reservoir permeability, porosity and total dissolved solids tend to be a function of temperature. Permeability and porosity generally decline with increasing temperature, while the concentration of dissolved solids increases with increasing temperature, reflecting a general increase in mineral solubility. A possible explanation of decreasing permeability with temperature is a local increase in crustal stresses caused by thermoelastic phenomena. Thermal expansion of the reservoir rocks will reduce the number voids and cracks in the rock matrix and hence reduce permeability. Another major factor that affects the permeability is mineral deposition. For example, the solubility of calcite decreases with increasing temperature, causing clogging of pore spaces at high temperatures. All the above demonstrates that an EGS is a complicated Thermal-Hydro-Mechanical-Chemical (THMC) coupled system, which requires more comprehensive understanding and modelling of coupled processes than is commonly done in standard reservoir engineering.

Recent studies on computer modelling

Recent studies on computer modelling the conventional geothermal reservoir engineering and the EGS/HDR system are reviewed by O'Sullivan et al. (2001) and Sanyal et al. (2000) respectively. They show that computer modelling is routinely applied in conventional hydrothermal reservoir engineering, but it is comparatively premature in EGS simulation which still rely much on the EGS expertise and feedback of practical active modellers and engineers. Based on the above and other recent studies, existing simulators are faced with following challenges: (1) Geomechanical deformation/rock stress and its fully coupling with the multiphase thermal-fluid flow and chemicals are not addressed yet. Such coupled models are critical for analysing the geothermal reservoir system especially for EGS. Further research is needed in exploring different approximations for coupled processes with vastly different intrinsic spatial and temporal scales. Such a coupled treatment can potentially provide a more realistic description of geothermal reservoir processes during natural/stimulated evolution as well as during exploitation. It can also provide added constraints that can help reduce the inherent uncertainty of geothermal reservoir models; (2) a reliable fully-coupled treatment of 3D fluid flow and mass transport with detailed chemical interactions between aqueous fluids, gases, and primary mineral assemblages still requires further research. This is currently available in hydrothermal code TOUGH2, but not

available in the other codes including all the HDR simulators/FEM simulators; (3) the relevant reservoir model generation and meshing are still difficult and time consuming especially for fracture dominated EGS. The finite differential method is widely used in geothermal modelling but requires regular rectangular mesh structure. The popular geothermal code TOUGH2 may handle irregular meshes theoretically, but most of models set up using TOUGH2 contain some structure, such as layering. It is impossible to explicitly describe the complicated fractures in an EGS reservoir with such mesh structures. Unstructured mesh may be a better choice, but no unstructured mesh based solver-finite element solver- as powerful as such as TOUGH2 is available for geothermal simulation yet; (4) no module for visualizing microseismicity and evaluating the relevant rupture and permeability distribution for the further simulation has been integrated into the simulator so far; (5) No multiscale computing or parallel computing involved in the widely available geothermal simulators yet despite their well-studied and widespread application in other fields.

In conclusion, further computational model and code developments are urgently needed to improve our understanding of geothermal reservoir and the relevant natural and/or enhanced evolution such as of enhanced geothermal reservoir system, and achieve a more accurate and comprehensive representation of reservoir processes in more details, to reduce the uncertainties in models, and to enhance the practical utility and reliability of reservoir simulation as a basis for field development and management (e.g. O'Sullivan et al., 2001, Sanyal et al., 2000). This presentation will focus on our research efforts towards high performance simulation of enhanced geothermal reservoir systems.

An Integrated Geothermal Reservoir Simulator

PANDAS - Parallel Adaptive static/dynamic Nonlinear Deformation Analysis System - for simulating the coupled geomechanical-fluid flow-thermal systems involving heterogeneously fractured geomaterials is being developed using finite element method (FEM). It addresses the key scientific and technological challenge in developing enhanced geothermal energy. Namely, it is targeting a new predictive modelling capacity spanning different temporal and spatial scales with the potential to yield breakthroughs in understanding how to enhance the flow of water through the enhanced geothermal field and how to sustain it over decades such that the trapped heat energy can be extracted.

Currently, PANDAS includes the following five key components: Pandas/Pre (for visualizing and evaluating microseismic events and the relevant ruptured zone and permeability, mesh generation), ESyS_Crustal (FEM solver for an interacting fault system), Pandas/Thermo (FEM thermal solver), Pandas/Fluid (FEM solver for porous media flow) and Pandas/Post (for visualizing computing results). All the above modules can be used independently or together to simulate individual or coupled phenomena (such as interacting fault dynamics, heat flow and fluid flow) with or without coupling effects. It aims to provide (a) visualization the recorded microseismic events and further evaluation of the fracture location and evolution, geological setting, the reservoir characteristics (e.g. permeability) and mesh generation; (b) a non-linear finite element based numerical solution to model and evaluate a certain geothermal reservoir under various affecting factors. For more details, refer to Xing et al (2002; 2006a; 2006b; 2007; and 2008).

Benchmark and Application Examples

PANDAS has been applied in several different cases. We list a few of examples to show its accuracy, stability, usefulness and efficiency in simulating the enhanced geothermal reservoir system.

Benchmark of computational model

Verification and benchmark testing of our finite element based geothermal code PANDAS are accomplished by comparing the available analytical solutions and/or the widely accepted results with those calculated by PANDAS. So far, the following cases have been tested; only the case 3) is further described here.

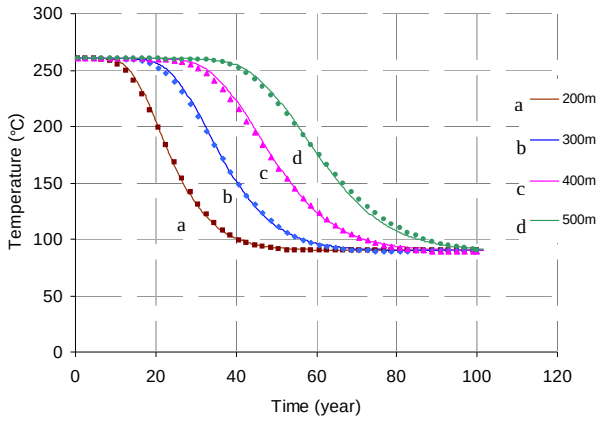

Figure 1: Comparison of FEM result with analytical one (curves) on thermal-fluid flow in fractured rocks. It shows the fluid temperature evolution at different positions of the fractured zone. Around the production well (500m), the temperature remains above 150℃ at 60 years. Assuming an allowable maximum temperature decrease of 40℃ at the projection well, it will last up to 50 years with the injection rate of 0.017litre/s. Refer to Xu et al., (2007) for the detailed model description.

1) Heat transfer/Darcy flow in porous media (analytical solution available)
2) Convection dominated thermal-fluid flow in porous media (analytical solution available)
3) Thermal-fluid flow in fractured rocks (analytical solution available for a single fracture)
4) Two phase thermal-fluid flow in porous media (water and vapour, DOE (Department of Energy, USA) benchmark result).

Fluid flow in most enhanced (HDR/HFR) geothermal reservoirs is dominated by fractures and their distribution, which corresponds to the benchmark case 3). How the fractures affect the heat transfer between the fluid and the rock mass during injection process must be critically addressed. To investigate the advancement of the thermal fluid during the injection process into the fractured reservoir system, PANDAS is verified through comparison with the analytical solution of a simplified reservoir system consisting of a horizontal fracture intersecting an injection well and a production well as detailed in Xu et al. (2007). The analysed zone spans 30m thickness along the vertical direction and is composed of a main horizontal fracture and a permeable rock mass. To be analysed by both the analytical and finite element methods, in which the permeability of the 30m thick (D=15m) fracture zone is taken as 1.0E-30 in FEM simulation (close to zero to compare with the analytical solution). The transmissibility of the main fracture with the aperture H=0.01m down the middle of the fracture zone is 1 Darcy metre; and the temperature of injected fluid is 90℃, the initial temperature of rock matrix is 260℃. Figure 1 shows the benchmark result of two wells with the distance of 500m. The FEM calculation result agrees well with the analytical solution.

Microseismicity and EGS reservoir

Hydraulic stimulation is a basic concept of improving the residual permeability of the in-situ rock mass at depth and still remains the main mechanism to be envisaged for the creation of an enhanced geothermal reservoir (i.e. HDR/HFR/HWR). PANDAS has been developed and applied to visualize the microseismic events, to monitor and determine where and how the underground rupture proceeds during a hydraulic stimulation process, to determine the domain of the ruptured zone and to evaluate the material parameters (i.e. the permeability) for the further numerical analysis. Figure 2 shows the permeability distribution of a geothermal reservoir calculated from the microseismic events recorded during a hydraulic stimulation process. A virtual 8-well geothermal reservoir (i.e. 1 injection well + 7 production wells in a reservoir with the dimensions of Length x Width x Height:

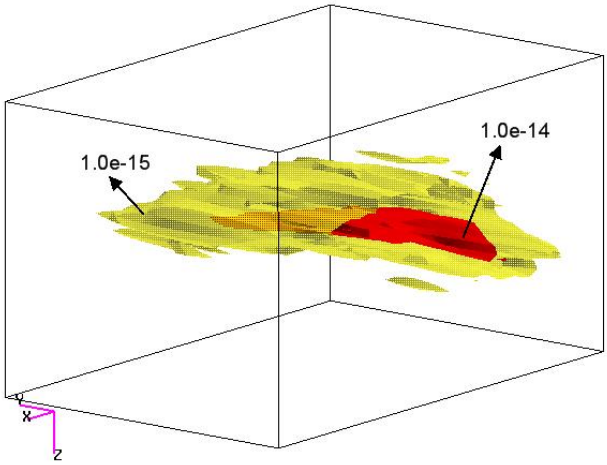

Figure 2: An example of the calculated permeability distribution of a geothermal reservoir thorough the microseismic events recorded during a hydraulic stimulation process.

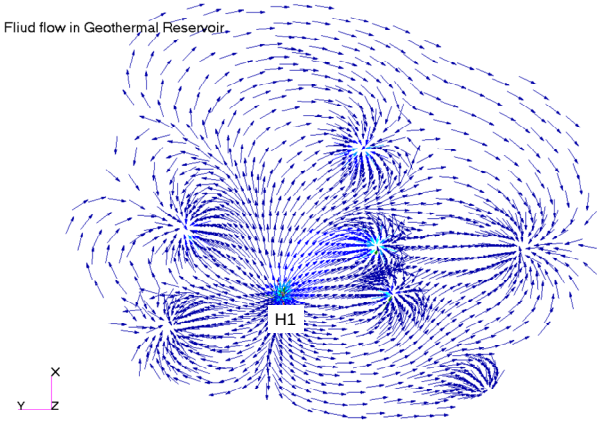

Figure 3: The simulated fluid flow in a certain fractured geothermal reservoir with 7 production wells and 1 injection well H1. It is calculated in 3D but shown in a certain cross-section here.

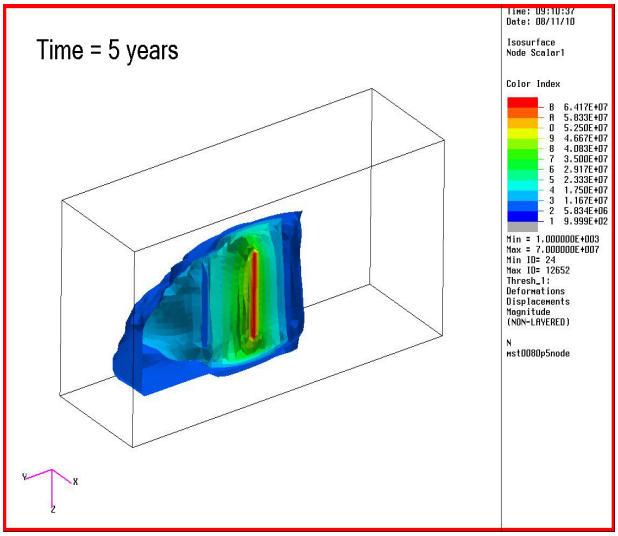

Figure 4: The simulated hydraulic pressure distribution at 5 years in a certain fractured geothermal reservoir with 7 production wells and 1 injection well H1(Figure 3).

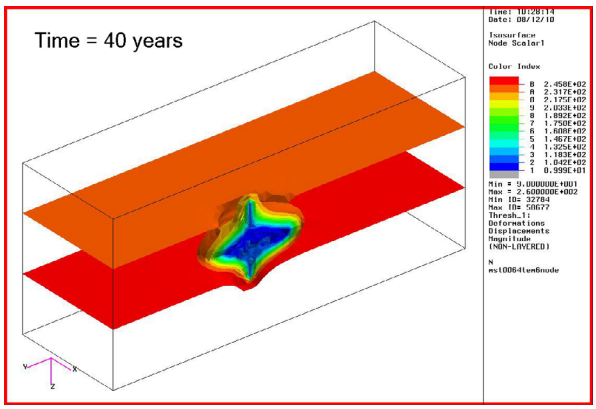

Figure 5: The simulated temperature distribution at 40 years in a certain fractured geothermal reservoir with 7 production wells and 1 injection well H1 (Figure 3)

4000 m x 3000 m x 1750 m) is designed and further analysed using PANDAS. The snapshots of the relevant results are shown in Figures 3, 4 and 5 with one injection well located at H1 (Figure 3).

Summary

We discuss the key improvements required in simulating an enhanced geothermal reservoir system (HDR/HFR/HWR) for further improving our understanding of geothermal reservoir and the relevant natural and/or enhanced evolution such as of EGS based on relevant studies. The goal is to achieve a more accurate and comprehensive representation of reservoir processes in more detail and reduce the uncertainties in models, and enhance the practical utility and reliability of reservoir simulations as a basis for field development and management. Our research in PANDAS towards high performance simulations of enhanced geothermal reservoirs is introduced and then verified using relevant benchmarks. It is further applied in a virtual design and assessment of a multiple well reservoir system based on the permeability distribution calculated from the recorded microseismic events. Both benchmark and application examples demonstrate its accuracy, stability and potential usefulness in simulating the enhanced geothermal reservoir system. PANDAS will be further developed for a multiscale simulation of multiphase dynamic behaviour for a specific geothermal reservoir system. More details and additional application examples will be given during the presentation.

Acknowledgements

Support is gratefully acknowledged by the Australian Research Council and Geodynamics Limited through the ARC Linkage project LP0560932. The authors are grateful to Dr Doone Wyborn of Geodynamics Limited for his constructive advice and support, to Dr Hehua Xu, Mr Wenhui Yu and Dr Enlong Liu for their collaborations in the relevant research.

References

Bjornsson, G. and Bodvarsson, G. 1990, A Survey of Geothermal Reservoir Properties: Geothermics, v. 19, no. 1, p. 17-27.

Brown, D., DuTeaux, R., Kruger, P., Swenson, D. and Yamaguchi, T. 1999, Fluid circulation and heat extraction from geothermal reservoirs: Geothermics, v. 28, p. 553-572.

O'Sullivan M. J, Pruess, K. and. Lippmann, M. J. 2001, State of the art of geothermal reservoir simulation: Geothermics, v. 30, p. 395–429

Sanyal, S K, Butler, S J, Swenson, D and Hardeman, B. 2000, Review of the state-of-the-art of numerical simulation of enhanced geothermal systems: Proceedings World Geothermal Congress 2000, Tohoku, Japan, May28-June 10. p. 3853-3858.

Xing, H.L., and Makinouchi, A. 2002, Three dimensional finite element modelling of thermomechanical frictional contact between finite deformation bodies using R-minimum strategy: Computer Methods in Applied Mechanics and Engineering, v. 191, p.4193-4214

Xing, H. L., Mora, P. and Makinouchi, A. 2006a, A unified frictional description and its application to the simulation of frictional instability using the finite element method: Philosophical Magazine, v. 86, no.21-22, p. 3453-3475.

Xing, H. L., Mora, P. 2006b, Construction of an intraplate fault system model of South Australia, and simulation tool for the iSERVO institute seed project: Pure and Applied Geophysics, v. 163, p. 2297-2316. DOI 10.1007/s00024-006-0127-x

Xing, H. L., Makinouchi, A. and Mora, P. 2007, Finite element modeling of interacting fault system: Physics of the Earth and Planetary Interiors, v. 163, p. 106-121. doi:10.1016/j.pepi.2007.05.006

Xing, H. L. 2008, Progress Report: Supercomputer Simulation of Hot Fractured Rock Geothermal Reservoir Systems: ESSCC/ACcESS Technical Report, The University of Queensland, p.1-48

Xu, H, Xing, H. L., Wyborn, D and Mora, P. 2007, Analytical and numerical investigation of thermo-fluid flow of fracture dominated geothermal reservoir, in Yong Shi, Geert Dick van Albada, Jack Dongarra, and Peter M.A. Sloot (eds), Lecture Note in Computer Science (LNCS) 4489 (Computational Science-ICCS2007), Springer-Verlag, Berlin, Heidelberg. P. 1156-1163,

Fracture Simulation for Deep Crystalline Rock

Chaoshui Xu[1] and Peter A. Dowd[2]*
[1] School of Civil, Environmental and Mining Engineering, University of Adelaide
[2] Faculty of Engineering, Computer and Mathematical Science, University of Adelaide
* Corresponding author: Peter.Dowd@Adelaide.edu.au

This paper describes the application of simulated annealing for fracture modelling in crystalline rock. The technique is capable of incorporating the spatial correlations of fracture properties within a fracture set or across different fracture sets so that more realistic fracture systems can be simulated.

Keywords: marked point process, discrete fracture network, *K*-function, simulated annealing

Introduction

Realistic fracture models are crucial for the design and performance assessment of geothermal reservoirs, especially in hot dry rock (HDR) applications. The model is the fundamental input required for the modelling of fluid flow through the 3D fracture network comprising initial fractures and new fractures created by hydraulic stimulation. The characterisation of rock fracture networks is an extremely difficult problem not least because accurate field measurement of a single discontinuity is difficult and measurement of all discontinuities is impossible. For these reasons, in practical applications, there is no observable reality of the 3D network on any meaningful scale and the only realistic approach is via a stochastic model informed by sparse data and/or by analogues.

The first step in stochastic fracture modelling is data collection and statistical analysis, from which model parameters are derived. Data normally come from surveys of analogues, such as rock outcrops, or from direct or indirect observations of the rock mass such as drill cores, borehole imaging, geophysical surveys or seismic monitoring during fracture stimulation. In general, the outcomes of this step include the identification of fracture sets, the distribution characteristics of fracture locations, and statistical distributions of fracture properties, such as orientation, size and aperture. On the basis of these parameters it is then possible to generate a 3D fracture network for the reservoir, which is a possible "reality" in the sense that all statistical characteristics of the network are reproduced.

The two most commonly used mathematical methods for stochastic fracture simulation are Poisson planes (Dershowitz and Einstein, 1988) and random object models (Stoyan et al., 1995, Molchanov, 1997), with the latter more popular because of its flexibility for adaption to a wide range of applications. Current practice in random object models is to generate fractures via a Boolean-type approach (Stoyan et al. 1995, Molchanov 1997, Chilès and Delfiner 1999). The fractures are divided into sets and parameters for location, size and orientation are modelled separately for each set. The final fracture model is the combination of each set of fractures generated independently. Spatial correlation is considered only for modelling the fracture intensity which defines the number of fractures in a particular area (2D) or volume (3D). Other spatial correlations, either auto-correlation for an individual variable or cross-correlations between pairs of variables, within a fracture set or between different fracture sets, are generally ignored. These correlations, however, must be included to generate realistic fracture models.

Boolean object model

It is common practice to classify observed fractures (traces) into sets according to their orientations and to study each set independently. The separation of fractures into different sets is based on the belief that fractures formed by tectonic activity are likely to be oriented in approximately the same direction and to display similar properties (e.g., size, aperture). It is therefore reasonable to study the sets individually.

The generation of a Boolean object model is relatively straight-forward (Xu and Dowd, 2009). For a given fracture set, the fracture locations are generated first, usually by a Poisson distribution in which fracture intensity for a particular area (2D) or volume (3D) is either assumed to be constant or is derived from geostatistical estimation or simulation. Secondly, the orientation of each fracture is generated, most commonly from a Fisher distribution. Finally, the size of each fracture is generated from a specified distribution, the most common being exponential, lognormal or gamma. Other fracture properties, such as aperture and joint strength, can then be added into the network by additional Monte Carlo steps. Options for fracture intersections and termination/truncation can also be incorporated. Additional fracture sets can be generated in a similar fashion (independent simulation) to produce the final fracture model.

A common approach to the statistical analysis of fracture models is to use marked point processes. Fracture locations are represented by points (centre point or a random point on the fracture) in space and all fracture properties, such as orientation, size and aperture, are represented by marks associated with the points. In this context a Boolean object model can be described as a

realisation of a point process with independent markings. A two-dimensional example is given in Figure 1, which shows fracture traces on a Yucca Mountain outcrop, as mapped by Barton and Larson (1985). Similarly, three-dimensional representations of fractures by marked points can also be constructed provided the shapes of the fractures are assumed.

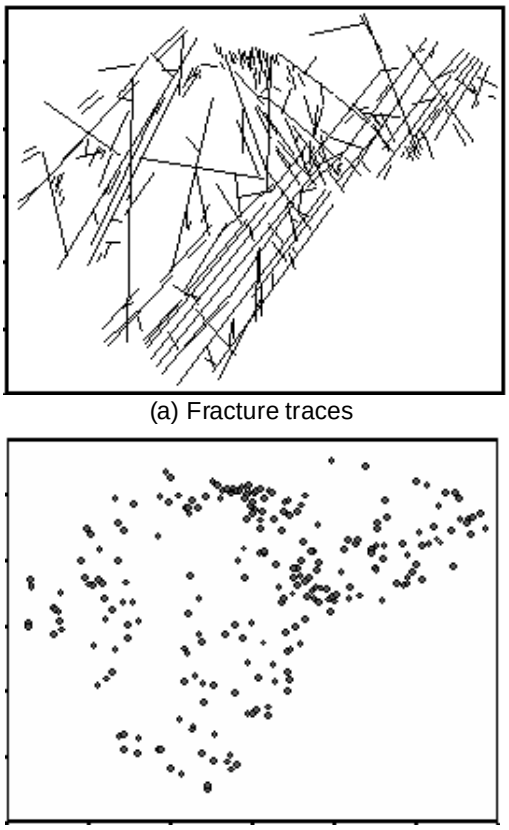

(a) Fracture traces

(b) Point representation

Figure 1 Two-dimensional fracture pattern and the corresponding point representation, Barton and Larson (1985)

This simplistic fracture model assumes no spatial correlation among the fracture sets, and no spatial correlation between fracture properties and fracture locations and among fracture properties themselves. The only spatial correlation model included in the model is the fracture point density defined as the number of fracture representation points per unit area (2D) or per unit volume (3D). This correlation is imposed either by using a geostatistical model to simulate the fracture point density or implicitly by various types of point patterns (homogeneous, non-homogeneous, cluster or Cox point process).

Spatial correlations in fracture modelling

In general, fractures sets tend to be correlated (Chilès and Marsily, 1993). This is supported by the observation that different fracture sets may be formed by different tectonic events active at different times, which raises the possibility that the formation of newer fractures is likely to be influenced by existing fracture networks. The extent and significance of the correlations can vary but can cover various aspects of the fracture properties. For example, five fractures sets are identified for the fracture pattern in Figure 1a; the auto- and cross- ***K***-functions of the fracture locations shown in Figure 2a and b (Xu and Dowd, 2008) show that the fracture locations of different fracture sets have some association and are not independent. Either a hierarchical model (Lee et al. 1990) or plurigaussian simulation (Dowd et al. 2007, Xu & Dowd 2008) can be used to incorporate these correlations into the fracture model. A cluster point process is another type of model that can takes the correlation of fracture locations into account during fracture model construction.

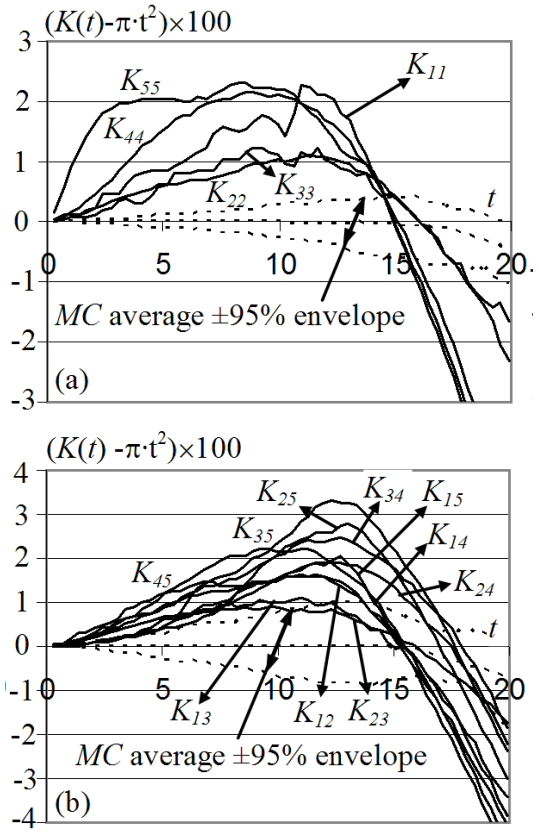

Figure 2 Auto- and cross- ***K***-functions for the point dataset Figure 1b

Fracture properties can also be correlated and the correlation can be among fractures in the same set or across different sets. These correlations are ignored in the Boolean object model, i.e., marks generated in the model are spatially independent. Practical observation and statistics (Priest 1993, Lee and Farmer 1993, Baghbanan and Jing 2007, Chilès and de Marsily, 1993) suggest high correlation between fracture size and aperture. Sizes and locations of fractures are always spatially correlated, even if the fractures belong to the same fracture set. The general practice of classifying fractures in sets and their

independent treatment is an indication that fracture properties are highly correlated with orientation. For realistic fracture modelling these correlations cannot be ignored.

Demonstration of the incorporation of correlations in fracture model

Figure 3a shows a simulated 3D fracture system generated in a volume of interest of size 100×100×100. In reality, such an image is difficult to obtain and we are restricted to the use of exposed 2D images such as rock outcrops or quarry faces. An example of this type of image is shown in Figure 3b, which was obtained by cutting Figure 3a by a north-south vertical cross-sectional plane (shown), thus simulating an exposed quarry face. The fracture trace lines on the image can now be analysed to construct a possible model to describe the pattern. Using the mid-points of the trace lines, the corresponding point dataset for the fractures is shown in Figure 3c.

We consider here two marks for each point, the fracture trace length, ξ, and orientation α. Angle α is measured clockwise from the vertical direction and it is, therefore, necessary to make the transform to $\beta = |\alpha - \pi/2|$ $(0 \le \beta \le \pi/2)$ for the convenience of analysis. After this transformation, small β values correspond to near horizontal lines (parallel to Northing direction in Figure 3a) and large β values suggest the lines are nearly vertical (parallel to vertical direction in the Figure 3a).
The correlation coefficient between ξ and β is estimated as 0.48 and the distributions of ξ and β are estimated using a kernel density estimate which show lognormal and uniform types respectively. We fit an approximate lognormal distribution with a mean of 0.8 and a variance of 2.0 in logarithmic scale for ξ. The positive correlation between β and ξ indicates that the two marks are highly correlated, i.e., vertical fractures tend to be longer than horizontal ones. In summary, for the example,

1. ξ follows a lognormal distribution (with estimated mean of 0.8 and variance of 2.0 in logarithmic scale).
2. α and β follow a uniform distribution on the interval [0, π].
3. ξ and β are positively correlated with correlation coefficient 0.48, i.e., in physical terms vertical fractures tend to be longer.

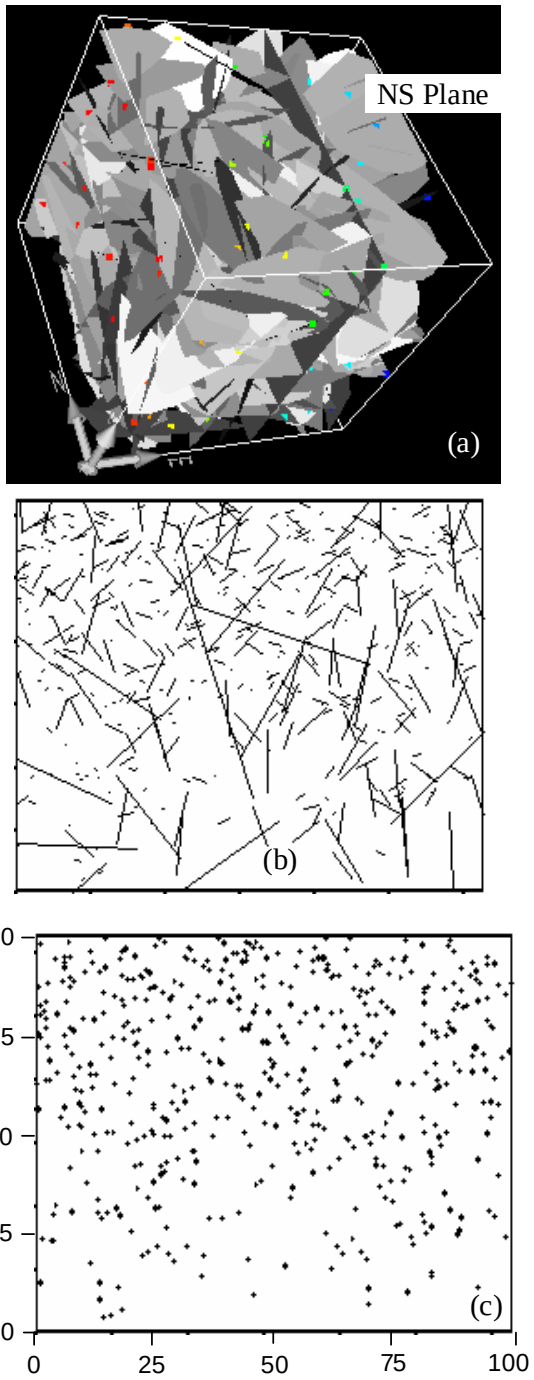

Figure 3 Simulated example: (a) 3D fractures, (b) Fracture traces on the plane, (c) Representing point pattern

To quantify the spatial correlations between ξ and β, we use the cumulative spatial mark correlation function introduced by Xu et al. (2007):

$$K_m(t) = \frac{1}{K(t)\,\bar{f}_m}\,\frac{g w_g}{\lambda^2}\int_0^t u^{g-1}\lambda_2^{(f)}(u)\,du$$

where $w_g = \sqrt{\pi^g}\,/\,\Gamma(1+g/2)$ is the volume of the unit ball in $\Re^g$, $K(t)$ is the second order ***K***-function, λ is the point density, $\lambda_2^{(f)}$ is the second order *f*-product density function for the point field and *f* in this definition is the application-dependent mark function. Based on this

definition, $K_m(t) \equiv 1$ if there is no correlation between marks at distance t.

For the example (Figure 3), Figure 4a shows the spatial auto-mark correlation function for fracture line length ξ and Figure 4b shows the spatial auto-mark correlation for fracture orientation β. The spatial cross-mark correlation function between ξ and β is given in Figure 4c. The Monte Carlo (MC) simulation envelope (average value and ±95% bounds) for the case of spatially uncorrelated marks is also plotted on the graphs. These three figures reveal some important spatial characteristics between the marks in the simulated example dataset; briefly:

4. Smaller values of $\hat{K}_{\xi}(t)$ for small t indicate that fractures (points) close to each other tend to be shorter (smaller mark ξ). In physical terms, aggregated fractures tend to be shorter in length. Although this feature is not apparent in Figure 3b, it is widely observed in practice that short fractures in rock tend to occur in clusters as the result of local thermal effects and long fractures caused by geological movement (forces) tend to be more isolated or sparsely distributed.
5. Smaller values of $\hat{K}_{\xi\beta}(t)$ for small t suggest that fractures (points) close to each other tend to be horizontal and shorter. In physical terms, aggregated fractures in this particular dataset are more horizontally oriented and longer fractures tend to be more vertically oriented and more sparsely distributed.
6. The flat appearance of $\hat{K}_{\beta}(t)$ suggests that, in terms of fracture orientation, there is no preferential direction of the pattern of fracture aggregation.

The aim of simulating a fracture set that resembles Figure 3b now becomes two fold:

i). The point pattern of the simulated fractures must resemble the point pattern in Figure 3c in such a way that the point intensity field $\lambda(X)$ and the first and second moment measures, such as the inter-event distance function $H(t)$ and the K-function $K(t)$, are honoured (Stoyan et al. 1995).
ii). The simulated fractures must follow the mark distribution, the multivariate mark correlation and their spatial auto- and cross-mark correlations as described in 1 – 6 above.

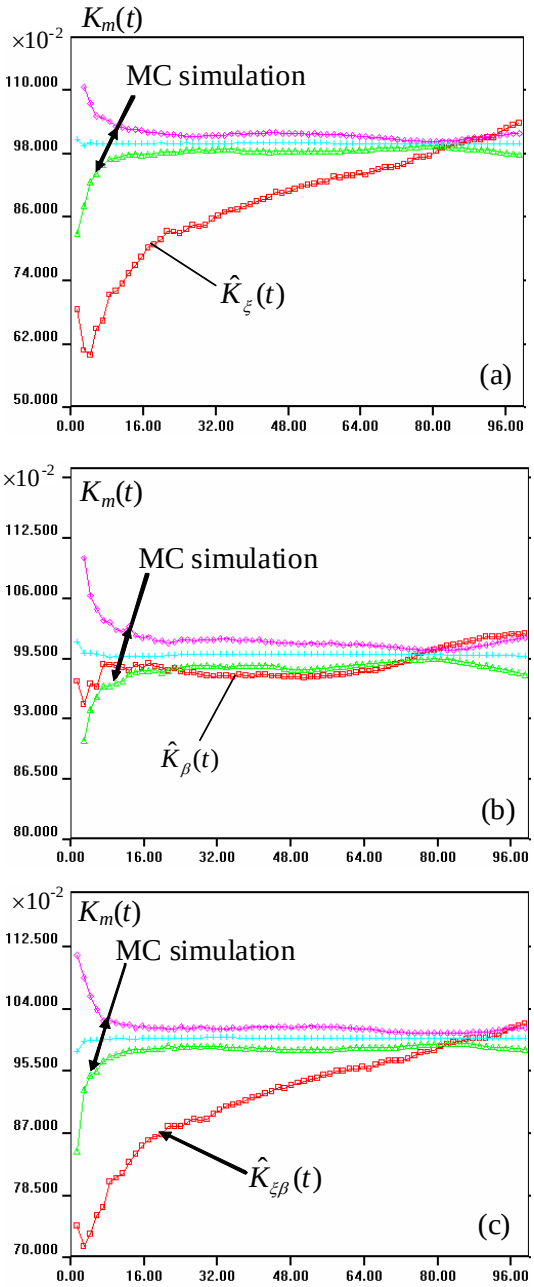

Figure 4 Corresponding cumulative mark correlation functions $\hat{K}_{\xi}(t)$ vs distance t (a), $\hat{K}_{\beta}(t)$ vs t (b) and $\hat{K}_{\xi\beta}(t)$ vs t (c) for the simulated example (Figure 3). The Monte Carlo (MC) simulation envelops shown are obtained for spatially uncorrelated marked point process

Problem i) can be solved, for example, by fitting an optimal non-parametric model (Xu et al., 2003). The second problem, however, cannot be easily resolved. Conditions 1 - 3 can be met by using a joint probability density function of ξ and β (α) for mark generation. We use simulated annealing to incorporate the spatial auto- and cross-correlation conditions (e.g., 4 - 6 above), as proposed in Xu et al. (2007).

Figure 5a shows a point realisation of the marked point process using a non-parametric model. This realisation is generated by a Boolean object

model and therefore initially the spatial auto- and cross-mark correlations of ξ, β and between ξ and β are non-existent. The realisation is then refined by simulated annealing and, after 1300 mark swaps, the final spatial mark correlation functions are given in Figure 6a and 6b, which indicate that the spatial mark correlation functions are closely reproduced at the end of the annealing process.

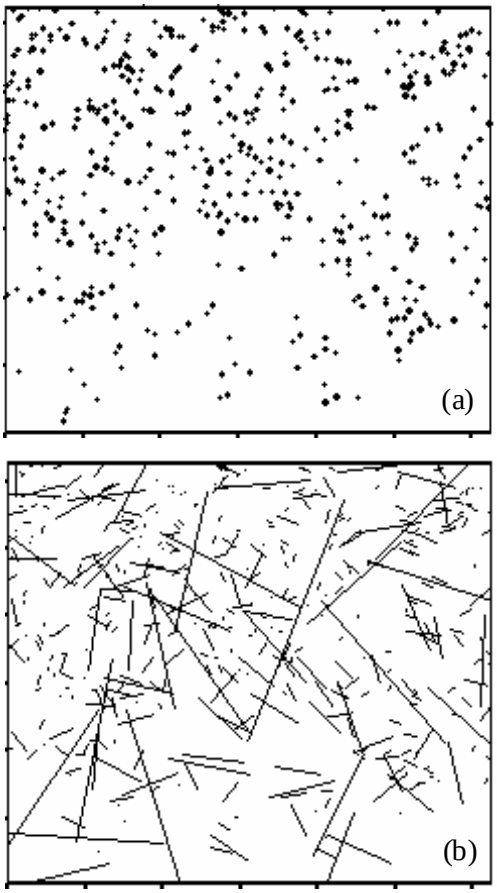

Figure 5 Simulated annealing process for the example shown in Figure 3 (a) One realisation from non-parametric model, (b) One realisation of the simulated fractures after annealing,

The final image of the simulated fractures, shown in Figure 5b, is not an exact replica of the original data (Figure 3b), but resembles the original data in the sense that the first and second moments of the characteristics of the corresponding marked point process (first and second order point intensity characteristics, mark distributions, multivariate mark correlations and spatial mark correlation functions) are reproduced.

Conclusions

Parameters of rock fractures (e.g., locations, orientation, size, aperture) are in generally spatially correlated. The correlations must be incorporated into the fracture model for realistic simulation of rock fracture system. The correlations can be quantified by cumulative spatial mark correlation function and the correlations can be effectively incorporated in the fracture model by simulation annealing.

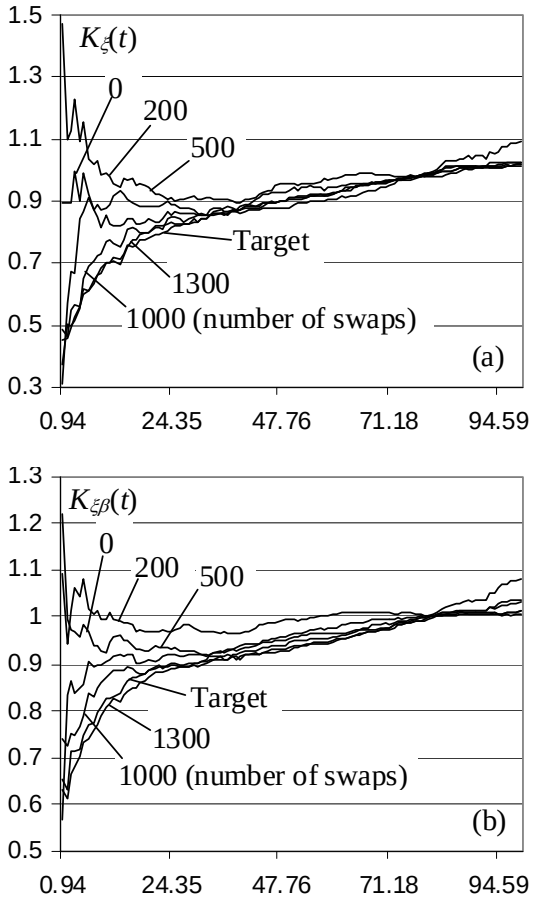

Figure 6 Simulated annealing process for the example shown in Figure 3 (a) $\hat{K}_\xi(t)$ vs distance t, (b) $\hat{K}_{\xi\beta}(t)$ vs t, (e)

References

Baghbanan, A. and Jing, L., 2007, Hydraulic properties of fractured rock masses with correlated fractures length and aperture, *International Journal of Rock Mechanics and Mining Science*, v. **44**, p. 704-719.

Barton, C.C. and Larson, E, 1985, Fractal geometry of two-dimensional fractures networks at Yucca Mountain, Southwest Nevada, proceedings of the International Symposium on Fundamentals of Rock Joints, O. Stephanson (ed.), Centek Publishers.

Chiles, J.P. & de Marsily G., 1993, Stochstic models of fracture systems and their use in flow and transport modelling, in *Flow and Contaminant Transport in Fractured Rock*, eds: Bear J., Tsang, C-F, and de Marsily, G., Academic Press.

Dershowitz, W. S. and Einstein, H. H., 1988, Characterizing rock joint geometry with joint system models, Rock Mechanics and Rock Engineering, v.**21**, p. 21-51.

Dowd, P. A., Xu, C., Mardia, K. V. and Fowell, R. J., 2007, A comparison of methods for the simulation of rock fractures, *Mathematical Geology*, v.**39**, p. 697 – 714.

Lee, C. H. & Farmer, I., 1993, *Fluid Flow in Discontinuous Rocks*, Chapman & Hall, London.

Lee, J. S., Veneziano, D., & Einstein, H. H., 1990, Hierarchical fracture trace model. Rock mechanics contributions and challenges, Proceedings of the 31th US Rock Mechanics Symposium, Hustrulid, W. & Johnson, G. A. (eds.), Balkema, Rotterdam.

Molchanov, I., 1997, Statistics *of the Boolean model for practitioners and mathematicians*, Wiley Series in Probability and Statistics, Wiley.

Priest, S. D., 1993, *Discontinuity Analysis for Rock Engineering*, Chapman & Hall, London.

Stoyan, D., Kendall, W. and Mecke, J., 1995, *Stochastic geometry and its applications*, 2nd edition, John Wiley & Sons, 436p.

Xu, C. and Dowd, P. A., 2009, A new computer code for discrete fracture network modelling, *Comps & Geosc.* (in press).

Xu, C. and Dowd, P. A., 2008, Plurigaussian simulation of rock fractures, *Proceedings of the Eight International Geostatistics Congress*, (eds. J.M. Ortiz and X. Emery), pub. Gecamin Ltd., ISBN 978-956-8504-17-5; v. **1**, p. 41-50.

Xu, C., Dowd, P. A., Mardia, K. V., Fowell, R. J. and Taylor, C. C., 2007, Simulating correlated marked point processes, *Journal of Applied Statistics*, v.**34**, 9, p. 1125 – 1134.

Xu, C., Dowd, P.A., Mardia, K.V. and Fowell, R., 2003, Stochastic approaches to fracture modelling. Internat. Assoc. for Mathematical Geology Conference, Sept., Portsmouth, UK

Habanero Tracer Tests in the Cooper Basin, Australia: Key Results for EGS Development

Norio Yanagisawa[1]*, Peter Rose[2] , Doone Wyborn[3]
[1] National Institute of Advanced Industrial Science and Technology,1-1-1,Higashi, Tsukuba, Ibaraki, 305-8567,Japan.
[2] Energy and Geoscience Institute, University of Utah, 423 Wakara Way Suite 300, Salt Lake City, Utah, USA
[3]Geodynamics Ltd, Suite 6, Level 1, 19 Lang Parade, Milton, QLD 4064
* Corresponding author: n-yanagisawa@aist.go.jp

The first tracer test of an Enhanced Geothermal System (EGS) in Australia was conducted in December 2008 and January 2009. The test involved circulating fluid (~14 kg s^{-1}) between an injection well, Habanero #1, and a production well, Habanero #3, for about 66.5 days through a closed-loop system in order to characterize the connection between the wells (560 m separation) and to estimate the tracer-swept volume of the reservoir. Two tracers were used: uranine and 1,3,5-naphthalene trisulfonate.
The tracer 'breakthrough' occurred after 4 days and the peak concentration occurred at 9 days. The tracer-swept pore volume was calculated to be 18,500 m^3 which is comparable in size to the reservoir of an EGS project located in Soultz-sous-Forêts, France.

Keywords: Cooper Basin, Australia, EGS, HDR, granite, tracer, fluorescien, uranine, naphthalene trisulfonate, circulation

Introduction

Geodynamics Ltd began developing its EGS project in the Cooper Basin, South Australia, in 2002. Since then Geodynamics has drilled 4 deep wells (Habanero #1, #2 and #3 and Jolokia #1), commenced drilling a fifth (Savina #1), and has constructed the Habanero closed-loop system. The project site is located in the remote north-east of South Australia as shown in Figure 1.

In March 2008, an open loop test was carried-out achieving a 20 kg s^{-1} production rate at Habanero #3. On 9 December 2008 a six week circulation test commenced. The test involved the circulation of 12 to 15 kg s^{-1} of geothermal fluid from Habanero #1, through the reservoir (at a depth of ~4,200 m) to Habanero #3 located 560 m away. A week later a tracer test was initiated with the aim of estimating the reservoir tracer-swept pore volume. Tracer testing is considered useful for estimating EGS and Hot Dry Rock (HDR) reservoir volumes (e.g., Robinson at al., 1987; Matsunaga et al., 1996). Reservoir volume is important because it influences the efficiency of heat extraction and the thermal and economic potential of EGS and HDR projects. This paper presents the results of the first tracer test at the Habanero well field in the Cooper Basin,

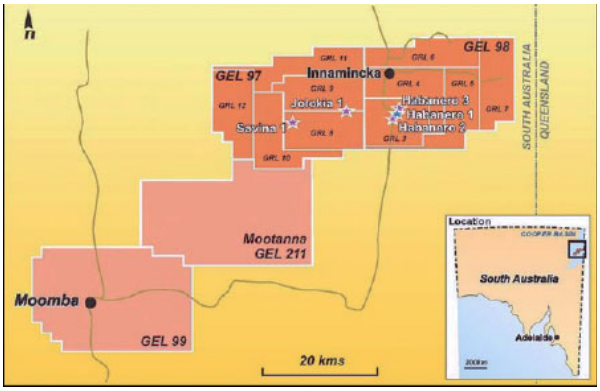

Figure 1: Location of the Geodynamics Limited Cooper Basin geothermal exploration sites

Method of tracer test

The tracer test was designed with two tracers: 1,3,5-naphthalene trisulfonate (1,3,5-NTS) and sodium fluorescein ('uranine dye'). The 1,3,5-NTS dose was 100 kg in 800 l of water, and the sodiuim fluorescein dose was 50 kg, resulting in a total tracer-mix volume of ~900 l. There were no fluid losses and the background concentrations of 1,3,5-NTS and sodium fluorescein were negligible. The tracer mix was injected into Habanero #1 and the circulation pump was restarted at 16:00 on 17 December 2008. The tracer injection and system is shown in Figure 2.

Figure 2: The tracer injection system at the Habanero site

Figure 3: The fibre-optical fluorometer (left hand side) and fluid sampling panel (right hand side) used in the test carried out at the Habanero site.

Tracer concentrations in the Habanero closed-loop were monitored for about 66.5 days. A fibre-optic fluorometer and fluid sampling panel are shown in figure 3. The fibre-optic fluorometer was used to used to obtain real-time fluorescence 'counts' which is useful for optimizing the bottled-sample sampling-rate and for comparing with laboratory measurements (Matsunaga et al.,2001, Matsunaga et al.,2002, Yanagisawa et al.,2002, Yanagisawa et al.,2003). Fluid samples were taken from sampling panel located downstream of the cooling tower. The bottled samples were sent to AIST, Japan, and to the University of Utah, USA, for chemical analysis.

Results

Results of the Continuous Field Sampling

Fluorescence counts were made at 5 minute intervals between 18 December and 25 February 2009 (see Figure 4). Mineral scale formed on the optical fibre (the fluid pH was about 5.5) causing the fluorescence counts to be relatively low and spiky. The presence of barite drilling mud and other particles in the fluid may have also contributed to the scatter.

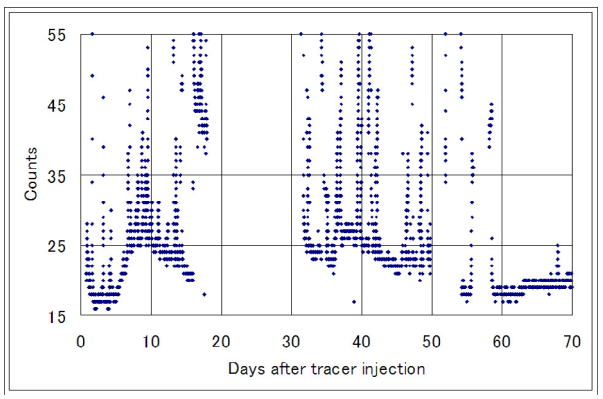

Figure 4: Habanero tracer test, fluorescein counts by optical fibre analyzer

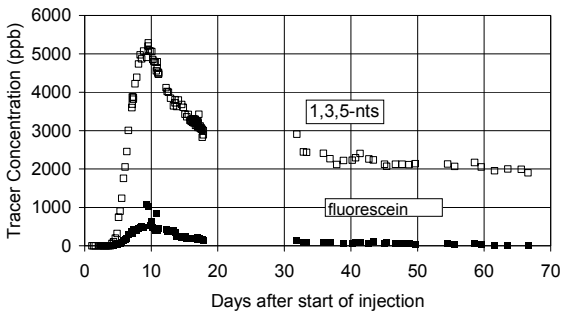

Figure 5: 1,3,5-NTS and fluorescein concentrations versus days after start of injection measured in samples taken from the sampling panel

The fluorescence record shows a tracer breakthrough at 4 days and a peak concentration at about ~9 days.

Results of the Laboratory Analysis

Fluorescein and 1,3,5-NTS concentrations of the samples collected over the 66.5 day sample period are shown in Figure 5. Due to unscheduled pump stoppages and the need to remove scale from the optical fibre, the circulation was stopped temporarily on several occasions during the tracer test. Hiatus periods included 4 to 18 January and 4 to 10 February. The data shown in Figure 5 are based on actual sampling time regardless of whether the fluid was circulating or not.

After 4 days of circulation the tracers were detected and concentrations reached a peak at about 9 days, consistent with the real-time monitoring results. An adjusted time curve (i.e. with hiatus periods removed) was calculated by assuming a flow rate of 14 kg s^{-1} and by dividing the total produced mass by the mass flow rate at each point in flow-time (see Figure 6).

Figure 6 shows the total flow volume at tracer breakthrough was about 4000 m^3 and was about 9000 m^3 at the peak concentration.

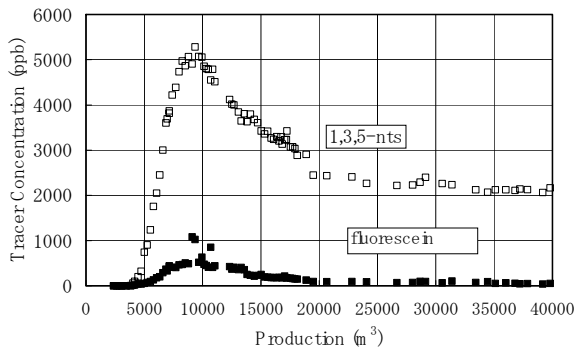

Figure 6: 1,3,5-NTS and fluorescein concentrations versus total fluid production measured in samples taken from the sampling panel

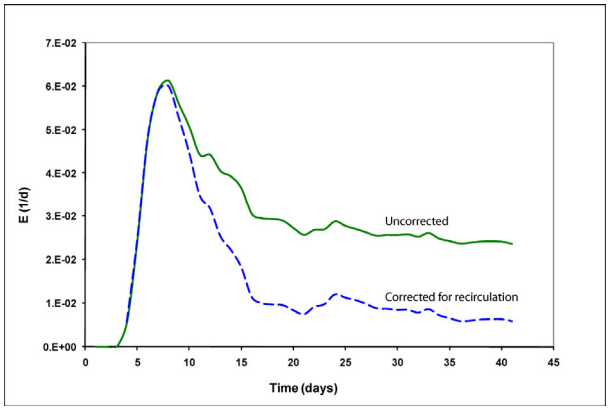

Figure 7: Plots of the residence time distribution function E(t) (upper curve) and the deconvoluted E(t) (lower curve) versus time

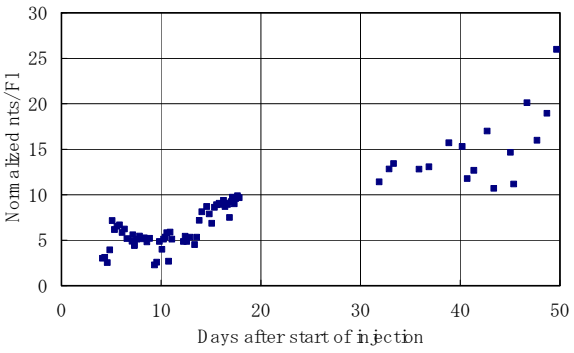

Figure 8: Normalized tracer concentration ratio 1,3,5-nts (nts) and fluorescein (fl) versus time.

To compare this with the Hijiori HDR volumes: at the first tracer test of Hijiori site, the tracer peak volume between HDR-1 and HDR-3 occured about half month after starting the long circulation test, and was about 100 m^3. This is 90 times smaller than the tracer peak volume at Habanero. However, the separation distance of the Habanero wells (560 m) is four times greater than for the Hijiori HDR-3 site (130m).

Estimation of Reservoir Tracer-Swept Pore Volume

The tracer-swept pore volume at the Habanero site was calculated using a program developed at Idaho National Laboratory (INL) that provides a standardized method of interpreting tracer return curves (Shook and Forsmann, 2005).

The program first calculates a residence time distribution function E(t):

$$E(t) = \frac{C(t) \cdot \rho \cdot Q}{M_t} \qquad \text{Equation 1}$$

where C(t) is tracer concentration, ρ is fluid density, Q is mass flow rate, and M_t is the mass of tracer injected. The program then conducts a "de-convolution" calculation, which subtracts the effects of tracer recirculation to create a new E(t) function.

This calculates what the tracer return curve would look like if the tracer had been removed from the circulation fluid at the production well after making only one pass through the reservoir. The program then extrapolates the return curve to infinite time assuming exponential decay. It then calculates the fraction of tracer-returned, a mean reservoir-residence time and the reservoir pore volume.

As described above, a constant flow rate of 14 kg s^{-1} was assumed for the duration (41 days) in which 50.4 tonnes of brine was circulated. Shown in Figure 7 (upper curve) is a plot of the residence time distribution function E(t). The lower curve is the de-convoluted E(t) curve.

Based on the assumptions described above, the mean residence time was 23.7 days and the fraction of tracer returned was 0.78. The calculated tracer-swept pore volume was 18,500 m^3. For comparison, a calculation using the same software and the tracer and flow data associated with the 1997 GPK1-to-GPK2 doublet test at Soultz-sous-Forêts, France, yielded a pore volume of 16,000 m^3 (Rose et al, 2006). The distance between production and injection well of the Habanero site is around 560 m and similar to the Soultz site.

Estimation of Reservoir Temperature

Fluorescein will decompose at temperatures greater than 200°C, whereas 1,3,5-NTS is thermally stable. From the ratio of 1,3,5-NTS concentration to fluorescein concentration, the reservoir temperature may be estimated with prior knowledge of the temperature-to-half-life relationship for fluorescein.

The concentration ratio of 1,3,5-NTS and fluorescien normalized by injected tracer amount is shown in Figure 8. At about 13 days, the concentration ratio rapidly changed from 2.2 to 7 and after 13 days, the ratio gradually increased from 7 to 10. This means that the half-life of the fluorescein was ~3 days and the reservoir temperature was approximately >250 °C.

The scatter in the chart may have been due, in part, to the cooling effects of re-injection (refer Figure 7).

Summary

The first EGS tracer test in Australia was carried out at the Habanero well field in the Cooper Basin, South Australia, in 2008-2009. The main results of tracer test are as follows:

1) Tracer breakthrough occurred 4 days after tracer injection and tracer peak occurred about 9 days after tracer injection;

2) Based on an average flow rate of 14 kg s^{-1} the total flow volume at tracer breakthrough was ~4,000 m^3 and the total flow volume at tracer peak-concentration was ~9,000 m^3;

3) The tracer-swept pore volume of the Habanero reservoir is about 18,500 m^3 and is comparable in size to the Soultz-sous-Forêts EGS reservoir; and

4) Based on the thermal properties of fluorescien and 1,3,5-NTS, the reservoir temperature is estimated to be >250°C.

Acknowledgements

The research described in this paper has been supported by Geodynamics Ltd. The authors would like to thanks Kevin Brown, Lew Bacon, Leonard Spencer and Bill Austin for helping our tests and providing samples and data.

References

Matsunaga, I., Tao, H and Kimura A.,1996, Preliminary Characterization of the Hijiori HDR Deeper System by Fluid Geochemistry and Tracer Experiments of a One-Month Circulation Test, Proceedings of 3rd International HDR Forum, p. 25-26.

Matsunaga, I. Sugita. H., and Tao, H., 2001, Tracer Monitoring a Fiber-Optic Fluorometer During a Long-Term Circulation Test at the Hijiori HDR Site, Proceedings of 26th Stanford Workshop on Geothermal Reservoir Engineering, p.74-77.

Matsunaga, I., Yanagisawa, N., Sugita. H., and Tao, H., 2002, Reservoir Monitoring by a Tracer testing During a Long-Term Circulation Test at the Hijiori HDR Site, Proceedings of 27th Stanford Workshop on Geothermal Reservoir Engineering, P.101-104.

Robinson, B.A., Aguilar, R.G., Kanaori, Y., Trujillo, P., Counce, D., Birdsel, S., and Matsunaga, I., 1987, Geochemistry and tracer behavior during a thirty day flow test of the Fenton Hill HDR reservoir, Proceedings of 12th Workshop on Geothermal Reservoir Engineering, 121-135.

Rose, E. P.,1998, The Use of Polyaromatic Sulfonates as Tracers in High Temperature Geothermal Reservoirs, Proceedings of 20th NZ Geothermal Workshop, p.239-243.

Rose, P.E., Mella, M., and McCullough, J., 2006, A Comparison of Hydraulic Stimulation Experiments at the Soultz, France and Coso, California Engineered Geothermal Systems, Proceedings, Thirty-First Workshop on Geothermal Reservoir Engineering, Stanford University, SGP-TR-179.

Shook, G.M. and Forsmann, J.H., 2005, Tracer Interpretation Using Temporal Moments on a Spreadsheet, Idaho National Laboratory Technical Report.

Yanagisawa, N., Matsunaga, I., Sugita, H. and Tao, H., 2002, Reservoir Monitoring by Tracer Test of a 2001 Long Term Circulation Test at the Hijiori HDR site, Yamagata, Japan, Geothermal Resources Council Transactions, 26, p.267-271

Yanagisawa, N., Matsunaga, I., Sugita, H. and Tao, H., 2003, Reservoir Monitoring by Tracer Test of a 2002 Dual Circulation Test at the Hijiori HDR site, Yamagata, Japan, Geothermal Resources Council Transactions, 27, p.785-790

Two Basic Problems for Hot Dry Rock Reservoir Stimulation and Production

Xi Zhang, Rob Jeffrey*, and Bisheng Wu
CSIRO Petroleum Resources, Melbourne, Australia
*Tel: 03-95458354, E-mail: rob.jeffrey@csiro.au

A numerical analysis is made for heat extraction from a geothermal reservoir in a naturally fractured rock mass. We consider in particular two issues: long-term prediction of fluid temperature around a single fracture and the initial stages of fracture development in a naturally fractured rock. For the first problem, the evolution of outlet fluid temperature is considered as a function of time and injection rate. The rock temperature around a single fracture in the reservoirs is also calculated. The second problem is motivated by the fact that injection pressure is highly dependent on the details of fracture geometry near the borehole. High treatment pressure are associated with the formation of opening mode hydraulic fractures in naturally fractured rock and recent result that can explain the origin of these pressures are applied here to the problem of high injection impedance at pressures below the jacking pressure.

Keywords: Hot Dry Rock, fluid flow, thermal effect, crack growth, numerical method

Introduction

In stimulation and operation of an Enhanced Geothermal System (EGS), fluid circulation is influenced in both the short and long-term by thermal-hydro-mechanical deformation. In other words, the efficiency for hot-dry-rock reservoir stimulation and production depends on fracture interconnectivity and thermal flux interchanges between rock and fluid coupled to fracture permeability (Bodvarsson, 1969; Hallow and Pracht, 1972; Gringarten, et al., 1975; Abe et al., 1976; Cheng et al., 2001). We present results from two problems that, at this point, include limited coupling. The first problem involves calculation of the evolution of heat transfer between rock and fluid over a long period of time and the second problem considers the effect of pre-existing fracture interconnectivity along a non-planar path on injected fluid pressure and crack growth. Both problems are useful in demonstrating the importance of coupled processes, e.g., thermal-hydraulic coupling for the first problem and hydraulic and mechanical deformation coupling for the second problem. We are working towards a thermal-hydraulic-mechanical coupled analysis of both problems.

We first address the interaction between the long-term heat extraction and fluid flow and heat conduction in both rock and fluid. The cooling of rock around an axisymmetric reservoir containing a single conductive fracture is discussed. In the second part of this paper we give a detailed study on how a fracture propagates through a fracture network that guides its path. The spatially varying fracture conductivity that results from stress-dependent fracture permeability has a strong effect on the fluid pressure distribution. As a result, the injection pressure is found to be elevated.

Thermal Analysis of Penny-Shaped Fracture Reservoirs

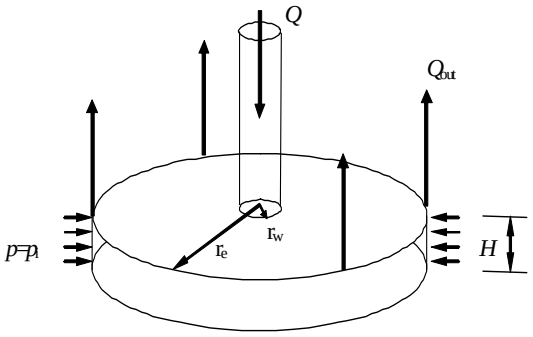

Figure 1: An axisymmetric penny-shaped geothermal reservoir.

Fracture conductivity and fluid flow

For a large naturally fractured geothermal reservoir, Pine and Batchelor (1984) found that the fracturing during injection was dominated by shear and associated dilation. For simplicity, shear deformation caused by far-field stresses interacting with the injected fluid pressure is not considered in this simple thermal-fluid model presented here and the reservoir is considered to consist of a impermeable layer of a finite thickness H, as shown in Fig.1. The reservoir layer is assumed to axisymmetric, with production wells located at the periphery of a circle with a radius r_e. The conductivity between the injection and production wells is provided by a single conductive fracture located at the midplane of the reservoir for the analysis of fluid flow and heat conduction. Practically, this closed but conductive fracture model, which uses an effective hydraulic aperture (<1 mm in most cases) held constant along its extent, is useful in studying the thermal-fluid system. The fracture aperture, in real natural fractures, has been shown to vary along the fracture with, surface roughness, effective stress, temperature and chemical processes (Min, et al., 2008). The fracture conductivity then is modelled by the cubic law with the fracture permeability given as follows (Tsang and Witherspoon, 1981)

$$k = \frac{w_0^{\,2}}{12} \qquad (1)$$

where k is the fracture permeability and w_0 is the effective hydraulic aperture for the closed natural fracture. We assume that the small roughness present and induced changes in the hydraulic aperture along the natural fracture can be ignored because the aperture change occurs with a small slope so that the cubic law is still valid (Brown et al. 1995).

Darcy's law is used to describe fluid flux in response to fluid pressure gradient ∇p_f

$$q_f = -\frac{k}{\mu}\nabla p_f \qquad (2)$$

where μ is the fluid dynamic viscosity.

Problem statement

As shown in Fig. 1, a fluid (at temperature T_i) is injected into the reservoir at a constant rate Q. The production wells are assumed to be uniformly distributed along the periphery of the reservoir with a constant production pressure p_o, so that the fluid flow and temperature change distributions are axisymmetric. The reservoir height is *H,* which also represents the spacing between conductive fractures in the reservoir or the designed fracture interval.

Based on fluid mass continuity, the governing equation for pressure diffusion in the axisymmetric fracture is given by

$$\frac{\partial p_f}{\partial t} = c\left(\frac{\partial^2 p_f}{\partial r^2} + \frac{1}{r}\frac{\partial p_f}{\partial r}\right) \qquad (3)$$

where $c = k/\chi\mu$ and χ is the elastic pore compressibility.

The solution to the above equation at given boundary and initial conditions can be found in the monograph by Carslaw and Jaeger (1959).

Let q_h denote the heat flux from rock to fluid at the fracture surface. Based on previous studies (Abe et al., 1983; Cheng, et al., 2001), the heat dissipation and storage along the fracture can be neglected. For the axisymmetric problem posed above, the heat transfer equation along the fracture surface can be written as (Abe et al., 1983; Cheng, et al., 2001)

$$\rho_w c_w q_f . \frac{\partial T_f}{\partial r} + q_h = 0 \qquad (4)$$

where T_f is the temperature along the fracture, and ρ_w and c_w are the mass density and specific heat of the fluid.

In the presence of heat exchange between rock and fluid, the rock temperature will vary in the form of

$$T_r = T_\infty + \frac{2}{\sqrt{\pi}}\int_0^t \frac{1}{[4\kappa_r(t-t')]^{3/2}}\int_{r_w}^{r_e} q_h I_0\left(\frac{rr'}{2\kappa_r(t-t')}\right) \exp\left(-\frac{r^2+r'^2+z^2}{4\kappa_r(t-t')}\right) r'dr'dt' \qquad (5)$$

where T_∞ is the initial uniform temperature of the rock, the rock thermal diffusivity is $\kappa_r = K_r/(\rho_r c_r)$ in which K_r is the rock thermal conductivity, and ρ_r and c_r are the mass density and specific heat of the rock. Finally, I_0 is the modified Bessel function of the first type.

Based on the continuity of temperature across the fracture surface, the governing equation for temperature change can be established by considering the equivalence of fluid temperature calculated by Eq. (4) and the rock temperature at the fracture surface by Eq. (5). This leads to an integral equation, which can be solved numerically by the collocation method. Moreover, the corresponding initial and boundary conditions are not listed here to save space.

Numerical results

As an example, we consider the case of reservoir radius r_e =300 m and wellbore radius r_w =0.1 m, and initial rock temperature of 270°C (or 543 K). Water with a constant viscosity μ =0.0004 Pa·s, although we recognise that the viscosity will depend on temperature, is injected into the fracture at a constant rate *Q*=20 l/s and at an initial temperature of 70°C (or 343 K). The reservoir height or thickness is H=0.5 m. The fracture hydraulic aperture w_0 is 1 mm. The rock thermal conductivity K_r =2.4 W/m·K, and the rock mass density and heat capacity are ρ_r =2700 kg/m^3 and c_r =1000 J/kg·K, respectively. The fluid temperature at the outlet is plotted against elapsed time in Fig. 2 and the temperature contours in the rock, at 1.92 and 14.26 years after the start of injection, are shown in Fig. 3.

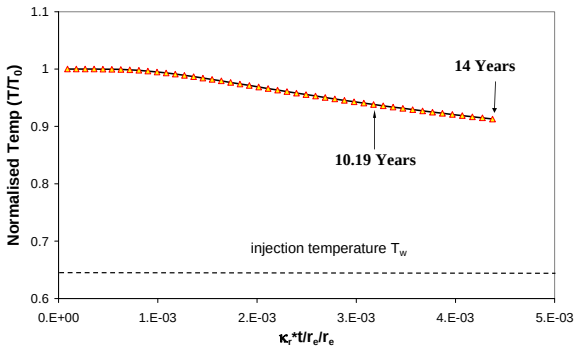

Figure 2 Normalised fluid temperature at production well against time

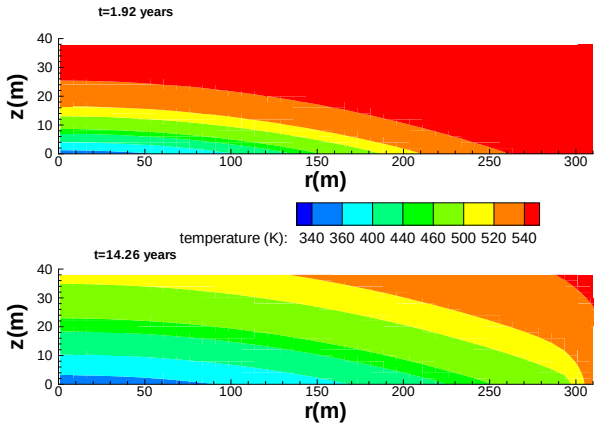

Figure 3 Temperature contours in the reservoir rock between the injection and production wells. The production well is at r=300 m.

Fracture Growth along an Offset Natural Fracture

As the geothermal reservoir is comprised of naturally fractured rock, the injected fluid will more or less follow the path defined by existing conductive fractures. In particular, injected water may reach a pressure sufficient to open some portions of natural fractures near the injection wellbore. The fluid flow is guided by the conductive channels and analysis of this problem involves tracking the strong coupling between rock deformation and fluid flow. The induced near-bore inflow restriction can limit fluid production eventually. To start, we idealise the fracture geometry as shown in Fig. 4. We consider the pressure and crack opening responses when injection is located at the start of a natural fracture that contains several offsets along its path (Fig. 4). The fracture geometry including the step and offset sizes and their intersection angle θ are shown in the figure, along with the far-field stresses and material constants used. The closed natural fracture is assumed to be conductive with an initial hydraulic aperture w_0. In this section, w_0 is 0.01 mm for all cases, unless otherwise specified. Although the real situation results in a 3D problem, it is here treated as a plane strain problem instead.

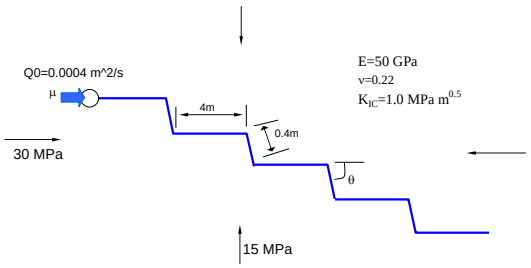

Figure 4 Schematic of an offset natural fracture with fluid injected at one end. K_{IC} is the fracture toughness of the rock.

Fracture slip model

Fracture frictional slip along parts of the fracture can be important in this case since there is a strong horizontal compressive far-field stress. We use the Coulomb frictional law, which is applied locally to the cohesionless, but frictional fracture, to provide a limit on the frictional stress τ_s in terms of the normal effective compressive stress, $\sigma_n - p_f$,

$$|\tau_s| \le \lambda(\sigma_n - p_f) \qquad (6)$$

where λ is the coefficient of friction and $\lambda(\sigma_n - p_f)$ is the frictional strength. For the dry portion of the fracture $p_f = 0$. In this paper, λ=0.8 for all cases.

Hydraulic fracturing model

As fractures can be opened by fluid pressure, elastic deformation associated with fluid flow must be considered here. The governing equation for fracture equilibrium is given as follows in the presence of multiple cracks,

$$\sigma_n(\boldsymbol{x},t) - \sigma_1(\boldsymbol{x}) = \sum_{r=1}^{N}\int_0^{l_r}[G_{11}(\boldsymbol{x},s)w(s) + G_{12}(\boldsymbol{x},s)v(s)]\mathrm{d}s \qquad (7)$$

$$\tau_s(\boldsymbol{x},t) - \tau_1(\boldsymbol{x}) = \sum_{r=1}^{N}\int_0^{l_r}[G_{21}(\boldsymbol{x},s)w(s) + G_{22}(\boldsymbol{x},s)v(s)]\mathrm{d}s \qquad (8)$$

where N is the number of cracks, $G_{\alpha\beta}$ (α,β =1,2) are Green's functions, w,v are opening and shearing displacement discontinuities across the fracture surface, and σ_1,τ_1 are the normal and shear stresses, respectively, acting along the fracture direction at location $\boldsymbol{x}$ generated by the far-field stresses.

In the existence of fracture opening (hydraulic fracturing), the fluid flow along the fracture can be

described by Reynolds' equation as follows (Batchelor, 1967)

$$\frac{\partial(w+\varpi)}{\partial t} = \frac{\partial}{\partial s}\left[\frac{(w+\varpi)^3}{\mu'}\frac{\partial P_f}{\partial s}\right] \qquad (9)$$

where $\mu' = 12\mu$. It should be noted that the total hydraulic opening is the sum of fracture mechanical opening and initial hydraulic aperture ϖ. Furthermore, the hydraulic aperture can vary with the effective stress in the closed fracture based on a liner spring model, that is,

$$d\varpi / dp_f = \gamma\varpi \qquad (10)$$

in which γ is a small constant for characterizing the compliance of a natural fracture with respect to pressure change (1/Pa), and is assumed to be less than 10^{-8} /Pa for most cases.

The above system of equations provides all governing equations for hydraulic fracture growth. The required initial and boundary conditions are not given here and the reader can refer to our previous work for more details (Zhang et al, 2008; Zhang and Jeffrey, 2008).

Numerical results

For the case that water is used as injection fluid, the fracture opening along the offset fracture is shown in Fig. 5, at a time when the fluid just reaches the fracture tip. It is clear that there is a narrow channel at the offset locations. An increase in the offset angle results in a narrower opening in this portion of the fracture (Fig. 5).

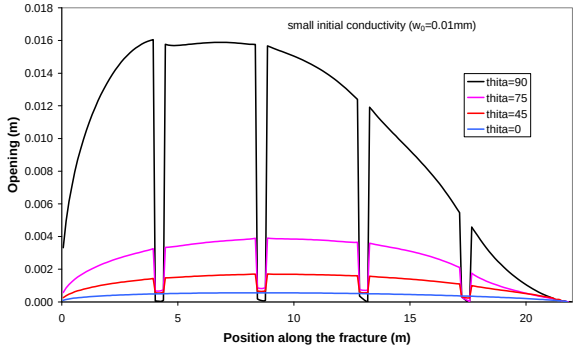

Figure 5 Fracture opening along the offset natural fracture when a hydraulic fracture is growing along it.

Figure 6 shows the time-dependent variation of the injection pressure for the offset natural fracture. Although the pressure decreases smoothly in time for a hydraulic fracture and for opening of a natural fracture without offset, it oscillates at an elevated level in the case of offset natural fractures. This reflects the different resistance for fluid flow along steps and offsets. When the fluid propagates along the steps, it will move at a lower pressure gradient. This results in pressure decreasing with time, in contrast to the increase in pressure occurring when flow is through the narrow offsets, which have lower opening compliance and are subjected to higher confining stresses.

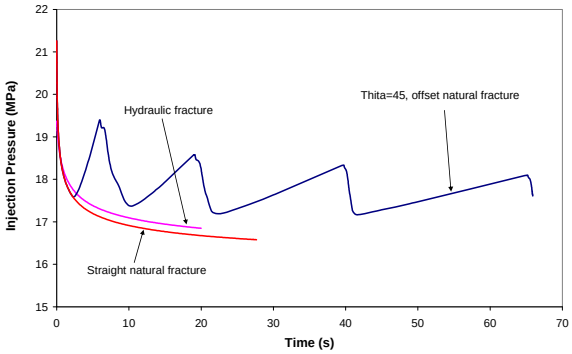

Figure 6 Pressure at the borehole against time corresponding to the cases shown in Fig. 5.

The effect of narrow offsets on the injection pressure, at pressures below the opening pressure, can be seen in Fig. 7 where the fluid is injected into the fracture at a very low injection rate Q_0=1E-7 m^2/s. The initial hydraulic aperture w_0 of the steps is increased to 0.05 mm to account for the relatively lower confining stress acting across them. Fig. 7 shows the variation of injection pressure against time when the kink angle is 45 degree. Even though the injected fluid pressure is below the confining stress so that no fracture opening occurs, a pressure increase is evident when the fluid front crosses the narrow offset region. Near-wellbore injection impedance may partly result from the injected fluid flowing along such tortuous pathways.

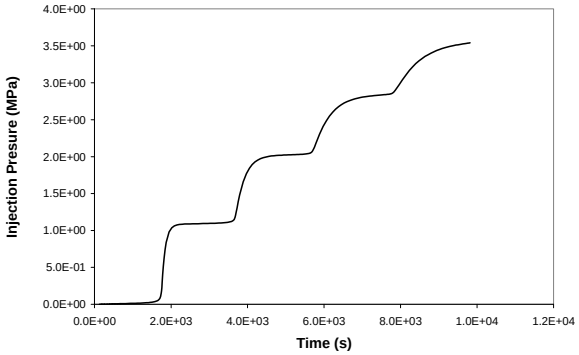

Figure 7 Pressure at the borehole against time in the case of low injection rate.

Summary and Discussion

We have presented numerical results for two basic problems, which are associated with the thermal-fluid coupling and fluid-mechanical coupling problems that arise in predicting temperature and fluid flow through a naturally fractured hot rock reservoir. From the analyses, the coupling between different mechanisms plays an important role in correctly predicting the temperature and fluid pressure changes. We

intend to next implement thermoelastic coupling in the 2D model used above.

In the first model, we have not considered the effect of elastic deformation. As we know, shear deformation assisted by surface roughness can induce fracture shear-induced dilatation that increases the fracture conductivity. Also, the reduction in effective stress caused by fluid pressure and the thermoelastic deformation resulting from cooling of rock can increase the fracture permeability. Chemo-mechanical processes should also be considered. These effects have been studied by coupled reservoir models (Min et al., 2008). Our approach is to extend our 2D hydraulic fracture model to include thermoelastic effects and apply it to the coupled mechanics of complex fracture geometries to analyse mechanism leading to local near-wellbore elevation of injection impedance. The results of this detailed mechanical modelling can then be incorporated in a more simplified way into reservoir-scale models.

References

Abe, H., Mura, T., and Keer, L. M., 1976, Growth rate of a penny-shaped crack in hydraulic fracturing of rocks, J. Geophysical Research vol 81, p5335-5340.

Abe, H., Sekine, H. and Shibuya, Y., 1983, Thermoelastic analysis of cracklike reservoir in a hot dry reock during extraction of geothermal energy, J of Energy Resources Technology vol 105, p503-508.

Batchelor, G.K., 1967, An Introduction to Fluid Dynamics, Cambridge University Press, Cambridge, U.K.

Bodvarsson, G., 1969, On the temperature of water flowing through fractures', J Geophysical Research vol 74, p1987-1992.

Brown, S. R., Stockman, H. W. and Reeves, S. J., 1995 Applicability of the Reynolds equation for modelling fluid flow between rough surfaces, Geophysical Research Letter vol 22, p2537-2540.

Carslaw, H. S. and Jaeger, J. C. 1959, Conduction of heat in solids, Oxford University Press, Oxford, U. K.

Cheng, A. H.-D., Ghassemi, A. and Detournay, E., 2001, Integral equation solution of heat extraction from a fracture in hot dry rock, Int. J. for Numerical and Analytical Methods in Geomechanics vol 25, p1327-1338.

Gringarten, A. C., Witherspoon, P. A. and Ohnishi, Y., 1975 Theory of heat extraction from fractured hot dry rock, J. Geophysical Research 80, p1120-1124.

Hallow, F. H. and Pracht, W. E. 1972 A theoretical study of geothermal energy extraction, J. Geophysical Research vol. 77, p7038-7048.

Min, K.-B., Rutqvist, R., and Elsworth, D., 2008, Chemically and mechanically mediated influences on the transport and mechanical characteristics of rock fractures, International Journal of Rock mechanics and Mining Science vol. 46, p80-89.

Pine, R.J. & Batchelor, A.S., 1984, Downward migration of shearing in jointed rock during hydraulic injections, International Journal of Rock mechanics and Mining Science and Geomechanics Abstract vol. 21, p249–263.

Tsang, Y. W. and Witherspoon P. A., 1981, Hydromechanical behavior of a deformable rock fracture subject to normal stress, Journal of Geophysical Research vol. 86, p9287-9298.

Zhang, X. Jeffrey, R. G. and Thiercelin, M., 2008, Escape of fluid-driven joints from bedding interfaces: A numerical study, J. Structural Geology vol. 30, p478-490.

Zhang, X. and Jeffrey, R. G., 2008, Re-initiation or termination of fluid-driven fractures at frictional bedding interfaces, J. Geophysical Research vol 113, B08416.

The Feasibility of a Nocturnal Radiative Heat Dissipation System for Remote Geothermal Applications

Joshua S Brimblecombe, Thomas J Vos.
University of Queensland, Q 4067
Supervisor: Hal Gurgenci

As the worldwide demand for energy increases, focus has shifted from conventional coal or gas fired plants towards the development of sustainable 'green' energy sources such as solar, hydroelectric, wind and geothermal. Energy sources can be deemed sustainable if the rate at which energy is replenished is greater than the rate of energy used. Geothermal energy has advantages over solar and wind in that operation of a geothermal plant is not sensitive to the weather conditions. Geothermal power stations use the heat from beneath the surface of the earth to operate a power cycle rather than the burning of hydrocarbons.

Types of Geothermal Energy

There are four main types of geothermal source – hydrothermal, geopressured, magma and hot fractured rocks (HFR). Of these, the only technology currently in use in power stations is hydrothermal. A hydrothermal plant uses a naturally occurring underground artesian aquifer to provide heat to the cycle. Two bores are drilled to allow the hot brine to be pumped to the surface. The concept of hydrothermal power is not new with many plants operating in countries around the world. There is currently an estimated 45000MW of generating capacity in hydrothermal geothermal resources worldwide (RISE 2008).

Hot Fractured Rocks

Most of Australia's geothermal potential, however, is in HFR. HFR geothermal energy is the only known source of renewable energy able to continuously meet base load power requirements. For a site to be acceptable for HFR energy extraction, however, it has to meet certain important criteria. The geology of the site must consist of hot granite (at least 250°C) at a depth of around 4km beneath the surface of the earth. This "Hot rock" layer must be insulated by at least 3km of sedimentary rock.

Figure 2 shows the crust temperature variation throughout Australia at a depth of 5km. At a typical site, two holes would be bored into the crust. Cold fluid would be pumped down one side, heated by the hot granite layer and drawn up the other side. Typically, granite layer temperatures in Europe are around 180°C, illustrating the potential Australia has for this sort of power generation.

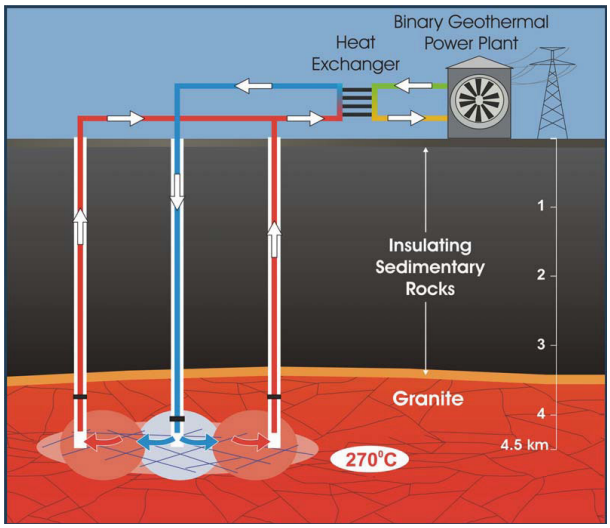

Figure 1 - Typical geological layout of a HFR site. This diagram can be obtained from the Geodynamics website: http://geodynamics.com.au/IRM/content/educationroom.html

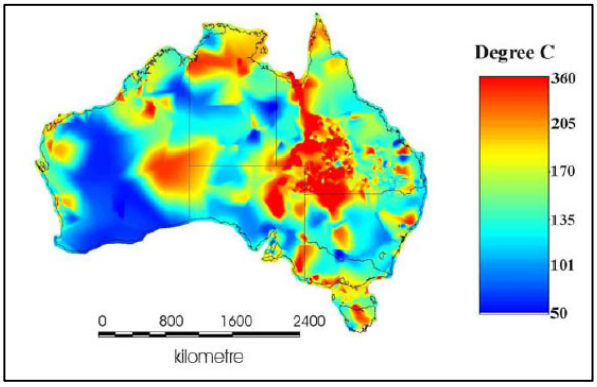

Figure 2 – Crust temperature at a depth of 5km. This image can be downloaded from the Research Institute for Sustainable Energy at: http://www.rise.org.au/info/Res/geothermal/index.html. After Somerville et al. 1994.

It is only recently, with research into Hot Fractured Rock technology, that the implementation of geothermal energy in Australia has become feasible. Potential sites have been identified throughout Australia for the development of geothermal power. The Cooper Basin is one of the largest geothermal resources in the world with an estimated 1.9×10^{21}J of available energy (Somerville et al. 1994).

Design Challenge

The remote location of Australia's geothermal resources presents a problem with respect to cooling. Typically, a power station will use a wet

cooling tower to dump waste heat from the power cycle. In Australia alone, coal fired power plants consume 300 gigalitres of water per year – quantities which are not feasible at these locations. In order to operate an efficient geothermal plant, a new method of cooling must be developed.

One potential solution is the implementation of a nocturnal cooling system (NCS). Central Australia typically experiences minimal cloud cover. This, combined with low humidity, allows for large radiative heat losses at night time. This is commonly referred to as nocturnal cooling. A NCS makes use of these conditions at night to dissipate heat from a coolant fluid and store the "coolth" for use during the daytime.

Investigation

The aim of this investigation is to explore the feasibility of a nocturnal radiative cooling system for a remotely located geothermal power plant in Australia. This has been aided by the consideration of the following aspects:

- Theoretical and experimental effectiveness of radiative heat dissipation techniques,
- Evaluation of coolant mass options, and
- Associated heat exchangers.

This investigation will look into the performance of a test facility operating under specified conditions at a location near Innamincka. Weather conditions for the nearby town of Moomba were assumed to be indicative of ambient conditions in this area.

This investigation will consider a binary geothermal system heating brine to 225°C to supply heat to a transcritical CO_2 Brayton cycle for the generation of work (Dostal, Driscoll and Hejzlar 2004). The details of the design point cycle are included in Table 1.

Table 1 - Cycle Properties

Design Parameters		Value
Ambient Temperature	T_a	30°C
Brine Temperature	T_b	225°C
H-Ex Pinch Points	ΔT	8 °C
Cold-side Pressure	P_c	8 MPa
Hot-side Pressure	P_h	22 MPa

In order to operate successfully, a power plant must have a constant power output. One of the key disadvantages of the transcritical CO_2 cycle is its high sensitivity to ambient conditions. For the purpose of this investigation, the design point ambient temperature is 30°C. With ambient temperatures peaking at almost 50°C, it can be seen that the power generation from the plant drops to almost 30% of the design power. It becomes apparent that a secondary system is required to maintain design performance.

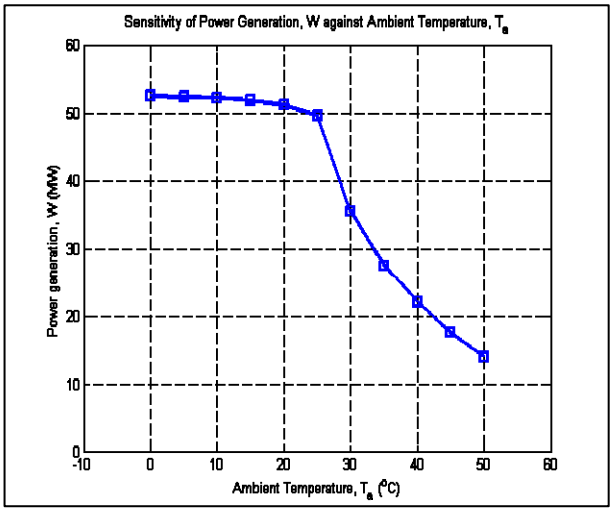

Figure 3 - Sensitivity of Power Generation against Ambient Temperature

As such, a two stage cooling system was investigated with the assumption that a dry cooling tower exists with the capacity to cool the cycle fluid to within 8°C of the ambient temperature. The design of such a tower, however, is not within the scope of this report.

Experimental Investigation

The purpose of the experimental analysis is to assess the cooling capacity for a typical night time period in Brisbane by estimating the effective sky temperature. This directly influences the radiative heat flux.

Experimental setup involves measuring the temperatures of a flat plate exposed to the night time sky. The plate, acting as a lid, is positioned on top of an insulated enclosure that is kept at a constant temperature throughout the testing period. It is expected that radiation rather than convection will dominant the heat loss from the surface.

The test plates are approximately 35 x 25 cm and are made of mild steel (coated and uncoated) and PVC. Emissivity is influenced by material properties as well as the surface finish. As heat loss due to radiation is proportional to emissivity (see Equation 1), different test plates are expected to have different heat fluxes.

$$q''_{rad}(W/m^2) = \varepsilon\sigma\left(T_s^4 - T_{sky}^4\right) \quad (1)$$

Since the walls and bottom of the enclosure are insulated, all heat will be dissipated through the test plates. At equilibrium, the boundary conditions for the setup can be described according to equation 2:

$$q''_{cond} = q''_{rad} + q''_{conv} \quad (2)$$

The heating for the experiment is supplied by two incandescent light bulbs.

Ideal testing conditions are when the sky is clear, humidity levels are low, and little wind is experienced. Using that data gathered from the experiments, a statistical analysis will provide estimates for the effective night time sky temperature. The results will be compared to empirical relations set out by Berdahl and Martin (1984).

Tests will be conducted on the roof of the Hawken Engineering building at the University of Queensland.

Coolant System

The aim of the proposed NCS is to maintain a constant compressor entry temperature of T_c=38°C both during the day and night throughout the entire year. The proposed system consists of a number of separate components, including:

- Coolant mass,
- Coolant storage system,
- Heat exchangers, and
- Radiative arrays

A detailed performance analysis has been carried out on the completed system for the purpose of evaluating the steady-state performance under varying atmospheric conditions. Figure 4 shows the typical power output throughout the year for a particular design solution. Dark points represent a power output below the design point (35MW).

Coolant Mass and Storage system

A simple coolant system with a fixed coolant flow rate has been considered in this case. It was found that the flow rate of coolant through the radiative arrays had only a minor influence on the amount of heat dissipated, so long as the flow rate was sufficiently high as to avoid large changes in temperature in the coolant.

Simulations carried out with moderate coolant tank sizes give reasonable results – almost 100% design point operation can be attained with 10^8kg water. Moderate operation, however, is achievable with masses as low as 4×10^7kg with 3% operation below design point and a minimum output work of 32MW (DP=35MW).

Radiative Arrays

In order to dissipate heat, a simple tube-fin radiative system was assessed. A pipe of length (L) has two radial fins (each of length x and thickness t). The temperature distribution (and hence heat flux) through these fins is governed by Equation 3.

$$\frac{d^2T}{dx^2} = \frac{\sigma}{A_c k}\frac{dA_s}{dx}\left(T^4 - T_e^4\right) \qquad (3)$$

Equation 3 is solved numerically to yield the temperature distribution along the radial direction of the fin. A typical temperature distribution described by this equation is shown in Figure 5. Note that heat flux along the direction of the pipe was considered negligible. This is a valid

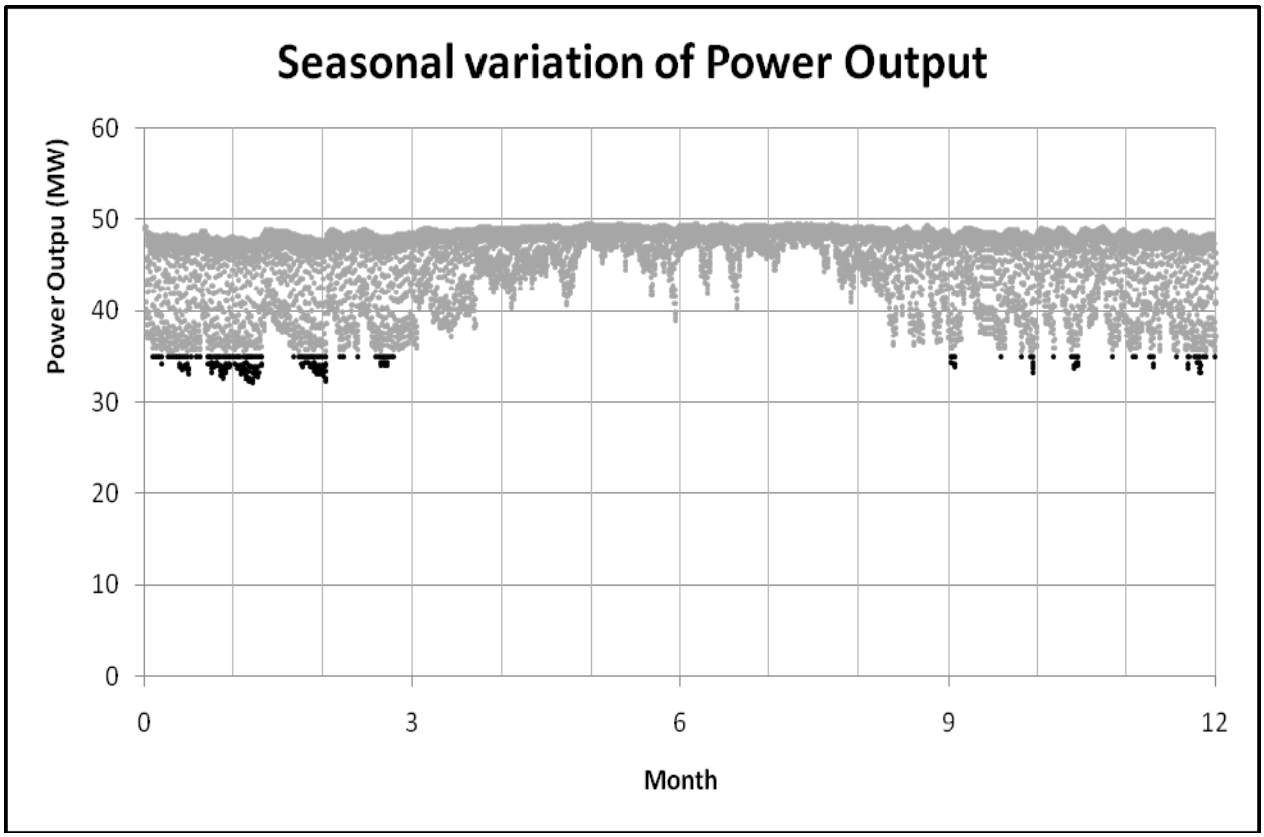

Figure 4 – Typical Seasonal variation of power output for M_c=6.4x10^7kg coolant, Pipe length, L=100m,

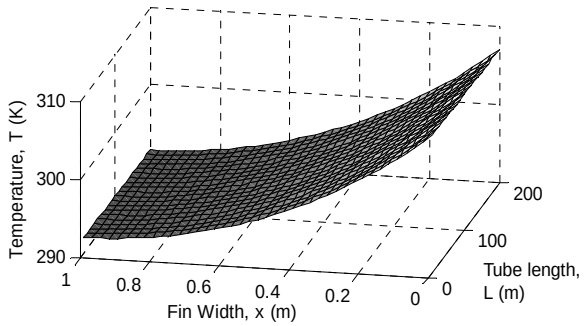

Figure 5 – Typical Temperature Distribution

assumption, as the temperature gradient is approximately 0.02 K/m whereas the gradient along the fins is on the order of 10 K/m. For the purpose of this investigation, both copper and steel plates were considered with a surface finish giving an emissivity of 0.8.

Economic Evaluation

Evaluation of this system and recommendations will be based on both power output and economic cost. Estimates of the initial capital and maintenance costs for each section of the station are to be made. Also included will be the revenue from the power generated with the aim of providing a break-even date.

Summary

Because of the remote arid location of Australia's main geothermal sources, conventional cooling processes are not feasible. The climatic conditions in this area, however, are ideal for nocturnal cooling. This investigation will examine the viability of nocturnal radiative cooling in combination with thermal storage.

References

Dostal, V, Driscoll, M, Hejzlar, P 2004, 'A supercritical carbon dioxide cycle for next generation nuclear reactors', PhD Thesis, Massachusetts Institute of Technology, Massachusetts.

Geodynamics 2006, HFR Geothermal Energy Fact Sheet, viewed 2nd April 2009, <http://www.geodynamics.com.au/IRM/content/home.html> .

Laird, J 2008 Optimisation of a Solar-Geothermal Hybrid Power Plant, Undergraduate thesis, The University of Queensland, Australia.

Massachusetts Institute of Technology 2006, Future of Geothermal Energy, U.S. Department of Energy, Idaho .

Parker, D 2005, Theoretical Evaluation of the NightCool Nocturnal Radiation Cooling Concept, FSEC-CR-1502-05, Florida Solar Energy Centre, Cocoa.

Research Institute for Sustainable Energy 2008, *Geothermal Energy*, Murdoch University, Australia.

Somerville, M., Wyborn, D., Chopra, P., Rahman, S., Estrella, D. and Van der Meulen, T. 1994. Hot Dry Rocks Feasibility Study. Energy Research and Development Corporation. Report 243. 133pp.

Low Temperature Difference Electricity Generation Using ORC

Dr. Matthew Bryson[1*], Simon St Hill[2], Vikram Joshi[2], Chris Dixon[1]
[1]RMIT University, PO Box 71, Bundoora, Vic 3083.
[2]Air International Thermal Systems, 80 Turner Street, Port Melbourne, Vic, 3207.
* Corresponding author: matthew.bryson@rmit.edu.au

Many geothermal sites in Australia have low temperature water as an available heat source. Often this temperature is under 75°C, in conditions where ambient temperatures can climb into the mid 30°s on a regular basis. These heat sources have often been considered to have an insufficient temperature difference, with respect to the atmospheric heat sink, to be worthwhile for driving a heat engine. As the temperature difference reduces, the maximum achievable efficiency must also reduce as demonstrated by classical thermodynamics. Thus, as the temperature difference drops, it is a matter of improving component efficiencies while reducing costs to make such systems viable. Lower temperature systems frequently use an Organic Rankine Cycle (ORC) heat engine. As the temperatures drop, the key parameters in the design of such systems become cost and efficiency. Of prime importance is the cost of the expander, efficiency of the heat exchangers, and the precision of the control system. The main investigations presented are:

- The reduction in system cost through selection of alternatives to turbine expanders.
- The selection of an optimised working fluid for low temperature operation.

Keywords: Organic Rankine Cycle Heat Engine, low grade heat, low temperature difference electricity generation, hydrothermal energy, low temperature geothermal.

Low Grade Heat Sources in Australia

Low grade heat (LGH) sources, here defined as below 100°C, are available throughout Australia. The utilisation of renewable energy sources (such as geothermal and solar thermal power) has been a topic in vogue recently and these sources lend themselves cost effectively to providing LGH that can then be transformed into other forms of energy. Low grade waste heat sourced from industrial processes can also be converted into electricity and therefore improve the efficiency of these industrial processes and consequently advance the pursuit of cost reduction and sustainability in industry. LGH is widely available from these industrial sources and includes the heat energy not utilised in absorption chillers, process condensate and cooling water from a range of industrial processes.

Australian hydrothermal resources

Australia has hydrothermal resources at a number of locations throughout the continent. Notable areas where hydrothermal energy is easily accessible include the Otway and Gippsland Basins (King et al 1985; Sinclair Knight Mertz 2005), the Perth Basin (Ghori 2008) as well as the Great Artesian Basin (Burns et al. 1995; Pirlo 2004). Direct heating applications have been applied to the heated waters of the Gippsland and Otway Basins (Burns et al. 2000) and the Great Artesian Basin has been used to produce electricity on a small to moderate scale with the Mulka Station (now closed) and Birdsville ORC installations (Sawyer 1991; Burns et al. 1995; Burns et al. 2000). The Great Artesian Basin geothermal resource, used as the heat source for the Birdsville plant, has the highest temperature of the resources described. The power station utilises a 1230m deep bore delivering 27l/s of 98°C water to provide heat energy to the plant (EPA Qld 2005). The other three hydrothermal resources mentioned previously in this section have considerably lower temperatures associated with them. The reason for exploiting these low temperature hydrothermal resources is to capitalise on the relative ease in accessing them and thus save on drilling costs.

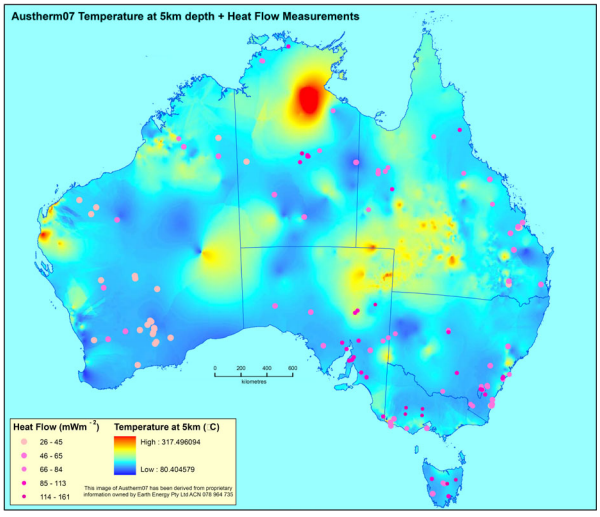

Figure 1: Map of projected temperatures at 5km depth and heat flows for Australia. The areas of darkest blue indicate a temperature of 80°C at 5km depth. The image of Austherm07 from proprietary information owned by Earth Energy Pty Ltd (sourced from Geoscience Australia 2007).

Figure 1 is a diagram that many people are familiar with and is a projection of the temperatures at a depth of 5km. It can be observed from the figure that for most of the continent, the projected temperature at that depth

is around 80°C. It can also be seen that these low temperature areas cover the national population centres and the higher projected temperatures are a considerable distance from the major cities.

In 1999 Kanoglu and Cengel calculated that the cost of drilling to a depth of 5km could cost 2 ½ times the cost of the power plant itself. Ruge (1999) contended that to drill 3.5 km into the Dilwyn Aquifer in the vicinity of Portland Victoria would cost A$1.98 million. For current projects, drilling to the depths to utilise 'hot dry rock' energy in Australia would be between A$15 million and A$37 million according to Goldstein et al (2008). This costing is backed up by a report prepared for the Australian Geothermal Energy Association by the consultants McLennan Magasanik Associates Pty Ltd (2008). One proponent of the study conducted by McLennan Magasanik Associates Pty Ltd (2008) suggested 'the cost of drilling to 4,500 metres was four times the cost of drilling to 3,000 metres'. One way to avoid the high costs of deep drilling is to avoid going to such depths as is required with Australia's geology to source high grade heat. Instead, it may be more cost effective to instead utilise lower grade heat.

Heat Engines for Electricity Generation from Low Grade Heat Sources

Currently, the lowest cost method of converting high grade heat into electricity is through the use of a heat engine. This statement holds true for lower temperature heat sources as well, but as heat source temperatures drop, the units have to be scaled up to achieve the same output. This is due to the compounding effects of 1) the amount of energy contained in lower temperature streams being less and 2) the efficiency of conversion being lower. The result is increased capital costs per unit output. The way to improve the utilisation of lower temperature heat sources, and thereby make use of underexploited resources or reclaim wasted energy, is to reduce the costs of employing heat engines for converting lower grade heat into a higher form of energy such as electricity. Investigations have been conducted into the cost drivers for ORCHEs by those such as Schuster et al. (2009) and Leibowitz et al. (2006), albeit for source temperatures around 100°C and above. These studies showed the possibility of designing commercially viable heat engines for those temperatures. Care has to be taken with the design of the employed cycle and the selection of components for use within these heat engines as the capital cost makes up the vast majority of the lifecycle cost of the equipment.

Thermodynamic cycle selection

One of the more fundamental design decisions to be made when developing a heat engine for use with LGH is the choice of thermodynamic cycle around which the machine will be based. Considerable amounts of research have been conducted looking at various cycles that are applicable to LGH and some of the more recent investigations include examinations of transcritical cycles (Cayer et al 2009), the trilateral flash cycle (Bryson 2007) and the Rankine cycle (Mago et al. 2008). Trials of various working fluids for use in low temperature heat engines have also been conducted and include Tchanche et al. (2009) investigating pure fluids, and Wang et al. (2009) studying zeotropic mixtures. The available research suggests that the Rankine cycle, using a low boiling point working fluid, provides the lowest price (per unit output of electricity).

Working fluid selection

The use of less traditional working fluids, either pure or in mixtures, is another topic that has seen a considerable amount of research being conducted over a number of years. Recently, Tchanche et al. (2009) have examined a range of fluids for use with an ORC utilising LGH and concluded (as have many before them) the ideal working fluid would be one which exhibits high cycle and heat exchange efficiencies, low turbine outlet volume flow rate, manageable high side and low side pressures, develops a favourable pressure ratio upon evaporation, no ozone depletion potential, low global warming potential and is non-flammable, non-toxic and should have no material compatibility problems. Also to be considered are: the specific volume of the liquid working fluid, the thermal conductivity, the viscosity, the surface tension, the thermal stability as well as the cost and availability of the fluid. Availability of the working fluid has become more of a concern in recent times due to the restrictions put on ozone depleting substances and the restrictions on the use of working fluids with a high global warming potential.

When selecting the working fluid for use within a particular heat engine that operates on a chosen cycle, the most critical variables upon which to base the choice are the heat source and sink temperatures. The heat source is usually fixed by what is available at the source of the heat energy, although, in the case of geothermal energy, there is the option of expending more on the drilling costs and accessing a higher temperature. In the case of the low temperature heat sink that must be used to make the engine function, this is usually dictated by the site of the plant (usually a function of a wet or dry bulb temperature or an available watercourse temperature). The working fluid choice, amongst other things, then dictates (for a given heat exchanger effectiveness) the pressures experienced by the high pressure side

and the low pressure side of the engine, the resulting pressure and volumetric ratios, the pumping power required to circulate the fluid and the efficiency of the conversion of heat energy into mechanical energy and then ultimately into electricity.

Figure 2 is a plot of the gross thermal efficiency of a regenerative Rankine cycle with refrigerant top temperatures between 50°C and 100°C. The model presented, developed by Air International Thermal Systems (AITS), has been run with a stipulation of 0°C expander entry superheat and a 20°C condensing temperature. In order to keep the unit from falling below atmospheric pressure in the condenser, a minimum condenser pressure of 130 kPa (absolute) was set. If, at 20°C condensing temperature, the pressure in the condenser (for the fluid being trialled) resulted in an absolute pressure below the set minimum of 130kPa, then the condensing temperature used was the saturation temperature of that of fluid at that minimum pressure. The requirement that the heat engine not fall below the minimum pressure is to avoid the possibility of air being drawn into the machine and consequently prevent the cycle attaining the design pressures. This is a problem experienced by conventional steam plants and various strategies are employed to allow for the removal of the trapped non-condensable air.

It can easily be seen from Figure 2 that, within the temperature range examined, that neopentane gives the highest cycle efficiency over the entire range. The fluids with the next highest efficiency (within 1% of neopentane at 75°C) are in descending order: R114, n-butane, RC318, isobutane, R236ea, R236fa, R227ea, R124, R245fa and R142b. The Carnot efficiency has been included on the plot to give a benchmark.

In accordance with the list of working fluid selection criteria mentioned previously, several of the working fluids examined can be immediately discounted from anything but academic consideration. This list includes the fluids controlled under the Montreal Protocol due to their ozone depletion potential (R114, R124 and R142b). Consideration must also be given to the long term availability of working fluids with high global warming potential (the hydrofluorocarbons RC318, R227ea, R236ea, R236fa and R245fa)) as these fluids are coming under more and more stringent regulatory control. This elimination leaves the naturally occurring hydrocarbons, with their lack of ozone depletion potential and no direct global warming potential, as the remaining choices from this process. There is the concern about the flammability of these substances and also a heat engine must be designed with their cost and availability in mind.

Rankine cycle heat engine components

A simple schematic diagram of a heat engine using a regenerative Rankine cycle can be seen in Figure 3. As can be seen from the diagram, such a device is made up from six major components. The largest expense for a single item is the expander for most systems.

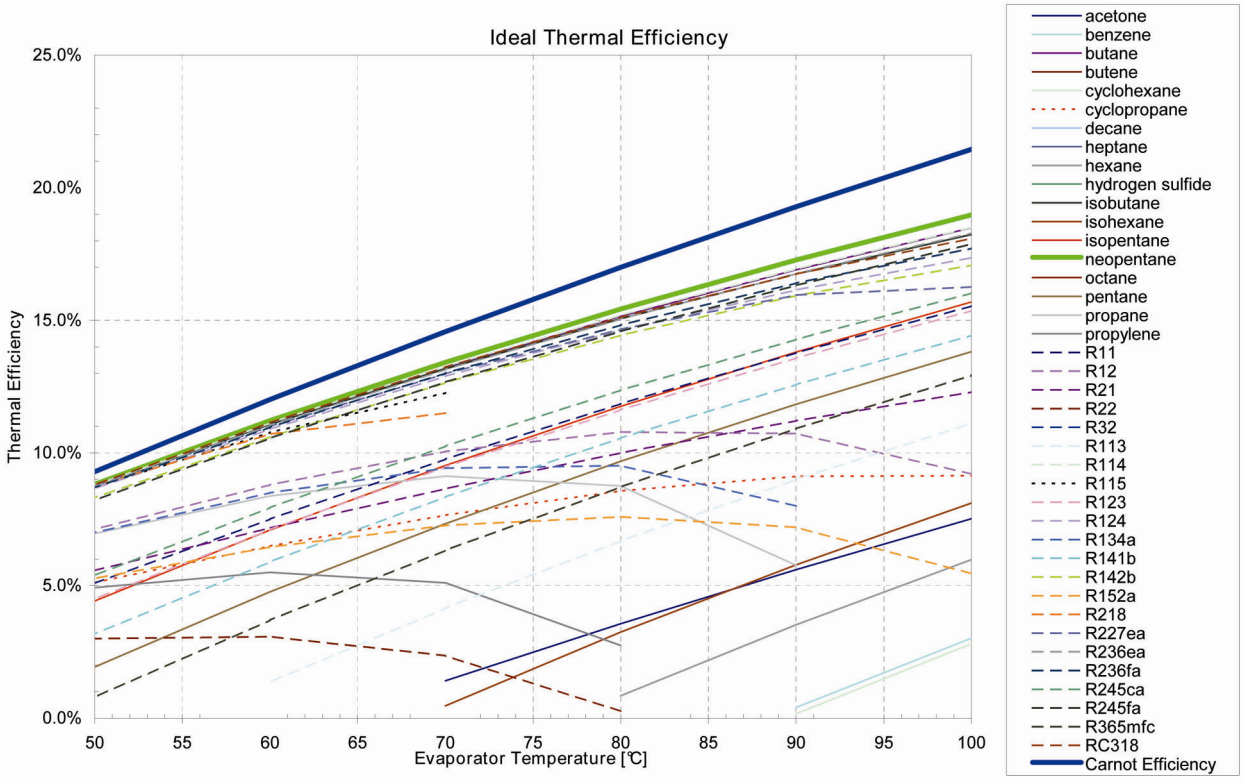

Figure 2: Efficiency figures for an ideal Rankine cycle with a 20°C condensing temperature (or a 130 kPa-abs condensing pressure if the saturation temperature is below this at 20°C) for a range of potential working fluids neglecting any parasitic loads.

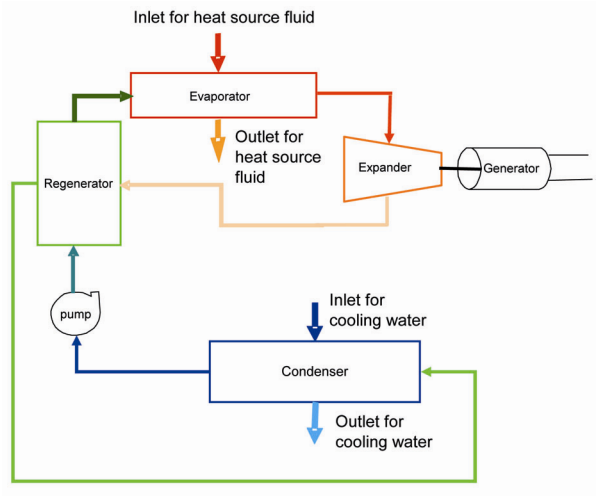

Figure 3: Simple schematic diagram of components used in a regenerative Rankine cycle heat engine.

From the diagram it can also be seen that in a regenerative Rankine cycle, there are three components responsible for heat exchange these being the evaporator, condenser and the regenerator. It is obvious that there is a requirement for the expander and the three heat exchangers to be sourced cost effectively, whilst still performing to an acceptable level, in order for the low temperature heat engine to be a commercially viable option for converting heat into power.

The goal for the design of a heat engine is to produce electricity at the lower price possible per unit of energy sent out. This leads to the two competing design drivers being the maximising of efficiency of energy conversion while minimising the capital outlay. It is usual to find that a more efficient or effective a component is, the more expensive it is. Therefore an optimal balance has to be sought between component efficiency and cost.

Expanders for use with organic Rankine cycle heat engines

As mentioned previously, the single component that has the greatest bearing on the viability of a low temperature heat engine is the expander. Depending upon the configuration, design and materials chosen the cost of sourcing a state of the art expander can easily cost more than the rest of the components combined. Most commercially available turbines developed for power production purposes were designed for service with steam power plants and are now in mass production making them relatively inexpensive to purchase. These units are not, however, suitable for use with many low boiling point working fluids such as hydrocarbons. This is due to the significantly higher molecular mass of the low boiling point working fluids requiring the shafts to carry significantly higher torque at substantially lower rotational speeds. While it is possible to source such a turbine with a very high efficiency, the relatively low numbers in production cause such a unit to be sold at a price high enough to make the ORC unit economically unviable.

Scroll and screw type compressors lend themselves well to operating in reverse as ORC expanders. They are both mass produced leading to their cost effective application to low temperature ORC units. Scroll compressors are widely used in the refrigeration and air conditioning industries and from experience gained in those industries, some concerns have been raised about the durability of the scroll end “tips”. There is not the same concern regarding screw compressors. In addition to this, experience has shown that the largest size of scroll compressor able to be sourced cost effectively on a commercial scale is 500kW. This is significantly smaller than that required for most commercial power production applications. The use of low temperature heat sources allows the selection of screw machines whose normal duty would be compressing gases such as air. There are many of these units produced each year and so their selection means that they are a cost effective part for use in ORC engines.

ORC Experimental apparatus

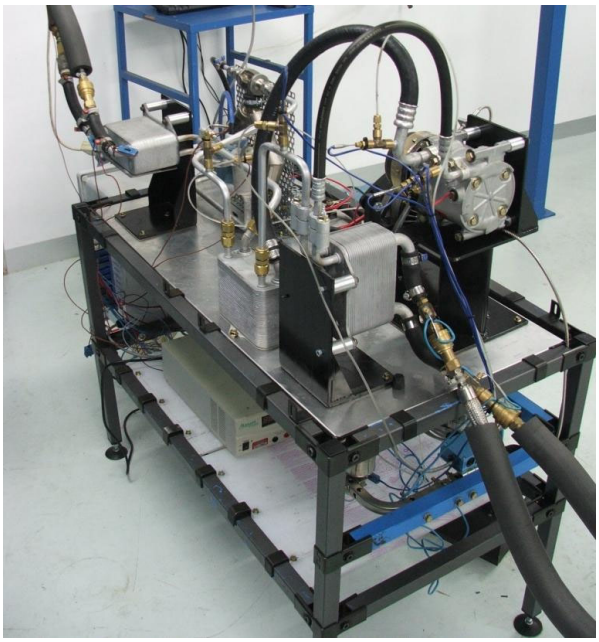

Figure 4: Photograph of the AITS ORC test apparatus.

In order to conduct a parametric experimental investigation of a small scale ORC, AITS has built and instrumented a unit by adapting parts manufactured for other purposes. A photograph of the experimental unit, as tested by RMIT and

AITS, appears in Figure 4. The heat engine, constructed almost entirely from automotive parts either built or supplied by AITS, includes a range of pressure and temperature probes and is part of a closed loop automated system that ensures that the required test parameters are controlled to within the testing tolerance specification. The system uses an air conditioning scroll compressor, operating in reverse, as an expander. A range of tests have been performed and include (amongst others) a charge determination procedure and an evaporator exit superheat sensitivity trial.

Results from the AITS experimental ORC rig

For the purposes of exploring the effect of varying the heating source fluid temperature upon this specific unit, experiments were conducted where the heat source fluid temperature was varied while holding the cooling source fluid temperature at 14.3°C ±1°C and the superheat of the working fluid was maintained at 10°C ±1°C. The amount of working fluid superheat was controlled to within its tolerance band by the computerised control system via varying the flow rate of the working fluid pump. It should also be noted that the fluid flow rates of the heat source and sink were held constant for all of the tests. Figure 5 shows a plot of the power output as the heat source fluid is varied. The output power is given a normalised percentage of the output power of the apparatus when the heat source fluid temperature was 75°C.

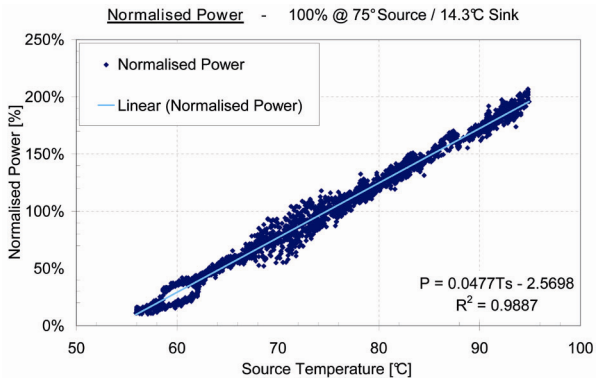

Figure 5: Normalised power output as a function of the heating source fluid temperature for a constant cooling source temperature.

Figure 5 indicates that there is a high degree of linearity in the relationship between the normalised power and the temperature of the heating source. The figure also shows that, for the experimental apparatus examined, the power output at 95°C source temperature is approximately double that at 75°C, while at a source temperature of 64°C is approximately half that produced at 75°C.

Tests trialling the sensitivity of the power output of the apparatus to the temperature of the cooling source fluid were also undertaken. The experiments were conducted with a 75°C ±1°C heating source temperature throughout the tests and the superheat of the working fluid was maintained at 10°C ±1°C. As with the tests examining the sensitivity of the unit to the heat source temperature, the amount of working fluid superheat was controlled in the same manner as for the heat source sensitivity tests. Figure 6 shows a plot of the power output as the cooling fluid temperature is varied. The power out is presented as a normalised percentage of the output power of the apparatus when the cooling source fluid temperature was 14.3°C.

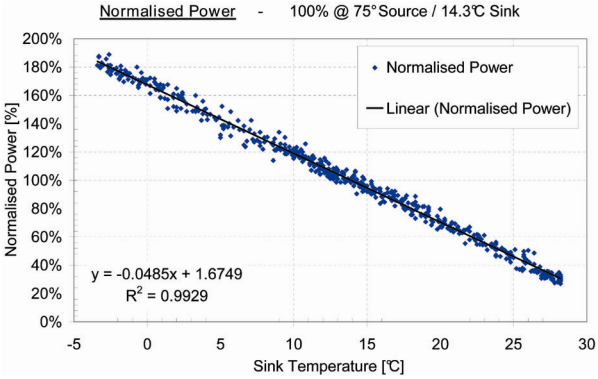

Figure 6: Normalised power output as a function of the cooling source fluid temperature for a constant heat source temperature.

Figure 6 also shows a high degree of linearity in the relationship between cooling fluid temperature and the output power of the rig. At a cooling fluid sink temperature of -3°C, the output of the rig is approximately 1.8 times that of the 14.3°C benchmark trials. At the top cooling fluid temperature of 28°C the output is approximately 30% of the nominal power output.

Conclusions

The available literature on the cost effective production of electricity using ORC heat engines that employ low temperature heat sources is limited. Although the preliminary results of this investigation have been concerned with the performance of the ORC, the indications are that it is cost effective to recover and convert low grade heat to electricity. For heat source temperatures of 75°C and below, the selection of the expander is a key concern due to the trade off between efficiency and capital cost. The selection of a working fluid that achieves a favourable ideal cycle efficiency is also of great impact upon the viability of these machines that utilise low grade heat. Results from the experiments jointly conducted by Air International Thermal Systems and RMIT University show a direct proportionality between achieved power output and heat source temperature within the range examined. It was

also found that, within the range examined, there was also a direct proportionality between the heat sink temperature and the achieved power output. Also notable is the fact that power was able to be produced by the experimental unit from around a 55°C heat source temperature while using a 14.3°C heat sink.

References

Bryson, M.J., 2007, The conversion of low grade heat into electricity using the Thermosyphon Rankine Engine and Trilateral Flash Cycle, [Ph.D. thesis]: Melbourne, RMIT University.

Burns, K.L., Creelman, R.A., Buckingham, N.W., and Harrington, H.J., 1995, Geothermal development in Australia: Proceedings of the World Geothermal Congress 1995, Florence, Italy, p. 45-50.

Burns, K.L., Weber, C., Perry, J., and Harrington, H.J., 2000, Status of the geothermal industry in Australia: Proceedings of the World Geothermal Congress 2000, Kyushu - Tohoku, Japan, p. 99-108.

Cayer, E., Galanis, N., Desilets, M., Nesreddine, H., and Roy, P., 2009, Analysis of a carbon dioxide transcritical power cycle using a low temperature source, Applied Energy, v. 86, p. 1055-1063.

EPA Qld, 2005, Fact Sheet – Birdsville Geothermal Power Plant, EPA Qld, viewed 1 May 2009, <http://www.epa.qld.gov.au/publications/p00834aa.pdf/Birdsville_geothermal_power_station.pdf>.

Geoscience Australia, 2007, Australian radiogenic granite and sedimentary basin geothermal hot rock potential map, viewed 1 July 2009, <http://www.ga.gov.au/image_cache/GA10332.pdf>

Ghori, K.A., 2008, Western Australia's geothermal resources, 2008 American Association of Petroleum Geologists Annual Convention & Exhibition, San Antonio, Texas.

Goldstein, B.A., Hill, A.J., Malavazos, M., Coda, J., Budd, A.R., and Holgate, F.L., 2008, Hot rock energy projects - Australian context, SPE International Thermal Operations and Heavy Oil Symposium 2008, Calgary, Alberta.

Kanoglu, M., and Çengel, Y.A., 1999, Economic evaluation of geothermal power generation, heating and cooling, Energy, v. 24, no. 6, p. 501-509.

King, R.L., Ford, A.J., Stanley, D.R., Kenley, P.R., and Cecil, M.K., 1985, Geothermal resource of Victoria - a preliminary study, Department of Industry, Technology and Resources and the Victorian Solar Energy Council, Melbourne.

Leibowitz, H., Smith, I.K., and Stosic, N., 2006, Cost effective small scale ORC systems for power recovery from low grade heat sources, 2006 American Society of Mechanical Engineers International Mechanical Engineering Congress and Exposition, Chicago, Illinois.

Mago, P.J., Chamra, L.M., Srinivasan, K., and Somayaji C., 2008, An examination of regenerative organic Rankine cycles using dry fluids, Applied Thermal Engineering, v. 28, p. 998-1007.

McLennan Magasanik Associates Pty, 2008, Installed capacity and generation from geothermal sources by 2020, Infrastructure Australia, viewed 13 July 2009, <http://www.infrastructureaustralia.gov.au/public_submissions/published/files/374_agea_SUB3.pdf>.

Pirlo, M.C., 2004, Hydrogeochemistry and geothermometry of thermal groundwaters from the Birdsville Track Ridge, Great Artesian Basin, South Australia, Geothermics, v. 33, p. 743-774.

Ruge, P., 1999, An Overview of the potential for production of geothermal electricity at Portland, Glenelg Shire Council, Portland.

Sinclair Knight Mertz, 2005, The geothermal resources of Victoria, The Sustainable Energy Authority of Victoria, viewed 1 June 2009, <http://www.sustainability.vic.gov.au/resources/documents/SKM_Geothermal_Report.pdf>.

Schuster, A., Karellas, S., Kakaras, E., and Spliethoff, H., 2009, Energetic and economic investigation of organic Rankine cycle applications, Applied Thermal Engineering, v. 29, p. 1809-1817.

Tchanche, B.F., Papadakis, G., Lambrinos, G., and Frangoudakis, A., 2009, Fluid selection for a low temperature solar organic Rankine cycle, Applied Thermal Engineering, v. 29, p. 2468-2476.

Wang, X.D., and Zhao, L., 2009, Analysis of zeotropic mixtures used in low-temperature solar Rankine cycles for power generation, Solar Energy, v. 83, p. 605-613.

Seasonal Storage of Air Cooled Water for Arid Zone Geothermal Power Plants

Robert Collins
Enreco Pty Ltd P.O. Box 690 Alice Springs NT 0871
Email: enreco.geothermal@gmail.com

This paper presents a new option for heat rejection from geothermal plants. Our 20 years experience with small geothermal plants at Mulka Station and Birdsville has convinced us that heat rejection is a major issue in Australian conditions. In arid zones air cooling has been the option of choice due to lack of water and the availability of industrial air condensers. This option has proved expensive, with costs in the U.S. of 20 - 30% of the total capital costs, including wells for 5 major geothermal plants

As noted previously by several authors this option also comes with severe performance penalties due to the extreme summer daytime temperatures. When the demand for electricity is greatest the geothermal electric output will drop by up to 40%. The geothermal industry needs to begin development and testing of new heat rejection options to solve this problem.

Just as the desert presents problems with high daytime temperatures, it offers opportunities with very low night time temperatures, large areas of land available and in most regions, shallow, saline aquifers suitable for water storage. A simple heat rejection system taking advantage of these characteristics is illustrated in Figure 1. A water cooled condenser using saline water from a shallow aquifer provides the heat rejection sink for the geothermal plant. The area of the aquifer used is sized to provide approximately 6 months of cooling water. The water that is returned to the aquifer is intermittently cooled by air coolers when the air temperature is below a set value. As long as the heat rejected to the air during cooler periods matches the heat going into the water form the condenser over the year, a constant water temperature will be maintained.

While the conditions necessary for this concept to work occur in most desert regions, the focus of this paper is on the geothermal areas of interest in the North East of South Australia above the Cooper Basin. Details of this concept, along with advantages and issues, and a design for an illustrative 2 MW geothermal plant cooling system are provided below. Also the matching of this concept with CO_2 as the geothermal fluid as well as plant working fluid is considered

SYSTEM CONCEPT

The system has 3 separate energy loops. The first is the circulation of the saline groundwater from production bores through the geothermal plant condenser and into the reinjection bores. The second energy loop is the intermittent air cooling of the groundwater after it leaves the condenser. This loop rejects to the atmosphere during cooler periods of the year, the heat from the condenser. The third energy loop is also an intermittent air cooling of the groundwater. This loop takes groundwater part of the way between the production and re injection bores and also cools it intermittently during cooler periods. The purpose of this third loop is to provide the extra cooling capacity to compensate for the intermittent operation.

The massive energy storage capacity of the shallow aquifer means that the heat rejected by the condenser can be balanced out over the year by the heat rejected to the atmosphere from the aquifer. The temperature of the water reinjected into the aquifer will vary from 40 °C on a summer day to due to no air cooling to 15 °C on a winter night with air cooling. These temperature variations will be smoothed over the year as the water slowly migrates in the aquifer from the reinjection to production bores.

The air coolers used for aquifer water cooling will be air to water coolers rather than air condensers. This will allow more efficient counter flow heat exchange compared to constant temperature condensing. However, they will have to transfer the same amount of heat only operating intermittently for 1/2 of the year. A major benefit of the intermittent operation is that they can be operated when desired during periods of minimal demand. This will remove the heavy parasitic power load during peak periods, increasing the net power output of the geothermal plant by 10-15% above its rated capacity.

Using saline ground water for cooling should not be a problem as seawater fed condensers operate around the world. Scaling problems should be minimal if the water temperature is kept below 40 °C. The 2 potential scaling problems with this groundwater are silica and calcium compounds. Both can be serious if there is any evaporation which brings them closer to saturation in the solution. Calcium can be a problem if there is heating beyond 40 °C as its saturation limit rapidly declines above this. Neither condition exists for this concept.

The cost of this complete condensing system will be greater than a standard air cooled condenser. The air to water coolers will have to have double the heat rejection capacity of an standard

continuously operating air condenser, since they will only be operating ½ the time. There will also be additional components such as the water cooled condenser, the saline aquifer bores, and submersible pumps. We estimate the cost for the complete system will add approximately 10% to the cost of a geothermal plant. The benefits far outweigh this cost. Instead of a 2 MW plant producing 1.2 MW on a hot day due to higher condensing temperatures, it would produce its rated 2 MW plus an extra 0.3 MW of reduced parasitic power loss not required for air cooling fans. Thus the useful output is nearly doubled when it is most needed and high value.

SALINE AQUIFERS

Shallow saline aquifers are nearly ubiquitous in the areas of interest above the Cooper Basin.

This is not surprising as Cooper Creek is part of the Lake Eyre Basin, which is the largest internal drainage basin in the world. Cooper Creek spreads out into a vast meandering area of ephemeral channels that are normally dry.

Saline groundwater is normally found at depths of 10 - 100 metres and even closer to the surface near salt pans. Aquifers can be 10s - 100s of metres thick. This water is of no economic value because it usually has too high a salt content for stock watering or cropping. Salt content is quite variable.

The bores for production and reinjection would be approximately 40 metres deep and cased with slotted PVC pipe. For a 2 MW geothermal plant approximately 20 of each would be required. These shallow bores should be relatively cheap to drill at 50 metre spacings. There are many suitable patterns for the bores, but probably the simplest is 2 parallel lines of bores separated by a suitable distance for the required 6 months storage requirements. For the other air cooling loop an additional 20 production and re injection bores would also be required

If we assume an aquifer thickness of 30 metres, soil porosity of 30%, then there is 10 thousand mega litres of water available per km^2. Thicker aquifers are better as they provide greater storage in the same area and also have higher flow rates/bore, requiring less bores. Typical shallow aquifer water temperatures in the Cooper basin are 23 °C. This is a substantial cold water storage system that is freely available.

Pumping from the aquifer would be via submersible pumps in the production bores. Since it is a closed circulation system, the head required would be primarily friction losses in piping, the condenser and air cooler. Total pumping head for the cooling system is estimated at 20 metres.

2 MW GEOTHERMAL PLANT OPERATION

A 2 MW geothermal plant has been chosen to illustrate the cooling concept. Assumed design parameters are 15% thermal efficiency and a working fluid condensing temperature of 40 °C. The heat rejection rate required is 11.3 MW. For water entering at 23 °C and exiting at 40 °C the required flow rate to capture this heat is 159 litres/sec. To provide 6 months storage requires 2514 mega litres.

Assuming the saline aquifer parameters described in the preceding section, we require an aquifer area .25 km^2 or a square 500 metres on a side. This could be satisfied by our parallel lines of production and reinjection bores spaced 600 metres apart. The geothermal plant would be in the middle between these 2 lines. A single large diameter pipe would connect the 2 lines of bores to the geothermal plant, so that a top view looked like the letter H. The bores would be spaced 50 metres apart on 1 kilometre lines forming the sides of the H.

To make up for the intermittent cooling, a second identical set of bores would be placed inside the H, forming a smaller H. These would operate at the same time to double the air cooling capacity. The production bores and re injection bores would be 200 metres apart and the 2 lines of these would be 200 metres inside the lines of the first set of bores.

These bores would operate counter flow to the first set of bores. They would provide additional cooling to aquifer water that had been reinjected several months before. This would make up for the intermittent operation of the cooling system. The relatively huge capacity of the aquifer and soil would smooth out the daily and seasonal temperature variations of reinjected water.

The power requirement to pump 159 litre/sec flow rate against a 20 metre head would be 50 kW or 2.5% of the plant capacity. This would be full time. The air cooler fans (300 kW) would operate intermittently when air temperatures were below 25C and when power demands allowed. Use of variable speed drives on the fans would allow even greater flexibility to cool the water at the optimum times.

The total fan power and pump power for both sets of bores and air coolers would be approximately 700 kW or 35% of the plant capacity to provide double the normal heat rejection to the atmosphere. Based on climate data from Moomba South Australia the fans would run approximately 1/2 of the year, during cooler, lower demand periods.

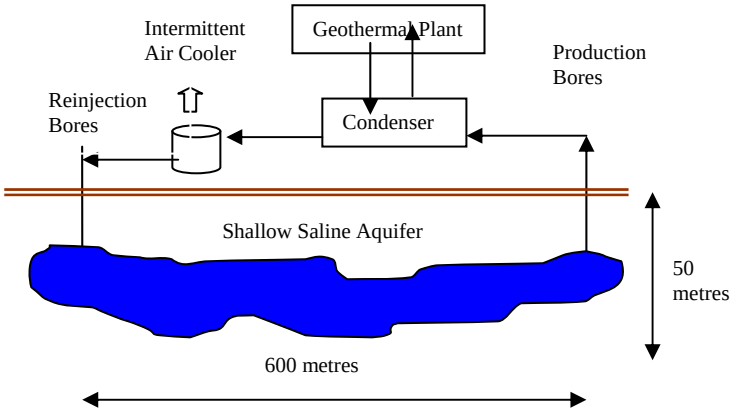

Figure 1. 2 MW geothermal plant cooling system using air cooled water with a shallow saline aquifer

CO_2 GEOTHERMAL SYSTEMS

CO_2 geothermal systems, where CO_2 is used as both the geothermal fluid for heat extraction, and as the working cycle fluid, offer significant advantages. There is a very big issue on the cooling side as the supercritical temperature for CO_2 is 31 °C. Above this temperature there is a huge performance penalty on the plant of up to 40%. Conventional air cooling systems could not meet this requirement most of year in the Cooper basin. The proposed cooling system in this paper could provide the necessary cooling to condense the CO_2 below its critical temperature. This would be critical during the summer periods of peak electricity demand.

CONCLUSIONS

The seasonal storage of water with air cooling offers a possible solution to the significant problem of summer heat rejection from geothermal power plants in arid regions. The presence of shallow saline aquifers in the Cooper Basin appears to offer a straight forward implementation of this concept in this region.

The additional costs are more than compensated for by the much greater plant output in peak periods and the flexibility to schedule parasitic cooling loads. The same benefits accrue to CO_2 geothermal systems.

Heat rejection is a major issue for geothermal plants in terms of capital cost, performance, and maintenance costs in Australian conditions. New concepts beyond just simple air condensers need to be developed and tested.

Feasibility Assessment of Underground Cooling for Geothermal Power Cycles

Bassam Dally*, Graham Nathan, Sean Watson, Andrew Heath and Carl Howard
[1] School of Mechanical Engineering, The University of Adelaide, SA, 5005.
* Corresponding author: bassam.dally@adelaide.edu.au

Geothermal heat sources offer significant potential for electricity generation in Australia by Hot Fractured Rock, HFR, technology and other approaches. However, all of the sites of greatest geothermal potential are situated remote from any significant surface water source, which poses a significant challenge to the method by which the working fluid in the power cycle will be cooled. The need for cooling in any thermal power cycle has driven many conventional power plants to be located close to a river, lake, or ocean to provide an environmental heat sink (Department of Environment, 2001). Where this is not realistic, cooling towers are almost invariably used to provide greater cooling than is possible by air-cooling alone, utilising the evaporation of water, much like a large evaporative air cooler. However, the water consumption due to evaporation and fouling losses, even for a conventional power station with comparatively high efficiency, is typically 1363 L/MW.h per day (Ricketts et al., 2006), and will be greater for typical geothermal plants owing to their low thermodynamic efficiency.

Indeed, the recent increase in demand for air-cooled condensers is a direct result of water shortages at potential plant sites and increasing government legislation limiting the use of water in the wet cooling systems (Ricketts et al., 2006). As noted above, the regions in which geothermal heat is the most viable are arid or semi-arid, with no readily available source of surface water for cooling. While underground water is present, notably from the Great Artesian Basin, it is unlikely that environmental regulators will allow it to be utilised because of the very large water consumption required by any large thermal power plant. Therefore, alternatives to conventional water-based cooling methods are expected to be required for these power plants.

The present commercially available alternative method of heat dissipation is through the use of conventional fin-and-tube air cooled heat exchangers. Fins on the surface of the heat exchanger are typically used to improve the heat transfer by increasing convection and radiation away from the surface. Such systems are used in a number of geothermal plants, e.g. in the Mokai plant in New Zealand. However, in the areas of interest, such as the Cooper Basin, daily ambient air temperatures can reach 45ºC in the summer, in which case the minimum temperature of the working fluid temperature must be in the range 48-50ºC, owing to the fact that the effectiveness of a heat exchanger is always less than 100%. Such high condenser temperatures result in a low efficiency of the power cycle. For example, Langman et al (2008) estimate that the output from a geothermal plant at a typical site in South Australia would drop by 40% as the ambient air temperature is increased from 15 to 45ºC. Furthermore, the peak demand, and hence peak prices, in the national grid are greatest during the very time when the output is lowest. Such a scenario could significantly influence the economic viability of a plant. Fans may be employed to force air over the fins to improve the performance of the heat exchanger, but consume large amounts of energy and hence reduce the net amount of electricity produced by the plant.

A potential solution to the problem of cooling the working fluid is to install a heat exchanger underground where temperatures are lower and more stable. Heat in the working fluid may then be rejected to the soil and in turn dissipated to the atmosphere. For this reason, the aim of the present investigation is to assess the feasibility of underground cooling for such a geothermal plant.

Keywords: geothermal, power cycle, condenser, underground cooling.

Approach and Methodology

The heat transfer processes within an underground heat exchanger are time dependent and three dimensional. Analytical solutions are unable to account for such variations in soil and atmospheric conditions. Hence we opted for a modelling strategy that accounts for temperature variation and heat flow over 24-hour period, repeated for many days. In this approach we are able to account for the radiation in the day and night and the temperature variation of soil and the air over an extended period.

In order to simplify the problem while maintaining the core issue intact, the following assumptions were made:

- the soil is homogeneous;
- there are no phase changes in water, and no latent heat effects;
- the soil emissivity, absorptivity and reflectivity are constant;
- convection over the surface is a function of wind speed, which is fixed;
- the pipe depth is fixed, and

- the effects of the pipe wall on conduction are negligible.

A block of soil with sides of approximately equal length, shown in Figure 1, is analysed. A pipe representing the heat exchanger is buried underground at a certain depth, ***l***, and the working fluid of the power cycle is passed through the pipe at a temperature T_i. Since the soil is at a lower temperature than the pipe, heat energy is lost to the soil, such that the fluid exits the pipe at some lower temperature T_o. It should be noted that the boundaries of the block of soil are assumed to be semi-infinite, and thus heat may be lost through the faces of the block with negligible resistance.

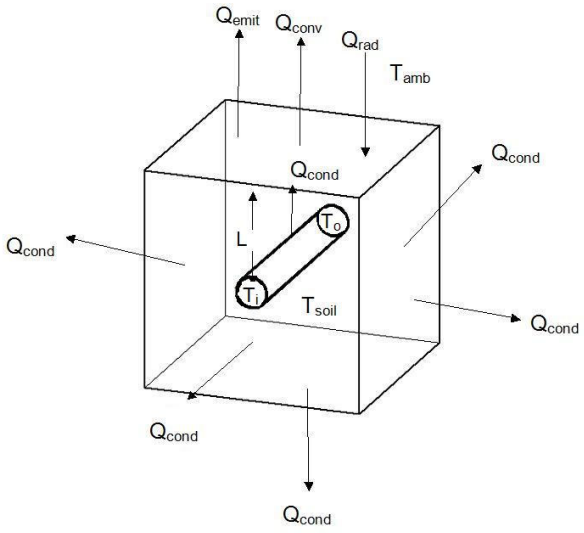

Figure 1: Schematic diagram of a pipe buried in soil

The pipe depth ***l*** is an important parameter and will have a crucial effect on the behaviour of the model. It is known that fluctuations in temperature over a period of time decrease with soil depth, depending on the properties of the soil (Pavelka et al. 2006). The measured change in temperature over the period of one day for various soil depths is presented in Figure 2. Thus, at a depth of just 30cm the temperature fluctuation for soil over a day can be small (typically 1 to 2ºC).

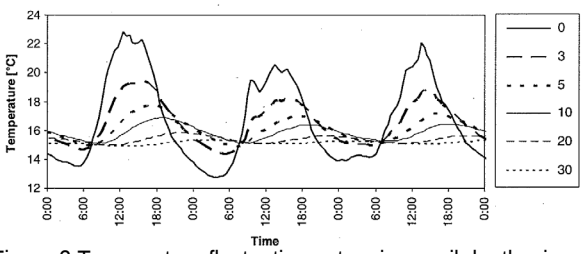

Figure 2 Temperature fluctuations at various soil depths, in cm, over 24 hours period [Paveleka et al., 2006]

For the present comparative assessment, it is sufficient to assume a typical temperature for the working fluid entering the condenser. We have chosen this to be 100ºC. This is typical of the temperature at which the geoliquid is expected to be returned underground from Enhanced Geothermal Systems (EGS) under conditions in central Australia (Langman et al, 2008). While being somewhat higher than expected condenser temperatures, for the present comparative purposes it is sufficient to ensure that both the geothermal and air-cooled temperatures are based on the same reference condition. The heat being lost to the soil through conduction is termed $\mathbf{Q_{cond}}$ in Figure 1 and depends on a number of parameters, including the conductivity of the soil. The conductivity of soil changes as the moisture content of the soil increases or decreases and is largest when the soil is wet. However, as rain is rare in the arid regions being considered, the soil conductivity is assumed to be that of dry soil, and is assumed to be constant. Note that this assumption is conservative, since the presence of moisture will increase the thermal conductivity. One report suggests that thermal conductivity values for sandy loams range from 0.54W/mK to 1.94W/mK (Abu-Hamdeh and Reeder, 2000). Exact data for the geomorphology of the Cooper Basin region is difficult to obtain, as reports suggest that the region contains both wetlands and desert, which have widely varying soil properties (Burdon, 2006). To allow for a conservative solution for conduction then, it was decided to use a value of 0.75W/mK for the thermal conductivity of all models, which is typical of sandy loam soils.

The heat transferred to the surface by radiation from the Sun during the day is termed $\mathbf{Q_{rad}}$, shown in Figure 1. Solar radiation is made up of two components, namely direct radiation and indirect radiation. For the purposes of the present model, the direct and indirect radiation are grouped into a single quantity. Measured data for the daily and seasonal variation in $\mathbf{Q_{rad}}$, are readily available.

The infra-red radiation from the soil is shown in Figure 1 as $\mathbf{Q_{emit}}$. It is assumed that the soil is a gray body and will emit radiation as a function of the emittance of the soil and the temperature difference between the soil and the air. The emittance of the soil is assumed to be constant and equal to 0.75 (Mills, 1999). Radiant losses are assumed, conservatively, to be to the air at ambient temperature. Measured data for the daily and seasonal variation in ambient temperature are readily available.

Heat is also dissipated through convection from the surface, termed $\mathbf{Q_{conv}}$ in Figure 1. This depends on the wind speed of the air flowing over the surface and the ambient air temperature. The average daily wind speeds for the month of January were obtained from Energy Efficiency and Renewable Energy (2008) and were averaged to provide a monthly average value.

This monthly average value was used to calculate the convective heat transfer coefficient.

The finite quadrilateral elements for the 2-dimensional longitudinal cross section model with a 50mm diameter pipe, 0.1m deep and 50m long is shown in Figure 3. Owing to constraints of the ANSYS package (ANSYS, 2007), to model an infinite boundary condition, it is necessary for the boundary of the problem to be circular as shown in the model below.

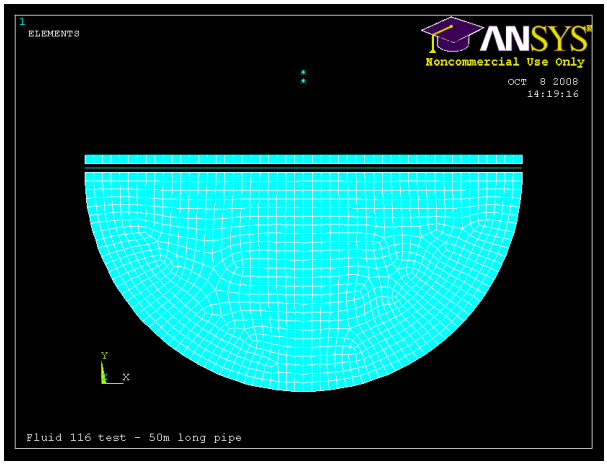

Figure 3 Finite element model of the 2-D Longitudinal Cross Section. Pipe diameter 0.05m, depth 0.1m and length 50m.

The thermal properties of the soil and the air, used in the model, are shown in Table 1.

Table 1: Soil and air thermal properties

Symbol	Soil	Air
k(W/mK)	0.75	0.0271
C(J/kgK)	1000	1900
ρ(kg/m³)	1500	1.225
ε	0.77	-

The inlet temperature of the water was assumed to be 373K. The heat dissipated by the underground pipe system was set to 5MW. The mass flow rate of water in the 0.005m diameter pipe was assumed to be 16 kg/s. The heat transfer coefficient inside the pipe was calculated using the Dittus-Boelter correlation for turbulent flow inside a smooth pipe.

$$Nu_D = 0.023 \mathrm{Re}_D^{0.8} \mathrm{Pr}^{0.4}$$

The pipe thermal conductivity is estimated at 0.41 W/mK. Thermal resistance between the soil and the pipe was assumes to be negligible. In practical systems this resistance can be minimized through proper compactness of the soil surrounding the pipes.

Weather data including the hourly average ambient temperature and an average hourly radiation for all days in the month of January were obtained from a weather station in the town of Oodnadatta, which is representative of summer conditions in the Far North East of the state of South Australia (EERE, 2008). The choice of January was due to it being in the middle of summer with the hottest daily temperatures. This corresponds to the worst loading conditions for the heat exchanger.

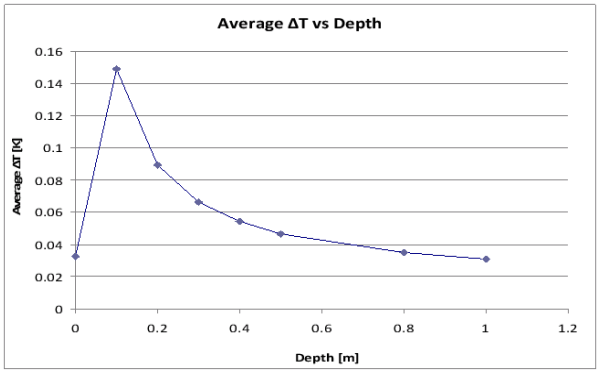

Figure 4: Water temperature drop plotted against the pipe depth after 20 days. Pipe diameter 0.05m, pipe length 50m.

The daily average wind speed for the month of January was used to calculate the heat convection coefficient to be 23.6W/m^{2}K.

Results and Discussions

Presented in Figure 4 is the temperature at the pipe exit plotted versus the pipe depth at end of a 20-day period. The 20-day period ensures that the temperature reaches pseudo-steady state conditions. It is clear from the figure that a depth of 10 cm is the most appropriate and provides the highest temperature loss for a fixed length of pipe.

The drop in temperature appears to be quite small for the 50 m length of the pipe amounting to 0.15K. However this amounts to 10 kW of heat which was dissipated away from the pipe and into the atmosphere. Worthy of note too, is that there was no attempt to enhance the pipe design which would have increased the amount of heat lost per length of pipe. Such enhancement can include fins, surface protection from sun radiation and other methods to increase heat loss during the night.

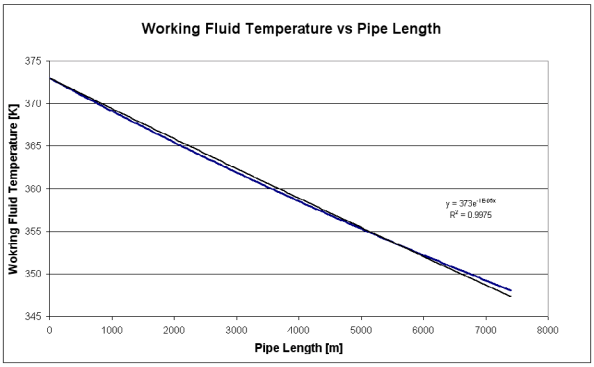

Figure 5: Calculated Temperature drop along a 50m length, repeated over a 7.4km length of pipe

The longitudinal model was also used to obtain an estimate of the overall pipe length to dissipate 5MW of heat. The 50m geometry, in Figure 3, was looped multiple times to calculate a temperature drop over 7.4km. In other words the exit temperature from the first 50m pipe after 20 days was used as inlet temperature to the second 50m pipe and the process was repeated 148 times to give the exit temperature at accumulated lengthy of 7400m. The exit temperature from each run is presented in Figure 5 for every 50m. A trend-line has been applied to this data and the equation of the trend-line is also shown on the graph.

Noteworthy is that the temperature difference between the pipe and the surrounding soil, which drives the potential for heat transfer, drops and hence the effectiveness of a meter length of pipe drops too. Hence extrapolating the curve generated above to longer pipes may not be accurate. Nonetheless, the curve fit is for almost half of the temperature reduction required (70ºC) and a reasonable estimate can be generated using this method. Thus, solving for length, and using a value of 300K (27ºC) for the pipe exit temperature, the length of pipe required is approximately 22km. To account for the issues discussed above a conservative estimate was deemed to be prudent and a factor of safety was introduced. Hence for the cost analysis, the overall length of pipe required for the underground cooling process was set to 25km.

The present preliminary cost estimate was undertaken for the above conditions without any specific reference to a relevant geothermal thermal cycle. That is, it does not consider the influence of the cooling cycle on the performance of the power plant. Nonetheless, these rough estimates, which considered worse weather conditions, have shown that in comparison to air cooled heat exchanger our approach is highly cost effective both from the initial investment and operating cost. It is anticipated that with further optimisation and accounting for year long weather conditions the above conclusions will hold.

Future work will focus on proving this concept experimentally and expanding the modelling work to a specific location accounting for local soil properties, likely thermal cycle and adopting standing heat transfer enhancing methods such as fins. This work will then give us further grounds to build a prototype to accurately quantify the benefits.

Summary

A preliminary assessment has been undertaken of the technical and economical feasibility of using soil to store energy during the day and dissipate it during the night. The assessment is based on conditions in the Copper Basin region of South Australia. Several approaches were used to calculate the rate of heat transfer and the viability of the concept, including analytical and an advanced computational technique, Finite Element Analyses, (FEA). It was estimated that the optimal depth to burry the heat exchanger pipes is about 0.1 m. This depth was arrived at through modelling the soil absorption of the heat dissipated from the pipe and the impact of the sun radiation, air temperature and wind speed on heat transfer from the soil to the atmosphere.

A two dimensional longitudinal model was used to estimate the length of pipe required to dissipate 5MW of heat by cooling a working fluid (Water) from 100ºC to 30ºC. The model revealed that an approximate length of 25km of 50mm diameter pipe is required to achieve the required heat transfer. The cost of dissipating heat through a water-based system at low pressure was estimated to be less than that of a conventional air cooled heat exchanger. Several other advantages are anticipated, such as avoiding the need for fans and a power output that is much less dependent on ambient temperature. However, a detailed assessment of its impact on the performance on the plant, or the economic feasibility is yet to be undertaken.

In addition, as with all models, a number of simplifications and approximations have been required, so that further model development and experimental validation are required to help better estimate the benefits. Further work is also required to optimise the design and consider its integration into specific geothermal cycles with a view to justifying a demonstration prototype.

Acknowledgements

The authors acknowledge the financial support of the Primary Industry and Resources in South Australia, PIRSA under the Australian Geothermal Energy Group Tied Grant scheme.

References

Somerville, M., Wyborn, D., Chopra, P., Rahman, S., Estrella, D. and Van der Meulen, T., 1994, Hot Dry Rocks Feasibility Study, Energy Research and Development Corporation, Report 243, 133pp.

Abu-Hamdeh, N. H., & Reeder, R. C. (2000). Soil Thermal Conductivity: Effects of Density, Moisture, Salt Concentration, and Organic Matter, Soil Science Society of America Journal , Vol. 64, No. 4, pp1285-1290.

ANSYS. 2007, ANSYS v11.0 Release Documentation, v.11.0, computer program, ANSYS Inc., Pittsburgh, PA, USA

Burdon, A 2006, 'The Strzelecki Track', Australian Geographic, Issue 82, pp42-57

Australian Government, Department of Environment, Water, Heritage and the Arts, 2001,

<http://www.environment.gov.au/education/publications/greenhouse.html>

Energy Efficiency and Renewable Energy (EERE) 2008, Statistics for SA Oodnadatta Airport, Department of Energy, USA

Langman, A.S., Nathan, G.J., Ashman, P.J. and Battye, D. (2008) “Preliminary Investigation of the Mech. Systems Needed to Extract Geoth. Energy from a Typical South Australian Site”, Report to: Electricity Supply Industry Planning Council, Consulting Report MECHTEST MT-0949, School. Mech. Eng., University of Adelaide.

Mills, A. (1999). Heat Transfer 2nd Edition. New Jersey: Prentice Hall

Pavelka, M., Acosta, M., Marek, M., Kutsch, W., & Janous, D. (2006). Dependence of the Q10 values on the depth of the soil temperature measuring point, Plant & Soil , Vol. 292, 1/2, pp175

Ricketts, C, Myint, M, Nirmalakhandan N & Gadhamshetty V 2006, Improving Air-Cooled Condenser Performance in Combined Power Cycle Plants, Journal of Energy Engineering, Vol. 132, No. 2, pp81-88.

Dry Cooling Technology in Chinese Thermal Power Plants

Zhiqiang Guan* and Hal Gurgenci
The Queensland Geothermal Energy Centre of Excellence (QGECE), the University of Queensland, St Lucia, Brisbane, Qld 4072
* Corresponding author: guan@uq.edu.au

Design of efficient dry cooling system is of critical importance for geothermal power conversion technologies. In fact, dry cooling may be the only option for most geothermal power plants planned to be established in areas with limited access to water. The heat exchange performance, flow geometry optimisation and cost are key factors in determining suitability of dry cooling towers for geothermal power plants.

China has made advances in recent years in R&D, manufacturing, and utilisation of dry cooling towers in its coal rich but water scarce Northern provinces. One driver for the surge in applications of dry cooling systems is the government regulation that requires all new coal-fired power plants built in Northern China region to use dry cooling systems. Northern China has plenty of coal but no water for wet cooling in its coal-fired power plants.

A straightforward copying of the technology from coal-fired power industry to geothermal power industry is not expected to deliver a cost-effective solution and should be avoided. Benefits would be gained by reviewing the development of dry cooling technologies in Chinese coal-fired power plants. The Queensland Geothermal Energy Centre of Excellence (QGECE) has supported Dr Zhiqiang Guan to apply for the Queensland International Fellowship aiming to review the advance of the dry cooling technology in China. In this paper a summary of dry cooling technology will be given with a focus on the Chinese practice.

Keywords: Geothermal energy, Cooling tower, natural draft cooling technology, Coal-fired power plants.

Cooling Technology in Thermal Power Plant

Thermal power plants make use of a steam cycle to transport energy from large boilers to turbo-generators. An important part of this steam cycle is the condensation of the steam downstream of the turbine. A Cooling Tower is a heat rejection device that extracts waste heat to the atmosphere by either cooling a stream of hot water from the condenser (indirect wet or dry cooling) or cooling (condensing) the steam downstream of the turbine directly (direct dry cooling). Cooling towers are classified as either wet or dry cooling.

A wet cooling is a recirculation water system that accomplishes cooling by providing intimate mixing of water and air, which results in cooling primarily by evaporation. As shown in Fig.1, the hot water leaving the condenser is piped to the cooling tower and is pumped and distributed across the distribution deck where it flows through a series of nozzles onto the top of the tower's fill material. Fill material is used in cooling towers to create as much water surface as possible to enhance evaporation and heat transfer. The water, after being cooled by a combination of evaporation and convective heat transfer, is pumped through the condenser to condense the turbine steam in a continuous circuit.

Wet cooling towers are characterised by the means by which air is moved. Mechanical draft cooling towers rely on power-driven fans to draw or force the air through the tower. Natural draft cooling towers use the buoyancy of the exhaust air rising in a tall chimney to provide the draft.

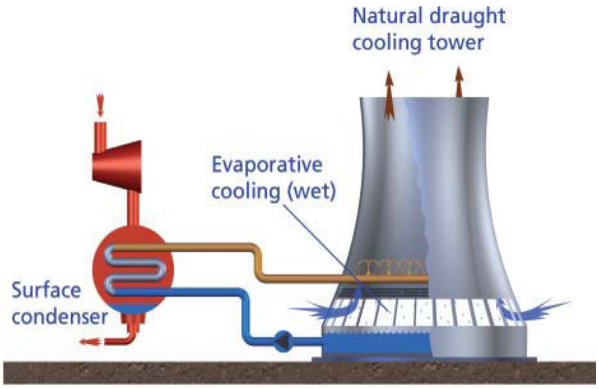

Fig.1 Wet cooling tower [GEA Aircooled Systems (Pty) Ltd]

Dry cooling towers rely on convection heat transfer to reject heat from the working fluid, rather than evaporation. The cooling takes place through air-cooled exchangers similar to radiators. Fig.2 shows configuration of natural draft dry cooling tower used by the thermal power plants.

In natural-draft cooling towers, the volume flow rate of air across the heat exchanger bundle is directly proportional to the height of the cooling tower. There are some options in natural draft cooling tower to use fans to enhance the air flow through the tower.

If fans are used as the mechanism to circulate air, then there is no need for a tall tower as shown in Fig.3. While such systems are cheaper to build, the power needed to drive the fans is significant, especially in low-efficiency cycles where proportionally more heat must be dumped for each MW of electricity generated.

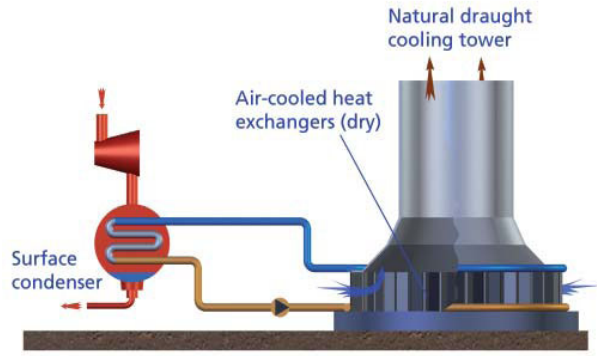

Fig.2 Natural draft dry cooling [GEA Aircooled Systems]

Fig.3 Zhenglan Inner Mongolia Province — ACC for 4 x 600 MW Coal Fired Power Plant

Wet / Dry Cooling Towers

Theoretically a wet cooling tower could cool the water to a temperature approaching the ambient air wet bulb temperature. This cooling system is more efficient, relatively cost effective to install and easy to operate. They are, however, becoming less attractive since they consume large amounts of water through evaporation and high blowdown rates. Dry cooling towers, on the other hand, cools the water to a temperature governed by the ambient air dry bulb temperature. No water is used and therefore the operating costs are lower due to the savings on the cost of water and the water treatment. Since the dry bulb temperature for air is higher than the wet bulb temperature, dry cooling towers require significantly larger heat exchange areas and they are more expensive to build than wet towers.

Water consumption

Coal-fired plant using wet cooling system would require huge amount of water annually to replace cooling tower evaporation, blowdown and drift losses. Under certain conditions, a wet cooling tower plume may present fogging or icing hazards to its surroundings. Fig.4 is a photo of natural draft wet cooling towers at a power plant.

Zhu and Guan (2006) have studied water consumption by comparing the water usage between two wet and dry cooling coal-fired power plants in China. The plants have the same power generating capacity of 2x600 MW. The study assumed the plants operate 5500 hours yearly and the results are shown in Table 1. It is seen that the water saving is 8.8×10^6 m^3 per year from the dry cooling system. This is based on the factor that the water consumption for other equipments in the plants is the same.

Fig.4 Natural draft wet cooling tower in power plant

Table 1. Comparison of water consumption between wet and dry cooling systems

	Dry cooling	Wet Cooling
Water consumption Index (m^3/s.GW) (yearly average)	~0.13	~0.5
Water consumption hourly rate (m^3/hrs) (yearly average)	560	2160
Total water consumption in a year (m^3)	3.08×10^6	11.88×10^6
Water saving (m^3)	8.8×10^6	

Coal consumption

Since evaporation process is governed by the ambient air's wet bulb temperature, which is significantly lower than its dry bulb temperature, power plant using a wet cooling system is more efficient than a similar power plant using a dry cooling tower – if the same size of cooling tower is used in both cases. Zhu and Guan (2006) have studied the coal consumption of the above two generators and the results are shown in Table 2. The cooling towers are of the same size but one plant uses a dry cooling tower, the other is wet.

The result shows that, for a 2x600MW power plant operating 5500 hours in a year, the wet cooling plant uses 145200 tonnes less coal than the dry cooling plant.

Table 2. Coal consumption between wet and dry cooling systems

	Dry cooling	Wet cooling
Sub critical generator Coal consumption (g /(kW*h)	332	310
Super critical generator Coal consumption (g /kW*h)	317-320	298

Capital cost

Chai (2006) conducted a cost study on four 2x600MW power plants, one with wet cooling and the other three with dry cooling systems. The result is shown in Table 3.

Table 3. Capital cost comparison (10^6 Chinese Yuan)

	Stand wet cooling plant	Datong power plant	Toketo power plant	Yang Chen power plant
Equipment cost	135.66	492.11	346.40	420.70
Construction cost	58.98	69.80	122.16	145.29
Installation	58.98	68.66	96.68	68.11
Total	256.82	630.57	565.24	634.10

Results of a similar analysis conducted for US plants was presented by Maulbetsch (2008) in an Advanced Cooling Workshop in Charlotte, NC and the US results according to this study are presented in Fig.5. Based on these limited samples, in US, the capital costs of dry cooling systems appear to be about 3.0 - 3.6 times higher than wet cooling systems and, in China 2.0 - 2.5. It should be noted that the operating cost will vary depending the cost of water and water treatment.

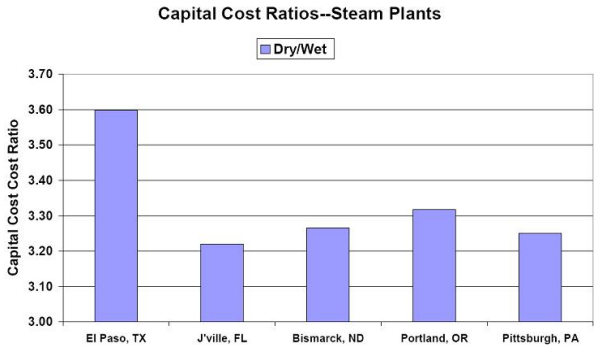

Fig.5 Cost comparison by Maulbetsch (2008)

Market Potential of Dry Cooling in China

Based on the current GDP growth rate in China, the demand for electrical power is significant. It has been predicted that the increase of the electricity must be at least 7% to maintain the country's GDP growth. Reportedly using conservative assumptions, Liu (2007) predicts the total electric energy demand for 2010 and 2020 to be 818 GW and 1186 GW, respectively, as shown in Table 4.

Chen (2008) predicts the demand for dry cooling systems for heat exchanger manufactures as shown in Table 5. Based on his prediction, there will be about 30 new dry cooling power plants in 2007, 40 in 2008, 45 in 2009 and 45 in 2010 with average capacities equivalent to 600MW, to be requiring heat exchangers for their dry cooling systems. The market is expected to get even bigger if water becomes more expensive.

Table 4. Electricity demand predicted by Liu

Year	2006	2010	2020
Total power (GW)	622	818	1186
Coal Power (GW)	484.05	624.5	780
Hydraulic (GW)	128.57	180	320
Nuclear (GW)	6.7	8	40
Wind (GW)	2.589	5	40
Other (GW)	0.091	0.5	6

Table 5. Air cooling power plant potential

Year	2007	2008	2009	2010
New installed air cooling plant (GW)	18	24	27	27

Heat Exchanger Manufacturers

Heat exchangers are the most expensive and the most critical components in dry cooling systems of thermal power plants.

Due to the attractive market potential for heat exchangers, international and local Chinese companies are competing to produce high performance and cost-effective heat exchangers and cooling towers. Two leading international companies, SPX and GEA, have set up production lines and factories inside China. There are four major Chinese local manufactures that have emerged in recent years in competition to SPX and GEA.

Finned tube bundle design shown in Fig.6 is the only heat exchanger element used in thermal power plants. In this figure, extended surfaces or fins are used to increase the heat transfer surface area. The challenges for the manufacturers are to produce low-cost finned surfaces that must resist corrosion, be lightweight but have adequate mechanical strength.

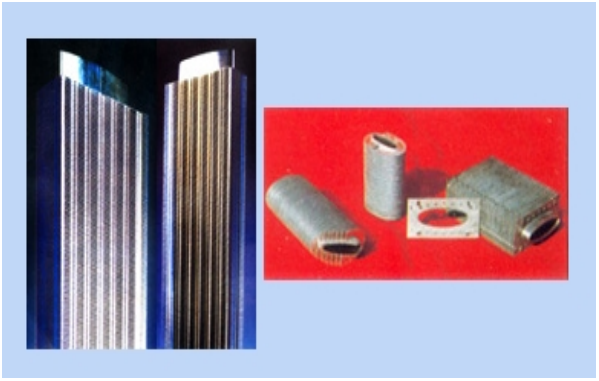

Fig.6 Finned tube heat exchanger

SPX Cooling Technologies is the leading full-line, full-service cooling tower and air-cooled

condenser/heat exchanger manufacturer. SPX has set up finned tube heat exchanger plants in Zhang Jia Kou and Tianjing respectively. Their market share is almost 35% in Chinese coal-fired power plants.

GEA has also set up a subsidiary in Longfan to manufacture finned tube heat exchangers. It also has two joint ventures with local Chinese partners in Shang Xi and Changshu. The market share of GEA is about 30%.

Harbin air conditioning Co., Ltd. is the largest local heat exchanger manufacturer in China. Their dry cooling products cover about 20% in coal-fired power plants and about 50% in the petroleum and chemistry processing plants.

Other heat exchanger manufacturers in China include Beijing Longyuan Cooling Technology Co., Ltd., Shouhang IHW Cooling Technology (Beijing) Co., Ltd. and Jiangsu ShuangLiang Air-conditioning Equipment Co., Ltd.

Dry Cooling Research and Cooling Tower Design

While most large heat exchange manufacturers can provide design, manufacture and installation for the entire cooling system including heat exchangers and the cooling tower, most of the natural draft cooling tower design and installation are done by power design and research institutes in China.

The China Institute of Water Resources and Hydropower Research (IWHR) is a comprehensive research organization in thermal and nuclear power. The institute has a division specializing in cooling tower design, cooling processing optimization, efficiency improvement of heat exchange and the cooling tower simulation.

IWHR has conducted intensive studies on the optimisation of the natural drafting cooling towers to improve the cooling efficiency.

Beijing University and Tsinghua University play a leading role in CFD, heat exchanger research and natural draft cooling tower optimisation.

Other universities specialised in heat exchange and cooling tower related research include North China Electric Power University, Chongqing University, Harbin Institute of Technology, and Xi'an Jiaotong University.

Cooling Tower in Geothermal Power Plant

The heat rejection per kWh(e) of net generation from geothermal power plants will be four or more times as great as from fossil-fuelled plants (Kroger, 2004). This will require larger cooling towers at higher costs.

Water shortage exists in most proposed Australian geothermal sites. The dry cooling will be the only option for these geothermal power plants. Mechanical draft consumes a large amount of power for driving fans so natural draft cooling system may be more attractive, provided the capital cost is acceptable.

Surrounding environment conditions have also a significant impact on the performance of power plants with dry cooling systems. Most proposed geothermal sites experience large daily temperature differences. An excessive rise in cooling water temperature during periods of peak ambient temperature will result in a loss of efficiency. In this case, hybrid cooling tower combining dry and wet cooling system (such as the system shown in Fig.7) may prove more cost-effective. In this design, both dry and wet sections are operated at the peak ambient temperature while only the dry section is used for the rest of time.

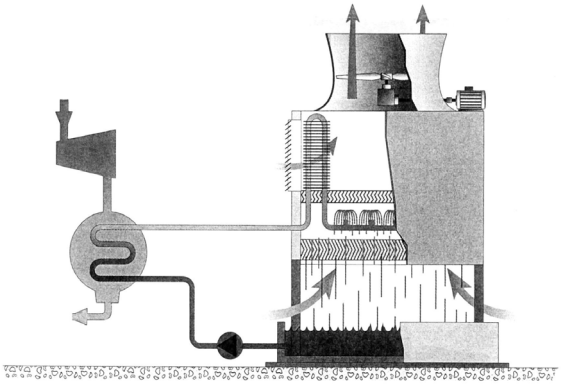

Fig. 7 Natural draft hybrid cooling system

Other options for geothermal plant cooling include precooling the entering air by humidification or deluging the air side of the heat transfer surface with water during the high cooling demand.

Fans may also be used to enhance the natural cooling during high ambient temperature.

Summary

An appropriate and well-designed cooling system can have a very significant positive impact on geothermal power plant performance and profitability.

The combination of theoretical and experimental studies as well as extensive practical experience in dry cooling technology in Chinese coal-fired power industry may offer good examples towards a cost-effective design and operation of such cooling systems for Australian geothermal power industry.

References

Zhu, X, and Guan, X., 2006, Economic analysis of dry cooling on supercritical generator, thermal power, December, 2006.

Chai, Q. Y., 2006, Application of dry cooling and economic analysis in thermal power plants, Proceedings on water saving technology in power plants 2006, Qindao, China, October 2006.

Liu, J. X., 2007, Harbin air conditioning Co., Ltd business report, Sinolink Securities, September 2007.

Chen, Y. C., 2008, Introducing air cooling industries, Southwest Securities, July 2008.

Kroger, D. G., 2004, Air-cooled heat exchangers and cooling towers, PennWell Corporation, Tulsa, Oklahoma.

How to Increase Geothermal Power Conversion Efficiencies

Hal Gurgenci
Queensland Geothermal Energy Centre, School of Mech. and Mining Engrg, The Uni. of Queensland
h.gurgenci@uq.edu.au

Geothermal power plants in dry regions typically use air cooling and consequently suffer from reduced efficiencies during hot days. In this paper, it will be demonstrated it may be possible to use solar boosting to maintain the geothermal plant power generation in such instances. It will be shown that commercial feasibility of solar boosting is improved when the cycle fluid is heated over a variable temperature range instead of the steam or organic Rankine cycles with fixed evaporation points. Results with supercritical CO_2 cycles will be compared against more conventional alternatives.

Keywords: power conversion; supercritical cycles; solar energy; hybrid plants; hot rock geothermal.

Introduction

Two factors prevent widespread adoption of HFR (Hot Fractured Rock) geothermal power in Australia:

- Compared to other renewables, there is a higher technical risk in HFR projects, namely in locating, establishing and exploiting a reservoir. This risk will be constrained with progress but will never disappear since each new prospect will be unique.
- Compared to coal- or gas-fired plants, geothermal plants need to dump several times more waste heat per MW of electricity generated. Without easy access to water, this can be a problem.

Higher potential rewards make risks more affordable. The reward from HFR investment is the electricity generation. If this reward can be increased, then higher risks would be acceptable to the investors.

The electricity generation from a given geothermal fluid source depends on:

- the fraction of the heat extracted from the geothermal fluid; and
- the efficiency of converting the extracted heat to electricity.

Let us start with the second one, a.k.a. the thermal efficiency. The thermal efficiency for a power conversion cycle is defined as the net turbine shaft power divided by rate of heat input into the cycle working fluid. The theoretical limit on thermal efficiency is the efficiency of the Carnot cycle, which represents ideal power conversion conditions. The actual efficiencies are usually much lower than the theoretical efficiency due to unavoidable losses. A good indicator of the maturity of a technology is what fraction of its Carnot efficiency it is able to deliver in actual operations.

In Figure 1, we plot the fraction of the corresponding Carnot efficiencies realised by operating geothermal, nuclear, coal, and combined-cycle gas turbine plants. The geothermal plant efficiencies are for binary plants calculated from data provided in Tester (2006) and the other plant data are from Willson (2007).

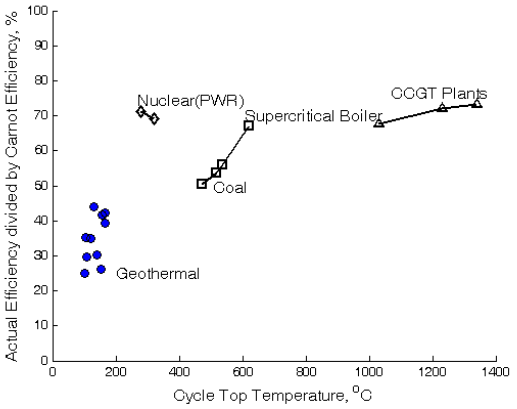

Figure 1: Fraction of the theoretical limit realised by different power generation technologies.

The important message from Figure 1 is that less than 40% of the ideal efficiency is realised in actual geothermal practice and the ratio is as low as 30% for low reservoir or high ambient temperatures. In contrast, any other modern power technology is able to enjoy around 70% of its ideal efficiency limit. Clearly, the geothermal energy practice has room to improve.

A significance source for efficiency loss in geothermal power plants is the irreversibility in the heat exchangers, e.g. see Demuth(1979), Larjola(1996), Vargas(2000), Chen(2006), Bronicki(2008).

Such irreversibilities can be significantly reduced by continuously matching the cycle fluid temperature against the temperature of the geothermal fluid during the heat exchange process. This is not possible in a conventional Rankine-cycle plant but easy in a supercritical cycle.

Case Study Definition

The analysis will be based on conditions that can be found in a typical Cooper basin HFR geothermal reservoir. We are assuming that hot brine is produced from a number of production wells at a temperature of 250°C at the rate of 500 l/s. The ambient air temperatures change from

about 0 °C during a cold winter night to 45 °C on a hot summer day.

We will consider two power plants to exploit this resource. One will be based on a supercritical CO_2 cycle and the other on a steam cycle. The steam cycle is conventional technology although it is usually employed at higher temperatures. The supercritical CO_2 cycle is a new technology development being pursued by the Queensland Geothermal Energy Centre of Excellence.

Supercritical Cycle vs Conventional Technology

Figure 2 shows the supercritical CO_2 diagram on temperature-entropy coordinates. A regenerator is used to recover some of the heat in the turbine exhaust stream.

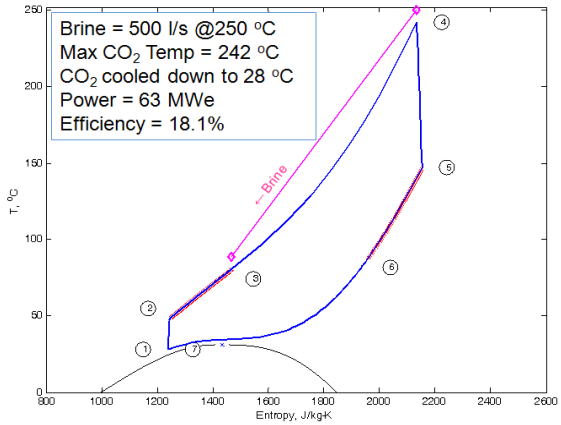

Figure 2. The supercritical CO_2 cycle

The case study temperatures are too high for an organic rankine cycle. The conventional technology for this temperature range is offered by a steam Rankine cycle. This is shown in Figure 3.

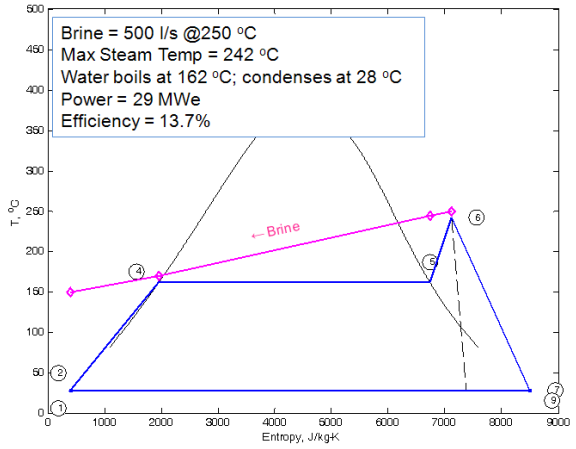

Figure 3. Conventional steam cycle

Cycle computations indicate that a power plant based on the supercritical CO_2 cycle has the capacity to generate 63 MWe at an efficiency of 18.1%. In comparison, the proven technology could only generate 29 MWe from the same reservoir and have an efficiency of 13.7%.

In other words, the supercritical CO_2 plant produces than more than twice the amount for the same resource. The performance varies through the year with the ambient temperature and the supercritical plant is more sensitive to the ambient temperature than the steam plant. Nevertheless, the expected annular electricity generation by the supercritical plant is 50% higher than that by the steam plant for the same geothermal resource and the same climate. The full comparison between the supercritical plant and the conventional technology is shown in Table 1.

Table 1. Comparison of supercritical CO_2 cycle and conventional plant performance

	CO_2 cycle	Steam cycle
Brine temperature, °C	250	250
Brine flow rate, kg/s	500	500
Brine return temperature, °C	89	150
Design-point power generation, MWe	63	29
Annual generation, GWh	401	256
Waste heat, MWth/MWe	4.5	6.4
Wet cooling tower water use, kg/kWh	8.0	8.2

Both plants operate on the same geothermal resource with the same subsurface investment. At an electricity sale price of 10¢/kWh, the difference in annual revenue would be about A$15m.

The water usage in Table 1 is provided only for comparison purposes. Otherwise, the analysis in this section assumes conventional dry cooling tower technologies with a heat exchanger approach temperature difference of 8oC. On hot days, this reduces the plant output significantly. Using innovative cooling technologies as explained in the next section, this vulnerability to high ambient temperatures can be minimised.

Dry Cooling Tower Technologies

Whether one uses new technology or established technology, for each MW generated several multiples of that amount must be dumped at waste heat. A more efficient plant would dump a lesser amount per MWe but large amounts heat must be dumped for either cycle.

In many geothermal plant locations, water is scarce and air cooling is the only option. Air cooling can be done by using fans or by using natural draft through a cooling tower. The fan-driven systems can be built quickly and at relatively low cost but their operating costs are higher due to their higher maintenance

requirements and the parasitic losses associated with running the fans.

The Queensland Geothermal Energy Centre of Excellence will do system studies, develop advanced heat exchanger technologies, and explore innovative systems towards better natural draft cooling towers. One of the options considered by the Centre is a low-cost air-lift cooling tower as depicted in Figure 6.

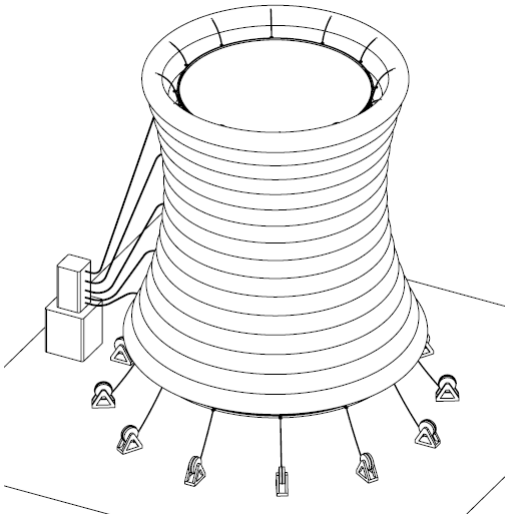

Figure 4. Innovative cooling tower design

Figure 4 shows an innovative cooling tower concept being investigated by the Queensland Geothermal Energy Centre of Excellence.

The tower is built as a flexible shroud and is held in place in tension by the buoyancy force acting on the toroidal rings filled with lighter-than-air gas.

There are a few issues associated with this concept but the Centre is expecting to be ready to build a prototype by mid-2010.

The motivation for the air-lift cooling tower shown in Figure 4 is to enable construction of very tall cooling towers at an acceptable cost.

Taller towers would increase the suction air velocity and the heat transfer at the heat exchangers and they also would enjoy lower tower exit temperatures.

Another system innovation under consideration targets the exploitation of clear and dry nighttime skies typically found in the Australian outback.

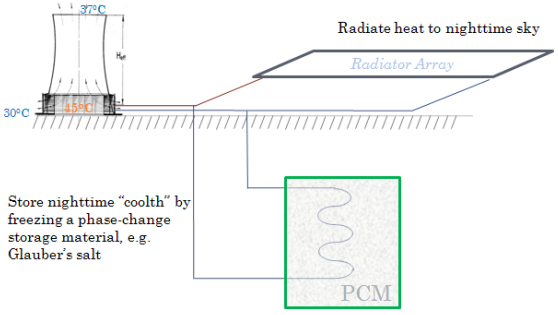

Figure 5. Nocturnal cooling for power plants

The system depicted in Figure 7, aims to cool a stored medium by using radiative coolers at night.

The night-time sky temperature is about 0 ^{o}C through the year in most of Central Australia.

Either sensible or latent storage can be used to extend nighttime cooling through the day. The required investment is smaller for a supercritical cycle where the first ΔT of cooling can be done by air (e.g. from 90 ^{o}C to 40^{o}C) and the second ΔT by the stored coolth (e.g. from 40^{o}C down to 20^{o}C).

Supercritical Rankine Cycle

If a geothermal plant has access to cold water or if some of the cooling technologies of the previous section can be judiciously implemented, it might be possible to design a plant at an even higher efficiency. In a supercritical Rankine cycle, CO_2 would condense at a temperature below 30 ^{o}C and it would then be heated to supercritical temperatures and expanded as a supercritical gas. The temperature-entropy diagram for a supercritical CO_2 Rankine cycle is shown in Figure 6.

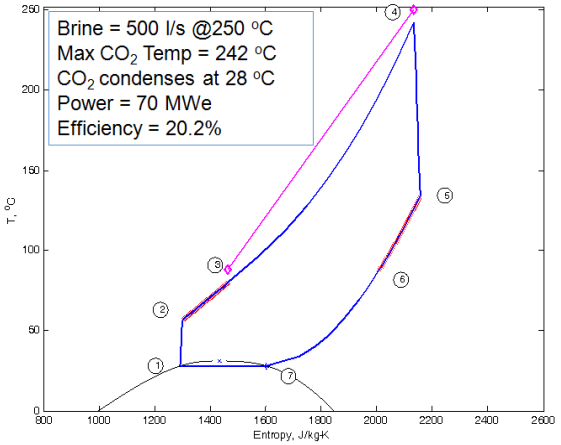

Figure 6. Supercritical CO_2 Rankine Cycle

The cycle shown would deliver even higher power. Since the critical point for CO_2 is about 30 ^{o}C, this plant would require access to a cooling medium well below 30 ^{o}C.

That is why a supercritical Rankine cycle may not be feasible for most Australian geothermal plant locations unless it is combined with other innovative cooling options as described elsewhere in this paper.

Geothermal + Solar Hybrid Plants

Another interesting opportunity with supercritical cycles is to use solar heat to maintain the plant output on hot days.

For example, by adding solar boosting to the plant of Figure 2, one can maintain the design output at ambient temperatures as high as 45^{o}C. The supercritical cycle with solar boosting under these conditions is shown in Figure 7.

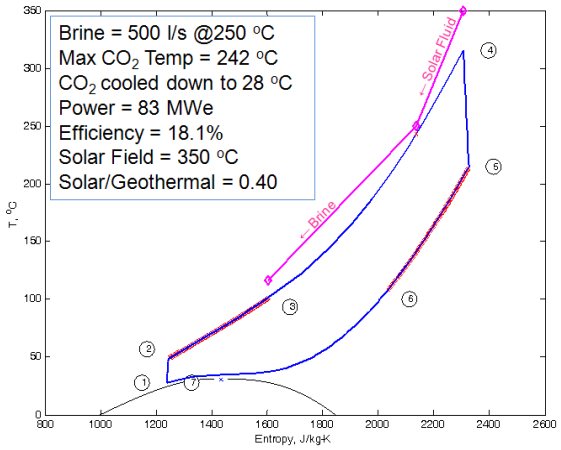

Figure 7. Supercritical CO_2 Brayton cycle with solar boosting

It is difficult to make solar boosting economically feasible with steam plants. This is because most of the heat added to the Rankine cycle is latent heat at the saturation temperature corresponding to the turbine design inlet pressure. It is not possible to significantly shift this temperature upwards without changing the turbine inlet pressure. Changing the pressure requires a separate turbine. Therefore, solar boosting of a geothermal plant based on a steam cycle requires two turbines: one for geothermal-only operation and the other for geothermal + solar. Even then, the optimum operating point would be elusive because of variable solar incidence and the inability of the plant to optimally track such variations. In a supercritical cycle, the turbine inlet temperature and the pressure are not linked and the solar heat can be added to the cycle fluid on the same pressure line as shown in Figure 7.

Supercritical CO_2 Geothermal Siphon

The use of CO_2 as a geothermal heat exchange fluid has been proposed by Brown (2004) and Pruess (2006). Gurgenci (2008) and Atrens (2008) and Atrens (2009) expanded the concept to include the power conversion using a supercritical CO_2 cycle. A supercritical CO_2 cycle achieves higher efficiencies but even then hardly catches up to the maturity of technology available to coal- and gas-fired power plants. For example, the supercritical CO_2 Rankine cycle of Figure 6 has a thermal efficiency of 20.2%, which is 49% of its theoretical limit. This is much better than the second law efficiency of 33% for the steam cycle of Figure 3 but still below the 60-70% enjoyed by coal and gas plants as shown in Figure 1.

By using a supercritical cycle, the heat exchanger irreversibility is reduced but not eliminated. The heat exchanger irreversibilities can only be eliminated when we do not use heat exchangers. This is possible if we use the same CO_2 for geothermal heat exchange in the reservoir and expand it through the turbine when it comes to the surface and send it back to the reservoir after cooling it. The cold CO_2 would sink in the injection well and the hot CO_2 would rise in the production well. No significant compression input or downhole pumping would be necessary to drive the system described in Figure 8.

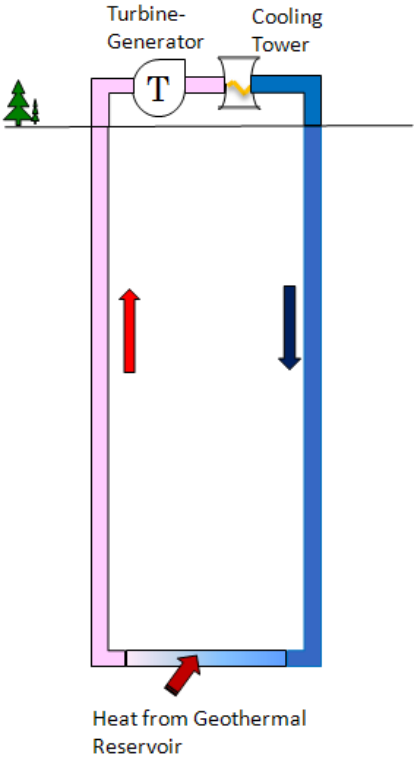

Figure 8. Operation of the supercritical CO_2 geothermal siphon

This is a new concept where supercritical CO_2 extracts reservoir heat, rises to the surface and drives a turbine, and then is cooled and sent back underground to close the cycle.

The concept offers the following intrinsic advantages over the alternatives:

- Driven by the buoyancy of the hot fluid, it does not need a submersible pump
- Removing the binary plant heat exchanger increases efficiency and lowers capital costs
- Better geothermal heat extraction enables larger well separation and longer plant life

Access to large quantities of CO_2 is essential, first, to start the reservoir and, then, possibly to make up for underground capture. The cost of such access could be defrayed by the CO_2 sequestration benefits.

Conclusions

The Queensland Geothermal Energy Centre of Excellence (QGECE) of The University of Queensland is working towards the following research outputs in the next two years:

- Supercritical CO_2 turbines for high-grade geothermal resources and solar/geothermal hybrids

- Better dry cooling technologies for geothermal and solar thermal power plants in arid regions
- Delivery of these outputs will quicken the large-scale adoption of HFR geothermal energy in Australia and around the globe.

In this paper, we compare the proposed technologies to present alternatives and identify and quantify the potential benefits from such research.

Comparing geothermal power against more mature technologies such as nuclear, coal power plants, and gas turbines, we first identify a clear potential to increase geothermal power conversion efficiencies by at least 50%. Incremental improvements cannot realise such a potential. A fundamentally new approach is needed. Supercritical cycles offer such a fundamentally new alternative.

A supercritical CO_2 cycle is the superior alternative at geothermal fluid temperatures above 200 ^oC. These temperatures are too hot for organic fluids but not hot enough for steam cycles. At 250 ^oC, for example, we demonstrate that a supercritical cycle would double the power available from conventional technology. For a geothermal plant based on a 500 l/s hot brine resource, this means and additional revenue of $15m per year at an electricity sale price of 10¢/kWh.

Most of the components in a supercritical CO_2 cycle are off-the-shelf technology except for the turbine. To deliver the missing link, QGECE is aiming to demonstrate a 5-kW prototype demonstrated in the laboratory by mid-2011 and develop the funding and the partnership for a 1-MWe demonstration project by mid-2013.

Even then, HFR geothermal plants may still be unviable in hot and arid regions without better dry cooling technologies. QGECE is pursuing advances in this area through incremental research and system innovations. Some of the target innovations are described in this paper.

References

Atrens, A D, Gurgenci, H, Rudolph, V, “Carbon Dioxide Thermosiphon Optimisation”, 2008 Australian Geothermal Energy Conference, Melbourne.

Atrens, A.D., Gurgenci, H., and Rudolph, V.: CO_2 Thermosiphon for Competitive Geothermal Power Generation, *Energy & Fuels*, **23** (2009) 553-557.

Brown, D.W.: A Hot Dry Rock Geothermal Energy Concept Utilizing Supercritical CO_2 Instead of Water, Proceedings, 25th Workshop on Geothermal Reservoir Engineering, Stanford University, Stanford, CA (2000).

Bronicki, L.Y.: Advanced Power Cycles for Enhancing Geothermal Sustainability, IEEE PES General meeting, Pittsburgh, PA (2008).

Chen, Y., Lundqvist, P., Johansson, A., and Platell, P.: A comparative study of the carbon dioxide transcritical power cycle compared with an organic rankine cycle with R123, *Applied Thermal Engineering*, **26** (2006) 2142–2147.

Demuth, O.J.: Analysis of Binary Thermodynamic Cycles from a Moderately Low-Temperature Geothermal Resource, Report #TREE-1365, Idaho National Energy Laboratory (July 1979).

Gurgenci, H., Rudolph, V., Saha, T., and Lu, M.: Challenges for Geothermal Energy Utilisation, *Proceedings,* 33rd Workshop on Geothermal Reservoir Engineering, Stanford University, Stanford, CA (2008).

Gurgenci, H.: Electricity Generation Using a Supercritical CO_2 Geothermal Siphon, *Proceedings,* 34th Workshop on Geothermal Reservoir Engineering, Stanford University, Stanford, CA (2009).

Larjola, L.: Electricity from Industrial Waste using High-speed Organic Rankine Cycle, Int J Prod Economics, **41** (1995) 227-235.

Pruess, K.: Enhanced Geothermal Systems (EGS) using CO_2 as Working Fluid – A Novel Approach for Generating Renewable Energy with Simultaneous Sequestration of Carbon , Geothermics, 35 (2006), 351-367

Tester, J.: The Future of Geothermal Energy, *MIT Press*, (2006)

Vargas, J.V.C., Ordonez, J.C., and Bejan, A.: Power extraction from a hot stream in the presence of phase change, *Int J of Heat and Mass Transfer*, **43** (2000) 191-201.

Willson, P.: The Nu gas Concept – Combining Nuclear and Gas Power Generation, PB Power, http://www.imeche.org/industries/power/nugas-june-2007.htm (2007).

An Overview of GRANEX Technology for Geothermal Power Generation and Waste Heat Recovery

Behdad Moghtaderi* and Elham Doroodchi
Priority Research Centre for Energy, Chemical Engineering, School of Engineering
Faculty of Engineering and Built Environment, The University of Newcastle, Callaghan, NSW 2308, Australia
* Corresponding author: Behdad. Moghtaderi@newcastle.edu.au

This paper reports on the recent advancement of the GRANEX technology platform developed by our group for power generation from low-grade heat sources. The technology is particularly suited to applications involving geothermal power generation and waste heat recovery. By combining the concepts of heat regeneration and supercritical Rankine cycle into a unified process, GRANEX improves the thermal efficiency of the cycle and increases the net electrical output which can be recovered from a given low-grade heat source. The regeneration of the thermal energy in GRANEX is achieved through a novel heat regenerator invented and patented by our group in partnership with Granite Power Limited (GPL). Development of GRANEX dates back to early 2006 when a Research and Development Agreement was established between the University of Newcastle and GPL. In conjunction with a program of fundamental studies an applied program of work was undertaken for proof of concept and prototype development with the assistance of a REDI grant from AusIndustry (2007-2009). By 2008, a 1 kW prototype had been built and experimental trials of the system had been completed, demonstrating considerable advantages over conventional systems in terms of both thermal efficiency and power generation (about 40% improvement). This was followed by the design of a 100 kW pilot-plant in early 2009. The pilot-plant is currently under construction and is due to be commissioned by late November 2009.

Keywords: Geothermal power, waste heat recovery, GRANEX

Introduction

The growing world-wide concern about energy conservation and the global impact of greenhouse gases have prompted a series of new research and development activities focusing on renewable energy sources, particularly solar, wind, biomass, and geothermal energy. By and large the geothermal energy is an untapped energy resource despite its potential and clear environmental advantages (e.g. minimal CO_2 emissions) over other sources of energy, such as fossil fuels and nuclear energy. According to an estimate by the IEA (International Energy Agency), currently only 0.3% of the world's electricity is generated from geothermal sources (Priddle; 2002). However, geothermal power production is expected to steadily increase at a rate of 4.3% per year reaching a share of 0.6% of the global electricity production by the year 2030 (Priddle; 2002, Barbier; 2002, Bertani; 2005). Although the predicted growth in the geothermal power production sector should be considered as a positive sign of the worldwide move towards more renewable and environmentally friendly energy sources, the growth clearly falls short of expectations. The contribution of the geothermal energy to the world's electricity production by 2030 can be potentially one order of magnitude higher than the IEA's estimate, should the technical problems associated with the use of geothermal energy are resolved (Barbier; 2002, Bertani; 2005). Within this context, the study of geothermal power cycles is regarded as one of the key areas for major technological improvements since many of the problems associated with the geothermal power technology are underpinned by inefficient and often unsuitable heat exchange processes within power cycles. That is partly due to the fact that most power cycles currently employed in geothermal applications (with the exception of Kalina power cycle) were originally designed for large-scale power production from fossil fuels where higher temperature sources are available for heat exchange.

In recognition of these shortcomings, the Granite Power Limited (GPL) and the University of Newcastle initiated a joint R&D program in 2006 with the goal of establishing alternative and potentially more efficient ways of generating power from geothermal and other low-grade heat sources, such as industrial waste heat. Reduction of industrial waste heat will undoubtedly lessen the demand for energy that would otherwise be met, either directly or indirectly, by primary energy resources such as fossil fuels. Industrial sectors such as power generation, aluminium, iron, and steel manufacturing, petroleum refining, cement production, chemical processing, and pulp and paper manufacturing account for approximately 65% of all industrial waste heat.

Theoretical Considerations

The fraction of heat that can be converted to mechanical work and/or electrical power is limited by laws of thermodynamics (Cengel and Boles; 2002). This fraction is commonly expressed in terms of the so called "grade (or quality)" of the waste heat although from a thermodynamic point of view the correct terminology is "exergy" (the

useful work potential of a system at a given state). Source temperature rather than "quantity" is the primary consideration in determining the grade of a waste heat source. For instance no power can be generated from ambient air even though it contains huge quantities of thermal energy. Generally, waste heat streams with source temperatures within the range of 600°C-1700°C are considered high-grade while those within the temperature ranges of 250°C-600°C and 50°C-250°C are deemed medium-grade and low-grade, respectively. Geothermal sources have typically temperatures between 150-250°C and, hence, can be categorised as low-grade.

The principles of power generation from low to high-grade heat sources are not different and the constraints that apply to any power generation process equally apply to all. Three processes must be accomplished within the temperature range defined by the source (T_{so}) and sink (T_{si}) temperatures. These are: (i) heat addition from the source to power plant driven by the temperature differential $\Delta T_{so} = (T_{so} - T_H)$ where T_H is the absolute temperature at which energy is introduced into the plant, (ii) power generation by an expander (i.e. turbine) driven by the temperature differential $\Delta T = (T_H - T_L)$ where T_L is the absolute temperature at which heat is rejected to the sink, and (iii) heat rejection from the power plant to the sink driven by $\Delta T_{si} = (T_L - T_{si})$. Among temperature differentials ΔT is of significant importance since many key features of the plant depend on ΔT. For example, the required energy input per unit power (Q/W) and plant size per unit power (A/W) can be expressed in terms of ΔT using the following equations:

$$(Q/W) = (T_H / \Delta T) \quad (1)$$

$$(A/W) = (T_H / \Delta T^2) \quad (2)$$

For low-grade heat sources ΔT is inherently small, hence, for a given power a low-grade heat source is required to provide more energy than a high-grade source (Eq 1). The plant size corresponding to the low-grade heat source will be also much larger than that of the high-grade one (Eq 2).

The other major difficulty with low-grade heat sources is that, if not minimised, ΔT_{so} and ΔT_{si} will take significant fractions of the possible temperature drop (i.e. T_{so}-T_{si}) reducing ΔT and, thereby, the net power output and thermal efficiency of the plant. While the Carnot efficiency (η_C in Eq 3) defines the upper limit of thermal efficiency the actual efficiency is given by Eq (4):

$$\eta_C = (W_{Max}/Q) = (T_{so} - T_{si}) / T_{so} \quad (3)$$

$$\eta = (W/Q) = (T_H - T_L) / T_H = \Delta T / T_H \quad (4)$$

If ΔT_{so} and ΔT_{si} are minimised (T_I - T_R) will approach (T_{so}-T_{si}) and, hence, η and W move towards η_C and W_{Max}, respectively (see Eqs 3 and 4). Minimisations of ΔT_{so} and ΔT_{si} are particularly important for real-world finite capacity sources (and sinks) where T_{so} and T_{si} do not necessarily remain constant during the heat addition and/or rejection processes. Among conventional power cycles the Organic Rankine cycle (ORC) possess the largest source and sink temperature differentials (ΔT_{so} and ΔT_{si}) and, thus, suffers the most from problems associated with small ΔT. This is clearly illustrated in Figure 1 where the temperature entropy (T-S) plots of the ORC, Kalina cycle and Supercritical Rankine cycle (SRC) are shown by the thick solid lines while dashed lines represent the phase diagram of the working fluid. As can be seen, there are significant temperature differences between the source and the working fluid in an ORC during the heat addition process because the phase change of the working fluid takes place at constant temperature under the saturation dome.

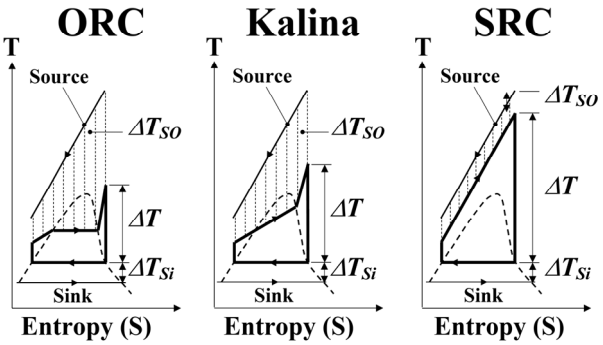

Figure 1: T-S plots of ORC, Kalina, and SRC.

Kalina cycle reduces the temperature mismatch between the source and the working fluid using a zeotropic mixture of ammonia and water with variable temperature phase change (Figure 1). While this approach increases ΔT, η and W, it requires a complex array of absorption and distillation hardware. The added complexity together with the high sensitivity of Kalina cycle to pressure and composition of the ammonia-water mixture, limits its application over a wide range of source temperatures and significantly adds to the capital and operating costs (DiPippo; 2005).

SRC also avoids the constant temperature phase change except that the heat addition and/or rejection processes are carried out under supercritical conditions using a single-component working fluid rather than a zeotropic mixture like that employed in the Kalina cycle (Figure 1). This approach not only results in a simple plant layout but a small ΔT_{so} and, hence, higher ΔT, η and W.

However, the constant pressure lines in the supercritical region are generally too close and as such the conventional SRC has a relatively low net power per unit of enthalpy change. Thus the turbine outlet stream in a conventional SRC may contain large amount of thermal energy which is typically wasted during the heat rejection process leading to thermal efficiency losses. Moreover, relatively high operating pressures may be

required to achieve a desired power output under supercritical conditions. As shown in the next section, GRANEX effectively resolves the above shortcomings of the conventional SRC in a relatively simple manner.

GRANEX Technology

Figure 2 shows the schematic representation of a GRANEX based power plant. The system is essentially a conventional SRC fitted with a heat regenerator. The inclusion of the regenerator resolves the issue of low net power per unit of enthalpy change by utilising the unused thermal energy of the turbine outlet stream in the heat-up of the cold working fluid exiting the pump. This version of SRC which is also referred to as "Regenerative Supercritical (RGSC) Rankine cycle" has higher thermal efficiencies than the conventional SRC. The issue of potentially high operating pressures is also overcome by selecting suitable working fluids with sufficiently low critical pressures. In addition, the patented design of the regenerator in GRANEX avoids the so-called maximum enthalpy points for which the driving force for heat transfer is zero. This ensures a much smoother heat exchange during supercritical operation.

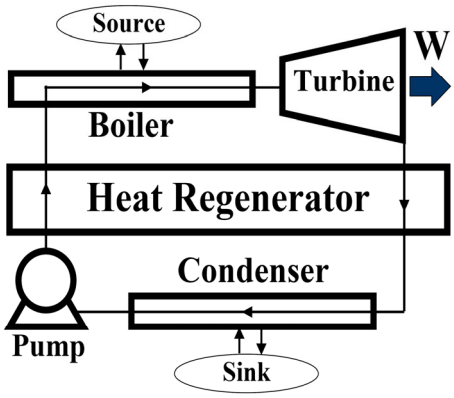

Figure 2: Schematic of GRANEX system.

Power Cycle Analysis

The performance of the GRANEX cycle was theoretically assessed by a numerical model developed using the process simulation software HYSYS. For a large selection of working fluids first- and second-law thermodynamic analyses of the cycle were carried out to determine the values of W (net power), η (thermal efficiency), and η_{II} (exergy efficiency) under a range of operating conditions in terms of heat source/sink temperature (that is $150^oC < T_{so} < 250^oC$ and $15^oC < T_{si} < 35^oC$). This was to establish the so-called envelop of operation for each fluid and rank them on the basis of thermal and exergetic efficiencies. The interplay between the sink temperature and condensation properties of the working fluid will be carefully examined to assess the impact of ambient conditions on the overall cycle performance. A series of calculations will be also performed to investigate the impact of molecular weight and density on key turbine (i.e. expander) characteristics such as number of stages, exit area, sonic velocity, and leave loss.

As part of these studies, the performance of GRANEX was compared with several existing geothermal power plants (Table 1). In each case the calculations associated with GRANEX were carried out using a working fluid referred to as "Fluid-6" under source and sink temperatures identical to that of the actual plant. The results have been summarised in Figures 3 to 5.

Table 1: List of case studies

Case	Case Description	Ref
1	Kalina	DiPippo; 2005
2	Otake	DiPippo; 2005
3	Nigorikawa	DiPippo; 2005
4	Heber (SIGC)	DiPippo; 2005
5	Brady (Double Flash)	Kanoglu & Cengel, 1999
6	Single Flash-1 (Nevada, US)	Kanoglu & Cengel, 1999
7	Single Flash-2 (Nevada, US)	Kanoglu & Cengel, 1999
8	Double Flash (Nevada, US)	Kanoglu & Cengel, 1999
9	Binary (Nevada, US)	Kanoglu & Cengel, 1999
10	Combined (Nevada, US)	Kanoglu & Cengel, 1999
11	Pseudo-SC (Nevada, US)	Gu & Sato; 2002

Figures 3 and 4 illustrate the plots of thermal conversion and exergetic efficiencies as a function of the temperature difference between the geothermal fluids at the production and reject wells, ΔT_{geo}. Plots have been drawn using the data shown in Table 1 for both conventional and RGSC (GRANEX) Rankine cycles.

As can be seen, the performance of the RGSC cycle is far superior to that of conventional cycles. For the range of investigated source temperatures, the thermal efficiency varies between 10-18% with an average of 16.5% for RGSC cycle whereas for conventional cycles, including Kalina, the thermal efficiency does not change and plateaus around a nominal value between 11 to 12%.

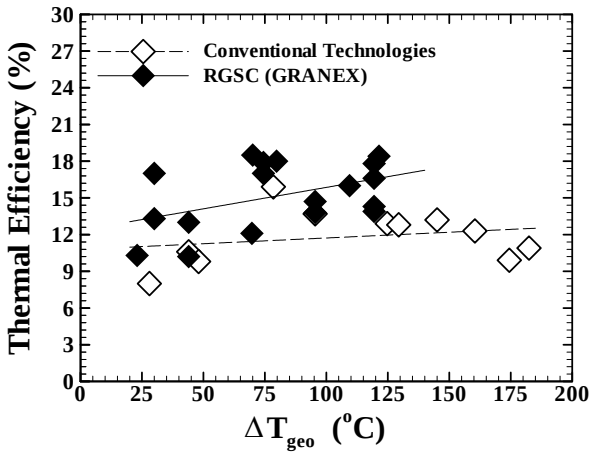

Figure 3: Comparisons of thermal efficiencies of the RGSC (GRANEX) and conventional cycles.

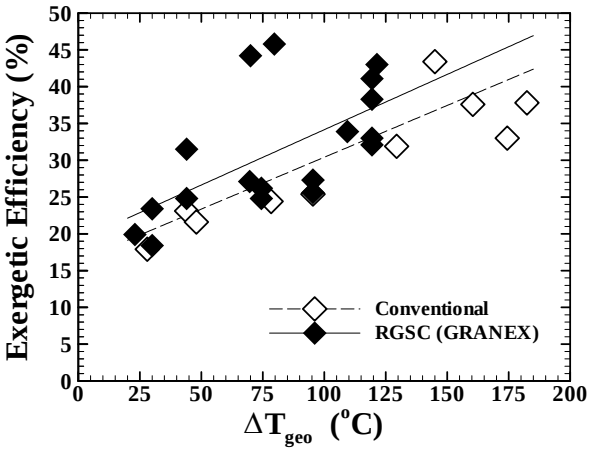

Figure 4: Comparisons of exergetic efficiencies of the RGSC (GRANEX) and conventional cycles.

The higher thermal efficiency of the RGSC cycle implies that more power can be generated from this cycle per unit of input energy than from a conventional cycle. This is quite evident from Figure 5 where the specific power (W_{spc}) has been plotted against ΔT_{geo}. The specific power is defined as:

$$W_{spc} = W_{net} / \dot{m}_{geo} \ . \qquad (5)$$

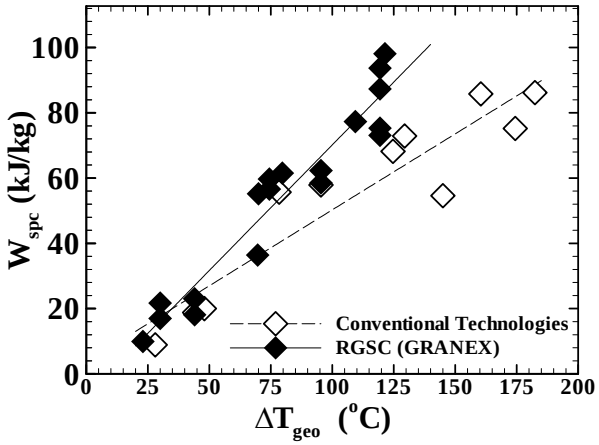

Figure 5: Plots of specific power versus ΔT_{geo}.

Experimental

Fifteen candidate working fluids were selected from power cycle analysis. The shortlist of selected fluids was shortened by eliminating fluids which in terms of W, η and η_{II} underperforming a reference ORC with iso-pentane as working fluid. The remaining fluids were experimentally studied over a range of source and sink temperatures ($150^oC<T_{so}<250^oC$ and $15^oC<T_{si}<35^oC$) in a 1 kW proof-of-concept (POC) plant.

The POC plant (Figure 6) is a unique facility in Australia which has been established using a $2,400,000 grant jointly funded by GPL and AusIndustry. The facility can be operated at pressures of up to 30 MPa and temperatures up to 300°C under GRANEX or ORC configuration. The prototype facility comprises a water chiller (i.e. heat sink), a condenser unit, a cycle pump with a maximum operating pressure of 28 MPa, a regenerator module consisting of 4 tube and tube heat exchangers fitted with our patented heat exchange technology, an electrical heater (i.e. heat source) with a 30 kW rated capacity, a boiler, and a turbine simulation unit fitted with a collection of valves and heat exchangers to reproduce the pressure and temperature drops of typical expanders. The facility is fully automatic (uses delta VB) and has been equipped with an array of sensors (T, P, and flow) and safety devices such as pressure relief valves, gas sensors, alarms, an air extraction system.

Measurements of pressure, temperature, and flow rate were taken in 20 different points around the plant at a frequency of 10 per minute using a sophisticated data acquisition system. For any given combination of operating conditions (working fluid, T, P, and flow rate), experiments were carried out over a 1.5 hours period and were repeated at least twice to ensure the statistical integrity of the results. The aim was to develop an experimental version of the operational envelop and compare it with that developed from theoretical predictions. About 650 individual experiments were completed over an eight months period to achieve the broad objectives of the project.

Figure 6: The picture of 1 kW POC plant.

Figures 7 and 8 show bar charts of experimental results obtained from the 1 kW plant for the net power and the thermal efficiency improvement. It can be seen from Figure 7 that for a given set of conditions GRANEX in conjunction with Fluids 1 to 6 can deliver higher net powers that those obtained from Kalina and ORC. Fluid 1, in particular reaches the prototype plant's rated output of 1 kW.

Figure 8 also clearly indicates that with respect to a reference ORC, improvements of up to 40% in thermal efficiency can be achieved when Fluids 1 to 6 are employed.

The efficiency improvement of GRANEX over Kalina cycle is approximately 20% owing to the fact that Kalina is a much more efficient process than ORC, although it has a complex hardware.

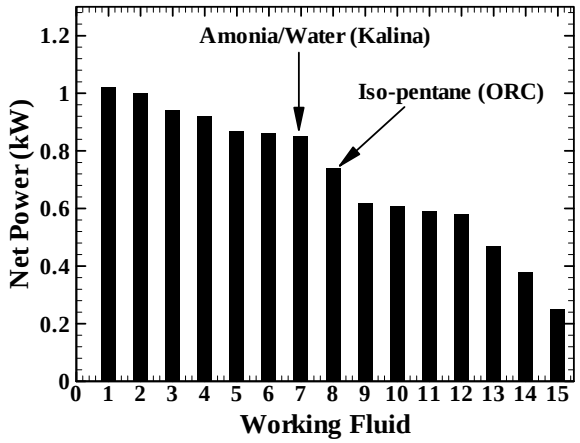

Figure 7: Measurements of net power from the 1 kW unit.

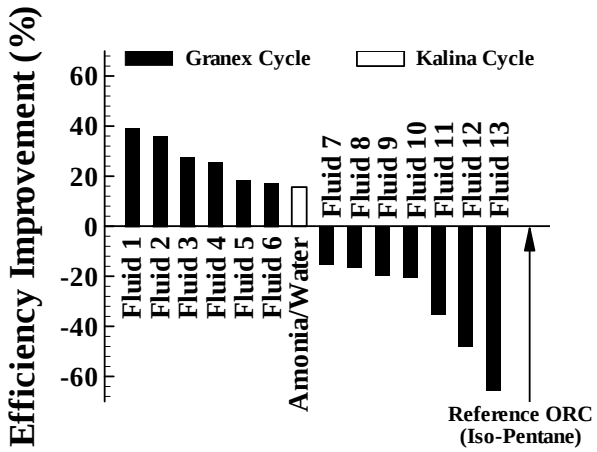

Figure 8: Efficiency improvement (%) with respect to a reference ORC.

Work in Progress

A set of experiments is being carried out using the 1 kW POC unit at temperature ranges between 80°C and 150°C. This lower temperature range is of more relevance to waste heat recovery applications. The preliminary findings indicate that GRANEX can maintain its advantage over conventional systems even at lower source temperatures if a suitable working fluid is employed.

Also, based on theoretical and experimental research conducted since 2006 on GRANEX for geothermal applications, the design of a 100 kW prototype has just been completed. The prototype which is currently under construction is due for commissioning by the end of Nov 2009. The prototype will be employed in a comprehensive series of pilot-scale experiments in early 2010 to develop the scale-up rules.

Conclusions

The present document summarises the result of a combined theoretical and experimental study on GRANEX technology. The study is part of a larger project aimed at developing a technology platform with thermal efficiency and economics superior to conventional system for power generation from low-grade heat sources. GRANEX combines the established concepts of supercritical power generation and heat regeneration into a unified platform. As shown in this document GRANEX, leads to significantly higher conversion efficiencies than those currently provided by conventional power cycles.

Owing to its simplicity, the RGSC cycle also offers a greater degree of flexibility and robustness, which in turn, will translate into much better economic characteristics when compared with conventional power cycles.

References

Priddle, R., 2002, Word Energy Outlook 2002, Second Edition, IEA report 2002.

Barbier, E., 2002, Geothermal Energy Technology and Current Status: An Overview, *Renewable and Sustainable Energy Reviews*, 6, p. 3–65.

Bertani, R., 2005, World Geothermal Power Generation in the Period 2001–2005, *Geothermics*, 34, p. 651–690.

DiPippo, R., 2004, Second Law Assessment of Binary Plants Generating Power from Low-Temperature Geothermal Fluids, *Geothermics,* 33, p. 565–586.

Kanoglu, M., and Cengel, Y., (1999), Retrofitting a Geothermal Power Plant to Optimize Performance: A case Study, *Journal of Energy Resource Technology*, 121, no 4, pp. 295-300.

Gu, Z., Sato, H., 2002, Performance of Supercritical Cycles for Geothermal Binary Design, *Energy Conversion and Management*, 43, pp. 961-971.

Cengel, Y.A., Boles, M.A., 2002, Thermodynamics: An Engineering Approach", 4th Ed, McGraw Hill, NY.

PureCycle® Product Development and Applications Update

Craig Morgan[1], Stephen Byers[2]
[1] Pacific Heat and Power, Level 14, 500 Collins Street, Melbourne VIC 3000
[2] Pratt & Whitney Power Systems, 400 Main Street, East Hartford, Connecticut, USA
* Corresponding Author: craig.morgan@pacificheatandpower.com, +61 3 9013 4425

When field trials were first conducted in 2006 the PureCycle® product introduced a new concept in modular, packaged, quick to market organic rankine cycle power generation systems. Over 2008 and 2009 the PureCycle® system was deployed in number of applications including waste heat capture, both small scale (500kW) and large scale (10MW) geothermal power plants. The systems have performed exceptionally well with over 98% availability and exceeded expectations. Nevertheless, system improvements continue to be made.

This paper summarises the overall performance of the systems currently in operation, product features and their performance in the field, and new technical innovations that are being offered and considered by Pratt & Whitney Power Systems.

Keywords: PureCycle®, Pratt & Whitney Power Systems, Pacific Heat and Power

PureCycle® applications to date

The first field trial for PureCycle® was conducted in 2006 in Chena Springs, Alaska. Since that time standard water-cooled systems using the non-flammable working fluid R245fa have been deployed in numerous applications:

- 10MW at Raser Technologies' Utah plant, USA operating on geothermal brine (Fluid - geothermal brine from a hot sedimentary aquifer; Temperature – 121°C; Flow Rate: approx 19 l/s per unit). The system is water cooled using a common cooling tower.
- 2 units on a greenhouse operation in the USA operating on geothermal brine (Fluid - geothermal brine from a hot sedimentary aquifer; Temperature – 108°C; Flow Rate: approx 29 l/s per unit). The system is water-cooled using a common cooling tower.
- 1 unit on waste heat from diesel jacket water in Guatemala (Fluid – ethylene glycol; Temperature – 99°C; Flow Rate: approx 60 l/s per unit). The system is water cooled using a cooling tower.
- 1 unit at the Oregon Institute of technology for the first geothermal plant in Oregon (Fluid - geothermal brine from a hot sedimentary aquifer; Temperature – 88°C; Flow Rate: 21.5 l/s). The unit is water cooled using a cooling tower.
- 2 units on a waste to energy plant in Massachusetts (Fluid – one on low pressure steam and one on ethylene glycol; Temperature – 105C; Flow Rate: 4500 kg/hr (steam) & 65 kg/s)
- 1 unit using the thermal energy from an oil and gas well and operating on R134a (Fluid – co-produced fluids from an oil and gas well; Temperature – 85°C; Flow Rate: 54 l/s)
- The rate of enquiries and equipment orders is increasing. Based on the existing pipeline of opportunities we would expect this number to substantially increase with the continued strengthening of geothermal markets, and increasing focus on waste heat recovery and energy efficiency in industrial and oil and gas markets.

Performance summary

To date the equipment across all applications is operating at > 98% availability. Power output has been consistent with the theoretical models developed in the UTC Research Centre in East Hartford, Connecticut.

Technical innovations on the Model 280

The product development team continue to make system improvements that increase efficiency, broaden the variety of suitable applications, and provide the ability to operate in with zero water for cooling. Key additions to the product include:

- Air condenser for use in areas with limited access to water. The refrigerant is condensed directly in the air-condenser to maximise heat transfer.
- Recuperator that improves the cycle efficiency on the air and water cooled systems. This works by capturing the waste heat from the turbine exhaust and pre-heating the incoming hot liquid prior to the evaporator.
- Coatings and equipment modifications such as those necessary for a high H2S environment in some international geothermal fields.
- High pressure evaporators may also be selected on a case by case basis for some applications.

Australian and New Zealand applications

Based on the previous 12-18 months of discussions with potential customers, the key applications for utilising low grade heat in Australia and New Zealand are:

- Waste heat from reciprocating engines operating on a variety of fuels (diesel, natural gas, landfill gas, sewage digester gas)
- Waste heat from biomass plants (sawmill waste and other mixed wastes)
- Waste heat from industrial processes and fossil fuel power generation (steel, aluminium, foundries, gas turbines)
- Low temperature geothermal applications

Analysis of the opportunities suggests that the following principles apply:

- Prices for the major generating plant in Australia are often more attractive than in New Zealand due to the relative strength of the AUD against the USD and Euro, making any internationally sourced equipment cheaper in Australia.
- High-priced diesel generation is attractive due to the high cost of fuel and low resource risk (the amount and flow of heat is easily quantified)
- The effective revenue gained from generating power on-site is higher than selling to the wholesale market
- Renewable energy certificates (RECs) improve the financial performance of projects developed in Australia where the waste heat is derived from renewable fuels.
- Waste heat is easier to quantify and more certain than geothermal resources, but less plentiful. There is some resource uncertainty as the waste heat is only available as long as the host industry continues to operate.

Figure 1 outlines a summary of where PureCycle® is likely to be most cost effective.

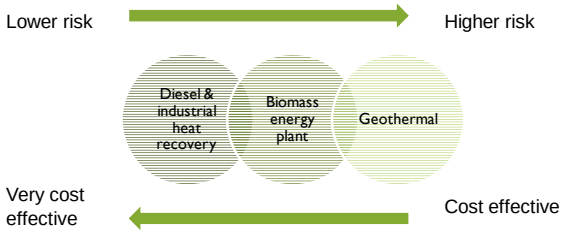

Figure 1: Cost effective PureCycle® applications

Nevertheless, the future looks bright for Australian and New Zealand geothermal, as well as waste heat applications.

The future and corporate update

PWPS has embraced and enhanced the PureCycle® model 280 since taking over the product from its sister company – UTC Power in early 2009. The PureCycle® sits alongside gas turbines in its industrial power division.

For geothermal applications, generation of power from the Next Generation PureCycle® using resource temperatures at top of hole of up to 175°C should be achievable. Target pricing is confidential, but has been set at a point to ensure competitiveness in generating primary utility-grade power from geothermal power plants. A firm release date has not yet been set.

Conclusion

There is a wide variety of economic applications available that suit the current PureCycle® Model 280, which continues to prove its reliability in the field, including waste heat from engines, geothermal, and industrial waste heat. Australia is generally a more attractive market than New Zealand due to the lower geothermal temperatures, better exchange rate, and supportive policy environment. The range of suitable applications is widening as the team at PWPS broaden the product offering and capability of the unit with technical innovations.

Natural Draft Dry Cooling Tower

Clare Murray[1]*
[1]School of Mechanical and Mining Engineering, The University of Queensland
* Corresponding author: clare.murray@uqconnect.edu.au

The location of geothermal power plants in central Australia raises the need for a cooling method that is not dependent on large volumes of water. The natural draft dry cooling tower is an alternative to conventional mechanically driven or evaporative systems. This design is being completed for a geothermal plant located in Innamincka, South Australia. The design of the cooling tower incorporates the arrangement of heat exchangers and the tower structure itself. This is dependent on the ambient conditions of the area and the required heat rejection rates.

In a natural draft dry cooling tower air acts as the cooling medium to condense steam that is pumped through heat exchangers. Air is drawn in at the base of the tower and passes through the heat exchangers. This heated air is forced up the tower by the pressure difference created between the warm air and the ambient conditions. The heat exchangers can be placed wither vertically around the perimeter or horizontally within the mouth of the tower. This is a suitable alternative as water is not evaporated to the atmosphere and is reheated to run through the turbine again. The cooling tower will operate most effectively with a larger temperature difference and a greater tower height.

Keywords: Natural Draft, Dry Cooling, Geothermal Energy, Australia

Alternative Cooling Methods

This system can be considered as an alternative to mechanically driven systems which incorporate large fans to drive the flow of air through the tower. There is an obvious advantage to this as the flow through the tower can be controlled independently of the temperature difference which increases the reliability of the system to cool. This means the cooling structure can be smaller requiring lower initial investment. The use of fans does require a significant power output of approximately 10-15% of the plant's output. They also require continuous maintenance and generate significant amounts of noise (Forgo 1979).

Another alternative, evaporative cooling is quite similar however water sprays are used as opposed to heat exchangers. This does result in a more efficient system as the latent heat of water removes more heat, resulting again in a smaller tower with a lower initial investment. There is significant water loss which can be up to 3 million litres annually which is not viable for central Australia. The run off created by wet cooling towers creates an environmental hazard due to chemical additives in the water and the wet plumes can be quite corrosive to the tower structure. Hence a natural draft dry cooling tower is most appropriate for the conditions of this power plant.

Tower Structure

The dimensions of the tower are dictated by the flow requirements for heat rejection at the ambient conditions. The shape and material selection are important to ensure the tower is strong against wind loading, buckling and vibration.

To reject the heat from a 23MW power plant at a 30°C ambient temperature the following dimensions listed in Table 1 are required the location of which are presented in Figure 1.

Table 1: Tower Dimensions

Outlet height	200 m	H5
Inlet height	16 m	H3
Throat height	170 m	Ht
Throat diameter	136 m	D5
Inlet diameter	170 m	D3

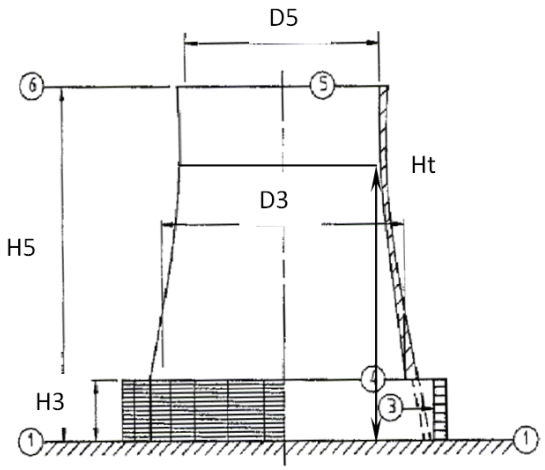

Figure 1: Outline of Tower Dimensions

The tower is hyperbolic up to the throat diameter and then extends straight up. The shell of the tower depends on material selection which is most commonly concrete or steel. This design is slightly different and incorporates a steel frame with square hollow beams that support a material shroud. The selected material covering must be sufficiently strong and stiff to withstand wind loading, durable and resistant to UV degradation.

Wind loading has been applied with a maximum gust speed of 27.8m/s at a height of 10m. Results from a static analysis indicate the maximum deflection would be 2.9m with a stress of 375MPa. Based on this the high strength low alloy

steel A582 (grade 65) has been selected. This has a yield strength of 450MPa which is sufficient for the loading conditions. A possible frame design has been modelled and loaded in Strand7 and is presented in Figure 2.

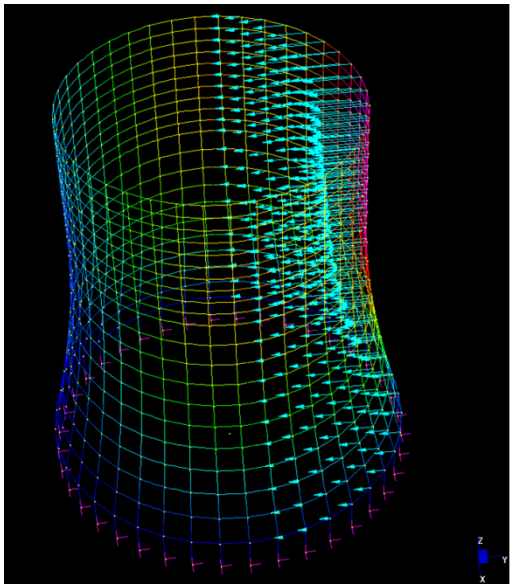

Figure 1: Strand7 model of a cooling tower under wind loading

There are advantages to a steel frame over a concrete shell. As there is a low possibility of seismic shocks due to the creation of fractured rocks underground the the shell must be strong against cracking. Steel is more likely to withstand ground vibrations without failure. Steel is also suitable as this is a dry tower so corrosion is not a major issue.

Heat Exchanger Design

The design of the heat exchangers requires the selection of the heat exchanger location as well as the design of the finned tubes within the bundles. The heat exchanger arrangement must be designed to minimise the pressure drop in air flow while maximising the heat transfer.

The bundles can be located either vertically around the circumference of the tower or horizontally within the mouth of the tower. Some of the common arrangements are presented in Figure 3. The difference in thermal performance between the various arrangements is quite minimal when considering one dimensional flow through the tower. It is only when considering the effect of wind flow around the tower that the difference in performance is observed (Moore 1978).

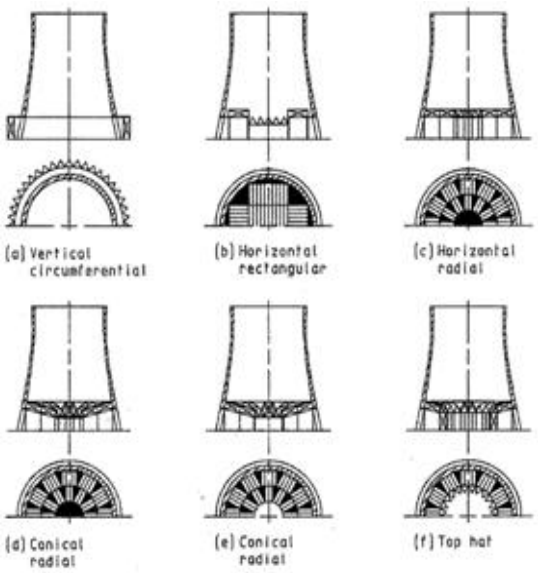

Figure 3: Common Heat Exchanger Arrangements (Kröger 2004)

For this tower design a vertical arrangement has been chosen as the bundles are self supported and arrangement is simple to model. The flow losses through the heat exchangers can be calculated analytically to determine the resistance to the air flow. A draft equation has been proposed by Kröger which equates the flow resistances to the pressure drop as the height increases.

$$\Delta P_s = (\rho_{atm} - \rho_{air})g\left[H_3 - \frac{H_3 + H_4}{2}\right] = \sum Flow\ Resistances$$

Equations for the resistances have been proposed and have been calculated iteratively to determine the mass flow rate through the tower and determine the size of the bundles.

Heat Exchanger specifications for this tower are listed in Table 2.

Table 2: Heat Exchanger Specifications

Number of Bundles	196
Total Number of Tubes per Bundle	1350
Rows of Tubes	9
Length of Tubes	15.6m
Number of Water Passes	2
Outside Diameter of Tube	40mm
Outside Diameter of Fin	80mm
Number of Fins per metre	60/m

The bundles are arranged vertically around the circumference of the tower at an angle of 60° to the tower. These results have been compared to the AspenTech Heat exchanger design program to ensure that the surface area of the finned tubes is sufficient.

Performance Analysis

The performance of the natural draft dry cooling tower is quite dependent on the weather conditions. As the ambient temperature increases the cooling capacity and the performance of the power plant decreases which is the primary concern in the use of natural convection. As the ambient temperatures will peak in the summer months when the power usage is often at its greatest, this requires some investigation to determine the viability of this method. There will also be significant temperature drop during the night so there will be some variation in the performance of the tower over a daily and monthly time frame.

Wind acting around the tower will also affect the cooling performance. The direction of air entering the tower changes due to the effect of wind as is evident in Figure 4. Ideally, air enters perpendicularly to the face of the heat exchanger to minimise the pressure drop in the flow. An investigation conducted by Moore (1978) to determine the effect of varying the angle found that for angles greater than 75° (from perpendicular) the flow is negligible. The use of wind break walls is proposed by Du Preez (et.al. 1995) and seems to minimise the effect of the wind.

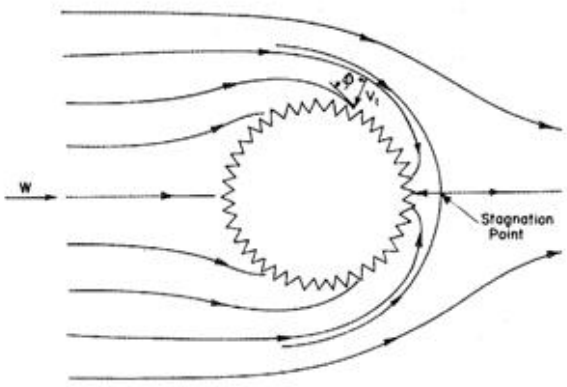

Figure 4: Possible wind streamlines (Moore 1978)

Summary

The natural draft dry cooling tower would provide an alternative cooling method when large quantities of water are not available. Investigation is required to determine whether it is suitable for a power plant in South Australia based on the ambient conditions of the location. A tower of 200m is required to cool the 23MW power plant in 30°C ambient conditions. Vertical heat exchangers are arranged around the circumference to allow for heat transfer.

References

Busch, D., Harte, R., Kratzig, W., Montag, U. (2002). "New natural draft cooling tower of 200 m of height." Engineering Structures **24**: 12.

du Preez, A. F. and Kröger, D. G. (1995). "The effect of the heat exchanger arrangement and wind-break walls on the performance of natural draft dry-cooling towers subjected to cross-winds." Journal of Wind Engineering and Industrial Aerodynamics **58**(3): 293-303.

Forgo, L. (1979). "Dry Cooling for Power Stations." IEEE Trans Power Appar Syst **98**(3): 1099-1103.

Kröger, D. G. (2004). Air-cooled Heat Exchangers And Cooling Towers: Thermal-flow Performance Evaluation And Design. Oklahoma, PennWell Corporation.

Moore, F. K. (1978). Aerodynamics of Heat Exchangers and Their Arrangment In Large Dry Cooling Towers. ASME Thermophysics and Heat Transfer Conference. San Francisco, California, ASME.

Singham, J. R. (1983). Natural Draft Towers. Heat Exchangers Design Handbook. E. Schlunder. Dusseldorf, Hemisphere Publishing Corporation. **3.12**.

Comparing the Tube Fin Heat Exchangers to Metal Foam Heat Exchangers for Geothermal Applications

Odabaee, M. , Hooman, K. and Gurgenci, H.
School of Engineering, the University of Queensland, Brisbane, Australia
Email: mostafa.odabaee@uqconnect.edu.au, K.hooman@uq.edu.au, H.gurgenci@uq.edu.au

This paper examines the application of two different heat transfer augmentation techniques to improve the performance of an air-cooled heat exchanger. The conventional finned-tube design is compared with a modern technique being the application of a metal foam heat exchanger applied as a layer to the outer surface of the tube. Both designs improve the heat transfer rate from the condensing fluid flowing in the tube bundle albeit at the expense of a higher pressure drop compared to the bare tube as our reference case. Considering the heat transfer enhancement as the benefit and the excess pressure drop as the cost, the two cases are compared against each other. In order to achieve this goal, results from two different sources have been compared being ANSYS-Fluent and ASPEN B-JAC. A number of correlations are also proposed to predict the cost (excess pressure drop) and the benefit (heat transfer augmentation) of the extended surface.

Introduction

Most of the geothermal resources of Australia are located in arid areas where there is not enough water to feed wet cooling towers to absorb the cycle waste heat. Air-cooled condensers provide the only economic choice in such places where the cycle fluid condenses inside the tubes cooled by air. The tubes have external fins to increase the air-side heat exchange surface. Fins improve the heat transfer performance but at the same time lead to higher pressure drop compared to bare tubes. As such, there always is a trade-off between these two opposing effects where the main goal is to remove the waste heat from the condenser.

Metal foams, an emerging technology in the field of heat exchangers, benefit from such advantages as low-density, high area/volume ratio, and high strength structure. Therefore, they have been applied in a variety of applications including cryogenics, combustion chambers, cladding on buildings, strain isolation, buffer between a stiff structure and a fluctuating temperature field, petroleum reservoirs, compact heat exchangers for airborne equipments, high power batteries, compact heat sinks for power electronics and electronic cooling, heat pipes and sound absorbers (Mahjoob and Vafai 2008). This study explores a comparison between thermo-hydraulic performance of finned-tubes and metal foam heat exchangers with specific attention being paid to the price, weight and manufacturing structure as a basis for future work.

Figure 1: Samples of metal foam heat exchanger and tube fin heat exchanger

Finned-Tube Heat Exchangers

A finned-tube heat exchanger is designed by the well-known commercially available engineering software ASPEN B-JAC for an air-cooled heat exchanger, as indicated by Table 1. This table presents a sample of our results for a binary cycle with Isopentane as the working fluid which is cooled by air in a geothermal power plant. Based on an efficiency of about 15%, 283 MW of heat should be dumped so that 50 MWe can be generated; see also (Ejlali et al 2008). Further details of the air-cooled heat exchanger, including fin thickness, type, and number density are presented in Tables 1 and 2 where the tube bundle configuration is illustrated in Figure 2.

Metal Foam Heat Exchangers

Performance of a metal foam-covered single tube as a representative, in cross-flow is examined numerically as illustrated by Figure 3 where the geometry and the applied mesh system is presented. As mentioned earlier, the commercially available CFD software Fluent is used to solve the full set of governing equations for different samples of metal foams (Calmidi and Mahajan 2000).

Similar to (Hooman and Gurgenci 2010), the thermo-hydraulic performances of the two different designs, finned-tube and metal foam-covered heat exchangers, are compared under similar conditions.

Summary and Conclusion

It is expected that metal foams heat exchangers have higher heat transfer rates compared to finned-tube ones. At the same time, metal foams can cause higher pressure drop. Interestingly, for a specific case where the same boundary conditions have been set for a metal foam covered tube and finned tube (air velocity = 3.34m/s, air temperature = 308K, tube temperature = 320K), according to our numerical results, the former is associated with 10% higher heat transfer rate at the same pressure drop. It is expected that an optimization study can further increase the heat transfer of metal foams so that the heat removal form a binary cycle in a geothermal power plant can significantly be improved with less parasitic losses compared to the existing technology.

References

Calmidi, V. V. and R. L. Mahajan (2000). "Forced convection in high porosity metal foams." Journal of Heat Transfer 122(3): 557-565.

Ejlali, A., Hooman, K., "A comparative study on dry cooling of different working fluids for geothermal applications," AGEC 2008, Melbourne, Australia.

Mahjoob, S. and K. Vafai (2008). "A synthesis of fluid and thermal transport models for metal foam heat exchangers." International Journal of Heat and Mass Transfer 51(15-16): 3701-3711.

Hooman, K. and H. Gurgenci (2010) Different heat exchanger options for natural draft cooling towers to be presented in World Geothermal Congress, Bali, Indonesia.

Table 1: The result of ASPEN B-JAC

Air-Cooled Heat Exchanger Specification Sheet

1	Company:						
2	Location:						
3	Service of Unit:		Our Reference:				
4	Item No.:		Your Reference:				
5	Date:	Rev No.:	Job No.:				
6	Size & Type	6243 / 1073155Type	Induced		Number of Bays	219	
7	Surf/Unit-Finned Tube	612786.1 m²			Bare Tube	56306.8	m²
8	Heat exchanged	283127000 W			MTD, Eff	15.22	℃
9	Transfer Rate-Finned	30.4 Bare, Service	330.4		Clean	354.3	W/(m² K)
10	**PERFORMANCE DATA - TUBE SIDE**						
11	Fluid Circulated					In/Out	
12	Total Fluid Entering	kg/s 858		Density, Liq	kg/m³	592.07/592.07	
13		In/Out		Density, Vap	kg/m³	2.71/2.71	
14	Temperature	℃ 46.85/46.85		Specific Heat, Liq	kJ/(kg K)	2.376/2.376	
15	Liquid	kg/s 857.9901/858		Specific Heat, Vap	kJ/(kg K)	1.766/1.766	
16	Vapor	kg/s 0.01/		Therm. Cond, Liq	W/(m K)	0.099/0.099	
17	Noncondensable	kg/s /		Therm. Cond, Vap	W/(m K)	0.017/0.017	
18	Steam	kg/s /		Freeze Point	℃		
19	Water	kg/s /		Bubble / Dew point	℃	/ 45	
20	Molecular wt, Vap	/		Latent heat	kJ/kg	330	
21	Molecular wt, NC			Inlet pressure (abs)	bar	1	
22	Viscosity, Liq	mPa s 0.182/0.182		Pres Drop, Allow/Calc		0.4/ 0.001	
23	Viscosity, Vap	0.009/0.009		Fouling Resistance	m² K/W		
24	**PERFORMANCE DATA - AIR SIDE**						
25	Air Quantity, Total	24000 kg/s		Altitude		m	
26	Air Quantity/Fan	97.545 m³/s		Temperature In	25	℃	
27	Static Pressure	25.26 mmH²O		Temperature Out	36.74	℃	
28	Face Velocity	3.34 m/s Bundle velocity	11.1 kg/s/m²	Design Ambient		℃	
29	**DESIGN-MATERIALS-CONSTRUCTION**						
30	Design pressure	1.448 bar	Test Pressure	Code	Design temperature	78.89	℃
31	**TUBE BUNDLE**		**Header**		**Tube**		
32	Size	6243	Type Plug		Material	CS	
33	Number/bay	2	Material		Specifications	Welded	
34	Tube Rows	5	Passes	1	OD	62 Min Thk.	1.65 mm
35	Arrangement		Plug Mat.		No./Bun	110 Lng	6 m
36	Bundles	2 par 1 ser	Gasket Mat.		Pitch	106.35 / 92.1	Staggered
37	Bays	219 par 1 ser	Corr. Allow.	3.18 mm	**FIN**		
38	Bundle frame	Galvanized steel	Inlet Nozzle (2)	50.8 mm	Type	Embedded	
39	**MISCELLANEOUS**		Outlet Nozzle(2)	50.8 mm	Material	CS	
40	Struct. Mount.		Special Nozzles		OD	100 Tks	0.91 mm
41	Surf.Prep		Rating		No.	197 #/m Des Temp	℃
42	Louvers		TI PI		Code		
43	Vibration Switches		Chem Cleaning		Stamp	Specs API 661	
44	**MECHANICAL EQUIPMENT**						
45	Fan,Mfr., Model		Driver, Type		Speed Reducer, Type		
46	No./Bay	1 RPM 134.67	Mfr.		Mfr.&Model		
47	Dia. mm	4572 Blade(s) 18	No./Bay		No./Bay		
48	Pitch	1.54 Angle	RPM		Rating		hp
49	Blade(s)	4572 Hub 2286	Enclosure		Ratio		
50	hp/Fan	32.83 Min Amb	V/Phase/Hz	/ /	Support		
51	Control Action on Air Failure-				Louvers		
52	Degree Control of Outlet Process Temperature						
53	Recirculation				Steam Coil		
54	Plot Area	m²	Drawing No.	Wt.Bundle	7889.5 Wt.Bay	18042	kg
55	Notes:						
56							
57							
58							

Table 2: Mechanical details of tubes and fins

Tube material		Carbon Steel	Fin material		
Tube length	m	6	Fin type		Embedded
Tube OD	mm	62	Fin OD	mm	100
Tube wall thickness	mm	1.65	Fin thickness	mm	0.91
Tube pitch face row	mm	106.35	Fin density	#/m	197
Tube pitch rows deep	mm	92.1	Fin segment width	mm	
Tube pattern		Staggered			
Pass type					
Area ratio Ao/Ai		11.49			

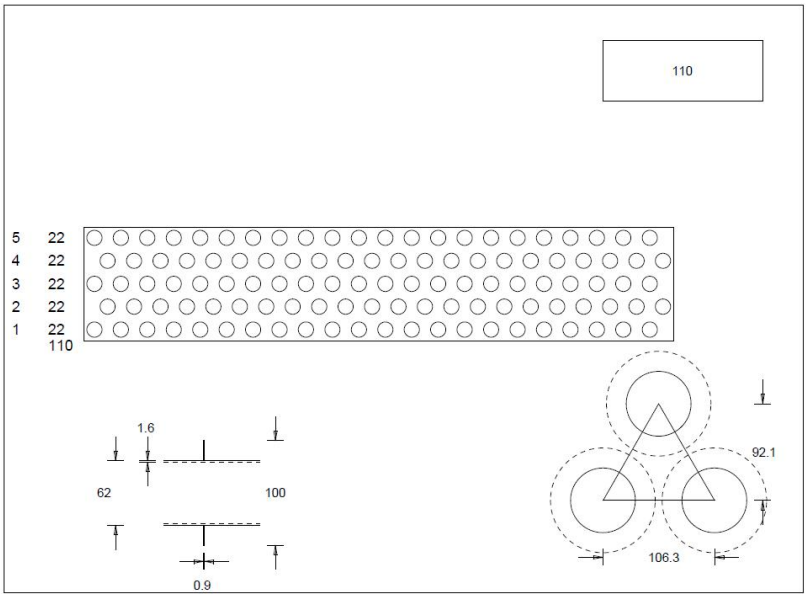

Figure 2: Mechanical details of tube layout

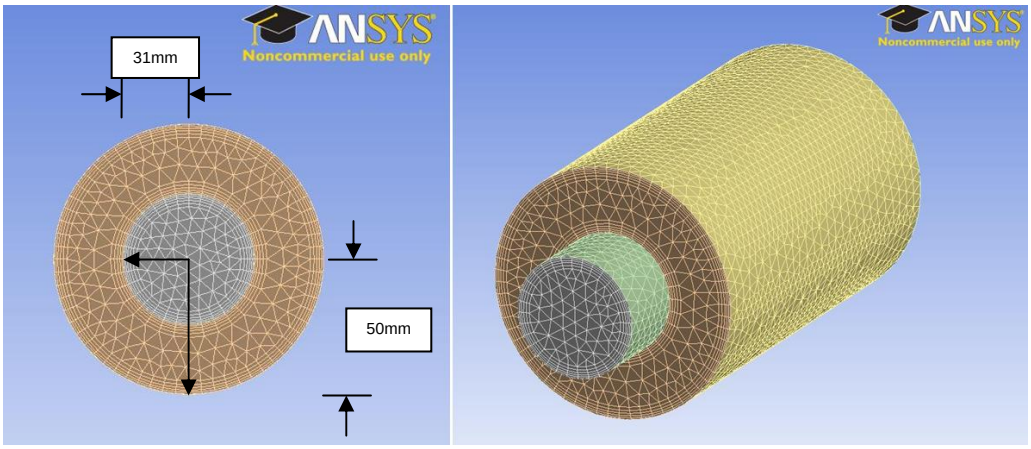

Figure 3: The metal foam-covered single tube in 2D and 3D views (the generated mesh in the flow region has not been shown for the visibility proposes).

Assessment of Current Costs of Geothermal Power Generation in New Zealand (2007 Basis)

Paul Quinlivan
Sinclair Knight Merz,
12-16 Nicholls Lane, Parnell, Auckland, New Zealand
pquinlivan@skm.co.nz

Sinclair Knight Merz (SKM) has completed a study for the New Zealand Geothermal Association (NZGA) which assesses the cost of developing typical greenfield New Zealand geothermal resources in single blocks of either 20 or 50MW capacity.

Figure 1 High temperature geothermal fields in New Zealand

The method used in the study consisted of the development of a spreadsheet financial model which was then applied to a band, or envelope, of estimated capital costs based on an assessed range of resource characteristics. Capital and operating costs were iterated across a diverse range of New Zealand geothermal industry participants until agreement on costs was obtained while avoiding disclosing confidential information. Using the model, electricity tariffs were derived for geothermal resources in a New Zealand setting from analysis of a total of 32 greenfield geothermal development scenarios.

Keywords: geothermal resource, capital cost, electricity selling price, greenfield, estimation, geothermal power generation

Development Scenarios

The 32 development scenarios derive from selected combinations of 4 resource variables critical in any given development: (i) resource temperature (3 cases); (ii) development size (2 cases); (iii) plant technology (4 cases), and; (iv) well flow rates based on permeability (2 cases). These variables and the rationale for their assumed values are described. A total of 16 cases at a high flow band (150 $kg.s^{-1}$) and 16 cases at a low flow band (50 $kg.s^{-1}$) have been studied. The cases are realistic in that there is over 50 years of experience in exploration, development and operation of New Zealand geothermal fields and so good data are available on which to base the resource performance characteristics.

A number of resource temperatures for developed and undeveloped geothermal resources, which may be available for development, are considered in the model. For New Zealand fields likely to be developed under the current regulatory and pricing regime, maximum resource temperatures at depths currently drilled in the natural state range from 230 to 330°C with an average value of around 280°C.

Accordingly, four development cases have been allowed for resource temperatures, well deliverability and development size. Wells are assumed to self-discharge rather than be pumped. The first development case is for a high temperature and highly productive resource (Mokai, Rotokawa and Kawerau) with resource temperatures in excess of 300°C. In this case, wells have some excess enthalpy, which is assumed to be 10% above the enthalpy of water at 300°C, and high well head delivery pressures of typically 20 barA. The development size is assumed to be 50 MWe.

The second development case includes medium temperature and moderate productivity resources (Wairakei, Ohaaki and Tauhara), and the lower temperature zone of higher temperature fields with resource temperatures averaging 260°C. In this case, liquid reservoir conditions prevail with no excess enthalpy, and wells have moderate wellhead delivery pressures of about 5 barA. The development size is set at 50 MWe. The third case is the same as the second case, but the assumed development size is set at 20 MWe.

The fourth case includes lower temperature and moderate productivity resources such as Ngawha and outflow zones of higher temperature resources, with resource temperatures averaging 230°C. In this case liquid reservoir conditions prevail with no excess enthalpy, and wells have low wellhead delivery pressures of about 3 barA. The development size is limited to 20 MWe.

Four classes of plant technology commonly used in the generation of power from geothermal energy were selected in order to estimate costs for this study. These include: (i) Single flash steam Rankine cycle direct contact condensing plant; (ii) Double flash steam Rankine cycle direct contact condensing plant; (iii) Organic Rankine cycle (ORC) power plant, and; (iv) Hybrid steam-binary cycle plant.

Historical data indicate that the outputs of New Zealand geothermal wells vary up to a maximum of about 30 MWe per well, with the average value skewed to a relatively low value of about 4 to 5 MWe. This probably reflects that many of the wells were drilled between the 1950's and 1970's when hole depths were typically limited to 1,200 m and only rarely to depths greater than 2,000 m, and some, such as the early wells at Wairakei and Kawerau, were of smaller diameter than is now considered standard.

Outputs of wells drilled subsequent to these early wells are often higher due to being drilled to greater depth thus benefiting from both shallow (high enthalpy) and deep (liquid) production zones, and in some cases from having larger diameter production holes and production casings. Future geothermal wells in New Zealand and internationally should prove to be better than this past average for the same reasons. Given this historical data it is considered reasonable to assume future geothermal wells in New Zealand will have an average output in the range of 5 to 10 MWe, i.e. somewhat greater than wells typical of the Wairakei and Ohaaki developments, but significantly less than the larger output wells encountered in the higher temperature, central parts of the Mokai, Rotokawa and Kawerau fields. In each case the specific energy output of the wells was calculated from the flow rate.

Methodological Approach

Considering the range of resource characteristics discussed above and that the development options to be costed need to include a number of different power plant cycle types with cycle efficiencies that vary in response to plant inlet pressure, and well enthalpies (which dictate steam and brine flows), it is not very useful for comparative purposes to assign a single average MWe rating to wells drilled into the above four resource scenarios. Instead, the approach taken follows that of Barnett (2006 and 2007) in which the number of production and injection wells required at time 0 was calculated, while ensuring that those wells at time 0 covered not less than 110% of the selected capacity. Well capacity decline with time was modelled using a harmonic decline equation. An additional make-up production well was added whenever the capacity in a subsequent year would drop below the 10% reserve margin.

The method allows for investigation of the cost performance of the various options. This performance varies considerably depending on resource temperature and well flow rate. Total capital cost, specific capital cost (SCC) and the required Year 0 electricity tariff ($NZc.kWh^{-1}$) have all been estimated for each option and financial models developed for each of the 32 cases.

The estimated capital costs for each project scenario are inputs to this model together with operations and maintenance costs (O&M) and make-up and replacement wells, assessed over the operating life of the project which is assumed to be 30 years. Net delivery at the sales point is determined on a year-by-year basis, with assumptions made for scheduled and unscheduled outages, semi-annual inspection shutdowns, and recoverable and unrecoverable performance degradation.

Results

Full results are presented in Table 1 (Appendix 1). The relative rankings for thermal and financial performance are summarised below and presented in Figures 2 to 4:

Thermal performance (based on gross generation)

High temperature:
ORC < Single Flash < Hybrid < Double flash
Low temperature:
Single Flash < Double Flash < ORC < Hybrid

Financial performance
Low Temperature (20 MWe gross)
Specific capital cost:
Single flash < Hybrid < ORC < Double Flash
Electricity tariff:
Single flash < Double flash < Hybrid < ORC
[Range 10 to 14.5 NZc/kWh real]

High Temperature (50 MWe gross)
Specific capital cost:
Single flash < Hybrid < Double flash < ORC
Electricity tariff:
Single flash < Double flash < Hybrid < ORC
[Range 7 to 11 NZc/kWh real]

The ranking of the power cycle options in terms of thermal performance (gross) is quite different to the ranking in terms of financial performance. The advantage enjoyed by the binary plant options in terms of thermal performance at low temperature is not able to be translated into a financial advantage. There are two reasons for this, the

first being that the binary plant options have somewhat higher plant parasitic loads which decrease their net thermal performance and thus their respective revenue streams, and although they have similar SCCs to double flash at low temperature (based on the cost assumptions made in the study), this is not enough to give them a levellised cost advantage.

Nevertheless, the range is quite close and innovative approaches to equipment marketing and financing may be enough to tip the balance in favour of one technology over the other, as can be witnessed by the market success of ORC and hybrid plants in New Zealand over the past 15 years.

Double flash plants have higher specific capital costs than the single flash steam or hybrid plant options, in spite of double flash plant having good thermal efficiency at all of the reservoir temperatures examined. This is due to the greater complexity and thus cost required within the steamfield and power plant to accommodate the second stage steam flash separators and piping / instrumentation and the additional cost for fitting out a turbine with two steam inlets. It is these additional costs which penalise the double flash option relative to the single flash and hybrid options.

The analysis undertaken here for the double flash option is relatively conservative conservative being constrained by limiting second stage flash pressure to control silica scaling potential. A more aggressive approach could be taken through reducing the second stage flash pressure further to generate a greater steam flow from the second stage flash step. This would improve the cost performance of this option, however, this would be at the risk of silica super saturation in the waste brine in excess of 130% with increased potential for scale deposition even with chemical treatment.

The key outputs from the model runs are estimates of the required “electricity tariff” for each project development option for a variety of financial assumptions of which corporate tax rate (30%), depreciation (straight line, 8 years), inflation (0%) and equity content (100%) are the most important. These tariff values are equivalent to the year 0 selling prices required to achieve the financial hurdle After Tax Internal Rate of Return (IRR) assumed in the model (10% real). Intermediate model outputs are specific capital cost (NZ$.kWe(gross)$^{-1}$) and thermal performance (the ratio of thermal power supplied to gross electrical power generated).

The costs developed here (and presented in Figure 2) are in New Zealand dollars. They are based on 2007 values, and were internally calibrated against costs being incurred for New Zealand geothermal developments, of which there were a number in progress at that time, and several overseas geothermal projects which were also in progress at that time.

This study did not consider greenfield developments greater than 50 MWe. The main reason is that a greenfield developer would most likely not be able to attract the funds required for a larger development until some experience with the particular resource was gathered and the risks associated with a larger development were able to be well quantified. Furthermore a greenfield development of over 50 MWe may struggle to obtain resource consents in New Zealand, given the conservatism of regulatory authorities and their preference for staged developments, for the same reasons.

This contrasts with the current situation in New Zealand where large developments of medium to high temperature resources are occurring at brownfield sites (100 MWe at Kawerau and 132 MWe at Nga Awa Purua (Rotokawa)). Being brownfield sites, these larger, second stage developments are then appropriate. This implies that the anticipated returns on these larger investments within the current electricity market in New Zealand are attractive – and developers are on record as stating that “Geothermal is the lowest cost source of new generation for New Zealand” (Baldwin, 2008).

For several years prior to 2007, geothermal development costs rose steadily in line with global market commodity and equipment price rises. These rises continued until the middle of 2008 when the current global financial crisis occurred and commodity prices fell back to 2003 levels. It is not certain that there is enough market data available yet to determine what is currently happening to geothermal power plant, steamfield and well costs to be able to compare current (2009) costs with the 2007 estimates used in this study.

Applicability to Australia

The results of this study should be applied with caution to Australian geothermal projects. Although we consider the method to be robust and suitable for Australian projects, there are very real differences between the two countries which make the specific results inapplicable. Quite apart from the need to escalate costs to 2009, the general tendency will be for the differences to make New Zealand projects lower cost that Australian.

Significant differences include:

- The volcanic geothermal setting of New Zealand is demonstrably well suited to the occurrence of exploitable geothermal systems
- With an industry history of 60 years, exploration of New Zealand geothermal

resource is well advanced, reducing resource risks greatly
- New Zealand resources are generally hotter and much shallower than in Australia
- Some New Zealand wells encounter higher permeability than will be typical in Australia, and hydro fracturing and stimulation as necessarily required in the development of Enhanced Geothermal Systems (EGS) in Australia are not required in the New Zealand volcanic setting
- Wells in New Zealand do not generally need pumping whereas all Australian geothermal projects of the EGS and HSA (Hot Sedimentary Aquifer systems) types, with the possible exception of some in the Great Artesian Basin, will require both production and injection well pumping
- There is a highly developed and competitive geothermal drilling and service industry in New Zealand
- Use of evaporative cooling towers is common (for the non-ORC cases), and
- Distances to grid connection points are not great.

However, the method is equally applicable to the Australian context as to the New Zealand context when the above differences are taken into account.

To assist with transfer of costs, there are assessments of locally-sourced costs versus imported costs. Australian labour and materials costs can readily be substituted.

Acknowledgement

The input to this study of Peter Barnett, previously of Sinclair Knight Merz, and currently with Hot Rock Limited, is gratefully acknowledged.

References

Baldwin, D. (2008). Chief Executive's Review. http://www.contactenergy.co.nz/web/pdf/financial/ar_20080923_chairman_ceo_review.pdf

Barnett, P. (2006). *Assessment of the Current Costs of Geothermal Power Development in New Zealand.* Proceedings of 28th New Zealand Geothermal Association Workshop, 2006. http://pangea.stanford.edu/ERE/db/IGAstandard/record_detail.php?id=5119

Barnett, P. (2007). *Costs of geothermal power in New Zealand - 2007 Update.* Proceedings of 29th New Zealand Geothermal Association Workshop, 2007. http://www.nzgeothermal.org.nz/publications/Reports/Workshop2007/GeothermalCosts2007.pdf

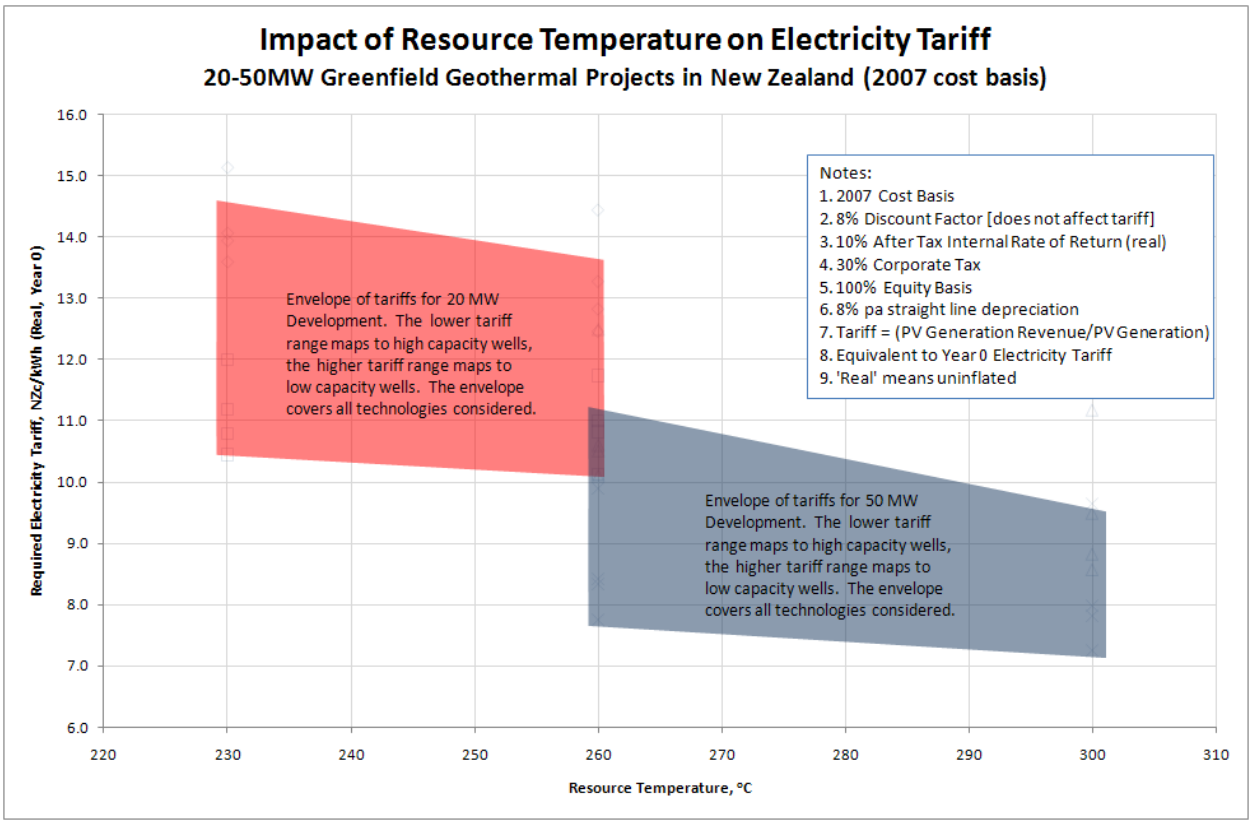

Figure 2 Electricity tariffs required for greenfield geothermal developments in New Zealand (2007 basis)

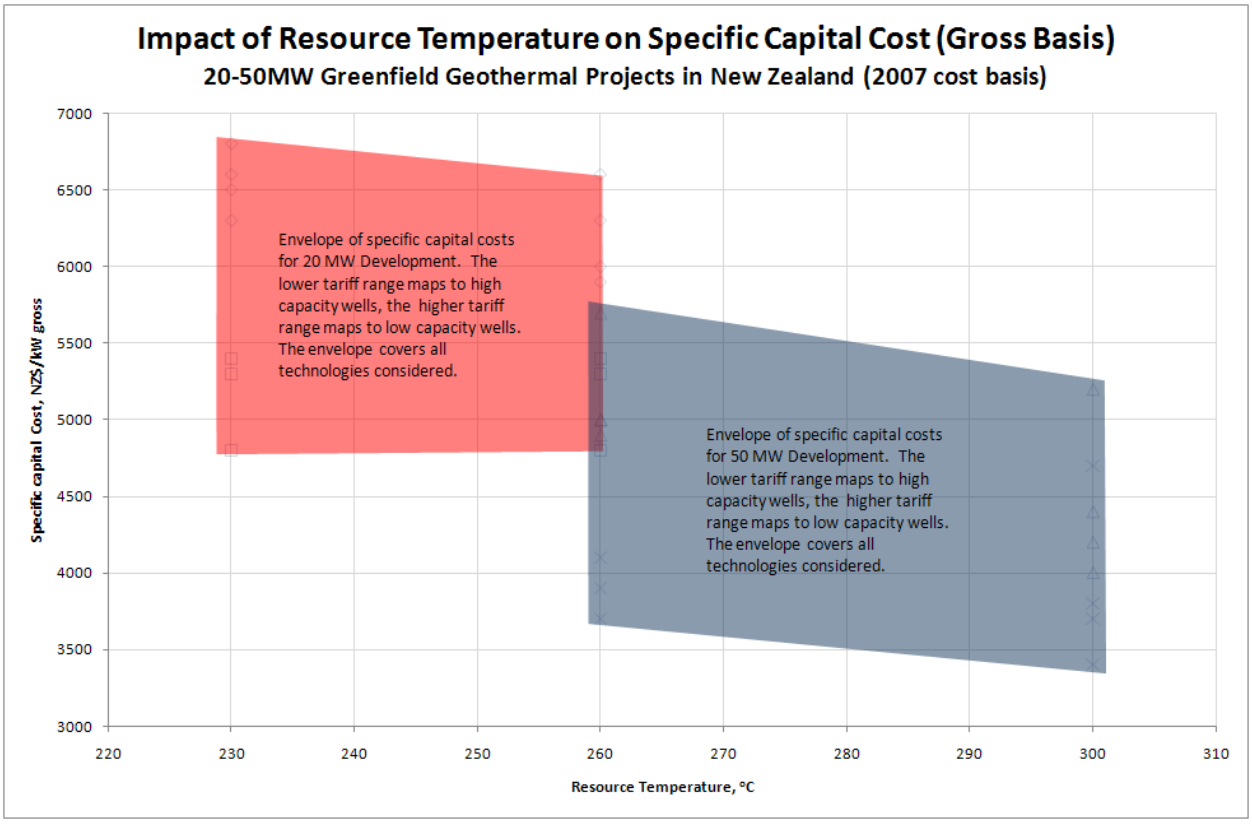

Figure 3 Specific capital costs of Greenfield geothermal developments in New Zealand (2007 basis)

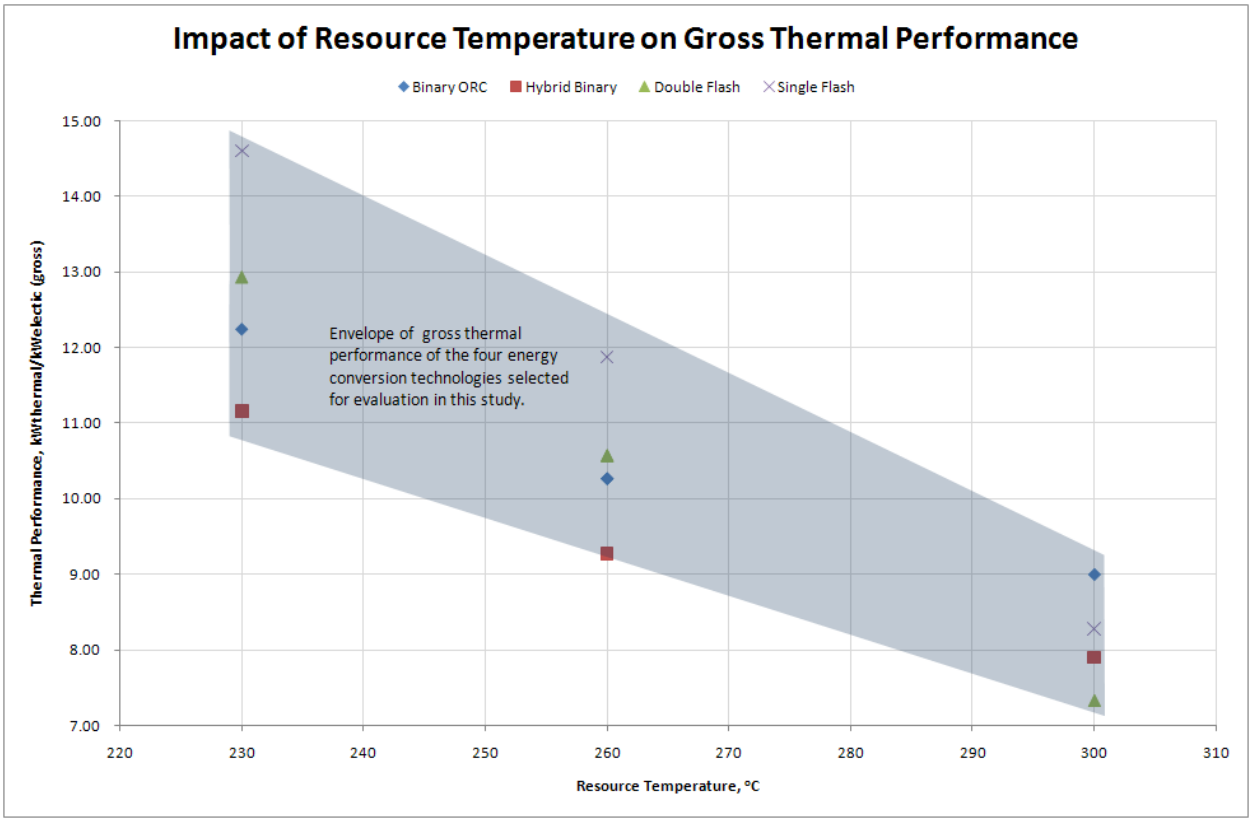

Figure 4 Thermal performance of the energy conversion options reviewed in this study

Appendix 1

Table 1 Outputs from study

Option	Well Capacity Envelope	Reservoir Temperature	Development Size	Power Plant Technology	Year 0 Tariff (Real)	Specific Capital Cost	Thermal Performance
#	High=150kg.s^{-1} Low=50kg.s^{-1}	^{o}C	MWe(gross)		NZc.kWh^{-1} (2007 basis)	NZ$.kWe(gross)$^{-1}$ (2007 basis)	kWthermal. kWe(gross)$^{-1}$
1	High	300	50	SF	7.3	3400	8.3
2	High	260	50	SF	7.8	3700	11.9
3	High	260	20	SF	10.1	4800	11.9
4	High	230	20	SF	10.5	4800	14.6
5	High	300	50	DF	7.8	3800	7.3
6	High	260	50	DF	8.3	4100	10.6
7	High	260	20	DF	10.8	5300	10.6
8	High	230	20	DF	10.8	5300	12.9
9	High	300	50	Hybrid	8.0	3700	7.9
10	High	260	50	Hybrid	8.4	3900	9.3
11	High	260	20	Hybrid	11.0	5300	9.3
12	High	230	20	Hybrid	11.2	5300	11.2
13	High	300	50	ORC	9.6	4500	9.0
14	High	260	50	ORC	9.9	4700	10.3
15	High	260	20	ORC	11.7	5400	10.3
16	High	230	20	ORC	12.0	5400	12.2
17	Low	300	50	SF	8.6	4000	
18	Low	260	50	SF	10.1	4900	
19	Low	260	20	SF	12.5	5900	
20	Low	230	20	SF	13.6	6300	
21	Low	300	50	DF	8.8	4200	
22	Low	260	50	DF	10.5	5000	
23	Low	260	20	DF	12.8	6000	
24	Low	230	20	DF	13.9	6800	
25	Low	300	50	Hybrid	9.5	4400	
26	Low	260	50	Hybrid	10.6	5000	
27	Low	260	20	Hybrid	13.3	6300	
28	Low	230	20	Hybrid	14.1	6500	
29	Low	300	50	ORC	11.2	5200	
30	Low	260	50	ORC	12.5	5700	
31	Low	260	20	ORC	14.4	6600	
32	Low	230	20	ORC	15.1	6600	

Analysis of Reinjection Tests in a Bedrock Geothermal Reservoir, Tianjin, China

Zhu Jialing*[1] and Wang Kun[2]
[1]Tianjin Geothermal Research & Training Center, Tianjin University, Tianjin, China
Weijin Road 92, Nankai District, Tianjin 300072 China
[2]Geothermal Management Division, Bureau of the City Plan and Land Resource, Tianjin,
Email:zhujl@tju.edu.cn

By the end of 2008 there were about 245 production wells and 12 reinjection wells operating in Tianjin. The annual production rate is 25 million m^3 and the reinjection rate is 4.2 million m^3. Reinjection is expected to gradually cool the reservoir and so it is important to carefully design and manage the well fields and this involves estimating the thermal breakthrough time for different well separation distances. This paper describes the 2-D mass and heat transfer in the heterogeneous fractured rocks. Equations that arise for each grid block were linearised and anumerical model of the geothermal system was developed with TOUGH2. This model was then used to analyse the reservoir pressures and temperatures with special emphasis on simulating break-through of cooling at the production well. The tracer test is shown to be important for improving our understanding of the tracer and heat transport processes and reservoir (channel/fractured/karst) porosity, and for enabling the estimation of future reservoir cooling caused by fluid reinjection.

Keywords: Geothermal reservoir, Simulation, Heat break-through, Doublet system

Introduction

Tianjin is located at the north-east of the Hua-Bei plane in China, with the Yanshan Mountains at its north and Bohai Bay at its east. The total region area is 11305 km^2. The bedrock outcrop is limited to the mountain area of the north JI County[1].

In Tianjin, the main productive reservoirs are porous reservoir in the sandstone (two productive zones) and karst/fractured reservoir in bedrock (three productive zones). The top depth of the karst /fractured reservoir in bedrock is over 950 m. The discharge rate of the single well is more than 100 m^3/h, the wellhead temperature is 55-100 °C. The waters are mainly used in space heating, physical therapy, bathing, fish farming etc.

Since 1996, the reinjection test started in the basement reservoir in Tianjin. Till now there are 27 doublet (reinjection/production) geothermal wells, and 10 of them are located in Tianjin urban area. These doublet wells are significant for the protection of the geothermal resource in Tianjin.

By the end of 2008, there were about 245 production wells (including 27 reinjection wells). The annual production rate is 25 million m^3 and the reinjection rate is 4.2 million m^3. The static water level is between –35m and –90m, the annual draw down rate is 6-9m.

Analysis of the Tests in the Basement Geothermal Reservoir

Geological modelling of the doublet system

The system of WR45 is the second production-reinjection doublet well in the basement reservoir of Tianjin, which was drilled in 1995. Production and reinjection wells were drilled into the Wumishan formation of the Jixian series of the Proterozoic group.

Analysis of the reinjection tests in WR45

The productive zone of the doublet WR45 is Wumishan formation of the Jixian series in Proterozoic group. The main lithologic characteristic is the dolomite and limestone. The karst fissure is well developed in this area.

The first reinjection test was carried out with the pressurization pump in Oct. 1996. Figure 1 shows the monitoring data for the test. Removing the abnormal data that may cause by some equipment problems, the reinjection flow-rate was inverse proportional to the re-injective pressure during the test. When the pump pressure was 0.02 MPa, the reinjection rate was 100m^3/h. But the re-injective rate decreased to 86 m^3/h when the pump pressure increased to 0.05 MPa. During the last stage, the pump pressure was 0.09MPa, the re-injective rate settled at 50m^3/h more or less.

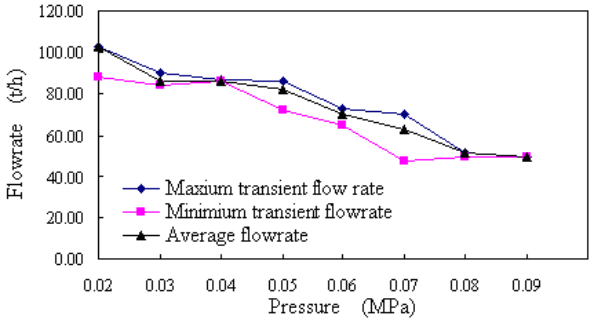

Figure1 Relationship between re-injection pressure and flow rate.

The doublet well of the WR45 is located at the well-developed karst fissure area in Wumishan reservoir, which is the porous-fracture medium of doubling porosity. At the beginning of the reinjection test, the flow along the fissure takes

the leading effects. The pump pressure influences a little on the reinjection rate. The reinjection fluid transfers the aquifer quickly because of the increasing of the pressure gradient between the reinjection and production well. As the reinjection time extended, the seepage flow in porous medium took more and more effects. The velocity of reinjection fluids in the reservoir became slowly, and the re-injective was decreased. As a whole, the pump pressure increased and the injection rate decreased gradually as the reinjection test continued.

During the space-heating period from Nov. 1999 till March 2001, the doublet WR45 has been run under the natural state without pressure pump. All the released geothermal water was reinjected into the reservoir quickly after the heating cycling. Because several geothermal production wells were used for space heating simultaneously around WR45, the reservoir pressure decreased fast. It would be of influence to the water level of the reinjection well. For the case, it may be easier to reinject. However, the temperature changes of the production zone should be monitored so that the rate of reinjection can be adjusted. By the 2002, the temperature changes have not observed in surrounding the production geothermal wells.

Tracer Test in Fractured Medium Reservoir

The tracer test is very important to understand the transport state and channel/space in the production/reinjection zone. And it is a very important stage to simulated heat transfer in the reservoir. To investigate the connective channel between the reinjection and production well of doublet WR45, the tracer tests have been done in the winter of 1998-1999. 10kg of iodide of potassium (KI) is selected for the first stage as the tracer. A series of instruments are installed surrounding wells to monitor the water quality for a long period. The detailed data is listed in Figure 2.

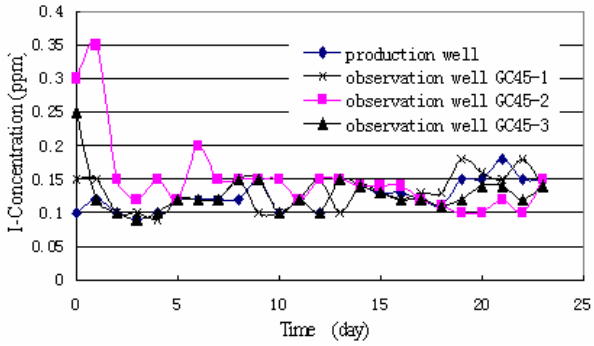

Figure 2 Observed concentration breakthrough curves of the tracer test.

The monitoring data shows that the tracer concentration is almost constant in production wells, in the other hand the observation well GC45-2 is more sensitive to the iodine. It means that the hydro-geological connection between the production and reinjection well of doublet WR45 is indirect, and maybe there is a direct or fast migration channel between the reinjection well and the other geothermal production well, like the production well GC45-1, which is about 2.5 km away from reinjection well. The test results in the well of GC45-2 were simulated by the mathematics model in order to understand the geometry structure of the fracture passage between GC45-2 and reinjection well (See Figure 3 and Table 1).

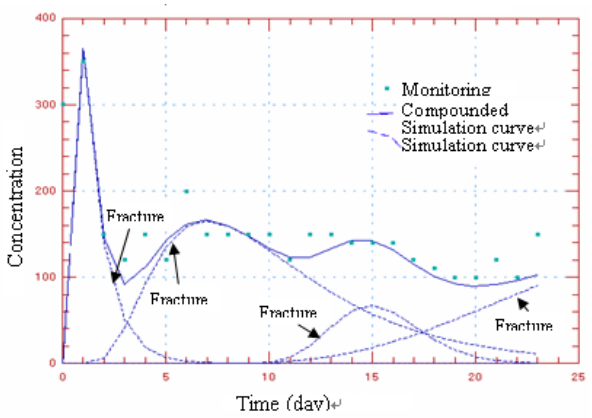

Figure 3 Simulated breakthrough curves compared with the results of the tracer test.

Table 1 Calculated parameter of the tracer test

	Cross section area Aφ	Dispersion α_L	Recovery mass (%)
Fissure 1	1.50	355.50	20.35
Fissure 2	15.74	142.25	38.90
Fissure 3	29.51	10.06	10.27
Fissure 4	54.68	161.38	21.90

Table 1 shows a comparison of the simulation curves and calculation data. One simulation curve compounded by 4 pulse curves is derived from the modelling. When the tracer was injected into the aquifer, it would quickly travel along the most direct/fast pathway, which has the smallest cross section and biggest disparity. Then the tracer would move to the production well quickly and its concentration will reach the maximum value in a very short time. If the reinjection water diffuses into a large space, only a small fraction of the tracer will be detected and the time reach the peak value will be longer. The heat breakthrough time will not be a problem in doublet system if the distance is more available between the production and reinjection well.

Model and Constitutive Equations

The main side effect anticipated from reinjection is a cooling of the reservoir [2]. It is necessary to

estimate the thermal breakthrough time for different injection-production well spacing, i.e. the time from initial injection until a significant cooling is observed in a production well [3].
The mass conservation equation

$$\frac{\partial \phi \rho}{\partial t} = \frac{-\partial \phi S \rho_v}{\partial t} + \frac{\partial \phi (1-S)\rho_l}{\partial t} = -\nabla F + q_\rho \quad (1)$$

l = liquid phase; v = vapour phase; F = vector of mass matrix; q_ρ = external energy; ρ = density; ϕ = porosity; S = vapour saturation.

The energy conservation equation (conductivity and convection):

$$\frac{\partial(\frac{Q}{V})}{\partial t} = \frac{\partial(u\rho\phi + u_s\rho_s(1-\phi))}{\partial t} = -\nabla G + (\frac{F_v}{\rho_v} + \frac{F_l}{\rho_l})\nabla P + Q_u \quad (2)$$

S = solid phase; u = internal energy; G = energy matrix; Q = energy; V = volume of reservoir; Q_u = external energy.

Set of equations (l) and (2) is related to one or two phase filtration in a porous or fractures medium where rock matrix and fluid are considered to be in local thermal equilibrium. For a block of micro volume Vn of the field, the transfer equation of mass and energy (5) call be interpreted by equations (3) and (4).

$$\frac{\partial \phi \rho}{\partial t} = \sum_{m=1}^{N} \frac{F_m A_m}{\tau} + q \quad (3)$$

$$\frac{\partial u_s}{\partial t} = (\frac{\partial u_s}{\partial t})_\rho \frac{\partial u}{\partial t} + (\frac{\partial u_s}{\partial \rho})_u \frac{\partial \rho}{\partial t} \quad (4)$$

$$\Delta U_n = \Delta t \frac{\frac{1}{V_n}\sum_{m=1}^{N} A_{nm}(G_{nm} - u_n F_{nm}) + (Q_n - Q_n')}{\phi\rho + (1-\phi)\rho_s\{(\frac{\partial u_s}{\partial u})_\rho + (\frac{\partial u_s}{\partial \rho})_u \frac{\alpha\rho/\partial t}{\partial u/\partial t}\}} \quad (5)$$

At present, the main reinjection math model in Tianjin has been simulated by a program called TOUGH2[4]. The results would be helpful to analyse changing of the temperature field and predict the pressure and temperature alteration later than 10 years in the Wumishan aquifer. Fig 4 is a sketch map of another doublet WR82/83. Considering the heat transfer between the reservoir and the other stratum at the top or bottom, a multi-aquifers model is set up to predict the temperature changes in reservoir during the reinjection test. The parameters used in modelling are listed in Table 2.

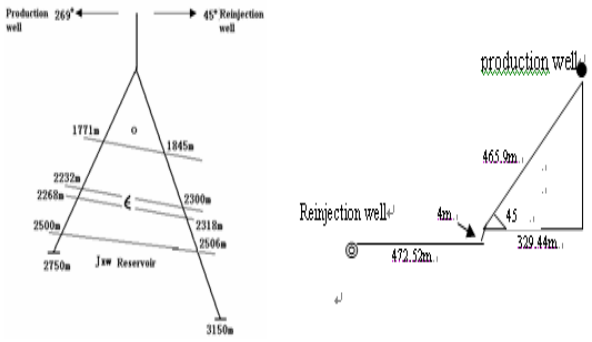

Fig. 4 The Conceptual Model of WR82/83.

Table 2 The parameters in the modelling

Reservoir temperature	87℃
Reservoir thickness	900m
Permeability of aquifer	0.2-200Darcy
Porosity of aquifer	0.03-0.5
Temperature of aquifer	85℃-90℃
Reinjection temperature	30℃
Reinjection/production rate	26.78kg/s
Rock density	2550-2770kg/m3
Heat capacity of reinjection fluid	4100J/kg℃
Density of reinjection fluid	995.62kg/m^3
Specific enthalpy of reinjection fluid	125.7kJ/kg
Specific enthalpy of production fluid	419.1kJ/kg
Reservoir's average heat capacity	1200J/kg℃
Rock specific heat	800-999J/kg℃
Rock heat conductivity	1.9-3.5W/m℃

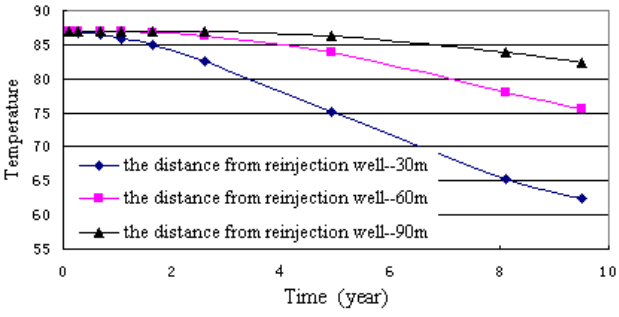

Figure 5 Temperature drawdown curves

The Figure 5 shows the simulation results. It appears that locating reinjection wells at a distance of about 100m from production well should not cause a thermal break-through in less

than 10 years. It should be pointed out that the reinjection would only be carried out in wintertime here. The reinjected water will extract more thermal energy from the rock matrix when geothermal wells are shut down in summer, resulting in slower cooling rates. However, the result is highly uncertain because the flow channel dimensions are unknown. So, more tracer tests are recommended in future research.

Summary

An important process in geothermal energy extraction is the gradual cooling of the reservoir by the reinjection fluid when reinjection is involved. The thermal breakthrough time at the production well is related to the geologic structure, hydraulic and thermal properties of the reservoir, and the reinjection rate. If the reinjection water is diluted by a large volume of reservoir fluid then tracer return concentrations will be low and cooling breakthrough is expected to be less problematic.

The reinjected water will receive more thermal energy from the rock matrix when geothermal wells are shut down in summer. This will slow the reservoir cooling process somewhat. Interpretations and predictions regarding reservoir cooling are difficult to make because the geometry of the pore space and major flow channels is the most unknown. Tracer tests provide the best means of characterising reservoir advection and dispersion between injection and production wells and are recommended for estimating the future cooling trends. It is also recommended that long-term monitoring of the Tianjin geothermal field be carried out to detect and record temperature changes caused by reinjection.

References

[1] Somerville, M., Wyborn, D., Chopra, P., Rahman, S., Estrella, D. and Van der Meulen, T., 1994, Hot Dry Rocks Feasibility Study, Energy Research and Development Corporation, Report 243, 133pp.

[2] Ouyang, J. Wang, K. and Dong, Z. The reinjection test and its numerical modeling in low-medium temperature geothermal field. Dagang, Tianjin: TDE&DI report. 1990. 100pp.

[3] Axelsson, G., Bjornsson G., Flovenz, O.G., Kristmannsdottir H. And Sverrisdottir G., Injection experiments in low temperature geothermal areas in Iceland. Proceedings of the World Geothermal Congress 1995, Florence, Italy: May 1995.

[4] Zhu Jialing, Wang Kun, Lei Haiyan, Beijing: Studies of the Reinjection Test in the Wuqing Geothermal Geothermal Field, Tianjin, China. Transactions of Tianjin University. 2002.2。

Low and Moderate Enthalpy Geothermal Resources to Desalinate Sea Water and Electricity Production

Héctor Gutiérrez[1], Salvador Espíndola[2*]
[1]Comisión Federalde Electricidad, México
[2]Instituto de Ingenieria, UNAM, México
[*]Corresponding Author: sespindolah@iingen.unam.mx

Baja California, on the northwest part of Mexico and close to the border with the largest economy of the world, has shown a rapid and continued growing of its industrial and touristy activity triggered for real state demand, since thousands of retired Canadian and American people are moving south searching for nice ocean view places and warmer weather along the Mexican coast. This baby-boomers phenomena is producing a strong increase of goods and services in the region but, specifically on the fresh water demand, in a zone where this resource is highly stressed and not easy to access or supply.
On the other hand, this though and arid region with extreme temperatures, 0ºC in winter up to 50ºC during summer, has been blessed with abundant renewable energy sources. Solar, wind, geothermal, tidal, hydrothermal vents, and other resources are widely spread along the 1,200 miles through the Baja Peninsula. That is why the National University of Mexico (UNAM) formed three years ago a professional-multidisciplinary research group –IMPULSA IV- in order to promote and implemented technological solutions to desalinate sea water through the use of renewable energy sources, Alcocer, et al (2008).
It is well known that in a traditional thermal desalination plant, the main component of the cost of the desalinated water comes from steam extracted from a power generating plant or power taken from the grid. In the case of Baja California, geothermal heat that rises from geological faults has already increased temperature of water near to the boiling point. In IMPULSA project a combined analysis of multiple effect distillation plant (MED) and a multi stage flash plant (MSF) was performed in order to be able to desalinate sea water using the hot geothermal fluid instead of the traditional steam supply from a thermal plant.

Keywords: Desalination, Low Enthalpy, MED.

Baja California Geothermal Resources

For purposes of this paper, we have divided the Baja California Peninsula in three arbitrary zones in order to present a summary of the principle sites with geothermic potential in the Peninsula (Fig.1). The northern zone is comprised of the area from the U.S. border on the northern part to the 30th parallel. The mid zone, comprised of the area between the 30th and 26th parallel, and the southern zone is from the 26th parallel to the south end of the Peninsula.

Northern Zone, Mexicali Valley

There are at least 20 sites in the northern part of the Baja California Peninsula in which there is geothermic manifestation. The most well known and largest are the Cerro Prieto Geothermal Fields, in Municipal Mexicali, where the state owner power company, Comision Federal de Electricidad (CFE) has drilled more that 300 wells to extract steam necessary for power generation. At Cerro Prieto field it is installed 720 MW of geothermal power capacity that means up to 45% of the electric energy consumed in the cities of Mexicali, Tijuana, Tecate and Rosarito.

A few kilometers from Cerro Prieto it has been identified at least five geothermal sites; all associated with the Pull-apart system between the Imperial and Cerro Prieto faults systems. However, in none of them it has been successful in obtaining sufficient temperature to be able to use them for power generation, even for example, the Tulecheck Field, where a temperatures of 165ºC has been registered, in the Airport field 112ºC and in Guadalupe Victoria up to 230ºC in a well 3,100m deep.

In the western part of the Cucapah Mountains there is a large plain, Laguna Salada (Salted Lagoon) where a multiple geothermal and geophysical soundings has been found and three deep exploratory wells where drilled. However, the maximum temperature reported in one of them was only 101ºC. To the south of this plain, it is reported agricultural wells with estimated temperatures up to 250ºC.

Ensenada

In the western part of the Baja California Peninsula, south of the city of Ensenada, several geothermal sites have been identified (Alvarez, 1993), springs appearing, hot soil, steam escaping, wells and hot norias, where geothermal potential has been identified from direct measurements of the natural discharges and in the wells of the area, particularly in the Maneadero Valley, Punta Banda, Santo Tomas and San Carlos, all of them associated with the occurrence of Agua Blanca Fault, one of the regional structures predominately oriented NW 48º.

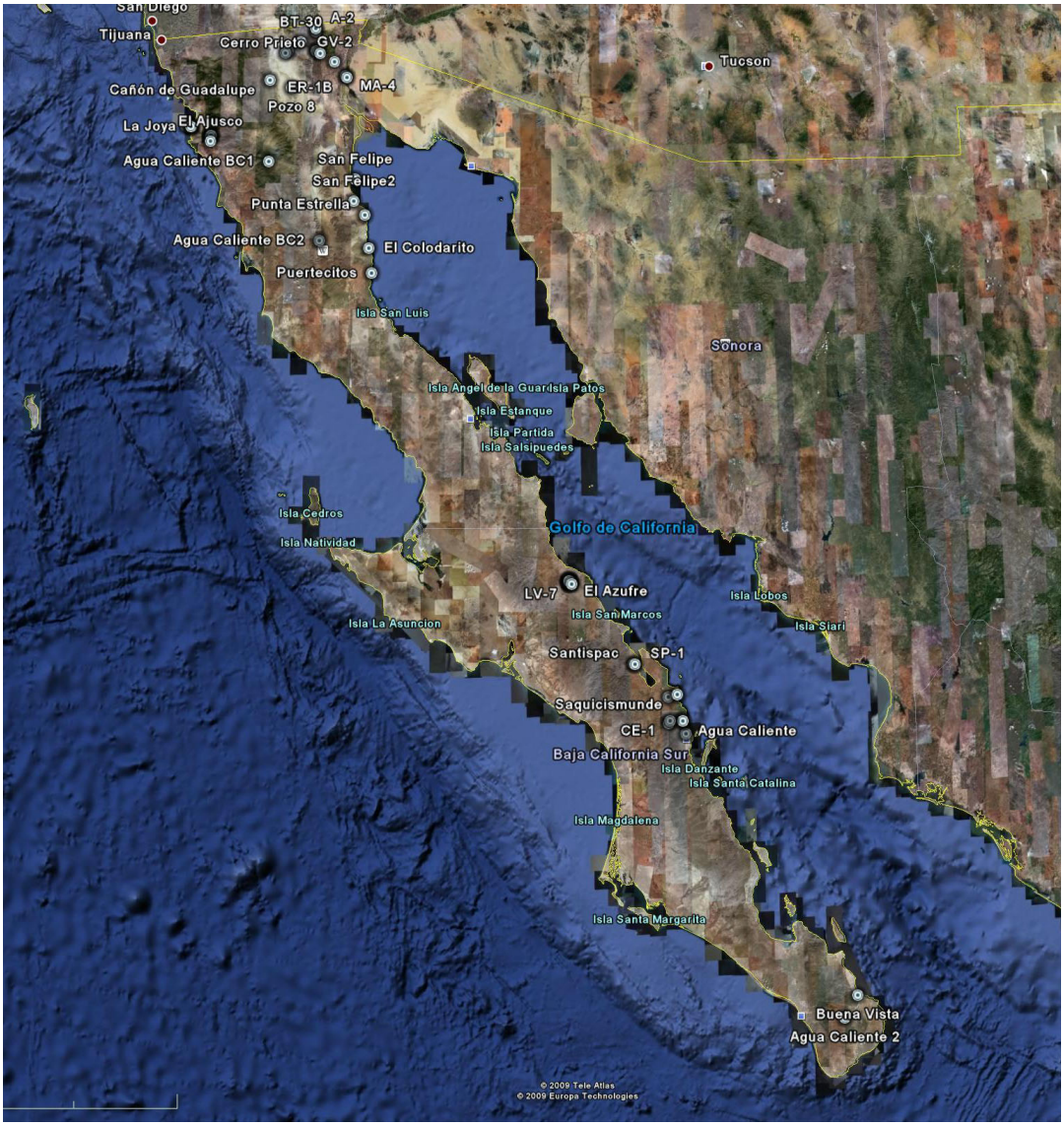

Figure 1 Baja California Geothermal Resources. Impulsa, UNAM, showing main geothermal fields Cerro Prieto (720 MW) and Las Tres Vírgenes (10MW) operated by Mexican National Utility, CFE. Also most of places with geothermal features a long of the sea shore.

Given that the zone described has been changed into a tourist development, the major part of the usage of thermal water is utilized directly for use in the tourist areas along the coast of the Maneadero Valley, there are various beaches where at low tide you can see springs of water with boiling temperatures that have been measured on the surface, resulting in the study of these sites in order to start projects of desalination of seawater through the use of thermal energy. The main locations are:

Punta Banda-Maneadero

This area is characterized by the intense hydrothermal activity, submarine as well as the length of the coast, showing emanations of steam and hot water in the sea bed having temperatures of 102ºC to 110ºC at a depth of 30 meters, as well as at diverse tourist camps along the coast where some norias have been dug that provide temperatures of 45ºC to 98ºC just at depths of 1.5 meters and in wells dug in the area. The most distinctive sites are in the area of La Joya, Agua Caliente and the Bufadora.

Ejido Uruapan

On this area there are a group of springs located on the margins of the arroyo that drops into the Cañon de la Grulla, located some 3 kilometers NE of the Agua Blanca Fault. One channel of this spring has been measured as from 250 liters per minute with temperatures of 50ºC to 65ºC. This water is used by the residents of the village as thermal baths and laundries and they have built pools and pits for the purpose.

Santo Tomas-Ajusco

Along the length o the Santo Tomas Valley and Canyon, are thermal springs during the rainy seasons. There are reports of springs with

temperatures of about 47ºC and in one thermal noria they measured temperatures of 176ºC by using geothermometers.

San Carlos – Ensenada

To the NE of the Maneadero Valley is the San Carlos Canyon where there the springs of San Carlos and Agua Caliente, reporting temperatures of 47ºC to 50ºC. In the same city of Ensenada there are springs and norias that have been used for years in the public baths of Acapulco, Lourdes and La Providencia.

To the Gulf of California or Sea of Cortes, is the volcanic providence of Puertecitos, where recent tectonic activity and the volcanic and rock activity of the zone have given rise to various thermal springs along the coast (Figure 1). This desert zone in the north of the peninsula of Baja California has been converted into an important tourist development area, where there are several sites along the coast in the upper part of the gulf, the majority of which are aimed at recreation and fishing. The main sites are:

San Felipe-Punta Estrella

In the port of San Felipe, around the Machorro hill area, there are various manifestations of thermal activity located along the coastline, where there is at least one spring with 50ºC and a noria where a temperature of 30ºC has been found at a depth of only 2m. At this site, apart from the thermal resources, there have been several studies done for the feasibility of installing a solar power plant, owing to the high degree of iridescence in the area, for which many residents of the area have solar panels for the energy in their houses. 25 kilometers to the south of San Felipe, in Punta Estrella, there is a thermal spring that has given readings of 33ºC.

Puertecitos-El Coloradito

The geothermic area of Puertecitos is located on the east coast of Baja California Peninsula, 76 km south of the port of San Felipe. This area is considered as a place of geothermic interest owing to the presence of recent volcanic action in surrounding areas and for the existence of springs in the inhabited areas as along the coast as well, registering temperatures in the range of 55ºC to 77ºC. An exploratory well has been drilled on this site but only got to a depth of 375m when they started to have problems drilling. The maximum temperature registered there was 44ºC. To the north of Puertecitos, on the coast and some 30km inland there is a hydrothermal manifestation in an area known as Coloradito, where abundant hydrothermal alteration has been observed in the outlying rocks around the spring where 56ºC has been registered.

Central Zone of the Peninsula

Tres Virgenes

This geothermic area is located some 33 miles northeast of Santa Rosalia, Baja California Sur (BCS), in an ample area remarkable for the hydrothermal activity in the middle of the region of the Tres Virgenes, as the three main volcanoes are known, La Virgin, el Azufre and La Reforma. In this area are numerous thermal zones where small boiling pots are seen, hot soil, hot water springs, smokers and a large zone of hydrothermal alteration. This area has been widely studied (Lira, 1985) and developed by CFE, the national power company, installing on site a 10 MW power plant, operating on the steam extracted from the wells drilled in the geothermal field.

Santispac

20 kilometres to the south of Mulegé, in the central part of the Bahia de Conception, a hot spring has been identified (44ºC) on the beach of the inlet at Santispac, in an area influenced by the fractured region of NW-SE which allows the overflow of hot water to mix with the sea water. Through the use of geo thermometers it is estimated that the temperatures of formation can be on the order of 180ºC. At this site a slim hole was drilled to a depth of 500m where the temperature was registered at 85ºC maximum.

San Nicolás-El Volcán

This is an area of thermal manifestations of 65ºC- 70ºC temperatures located 70 km to the north of Loreto, BCS, and 9 km southeast of San Nicolás. On this site various hydrothermal activities have been observed, steaming ground and hot water discharges in the arroyo of San Nicolás. A little further south in the area known as Puerto Púlpito there have been manifestations of steam on the sand of the beach, the sea invading the area makes it difficult to measure actual temperature.

El Imposible-El Centavito

There is a hot water well located in the San Juan Valley, 30 km northeast of Loreto that averages 46ºC. From the chemical analyses of this well, we know that it is a sodium-chlorate composed and a temperature estimated to be between 181ºC and 262ºC estimated by geo-thermometers.

Agua Caliente-Comondú

In this area there is a hot spring (59ºC) located some 25 km to the north of Loreto in the El Caballo Arroyo and 3.5 km from Boca Bataques beach. This spring flows through a fracture parallel to the structural system of the zone, and owing to the presence of recent volcanic action there is an area of high geothermic interest, however, in a slim hole drilled by CFE it only

registered 97ºC at 500m depth. The temperatures estimated by geo-thermometers at this site are on the order of 176ºC.

Southern zone of the Peninsula

Buena Vista

In front of the Bahia de Las Palmas some 60 km NE from San José del Cabo BCS, there is the Hotel Buena Vista where they found a hot water well (58ºC) inside of the property some 200m from the beach. This hot well was abandoned because they were searching for fresh cold water well to be use at the Hotel.

Agua Caliente-La Paz

4 km to the west of the town of Agua Caliente, between the towns of Miraflores and Santiago, in municipal La Paz, there is a hot water spring (50ºC) with water bubbling up over the granite rocks.

Los Cabos

At the southern extreme of the Peninsula of Baja California, is one of the major tourist zones in Mexico, where an impressive development of hotels and the service infrastructure has been built in the last 10 years, increasing drastically the need for water and energy in the area. The operator of the municipal water system has a 200 lt/sec desalination plant fed by beach wells. At the beginning they drilled some wells registering temperatures of 35ºC to 72ºC (Lopez, et al, 2006) including an 84ºC well but they were not able to use that hot water in the reverse osmosis process.

Hot water technological Developments

IMPULSA project has implemented two programs in order to desalinate water. 1) In case of low temperature of geothermal resource (under 140ºC) we can desalinate sea water through a thermal process (LE-MED). 2) In case of hot water resources (>140ºC) it can be use to generate electricity with a PWG system and then that power feed a reverse osmosis plant to desalinate sea water.

LE-MED (Low Energy-Multi Effect Distillation)

The LE-MED system is an original IMPULSA design that comes from the technological mixture of a MED and a MSF thermal desalination plants. The operation basics of traditional MSF and MED plants started preheating sea water to its boiling point using steam usually extracted from a thermal power generator, then the preheated sea water is evaporated and the steam free of salts is condensate as fresh water. The remaining water leaves the plant as concentrated brine. The new IMPULSA LE-MED does not use steam in the process at all, instead geothermal hot water is use as an energy source to run the system. The main idea with this LE-MED system is to avoid the use of fossil fuels sources in the scheme of the desalination process. These would reduce significantly the desalinated cubic meter cost.

We consider this is one of the most relevant themes in the IMPULSA project. It is a rare case in the world that allows a big savings in energy yielding desalination into a sustainable concept. The price of desalinated cubic meter by this process taking advantage from the geothermal natural heat will depend strongly on the materials required and additional sources of energy for pumping and vacuum.

For the design of the LE-MED IMPULSA plant, several computer programs have been developed in order to assess mass and thermodynamics balance, heat exchange areas, pumping and vacuum power. At this stage IMPULSA project is studying various ways for future incorporation of the problems related with scaling. Later on it will comes the construction of a laboratory prototype to test the whole system.

The principle benefit of this proposal is to avoid the use of steam in the thermal desalination process and in its place, use renewable resources (hot geothermal water) abundant in the Baja California Peninsula. Thereby not using fuel to generate steam for desalination could save up to 30 to 40% of the desalinated cubic meter cost; this corresponds to the cost of the fuel to produce steam by traditional desalination methods (Figure 2).

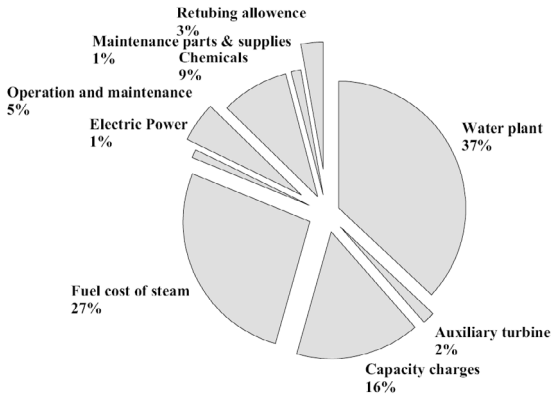

Figure 2 Integrated Cost of a Thermal Desalination Plant. (Semiat, 2000).

The continuous economic results of the project estimate that it can lower the cost up to 30% of cubic meter desalted with thermal technologies through the use of hot seawater as a source of energy for desalination.

Geothermal electricity generation, PWG. (Pressure Water Generation).

The following project proposes the use of the hot geothermal water located in abundance in the

Baja California Peninsula, as part of distributed generation for small plants that in many cases won't be connected to the grid. Under this plan the IMPULSA project of UNAM has developed exploratory surveys to locate, characterize and estimate the potential of hot sources in the Peninsula. The main idea of this project is to generate electricity with the PWG plant, the proposal is the generation of electrical energy by heat transference from a geothermal source into a working compressed liquid (water).

The binary geothermal generation technology that is installed in many parts of the world with organic fluids which are basically preheated and evaporated through heat exchangers (shell and tube system) is already well known. The main difference of the proposal with respect to a traditional binary cycle is the elimination of the heat exchange evaporator, proposing a flash system so that the fluid vaporization is done by the pressure lowering, thereby in order to pre heat the working fluid its is possible to use a heat plate exchanger that is easier to maintain and operate. Also the turbine proposed for the PWG is a high speed turbine with a reduced diameter but higher revolutions. This proposal meets these objectives, having the main goal of generating electricity in a more efficient, sustainable and economically competitive way.

The IMPULSA group has developed a new thermodynamic cycle for the efficient use of geothermal low enthalpy resources. On this design the secondary fluid is water at high pressure and a temperature. Fist the working pressurized fluid is pre heated in the heat plate exchanger, then it is flashed into a separation tank, the steam runs the high speed turbine. Finally the exhausted steam from the turbine is condensate and mixed with the hot water that did not flash in the tank, the mixture is pressurized and the cycle starts again.

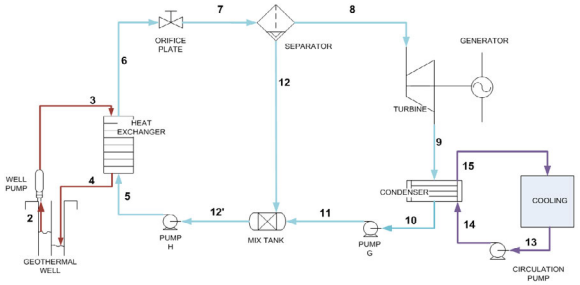

Figure 3 PWG cycle design, (IMPULSA).

The conventional systems of binary generation use great chambers of heat exchange to preheat the working liquids, which are generally organic fluids such as isopentane and isobutane and other heat exchangers to vaporize the fluid and activate the turbine, constants stops, are required for service and maintenance of the shell and tube heat exchangers.

The proposal consists of the installation of plate type heat exchanger that will improve the heat transfer, takes less space and are easy maintenance. The proposed cycle will be water-to-water (pressurized) generating steam by a pressure decrease. The IMPULSA turbine design will be small diameter (10 to 20 cm diameter) and high velocity (30,000 rpm) integrating the most advance turbine design.

The PWG system could generate energy at prices of 5 to 9 Aus ¢/kWh (4 to 6 US ¢) strongly depending of the installation equipment's cost, well drilling and operation and maintenance costs.

Case Study, La Joya, BC.

As a demonstration project, IMPULSA is planning to install two small scale prototype plants in La Joya, a recreational camp, south of the city of Ensenada, BC in order to take advantage of the geothermal resources (98ºC) that has been identified on this beach. Drilling a geothermal shallow (150 m) well near the coast it would produce enough thermal output (140ºC) to run a small power generator, then by use this electricity install and operated a reverse osmosis plant to desalinate sea water. Main target of this project is to assess geothermal reservoir's response at La Joya and at the same time, test and evaluate global performance of both plants for a period of on year. General features of this project are:

Power Generator (PWG)

A 7 kW binary plant will be installed at La Joya Camp, using a geothermal hot water from a well drilled at this resources to produce electricity by this way, a levelized power cost of 8 Aus ¢/kWh has been estimated, which even it is not cheap is lower than electricity tariff on that region 25¢ Aus/kWh (20 US¢/kWh).

Thermal Desalination (LE-MED)

In order to use the power produced on site, a 20 m^3/day desalination plant (LE-MED) is going to be installed at La Joya Camp.

Prototype LE-MED desalination plant has been designed and constructed by IMPULSA group and will be tested and gain some practical experience on scaling, heat rate, heat performance, etc.

Final Remarks

Intensive use of the cost line geothermal resources in Baja California is one of the big challenges for IMPULSA group in Mexico, helping to solve the power and fresh water scarcity on this region of the county. Since it is located in a very arid zone but with abundant natural resources like solar, wind and geothermic as well.

At the same time, an enthusiastic and promising engineering group has been consolidated at the National University; UNAM committed with the use of renewal energies meanwhile several research project of IMPULSA allow post graduated students to finish their Engineering degrees.

Desalination of sea water by using renewable energy is the main goal of the IMPULSA team that through scientific and technological research, the group is promoting the use of clean and environmental friendly energy sources, like the PWG and LE-MED prototype developments.

References

Alcocer, S. M. and Hiriart L. G. (2008). An Applied Research Program on Water Desalination with Renewable Energies. American Journal of Environmental Sciences. 4 (3): 190-197. 2008.

Alvarez, R. J. (1993). Reconocimiento geotérmico en el área de Ensenada, B.C. Comisión Federal de Electricidad. Residencia General de Cerro Prieto. Internal Report.

Arango-Galván, C., Flores-Márquez, E.L., Prol-Ledesma, R.M., (2007). “Geoelectrical image of Punta Banda (Baja California) using CSAMT and ERT data”. Proceedings 13th European Meeting of Environmental and Engineering Geophysics of the Near Surface Geoscience Division of EAGE (Istanbul, Turkey). 5 pp.

Lira, H. H. (1985). Reconocimiento y evaluación de focos termales en el estado de Baja California Sur. Comisión Federal de Electricidad. Gerencia de Proyectos Geotermoeléctricos. Depto. De Exploración. Internal Report.

López, S. A., Báncora A. C., Prol Ledesma R.M., Hiriart L.G. (2006). A new geothermal resource in Los Cabos, Baja California Sur, México. Proceedings 28th New Zealand Geothermal Workshop. 2006.

Semiat,R. (2000) “Desalination: Present and future”. IWRA, Water International, Volume 25, Number 1, March 2000.

Torrez, R. V. (2000). Geothermal Chart of México. Proceedings World Geothermal Congress 2000. Kyushu-tohoku, Japan.

Direct GeoExchange Cooling for the Australian Square Kilometer Array Pathfinder

Donald J. B. Payne[1,2*], Grant Hampson[3], Dezso Kiraly[3], and Evan Davis[3]
[1] School of Physics, University of Melbourne, Parkville, VIC, 3010.
[2] Direct Energy Pty. Ltd., 6 Alma Rd, St Kilda, VIC, 3182.
[3] Australia Telescope National Facility, CSIRO, Corner Vimiera & Pembroke Rd, Marsfield, 2122.
* Corresponding author: Donald.Payne@gmail.com; 0423 776 996

Direct Geoexhange Heat Pumps (DGHPs) provide chilling via refrigerant-carrying copper loops buried in the ground which act as a condenser and achieve higher efficiency than equivalent air source heat pumps because of the ground's constant heat capacity. DGHPs are particularly suited to desert environments with more extreme ambient temperatures. The Australian Square Kilometer Array Pathfinder (ASKAP) radio telescope will be an array of 36 x 12-m diameter parabolic dish antennae situated in the WA desert each requiring 5 – 7 kW_{th} cooling for computer equipment. A direct geoexchange system installed at the CSIRO facility in Marsfield, NSW provides chilling to prototype equipment via a 160 L water buffer. Preliminary results indicate a Coefficient of Performance (COP) 5 for chilling water to 15 C. We describe the results from this prototype in detail.

Keywords: Direct Geoexchange, Direct Use, Geothermal Heat Pump

Direct Geoexchange

The emerging geothermal industry in Australia is focused on producing electricity ("indirect use") and should begin delivering substantial results over the next decade. *Direct Use* geothermal energy is more efficiently available as it entails only one energy conversion (absorption or radiation of heat), rather than the several that occur in electricity generation and usage, with each step losing a percentage on conversion. Geothermal Heat Pumps (GHPs) are a direct use of geothermal energy which involve circulating a fluid (water, brine or refrigerant) through earth loops (poly pipe or copper) a few tens of metres deep (Fig. 1, Payne et al. 2008).

Direct Geoexchange Heat Pumps (DGHPs) which circulate refrigerant through copper loops have greater efficiency than water-loop GHPs because:

- copper is more thermally conductive than insulating plastic;
- latent heat transfers directly with the ground on evaporation or condensation; and
- an intermediate water-to-refrigerant heat exchanger between the ground loops and compressor is not required.

DGHPs transfer heat via 30-metre deep, 75-mm diameter bore holes compared with 100-metre deep, 150-mm diameter bores used for water-loop GHPs. A continuous, closed loop of copper piping is inserted and sealed with a thermally conductive grout (cement). Below 5 metres the Earth remains at a stable temperature all-year-round (16-17^{o} C at Marsfield, NSW). The smaller temperature difference between the heat source/sink and the building or water to be heated/cooled results in lower head pressure and energy requirement of the compressor compared to conventional heating and cooling systems. A "desuperheater" may be employed in chilling applications to further optimise the performance and produce hot water or air which can be used usefully elsewhere.

Figure 1: Copper earth loop, liquid & vapour manifold.

ASKAP

The Australian Square Kilometer Array Pathfinder (ASKAP) radio telescope will be an array of 36 x 12-m diameter parabolic dish antennae situated in Boolardy WA (Fig. 2) with construction due to commence in early 2010 and is a precursor to the Square Kilometer Array (SKA) of several thousand 12-m dishes. A prototype of the Electronics Systems (ES) and Phased Array Feed (PAF) package to be cooled has been installed at the CSIRO Australian Telescope National Facility (ATNF) headquarters in Marsfield, NSW. These two components should not exceed 20 - 30^{o} C under all operating and weather conditions and require an estimated heat dissipation of 5 – 7 kWth. Various cooling methods have been considered and the extreme desert temperatures and high price of diesel generated power strongly favour a DGHP solution. The results of testing of a DGHP are summarised in this paper.

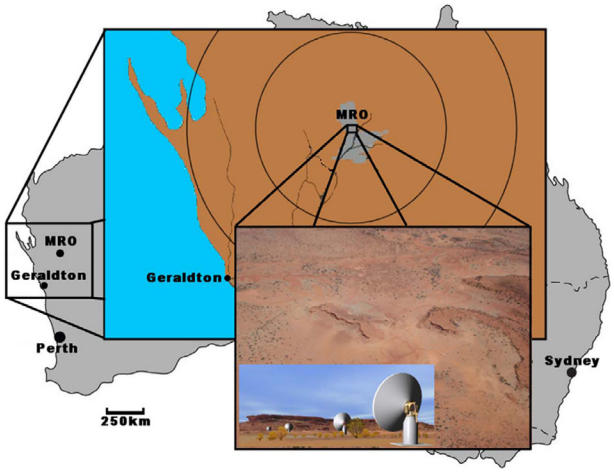

Figure 1: Location of ASKAP

System Design

Cooling is provided by a 10.5 kWth DGHP which circulates refrigerant (R407C) through 4 x 30-m copper earth loops to a refrigerant-to-water, braised-plate heat exchanger. Water is circulated through this heat exchanger into a 160 L buffer tank and is chilled to 7 – 15^{o} C (the "primary" circuit). Water is circulated from this buffer tank to the PAF & ES to deliver the required cooling to the heating load (the "secondary" circuit). The design of the secondary circuit is beyond the scope of this paper – here the performance as a function of thermal load is explored. A controller achieves the specified water temperature.

Earth Loop Installation

The 10.5 kW_{th} system requires 4 x 30-m copper earth loops (½-inch vapour and ¼-inch liquid) with PVC insulation on the upper 15-m of the liquid line to minimise heat transfer between the two and stop flashing of the liquid refrigerant. 75-mm diameter holes are drilled vertically 30-m deep in a square configuration with at least 3-m spacing between them to allow sufficient thermal diffusion through the ground. After insertion of the loops the holes are filled with a thermally conductive (geothermal) grout (e.g. 111-mix, Therm-Ex, IDP-357, Barotherm) ensuring that there are no air pockets. The liquid & vapour lines from the earth loops are braised to their respective manifolds (½-inch liquid & 7/8-inch vapour) using a 15% silver braising alloy. The lines are insulated with ½-inch non-corrosive insulation material (e.g. Armaflex, Insul-Lock) and run towards the heat pump (compressor) with a maximum length of 40-m. Figure 3 shows the drilling and site at Marsfield.

Buffer Tank, Heat Exchanger & Flow Rates

For chilling in the primary circuit, the braised-plate heat exchanger acts as an evaporator and it is crucial to have sufficient water flow over it to fully evaporate the refrigerant else performance will be compromised. The change in water temperature across the heat exchanger should not exceed 5 C and is ideally below 3 C. A minimum flow rate of 0.6 L/s (36 L/min) is required to achieve this. It has proven important to have large diameter (1.5-inch) water pipe between the evaporator and buffer tank. An alternative design has a refrigerant coil evaporator dwelling in the buffer tank and eliminates the need for a circulation pump – this will be investigated.

Heat Pump Design & Refrigeration

Figure 3: Installation of earth loops at CSIRO Marsfield.

The internal design of the heat pump refrigerant system is illustrated in Figure 4. The components are described in turn.

Compressor: A 3-phase Scroll compressor drives the heat pump with compression ratio of 4. Its efficiency is a function of the evaporating and condensing temperatures (pressures).

Active Charge Control (ACC): This:

- prevents liquid refrigerant from reaching the compressor by acting as a reservoir;
- evaporates refrigerant to keep the system properly charged and to eliminate superheat;
- improves volumetric efficiency, reduces power draw, and lets compressor run cooler;
- enables passage of oil entrained in refrigerant;
- indicates refrigerant level via 3 sight glasses.

Liquid Flow Control (LFC): This is an efficient Thermal Expansion Valve (TXV) which:

- Sets proper refrigerant flow rate based on condenser (upstream) operating conditions;
- Ensures zero sub-cooling so condenser is fully active;

- Reduces compressor discharge pressure and lowers power requirement;
- Prevents vapor from “blowing through”.

Oil Separator: Oil lubricates the compressor and the oil separator acts with the ACC to prevent oil from migrating down the earth loops.

Dryer: This filters and dries the refrigerant before it enters the LFC.

Reverse Cycle & Check Valve: This reverses the refrigerant flow between heating & cooling modes. For this specific cooling-only application this is redundant hardware and a specific GHP will be designed for the final application.

Refrigerant: R407C [HFC azeotrope: R32 (23%) + R125 (25%) + R134a (52%)]. Future work will explore other HFC and hydrocarbon refrigerants.

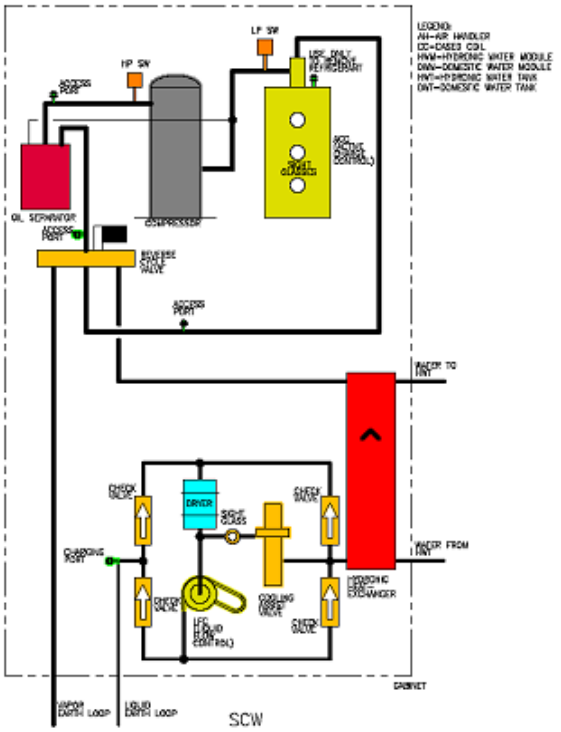

Figure 4: Internal components of DGHP.

Expected Performance

The Air-Conditioning, Heating and Refrigeration Institute (AHRI) has a well-established standard for DGHPs: ANSI/ARI Standard 870, 2001. Also, DGHPs are EnergyStar rated and endorsed by the Environmental Protection Authority (EPA). The DGHP manufacturer, EarthLinked, provides performance tables which are derived from both the Scroll compressor’s performance and field trials. For an earth temperature of 16^{o} C and chilling water to 15^{o} C, the expected Coefficient of Performance (COP = thermal energy removed/ electrical energy input) is 5.1. The theoretical maximum (Carnot cycle) performance for cooling is given by (Tcond –Tevap)/Tevap where Tcond is the condensing temperature and Tevap the evaporating temperature (Kelvin) and is 8.4 for Tcond = 37 ^{o} C and Tevap = 4 ^{o} C which correspond to the above conditions.

Methodology

To find the most efficient means of cooling, the COP is measured as a function of the controllable aspects of the system. The key controllable variables are:

Buffer Set Point ($T_{b\text{-}set}$): the temperature to which the buffer tank is controlled to be chilled – it is measured at the primary outlet of the buffer tank.

Buffer Maximum ($T_{b\text{-}max}$): the buffer tank temperature at which the controller switches on the chilling DGHP.

Cabinet Set Point ($T_{cabinet}$): the temperature to which the cabinet is cooled.

Secondary Load (P_{load}): the thermal power which is simulated with a set of heaters.

Tank Load (P_{tank}): the element of the tank can be turned on to act as a thermal load to the system.

Other input variables include:

Ambient Temperature: this includes both the wet (T_{wet}) and dry (T_{dry}) bulb temperatures.

Environmental Gain (P_{envt}): the tank & pipes are insulated but there is still environmental gain.
Tank Volume (V_{tank}): the buffer tank volume.

Water Volume (V_{water}): volume of water in the system: tank, primary & secondary pipes.

Output variables include:

Compressor Electrical Power (P_{comp}): the electrical power used by the compressor.

Cycle Time (t_{cycle}): the time between compressor start-ups.

Compressor Time (t_{comp}): the time the compressor is on during a cycle.

Duty Cycle (D): the percentage of time the compressor is on (t_{comp}/t_{cycle}).

Earth Loop Temperatures ($T_{5\text{–}30m}$): The temperatures measured at 5, 10, 15, 20, 25 & 30m.

Refrigerant liquid & vapour temperature (T_{liq}, T_{vap}): the temperatures to and from the earth loops

Suction, Head & Return Pressures (P_{head}, P_{suc}, P_{ret}): The pressures in & out of the compressor and returning from the earth loops.

Results

The default input values are: $T_{b\text{-}set}$ = 15^{o} C, $T_{b\text{-}max}$ = 17^{o} C, $T_{cabinet}$ = 23^{o} C, P_{load} = 5.2 kW_{th}, P_{tank} = 0,

V_{tank} = 160 L, V_{water} = 201 L. The ambient temperature varies between 10 and 35^{o} C during the test periods and future results will be calibrated against this. An estimate of the environmental gain was determined by cooling the buffer to 15^{o} C, leaving the system off and measuring the time taken (t_{envt}) for the temperature to increase a known amount (ΔT_{test}). $P_{envt} = C_{pw}.V_{water}.\rho_w.\Delta T_{test}/t_{envt}$ where C_{pw} = 4.2 kJ/(kg.K) is the specific heat of water, ρ_w = 1 kg/L is the density of water. It was found that for ΔT_{test} = 2 K, t_{envt} = 135 min giving P_{envt} = 208 W.

Figure 5 shows the temperature and pressure outputs for the above input conditions. From these results, the COP can be derived. We find t_{cycle} = 1645 sec, t_{comp} = 737.5 sec, giving D = 44.83%. There is a temperature overshoot of at least 0.75 K below $T_{b\text{-}set}$ and above $T_{b\text{-}max}$ giving ΔT = 3.5 K. The power required to reduce the system water temperature is $P_{water} = C_{pw}.V_{water}.\rho_w.\Delta T/t_{comp}$ = 4.01 kW_{th}.

The electricity consumed by the compressor is measured over a known number of cycles to give average power consumption. For this run, E = 210 MJ is consumed over n_{cycle} = 87.17 cycles (39.8 hr) giving an average power $P_{comp} = E/(t_{comp}.n_{cycle})$ = 3.268 kW_{elec}.

COP = $[P_{water} + (P_{load} + P_{envt})/D]/P_{comp}$ = 5.0. Note that D accounts for the fact that the load and environment are constantly delivering heat to the system which must be dissipated by the heat pump whilst on.

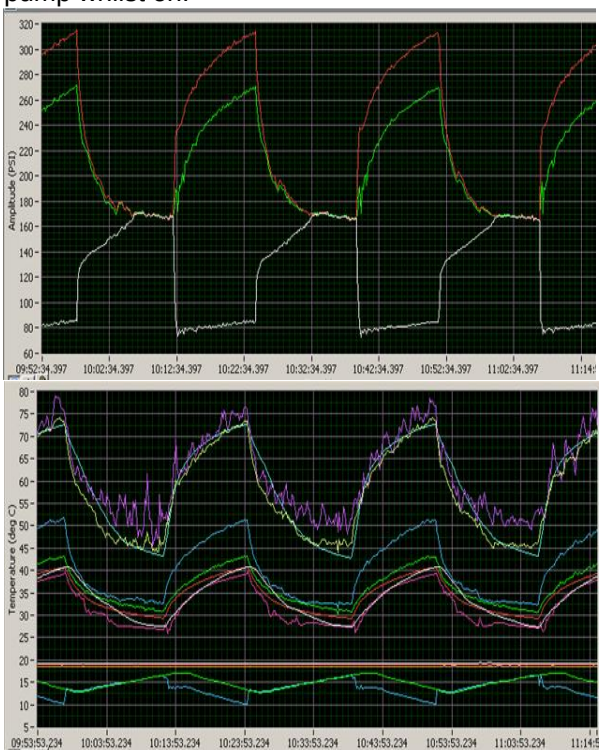

Figure 5: Temperature (top) and Pressure (bottom). From top to bottom, the lines are: T_{vap}, $T_{30\text{-}m}$, $T_{25\text{-}m}$, $T_{20\text{-}m}$, $T_{15\text{-}m}$, $T_{10\text{-}m}$, $T_{5\text{-}m}$, T_{liq}, spares, $T_{tank\text{-}out}$, $T_{tank\text{-}in}$. P_{head}, P_{ret}, P_{suc}.

Using this method, the COP is calculated as a function of load and DGHP configuration. Figure 6 shows a summary of average COP values as a function of secondary thermal load and Figure 7 displays COP as a function of the buffer water temperature.

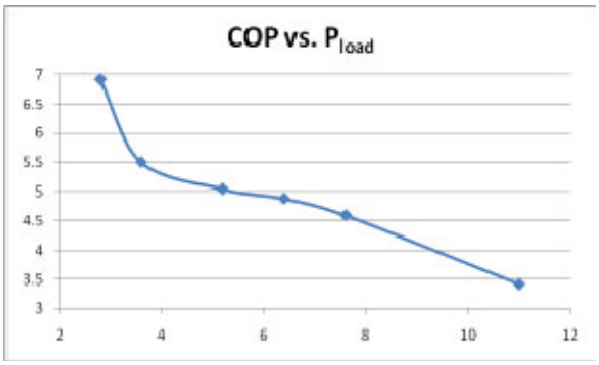

Figure 6: COP vs. P_{load}.

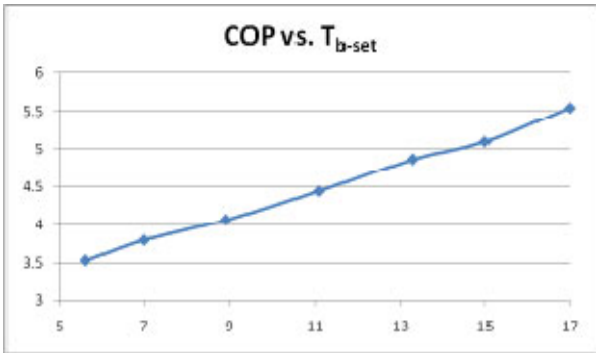

Figure 7: COP vs. $T_{b\text{-}set}$.

It is clear that the system should not be designed to run with a 100% duty cycle. An initial configuration of the system had the heat pump unit 30 m away from the earth loops. After moving the DGHP to within 4 m of the earth loops, the pressure drop across the earth loops was 5 – 15 PSI lower. Also, the manifold pit was initially exposed for testing and thus about 15 m of the copper earth loops was exposed to air and thus not efficiently dissipating heat. Backfilling the manifold pit boosted the performance.

Earth Loop Temperature

The ground temperature is measured every 5 m down one of the bore holes via thermocouples. As seen in Figure 5, after the compressor starts, the ground temperatures rise asymptotically towards saturation at which thermal output matches thermal dissipation in the ground. The no load condition is shown in Figure 8 along with the maximum load (11 kW_{th}) with saturated ground temperatures in Figure 9. In Figure 8 note that the manifold temperatures track the ambient temperature overnight as the pit was still open at the time this data was taken. From the no load graph it is clear that there are anomalous offsets in the ground temperatures. The precise

explanation for these is as-yet undetermined. It is suspected that the thermocouples used are unsuitable for use with the grout. In the absence of further details, the temperatures are calibrated by these offsets.

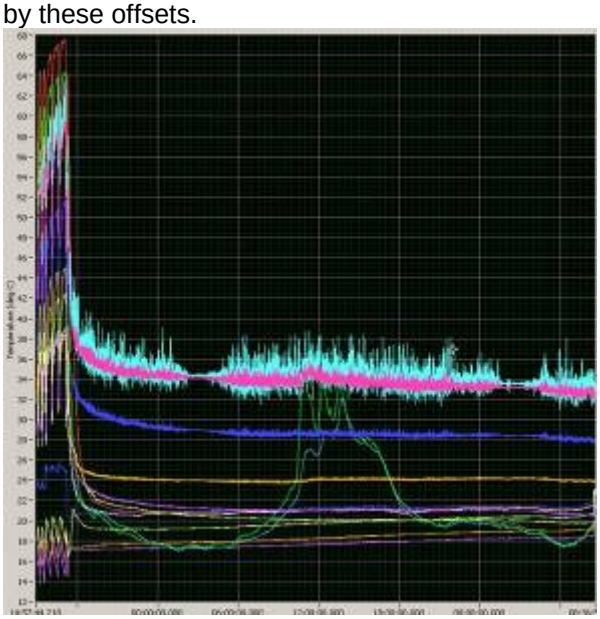

Figure 8: Temperatures for no load condition.

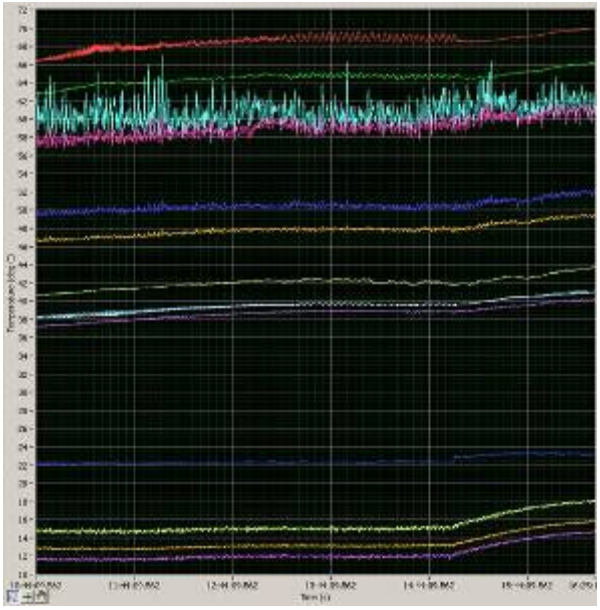

Figure 9: Temperatures for P_{load} = 11 kW_{th}.

Conclusions & Further Work

DGHPs are an efficient solution for heating and cooling and are particularly suitable for cooling in a desert environment with no power infrastructure. It has been shown that a DGHP achieves a COP exceeding 5 when chilling water to 15^{o} C in the primary circuit of a cooling system for a pedestal of the ASKAP – the prototype installation is at Marsfield NSW with a ground temperature of 16 - 17^{o} C. Furthermore, it has been demonstrated that COP decreases as a function of load in the secondary circuit (which determines the duty cycle) and buffer water temperature. Important factors which influence performance include the distance from earth loops to heat pump and the coverage of the manifolds.

Further results will be obtained for this configuration and additional experiments include:

- Use of a flooded evaporator within the buffer tank to eliminate the primary circulation pump.
- Use of a desuperheater between the compressor head and the earth loops.
- Use of alternative refrigerants.

These results are representative of expected behaviour in the field site at Boolardy, WA though slight variations will result from:

- An expected ground temperature of 20-21^{o} C at Boolardy.
- Different thermal conductivity of the ground.
- Different baseline thermal gain to the system.

Figure 10: Location of desuperheater, compressor & buffer tank.

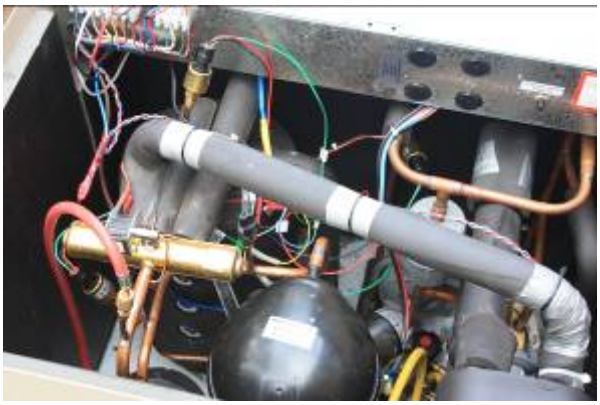

Figure 11: View inside heat pump unit.

References

Payne, D. J. B., Ward, M. And King, R. L., Position Paper: Direct Use Geothermal Applications, Australian Geothermal Energy Association (AGEA), Feb 2008.

Geothermal extraction from porous rocks - revisited

Michael Swift[1*], Johannes Muhlhaus [2].
[1] Applied GeothermEx Pty Ltd PO Box 3001, Norman Park, QLD, 4170
[2] Director, ESSCC The University of Queensland St Lucia, QLD 4072, Australia
* Corresponding author: geotherm1@bigpond.com

There are a growing number of studies of heat and temperature distribution in the crust that are indicative of pore fluid movement redistributing energy. In the subsurface there are incidental expressions of pore fluid flow: mineralization, hydrocarbon migration, tilted oil/water contacts, sediment compaction. There has been very little quantitative work undertaken to understand the larger heat and mass transfer systems in the shallow crust and subsequent exploitation strategies. Temperatures within these shallower geothermal reservoirs may be lower than the deeper more impermeable granite HDR reservoirs, but higher flow rates and higher sustainable fluid temperatures may yet prove a boon for geothermal energy exploitation. Although cooler they may offer higher flow rates and more sustainable fluid temperatures. Modelling studies are targeted to delineate natural geological features that will enhance pore fluid flow to overcome fluid extraction loses, diffusivity losses and injection cooling effects. There is a focus on developing an artificial geysering effect after drilling for enhanced production from porous reservoirs as a production model.

Keywords: Convection, porous rock, geothermal, geyser.

Balancing Heat Flow

Conservation of energy requirements mean that in any extraction system the total energy will fall unless there is some recharge mechanism. This geothermal extraction of heat reduces the local temperature. So how can heat flow be utilized to balance the heat flow anomalies and maintain high temperatures (if at all) ?

Geothermal anomalies are generally any phenomena which perturb the temperature or heat flow from the simply conductive explanation. In general any heat flow variation from the average of 87 milliW/m^2 or a shallow crust temperature gradient far from 25 °C/km is considered anomalous and this is generally ascribed an easy explanation; such as heat sources from intrusives, from radioactive decay and less frequently due to pore fluid movement. Generally, heat movement is a sum of three distinct process; conduction, advective-convective and radiation as part of the thermo-electromagnetic spectrum. Now in order of increasing amount, the approximate numbers are;

Q_{out} = 0.087 W/m^2 by body conduction

+/- 1400.0 W/m^2 by surface radiation

+200000.0 W/m^2 in body advection convection

Interestingly the earth's conductive heat flow is a very low, 87 milliW/m^2 outwards. This is largely fixed due to the surface of the earth's average temperature of about 20 degrees (above the black body radiation temperature of -25 degrees to the atmosphere and green house effects) and the effectively fixed temperature of about 5500 degrees at the core. Ultimately, the conduction level is defined by the temperature of the boundary (in Space there is nothing to conduct heat), in this case the surface of the earth. The temperature of the earth due to the sun is;

$$T_E=T_S \sqrt{((\sqrt{(1-\alpha)}R_S/2D)}$$

T_E is the Black Body temperature of the earth (250 °K) , T_S is the surface temperature of the Sun (5778 °K) D is the distance from the Sun 1.496 * 10^{11} m and α is the earths albedo 0.367 and R_S is the radius of the sun 6.96 * 10^8 m. Estimates are often based on the solar constant (total insolation power density) rather than the temperature, size, and distance of the sun. For example, using 0.4 for albedo, and an insolation of 1400 Wm^{-2}, one obtains an effective temperature of about 245 K. The point is that all the radiated heat is lost back to space, hence the +/- sign used above.

The conductive losses are converted into radiation losses, this conversion occurs in the top 30 cm of the crust where opacity starts to reduce to zero. The implication is that the heat flow out will always be about 0.087 W/m^2 in the short to medium term (geologically speaking) as the universal back ground temperature of -274 °C is still small relative to the earth's core temperature. This low conductive heat flow defines the minimum state for steady state geothermal extraction, unless of course is in part some redistribution due to advection-convection.

It can be seen that 'In body' advection-convection is the most efficient way to move heat, indeed all geothermal extraction methods are based on this. Referring to the mathematical development in Appendix 1 and looking at equation (1.1) it can be seen that for the advective-conductive term;

$$Q=\rho*c*V*T$$

So fluid velocity is very important in heat re-distribution because these can be quite low and still give rise to the instance where fluid flow is quicker than heat recharge / discharge via

conduction. Note that cooling as well as heating the country rock will occur by fluid flow.

Advection

Advection is generally used to describe fluid flow occurring in one direction, and generally implies an open system, and generally gravity head is the driving mechanism. It is a generalization and simplification of the convection models, which deal with circulating systems and have heat as the driving force. A good way to visualize the effect of fluid flow is the study the transient effects of drilling a well. Such as system is quasi circulation as mud is pumped, but considered advective here as it is an open system. The drilling of wells generally required the circulation of drilling mud to bring the rock cuttings to the surface. The circulating mud is generally surface ambient temperature at the top over well and as it is pumped down/up it warms, with a corresponding cooling of the country rock, see Figure 1 below. The main parameters are the temperature difference between the mud and the country rock and the time of exposure on the rock to the mud.

The country rock is cooled and after cessation of drilling, given time it will recover to the true pre-drill formation temperature. Example recovery curves are shown in Figure 2. The static drilling mud in the hole quickly equilibrates to the disturbed nearby country rock temperature. It then takes about 2 to 3 days for the mud/rock to recover. In this example there is a 60 litre/hour recharge in the well from an aquifer at 1205 feet. The Horner plot shows the theoretical steady state conductive recovery of about 14 days. Highlighting the efficiency of fluid flow to cool and heat.

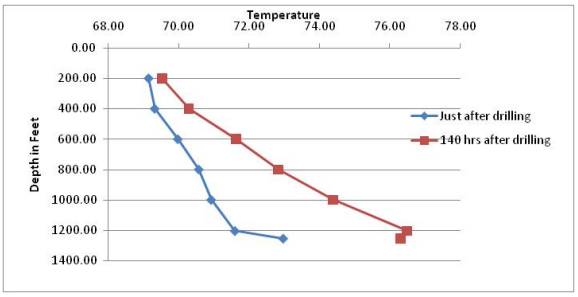

Figure 1 Schematic representation of temperature condition in bore hole immediately after drilling. Gretener 1981

Low Entropy Convection

There are many examples of natural pore fluid convection in the natural world. The first and most obvious are water wells or springs which are attached to aquifers and so refill with water. The recharge mechanism is local gravity drive from the water table or a confined aquifer. These waters may be hot if the aquifer has reached great depths. There are fewer examples of convective systems, some are discussed below.

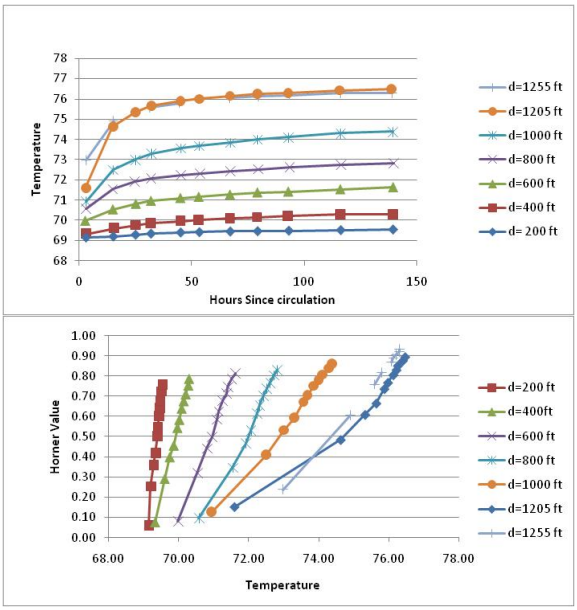

Figure 2 Restoration of thermal equilibrium and Horner plot. Gretener 1981

The surface heat flow of the Exmouth Plateau, offshore North West Australia has been mapped and the results are shown in Figure 3. The anomaly in this case is the heat flow low in the centre of the Plateau of 16 milliW/m^2. This anomaly has been explained by deep pore fluid convection in the sedimentary pile see Figure 4. This conclusion is supported by numerical modelling of the equations given in Appendix 1.

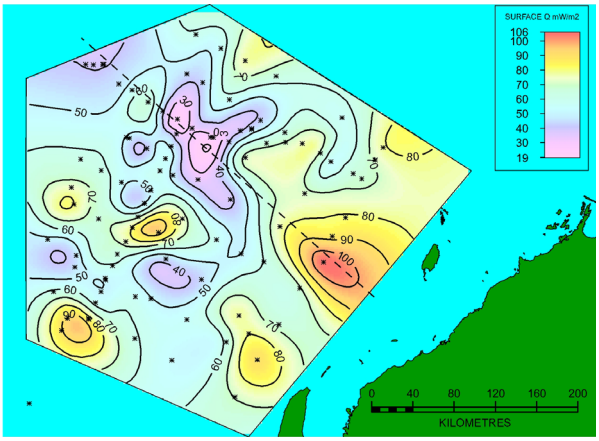

Figure 3 Surface Heat Flow map of Exmouth Plateau, (Swift 1991). Dash line is section in Figure 4.

The proposed driving mechanisms for pore fluid flow in this instance are horizontal temperature gradients. These gradients nearly always exist due to horizontal thermal conductivity contrasts, inherent in the basement/sediment architecture of basins. Importantly this implies convection within most sedimentary basins.

Modelling shows these systems to be self sustaining, that is, the horizontal gradient is actually greater than the conductive only component, thereby establishing steady state convection.

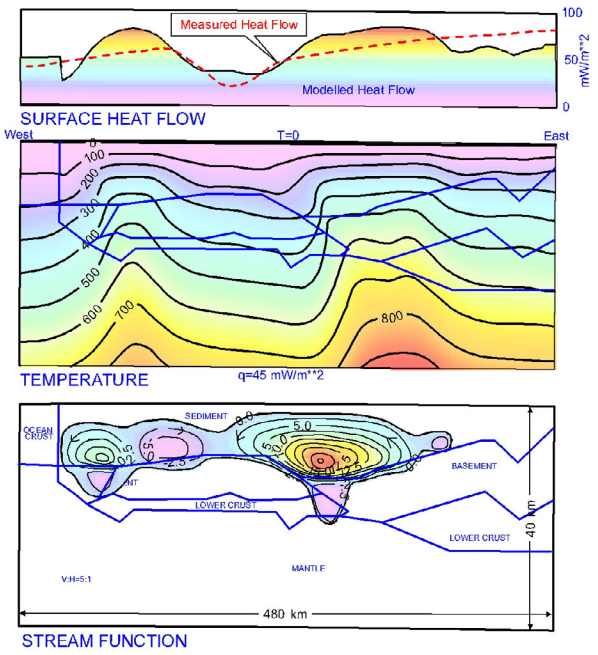

Figure 4 Subsurface temperature and fluid flow solution for Exmouth Plateau, Swift 1991

It is possible to characterize the convective system vigour with a modified Rayleigh Number *Ra ** (Hickox and Gartling, 1981) where;

$$Ra^* = g\alpha\rho ck(T_{hot} - T_{cold})W/\mu K$$

where in this case $(T_{hot} - T_{cold})$ is the lateral temperature difference over the width *W.* In this case there is no critical value that has to be exceeded for convection to occur. There will always be a driving force able to overcome resistive forces. It is under the conditions of this modified Rayleigh Number *Ra**, and not the classic Rayleigh Number *Ra (see high entropy discussion following)* that natural convection in the geological environment readily occurs.

Our modelling results in Figure 3 show there are elevated temperatures in the pore fluids, reaching about 300 degrees Celsius at 5.6 kilometres, approaching a gradient of 53 degrees per kilometre. Darcy velocities are derived from the stream function, which in turn can be used to calculate the pore fluid velocity, based on assumption regarding the porosity and permeability. In the example given Darcy velocity as high as 60,000 m/My or approximately 60 metres per year in a very low permeability environment (0.01 millli Darcy). There is an order of magnitude increase in velocity with order of increase in permeability. So in permeable sands, of the order of 50 milli Darcy velocities are up to 35 metres per hour! With pressure support and reasonable porosities, this is 3.5 tonne over a unit area.

This demonstrates that it is possible to have extensive and relatively vigorous subsurface pore fluid convection cells that are not detectable by surface heat flow measurements. This is due to the fact that if the cells are very deep, the perturbations in the temperature field may diffused out well before the heat flow passes through the top boundary, especially if these systems are local.

High Entropy Convection

The analytical solution for high entropy systems for the equations governing heat and mass transfer in a porous medium, given in Appendix 1, is based on the classic Rayleigh Number *(Ra)* analysis. Here only the vertical temperature gradient is considered. This is seen in the definition of the Rayleigh Number Ra as;

$$Ra = g\alpha\rho^2 ck\Delta TH/\mu K$$

where ΔT is the vertical temperature gradient over the height H (see Notation 1 for the definition of the other variables). Natural convection occurs when the *Ra* describing the system exceeds Ra_C for a homogenous medium $Ra_C = 4\pi^2$. In the geological environment the value of $k\Delta TH$ is more often than not too small for $Ra > Ra_C$ and so natural (forced) convection has historically not been considered as being a wide spread phenomena. As demonstrated above, there are convective systems possible where consideration is given to horizontal temperature gradients

Horowitz et al 2008 report values of Ra_C in the range 62 to 186 for the onshore Perth Basin. and imply manifested convection, although not modelled. It is suspected the Rayleigh criterion an inappropriate approach, however the variation in the mapped thermal gradient is consistent for pore fluid flow. The underlying inapplicability of applying classic convection theory to natural convection in the geological environment is that it fails to take any account of horizontal temperature gradients.

Hot water expulsion from geysers derives from a high entropy system where the Rayleigh criterion Ra_C does apply. In this instance the fluid flow is within fractures, a schematic is shown in Figure 5 below. The mechanisms of geysers are reasonable well understood, see Lu and Watson (2005) for the most recent review. The fundamental dynamics are; (a) dual water influx, hot and cold. into a reservoir, (b) a heating system to bring the water mix to the boil, (c) steam to be liberated, (the phase change alters the pressure environment to liberate more steam and more violent movement in the boiling water). The steam and entrained hot water move up to a lower pressure environment.

In terms of exploitation of geysers, a generalisation is that it takes about 1 tonne/hr of very hot water undergoing flashing to generate 1MW of energy.

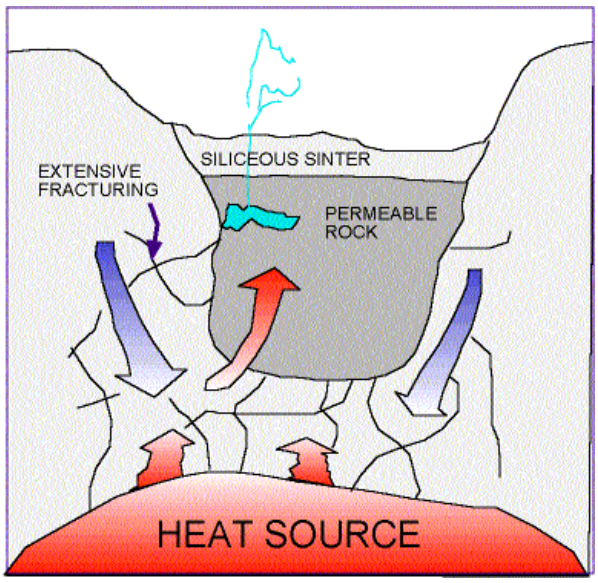

Figure 5 Schematic of geyser

Water has a specific heat of about 4200 J/kgK . or 1.16 w-hr/kgK or 1160 W-hr/tonne C so a turbine temperature drop of 250 to 90 degrees gives 0.162MW-hr for a water system. For a steam flash the heat content is higher at 2,100,000 j/kgK (500 times higher) or 81 MW-hr per tonne. This is easily achieved with an efficiency of say 2%.

How is it possible to get tonne/hr of hot water to generate 1MW in a porous system? The key requirement is the heating system. The essentials of the geyser system are seen to exist in deep pore fluid convective systems; hot enough to boil water, a recharge mechanism and fluid flow paths. Before drilling for these systems further numerical modelling is planned to first establish exploration criterion. There are questions on how to find these systems; by surface heat flow measurements or is structural configuration sufficient? There are questions on how to exploit these systems in such a manner that there are sustained high flow rates at sufficiently high temperature. There are engineering questions, notably on how to complete drilling in such a manner that "geysering" will occur from a single geothermal. It is planned that collaborative numerical modelling be undertaken at the Earth Systems Science Computational Centre of the University of Queensland to answer these questions.

Summary

In the geological environment there are low and high entropy convective systems within porous media. The planned research is to numerically model and understand pore fluid systems with a view to establish exploration criterion, drilling methodology and reservoir engineering of porous rocks for geothermal exploitation. Early results indicate that low entropy systems exist at depth, associated with and accentuating horizontal temperature gradients. The aim is the find and exploit more vigorous systems where recharge rates are very high. It should be reasonable to expect to discover pore fluid systems that will support long term geothermal exploitation.

References

Gretener, P.E., 1981, Geothermics: Using temperature in Hydrocarbon Exploration. AAPG Education Course Notes Series #17, 170pp.

Hickox, C.E. and Gartling, D.K., 1981. A numerical study of natural convection *in* a horizontal porous layer subjected to an end-to-end temperature difference. J. Heat Transfer, 103: 797-802.

Horowitz, F.G., Regenauer-Lieb, K.,Wellmann, J.F., Chua, H.T., Wang,X. and Poulet, T.2008 Evidence for Hydrothermal Convection in the Perth Basin, Australia, in: Gurgenci and Budd (editors),Proceedings of the Sir Mark Oliphant International Frontiers of Science and Technology Australian Geothermal Energy Conference, Geoscience Australia, Record 2008/18.

Xinli Lu and Arnold Watson, 2005, A Review of Progress in Understanding Geysers, Proceedings World Geothermal Congress 2005 Antalya, Turkey, 24-29 April 2005

Swift, M. G., 1991, Heat flow modelling: a generalized two-dimensional diffusive and convective numerical model for the Exmouth Plateau, offshore Northwest Australia, *Tectonophysics,* 194 (1991) 409-426. Elsevier Science Publishers B.V., Amsterdam

Appendix 1

Mathematical development

The system of two equations which govern pore fluid convection is:

Heat Transfer

$$(\rho c_p)^* \partial_t/T = \partial_x(K_x\partial_x T) + \partial_z(K_z\partial_z T) - \rho_f c_f \mu \partial_x T - \rho_f c_f \nu \partial_z T + S \quad \text{.....(1.1)}$$

Fluid Transfer

$$(1 + k_x/k_z)\,\partial_x^2\psi + (1 + k_z/k_x)\,\partial_z^2\psi - [\partial_x(k_z/\mu)\mu/k_z + \partial_x(\mu/k_z)k_z/\mu)]\,\partial_x\psi + - [\partial_z\,(k_x/\mu)\mu/k_x\partial_z(\mu/kx)k_z/\mu)]\,\partial_z\psi = (k_x + k_z)g/\mu\,\partial_x p \quad \text{.....(1.2)}$$

These need to be solved simultaneously, with the aid of the following definitions:

$$u = -\partial_z\psi = -(k_x/\mu)\,\partial_z P \quad \text{.....(1.3)}$$

$$v = \partial_x\psi = -(k_z/\mu)\,\partial_z P - (k_z pg/\mu) \quad \text{.....(1.4)}$$

$$\rho = \rho o\,[1 - \alpha(T - To)] \quad \text{.....(1.5)}$$

The governing equations are non-linear as the physical parameters can be temperature and pressure dependent, as well as being functions of position and direction (where such a distinction is appropriate). The solutions of these equations have no analytical expression, and so a solution can only be derived numerically.

NOTATION

Definition of variables *

Symbol	Description	Dimension
c	specific heat capacity	$Jkg^{-1}°K^{-1}$
g	gravitational acceleration vector	ms^{-2}
k	horizontal permeability	m^2
K	thermal conductivity	$Wm^{-1}°K^{-1}$
P	pressure	Pa
Q	heat flow	Wm^{-2}
Ra	Rayleigh number	
Ra *	Modified Rayleigh number	
S	internal heat production rate	W/m^2
t	time	s
T	temperature (Kelvin)	°K
	(Celsius)	°C
u	filtration velocity vector *(u, u)*	ms^{-1}
x	co-ordinate direction	m
z	ordinate direction	m
α	coefficient of thermal expansion of fluid	$°K^{-1}$
κ	thermal diffusivity	m^2s^-
Po	density of fluid at reference temperature	kgm^{-3}
p	density of fluid	kgm^{-3}
Ps	density of sediment	kgm^{-3}
μ	(dynamic) viscosity	Pa s
ψ	stream function	
∂	partial derviative	
φ	porosity	
(pc) *	sediment-fluid composite specific heat capacity	$Jkg^{-1}°K^{-1}$

* Subscripts: *f* = fluid, *s* = sediment, *z* = vertical direction,

Radiation associated with Hot Rock geothermal power

David L. Battye*, Peter J. Ashman
School of Chemical Engineering, University of Adelaide, SA 5005.
* Corresponding author: david.battye@adelaide.edu.au

Water in Hot Rock reservoirs is in contact with granites containing radioactive elements (radionuclides). The wider community is generally aware of this fact through publicity by the Australian geothermal industry. It is less clear to the public what radiation hazards may exist for Hot Rock projects, and how significant they may be. The aim of this study was to investigate likely radiation hazards associated with Hot Rock geothermal power, with a particular emphasis on radon emission. The study consisted of a review of literature and quantitative estimates of radon emission and dispersion from a typical Hot Rock reservoir. This information has been used to develop a fact sheet, published by Primary Industries and Resources South Australia (PIRSA, 2009).

Keywords: radiation, radon, radium, uranium, Hot Rock geothermal.

Dissolved radionuclides

The radionuclides of interest are those with long enough half-lives to travel to the surface from the reservoir, including isotopes of uranium, thorium, radium, and radon.

Uranium and thorium in granites are mostly found in monazite, zircon and allanite mineral phases. These phases are highly insoluble under most conditions, therefore the controlling mechanisms for radionuclide release are dissolution at the rock-water interface and alpha-recoil (ejection from the rock due to alpha-decay of the parent radionuclide).

Uranium solubility is a strong function of the oxidising or reducing nature of the geofluid. Uranium contents in granite groundwaters are frequently less than the recommended limit for drinking water (20 μg/L), but may exceed 800 μg/L in oxidising groundwaters (Gascoyne, 1989). Uranium does not emit gamma radiation, therefore it is only hazardous if ingested or inhaled.

The solubility of thorium is low since it tends to form the insoluble hydroxide. Thus, thorium concentrations in groundwaters rarely exceed 1 μg/L (Langmuir and Herman, 1980).

Radium is released from the rock by alpha-recoil, but is readily scavenged from solution by sorption onto mineral surfaces. Cations compete with radium for sorption sites, thus the solubility of radium increases strongly with total dissolved solids (TDS), as indicated by groundwater data shown in Figure 1. Where natural waters exist in Hot Rock reservoirs, they are typically quite high in dissolved solids, eg. TDS = 100 g/L at Soultz (MIT, 2006) and 21 g/L in the Cooper Basin (Wyborn et al, 2004). The TDS of water in an operational field will depend on the extent of dilution of natural water with injected water. At Fenton Hill, substantial dilution was achieved during open-loop operation (Grigsby et al, 1983). On switching to closed loop operation, the TDS reached a steady value of ~3 g/L. Thus, natural water in Hot Rocks may have radium activities at the upper end of the scale shown in Fig. 1, but the activity can be reduced to low levels by dilution of dissolved solids. To gain some perspective on what constitutes “low” levels, we note that groundwater sources for drinking water may contain radium at up to or exceeding 0.5 Bq/L (NHMRC, 2004), a level corresponding to TDS ≈ 5 g/L according to the trend in Figure 1.

Hot Rock reservoirs are at significantly higher temperatures than the groundwaters for which uranium, radium and thorium data exist. Solubility is typically enhanced by increasing temperature and higher concentrations of these radionuclides than cited above are therefore possible, depending on the other contributing factors. The Hot Rock geothermal literature reports measurements of radon in solution but not other radionuclides of interest. Such measurements in current and future projects would be of scientific value, and would directly address radiation concerns.

Deposition in surface equipment

The Hot Rock geothermal power concept involves circulation of water through an artificial reservoir and surface equipment in a closed loop. Cooling and depressurising of water in surface equipment may lead to solid deposits in the form of scales and sludges. There is potential for these deposits to be radioactive due to inclusion of precipitated radionuclides. This problem is encountered in the oil and gas industry, where highly saline produced waters with significant dissolved radium are handled. These waters tend to be saturated with barium and strontium sulphates, which precipitate as scales and sludges. Dissolved radium readily substitutes for barium and strontium in the solids, creating a radioactive waste material which must be periodically removed. Workers are exposed to gamma radiation, which is able to penetrate pipe and vessel walls. Additionally, inhalation of radioactive dust is an exposure hazard when removing the deposits. Hamlat (2001) provides estimates of radiation doses received by workers in the oil and gas industry which suggest that the

exposure is low - generally < 1 mSv per year - compared with the Australian occupational dose limit of 20 mSv per year (ARPANSA, 2002), provided that appropriate protective measures are taken. This level of exposure is less than the average background radiation dose in Australia of 1.5 mSv per year (ARPANSA, 2009).

The levels of dissolved solids, radium, and of strontium and barium sulphates are expected to be lower for Hot Rock waters than generally encountered in the oil and gas industry. Hence, lesser quantities of radioactive deposits are anticipated, with lower concentrations of precipitated radium. The gamma radiation hazard associated with solid deposits may therefore be small compared to that managed in the oil and gas industry. The data of Fisher (1995) in Fig. 1 is representative of waters produced from oil and gas fields, which frequently have TDS in excess of 100 g/L. Diluted water circulating in Hot Rocks is expected to have at least 10 times less TDS than this, and therefore 7 times less radium activity according to the trend in Fig. 1. The same reduction in radioactivity of the barium and strontium sulfate deposits can be expected. Considering that the occupational radiation exposure in the oil and gas is already relatively low, the exposure from Hot Rock geothermal power plants is therefore likely to be very small. However, the ALARA (As Low As Reasonably Achievable) principle of radiation protection will still apply, which calls for monitoring of exposure and protective measures. In particular, workers involved with removing solid deposits from equipment will need to avoid inhaling dusts.

Radon

Radon is an inert radioactive gas which is formed by the alpha-decay of radium. It is normally present at low levels in ambient air. The average radon level in Australian homes is 10.5 Bq/m3 (ARPANSA, 2009). The decay products of radon can lodge in the lungs if inhaled, exposing them to ionizing radiation and increasing the risk of lung cancer. The action limits for radon in air are 200 Bq/m3 in dwellings and 1000 Bq/m3 in workplaces (ARPANSA, 2002).

In a geothermal reservoir, radon enters solution predominantly by alpha-recoil and remains dissolved until its decay. The maximum radon content is achieved when the rates of solution and decay are equal This occurs if the residence time of water in the reservoir exceeds 25 days (222Rn has a half life of 3.8 days). Radon activity in water was a maximum of 500 Bq/L at Fenton Hill (Grigsby et al, 1983) and 200 Bq/L at Rosemanowes (Richards et al, 1992).

Radon emission and dispersion

Radon emissions will occur during open-loop circulation testing of newly created reservoirs, from uncontrolled flows of geothermal water, or from venting of light gases from steam condensers.

If the Hot Rock reservoir is assumed to consist of planar, parallel fractures with even spacing, the radon emanation rate, R (atoms/s) is given by:

$$R = \frac{2FV}{S}$$

where F is the radon flux from fracture surfaces (atoms s^{-1} m^{-2}), V the fractured rock volume (m^3) and S the fracture spacing (m).

The radon flux from plane surfaces of Carnmenellis granite cubes in water was measured at 30 atoms s^{-1} m^{-2} by Andrews et al. (1983). The granite had an average uranium content of 13.5 ppm, and we have assumed that a similar flux value is appropriate for Cooper Basin granites, which typically contain 16 ppm of uranium (Geoscience Australia, 2008).

Kruger (1995) inferred a mean fracture spacing of 50 m from circulation tests at the Rosemanowes site.

Steady-state emission of radon from a field can be estimated by assuming that the emission rate at the surface is equal to the emanation rate. Decay of radon in the reservoir is neglected. Assuming the above cited values for fracture spacing and flux in the Cooper Basin, this method yields an emission rate of 1.2 billion atoms (2520 Bq) per second, per cubic kilometer of fractured rock.

Radon is emitted from steam-venting stacks during circulation testing, therefore downwind radon levels are of interest. A simple Gaussian dispersion model was used to predict the maximum radon activity at ground level downwind of a single emission source with respect to effective emission height (physical vent height plus an allowance for plume rise), and wind speed. Results for a 1 km^3 reservoir are shown in Figure 2. Radon levels are generally negligible for emission heights of 10 m or more, except in calm conditions (wind speeds less than 1.8 km/h). In the latter case, levels are expected to be less than the action limit for dwellings.

During an uncontrolled flow of geothermal water from a well, the effective emission height is close to ground level, eg. 2-5 m. Figure 1 suggests that for a 1 cubic kilometre reservoir, downwind radon levels would be significant but not exceeding the workplace action limit except under calm conditions. However, it should be remembered that Figure 1 is based on a steady-state emission rate. If the water in the reservoir has been still for a period, its radon content will be higher than during circulation. Therefore the initial emission rate will initially be higher than the steady-state value. For example, if still water in the reservoir

attains a radon level of 500 Bq/L, then a sudden flow of 50 L/s will cause an initial emission rate of 25,000 Bq/s, a value 10 times the steady value assumed for Figure 1 and therefore increasing downwind radon activities by the same factor.

Calm conditions usually occur at night in central Australia and may last several hours. Estimates suggest that during calm periods radon emission may be a significant hazard for the area within 200 m downwind of an uncontrolled flow. However, the simple Gaussian dispersion model results become spurious as wind speed approaches zero, and more advanced dispersion models are required to more accurately predict radon levels in calm periods.

Acknowledgements

This work was commissioned by Primary Industries and Resources SA (PIRSA). We wish to thank Alexandra Long and Michael Malavazos of PIRSA for their guidance throughout the project.

References

Andrews, J.N, 1983, Dissolved radioelements and inert gases in geothermal investigations, Geothermics, v. 12, no. 2/3, p. 67-82.

ARPANSA, 2009, Background radiation fact sheet, http://www.arpansa.gov.au/pubs/baseline/bg_rad.pdf (retrieved June 2009).

ARPANSA, 2002, Radiation Protection Series No. 1, http://www.arpansa.gov.au/publications/Codes/rps.cfm (retrieved June 2009).

Fisher, R., 1995, Geologic, geochemical and geographic controls on NORM in produced water from Texas oil, gas and geothermal reservoirs, Final report, US Department of Energy Report DOE/MT/92011-12.

Gascoyne, M., 1989, High levels of uranium and radium in groundwaters at Canada's Underground Research Laboratory, Lac du Bonnet, Manitoba, Canada, Applied Geochemistry, v. 4, p. 577-591.

Geoscience Australia, OZCHEM database, http://www.ga.gov.au/gda/ (retrieved October 2008)

Grigsby, C.O., Tester, J.W, Trujillo, P.E., Counce, D.A., Abbot, J., Holley, C.E., and Blatz, L.A., 1983, Rock-water interactions in hot dry rock geothermal systems: Field investigations of in situ geochemical behavior, Journal of Volcanology and Geothermal Research, 15, p. 101-136.

Hamlat, M.S., Djeffal, S., Kadi, H., 2001, Assessment of radiation exposures from naturally occurring radioactive materials in the oil and gas industry, Applied Radiation and Isotopes, 55, p. 141–146.

Kruger, P., 1995. Heat extraction from HDR geothermal reservoirs. Proceedings of the World Geothermal Congress, 1995, Florence, Italy, Vol. 4, pp. 2517-2520.

Langmuir, D. and Herman, J.S., 1980, The mobility of thorium in natural waters at low temperatures, Geochimica et Cosmochimica Acta, 44, p. 1753-1766.

MIT, 2006, The Future of Geothermal Energy, http://geothermal.inel.gov (retrieved October 2008).

NHMRC, 2004, Australian Drinking Water Guidelines, http://www.nhmrc.gov.au/publications/synopses/eh19syn.htm (retrieved June 2009).

PIRSA, 2009, Fact Sheet: Radon and Naturally Occurring Radioactive Materials (NORM) associated with Hot Rock Geothermal Systems, http://www.pir.sa.gov.au/__data/assets/pdf_file/0013/113341/090107_web.pdf (retrieved September 2009).

Richards, H.G., Savage, D. and Andrews, J.N., 1992, Granite-water reactions in an experimental Hot Dry Rock geothermal reservoir, Rosemanowes test site, Cornwall, U.K., Applied Geochemistry, v. 7, p. 193-222.

Wyborn, D., de Graaf, L., Davidson, S., and Hann, S., 2004, Development of Australia's first hot fractured rock (HFR) underground heat exchanger, Cooper Basin, South Australia, PESA Eastern Australasian Basins Symposium II, Adelaide, p. 423-430.

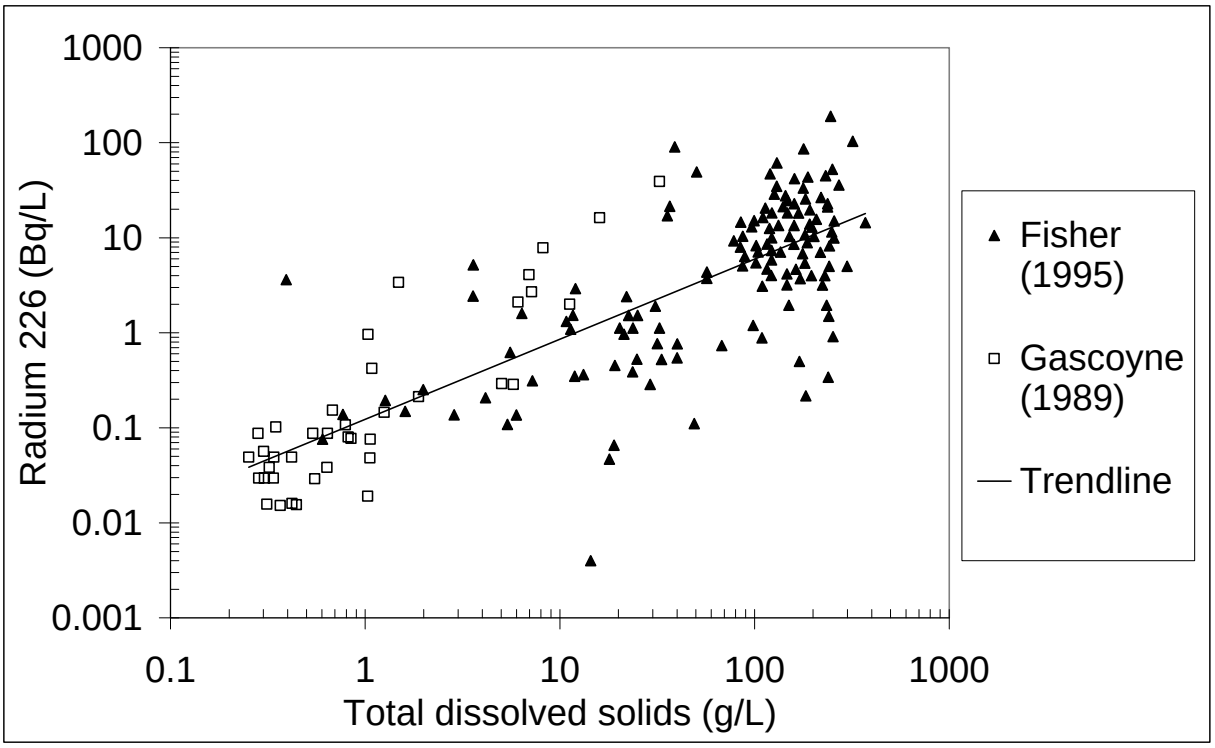

Figure 1: Radium-226 activity versus total dissolved solids in groundwaters. Fisher (1995): Oil, gas and geopressured-geothermal wells in Texas. Gascoyne (1989): Granite groundwaters, Whiteshell Research Area, Canada.

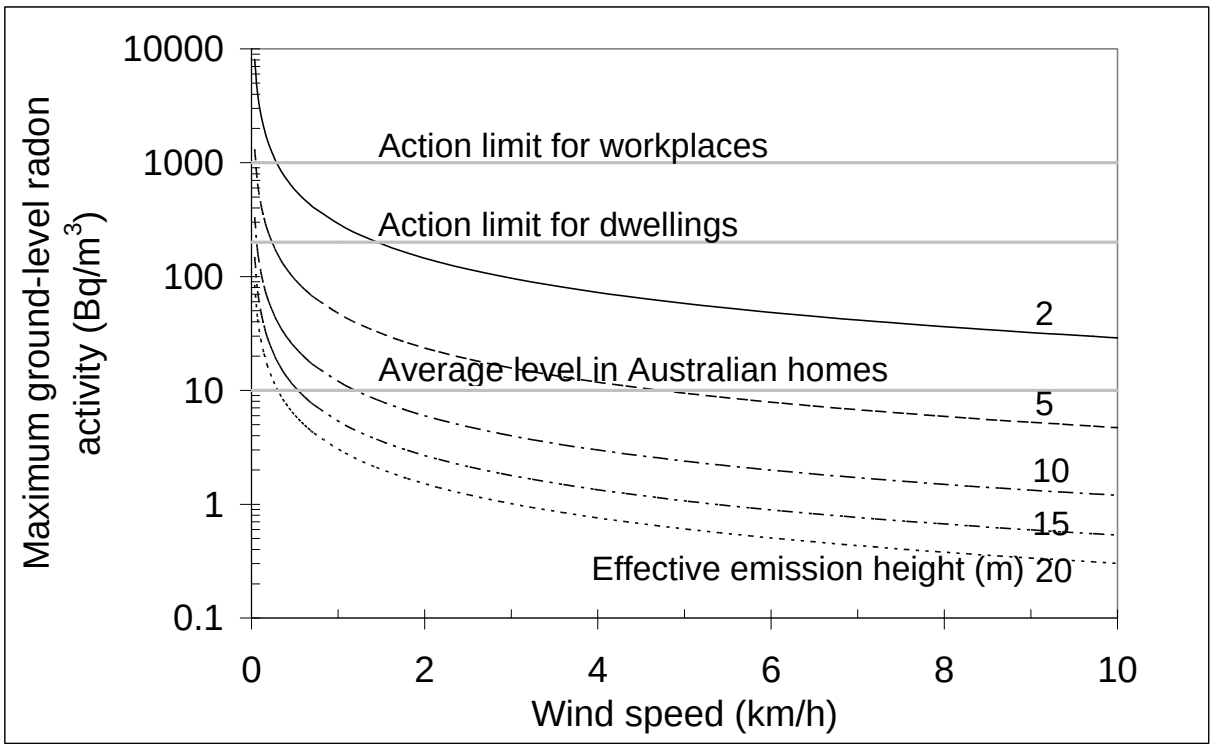

Figure 2: Maximum ground-level radon activity directly downwind of a single emission source, with respect to wind speed and effective emission height. Assumes an emission rate of 2520 Bq/s, based on steady-state emission from 1 km^3 of fractured rock, 50 m mean fracture spacing, 30 atoms s^{-1} m^{-2} radon flux from fractures, and neglecting decay of radon. To determine radon levels at another emission rate, E (Bq/s), multiply the radon level in the plot by E/2520.

Bringing large scale geothermal electricity to the National Grid

Tom R. Butler, Sharon Tissai-Krishna, *Anthony B. Morton
Senergy Econnect Australia
PO Box 16137, Collins St. West, Melbourne, Vic. 8007.
*Corresponding author: tony.morton@senergyworld.com

The Australian Greenhouse Accounts report that the Australian stationary energy sector is currently responsible for 50% of the country's total CO_2-e emissions. In order to mitigate this contribution to reach emissions reductions targets a significant portion of Australia's electricity generation is expected to be sourced by renewable energy sources in the near future. Although currently developed as a smaller contribution to electricity generation, recent developments in the area of Hot Rock Geothermal Energy have poised geothermal electricity generation for large scale developments. In Australia one of the major impediments faced by the development of large scale geothermal electricity generation is the ability to transfer large quantities of electrical energy from accessible geothermal resources to the 'local' electricity grid. This abstract outlines the potential issues of connecting large scale remote geothermal electricity generators to the 'local' electricity grid in the context of the National Electricity Market (NEM). These are discussed from the point of view of a hypothetical case study presenting large scale generation in the Cooper Basin on the border of South Australia and Queensland.

Keywords: Geothermal Electricity Generation, HVAC, HVDC, National Grid.

Issues to consider

In Australia the remote location of acceptable geothermal resources for large scale electricity generation, such as that found in the Cooper Basin, poses some significant issues for the delivery of electrical energy to the National Grid (Figure 1). Given that large scale generation requires large scale electricity transmission capacity to, and within, the National Grid, a connection to the closest possible point to a generator is rarely optimal. Such a connection must consider the following technical and regulatory aspects:

- The optimum connection point to the National Grid, considering the location and security of existing and proposed transmission network assets, and the impact of potential constraints on generating capacity (including interregional power transfer capacity);
- The preferred medium of energy transfer (HVAC or HVDC link);
- Potential transmission capacity sharing with adjacent proposed and existing generators;
- Voltage and frequency stability issues specific to large scale remote generation;
- Voltage levels and voltage drop over the distances involved;
- Network fault levels both at the point of connection to the NEM and generator; and
- State specific regulatory issues faced by a proposed generator connection.

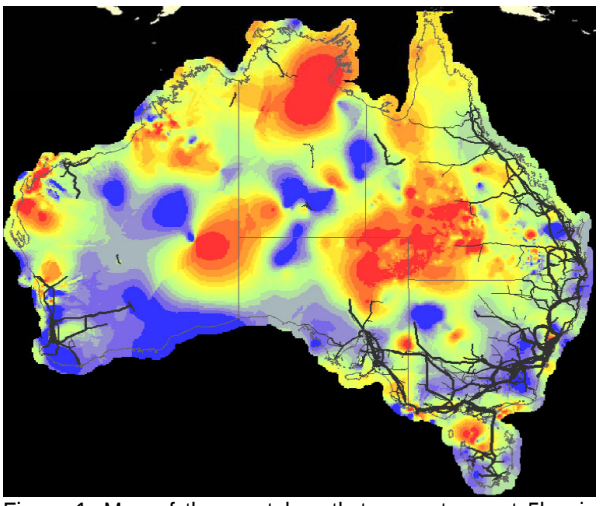

Figure 1: Map of the crustal earth temperatures at 5km in Australia. Red areas on the map indicate a temperature range of 194-319°C while grey lines show the National Grid. Courtesy of the Renewable Energy Atlas: www.environment.gov.au, 12/6/09.

Case study

A technical case study is presented here whereby a geothermal electricity generator with a capacity of 2-3GW is assumed to be installed in South Australia's (SA) remote Cooper Basin region. The proposed Cooper Basin Power (CBP) generator is located far from the National Grid and load centres, in order to draw out the technical issues involved with the various connection options. The following outlines the background information, issues and connection options for the hypothetical CBP project.

Proposed Generation

Given the vast distance between CBP and any potential points of connection (PoC), multiple large scale generation propositions have been identified in the 'vicinity' of CBP. In such scenarios, the potential exists for the connection of these generators to interact with the connection of the proposed generation or, alternatively, provide a benefit to both projects through a shared connection arrangement. Other generation projects to consider include:

Innamincka Geothermal Energy Project

The proposed 500MW Innamincka Geothermal Power Station site is situated within 100km of the CBP site. Geodynamics Ltd. is planning to build the project in three different stages with completion by the year 2013. Faced with similar difficulties to CBP, Geodynamics has identified three connection options for Innamincka:

Olympic Dam via a new 275kV circuit;

The 275kV network at Robertstown, north of Adelaide via a HVDC link; and

A connection to Braemar in NSW via a HVDC link.

Olympic Dam Geothermal Energy Project

Green Rock Energy has proposed a large geothermal generation project with staged development to a total capacity in excess of 400MW near the Olympic Dam mine in SA. The proposition includes the direct connection of the generator to the existing 275/132kV Olympic Dam West Terminal Station (TS) to supply the Olympic Dam mine.

Paralana Geothermal Energy Project

Petratherm are proposing a large scale geothermal generation project with a capacity in excess of up to 520MW located 370km to the east of the Olympic Dam mine in SA. Petratherm propose two separate connection options for their project:

A 275kV double circuit to connect directly into Davenport TS; or

Two single 275kV circuits: one direct to Davenport and another to Olympic Dam via Leigh Creek.

Silverton Wind Farm

Epuron has proposed to install a 1GW wind farm in the Silverton area approximately 25km north-west of Broken Hill. Stage 1 of the project (~400MW) received planning approval in June 2009 and is expected to connect directly into the 220kV network at Broken Hill TS. Once approved Stage 2 of the project (~600MW) will require an additional 220kV circuit from Broken Hill to Red Cliffs TS or Buronga TS.

Mildura Solar Concentrator

Solar Systems is developing a 154MW solar power plant in Mildura. The project has received Victorian and Federal Government grants with project completion proposed for 2013. However, recent events provided a great deal of uncertainty in Solar Systems progressing this project. Although unconfirmed, this project is expected to connect into the NSW 220kV network local to Buronga.

Other generators

In states adjacent to the proposed generation site, many other renewable generation projects have been proposed ranging in scale and technologies. Should any of these proposed projects be commissioned and connected to any CBP PoC identified here, the existing transmission network capacity will be reduced by the amount connected which may impose capacity constrains on CBP.

Technical Design Issues

A number of significant challenges are present in delivering the proposed power to the National Grid. Not only does the scale of CBP require significant power transfer capacity, but the distances involved to connect CBP to the grid bring a new set of challenges. Modern electricity transmission technologies provide two distinct design options for the connection.

HVAC

Transmission Network Service Providers are well versed in the installation, operation and management of HVAC electrical networks. One of the key advantages of HVAC is the ability to very easily integrate a new connection into the existing network with existing and available components and materials. An important disadvantage, however, is the significant cost of reactive plant required for voltage support when bulk power is transferred over long distances.

HVDC

For long distance transmission HVDC circuits have numerous advantages over HVAC:

HVDC conductors can carry 30-60% more power than a similar sized AC conductor, thus requiring smaller conductors and fewer circuits;

HVDC lines typically have lower losses over long distances;

Only two conductors are required thus needing smaller line easements;

Owing to the absence of reactance effects, DC lines have a much greater capacity to transfer active power over long distances without risking voltage instability; and

Particularly for the new voltage-source type of HVDC systems, there is little or no reactive power compensation required at AC/DC or DC/AC conversion stations.

HVDC experience in Australia

HVDC provides an efficient method of transmitting electricity over long distances with cables designed with carrying capacity up to 3GW. HVDC links are already commonly used in the NEM to provide interconnection between state transmission networks (**Error! Reference source not found.**).

Name	From/To	Voltage (kV)	DC Transmission Voltage	Installed Capacity	Transfer Capacity	Interconnector Length
		(From/To)	kV	MW	MW*	km
DirectLink	NSW/QLD	132/110	80	180	80/180	59
MurrayLink	VIC/SA	220/132	150	220	220/150	180
Basslink	VIC/TAS	500/220	400	600	480/600	290
* A/B, where A implies transfer capacity From/To and B implies transfer capacity To/From.						

Table 1: Summary table of HVDC interconnectors currently operating in the NEM.

Design of HVDC interconnectors varies widely depending on project specifications as they relate to specified transfer capacities and transmission distances.

A HVDC transmission link is usually composed of AC/DC and DC/AC converter stations, located at the sending and receiving ends with a DC transmission link connecting the two. As with traditional AC transmission, DC transmission links may be composed of overhead lines. However, as HVDC overcomes the reactive effects found in AC cabling, DC links can also be composed of overhead, underground or subsea cables.

It is for these reasons that proposed generation at a site such as CBP should fully investigate the use of HVDC should a PoC be favoured at a great distance from the site, in order to provide the greatest transfer capacity and network reliability.

Voltage Stability

HVAC power transfer capability is limited by voltage stability constraints rather than thermal constraints.

When heavily loaded, long transmission lines absorb a large amount of reactive power which causes voltage along the line to sag and may result in voltage collapse. Voltage stability can be maintained by absorbing reactive power when the line is lightly loaded and exporting reactive power when the line is heavily loaded. Hence, the maximum power transfer capability of HVAC lines can be increased with reactive support such as

- Shunt capacitors and/or reactors;
- Series capacitors and/or reactors;
- Static VAr systems (SVC, STATCOM, etc.); or
- Synchronous condensers.

HVDC transmission on the other hand is much less constrained by voltage stability limits and requires little or no additional reactive power compensation.

However, it is not just the transfer of power to the network where issues of voltage stability may arise. Given the proposed capacity it is expected that power will be transferred within the NEM over several hundred kilometres from the PoC before being completely used in load centres. Thus, in the case of CBP, the network surrounding the PoC would likely require the installation of significant reactive support.

Following consultation with network operators, detailed power system studies will need to be performed to determine the extent of this issue for any connection considered here.

Fault Levels

Network fault levels depend on many factors such as network configuration, length of lines and generator characteristics. In almost all cases, the addition of new generation increases network fault levels. Should the increased fault levels exceed that of the existing protection equipment design ratings, anywhere on the network, remedial action will be required in order to replace the equipment with that of an increased design rating.

Assuming that CBP will consist of multiple synchronous generators, the fault contribution will be approximately five times the installed generation capacity, totalling 15GVA. This could potentially have a significant impact on the selection of an appropriate PoC. However, in all cases the extent of this impact is limited by the amount of generation capacity able to connect to any PoC where the fault contribution is five times that capacity, not the maximum CBP capacity.

In all cases the full extent of fault level issues can only be determined through extensive power system studies and modelling.

Existing Infrastructure

Given the remote location of CBP, three immediately evident Points of Connection (PoC) 'local' to CBP have been identified in SA and New South Wales (NSW).

The three potential PoCs for CBP are the 275/132kV Olympic Dam West TS and the 132/33kV Leigh Creek Substation, which are 630km and 460km to the south west in SA respectively, along with the 220/22kV Broken Hill TS situated 555km to the south in NSW. These are shown in **Error! Reference source not found.** with (1), (2) and (3) respectively. However, although these connection points appear to be ideal none of them offer an immediately optimal solution as they are all limited in their transmission capacity. Considering the worst case summer conditions published by AEMO, in the case of (1) the combined 275kV and 132kV network to Olympic Dam along with the present mine load offer a maximum of 400MW of power transfer, the 132kV supply to (2) is limited to 20MW while (3) has the capacity for 420MW but this has effectively been allocated to Silverton Wind farm and is troubled with voltage stability issues.

Hence, the connection of 2-3GW of generation would ideally be to large load centres such as cities or large industrial loads. **Error! Reference source not found.** shows the nearest significant load centres as Melbourne, Adelaide, Brisbane,

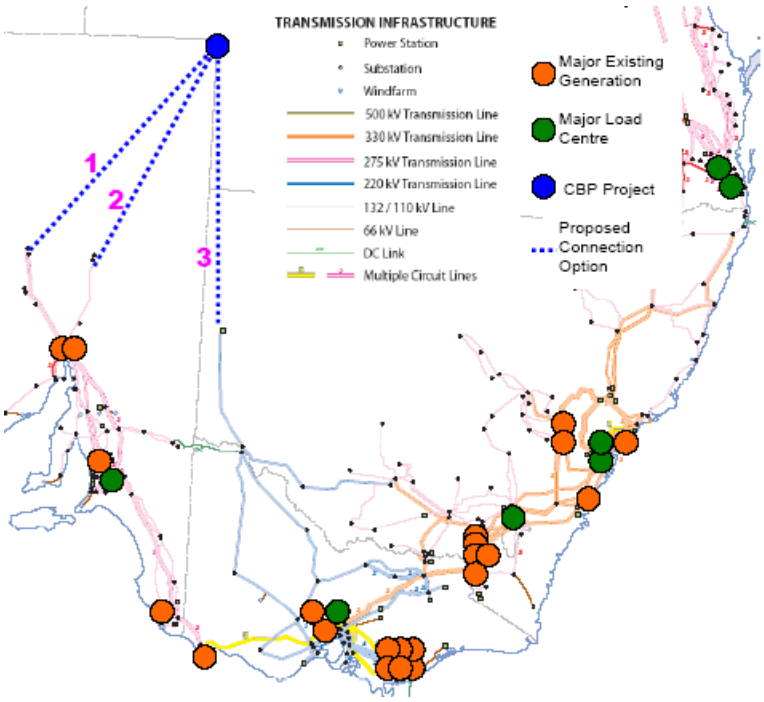

Figure 2: Map showing the major load centres and generators in the south of the NEM along with the location of the CBP project and the three immediately evident connection options. Background map courtesy of AEMO: www.aemo.com.au, 18/9/09.

Canberra, Sydney and the Hunter Valley all located a vast distance from CBP. We need to understand the network and available capacity in each state in order to understand the potential connection options adjacent to these load centres for CBP.

South Australia

The SA transmission system consists of a meshed network operating at 275kV and 132kV. The high capacity 275kV network transports power from the major generation plants in the Port Augusta region to Adelaide and further south, while the lower capacity 132kV network supplies smaller regional loads.

There are two major interconnections with the Victorian network; the Heywood connection in the south east corner of the state and the Murraylink connection in the Riverland region.

All transmission assets in SA are owned and operated by ElectraNet, with the exception of some 275kV network supplying Olympic Dam.

Victoria

The Victorian transmission system consists of a meshed 500kV, 330kV and 220kV system where the 500kV network transports bulk power from the major generation plants in the La Trobe Valley to Melbourne and then extends further west to Portland and the Heywood–SA interconnection. The 330kV network provides an interconnection with the Snowy region in NSW where major generation is placed. The 220kV network supplies Victoria's regional areas and the Murraylink SA interconnector. Further interconnection extends from the La Trobe Valley to Tasmania via Basslink.

The transmission network assets are owned by SP AusNet while VENCorp are responsible for transmission planning in Victoria. Connection to this network requires liaison with both utilities.

New South Wales

The NSW transmission network operates at 500kV, 330kV, 220kV and 132kV and is owned and managed by TransGrid. This network provides transmission capability between large scale generators, distributors and directly connected customers and includes interconnections with QLD and Victoria.

In NSW the 500kV and 330kV networks supply bulk power to regional load centres and provide interconnection to, and between, Victoria and QLD. As a result, any developments at this level have an effect on inter-regional power transfer capability. The 220kV and 132kV networks supply the regional areas around NSW.

Queensland

The 1,700km long QLD transmission network is mainly comprised of a 275kV radial transmission network from Cairns in the north to Mudgeeraba in the south, while the 110kV and 132kV meshed system also supplies regional QLD, while backing up the 275kV network. A small amount of 330kV network interconnects the major QLD generation to NSW through the QNI interconnector.

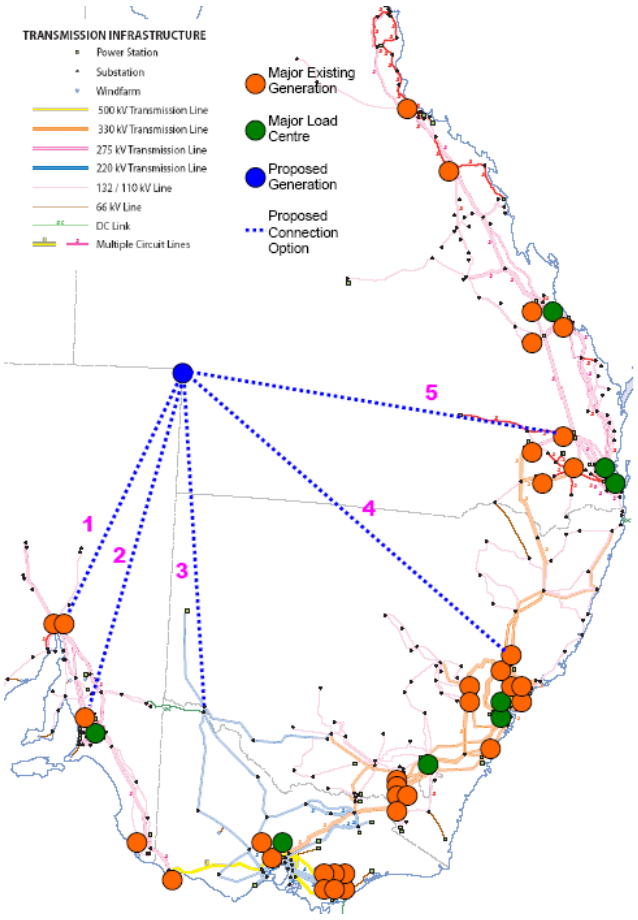

Figure 3: National Electricity Grid showing the major load centres and generators in the NEM along with the location of the proposed generation and the five potentially feasible connection options identified. Background map courtesy of AEMO: www.aemo.com.au, 18/9/09.

In QLD Powerlink owns, develops, operates and maintains the HV transmission network under appointment from the State Government as the transmission network planning body in QLD.

Connection Options

Following the initial assessment of the immediately evident PoCs, Leigh Creek and Broken Hill have been eliminated due to capacity constraints. Five alternative PoCs have been identified as shown in **Error! Reference source not found.**. All are discussed below.

1: Davenport 275kV Terminal Station

According to AEMO data, Davenport TS both supplies the Port Augusta region in SA and provides access to the National Grid for a significant amount of generation capacity located adjacent to it. Based on maximum demand in the region the available power transfer capacity at Davenport TS is in excess of 2.2GVA. However, existing generation in the area reduces this to 1,120MVA and could potentially reduce further to 720MVA should the Olympic Dam Geothermal Energy Project proceed to its full capacity.

From a high level analysis, connection to Davenport TS would require the construction of 655km of new transmission circuit from the proposed CBP site to Davenport TS and the possible expansion of Davenport TS to accommodate a step down substation or a DC/AC converter station.

A new transmission circuit for this connection could also upgrade the Leigh Creek supply, offering a cost saving to the CBP project. Furthermore, the proposed Innamincka and Paralana Power Stations would also be positioned adjacent to the new transmission line such that the connection cost could be shared to some extent. However, if both of these projects were also to proceed to their proposed capacity the available capacity for CBP would be reduced to zero without major augmentation of the SA transmission network.

In SA the potential exists for regulatory issues to arise owing to the limited capacity available to export from South Australia to the remainder of the NEM under low SA load conditions. Considering that the proposed CBP generation of 2-3GW is similar to the total SA 2009 minimum load these constraints become highly likely and are expected to have a significant impact on CBP.

Given an installed CBP capacity of 1,120MVA connecting to Davenport TS the fault contribution would be 5.6GVA. As there is already considerable generation in the Davenport region network design considers high fault levels and, based on this high level analysis, the only location where fault level mitigation works will be required is on the 132kV side of Playford TS.

2: Para 275kV Terminal Station

Para TS is a major hub in the SA transmission network supplying power to Adelaide. There are several 275kV circuits connecting to Para TS which interconnect the north-south power transfer capacity in SA, along with significant 132kV network. In all Para TS has a power transfer capacity of over 5GVA.

From a high level analysis, connection to Para TS would require the construction of 1,000km of new transmission circuit from the proposed CBP site to Para TS and the possible expansion of Para TS to accommodate a step down substation or a DC/AC converter station.

The connection of CBP to Para TS would again likely pass adjacent to the Innamincka and Paralana sites. However, in this case there is capacity at Para to accommodate all three projects and it may be possible to achieve some cost saving should the connection be shared.

As in the case of Davenport, it is highly likely that SA regulatory issues will constrain the generation capacity of CBP to some extent under low SA load conditions.

Considering the 275kV and 132kV network in the vicinity of Para TS it is apparent that almost all of the switchgear design ratings are able to manage the maximum proposed CBP fault level capacity of 15GVA. The only exception being Parafield West Gardens TS south of Para TS where mitigation works will be required.

3: Red Cliffs/Buronga 220kV Terminal Stations

Red Cliffs and Buronga TS both facilitate a major junction between the NSW, Victorian and SA transmission networks via the Murraylink and Victoria – NSW 220kV interconnectors. Collectively the total capacity available from the two stations combined is 1,260MVA which includes the 220MVA Murraylink DC interconnector. However, the planning approval given to Silverton wind farm implies that 800MVA of this will be offset by Silverton's generation entering and leaving the Red Cliffs / Buronga area.

Thus the total capacity available from the combined Red Cliffs and Buronga TS is limited to just 460MVA. A connection to this point in the National Grid would require approximately 900km of transmission circuit to accommodate the new generation, the reinforcement of the Victoria – NSW interconnector between Buronga and Red Cliffs and the probable expansion of both terminal stations. The potential also exists for a joint connection including Innamincka and the less probable Mildura Solar project but, given the limitations in network capacity imposed by Silverton, significant network augmentation would be required to accommodate either of these projects along with CBP.

Some network upgrades are proposed for the area including increasing the existing transmission network voltage from 220kV to 275kV up to Red Cliffs TS from NSW. While this upgrade would increase the capacity to the area it would only provide an additional 100MVA to a new total capacity of 560MVA.

Although small in comparison to the two previous connection options an additional 560MVA of generation at this point in the National Grid is expected to increase the network fault levels above switchgear design ratings at at least five Terminal Stations requiring significant fault level mitigation works.

4: Bayswater 330kV Terminal Station

Bayswater TS has a significant total power transfer capacity of 9.5GW and is interconnected with the 330kV NSW transmission network. The existing generation capacity connected to Bayswater TS is 2.6GW with a further 4.5GW in the areas surrounding Bayswater TS. Thus, the available capacity for the CBP project at Bayswater is around 2.4GW. However, the significance of this location in the National Grid requires detailed power system studies to determine the impact of connecting CBP to Bayswater TS.

From a high level analysis, connection to Bayswater TS would require the construction of 1,200km of new transmission circuit from the proposed CBP site to Bayswater TS and the possible expansion of Bayswater TS to accommodate a step down substation or a DC/AC converter station.

As the Bayswater TS is located in a very strong area of the National Grid, adjacent to significant existing generation, protection equipment is rated accordingly with high fault level design ratings. However, the addition of up to 12GVA of fault level from the CBP project is expected to exceed the fault level ratings of protection equipment in the central NSW and Sydney regions where mitigation works will be required.

5: Tarong 275kV Terminal Station

Tarong 275kV TS currently supports around 2GW of generation while being heavily interconnected within the QLD 275kV network and Tarong is instrumental in supplying Brisbane. Just south of Tarong TS, the QNI interconnector connects Queensland to NSW via Bulli Creek TS adjacent to Tarong TS. Given the level of interconnection at Tarong TS it has a total power transfer capability of 14.5GW. There is currently around 3GW of generation connected to Tarong TS and the adjacent 275kV network.

It is possible that the existing generation in the Tarong TS region may impose some constraints on the CBP project, however, given the capacity of the adjacent network this appears to be unlikely at this early stage. Hence, the available capacity is expected to accommodate the maximum of 3GW for the CBP project.

From a high level analysis, connection to Tarong TS would require the construction of 1,100km of new transmission circuit from the proposed CBP site to Tarong TS, and the possible expansion of Tarong TS to accommodate a step down substation or a DC/AC converter station.

Powerlink are currently planning for significant upgrade works on the QLD transmission system in order to accommodate rapidly increasing demand in the generation poor south east regions of the state. The proposed upgrades include the installation of some 500kV network and large scale generation capacity. Hence, it is expected that Powerlink would consider the connection of CBP to benefit their present network conditions.

Considering the existing fault level in the area the addition of the full CBP capacity at Tarong TS

would add a further 15GVA. At present much of the existing 275kV protection equipment at the terminal stations adjacent to Tarong TS is not rated for this increase. As such it is expected that this connection would require significant fault level mitigation works on the QLD 275kV transmission network.

Conclusions

Given the information presented it is evident that, while there are many options available for large scale geothermal generation to connect into the National Grid, few of these are considered to be optimal as existing transmission system design focusses around large load centres and existing large scale generation. Hence, all of the connection options considered here are expected to require significant network upgrades in order to accept the generation capacities considered in the CBP case study.

Based on the CBP case study it is evident that either northern South Australia or southern QLD present the greatest opportunity for the connection of large scale geothermal electricity, despite the significant transmission distances involved. HVDC transmission is expected to be able to assist here. Correspondingly, the availability of a shared connection over the distances considered would be expected to benefit all parties financially.

References

Australian Gov. Dept. of Climate Change, 2008, "Carbon Pollution Reduction Scheme White Paper: Summary"

The Australian Greenhouse Information System: Australia's Greenhouse Accounts www.climatechange.gov.au (10/8/2008)

Geodynamics Limited website: www.geodynamics.com.au (12/6/09)

Silverton Wind Farm website: www.silvertonwindfarm.com.au (12/6/09)

Green Rock Energy website: http://www.greenrock.com.au (12/6/09)

ABC, 03/11/2008, "Solar Future for Mildura": http://www.abc.net.au/local/stories/2008/11/03/2408915.htm

The Age, 26/02/2008, "Mildura power station to help cut emission levels":

http://www.theage.com.au/news/national/power-station-to-help-cut-emission-levels/2008/02/25/1203788246883.html

AEMO website:

http://www.nemweb.com.au/Reports/Current/Alt_Limits/ (13/6/09)

ElectraNet, 2008, "*Annual Planning Review 2008-2028*", www.electranet.com.au

TransGrid, 2004, "*2004 Data Book*", www.transgrid,.com.au

TransGrid, 2008, "Annual Planning Report",

www.transgrid.com.au

Powerlink, 2009, "*Planning a 500kV network to meet Growth in South East Queensland*", www.powerlink.com.au

Alternative Energy Carriers for Remote Geothermal Sources

Robert R. Dickinson[1,3]*, David Battye[2], Valerie Linton[1], Peter Ashman[2], and Graham (Gus) Nathan[1]
Schools of Mechanical Engineering[1] and Chemical Engineering[2], The University of Adelaide, and Hydricity SA[3]
The University of Adelaide, Australia, 5005
* Corresponding author: robert.dickinson@hydricity.com.au

Australia's geothermal industry will soon be ready to scale up its capacity from pilot-scale projects of one MW or less, to demonstration plants of several tens of MW. These scales are too small to justify construction of high-capacity long-distance electricity transmission lines connecting to the national grid. As illustrated in Figure 1, Australia's primary geothermal sources are much closer to the national Compressed Natural Gas (CNG) pipeline network than they are to the national electricity grid. This paper presents an assessment of the prospect of using large-scale electrolysis to convert the output of a geothermal demonstration plant to hydrogen and then to methane for direct injection into existing CNG transmission pipelines. The methanation step involves the consumption of carbon dioxide from CNG processing plants – a byproduct that would otherwise be vented to the atmosphere. A summary of energy flows is given towards the end of this paper, The key advantage of the use of hydrogen and methane as alternative energy carriers is that it would circumvent the dilemma: "What comes first -- commercially viable electricity transmission lines or a successful industrial scale demonstration plant?".

Keywords: geothermal source, electrolysis, hydrogen, methanation, CNG transmission pipelines

Outline of assessment

The assessment that we present here arose from the need to quantify and clarify the technical, engineering and economic feasibility of using an alternative energy carrier to transport energy from a geothermal source in northern South Australia (SA) to major energy consumers located in Olympic Dam and Adelaide. The outcome and conclusions from our assessment can be generalised to other regions.

For our quantitative assessment, we assumed that the net power from a geothermal demonstration plant would be 50 MWe. This provided the basis for estimating the scale of the electrolysis stack, the maximum rate of feedwater consumption, the hydrogen yield, and in turn, the maximum methane flow that would be injected into an existing CNG pipeline.

The following sections outline the main components of the system that we assessed: the water that is fed into the electrolysis system, the electrolysis system and its associated cooling system, and the methanation processing plant.

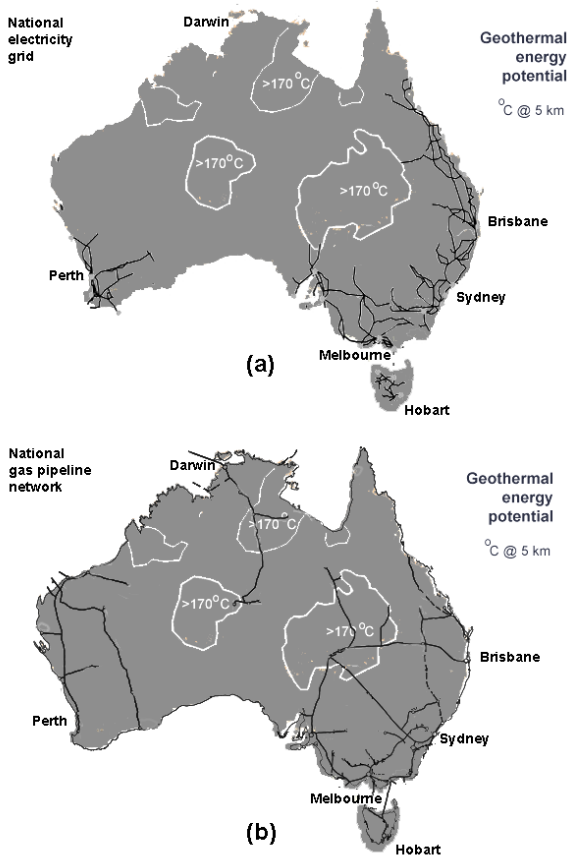

Figure 1: Australia's coastal electricity grid (a) is distant from primary geothermal sources, but overlaps with the national CNG transmission pipeline network (b). [Geothermal data adapted from AGEC (2009), electricity and gas networks adapted from ACCC (2008)]

Feedwater production

The feedwater for the electrolysis process is required to be purer than the groundwater that is typically available in central Australia. Figure 2 shows a proposed geofluid distillation plant that could be used to deliver a sufficient quantity of distilled water for input to the electrolysis process.

Electrolysis plant

The proposed electrolysis plant is based on an array of type 5040 electrolysers from StatOil Hydro's Hydrogen Technologies (previously Norsk Hydro)[1]. Each such unit yields an output of 0.135

1 We discarded the prospect of high temperature electrolysis ("HTE") because commercial systems are not yet available, and the marginal energy

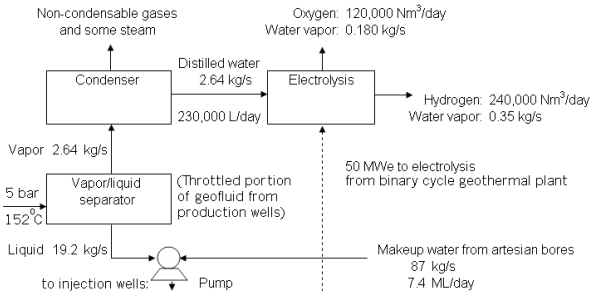

Figure 2: Proposed feedwater processing plant flow diagram

Nm^3/s (485 Nm^3/h) of hydrogen, and consumes 2330 kW, from a DC power supply of 5150 amps.

Waste heat from this electrolysis plant is removed by cooling water, in a water cycle that is completely separate from the feedwater production process. This cycle requires a means of reducing the temperature of the cooling water temperature by 10 °C. For this, we propose a refrigeration plant. We chose this after considering other more energy-efficient, options, including evaporative cooling (which would consume excessive groundwater) and underground pipe networks (which would have a high capital cost invested in an immovable infrastructure).

In theory, the methanation step shown in Figure 3 is optional. In practice it is likely to be the key to a successful alternative carrier implementation. We reached this conclusion based on consideration of the prospects for (1) direct use of hydrogen yield, (2) blending the hydrogen yield with CNG for transmission as HCNG and (3) methanation.

Prospects for direct use of hydrogen yield

In future, there may be opportunities for direct use of the hydrogen yield from an electrolysis plant such as the one proposed here. These may include domestic and export markets for 99.9% pure hydrogen. For example, McLellan (2009) presented an assessment of the prospect of large scale domestic consumption of hydrogen in the mining sector, but it is unlikely that such opportunities will arise within the proposed time frame for implementation of an alternative carrier scheme.

Prospects for transmission as HCNG

A quantitative assessment of the maximum hydrogen yield from the electrolysis plant relative to typical CNG flows, led us to consider direct injection of hydrogen for transmission as HCNG in a proportion of 5% H_2 to 95% CNG by volume.

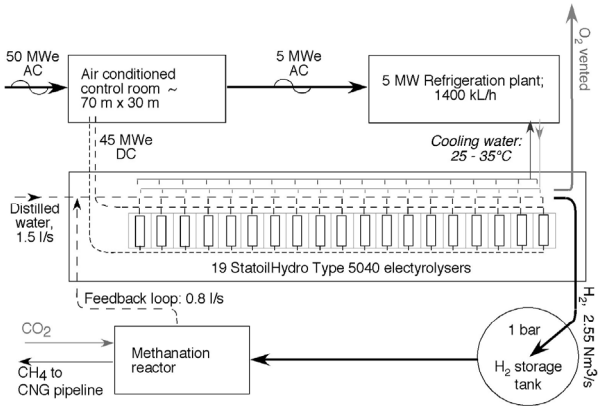

Figure 3: Proposed electrolysis plant layout

Our assessment of the effects of a blend of 5% hydrogen on the physical properties of HCNG fuel did not reveal any major limitations. Standards compliance would be near the limits of current gas pipeline content requirements, the risk to modern domestic appliances would be negligible, and the risk to gas engines would be small, while gas turbines would require a stable proportion of hydrogen. In contrast, our assessment of the effects of HCNG blends on the structural integrity of the existing CNG pipeline infrastructure led us to conclude that these could be significant limiting factors.

Hydrogen containment engineering is more stringent and challenging than CNG containment. The cost of new hydrogen pipelines of a given diameter are up to twice those of CNG pipes of the same diameter (Ball and Weitschel, 2009). Existing hydrogen pipelines in refineries and chemical plants to date have performed well (Zawierucha and Rana, 2005), but these pipelines are generally in small diameter, (Thompson and Bernstein, 1977), made from low strength steel, (Hayden, 2007) and operate at low pressures. Experience with such pipelines offers little guidance on the potential performance of high-pressure hydrogen transmission pipelines.

In contrast to containment of pure hydrogen, there presumably exists a theoretical proportion of hydrogen in an HCNG blend below which the marginal increase in engineering stringency is negligible. Our consideration of such issues as embrittlement, ductility, fracture toughness, fatigue life, fracture propagation, pressure (Haeseldonckx and D'haeseleer, 2007), and exposure duration, led to the conclusion that there would be a substantial risk that even a 5% blend might detrimentally affect the CNG pipeline steel in the long term. This risk would have to be taken into consideration when determining the operating, inspection and maintenance schedules for hydrogen-carrying pipelines.

conversion efficiency increase is very small for the low temperature range of 150-200 ºC at 5km that is typical of Australia's primary geothermal sources (Balta et al 2009).

Methanation

Methanation involves conversion of hydrogen and carbon oxides to methane. The two main reactions are:

$CO + 3H_2 <-> CH_4 + H_2O \quad \Delta H = -206$ kJ/mol (1)

$CO_2 + 4H_2 <-> CH_4 + 2H_2O \quad \Delta H = -165$ kJ/mol (2)

Both reactions are reversible and exothermic and both require a catalyst.

Reaction 1 (using carbon monoxide) is used on an industrial scale to produce synthetic gaseous fuel. A prominent example is the Great Plains Synfuels Plant in North Dakota, which converts lignite coal to methane at a rate of 1.5 billion Nm^3 per year.

Reaction 2 was discovered in the early 1900's by Paul Sabatier, and is often cited as the method for removing astronaut-exhaled CO_2 from space lab "air". It has not been developed on a large industrial scale to date, but researchers in Japan are working towards this end (Hashimoto et al 2009). The key advantage of using reaction 2 is that CO_2 is available in abundance at Moomba's gas processing facility, as a byproduct gas that is otherwise vented to the atmosphere.

Figure 4 shows a flow diagram for implementing reaction 2 in the context of the electrolysis plant.

Two or more methanation reactors in series would be required to ensure better than 90% conversion performance. Alternatively, the separation step at the bottom of the flow diagram could be used to reduce the delivered hydrogen proportion to a negligible amount.

Further work is required to confirm the ways and means by which suitably scalable methanation reactors can be built and applied for an electrolysis plant such as that outlined in Figure 3.

The output from a 45 MW electrolysis plant is estimated to yield an amount of methane equivalent to 2% by volume of the flow of natural gas from Moomba to Adelaide. This amount could lead to a net reduction of overall national greenhouse gas emissions, via displacement of natural gas from CO_2-emissions-intensive sources.

Summary of energy flows

The geothermal energy harvesting subsystem generates 70 MWe but loses 20 MWe in parasitic losses. Similarly, of the remaining 50 MWe the electrolysis plant loses 5 MWe in the cooling system. The remaining 45 MWe is converted to hydrogen and then to methane with a net efficiency of 56%. The methane yield (available for sale) is about 2.5 Nm^3/s, or 8.3 TJ/day if the plant is operated at full capacity.

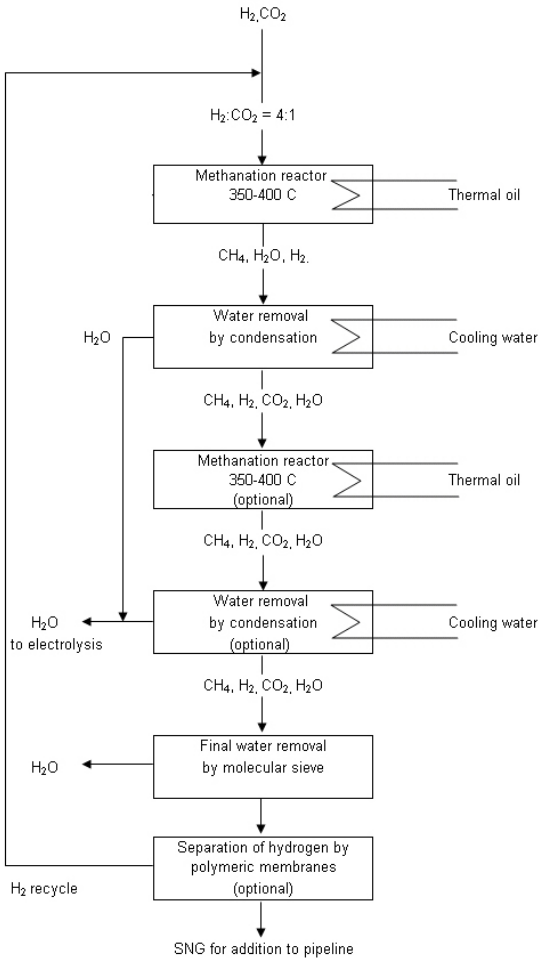

Figure 4: Proposed methanation flow diagram.

Relative cost assessment

The capital cost of the installed electrolysis and refrigeration plant and associated pipework is estimated to be of about 70 million dollars. This compares favourably with the hundreds of millions of dollars that would be required to construct a high-capacity long-distance electricity transmission line. For example, the cost of upgrading the SA – Victoria interconnector is expected to be about 400 million dollars, for a distance of about 300 km. This advantage is greatest if the geothermal plant is co-located with a CNG pipeline. The cost effectiveness of the electricity-to-methane process would have to be evaluated in detail on a case-by-case basis for each new demonstration geothermal plant, and would be influenced by the accessibility of CO_2 stocks as well as distance to electricity and pipeline networks.

By way of an example, the break-even electricity production cost (amortized capital cost compared to energy sales) for the 50 MWe electrolysis-based electricity consumer, is similar to the break-even production cost of a 400 MW geothermal plant sending electricity down a 400 MW 400 km electricity transmission line, despite the electricity

to methane energy losses and despite the difference in the value of electricity and methane per unit of energy. This is because such a transmission line would cost over three times the cost of the electrolysis plant.

Summary and conclusions

We reviewed the prospect of converting electrical energy from demonstration geothermal plants to hydrogen. We propose a system in which this energy would be shared in the ratio of 9:1 between an electrolysis plant and a refrigeration plant. An additional methanation step is required to avoid the risks posed by adding pure hydrogen to the existing CNG infrastructure. Apart from the the methanation reactor, all of these components are available as off-the-shelf items. Only the methanation reactor requires additional detailed design and further work to ensure the viability of this system. This system appears to offer a cost-effective circumvention of the geothermal business development dilemma: "What comes first -- commercially viable electricity transmission lines or a successful industrial scale demonstration plant?".

References

Australian Geothermal Energy Group (AGEG), Australian Geothermal Implementing Agreement Annual Report – 2008, 17 July 2009 http://www.pir.sa.gov.au/geothermal

Australian Competition and Consumer Commission, State of the Energy Market 2008, http://www.accc.gov.au/

Ball, M., and Wietschel, M., 2009, The future of hydrogen – opportunities and challenges, International Journal of Hydrogen Energy v. 34, Issue 2, p. 615 – 627.

Balta, M.T., Dincer, I., and Hepbasli, A., 2009, Thermodynamic assessment of geothermal energy use in hydrogen production, International Journal of Hydrogen Energy, v. 34 p. 2925-2939

Hayden,L.E., The ASME B31.12 Hydrogen Pipeline Code. Proceedings of the conference Transmission of CO2, H2 and Biogas: Exploring New Uses for Natural Gas Pipelines. Hilton Hotel, Amsterdam, 30-31 May, 2007.

Haeseldonckx, D. and D'haeseleer, W., 2007, The Use of the Natural-Gas Pipeline Infrastructure for Hydrogen Transport in a Changing Market Structure. International Journal of Hydrogen Energy v. 32 (2007) p1381 – 1386.

Hashimoto, K., Tako, Z., Kumagai, N., and Izumiya, K., 2009, Materials and Technology for Supply of Renewable Energy and Prevention of Global Warming, Journal of Physics: Conference Series 144 (2009) 012009, IOP Publishing

McLellan, B.C., 2009, Potential opportunities and impacts of a hydrogen economy for the Australian minerals industry, International Journal of Hydrogen Energy, v 34, issue 9, p 3571-3577

Thompson, A.W., and Berstein, I.M., 1977, Selection of Structural Materials for Hydrogen Pipelines and Storage Vessels. International Journal of Hydrogen Energy, v 2, p163-173.

Zawierucha, R., Xu, K. and Rana, M., 2005, Hydrogen Pipeline Steels. Proceedings of the MS&T'O5 Conference: Materials Science and technology.

What Contribution Can Geothermal Energy Make to Australia's Renewable Energy Target

Froome, C.W.
School of Chemical Engineering, The University of Queensland
Brisbane, Queensland, 4072, Australia
Phone: +61 7 3365 1574; Fax: +61 7 3365 4199; Email: c.froome@uq.edu.au

Geothermal energy provides the renewable energy sector with an opportunity to produce base load power, whilst meeting current government objectives in relation to greenhouse gas emission and renewable energy portfolio standards. Whilst the technology is not currently at an advanced stage of commercialisation when compared to other generation technologies utilising renewable sources such as wind or solar, the fact remains that it can provide continuous, rather than intermittent generation. Industry and renewable energy associations, together with government agencies are now including geothermal energy within their calculations of available generation capacity by 2020.

However, conflicting policy initiatives between State and Federal Governments, together with delays in proving commercial viability of the technology may see the sector miss out on many funding opportunities. This research looks at whether the current proposed Federal policies will provide the incentives needed to drive the deployment of geothermal energy within the 2020 timeframe or whether the current barriers will see deployment occur much later. This paper will also consider whether the delays may actually be advantageous given the conflicting policy objectives.

Finally the paper will consider the current development sites and whether policy could see deployment closer to the point of end use. Whilst the need to develop pilot plants is crucial, the need to develop sites closer to existing networks is also important given the costs associated with establishing grid connection, a cost that must be borne by the generator. This may see the need for additional State based policy measures to drive both additional development and deployment of those identified resources close to existing infrastructure.

For the purpose of illustration any examples will relate to the State of Queensland.

Keywords: Renewable Energy; Government Policy; Transmission

Renewable Energy in Australia

Australia's renewable energy sector is still in its infancy when compared to most other developed countries. For many European countries renewable energy started being deployed in the 1980's to combat energy security concerns. With Australia being resource rich, our renewable energy sector is being developed as a result of combating climate change concerns.

Current policy is aimed at the period to 2020 with the target being set at 45,000 GWh of renewable energy being generated annually at that time. In addition most electricity retailers are offering "green" electricity options, with that electricity sold not counting towards the portfolio standard, increasing the actual target above that required by the legislation.

Wind technology is at an advanced state of commercialisation and within Australia has been the most widely deployed large-scale renewable technology in the past decade. Most recent announcements on new renewable generation have also focused on this technology.

Whilst all renewable energy resources have benefited from REC income some renewable or clean energy technologies, such as solar and gas, have received additional financial subsidies at a State level. The deployment of wind has also occurred without the need for additional ongoing subsidies. The wind sector has also benefited from Australia's population being predominately located on the coast with this generally being the area of greatest wind potential. This has enabled the selection of wind farm sites close to existing grid infrastructure and due to the design of the electricity market they are able to ensure that all generation is dispatched.

Many State Governments are also providing additional incentives, in relation to the deployment of solar technologies through feed-in tariffs or equipment subsidies. Whilst most of the feed-in tariffs adopted are based on the net amount of electricity exported to the grid rather than gross generation, it has resulted in conjunction with equipment subsidies, a higher than expected uptake of the technology.

Geothermal energy can however provide base load generation capacity capable of replacing existing coal-fired plants, unlike their intermittent counterparts. The only other renewable technologies capable of this are hydro and biomass, however this supply has reached the upper end of possible deployment due to the lack of additional resources.

It must not be forgotten that geothermal is not a new energy source for power generation having been around for over a century, with the first

electricity generation plant constructed in Larderello, Italy in 1904 (Australian Institute of Energy, 2004). What is new is the technology surrounding how the available resource is to be exploited within this country. Whilst many of the current companies are looking at similar proposals, there is still a degree of differentiation.

The problems encountered by the geothermal sector are different to the other technologies noted above within Australia, due to the areas of greatest potential being located at great distance from the end point of energy use. However, as those sites where resources can be easily and economically exploited already taken, particularly in relation to wind, or where solar thermal becomes an economic option, development of sites further inland will become an option.

Government Policy

The Government has identified the policy measures that they believe will drive the deployment of renewable energy within Australia, being the Carbon Pollution Reduction Scheme (CPRS), a cap and trade system, together with the Renewable Energy Target (RET), being a portfolio standard.

In addition to these schemes, the various States are also introducing policy measures of their own, targeting resources where they have an economic advantage. These policy measures may actually benefit the geothermal industry with modelling undertaken to date showing that the increased deployment of wind and various small scale solar technologies will result in a surplus of REC's in the early years (particularly due to the multiplier effect to apply to small solar generation), as shown in Figure 1. The RET also includes electricity displacement options, such as solar hot water, as an accredited renewable energy generator.

Based upon the current position of technological development, large-scale deployment of geothermal is not anticipated until late in the next decade, which coincides with the shortfall in renewable generation. The industry will be in a position to meet this shortfall with an anticipated higher REC price than will be achieved in the earlier years.

If we consider PV deployment rates in Europe when their market was in a similar position of maturity, an annual growth rate of 10% is not considered unreasonable. Together with proposed wind farms would see a surplus in the REC market until 2017, based on no geothermal contribution.

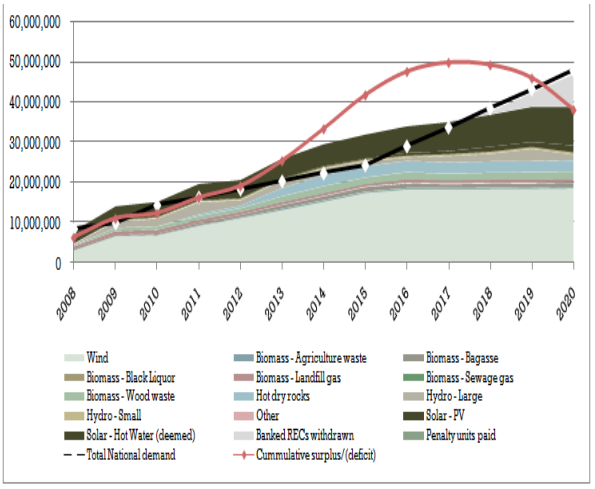

Figure 1 - National REC Supply v Demand (with banking) Source: (Herd, 2009)

In addition to the CPRS and RET discussed above, the Federal Government has also established the $50 million Geothermal Drilling Program as part of the $500 million Renewable Energy Fund. This program is merit based and is capped at $7 million per project, with the aim to provide funding to demonstration proof-of-concept projects in a number of locations. It was further stated that this program could make small-size plants possible, allowing for generation projects where sites close to current transmission infrastructure have been identified.

State Governments have also been active in their support for the geothermal sector, particularly in South Australia and Queensland.

Current Issues

There are two major issues currently facing the geothermal industry effecting their future contribution to Australia's renewable energy target. The first relates to the development of the technology to the point where it can be commercially deployed. Once the technology is proven, there will still be some delay before it can be deployed to the extent that it can make a contribution to base load generation. Until pilot plants are operational it is still hard to determine with any pinpoint accuracy this time frame.

Major investors in renewable, such as AGL (see www.agl.com.au) have also focused their attention on wind farms acquiring the rights to a number of sites still going through the planning stage. This will enable them meet their corporate renewable targets based upon existing technology with a known cost base.

The second (and more costly) issue is the construction of transmission networks, a cost which must be borne by the generation company. With existing coal and gas-fired plant, the actual generation plant relies upon the fuel being delivered to it, with on-site storage generally available. Geothermal, like most renewable

technologies requires that the generation plant be located at the site of the resource.

Similarly looking at the coal or gas sector, the majority of generation plant is based upon similar or the same technological design. The same may be true for the above-ground geothermal plant, however there are currently a number of proposed options as to how the underground resource can be best utilised.

Geodynamics (Grove-White, 2009) have already identified that the cost of transmission will be a major problem and that it may be better to bring the customers to the source of the generation, rather than vice-versa. Whilst this will allow for the generation to be scaled up on-site whilst delaying transmission infrastructure costs and assist in the meeting of the Federal portfolio standard, it will not reduce base load generation required from existing coal and gas-fired plant, supplying the major coastal population base, unless those customers are relocating from an existing site rather than establishing additional facilities.

The alternative to the construction of new transmission infrastructure is to locate geothermal power plants closer to existing infrastructure.

The issue of transmission and plant location will be discussed later in this paper.

Industry Outlook

A report by MMA (2008) on the capacity expectations of the industry by 2020 recognised that the technology deployed needed to be viable, with this being defined as being cost competitive with other renewable technologies, including a margin deemed sufficient by providers of capital.

A REC market that will be in surplus will result in a REC price that will be much lower than that currently anticipated. This may work to the ultimate advantage of the geothermal sector.

Figure 2 indicates that the installed geothermal capacity will start to increase significantly from 2015, however due to technical problems with some pilot plants; it is considered that this will be delayed by two to three years, which may provide opportunities for the sector.

The MMA report (2008) also identified that a substantial amount of the RET must still be available when geothermal projects are at the stage of being ready for deployment. Much of the current State and Federal policy has been aimed at the deployment of existing commercially viable technologies, such as solar PV and hot water systems, through the Federal Solar Bonus Scheme and various State schemes, focusing on hot water rebates and fees-in tariffs. As noted above, modelling set out in Figure 1 indicates that that this will create a surplus of REC's and dependent on the uptake of the technology, may result in this surplus remaining until 2017. The data presented allows for no geothermal energy being exported to the grid, but does show the shortfall of REC's that the geothermal sector can take advantage of.

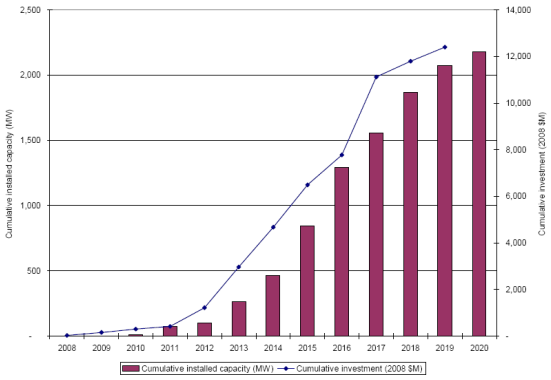

Figure 2 - Cumulative installed capacity and investment
Source: (McLennan Magasanik Associates, 2008)

Many electricity retailers also anticipate that wind generation will pick-up the shortfall, with an additional 29 wind farm projects currently under consideration, however, many of these may find that the wind availability in some of these areas under investigation is not economically viable particularly given that the majority are located in South Australia and Victoria where there is already a high presence of this technology.

Research has previously indicated (Froome, 2009) that existing and proposed Federal policy measures will not be sufficient by themselves to drive renewable energy deployment to the targets proposed. With retailers also offering 'green energy' programs, the actual shortfall will be much greater than indicated. Like the solar examples provided, additional State measures will be required, based upon the individual needs of the State in meeting their own economic and social policy objectives.

Looking specifically at Queensland the policy decisions being faced may be whether to provide support through a feed-in tariff to those generators located close to existing infrastructure or subsidise new infrastructure to those areas where the resource is more plentiful.

Transmission

The Queensland Government has already released 29 sites for tender as shown in Figure 3, with only one site west of Gladstone having already been awarded. There are currently a further 26 tenders under consideration by the Department of Mines and Energy. Whilst many of these sites are considerably smaller than the major sites being developed in South Australia, having existing transmission and distribution infrastructure in close vicinity, together with forecast demand growth for many of the regions surrounding these sites, the economic return

required or investment hurdle point will be much lower.

The information shown in Table 1 indicates the increased interest in geothermal energy, both through the number of tenders lodged compared with land releases and the number of companies ultimately gaining preferred tender status. There still remain two land releases (one from each of rounds one and two) that no tenders were received for.

However this will also result in competition for the limited amount of private funding available to progress the proposed projects.

	Rnd 1	Rnd 2	Rnd 3
Tender Closing Date	**3/06**	**4/07**	**2/08**
Land Released (No.)	6	10	35
Tenders Received (No.)	6	11	13
Preferred Tenders (No.)	5	9	13
No. Of Tendering Company's	2	3	6

Table 1 - Queensland Geothermal Tenders
Source: (Office Of Clean Energy, 2009a)

It is also interesting to note that the land released in round three is located furthest from the coast and will therefore incur greater capital requirements when considering transmission infrastructure costs, but all land releases progressed to the preferred tender stage.

Also looking at this from a Queensland perspective, locations that have been identified as suitable for new solar thermal or wind generation are also located near identified geothermal resources. This will provide a number of shared infrastructure opportunities.

If we consider where the Queensland Office of Clean Energy believes that our renewable resources may come from by 2020, as shown in Figure 4, there will be significant investment in both of the above technologies.

An interesting observation is the extent of the deployment of solar hot water (being a current Queensland Government priority) which is electricity displacement rather than generation, which adds weight to earlier conclusions in relation to the surplus of REC's in the early RET program.

Geothermal, solar thermal and wind are expected to add approximately 2,000 MW of generating capacity, with the majority of generation plant to be located in areas currently not connected to the transmission grid.

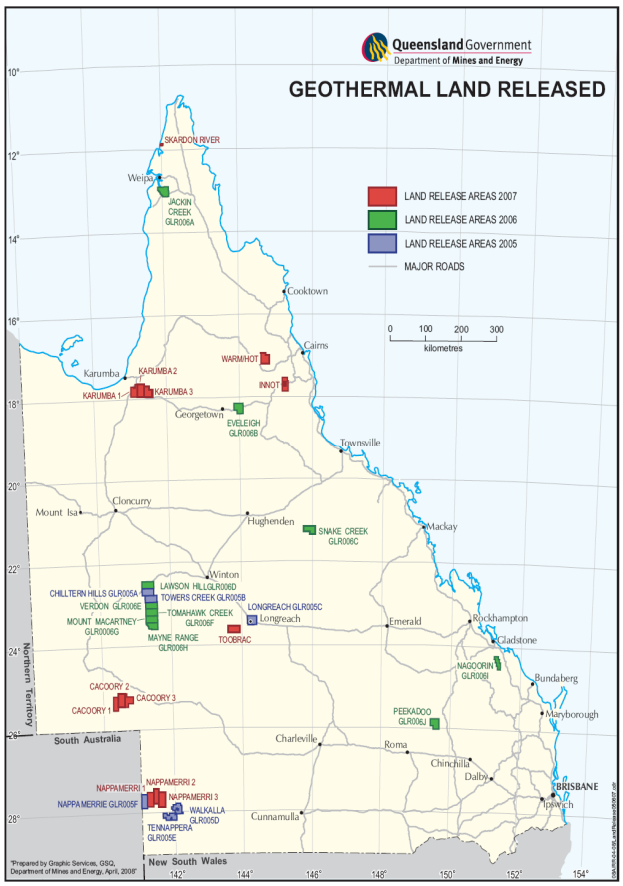

Figure 3 - Queensland's Geothermal Sites
Source: (Department of Mines and Energy, 2008)

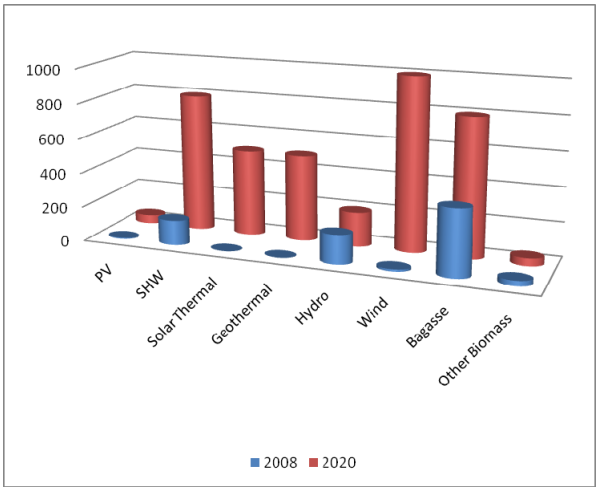

Figure 4 - Queensland's Clean Energy Future
Source: (Office Of Clean Energy, 2009b)

It may therefore be more appropriate to look at policy measures that fund additional transmission and distribution infrastructure to bring forward the deployment of these smaller sites, than looking at policy measures that support the final generation output.

Summary

Current policy measures would appear to be working well for the geothermal sector, with funding being made available for research, exploration and drilling. The deployment of other renewable technologies already commercialised will be driven by State subsidies and will keep the REC price relatively low in the early years due to anticipated deployment rates, stalling investment in those marginally economic technologies. Based upon industry forecasts, much of the planned geothermal generation plant will start to come on-line when the REC surplus has been expended and there is short-fall with the price increasing accordingly, resulting in greater 'profit' opportunities for this sector.

This paper has highlighted the need for further research looking at the effect that subsidised transmission and distribution infrastructure may have on the deployment rates of renewable technology. As other technologies, particularly wind and solar thermal also look at siting generation plant further from the coastal population bases, the need for a structured plan to develop the necessary infrastructure requirement of the national electricity market as a whole needs to be looked at in much greater detail.

The renewable energy sector cannot move forward without considerable support from all levels of government, but what the sector must determine what form that support should be.

References

Australian Institute of Energy, 2004. Fact Sheet 9: Geothermal Energy.

Department of Mines and Energy, 2008. Geothermal Land Released. Queensland Government, Brisbane.

Froome, C., 2009. Renewable Energy in Australia: 20% by 2020 - Can this be achieved? , Environmental Research Event, Noosa, Queensland.

Grove-White, G., 2009. Renewable Energy - How can Queensland lead the way, CEDA Forum, Brisbane.

Herd, D., 2009. National REC - Supply v Demand, in: Froome, C. (Ed.). People Planet Profit, Brisbane.

McLennan Magasanik Associates, 2008. Installed capacity and generation from geothermal sources by 2020. Australian Geothermal Energy Association, South Melbourne.

Office Of Clean Energy, 2009a. Geothermal Exploration Tenders, in: Energy, D.o.M.a. (Ed.), Brisbane.

Office Of Clean Energy, 2009b. Queensland's Clean Energy Future. Queensland Department of Mines and Energy, Brisbane.

Levelised Unit Cost – A Calculation and Reporting methodology

Alan Knights
Executive Director, Green Rock Energy Limited, PO Box 1177, West Perth, WA 6005
Honorary Secretary, Australian Geothermal Energy Association, PO Box 1048, Flagstaff Hill, SA 5159
aknights@greeenrock.com.au

To ensure there is no confusion, contradiction and a fair and meaningful comparison within the geothermal and investment community in relation to the use of unit generation costs, the adoption of a standardised methodology for cost calculations and reporting among different electricity generators is a prerequisite. The Australian Geothermal Energy Association, "AGEA", proposes to use Levelised Cost as the unit cost measure to be quoted when companies report average unit generation costs. Levelised Cost is the methodology used by the electricity generation industry and its use enables the comparison of the generation cost of different forms of electricity generation (such a coal, gas, wind, wave and geothermal) and of different projects using the same form of generation. The methodology to be adopted by AGEA for calculating and reporting average unit electricity generation costs when developing and/or operating geothermal power generators has not been finalised. This paper describes one method for calculating and reporting Levelised Costs. It has been prepared to facilitate discussion and consideration as AGEA moves to agreement on a desired methodology.

Keywords: Unit generation costs, Levelised Cost, calculating unit electricity generation costs, geothermal.

Introduction

Unit production costs are used for many purposes, ranging from internal management costing through to project evaluation. The methodology used in calculating the unit cost will depend upon its use. The Australian Geothermal Energy Association ("AGEA") is seeking the adoption of a standardised methodology for the calculation and reporting of unit electricity generation costs to ensure there is no confusion, contradiction and a fair and meaningful comparison can be made between alternative investments by the geothermal and investment community.

AGEA proposes the establishment Levelised Cost as the unit cost measure to be quoted when companies report average unit generation costs.

Levelised Cost is the methodology used by the electricity generation industry and its use enables the comparison of the generation cost of different forms of electricity generation (such a coal, gas, wind, wave and geothermal) and of different projects using the same form of generation.

This paper describes a methodology for calculating and reporting average unit electricity generation costs by companies developing and/or operating geothermal power generators. The methodology is currently open for comment before finalisation by AGEA.

Calculation of Levelised Cost

There are a number of ways of approaching the calculation of unit production costs. The electricity industry uses Levelised Cost which incorporates the investment in the plant and the fact that not one, but many units of electricity are produced during the life of the project.

The Levelised Cost is the time series of the capital and operating expenditures divided by the net power supplied, discounted to their present values.

The following sets out the main components of the Levelised Cost calculation methodology:

- Expenditures include all those required to deliver the net power supplied to the station busbar, where electricity is fed to the grid or end user. It does not however include the potential additional costs to the electricity network to cater for the impact of the power plant on the existing network;
- The time series covers the life of the power plant from evaluation through to decommissioning;
- Capital expenditures include all costs required for the development, commissioning and decommissioning of the geothermal power generator including the site preparation, evaluation, production and reinjection wells, the plant and machinery, administration and personnel buildings/accommodation and power lines and associated costs to connect to the grid or end user.
- Operating expenditures include all operation and maintenance costs on the wells, power plants and power lines including make-over or additional drilling costs to extend the project life, plus permit and licence fees, administration, insurances and any royalties payable for the extraction of geothermal energy;
- Capital and operating expenditures are to exclude income taxes, the benefits associated with the generation of renewable energy,

including Renewable Energy Certificates but are to include any costs associated with the generation of greenhouse gases. The costs are to be in constant monetary terms;

- Net electricity generated and supplied to the grid, or end user, takes into account the plant availability and variability due to the plant operating efficiency factors such as ambient temperatures, the parasitic power required for operating the well pumps and plant and machinery and the impact of thermal drawdown, if applicable, over the project life;
- The discount rate is the rate of return that could be earned on similar investments on a pre-tax basis.

The formulae to calculate the Levelised electricity generation Cost (LC), for each power plant, is the following:

$$LC = \sum_t [(I_t + M_t)\,(1 + r)^{-t}] \;/\; \sum_t [E_t(1+r)^{-t}]$$

Where:

LC	=	Average lifetime Levelised electricity cost per MWh
I_t	=	Capital expenditures in year t
M_t	=	Operating and maintenance expenditures in year t
E_t	=	Net electricity generation in year t
r	=	Discount rate
$\sum_t$	=	The summation over the life of the power generator including evaluation, construction, operation during the economic lifetime and decommissioning of the plant.

Reporting of Levelised Cost

When reporting of average unit generation costs a company should clearly state that the unit cost is a Levelised Cost and either $/MWh or c/kWh.

The company reporting should be prepared to disclose, as a minimum, the following information used in the calculation of the Levelised Cost:

- Total capital expenditure
- Average annual total operating and maintenance expenditure
- Average annual net electricity generation
- Life of the power generator
- Discount rate

Conclusion

This paper describes a methodology for calculating and reporting average unit electricity generation costs by companies developing and/or operating geothermal power generators. The methodology is currently open for comment before finalisation by AGEA.

Comments should be directed to the author at aknights@greenrock.com.au

References

McLennan Magasanik Associates: Installed capacity and generation from geothermal sources by 2020. Report to Australian Geothermal Energy Association, (August 2008).

Skills Issues and Training in the Geothermal Industry A New Zealand perspective

Juliet Newson[1] and Jane Brotheridge[2]

[1]Dept of Engineering Science, University of Auckland, Private Bag 92019, Auckland, New Zealand

[2]NZ Geothermal Association, PO BOX 11-595, Manners St, Wellington 6142, New Zealand

Geothermal electricity generation is expanding around the globe with total global capacity expected to rise to 11 GW by 2010. Many countries are investing in research and development of EGS and low temperature resources.

In New Zealand, 135 MWe geothermal has been added to the grid since 2005, with another 155 MWe under construction, with a further 120 MWe at the resource consent stage and over 500 MWe planned or under review. Personnel levels in a professional capacity have grown from 350 in 2005 to 450 today, with a total of over 600 people solely involved in the geothermal industry based in NZ. However, there are critical shortages of trained personnel worldwide.

The New Zealand Geothermal Association has developed a 'Skills Action Plan' to address some of these issues.

- MAKE: Grow professional and trade/technical skills for new entrants to the industry;
- FIX: On-the-job up-skilling for those already in the industry;
- BUY: Immigration – source skilled labour on the world market.

The aim of this plan is to present a way forward to increase the level of participation of skilled personnel in the industry. It also has the aim of raising the profile of this energy resource which often gets ignored in the bigger discussion on renewable energy in New Zealand.

The Geothermal Institute at University of Auckland ran a very successful year-long Geothermal Diploma course from 1979 to 2002. This course has been reshaped and revitalised and is now one-semester PGCert (Post-graduate Certificate), with additional short courses tailor-made to industry needs. From 2010 the Faculty of Engineering will also offer a Masters Degree course in Energy, with a specialisation in Geothermal Energy.

The framework already exists to design non-university trade and technical courses in geothermal energy topics which can be part of a nationally recognised qualification. School and community level education is also required.

Keywords: personnel shortages, skills action plan, specialised geothermal training, education

The Global Geothermal Industry

Trends in the global geothermal industry over the last several years reflect a strong upswing in interest in renewable energy which is being driven by two key factors – a growing recognition of the reality of global warming and the contribution that fossil fuel generation with high CO_2 emissions makes to this problem, and the very high fuel costs that had prevailed up to 2008. As a result of these factors, geothermal energy has become a favoured form of renewable power generation, being suitable for long term sustainable power with low CO_2 emissions, typically at a level of less than 20 % of that for fossil fuel generation.

The New Zealand Geothermal Industry is experiencing a period of growth which is expected to continue for the coming 10 years. A number of developers have built up critical levels of skill and confidence to be able to make geothermal investments as part of a broad portfolio of energy projects. Additionally, the geothermal industry in Australia is very buoyant with capital raising, surface exploration, exploration drilling and power development planning actively undertaken by a number of commercial entities.

Traditional international markets of the Philippines and Indonesia have recently undergone restructuring of the national electricity supply networks and of associated state-owned enterprises coupled with privatisation and asset sales. This has drawn in New Zealand consultants (and potential investors) into due diligence studies on behalf of multiple investors, and subsequent feasibility studies. Consultants have also provided advice on maintenance regimes for existing facilities. Major projects may follow.

Other developments that have required and will require New Zealand personnel include the Lihir project in Papua New Guinea, the San Jacinto project in Nicaragua, and Olkaria in Kenya. There are frequent calls on geothermal experience for due diligence and feasibility studies through parts of South East Asia and in Europe, and more recently through the Caribbean. Djibouti is one of the latest places for prefeasibility studies. There is growing interest in Central and South American development, including a recent strong drive by the Chilean government to encourage development in Chile.

Until now there have been almost no inroads into the US market but that could be about to change. The WGC 2005 country update for the USA showed there were approximately 725 professional personnel involved with geothermal activities in the US in 2004 compared with 440 similarly qualified geothermal professionals in New Zealand currently.

The US DOE has recently announced an investment of up to US$350 million targeted at geothermal demonstration projects; EGS research and development; innovative exploration techniques; and a National Geothermal Data System, Resource Assessment and Classification System. One of the expected program outcomes include demonstrating the ability to create an EGS reservoir capable of producing 5MW by 2015.

Close to US$155 billion was invested in 2008 in renewable energy companies and projects worldwide, not including large hydro. Of this, $13.5 billion of new private investment went into companies developing or scaling-up new technologies alongside $117 billion of investment in renewable energy projects from geothermal and wind to solar and biofuels. The 2008 investment is more than a four-fold increase since 2004 according to *Global Trends in Sustainable Energy Investment 2009*, prepared for the UNEP Sustainable Energy Finance Initiative.

Geothermal Personnel

Throughout the energy industry worldwide there is a shortage of skilled personnel, an ageing workforce and a reduction in graduates in relevant disciplines.

In 2005 a skills survey (NZGA 2005) of the geothermal industry reported a total 350 personnel engaged in the NZ geothermal industry as professional engineers, scientists and technically qualified plant operators. Four years on, and with an additional 135 MWe added to the grid from geothermal, there are almost 450 professionals plus over 150 technical and non-technical staff involved solely in the geothermal industry (NZGA 2009). Several geothermal companies in NZ have found a need to attract skilled professionals internationally and therefore must compete with others in the internation energy sector.

Future development in NZ alone has 155 MWe under construction, with 120 MWe with resource consents. Additional to these, over 500 MW is planned and under review. In the past 20 years much of the work NZ consultants (this includes large and small companies, individuals, Crown Research Institutes (CRIs) and universities) have been involved with is offshore. The NZ based work alone was not enough to sustain them. Yet with the growth of development in NZ in the last several years, and the growth in personnel, the geothermal industry in NZ is still facing shortages. This has been critical in the drilling sector.

The expertise of many NZ geothermal consultants is being called upon by the recent 'birth' of the geothermal industry in Australia where this industry is expected to provide between 1000 and 2000 MWe by 2020 (MMA 2008).

The MMA 2008 report noted that most of the personnel involved in the emerging geothermal industry in Australia have a strong background in minerals exploration and development, but they have less experience in generating and selling electricity, with only a few having geothermal development experience. It is particularly critical in areas such as drilling and reservoir engineering.

With the expansion and investment internationally in EGS, these areas will be in even higher demand.

Skills Action Plan

To address current and ongoing skill shortages a skills action plan is proposed. The Plan was developed by the New Zealand Geothermal Association (NZGA) on behalf of the Geothermal Industry in NZ. It is based on the 'Make, Fix, Buy' model developed by the Department of Labour and aligns with the New Zealand Skills Strategy.

- MAKE Grow professional and trade/technical skills for new entrants to the industry
- FIX On-the-job up-skilling for those already in the industry.
- BUY Immigration – source skilled labour on the world market

The aim of this plan is to present a way forward in increasing the level of participation of skilled personnel in the industry. It is also has the aim in raising the profile of this energy resource which often gets ignored in the bigger discussion on renewable energy in New Zealand. See Table 1 at end of paper.

'MAKE'

Education is central to the 'MAKE' section of the action plan. This involves: raising awareness of geothermal energy at a community level; school programs in scientific and cultural aspects of geothermal energy use; promotion of renewable energy studies at University; and as a desirable career path.

Development of a package for use in the school science curriculum is recommended for schools. Environmental awareness and sustainable development is now part of the school curriculum, and direct use of geothermal energy would fit well into this particularly at primary school level. It is a straight forward concept to explain and illustrated with a multitude of uses.

The geothermal industry needs a presence at community events raising awareness, and a package for static displays suitable, for instance, for libraries and foyers of community buildings. The geothermal industry needs to work with the Industry Trainings Organisations to develop trade and technical courses and qualifications to suit industry requirements. This may involve many interested parties, from Technical Institutes and even Universities for higher level technical skills, to in-house training for school leavers directly entering the workforce.

High level jobs involving tertiary education such as engineers and geoscientists are critical to current and future geothermal exploration and development. In the 2005 report on skills capability in the geothermal industry, the most common complaint from industry was the lack of training programs available to maintain a satisfactory inflow of younger staff or for further developing experienced staff. It was recommend that the former Geothermal Institute within the University of Auckland (UoA) be re-established but with tailored training programs to the NZ geothermal operator sector. In particular, focus on resource monitoring and management, steam field and power plant operational issues was sought.

For the long term it is suggested companies must consider actively recruiting graduates and mentoring/training them over a 2-4 year period to build up necessary experience. However, this is dependent on an increase in school leavers entering these disciplines at university. Programs promoting renewable energy and the green economy as viable career paths need to be targeted at senior school leavers.

'FIX'

On-the-job up-skilling is also vital. The benefits of on-the-job training include higher standards of safety, higher productivity, less down time, and employees feeling valued. Technological advancements require on-going training as well as the need to extend /expand the knowledge of workers moving to new areas of operation and up skilling those moving to supervisory or management roles. Employees report that they value training as long as it is delivered by someone experienced and knowledgeable who can transfer that knowledge in a way that learners can relate to, and is timely and that they have the opportunity to learn in group situations.

'BUY'

The energy industry as a whole needs to address the remuneration issue urgently and consider moves towards pay parity especially with Australia which is New Zealand's major competitor for skilled resources.

As a proportion of overall demand for skilled employees, the numbers are smaller and in the short term can be recruited in the global market. Companies will however have to prepare for a longer lead-in time to source experienced personnel because of the scarcity worldwide or to seek recruits from both traditional and non-traditional sources.

A major consideration for recruiting people from overseas is remuneration. Skills scarcity coupled with escalating demand has had the effect of adding premiums to wages and salaries for those employed within the sector. The general wage pressure is however wider than the NZ market, evidenced as a continued creep towards Australasian rates of pay for some skills and in limited circumstances, global pay rates for workers prepared to work in the more lucrative international day-worker market.

Current Status of Training in NZ

Because education comprises a significant section of the skills action plan, this section of the paper discusses the current state of geothermal training in New Zealand.

In response to perceived demand, and in anticipation of future demand, a new one semester post graduate course in geothermal science and engineering is now taught annually at the University of Auckland. For those who cannot afford the time away from work, specialist professional development short courses are offered.

The framework exists for training providers to design trade and technical courses for accreditation to a nationally accepted standard. At least one geothermal company has begun to work with Industry Training Organisations (ITO's) to enable workers to obtain a drilling qualification.

However, more needs to be done at a school and community level to promote geothermal energy.

Postgraduate Geothermal courses in NZ

The Geothermal Institute at University of Auckland ran a very successful year-long Geothermal Diploma course from 1979 to 2002 (Hochstein, 2005). Unfortunately support from the New Zealand Government for the Diploma course was withdrawn at the end of 2002. This was despite the growing concern over global warming and the required development of clean energy sources, concern among professionals over the loss of momentum in geothermal research and training in New Zealand, and a potential shortage of geothermal professionals (NZGA, 2005).

In 2006 Professor Mike O'Sullivan, leader of the Geothermal Reservoir Modelling Group in the Department of Engineering Science, and Associate Professor Stuart Simmons, Director of the Geothermal Institute, assembled a group of

geothermalists to teach a one-semester Post Graduate Certificate in Geothermal Energy Technology (PGCert).

The philosophy was to provide through the PGCert the backbone for a comprehensive geothermal training program involving university level papers, short lecture courses for professionals, graduate research degree courses and academic research programs. With the exception of Assoc Prof Stuart Simmons, the people initially involved in organising the course came from the Geothermal Reservoir Modelling Group in the Department of Engineering Science.

At the time when the decision to run the course was made the University was in the process of developing a cross-faculty research group called the Institute of Earth Sciences and Engineering (IESE). Geothermal energy was considered to be an important part of the research portfolio. However because of its research-only status within the University of Auckland the IESE cannot host University degree programmes and hence the PGCert course is hosted by the Department of Engineering Science in the Faculty of Engineering.

Support for the Course

Against the background of a small initial number of enrolments and no special financial support from government bodies, running the course relied heavily on the goodwill of:

- the Department of Engineering Science which provided lecture rooms, teaching support, and computer facilities;
- the retired staff of the old Geothermal Institute (Manfred Hochstein, Pat Browne, and Arnold Watson); and
- the New Zealand geothermal industry, who responded positively and contributed lectures, site visits, and scholarships for the course.

A feature of the inherited good will from the Geothermal Institute days has been a close connection between industry and geothermal teaching. There has been very strong industry support for the PGCert in 2007 and 2008. Contact Energy Ltd has supported the PGCert with six scholarships over the two years, with a total value of NZ$120,000, and Century Resources (now MB Century) has provided two scholarships with a total value of NZ$40,000. Sinclair Knight Merz (SKM) have donated fourteen hours of lectures each year, and GNS Science Wairakei have donated 12 hours of lectures and field tuition. In addition, Contact Energy, MB Century, Tuaropaki Power, and GNS Science, have given access to borefields, power stations, and geothermal areas, with staff accompanying groups of students for informal tours, training in taking field measurements, formal lectures, and student project supervision.

Chevron Geothermal (Indonesia) provided generous funding for three aspects of the training program:

- the development of one-week short-courses on geothermal geoscience and geothermal engineering;
- the development of course material for the PGCert; and
- archiving of course material from the Geothermal Diploma.

The success of the PGCert in 2007 and 2008 and the strong support from the geothermal industry was sufficient to convince the University of Auckland to continue support geothermal training for at least the next three years.

Teaching

Geothermal teaching at the University of Auckland involves four types of courses, all directed towards post graduate and professional training:

- the one-semester Post Graduate Certificate in Geothermal Energy Technology;
- professional short courses taught in New Zealand (one-week or four-weeks). These are planned to be part of staff professional development schemes;
- research studies for ME, MSc or PhD degrees; and
- professional short courses taught in other countries (one-week).

The University of Auckland is currently planning a one-year taught Masters of Energy degree, with a target start date of 2011. It will include geothermal energy as an option but will also allow for other specialisations such as wind, solar and bio-fuels. Courses from the PGCert will be available for this degree.

Post-Graduate Certificate in Geothermal Energy Technology

This one semester course includes lectures and assignments, field visits with data collection and interpretation, and a short research project. The minimum entry qualification is a Bachelors degree, preferably in Science or Engineering, and the University of Auckland also has strict English language requirements for post graduate courses.

Both geothermal geoscience and geothermal engineering topics are covered. All students are required to complete the first two lecture courses (papers) which are an introduction to ‘Geothermal Resources and their use’, and ‘Geothermal Energy Technology’. The class then splits: students must chose between a ‘Geothermal Exploration’ paper, and a ‘Geothermal Engineering’ paper, where specialist geothermal topics are covered in more depth. The final five

weeks of the course is devoted to a short research project resulting in a ~40 page research report. During the course there are two six-day long field trips to the Taupo Volcanic Zone, which involve lectures from geothermal experts and visits to power station, natural geothermal features, geological features, and geothermal energy direct use sites.

Professional Short Courses and PGCert Papers

One of the problems of specialist training courses for professionals is that many workers cannot take 5 months leave to attend a course such as the PGCert. In view of the lack of training courses worldwide in the last decade, causing an acute shortage of trained geothermal people, it is very difficult for those currently working in the geothermal industry to take training leave for longer than a few weeks. Our response to this problem has been to allow people to attend selected parts of the PGCert course as 'professional short courses'. These students do not attain a University qualification, but are still able to participate in modules of the course.

In 2008 the uptake for these courses was high, with an extra eighteen students attending sections of the course. Thus the number of students attending part of the PGCert course increased from one in 2007 to 18 in 2008.

Geothermal short courses are run according to demand in both in New Zealand and overseas. Some of these short courses were commissioned by companies as part of their staff development programs. For instance, in October 2008 staff from the IESE and the Department of Engineering Science spent two weeks in Indonesia delivering two short courses for Chevron Geothermal – one week each on Geothermal Geoscience and Geothermal Engineering attended by a total of 31 students. Similar courses were delivered in April 2009 in Auckland, and more courses abroad are being planned for late 2009.

Trade Qualifications and Certification

Trade/Technical skills are catered for in broad disciplines applicable to the energy industry eg. electricians, fitters etc, but not specific to the geothermal industry. However, the numbers of young people choosing to enter the trades is less than desired.

Industry Training Organisations (ITOs) have the mandate of the industry that they represent to develop training standards for their industry and to register these on the National Qualifications Framework. ITOs are funded by the Tertiary Education Commission to offer training subsidies for their industry. While not directly able to engage in training the ITOs determine which providers will be accredited to award qualifications for the industry and who will be recognised as an accredited assessor.

When necessary ITOs will respond accordingly if the geothermal industry identifies other needs or will adapt qualifications to meet any specific requirements. MB Century Ltd has been in talks with Extractives ITO EXITO to enable their in-house training be accredited by New Zealand Qualifications Authority NZQA. This new certificate will take about 6 months for a trainee to pass through the various steps in order to obtain the required credits.

Conclusion

The New Zealand geothermal industry has been experiencing a shortage of trade, technical, and professional staff. The New Zealand Geothermal Association has designed an action plan based on a model developed by the Department of Labour for the New Zealand oil and gas industry, which involves educating people for working in the industry (MAKE), further training for those already involved (FIX), and recruiting from abroad (BUY).

The 'make' and 'fix' components of the plan primarily involve education. Tertiary level geothermal training courses have been run annually at the University of Auckland since 2007, comprising the Post Graduate Certificate in Geothermal Energy Technology, and professional development courses. From 2010 the Faculty of Engineering will also offer a Masters degree course in Energy, with a specialisation in geothermal energy.

The framework already exists to design non-university trade and technical courses in geothermal energy topics which can be part of a nationally recognised qualification. One company is currently developing a drilling qualification but there is potential for further course development in this area. School and community level education is also required.

Implementation of aspects of the Action Plan is currently under discussion with the NZGA and various Stakeholders.

References

Akin, J., 2008, Workforce Management. Power, vol 152, No. 4, p 74-78.

NZGA Report prepared by SKM 2005, Review of Current and Future Personnel Capability Requirements of the NZ Geothermal Industry

NZGA Report prepared by Jane Brotheridge 2009, NZ Geothermal Industry Skills Report and Action Plan.

McLennan Magasanik Associates Pty Ltd., Aug 2008 Installed capacity and generation from geothermal sources by 2020.

Hochstein M.P. 2005. 25 years Geothermal Institute, Proceedings, World Geothermal Congress 2005, Antalya, Turkey.

Massachusetts Institute of Technology (MIT), 2006. The Future of Geothermal Energy. Impact of Enhanced Geothermal Systems (EGS) on the United States in the 21st Century. An assessment by an MIT-led interdisciplinary panel, prepared under Idaho National Laboratory Subcontract No 63 00019 for the US Department of Energy

MAKE General community education and primary to secondary educational level *(NERI findings in italics)*	**Who**	**Output (note – underlined is output already known to occur or planned for near future)**
There appears to be a shortfall in numbers of graduates in geothermal specializations, planning, policy analysis, mining specializations, corrosion sciences, surveying, physics, geology, ICT, human resources, law, resource management and project management needed to meet energy industry demand (NERI).	This appears to be part of a larger problem that extends over many engineering and science based industries. This requires long-term action from a range of educational and government organisations. The Geothermal industry should remain alert to the chance for input into relevant decisions.	Maintain a network of interested people who are in contact with regards this type of promotion – ie PR people in companies plus interested people at research and teaching organisations plus government departments/agencies.
A need to ensure that energy education in tertiary institutions includes sufficient focus on issue of strategic national importance (NERI).		
A need for better understanding of the stimuli external to universities that influence students' selection of courses, degree programmes and employment options (NERI).		
Market to school and tertiary sectors to promote employment opportunities in the sector	Currently GNS Wairakei and Kaikohe School. Industry	Assess and collate all existing marketing material Work alongside other stakeholders to develop relevant material. <u>Some development underway with GNS Wairakei & Kaikohe school.</u>
Development of a package for use in school science curriculum - approach schools to assess interest. Funding needs to sought.	University or research company/government department/agency.	Package developed.
Target one school then extend to three schools in 2 years time	As above.	Identify a pilot school for package. Roll to more schools in future
MAKE Tertiary education (*NERI findings in italics*)	**Who**	**Output**
Increase numbers participating in university programmes relevant to the sector (note that specialisation would occur in 3rd or 4th year of Bachelor Degree). Recruit graduates for the geothermal industry. *To meet current energy industry demand, an increase is needed in the number of university graduates from engineering, commerce, science and geography entering employment in the*	Industry/NZGA/Universities	List of contact people from each University/faculty, who organise careers presentations. Company participation in career/recruitment days. Career evening presentations hosting the Geothermal Industry as a

energy sector (NERI).		whole. Geothermal research promoted for Postgraduate topics.
Development of specific qualifications, specialist papers and projects	Universities/Industry/NZGA	Courses at the University of Auckland since 2007
Build internal expertise by collaborating/developing relationships eg. universities and utilities/developers. *A desire by energy stakeholders to have more contact with universities (NERI)*	Industry/Universities/NZGA	Develop a relationship that involves: • training using real-world scenarios • encouraging students to engage with the industry • Student projects • Course support • Fund research
Support increased numbers of MSc and PhD projects	Industry/Universities	Currently Masters and PhD research in geothermal topics at several institutions. Industry is already supportive, can always provide more research topics and funding for projects. 'Real world' topics can justify paying a student to research them.
Provide work experience/mentor graduates to build industry experience. *University graduates' relevant work experience does not appear to be sufficient to meet the work experience demanded by employers in the energy industry (NERI)*	Industry	Internship programs. Already some in the industry do this, needs more coordination with students and industry
A need for understanding of iwi perspectives on tertiary level energy education (NERI).	TPK/Universities	Input to Māori Geothermal Seminars, liaise with Māori groups on Campus, for instance UoA SPIES (South Pacific Island Engineering Students), liaise with other University groups researching wider Māori Energy Development.
There appears to be a need for cross-disciplinary university education relating to energy	Universities	Currently development of a Masters in Energy course at the University of Auckland starting 2010. Organised in the Faculty of Engineering but will have the potential for cross-disciplinary study.

MAKE Trade/Technical Qualifications (NERI findings in italics)	**Who**	**Output**
Trade level roles: Disseminate information to contractors and the community including iwi, to improve understanding of the current industry training system and how it compares with the former apprenticeship system. *A need for better information about the supply of non-university graduates for employment in such roles as field technicians and maintenance engineers in the energy industry (NERI)*.	ITO's/NZGA	Liaise with the engineering and electrical sectors for joint marketing of the industry as a career option Develop a communication strategy
Develop introductory pre-qualification packages for use in secondary schools.	ITO's/NZGA	Liaise with school careers advisors, ESITO etc. Establish relationship between these groups and industry to see what the needs are, and where the gaps are
Manage the relationships between schools and industry for work experience through the Gateway programme	Industry	Assess what marketing/promotional work needs to be conducted to increase industry participation in gateway. Work alongside schools to identify potential students.
Increase the number of apprentices/industry trainees	Industry	Liaise with industry to encourage the uptake of more trainees
FIX General culture of ongoing education	**Who**	**Output**
Employers in the industry need to ensure ongoing training	This is an ongoing obligation for all employers and for the self-employed	Regular widespread attendance at seminars and workshops Employees should be continuously adding to their skill base
Provision of suitable courses and topical seminars	NZGA, universities, technical institutes	Regular targeted seminars and workshops e.g. one day overview seminars useful for managers and non-technical people
Assist IESE in developing a business plan for their courses as the basis for a New Zealand/regional geothermal training facility	Industry, NZGA with some Government funding	Active and expanding training programme including input from experienced industry professionals
Ensure employees have a minimum of paid hours of training per year	Industry	Delivery of training

BUY Preparedness for Expatriate Workers	Who	Output
Individual employers should recruit internationally	Industry	Industry members are currently recruiting internationally
Where skill shortages are identified by employers, make submissions on behalf of industry to Immigration NZ's biannual shortage lists	NZGA, Industry	Shortage lists will address broad gaps, especially in trades
Utilising an independent remuneration consultant, promote a collaborative approach to benchmarking of NZ salaries. Include an assessment of the extent to which NZ geothermal compensation and benefits are aligned internally and regionally, and with the O & G sector, which are all competitors for skilled NZ geothermal workers	Industry and Government funding of an independent consultant managed by NZGA	Report on bench marked salaries, with repeat reports showing a move toward competitive values
Use Ministerial trade shows and trade fairs and international conferences to publicise the opportunities in the NZ geothermal industry	Industry/NZGA working with Government	NZ presence at wide range of events with booths highlighting opportunities

Table 1: Geothermal Industry Skills Action Plan

Power loss evaluations for long distance transmission lines

Mai Huong Nguyen, Tapan Kumar Saha*
Queensland Geothermal Energy Centre of Excellence
The University of Queensland, St Lucia, Brisbane - QLD 4072 Australia
* Corresponding author: saha@itee.uq.edu.au

Long distance power transfer is a major problem for renewable energy sources located far away from the major load centres. This issue in particular is more pronounced for the prospective geothermal power plants in Australia. This problem involves analysing the cost of investment and operation and types of interconnection used for transmitting the bulk power from a remote area to a major load centre. As the level of power transfer and the transmission distance increases, the power loss of the transmission line tends to increase. For these reasons, it is essential to carefully analyse the impact of interconnection on the total loss of a power system, subject to changes in operating conditions and varying transmission distances. The typical approach for very long transmission lines is to use high voltage (HV) based on either DC or AC. In theory, the HVAC line has higher resistance and reactance, therefore, it has a high loss in the line compared to the HVDC option. On the other hand, the HVDC scheme has a significant proportion of loss in its converter/inverter stations. Up to a certain distance called the "breakeven distance", HVAC is superior in terms of the total cost, loss and the stability margin. Above this distance, HVDC is the most favourable option. The main task in this paper is determining this "breakeven distance" for a particular electricity system based on static power flow analysis. In this paper we apply a four machine two area test system implemented in the PSS/E software environment to compare the impact of high voltage AC and conventional high voltage DC on total system losses. Further methodology will be developed to make this outcome more generalised for any electricity network..

Keywords: interconnection, HVDC, HVAC, loss evaluation.

Long distance transmission lines

The electricity systems from different areas are being connected by long transmission lines to achieve an economical benefit and to improve reliability. Such interconnections can connect regions in a country, from a country to another country or cover very large continental areas. They can also be used to transfer the power from remote renewable sources, such as off-shore wind farms, solar thermal systems or geothermal power plants in desert areas, etc. to the load centre. The advantages of long interconnections are the flexibility in deciding locations as well as in building larger and more economical power plants; creating the possibility of loss reduction by optimised system operation [1]. In the expansion of the electricity market all over the world, high voltage transmission lines over a long distance may offer considerable advantages in technical, economical and environmental aspects. In recent years, power industries all over the world supported many interconnections to enable the exchange of power among areas and transfer cheaper electricity over long distance to the customers.

HVAC and HVDC are the two interconnection schemes available for long transmission systems. There have been some publications on technical and economical evaluations for several types of interconnections using HVAC or HVDC technologies.

HVAC has been found to be the better solution for a distance less than the "breakeven distance", which can vary from 400km to 500km, between two synchronous regions [1-3]. However, for long transmission lines, HVAC must be facilitated by Flexible AC Transmission System (FACTS) devices for reactive power compensation.

Longer than the breakeven distance, HVDC becomes more preferable either with an overhead transmission line or an underground cable. Besides, HVDC is also suitable for the submarine cable, interconnections between AC systems of different or incompatible frequencies and for remote renewable energy resource connection.

Paper [4, 5] compared the total system losses due to the impact of HVAC, Line-Commutated Converter (LCC) HVDC and Voltage Source Converter (VSC) based HVDC connected to a large offshore wind farm (from 100 to 1000 MW) with varying distances up to 200km. Paper [4] concluded that the HVAC solution is superior for distances up to 70km. LCC HVDC is preferred in terms of reduced system losses above this distance. The "breakeven distance" for VSC HVDC in a loss point of view is around 200km. According to their results, the combination of different transmission systems never improves the total loss in the system. Paper [5] indicated that the HVDC solution is more expensive than the HVAC option with 100MW, 200MW and 500MW wind farms at the connection a distance of 60km due to higher investment cost and higher power loss. However, the HVDC option appears to be cheaper than the HVAC option while connected to a 100MW wind farm with a distance greater than 90km.

Nevertheless, these conclusions were based on the characteristics of HVAC and HVDC lines and on the experimental measurements data. The loss evaluation was carried within the interconnection, not in the whole system. Up to now, very few technical reports are available to compare the impacts of HVDC and HVAC on large power system performance. This paper will focus on the implementation of HVDC and HVAC options as a long transmission line for interconnecting between 2 large systems.

This paper is organised as follows: the first part of this paper introduces the load flow analysis for a power system using HVDC interconnections. The second part summarises loss evaluation and compares HVDC versus HVAC alternatives. The impacts of transmission length, number of interconnections, power transfer level and the sending end demand on the "breakeven distance" are also presented in this section.

HVDC analytical model

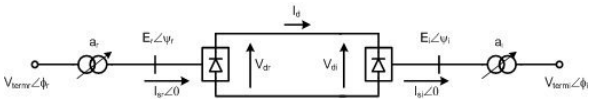

Fig. 1 Single diagram of a conventional HVDC link [1, 6].

The single line diagram of a HVDC system is depicted in Fig. 1. The steady state behavior of a AC-DC power system has been described in details by Arrilaga *et.al [6]*. The state variables for a HVDC system are: $[x] = [V_d, I_d, a, \cos\alpha, \phi]^T$ where V_d and I_d are the direct voltage and current, α and ϕ are the firing angle and the terminal voltage angle, respectively. For the inverter side, α will be replaced by γ, which is called the extinction angle.

The index *r* and *i* represent the parameters at the rectifier (converter) and inverter side, respectively.

In the PSSE software [7], the relationships between AC and DC voltages and currents at the rectifier side are expressed as:

AC-DC voltage:

$$V_{dr} = N_r \frac{3\sqrt{2}}{\pi} a_r V_{termr} \cos\phi_r \qquad (1)$$

$$= N_r \left(\frac{3\sqrt{2}}{\pi} a_r V_{termr} \cos\alpha - \frac{3}{\pi} I_d X_{cr} - 2R_{cr} I_d \right)$$

AC-DC current: $I_{sr} = \frac{\sqrt{6} N_r}{\pi} I_d \qquad (2)$

where R_{cr} and X_{cr} are commutation resistance and reactance, a_r is the transformer turn ratio, N_r is the number of bridges connected in series in a rectifier station.

The DC reactive and active power at the rectifier terminal is determined as follows:

$$Q_{termr}(DC) = V_{termr} I_{sr} a_r \sin\phi_r$$

$$= V_{termr} I_d a_r \sin\phi_r \frac{\sqrt{6} N_r}{\pi} \qquad (3)$$

$$P_{termr}(DC) = V_{termr} I_{sr} a_r \cos\phi_r$$

$$= V_{termr} I_d a_r \cos\phi_r \frac{\sqrt{6} N_r}{\pi} \qquad (4)$$

In this paper, the commutating resistance and transformer resistance are neglected, resulting in no active power loss in converter stations. Therefore, the DC active power at the rectifier terminal in equation (4) can be calculated as:

$$P_{termr}(DC) = V_{dr} I_d$$

The equations (1-4) can be applied to calculate the DC current, voltage and power at the inverter side, with $\cos\alpha$ and index *r* replaced by $\cos\gamma$ and index *i*, respectively.

The Jacobian matrix for load flow calculation of the HVDC system is determined by solving the following system of equations [1, 6]:

$$\overline{R}(\overline{x}, V_{term}) = 0 \qquad (5)$$

Where: $R(1) = V_d - \frac{3\sqrt{2}}{\pi} k a V_{term} \cos\phi$

$$R(2) = V_d - \frac{3\sqrt{2}}{\pi} k a V_{term} \cos\alpha - \frac{3}{\pi} I_d X_c$$

R(3) = f(V_d,I_d)
R(4) = control equation

The relationship between V_d and I_d, f(V_d,I_d), in this paper is: $V_{di} = V_{dr} - I_d R_d \qquad (6)$

where, V_{dr}, V_{di} is the dc voltage at the rectifier and inverter side respectively. R_d is the resistance of DC line.

The DC load flow algorithm based on the Fast Decoupled Power Flow method [6], which is used to solve the load flow problem with HVDC is briefly summarised as follows:

$$\frac{\Delta\overline{P}}{\overline{V}} = [B'][\Delta\overline{\theta}] \qquad (7)$$

$$\begin{bmatrix} \frac{\Delta\overline{Q}}{\overline{V}} \\ \frac{\Delta Q_{term}}{V_{term}} \\ R \end{bmatrix} = \begin{array}{|c|c|c|} \hline & & \\ \text{B''} & BB''_{ii} & \text{AA''} \\ & \text{BB''} & \text{A} \\ \hline \end{array} \begin{bmatrix} \Delta\overline{V} \\ \Delta V_{term} \\ \Delta x \end{bmatrix}$$

Where: $[AA''] = \frac{1}{V_{term}} \left[\frac{\partial Q_{term}(DC)}{\partial \overline{x}} \right]$

$$[BB''] = \left[\frac{\partial R}{\partial V_{term}}\right]$$

$$[BB''_{ii}] = \frac{1}{V_{term}}\left[\frac{\partial Q_{term}(AC)}{\partial V_{term}} + \frac{\partial Q_{term}(DC)}{\partial V_{term}}\right]$$

$$[A] = \left[\frac{\partial \overline{R}}{\partial \overline{x}}\right]$$

B'' and B'' are susceptance matrix of AC system

Loss evaluation

The test system used in this paper is a 2-area system shown in Fig. 2, which comprises of 4 generators and 2 large loads [8]. The two areas are connected to each other by two interconnection lines. In the original system, the interconnections are two 220km, 230 kV HVAC lines in parallel. The line parameters are:

R = 0.0529 (Ohms/km)
X = 0.529 (Ohms/km)
B = 33.1 x 10^{-6} (S/km)

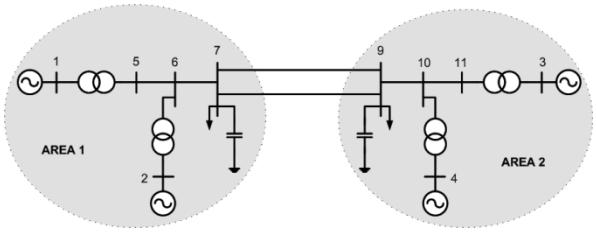

Fig. 2 System diagram [8]

The active and reactive power at system buses are presented in Table 1.

Bus	VM (pu)	V_{base} (kV)	P_G (MW)	Q_G (MVAr)	P_L (MW)	Q_L (MVAr)
1	1.03	22	700	0	0	0
2	1.01	22	700	0	0	0
3	1.03	22	700	0	0	0
4	1.01	22	700	0	0	0
7	1.00	230	0	200	967	100
9	1.00	230	0	350	1767	100

Table 1. System data bus, including voltage magnitude (VM), base voltage (V_{base}), active and reactive power generated (P_G, Q_G) and consumed (P_L, Q_L) at all buses in the system

We tested the original system with HVAC interconnections replaced by HVDC interconnections. The load flow results for the modified system are compared to that of the original system. The line resistance for the HVDC system is chosen to be the same as that of the HVAC system. In the HVAC case, bus 3 is the slack bus for the whole system; in HVDC interconnection case, bus 1 is the slack bus for area 1 and bus 3 is the slack bus for area 2.

The HVDC rated voltage is 230kV, the data of which is taken from [3]. The rectifier and inverter commutating reactance are 0.07 and 0.055 pu, based on a rated power of 890MW and a rated voltage of 230kV. The tap ratio at the converter transformer is maintained at 1.0 pu. The inverter is operated in constant extinction angle mode with $\gamma=22^0$. The maximum and minimum firing angle at the rectifier side is 12^0 and 8^0, respectively. Table 2 summarises load flow results obtained from using PSSE with HVAC and HVDC interconnection systems.

Bus	HVAC		HVDC (constant γ)	
	VM (pu)	Ang. (deg)	VM (pu)	Ang. (deg)
1	1.03	20.98	1.03	24.79
2	1.01	11.22	1.01	14.9
3	1.03	-6.8	1.03	-6.8
4	1.01	-16.93	1.01	-16.82
5	1.0066	14.51	1.0008	18.27
6	0.9785	4.43	0.9645	8.01
7	0.9618	-3.98	0.9367	-0.68
9	0.9751	-31.33	0.9604	-31.38
10	0.987	-22.98	0.9793	-22.92
11	1.0114	-12.74	1.0086	-12.7

Table 2. Voltage profile of the system, including voltage magnitude and voltage angle of all buses after solving load flow

The active power transfer from bus 7 to bus 9 was kept at 400 MW, resulting in 200MW active power transferred in each line. The load flow results are shown in Table 3 below.

	HVAC		HVDC (constant γ)	
	P (MW)	Q (MVAr)	P (MW)	Q (MVAr)
Gen. 1	700	184.05	635.78	180.19
Gen. 2	700	231.94	700	258.28
Gen. 3	718.74	164.93	772.30	202.10
Gen. 4	700	191.54	700	255.79
Total	*2818.74*	*772.46*	*2808.07*	*896.36*
L7	967	100	967	100
L9	1767	100	1767	100
Loss	*84.74*	*572.46*	*74.07*	*696.36*

Table 3. Power flow data, including active and reactive power generated at generator buses and consumed at load buses. See text below for loss calculation

Table 3 gives an initial comparison of the two interconnection options: HVDC and HVAC, with

the same active power transfer level. Both active and reactive power losses are calculated by subtracting the total active/reactive power consumed at the loads from the total generated active/reactive power. The active power loss is directly related to operating cost. The reactive power loss represents the additional reactive power the generators have to provide to the grid for maintaining the system voltage to a desired level. Reactive power generation is an important ancillary service in an electricity power market, and thus, also relates closely to the operating cost. As can be seen in Table 3, the active power loss in the HVDC system is smaller than that of the HVAC system. However, the HVDC system requires more reactive power than the HVAC system. In the following sections, active/reactive power loss of the HVDC and HVAC systems are compared at different power transfer levels and transmission lengths.

Impact of distance on system loss

The length of both interconnections is varied from 200 km to 350 km. The HVDC is operated in the power control mode. The power transferred from the rectifier station (bus 7) to the inverter station (bus 9) is kept equal to the power transferred in the HVAC case. The voltage magnitude and angle of bus 1 in the HVDC system is maintained equal to that in the corresponding HVAC case. The result is shown in Fig. 3.

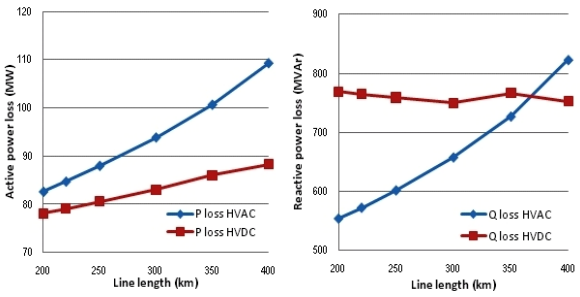

Fig. 3 Total system losses relating to transmission length

It can be seen from Fig. 3 that active and reactive power losses in the HVAC case steadily raise with the increase of the interconnection length. This is to be expected, as active/reactive loss on the interconnection line is an important part of the total AC system active/reactive loss. On the other hand, active/reactive loss in the HVDC system depends mainly on the losses in converter stations. The active power loss in the HVDC system is thus smaller than that in the HVAC system. Besides, the active power loss in the HVDC case does not increase as steeply as does the active power loss in the AC interconnection case when the transmission length increases. The reason is that the voltage profile decreases significantly for the HVAC case while the voltage profile of the HVDC system is slightly improved as the length of the line increases.

The reactive power loss in the HVDC system is slightly decreased with the increase in the length of the interconnection line, since the DC line does not consume reactive power. Moreover, in the HVDC scheme, the inverter is operated in constant γ mode, which keeps voltage at the inverter bus constant at 0.9604 pu (bus 9). As a result, when the transmission length is increased, the bus voltage at the rectifier bus will be increased in order to maintain the bus voltage at the inverter bus due to the relationship in equation (6). The voltage profile of the whole system, therefore, will be improved slightly resulting in lower reactive power loss.

When the line length is increased to 350km, to keep the power transferred on the HVDC line equal to that on the HVAC case, the HVDC needs to be operated in constant extinction angle mode $\gamma=23^0$ in order to increase the dc voltage (voltage at bus 9 is kept at 0.9581 pu). Therefore, we can see a slight increase in reactive loss of the HVDC line. When the length goes up to 400km, the extinction angle was kept at 23^0, thus the reactive power loss in the HVDC case continues to decrease slightly and becomes smaller than that in the HVAC case. Therefore, from both active power and reactive power loss points of view, the HVDC would be superior to HVAC after a distance of 360km.

Impact of power transferred in transmission line on the "breakeven distance"

The power transfer level is gradually increased from 150MW to 300MW per line. This is done by varying the load at the sending end (bus 7), from 1067MW to 767MW. Load flows are calculated for both AC and DC systems at each power transfer level. The results are presented in Fig. 4.

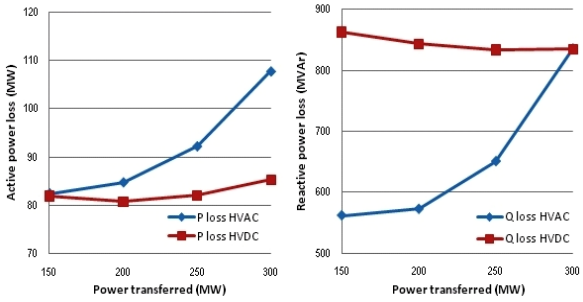

Fig. 4 Total system losses relating to power transferred in the interconnection

The loss in the HVAC system increases significantly as the active power transfer is increased. On the other hand, the reactive power loss in the HVDC system remains relatively unchanged (or even slightly decreases) as the power transfer is increased. In fact the slight reduction of reactive power loss does not relate to the DC link in this case. As the load at bus 7 is decreased, the current on the line 6-7 is reduced, therefore the total reactive power loss in area 1 is reduced slightly.

The “breakeven distance” for this case occurs around 600MW of power transfer (300MW per line). At this power transfer level, the reactive power loss in the AC system starts to surpass the reactive loss in the HVDC system. It should be noted that the two shunt capacitors at bus 7 and 9 help to reduce the reactive power transfer in both areas. The total reactive loss in the HVDC system could be further improved if one optimises the reactive power compensation at the two sending/receiving ends. Overall, reactive power compensation should be done locally, strategically placing shunt capacitors may help to greatly improve the efficiency of the HVDC system.

Impact of number interconnection on the “breakeven distance”

Load flow analyses are now carried out for the system with one interconnection line removed. The length of the transmission line is 200km. The HVDC is operated at $\gamma=22^0$. The system loss in this case was compared to the results of previous parts. Fig.5 illustrates the system losses with respect to the number of interconnection lines.

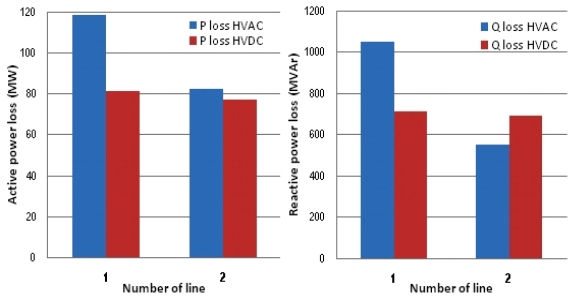

Fig. 5 Total system losses relating to number of interconnections

As is shown by Fig. 5, the loss in the HVAC system is significantly reduced when another interconnection is added. However, the loss in the HVDC system is slightly decreased. Again, one can see that the line loss in the DC link constitutes a very small part in the total system loss compared to the converter/inverter loss. It should be noted that this result is only based on loss evaluation. Adding a new AC line to reduce power loss may not be an overall cost effective solution.

Impact of receiving end load on the “breakeven distance”

The active load at bus 9 is gradually increased from 1667MW to 1967 MW. Active/reactive power loss for the AC and DC systems are shown in Fig. 6.

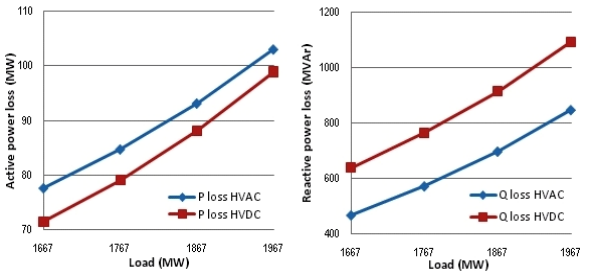

Fig. 6 Total system losses relating to the change in receiving end load

In this case, bus 3 is chosen as a slack bus, which is in the same area as bus 9. Therefore, the increase of active load at bus 9 is balanced by the increase of generating power at generator 3. There is not much difference between how the AC and DC link systems respond to the change in load bus 9. The increase of active/reactive power loss in Fig. 6 indeed comes from the increase of active/reactive power loss in the AC link of area 2. One can conclude that the “breakeven distance” does not depend on the load at the receiving end.

Conclusions

This preliminary work compares the DC and AC link options for a simple power system at various transmission lengths, load levels and interconnection strength.

Throughout the case studies, it is observed that the active power loss in the DC link constitutes a negligible part of the total system loss. Furthermore, the required reactive power for the HVDC system is quite independent of the interconnection strength and power transfer level. On the other hand, the AC system losses change considerably with the above parameters. Therefore, as the power transfer level and the interconnection length increase, the DC link gradually shows its superior performance. It should be noted that strategic placement of reactive power compensation can greatly improve the efficiency of a HVDC system. For the studied system in this paper, reactive power locations are obvious as there are only two important loads. For more complicated power systems, a thorough study of optimal reactive power compensation is essential, as it would strongly affect the outcome of the AC/DC comparison.

In this work, the “breakeven distance” is determined by comparing only the reactive/active power loss, which is closely related to the operating cost. If one takes into account the capital cost, the “breakeven distance” would be higher, due to the high cost of building HVDC systems.

One potential advantage of the HVDC system is its capability to enhance the total system dynamic stability. A comparative study of system stability with/without HVDC system is thus needed, and will be the subject of our future research.

References

[1] W. Breuer, D. Povh, D. Retzmann, and E. T. X. Lei, "Solutions for large Power System Interconnections" in CEPSI Shanghai, 2004.

[2] N. G. Hingorani and L. Gyugyi, Understanding FACTS: IEEE press, 2000.

[3] V. K. Sood, HVDC and FACT controllers: Klumer academic, 2004.

[4] N. B. Negra, J. Todorovic, and T. Ackermann, "Loss evaluation of HVAC and HVDC transmission solutions for large offshore wind farms" Electric Power Systems Research, vol. 76, pp. 916-927, 2006.

[5] P. Bresesti, W. L. Kling, R. L. Hendriks, and R. Vailati, "HVDC Connection of Offshore Wind Farms to the Transmission System" IEEE Transaction on Energy Conversion, vol. 22, March 2007.

[6] J. Arrillaga and B. Smith, AC-DC power system analysis: The Institution of Electrical Engineers, 1998.

[7] I. Siemens Power Transmission & Distribution, "PSSE help" in Basic Power Flow Activity Applications.

[8] P. Kundur, Power System Stability and Control: McGraw-Hill, 2006.

The Western Australian Geothermal Centre of Excellence

Klaus Regenauer-Lieb, Hui Tong Chua, Xiaolin Wang, Frank Horowitz, Florian Wellmann, Florian Fusseis, Thomas Poulet, Heather Sheldon, Mike Trefry, Klaus Gessner, Paul Wilkes, Thomas Hoskin, Simone Seibert, Peter Cawood, Steve Reddy, Moyra Wilson, Noreen Evans, Nick Timms, Chris Clarke, Geoff Batt, Oliver Gaede, Brent Mc Innes, Sean Webb, James Cleverley, Mehroz Aspandiar, Martin Danisik, Arcady Dyskin, Elena Pasternak, Ali Karrech, David Healy, Neil Prentice, Tim Shannahan, Charlie Thorn, Steve Harvey and Mike McWilliams

Western Australian Geothermal Centre of Excellence , UWA-CSIRO-CURTIN
ARRC 29, Dick Perry Avenue 6151 Kensington WA, PO Box 1130, Bentley WA 6102

In February 2008 the WA Government announced investment into the Western Australian Geothermal Centre of Excellence with co-funding from CSIRO, UWA and Curtin University. The Centres mission is to underpin a new era of energy development; to provide excellence in geological understanding and exploitation of geothermal fields; to foster a capable work force for the geothermal industry by providing world class training to students in geothermal energy systems and to promote the development of “geothermal cities”.

The Centre establishes capacity for the Australian industry to lead the exploration and exploitation of geothermal heat in a modern society. By exploring for and utilising low-grade heat in a permeable sedimentary environment the Centre addresses an overlooked opportunity for broadening the footprint of geothermal energy utilisation. We are particularly focussing on the geological setting of sedimentary basins like the Perth Basin, where exploitable heat is available right where it can be used. We suggest that geothermal groundwater in such basins provide a unique opportunity for the Australian geothermal industry. Owing to the high natural permeability there is no need for artificial hydraulic fracturing.

The Centre consists of the constituent institutions in Perth. Its researchers will provide relevant expertise in numerical modelling, geophysics, geology, geochemistry and engineering. The numerical modelling team will build the Australian capability for geothermal modelling. It will draw on the existing expertise of the CSIRO fluid/solid mechanics and reactive flow modelling group. With 25 researchers this group is the largest such group internationally and well respected in the hard rock mining community. However, it is currently overlooked in the emerging Australian geothermal sector. Modellers from this group will participate in the Centre and nucleate cross-fertilisation between the geothermal and mining communities.

The geophysical aspects of the research consist of a collaborative CSIRO-UWA-CURTIN team. The structural geology/ hydrogeology/ microstructure/ geochemistry will be performed through an existing Curtin-UWA-CSIRO collaborative team of ten researchers including personnel from the John de Laeter Centre. This interdisciplinary team will be unique in its breadth.

The above-ground engineering aspects will be led from the UWA Mechanical Engineering Department in strong collaboration with Earth Scientists from the other institutions. These researchers are focussing on novel exploitation technologies for low-grade heat. This is an essential step for broadening the utilisation opportunities of geothermal energy in the metropolitan urban environment. We investigate zero emissions Heating Ventilating and Air Conditioning (HVAC) technologies and geothermal desalination. Our aboveground strategy is complementary to the Queensland engineering based State Centre, which focuses on electricity generation and hot rock technologies.

Keywords: Geothermal Exploration, Deep Sedimentary Targets, Modelling and Simulation, Structural geology, Hydrogeology, Geochemistry, HVAC Direct Heat Use, Desalination

Geothermal Basin Exploration

Many of Australia’s major cities are built on sedimentary basins with naturally hot aquifer systems at shallow depth, often less than 3 km depth. Permeabilities can be extremely high making them an ideal target for geothermal energy extraction.

Classically sedimentary basins are investigated for petroleum exploration and a great host of knowledge exists for this field. In our COE we acknowledge the fact that petroleum geosciences only allows us to provide a first cut at geothermal exploration. There are two main reasons for this: 1) Economic constraints demand that geothermal exploration must do better than petroleum exploration because geothermal drilling cannot afford a ratio of one successful drillhole out of seven drilling projects. 2) Geothermal targets are deep aquifers. In the petroleum geoscience it is not standard to think of deep aquifers as potential targets. Consequently heat transferred through water motions in these deep aquifers is generally neglected. Petroleum geoscience consider sophisticated approaches for thermal/sedimentary evolution modelling of sedimentary basins. In

these models heat is thought of being transferred only through conduction or through tectonic movements of rock masses and little attention is paid to the possibility of fluid heat transfer.

This assumption squarely contradicts current geothermal practice where hydrogeology has been used as the science to focus better on the flow in hot aquifers. This approach has been used successfully in many places for the calculation of geothermal extractions for district heating systems such as those in the municipalities around Munich (Germany) where a hot aquifer in the Molasse Basin is the target at 3 km depth. Judging from such successful geothermal practice hydrogeological modelling appears to be at first sight the preferred method for geothermal. However, hydrogeology falls short in the science of dealing with geological faults, 3-D complexity and in particular the possibility of geothermally driven convection.

While clearly there is merit in marrying the sciences of petroleum and hydrogeology the basic underlying assumption of hydrogeology is still topography driven flow. In such models water follows the underground topography driven by its buoyancy defined by heat content and salinity. Hydrogeological software packages therefore are not designed for dealing with true 3D aspects but they are excellent for inherently layered aquifers extruded into 3-D. In addition hydrological models tend to overlook the possibility of thermally driven convection. There are a number of numerical codes that are designed for true 3-D geothermal flows and these would appear to be the preferred tool for assessing geothermal prospects. However, these codes have been mainly used in volcanic targets. A present shortcoming is that the 3-D complexity of sedimentary basins demands implementation on supercomputer systems, which is not widely available to date.

Using the example of the Perth basin we overcome this shortcoming and develop a workflow for geothermal modelling of geothermal flows in sedimentary basins, which we will lay out in the following subsections. The workflow consists of a straight coupling between structural geological modelling, regional numerical fluid flow modelling, reservoir scale modelling and geophysical inversion. Geophysical inversion is used to dispatch the loop of structure and fluid flow modelling for matching geophysical and geological data. A more detailed description of the first part of the workflow can be found in a companion abstract (Wellman et al., this volume).

3-D structural Modelling of the Perth Basin

The Perth Basin is a half-graben system to the west of the Darling Fault extending into the marine basin to the west. It comprises permeable sedimentary rocks down to 10-15 km depth, and is deeply dissected by normal faults. The structure of the basin is known through seismic and other geophysical and drillhole data. A 3-D structural model is compiled from these data using software packages such as Geomodeller or Gocad. This model serves as a basis for groundwater flow and convection modelling. The aim is to incorporate multiscale observations of sedimentology and structural characteristics, ranging from micro-scale CT scans up to field observations. By way of example we show a structure model (Figure 1) constructed for the Harvey ridge structure in the South Perth Basin built by Thomas Hoskin and Florian Wellmann. This model is based on a database using seismic, borehole, gravity, magnetic and structural data. This structure is close to the southern industrial precinct developed around Bunbury and a potential site for a CO_2 sequestration.

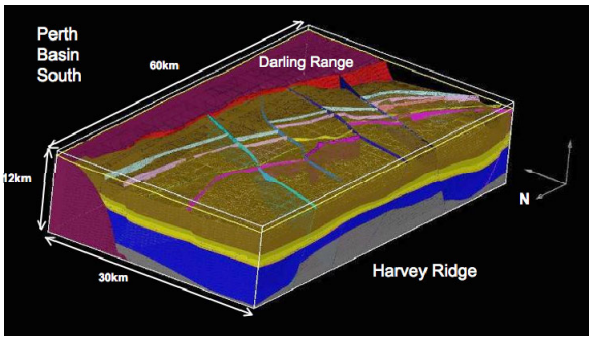

Figure 1 showing the Harvey Ridge structure in the southern part of the Perth Basin. Basement shown in grey, blue is Permian sediments, above the blue layer is the potential target for CO_2 sequestration.

3-D Numerical Regional Modelling of Fluid Flow and Heat Flow

The Perth basin comprises sediments of highly variable permeability ranging over several orders of magnitude from milli-Darcys to Darcys at several km depth. The Yarragadee aquifer is one of the largest fresh-water aquifers in the world, which is currently used to supply drinking water to metropolitan Perth. At greater than 1 km depth the temperature is too high for drinking water use (>50°C). The greater depth is the proposed target for extracting geothermal heat. The regional numerical flow modelling will use numerical models to explore the potential for fluid flow driven by heat, salinity and topography. The aim is to identify thermal upwellings and downwellings in the Perth Basin, which may be used for geothermal heat extraction/injection.

3-D Reservoir Scale Modelling

The exploitation of low-grade heat from shallow to intermediate depth aquifers is a new research field pioneered by the WA Geothermal Centre of Excellence. We intend to harness 90°C hot water for direct heat use applications, and re-inject water at ~40-50°C into the aquifer. There is no net water abstraction. The flow rate required for air conditioning large new housing developments

(e.g. 10 000 homes ca. 100 MWth base load) can be substantial and far in excess of 100-200 litres per second that are presently achieved in the water extraction bores from the aquifer. It will require an array of injection and extraction holes into the permeable Yarragadee aquifer. We will use reservoir engineering to optimise the layout of these wells using a novel approach for which a provisional patent is filed. This approach goes beyond the classical geostatistical modelling and will assimilate the outcomes of the structural, inverse and fluid flow modelling being conducted in the COE.

Geophysical Inverse Modelling

The structure of the Perth Basin is complex and not well constrained, particularly in the metropolitan area where seismic data is lacking. A detailed knowledge of the structure is required to reduce risk in exploring for geothermal heat resources. The aim of this project is to use inverse modelling techniques to refine the structural model of the Perth Basin as new data become available within the COE, e.g. from drilling and forward modelling of fluid flow. A software platform will be developed to enable calculations before drilling, and on-site data assimilation and inversion while drilling. This is in close collaboration with the CAGI (computer-aided geological inversion) initiative of CSIRO, Intrepid, BRGM, GA and UBC built around Geomodeller.

Deep Heat

This program is aimed at collaboration with the wider Australian industry and research activities focussing on high temperature geothermal activities, which is not an immediate target for the Western Australian Geothermal Centre of Excellence. We offer our leading capacity in solid mechanics, specifically for calculating high temperature fractures and high strain shear zones. We also supply our leadership in high temperature fluid dynamics, specifically chemically reactive flows, and contribute the outstanding geochemical facilities of the State Centre of Excellence John de Laeter Centre. We integrate this work with the Perth Basin by looking at the potential signature of higher temperature (paleo) systems in the Perth Basin. Extracting heat from these deeper and higher temperature systems requires an understanding of rock mechanics in the brittle-ductile transition, which is identified as the key problem in extraction of heat from “hot rock” geothermal systems. The two subprograms of the Deep Heat initiative are :

Identification of deep heat and its geochemical fingerprinting

This subprogram uses geochemical tools to define the thermal history of the Perth Basin. The mineralogy and isotopic signature of authigenic clay minerals within the basin sediments will be combined with low-T thermochronological analysis of basin sediments through (U-Th)/He and fission track dating of apatite samples to provide direct constraint of post-depositional thermal history within the temperature range relevant to geothermal circulation. This combination of analyses should be able to identify temperature variation and excursions of less than 30°C, revealing significant detail on the magnitude and temporal evolution of paleo-geothermal systems within the basin. Modelling of this geochemical data will also allow us to increase the robustness of the chemical simulation outlined in the other programs. This work will require the extraction of appropriate borehole sample materials from sandstone and siltstone units whose relationships to basin architecture can be well constrained through seismic data. $^{3}He/^{4}He$ analysis of deep fluids extracted from boreholes may also allow explicit constraint of fluid residence time in the aquifer.

Extraction of deep heat

One of the biggest challenges for the exploitation of deep geothermal power is understanding and enhancing the permeability structure at great depth. It was not the lack of heat that caused failure of the first Hot Dry Rock projects in Los Alamos and Cornwall, but the lack of pervasive permeability. We have now a lot of observations of high local permeabilities down to 9 km depth (e.g. the KTB borehole in Germany); however, we still lack understanding of what allows high permeability to exist at such high temperatures and pressures.

This subprogram targets just this problem from empirical and computational approaches. The computational approach is based on a recently developed thermodynamic formulation which allows for the first time to predict fracturing at high temperature in the brittle-ductile transition zone (Regenauer-Lieb et al., 2006). The approach predicts that most high temperature geothermal drillholes reach a depth where brittle and ductile processes are likely to compete. This critical temperature depends on rock composition (rheology), the loading rate and the presence/absence of fluids. For granite the critical temperature is of the order of ~270 °C in compression and ~230°C in extension (Figure 2).

We will pursue the fracture of hot granite and benchmark the predicted shear zones on the basis of available deep drillhole data including microstructural observations.

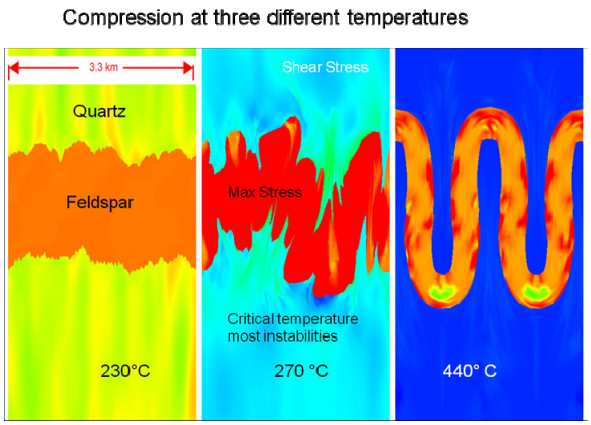

Figure 2 Numerical models of an isothermal quartz-feldspar composite slab with random thermal perturbations shortened from an initial configuration of 13.2 x 3 km to a final configuration of 3.3 x 12 km.

The empirical approach will assess the deeper Perth Basin and its likely basement to provide an assessment of the areas with deep geothermal potential. Microstructural analysis, utilizing scanning and transmission electron microscopes, X-Ray CT scans and a variety of other methods are used to examine competing deformational processes in rocks: for example the sliding of grains past each other and the formation of cavities along heterogeneous grain boundaries. The possible coupling of these mechanisms and their relation to fluid flow in deforming rocks is inferred from compositional and orientation variations in mineral grains. To this end we investigate these processes using bright X-Rays from a synchrotron source. Such sources can identify and map the 3-D connectivity of micro-sized microporosity (Figure 3). These studies are highly relevant to the high temperature shear zones modelled in Figure 2 because the microporosity under study serves as the nucleating damage for the larger scale high temperature flow of rock.

Above ground Technology

The above ground technology investigated in the Western Australian Geothermal Centre of Excellence has been the subject of the first AGEC presentation (Regenauer-Lieb et al., 2008) and shall not be repeated here. At present we focus on geothermal desalination (in cooperation with National Desalination Centre at Murdoch University) and geothermal air conditioning and cooling using geothermal fluids harvested in the Perth Basin.

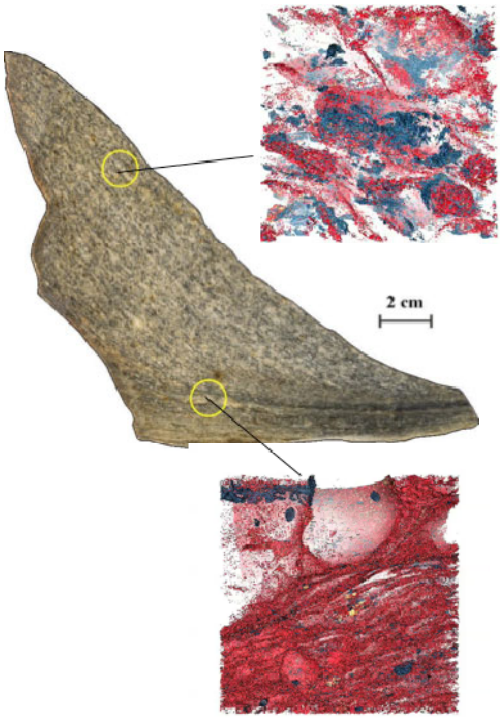

Figure 3 Hand specimen (Redbank Shear Zone) exhibiting a strain gradient from top to bottom. Representative sample series investigated by synchrotron (1.3 µm resolution) X-ray tomography are shown. Red is pore space, blue is mica and feldspar and quartz are rendered transparent. A dynamic mechanism for pumping of fluids through the shear zone centre has been identified (Fusseis et al., 2009)

Summary

We have described a tightly integrated research program for investigation of the Perth Basin Geothermal opportunity. We are particularly excited by the opportunity of intermediate to low temperature geothermal systems to contribute towards a zero emission energy supply.

References:

Fusseis, F., Regenauer-Lieb, K., Liu, J., Hough, R. and deCarlo, F., 2009. Creep Cavitation can establish a granular fluid pump through the middle crust Nature, 459: 974-977.

Regenauer-Lieb, K., Chua, H., Wang, X., Horowitz, F. and Wellmann, F., 2008. Direct-Heat Use for Australia, Australian Geothermal Energy Conference. AGEC.

Regenauer-Lieb, K., Weinberg, R. and Rosenbaum, G., 2006. The effect of energy feedbacks on continental strength. Nature, 442: 67-70.

Wellman, F, Horowitz, F, Regenauer-Lieb, K., Concept of an Integrated Workflow for Geothermal Exploration in Hot Sedimentary Aquifers, (this volume)

The development, launch and implementation of the Australian Geothermal Reporting Code and current developments

Malcolm Ward[1*], Graeme Beardsmore[2], Anthony Budd[3], Barry Goldstein[4], Fiona Holgate[5] Graham Jeffress[6], Adrian Larking[7], Jim Lawless[8], Peter Reid[9] and Adrian Williams[10]

[1] Geothermal Advisory Pty Ltd, [2]Hot Dry Rocks Pty Ltd, [3]Geoscience Australia, [4]Primary Industry and Resources, South Australia, [5]KUTh Energy Limited, [6]Australian Institute of Geoscientists, [7]Green Rock Energy Limited, [8]Sinclair Knight Merz, [9]Petratherm Limited, [10]Geodynamics Limited
*Corresponding author: PO Box 275, Orford, Tas, 7190, mward@geothermaladvisory.com

A joint committee of the Australian geothermal Energy Group (AGEG) and the Australian Geothermal Energy Association (AGEA) developed the world's first reporting code for geothermal resources, reserves and exploration results in 2007-2008. This paper, by the Geothermal Code Committee, outlines the development of the code, its basic structure and principles, implementation since August 2008 and developments since its launch.

Keywords: Geothermal reporting code, resources, reserves, exploration results, AGEA, AGEG, geothermal lexicon, ASX

History and Background

The Australian geothermal sector has expanded rapidly in the past decade, consisting now of some 11 stock exchange listed and 30 unlisted companies with geothermal exploration or development tenements. These companies are targeting Engineered Geothermal Systems (EGS), Hot Sedimentary Aquifer (HSA) and/or 'Direct Use' type geothermal plays within Australia and some are also looking at these and 'conventional' geothermal plays outside of Australia.

Australia has long had an active capital market supporting the mining and energy sectors and resources companies account for a significant proportion of the market capitalisation of companies listed on the Australian Securities Exchange (ASX). The Listing Rules of the ASX have developed alongside these traditional resources sectors to bring about a Public Reporting regime in which investors have confidence in the consistency of terminologies and mechanisms of accountability. This has greatly facilitated the raising of both debt and equity by the companies concerned.

Specifically, the Listing Rules of the ASX incorporate aspects of the Society of Petroleum Engineers (SPE) regime and, for the mining sector, the entire indigenous Joint Ore Reserves Committee (JORC) Code, which governs how Australian publicly listed mining and exploration companies may make Public Reports concerning their Mineral Resources, Ore Reserves and Exploration Results.

In 2007 a group was formed comprising stakeholders from companies, regulators and technical agencies to produce a Code to regulate Public Reporting by geothermal companies in Australia. This group is now constituted as a committee under the technical umbrella group the Australian Geothermal Energy Group and the company organisation, the Australian Geothermal Energy Association.

Development of the Geothermal Reporting Code and the Geothermal Lexicon

After considering a number of models, the 'Geothermal Code Committee' chose to base the new Australian Geothermal Reporting Code on the JORC mineral code model (Joint Ore Reserves Committee, 2004), for four main reasons:

- It had been developed and revised for more than 20 years and found to be very robust;
- Australian regulators were accepting of it;
- Mineral sector investors around the world were familiar with it and it has been formally accepted for use in some overseas jurisdictions; and
- It was desirable to minimise the introduction of new terminologies and concepts.

The scope of the new Code was designed to accommodate all forms of geothermal energy (excluding heat pumps), including 'conventional' geothermal plays.

During 2008 the Geothermal Code Committee met to resolve many issues arising in the adaptation of a minerals reporting code to the geothermal environment, whilst preserving the key terms and principles. One of the key determinations was in respect of reportable energy units, as follows:

- Thermal energy in place in Petajoules for Inferred Resources;
- The same for Indicated and Measured Resources, optionally also as recoverable thermal energy in Petajoules. These categories may also be reported as assumed electricity generation and rates

as MW_e for a defined period or GWh in total;

- Probable and Proven Reserves are reported as thermal energy in place and recoverable thermal energy (Petajoules). Electricity generation should be presented as net electricity output (MW_e) for a defined period or GWh in total.

In all cases all key assumptions should be stated alongside the energy totals and in the case of electricity generation figures, a statement on the technological pathway proposed for the energy extraction/conversion.

Another issue that called for additional consideration was the definition of the lowest confidence category, Inferred Resources. Given the high cost of drilling test wells into a reservoir, it was decided that, to allow junior companies to report early stage reservoir definition in a controlled manner, an Inferred Resource could be estimated and reported without any direct well penetration into the reservoir.

The Code governs how geothermal resources, reserves and exploration results are publically reported, but not the method of computation or estimation. However as the sector is new in Australia, the committee decided also to compile a Geothermal Lexicon which would describe good practice in estimation methodology. The Lexicon is not required to be used under the Code, but if the methodologies outlined in it are not broadly followed, then this must be stated in the Public Report.

Implementation of the Code

The Geothermal Reporting Code 2008 Edition was launched in August 2008 and was adopted as mandatory for AGEA members for a six month trial. The Geothermal Code Committee established a Compliance sub-committee which periodically reviewed Public Reports made by AGEA members and then offered confidential feedback to those companies. A number of Practice Notes were also compiled and circulated by the Geothermal Code Committee to inform AGEA members on 'best reporting practice' in respect of particular aspects of the Code.

The main issues that have been identified in the early application of the Geothermal Code include the following.

- Generation and reporting of large Inferred Resource figures which have the potential to mislead if the confidence level of the estimation is not understood by the reader. This issue comes about through the definition not requiring a direct penetration of the reservoir, allowing the energy in place of large volumes of reservoir to be reported and also because recovery factors and conversion efficiencies are not required to be made. This issue will likely be mitigated by the eventual requirement to apply a plausible recovery and conversion factors to the raw Inferred Resource figure(s). In combination, these could reduce the reportable figure to as little as 1% of the energy in place.
- Lack of understanding by companies of the role of the Competent Person in the drafting and sign-off of various types of Public Reports, such as derivative summaries of reserves and resources as might appear in Annual or Quarterly Reports. The answer here found in the Code is that each and every report of data involving a Competent Person's estimation of Resources, Reserves or exploration results must be agreed to in writing by the Competent Person.
- The amount of technical detail required in Public Reports; some reports have been very brief whilst some companies released the entire original internal technical report on the resource estimation. Ultimately it is up to the Competent Person to agree to the content of any Public Report based on their work. A very brief report will likely not contain enough information to allow the confidence on the 'bottom line' figure to be assessed, while a full report is unlikely to be comprehended by the target audience of investors. In early reports, as an education exercise, the Geothermal Code Committee has suggested more information is better than less, and a resources or reserve report of between 10 and 20 pages would be adequate, with the length of report probably decreasing over time.

The Geothermal Code has been disseminated to organisations and experts around the world and feedback has been constructive and positive. A number of comments or queries have come from technical persons concerned with the possibility of their technical freedom being restricted or bringing up particular circumstances where there is ambiguity with data or interpretation, for instance which temperature(s) in and around a reservoir should be used. In nearly all cases it can be shown that the Geothermal Reporting Code in no way limits any estimation methodology or choice of data, as long as those choices are clearly stated in the Public Report and can be justified by the Competent Person, if called upon to do so.

The Competent Person must also make judgments as to the classification of the resources and/or reserves. Again, there are no 'rules' laid out but check-lists and prompts are given in the

guidelines and at the end of the day, the experience of the Competent Person is relied upon, as is their preparedness to defend their choices.

In discussing and reporting geothermal reserves and resources, the term 'estimation' is preferred over terms such as 'measurement' to emphasise that the computation is not exact.

With use, a number of possible improvements were identified and a Second Edition of the Code will be launched in November 2009. Following the successful trial, AGEA has begun the process of having the Second Edition formally incorporated into the ASX Listing Rules.

International application

It is hoped that in co-operation with other national geothermal organisations, this Code might form the basis of a uniform, or at least a harmonised international geothermal reporting code, which will greatly assist cross-border investment and understanding based on recognised heat flow provinces.

Over-view of the Geothermal Reporting Code

The Code seeks to govern how Public Reports of Listed Companies are worded and presented. It does not govern how resources and reserves are estimated, although if methodologies deviate significantly from the conventional techniques outlined in the Geothermal Lexicon, then that must be stated.

The governing principles of the Code are:

a) **Transparency**. This requires that the reader of any Public Report is provided with sufficient information, clearly and unambiguously presented, to understand the report and not be misled;

b) **Materiality**. This requires that a Public Report contains all the relevant information which investors and their professional advisors would reasonably require, and reasonably expect to find in the report, for the purpose of making a reasoned and balanced judgment regarding the material being reported; and

c) **Competence**. This requires that the Public Report be based on work that is the responsibility of suitably qualified and experienced persons who are members of recognised, relevant professional organisations and subject to accountability and a professional Code of Ethics.

Under the Code, the writer or compiler of a technical report on either geothermal exploration results, or the estimation of geothermal resources or reserves must be a 'Competent Person' (CP), who is defined as having at least five years of relevant experience in the type of geothermal play under consideration. If a company then wishes to make a Public Report based on that work, the CP concerned must be satisfied as to the form and content of the Public Report and then must consent in writing to be personally identified as such in the report. This places a dual onus on the reporting company and the CP to produce a Public Report that is transparent, material, competent and defendable.

The categorisation of resources and reserves under the Code is illustrated as follows.

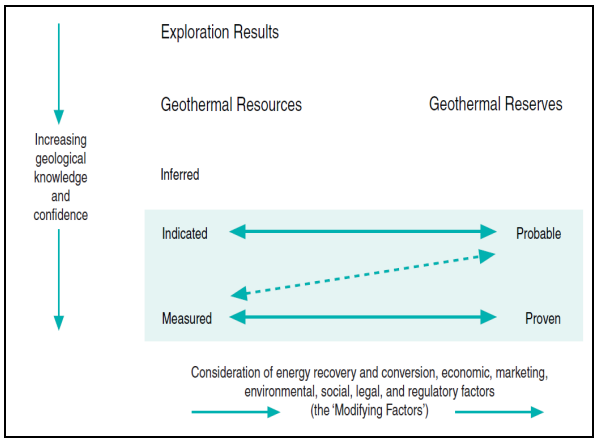

Figure 1 Structure of the Geothermal Reporting Code

With increasing levels of technical knowledge and confidence, geothermal resources progress from Inferred to Indicated to Measured. There is no claim or implication of the ability to economically extract any of the estimated resources at the time of reporting (i.e. for electricity production or 'direct use'), however there should be some expectation that reported resources may be economic under plausible circumstances in the future.

If studies into energy recovery and conversion, economic, marketing, legal and other factors are undertaken, so as to demonstrate energy extraction at a profit, then Indicated Resources may be converted into Probable Reserves and Measured Resources may be converted into Proved Reserves. The level of knowledge regarding Inferred Resources is always such that they may never convert directly into reserves. Reserves may fall back to resource status if the economics of the project decline.

Current developments (late 2009)

The 2008 Edition of the Code was reviewed during 2009 via appraisal of its performance, effectiveness and the technical outcomes resulting from its implementation and via extensive consultation with industry. The major outcome from this review will be enshrined in a Second Edition of the Code, to be launched at the November 2009 Brisbane Conference. The major effect was to change the definition of Resources and Reserves from thermal energy in place to recoverable thermal energy; units remain as PJ_{th} or MW_{th}-years. All estimates must quote a recoverable figure and state assumptions such as

recovery factor(s), base and cut-off temperatures and other key inputs. An estimate of the resource or reserve in terms of total electrical generation (in PJ_e or MW_e-years) or electrical generation over a period (X MW_e for y years) may also be quoted but only in addition to the recoverable thermal energy figure. Again, conversion factors and major assumptions must be stated.

The requirements for Competent Person statements and sign-offs did not change in the Second Edition of the Code, but were made more explicit.

Discussions are continuing with the ASX regarding having the Geothermal Reporting Code incorporated into the ASX listing rules, thereby bringing in mandatory use of the Code for ASX listed geothermal companies via the force of federal law.

The Canadian Geothermal Association, CanGEA have released a draft Geothermal Reporting Code for Canada, which is based on the Australian Reporting Code.

The authors thank the AGEG and AGEA for their encouragement in developing the Australian Geothermal Reporting Code and for permission to present this paper.

Reference

Joint Ore Reserves Committee, 2004, Australasian Code for Reporting of Exploration Results, Mineral Resources and Ore Reserves; The JORC Code 2004 The Australasian Institute of Mining and Metallurgy, the Australian Institute of Geoscientists and the Minerals Council of Australia.